Locomotor Function and the Evolution of the Primate Pelvis

by

Kristi Lynn Lewton

A Dissertation Presented in Partial Fulfillment
of the Requirements for the Degree
Doctor of Philosophy

Approved October 2010 by the
Graduate Supervisory Committee:

Mark A. Spencer, Chair
Kaye E. Reed
Gary T. Schwartz
Carol V. Ward

ARIZONA STATE UNIVERSITY

December 2010

ABSTRACT

The bony pelvis is a pivotal component of the locomotor system, as it links the hindlimb with the trunk and serves as anchorage for the primary propulsive musculature. Its shape is therefore expected to be adapted to the biomechanical demands of habitual locomotor behavior. However, because the relationship between locomotor mechanics and pelvic morphology is not well understood, the adaptive significance of particular pelvic traits and overall pelvic shape remains unclear.

This study used an integrative, dual approach to elucidate the relationship between form and function in the primate pelvis. A biomechanical cylinder model of pelvic stress resistance was tested using in vitro strain analysis of monkey and ape cadaver specimens. These results were used to refine adaptive hypotheses relating pelvic form to locomotor mechanics. Hypotheses of adaptation were then tested via univariate and geometric morphometric methods using a taxonomically broad, comparative sample of 67 primate taxa.

These results suggest that the pelvis exhibits some iliac and ischial adaptations to stress resistance that are associated with the biomechanical demands of habitual locomotor loading and of body size. The ilium and ischium exhibit relatively low levels of strain during experimental loading as well as adaptations that increase strength. The pubis exhibits relatively high strains during loading and does not vary as predicted with locomotion. This integrated study clarifies the relationship between strain and adaptation; these results support the

hypothesis that bones adapted to stress resistance exhibit low strains during typical loading.

In general, the cylinder model of pelvic biomechanics is unsupported. While the predictions of loading regimes were generally rejected, the inability of these methods to test the possible occurrence of overlapping loading regimes precludes outright rejection of the cylinder model. However, the lack of support for predicted global responses to applied loading regimes suggests that pelvic stress resistance may be better explained by a model that accounts for local, functional subunits of pelvic structure. The coalescence of a localized model of pelvic biomechanics and comparative morphometrics has great potential to shed light on the evolution of the complex, multi-functional structure of the pelvis.

ACKNOWLEDGMENTS

I extend the sincerest thanks to my committee, Mark Spencer, Kaye Reed, Gary Schwartz, and Carol Ward, for their support, encouragement, and guidance. I am especially grateful to my committee-chair, Mark Spencer, for his patience and enthusiasm during the early stages of project development, his meticulous editorial eye towards my grant proposals, and his remarkable aptitude at engineering various contraptions to facilitate data collection. I thank Kaye Reed for incredible field experiences, Gary Schwartz for always reminding me of the big picture, and Carol Ward for many enthusiastic conversations on pelvic functional morphology.

I greatly appreciate the assistance of various museum curators, collection managers, and laboratory technicians. Darrin Lunde and Eileen Westwig (American Museum of Natural History), Linda Gordon (National Museum of Natural History), Judy Chupasko (Museum of Comparative Zoology), Lyman Jellema (Cleveland Museum of Natural History), Bill Stanley (Field Museum of Natural History), Paula Jenkins and Louise Tomsett (Natural History Museum, London), Christine Lefèvre and Josephine Lesur-Gebremariam (Muséum national d'Histoire naturelle, Anatomie Comparée, Paris), Jacques Cuisin and Julie Villemain (Muséum national d'Histoire naturelle, Mammifères et Oiseaux, Paris), and Jacky Youssouf and Andry Randrianandrasana (Beza Mahafaly Special Reserve, Madagascar) provided access to osteological collections. For laboratory access and assistance with strain data collection I thank Neil Crawford, Anna

Brantley, Phillip Reyes, and Andy Baek at Barrow Neurological Institute's Spinal Biomechanics Research Laboratory.

This project would not have been possible without funding by The National Science Foundation (BCS-0752575), The L.S.B. Leakey Foundation, the Graduate and Professional Student Association at Arizona State University, the School of Human Evolution and Social Change at Arizona State University, and Sigma Xi. Other financial support was provided by a fellowship from the National Science Foundation's Integrative Graduate Education and Research Training in Neural and Musculoskeletal Adaptations in Form and Function.

I owe many, many thanks to my friends and family. Thanks to Kristen Hartnett McCann, Matt Tocheri, and Brian Villmoare and Amy Llanso for their hospitality during data collection trips. For discussions on primate anatomy and paleoanthropology, statistical and methodological assistance, and general camaraderie throughout graduate school, I thank Kate Ihle, Thierra Nalley, Teague O'Mara, Caley Orr, Terry Ritzman, Jeremiah Scott, Laura Stroik, Matt Tocheri, and Brian Villmoare. An extra thank you goes to Teague O'Mara and Laura Stroik for being there 24/7.

My family has been unendingly supportive of my pursuits. My parents, Cindy and Charles Lewton, encouraged my interests in natural history from the age of five. They accompanied a very young me to clean and prep fossil shells at the San Diego Natural History Museum (even though they could not imagine a more tedious activity) and much later in life they spent many evenings wandering the Sonoran desert looking for bones with me. Finally, my deepest gratitude goes

to my wife, Stephanie Meredith. I never dreamed that I would find her, my helpmate, and I still feel so lucky that I did; she brings a light to my life that does not exist without her. I cannot possibly thank her enough for her willingness to read countless drafts, her encouraging words, and her infinite patience.

TABLE OF CONTENTS

Page

LIST OF TABLES xv

LIST OF FIGURES xviii

CHAPTER

1 INTRODUCTION 1

2 BACKGROUND 7

Locomotor classification 7

Evolution of primate locomotion 11

Theoretical biomechanics 15

Biomechanics of primate locomotion 15

General quadrupedalism 15

Arboreal quadrupedalism 16

Terrestrial quadrupedalism 17

Vertical clinging and leaping 18

Suspension 20

Biomechanics of the primate pelvis 21

General models of pelvis stress resistance 23

Comparative primate pelvic morphology 25

Pelvic correlates of locomotor behavior 26

Ilium 26

Ischium 27

Pubis 28

CHAPTER Page

Acetabulum ... 28

Sacrum ... 29

Pelvic traits likely to reflect loading ... 30

Struts ... 30

Joints ... 31

Effects of body size on pelvic parameters ... 32

Summary and project overview ... 33

3 PATTERNS OF STRAIN IN THE PRIMATE PELVIS ... 36

Interpretation of strain patterns ... 38

Biomechanical hypotheses ... 43

Prediction A: Torsion ... 44

Prediction B: Dorsoventral compression ... 47

Prediction C: Dorsoventral bending ... 49

Materials and Methods ... 50

Sample ... 50

Specimen preparation ... 52

Gauge selection and application ... 53

In vitro strain data collection ... 55

Strain data analysis ... 59

Results ... 61

Macaca mulatta - a ... 67

Regional effects ... 67

CHAPTER Page

Strain orientation 67

Effects of angular limb position 68

Macaca mulatta - b 69

Regional effects 69

Strain orientation 69

Effects of angular limb position 70

Papio 75

Regional effects 75

Strain orientation 75

Effects of angular limb position 76

Ateles geoffroyi 80

Regional effects 80

Strain orientation 80

Effects of angular limb position 80

Hylobates lar 85

Regional effects 85

Strain orientation 85

Effects of angular limb position 86

Discussion 91

Regional and positional differences in strain patterns 91

Ilium 91

Ischium 92

CHAPTER Page

Pubis 92

Effects of angular position on strain patterns 92

Cylinder model of pelvic biomechanics 95

Conclusion 98

4 PELVIC ADAPTATIONS TO LOCOMOTION IN PRIMATES.. 100

Adaptive hypotheses 100

Linear dimensions of the pelvis 101

Traits related to pelvic stress resistance 101

Allometric scaling of pelvis traits 102

Overall pelvic shape 102

Specific predictions for locomotor categories 103

Morphometric sample 106

Morphometric data collection 110

Landmarks 110

Data acquisition 113

Measurement error 119

Missing landmarks 120

Calculation of univariate measures 121

Interlandmark distances 121

Pelvic diameters 121

Areal measures 122

Morphometric data analysis 123

CHAPTER Page

Geometric morphometric data 123

Generalized Procrustes Analysis 125

Principal Component Analysis 125

Phylogenetic analysis 127

Univariate data 128

Calculation of shape variables 130

Effects of phylogeny 131

Primate-wide analyses 136

Regression analysis 137

Statistical software 138

Hypothesis-rejection 138

Univariate results 139

Pairwise comparisons 139

Macaca fascicularis (AQ) v. *Macaca nemestrina* (TQ) ... 139

Macaca fascicularis (AQ) v. *Papio hamadryas* (TQ) 143

Otolemur crassicaudatus (AQ) v. *Galago senegalensis* (VCL) 147

Eulemur fulvus (AQ) v. *Propithecus verreauxi* (VCL) 150

Varecia variegata (AQ) v. *Propithecus verreauxi* (VCL) 155

Summary of pairwise comparisons 157

Primate-wide analyses 159

CHAPTER Page

Ilium length 160

Upper iliac height 163

Lower iliac height 166

AIIS to hip joint 170

Ilium width 173

Ischium length 177

Ischium dorsal projection 181

Acetabulum diameter 185

Superior pubic ramus length 188

Inferior pubic ramus length 191

Pubic symphysis length 195

Lower ilium cross-sectional area 199

Ischium cross-sectional area 203

Superior pubic ramus cross-sectional area 207

Inferior pubic ramus cross-sectional area 211

Auricular surface area 216

Pubic symphysis area 219

Anteroposterior diameter 222

Bi-iliac breadth 226

Biacetabular distance 230

Transverse diameter 233

Sacrum width 236

CHAPTER Page

Pelvis length 239

Summary of primate-wide analyses 248

Geometric morphometric results 250

All pelvic landmarks 250

Locomotor group patterns: PCs 1 and 2 251

Locomotor group patterns: PCs 3 and 4 252

Morphological patterns: PC 1 252

Morphological patterns: PC 2 253

Morphological patterns: PC 3 254

Morphological patterns: PC 4 254

Allometric scaling 255

Ilium landmarks 263

Locomotor group patterns: PCs 1 and 2 263

Locomotor group patterns: PCs 3 and 4 264

Morphological patterns: PC 1 264

Morphological patterns: PC 2 265

Morphological patterns: PC 3 265

Morphological patterns: PC 4 266

Allometric scaling 266

Ischiopubic landmarks 273

Locomotor group patterns: PCs 1 and 2 273

Locomotor group patterns: PCs 3 and 4 274

Morphological patterns: PC 1 274
Morphological patterns: PC 2 274
Morphological patterns: PC 3 275
Morphological patterns: PC 4 275
Allometric scaling 275
Hominoids 284
Locomotor group patterns: PCs 1 and 2 284
Locomotor group patterns: PCs 3 and 4 284
Morphological patterns: PC 1 284
Morphological patterns: PC 2 285
Morphological patterns: PC 3 286
Morphological patterns: PC 4 286
Allometric scaling 287
Summary of geometric morphometric results 291
Arboreal quadruped 291
Semi-terrestrial quadruped 291
Terrestrial quadruped 291
AQ/Slow climber 292
AQ/Leaper 292
Suspensory 292
Vertical clinger and leaper 292
Biped 292

CHAPTER Page

Discussion 292

Effects of allometry on pelvic shape 297

Effects of phylogeny on pelvic shape 300

Effects of locomotor classification on interpretation of pelvic shape 302

Conclusion 303

5 DISSERTATION DISCUSSION AND CONCLUSION 306

Evolution of the primate pelvis 306

Functional and evolutionary adaptation 306

General biomechanical model of the primate pelvis 312

Morphological integration and modularity 314

Conclusion 316

LITERATURE CITED 319

APPENDIX

A OSTEOLOGICAL SAMPLE FOR COMPARATIVE MORPHOMETRICS 347

B DISTANCE MATRICES FOR GEOMETRIC MORPHOMETRIC AND PHYLOGENETIC DATA 353

C BOX PLOTS OF PELVIC MEASURES FOR PAIRWISE COMPARISON ANALYSES 362

D POST HOC MULTIPLE COMPARISONS TABLES FOR UNIVARIATE ANALYSES 407

LIST OF TABLES

Table		Page
2-1	Napier and Napier's (1967) primate locomotion classification	10
2-2	Locomotor categories used in this project	11
3-1	Cadaver specimens used in bone strain analysis	51
3-2	Average and absolute maximum values of ε_1, ε_2, α, and γ across angular limb positions	62
3-3	ε_1, ε_2, angle of ε_1, and shear strains for each limb angular position.	64
3-4	Results from *Macaca mulatta* –a pilot specimen. ε_1, ε_2, angle of ε_1/ ε_2, and shear strains for each limb angular position	66
3-5	Predicted and observed average peak principal strains..	93
4-1	Predictions of univariate pelvic dimensions based on biomechanical requirements of locomotion.	105
4-2	Comparative morphometric osteological sample..	109
4-3	Three-dimensional pelvic landmarks..	112
4-4	Univariate measures of the pelvis..	116
4-5	Measurement error represented by minimum, maximum, and mean landmark deviations derived from data collection of ten replicate landmark configurations on one *Alouatta* pelvis..	120
4-6	List of taxa used in geometric morphometric analysis..	124
4-7	Ilium and acetabulum subset of landmarks.	126
4-8	Ischiopubic and acetabulum subset of landmarks..	127
4-9	List of taxa used in univariate analyses	129

Table Page

4-10 Estimates of λ- and K-statistics for phylogenetic signal in a subset of univariate measures.. 134

4-11 Taxa used in pairwise comparisons..... 136

4-12 Descriptive statistics and Mann-Whitney U results of comparison between *Macaca fascicularis* and *Macaca nemestrina* males.. 142

4-13 Descriptive statistics and Mann-Whitney U results of comparison between *Macaca fascicularis* and *Papio hamadryas* males..... 145

4-14 Descriptive statistics and Mann-Whitney U results of comparison between *Macaca fascicularis* and *Papio hamadryas* females.. 146

4-15 Descriptive statistics and Mann-Whitney U results of comparison between *Galago senegalensis* and *Otolemur crassicaudatus* males.. 149

4-16 Descriptive statistics and Mann-Whitney U results of comparison between *Eulemur fulvus* and *Propithecus verreauxi* males..... 152

4-17 Descriptive statistics and Mann-Whitney U results of comparison between *Eulemur fulvus* and *Propithecus verreauxi* females.. 153

4-18 Descriptive statistics and Mann-Whitney U results of comparison between *Eulemur fulvus* and *Propithecus verreauxi* unknown sex..... 154

4-19 Descriptive statistics and Mann-Whitney U results of comparison between *Varecia variegata* and *Propithecus verreauxi* males and females.. 156

Table Page

4-20 Results of reduced major axis scaling analyses for the primate-wide and individual locomotor group samples.. 243

4-21 PCA results for all landmarks; *Homo sapiens* excluded.. 256

4-22 Results of least squares regression of principal component scores on ln centroid size.. 261

4-23 PCA results for ilium and acetabulum landmarks; *Homo sapiens* excluded.. 267

4-24 PCA results for ischiopubis and acetabulum landmarks; *Homo sapiens* excluded.. 277

4-25 PCA results for all landmarks; hominoids only.. 288

LIST OF FIGURES

Figure Page

2-1 Representation of Kummer's (1975) two-armed lever model of the pelvis.... 24

3-1 Feedback loop demonstrating the processes by which bone maintains optimal strain levels. Adapted from Lanyon (1982) and Rubin (1984)... 41

3-2 Predictions of compressive and tensile strains during torsion of (a) a generalized cylinder or beam and (b) a primate pelvis in ventral view..... 46

3-3 Predictions of compressive and tensile strains during dorsoventral compression of (a) a generalized cylinder or beam and (b) a primate pelvis in transverse view..... 48

3-4 Predictions of compressive and tensile strains during dorsoventral bending of (a) a generalized cylinder or beam and (b) a primate pelvis in sagittal/lateral view..... 50

3-5 Gauge locations ("R" represents the reference gauge)... 54

3-6 Materials testing system with the *Ateles* specimen in the 90° limb position... 56

3-7 Angular limb positions during hindlimb loading by the materials testing system... 58

3-8 Raw strain data plotted against time, ε_1 is positive, ε_2 is negative.... 58

3-9 Gauge locations for the *Macaca mulatta* –a specimen... 68

Figure Page

3-10 Average absolute maximum values of maximum (ε_1) and minimum (ε_2) principal strains across limb positions for *Macaca mulatta* –b... 71

3-11 Maximum shear strain for each limb position, by gauge, for *Macaca mulatta* –b... 72

3-12 Right anterior (a) and right medial (b) views of a pelvis depicting the angular orientation of the average maximum principal strains (ε_1) recorded by each strain gauge on the *Macaca* specimen..... 73

3-13 Average absolute maximum values of maximum (ε_1) and minimum (ε_2) principal strains across limb positions for *Papio*.... 76

3-14 Maximum shear strain for each limb position, by gauge, for *Papio*.... 77

3-15 Right anterior (a) and right medial (b) views of a pelvis depicting the angular orientation of the average maximum principal strains (ε_1) recorded by each strain gauge on the *Papio* specimen..... 78

3-16 Average absolute maximum values of maximum (ε_1) and minimum (ε_2) principal strains across limb positions for *Ateles*.... 81

3-17 Maximum shear strain for each limb position, by gauge, for *Ateles*.... 82

3-18 Right anterior (a) and right medial (b) views of a pelvis depicting the angular orientation of the average maximum principal strains (ε_1) recorded by each strain gauge on the *Ateles* specimen..... 83

Figure Page

3-19 Average absolute maximum values of maximum (ε_1) and minimum (ε_2) principal strains across limb positions for *Hylobates*.... 87

3-20 Maximum shear strain for each limb position, by gauge, for *Hylobates*.... 88

3-21 Right anterior (a) and right medial (b) views of a pelvis depicting the angular orientation of the average maximum principal strains (ε_1) recorded by each strain gauge on the *Hylobates* specimen..... 89

3-22 Maximum shear strain for each limb angular position, by gauge and specimen..... 94

4-1 Lateral (a), anterior (b), and posterior (c) views of a pelvis depicting the three-dimensional landmarks used in this study. Some landmarks are shown in multiple views..... 113

4-2 A consensus phylogeny of the taxa used in this study derived from GenBank data (from the 10kTrees website, Arnold et al., 2010)..... 135

4-3 Box-and-whiskers plots comparing the medians and ranges of the ilium length shape variable for each locomotor group..... 161

4-4 Box-and-whiskers plots of medians and ranges of the ilium length shape variable for each taxon..... 162

4-5 Bivariate plot of ln-ilium length on ln-body mass$^{1/3}$.... 163

4-6 Box-and-whiskers plots comparing the medians and ranges of the upper iliac height shape variable for each locomotor group..... 164

Figure Page

4-7 Box-and-whiskers plots of medians and ranges of the upper iliac height shape variable for each taxon.... 165

4-8 Bivariate plot of ln-upper iliac height on ln-body mass$^{1/3}$..... 166

4-9 Box-and-whiskers plots comparing the medians and ranges of the lower iliac height shape variable for each locomotor group..... 168

4-10 Box-and-whiskers plots of medians and ranges of the lower iliac height shape variable for each taxon.... 169

4-11 Bivariate plot of ln-lower iliac height on ln-body mass$^{1/3}$..... 170

4-12 Box-and-whiskers plots comparing the medians and ranges of the AIIS-to-hip joint shape variable for each locomotor group..... 171

4-13 Box-and-whiskers plots of medians and ranges of the AIIS-to-hip joint shape variable for each taxon 172

4-14 Bivariate plot of ln-AIIS-to-hip joint on ln-body mass$^{1/3}$..... 173

4-15 Box-and-whiskers plots comparing the medians and ranges of the ilium width shape variable for each locomotor group..... 175

4-16 Box-and-whiskers plots of medians and ranges of the ilium width shape variable for each taxon.... 176

4-17 Bivariate plot of ln-ilium width on ln-body mass$^{1/3}$.... 177

4-18 Box-and-whiskers plots comparing the medians and ranges of the ischium length shape variable for each locomotor group..... 179

4-19 Box-and-whiskers plots of medians and ranges of the ischium length shape variable for each taxon.... 180

Figure Page

4-20 Bivariate plot of ln-ischium length on ln-body mass$^{1/3}$.... 181

4-21 Box-and-whiskers plots comparing the medians and ranges of the ischium dorsal projection shape variable for each locomotor group..... 183

4-22 Box-and-whiskers plots of medians and ranges of the ischium dorsal projection shape variable for each taxon..... 184

4-23 Bivariate plot of ln-ischium dorsal projection on ln-body mass$^{1/3}$.... 185

4-24 Box-and-whiskers plots comparing the medians and ranges of the acetabulum diameter shape variable for each locomotor group..... 186

4-25 Box-and-whiskers plots of medians and ranges of the acetabulum diameter shape variable for each taxon.... 187

4-26 Bivariate plot of ln-acetabulum diameter on ln-body mass$^{1/3}$.... 188

4-27 Box-and-whiskers plots comparing the medians and ranges of the superior pubic ramus length shape variable for each locomotor group..... 189

4-28 Box-and-whiskers plots of medians and ranges of the superior pubic ramus length shape variable for each taxon.... 190

4-29 Bivariate plot of ln-superior pubic ramus length on ln-body mass$^{1/3}$..... 191

Figure Page

4-30 Box-and-whiskers plots comparing the medians and ranges of the inferior pubic ramus length shape variable for each locomotor group..... 193

4-31 Box-and-whiskers plots of medians and ranges of the inferior pubic ramus length shape variable for each taxon.... 194

4-32 Bivariate plot of ln-inferior pubic ramus length on ln-body mass$^{1/3}$.... 195

4-33 Box-and-whiskers plots comparing the medians and ranges of the pubic symphysis length shape variable for each locomotor group..... 197

4-34 Box-and-whiskers plots of medians and ranges of the pubic symphysis length shape variable for each taxon..... 198

4-35 Bivariate plot of ln-pubic symphysis length on ln-body mass$^{1/3}$.... 199

4-36 Box-and-whiskers plots comparing the medians and ranges of the lower ilium cross-sectional area shape variable for each locomotor group..... 201

4-37 Box-and-whiskers plots of medians and ranges of the lower ilium cross-sectional area shape variable for each taxon.... 202

4-38 Bivariate plot of ln-lower ilium cross-sectional area on ln-body mass$^{1/3}$.... 203

Figure Page

4-39 Box-and-whiskers plots comparing the medians and ranges of the ischium cross-sectional area shape variable for each locomotor group..... 205

4-40 Box-and-whiskers plots of medians and ranges of the ischium cross-sectional area shape variable for each taxon.... 206

4-41 Bivariate plot of ln-ischium cross-sectional area on ln-body mass$^{1/3}$.... 207

4-42 Box-and-whiskers plots comparing the medians and ranges of the superior pubic ramus cross-sectional area shape variable for each locomotor group..... 209

4-43 Box-and-whiskers plots of medians and ranges of the superior pubic ramus cross-sectional area shape variable for each taxon.... 210

4-44 Bivariate plot of ln-superior pubic ramus cross-sectional area on ln-body mass$^{1/3}$.... 211

4-45 Box-and-whiskers plots comparing the medians and ranges of the inferior pubic ramus cross-sectional area shape variable for each locomotor group..... 214

4-46 Box-and-whiskers plots of medians and ranges of the inferior pubic ramus cross-sectional area shape variable for each taxon.... 215

4-47 Bivariate plot of ln-inferior pubic ramus cross-sectional area on ln-body mass$^{1/3}$.... 216

Figure Page

4-48 Box-and-whiskers plots comparing the medians and ranges of the auricular surface area shape variable for each locomotor group..... 217

4-49 Box-and-whiskers plots of medians and ranges of the auricular surface area shape variable for each taxon..... 218

4-50 Bivariate plot of ln-auricular surface area on ln-body mass$^{1/3}$..... 219

4-51 Box-and-whiskers plots comparing the medians and ranges of the pubic symphysis area shape variable for each locomotor group..... 220

4-52 Box-and-whiskers plots of medians and ranges of the pubic symphysis area shape variable for each taxon..... 221

4-53 Bivariate plot of ln-pubic symphysis area on ln-body mass$^{1/3}$..... 222

4-54 Box-and-whiskers plots comparing the medians and ranges of the anteroposterior pelvic diameter shape variable for each locomotor group..... 224

4-55 Box-and-whiskers plots of medians and ranges of the anteroposterior pelvic diameter shape variable for each taxon..... 225

4-56 Bivariate plot of ln-anteroposterior pelvic diameter on ln-body mass$^{1/3}$..... 226

4-57 Box-and-whiskers plots comparing the medians and ranges of the bi-iliac breadth shape variable for each locomotor group..... 228

4-58 Box-and-whiskers plots of medians and ranges of the bi-iliac breadth shape variable for each taxon..... 229

4-59 Bivariate plot of ln-bi-iliac breadth on ln-body mass$^{1/3}$..... 230

Figure Page

4-60 Box-and-whiskers plots comparing the medians and ranges of the biacetabular diameter shape variable for each locomotor group..... 231

4-61 Box-and-whiskers plots of medians and ranges of the biacetabular diameter shape variable for each taxon..... 232

4-62 Bivariate plot of ln-biacetabular diameter on ln-body mass$^{1/3}$..... 233

4-63 Box-and-whiskers plots comparing the medians and ranges of the maximum transverse diameter shape variable for each locomotor group..... 234

4-64 Box-and-whiskers plots of medians and ranges of the maximum transverse diameter shape variable for each taxon 235

4-65 Bivariate plot of ln-maximum transverse diameter on ln-body mass$^{1/3}$.... 236

4-66 Box-and-whiskers plots comparing the medians and ranges of the sacrum width shape variable for each locomotor group..... 237

4-67 Box-and-whiskers plots of medians and ranges of the sacrum width shape variable for each taxon.... 238

4-68 Bivariate plot of ln-sacrum width on ln-body mass$^{1/3}$.... 239

4-69 Box-and-whiskers plots comparing the medians and ranges of the pelvic length shape variable for each locomotor group..... 240

4-70 Box-and-whiskers plots of medians and ranges of the pelvic length shape variable for each taxon.... 241

Figure Page

4-71 Bivariate plot of ln-pelvis length on ln-body mass$^{1/3}$.... 242

4-72 Bivariate plot of principal component 1 on principal component 2 for the dataset containing all landmarks. Individuals are plotted (n = 794).... 257

4-73 Bivariate plot of principal component 1 on principal component 2 for the dataset containing all landmarks..... 258

4-74 Bivariate plot of principal component 3 on principal component 4 for the dataset containing all landmarks..... 259

4-75 Bivariate plot of principal component 3 on principal component 4 for the dataset containing all landmarks..... 260

4-76 Bivariate plot of principal component 1 on ln centroid size for the dataset containing all landmarks. Results of the Pearson's correlation are included..... 262

4-77 Bivariate plot of principal component 4 on ln centroid size for the dataset containing all landmarks. Results of the Pearson's correlation are included..... 262

4-78 Bivariate plot of principal component 1 on principal component 2 for the dataset containing ilium landmarks..... 268

4-79 Bivariate plot of principal component 1 on principal component 2 for the dataset containing ilium landmarks..... 269

4-80 Bivariate plot of principal component 3 on principal component 4 for the dataset containing ilium landmarks..... 270

Figure Page

4-81 Bivariate plot of principal component 3 on principal component 4 for the dataset containing ilium landmarks..... 271

4-82 Bivariate plot of principal component 1 on ln centroid size for the dataset containing ilium landmarks. Results of the Pearson's correlation are included..... 272

4-83 Bivariate plot of principal component 2 on ln centroid size for the dataset containing ilium landmarks. Results of the Pearson's correlation are included..... 272

4-84 Bivariate plot of principal component 4 on ln centroid size for the dataset containing ilium landmarks. Results of the Pearson's correlation are included..... 273

4-85 Bivariate plot of principal component 1 on principal component 2 for the dataset containing ischiopubic landmarks..... 278

4-86 Bivariate plot of principal component 1 on principal component 2 for the dataset containing ischiopubic landmarks..... 279

4-87 Bivariate plot of principal component 3 on principal component 4 for the dataset containing ischiopubic landmarks..... 280

4-88 Bivariate plot of principal component 3 on principal component 4 for the dataset containing ischiopubic landmarks..... 281

4-89 Bivariate plot of principal component 1 on ln centroid size for the dataset containing ischiopubic landmarks. Results of the Pearson's correlation are included..... 282

Figure Page

4-90 Bivariate plot of principal component 2 on ln centroid size for the dataset containing ischiopubic landmarks. Results of the Pearson's correlation are included..... 282

4-91 Bivariate plot of principal component 4 on ln centroid size for the dataset containing ischiopubic landmarks. Results of the Pearson's correlation are included..... 283

4-92 Bivariate plot of principal component 5 on ln centroid size for the dataset containing ischiopubic landmarks. Results of the Pearson's correlation are included..... 283

4-93 Bivariate plot of principal component 1 on principal component 2 for the dataset containing hominoid taxa only..... 289

4-94 Bivariate plot of principal component 3 on principal component 4 for the dataset containing hominoid taxa only..... 290

CHAPTER 1: INTRODUCTION

Locomotion is crucial to understanding extant and extinct primate biology because it is a fundamental component of daily activities such as foraging, travel, and predator avoidance (e.g., Morbeck, 1976; Rose, 1977; Mittermeier, 1978; Cant, 1986; Boinski, 1989; Oxnard et al., 1990; Dagosto, 1995; Garber and Preutz, 1995; Doran, 1996; Nekaris, 2001; Bitty and McGraw, 2007; Bezanson, 2009). The pelvis is a particularly important component of locomotor anatomy because it links the hindlimb locomotor system with the trunk and serves as anchorage for the primary propulsive musculature (Gray, 1918; Ankel-Simons, 2000). During locomotor behaviors, the pelvis is subjected to stresses produced by both muscle contraction and substrate reaction forces, which are transmitted through the hip and sacroiliac joints (Badoux, 1974; Dalstra and Huiskes, 1995; Levangie and Norkin, 2001). Pelvic form is therefore expected to be influenced by the differing mechanical requirements of alternate locomotor behaviors, and accordingly, previous workers have identified overall patterns of variation in pelvic morphology among some locomotor groups (e.g., Waterman, 1929; Steudel, 1981a; Berge, 1984; Ward, 1991; Fleagle and Anapol, 1992; Anemone, 1993; MacLatchy and Bossert, 1996; MacLatchy, 1998). Despite its central role in the locomotor system, our understanding of pelvic form and function is limited compared to knowledge of limb bone functional morphology (for a review of the relevant literature, see Ruff and Runestad, 1992; Ruff, 2002; Lieberman et al., 2004).

The pelvis has historically been examined for allometric effects (e.g., Schultz, 1949; Black, 1970; Gingerich, 1972; Leutenegger, 1973; Mobb and Wood, 1977; Steudel, 1981b; Leutenegger and Larson, 1985; Hager, 1989; Tague, 1991; Pissinatti et al., 1992; Tague, 1993, 1995; Hager, 1996; St. Clair, 2007) and the influences of obstetrical requirements and brain size on pelvic shape (e.g., Leutenegger, 1974, 1982; Abitbol, 1991; Bouhallier et al., 2004; Tague, 2005), especially in relation to the evolution of early hominins and the origins of bipedality (e.g., Reynolds, 1931; Dart, 1949; Le Gros Clark, 1955; Day, 1973; Lovejoy et al., 1973; Brain and Vrba, 1974; McHenry, 1975; Ashton et al., 1981; Berge, 1984; Berge and Kazmierczak, 1986; Rak and Arensburg, 1987; Hager, 1989; Berge, 1991; Rak, 1991; Fleagle and Anapol, 1992; Rosenberg, 1992; Berge, 1994; Ruff, 1995; MacLatchy, 1996; Macchiarelli et al., 1999; Marchal, 2000; Haeusler, 2002; Bouhallier et al., 2004; Lovejoy, 2005; Lovejoy et al., 2009; Weaver and Hublin, 2009; Ruff, 2010). While these other functional constraints on pelvic shape have been relatively well-studied, few studies have addressed the relationship between pelvic anatomy and locomotor behavior in non-human primates. Early workers described pelvic shape in select primate taxa (e.g., Mivart, 1867; Straus, 1929; Waterman, 1929; Schultz, 1930, 1936; Carleton, 1937; Washburn, 1942; Schultz, 1969; Zuckerman et al., 1973; Jouffroy, 1975), but many of these studies did not capture the full phylogenetic range of variation in primate pelvis shape and lacked a biomechanical framework. More recent studies on skeletal correlates of locomotor behavior in primate pelves (e.g., Ashton et al., 1981; Berge, 1984; Ward, 1991; Fleagle and Anapol, 1992;

Anemone, 1993; MacLatchy and Bossert, 1996; MacLatchy, 1998) have identified general suites of morphologies that correspond to locomotor behavior, but these correlations have typically been based on untested assumptions of pelvic mechanics, and did not examine three-dimensional aspects of pelvic shape, which could lend more insight into locomotor adaptations than just two-dimensional measures alone. Because pelvic correlates of locomotion are used to make inferences of locomotor behavior in fossil primates (e.g., Jungers, 1976; Ashton et al., 1981; Stern and Susman, 1983; McCrossin and Benefit, 1992; Ward et al., 1993; Fleagle and Simons, 1995; MacLatchy and Bossert, 1996; Anemone and Covert, 2000; Marivaux et al., 2008; Lovejoy et al., 2009; Berger et al., 2010), it is critical that their adaptive value and biomechanical context are appreciated (Ross et al., 2002).

It is important to note here that questions regarding adaptation and biomechanics are different; adaptive questions are evolutionary in nature, while mechanical questions are functional. This distinction may be better appreciated as questions that address ultimate (*i.e.*, adaptive) and proximate (*i.e.*, mechanical or functional) causes of structure. Ultimate and proximate causes of structure are, of course, linked because morphologies that result from mechanical or functional requirements are generally adaptive; the difference between these types of questions is in the perspective and scope of each. This project is concerned with both types of questions, and the theoretical approaches to addressing these questions follow below.

Identifying adaptation requires a correlation between trait and function, and a demonstration of a functional link between trait and function (Kay and Cartmill, 1977). To distinguish form-function correlations, the comparative method, which identifies adaptation via tests in comparative taxonomic samples, is typically used (Felsenstein, 1985; Harvey and Pagel, 1991; Ross et al., 2002). Although accurately inferring function from morphology can be difficult (Lauder, 1995), the strength of trait-function associations is increased when they can be demonstrated to occur repeatedly in a comparative sample. There are two approaches to demonstrating trait-function associations—the homology approach and the homoplasy approach—and within these there are several different criteria that are variably used (depending on one's definition of adaptation) to identify adaptations (e.g., see Rudwick, 1964; Bock and von Wahlert, 1965; Gould and Lewontin, 1979; Bock, 1980; Gould and Vrba, 1982; Baum and Larson, 1991; Coddington, 1994). The homology approach identifies adaptation through analysis of individual historical (cladogenic) events, but it does not address the possible effects of phylogenetic inertia (Coddington, 1994). The convergence (*i.e.*, homoplasy) approach (Coddington, 1994) requires multiple origination events (which increases the statistical power of analyses of adaptation) and is best-suited to the objective of identifying locomotor adaptations of the pelvis because it is more resistant to the possible (and likely) confounding effects of phylogeny (Lockwood and Fleagle, 1999). To minimize the effect of possible differences in morphology due to distant-relatedness (a problem inherent in the homoplasy approach), pairwise comparisons should be used in which several

pairs of closely related taxa that differ in behavior (and are therefore predicted to differ in functional adaptation) are compared in order to validate trait-function associations (as in, for example, Fleagle, 1976; Kay and Cartmill, 1977; Fleagle and Mittermeier, 1980; Fleagle and Meldrum, 1988; Tague, 1993; Spencer, 2003; Orr et al., 2007).

While pairwise comparisons may identify correlations between traits and functions, a more rigorous comparative approach also incorporates the formation and testing of *a priori* functional hypotheses (to show that the trait "has" the function) (Kay and Cartmill, 1977). Previous studies have proposed several hypotheses of pelvic adaptation to locomotion (e.g., Waterman, 1929; Schultz, 1969; Jungers, 1976; Jenkins and Camazine, 1977; Sigmon and Farslow, 1986; Ward, 1991; Fleagle and Anapol, 1992; Anemone, 1993; MacLatchy, 1998), but these have not been tested in a systematic manner. Additionally, many existing hypotheses are based on trait-function correlation alone, and not on predictions derived from the mechanical requirements of different locomotor behaviors (that is, traits hypothesized to be "adaptations" to locomotion have not been shown to perform the specified function). One way to demonstrate that a trait performs a function is by using optimality criteria to form predictions of morphology based on the biomechanics of the system (similar to Rudwick's [1964] paradigm method). It is in this way that the development of adaptive hypotheses relies on an understanding of a solid biomechanical foundation of the system. Although a biomechanical model of pelvic stress resistance in non-human primates has been proposed (Badoux, 1974; Kummer, 1975; Pauwels, 1980), it has not been

experimentally tested, which leaves its validity indeterminate. This project seeks to refine this biomechanical model and to test specific predictions of how the pelvis resists stress.

This project addresses two broad research questions: 1) how does the primate pelvis respond to loading? And 2) how does pelvic shape reflect locomotion within primates? Examining these questions requires the use of an integrative, dual approach that tests both evolutionary and mechanical hypotheses. This is accomplished by articulating experimental biomechanics (*in vitro* studies of mechanical stress resistance) with comparative morphometrics (measures of bony shape). In the current study, a theoretical model of pelvic mechanics was refined (from previous studies, see Badoux, 1974; Kummer, 1975; Pauwels, 1980) and predictions derived from it were tested using *in vitro* strain gauge methods on a small sample of primate cadavers. These results were used to identify those regions of pelvic anatomy that appear to be functionally relevant, and adaptive hypotheses regarding these regions were developed (or elaborated upon, in the case of existing hypotheses). These biomechanically-supported adaptive hypotheses of form-function relationships between both three-dimensional (3D) and 2D pelvic morphology and locomotion were then tested.. This was done using a large sample of 67 primate taxa and a comparative approach that incorporated control for the effects of phylogeny and body size on morphology. Using experimental and comparative approaches in tandem will necessarily contribute to a better understanding of primate pelvic functional morphology, which is particularly useful for reconstructions of locomotion in fossil primates.

CHAPTER 2: BACKGROUND

Theoretically, there is an interplay between ultimate and proximate questions, where answers to each inform study of the other. In this case, answering evolutionary questions about how the pelvis is adapted to locomotion first requires answers to questions regarding the proximate influences on pelvic shape. Study of just one set of these questions without the other results in an incomplete understanding of the form-function relationship between pelvic anatomy and locomotion (Autumn et al., 2002). In this study, the evolutionary and biomechanical sets of questions each have their own paradigms. This chapter details the relevant theoretical framework for both aspects of this work. Because this research aims to determine differences in pelvic shape according to locomotor mode, a brief discussion is offered, first, on the basis for the locomotor classification used in this study and on the evolution of primate locomotion. Then, a discussion of the biomechanics of locomotion in general and of the pelvis in particular is followed by a synthesis of previous work on primate pelvic adaptations to locomotion and a summary of how this study combines experimental and comparative approaches to answer questions related to the form and evolution of the primate pelvis.

LOCOMOTOR CLASSIFICATION

Primates are classified into locomotor groups as a means of simplifying the diverse behaviors they exhibit. As with all examples of categorization, some information is lost in the process of classifying the diverse locomotor behaviors of primates. Two primary methods of classification of primate locomotion have been

used—one based on behavior (*e.g.*, Napier and Napier, 1967) and the other based on functional criteria (Oxnard et al., 1990).

The behavior-based method of locomotor classification establishes locomotor categories on the *dominant* form of locomotion observed (that is, the behavior that is used the highest percentage of the time). As proposed by Napier and Napier (1967), this method defines four broad categories of locomotion: 1) vertical clinging and leaping, 2) quadrupedalism, 3) brachiation, and 4) bipedalism. Of these, quadrupedalism and brachiation each have subcategories of locomotion, for example, arboreal and terrestrial quadrupedalism (Table 2-1). This method of classification is often utilized because of its simplicity, but has been criticized (e.g., Prost, 1965; Oxnard, 1974; Oxnard et al., 1990). It overlooks rarely used but potentially important locomotor modes—for example, chimpanzees, a group of predominantly knuckle-walking taxa, also climb and use suspensory postures, which may be selectively important. It also lumps behaviors within a broad category even though they may be functionally distinct—for example, "vertical clinging and leaping" does not differentiate between the two biomechanically different forms of leaping exhibited by small and large-bodied leapers (Oxnard, 1974).

The functionally-based method of locomotor classification focuses on the musculoskeletal system as just that—a system composed of regional anatomies (*e.g.*, shoulder complex, hip complex, etc.) with biological roles in all aspects of life, including locomotion and feeding behavior. As such, it takes both behavior and anatomy into account (Oxnard et al., 1990). Oxnard et al.'s (1990) approach

to locomotor classification is unique in appropriately conceptualizing the diverse range of behaviors and morphologies exhibited by primates as a "behavioral-anatomical interface," (Oxnard et al., 1990), but it suffers from difficulties in discerning differences among major groups of taxa. It does not place taxa into discrete groups, but instead arranges them in a spectral pattern. Although the concept of using functional spectra to explain diverse primate morphologies is appealing, it is not the most pragmatic because it is analytically less tractable. First, precise data on locomotor behavior does not exist for all species of primates, which limits the available sample size. Second, considering both anatomy and behavior simultaneously precludes an understanding of the precise functional relationship between them.

In this dissertation, the locomotor groups used are similar to those proposed by Napier and Napier (1967) because of the simplicity of the method, and because it is hoped that the results from this research will be used to reconstruct locomotion in the fossil record, which, because of the lack of direct behavioral data for those taxa, requires identifying morphological differences among discrete groups (Table 2-2).

TABLE 2-1. Napier and Napier's (1967) primate locomotion classification.

Locomotor Category	Sub-type	Activity	Primate genera
Vertical Clinging and Leaping		Leaping in trees and hopping on the ground	*Avahi, Galago, Hapalemur, Lepilemur, Propithecus, Indri, Tarsius*
Quadrupedalism	Slow climbing	Cautious climbing—no leaping or branch running	*Arctocebus, Loris, Nycticebus, Perodicticus*
	Arboreal	Climbing, springing, branch running and jumping	*Aotus, Cacajao, Callicebus, Callimico, Callithrix, Cebuella, Cebus, Cercopithecus, Cheirogaleus, Chiropotes, Lemur, Leontideus, Phaner, Pithecia, Saguinus, Saimiri, Tupaia*
	Terrestrial	Climbing, ground running	*Macaca, Mandrillus, Papio, Theropithecus, Erythrocebus*
	NW Suspension	Arm-swinging with use of prehensile tail; little leaping	*Alouatta, Ateles, Brachyteles, Lagothrix*
	OW Suspension	Arm-swinging and leaping	*Colobus, Nasalis, Presbytis, Pygathrix, Rhinopithecus, Simias*
Brachiation	True	Gibbon type of brachiation	*Hylobates, Symphalangus*
	Modified	Chimpanzee and orang-utan type of brachiation	*Gorilla, Pan, Pongo*
Bipedalism		Striding	*Homo*

TABLE 2-2. Locomotor categories used in this project.

Locomotor Category	Sub-type	Exemplars
Arboreal Quadrupedalism		*Otolemur crassicaudatus, Macaca fascicularis, Cebus*
	AQ/Leaping	*Colobus, Nasalis*
	AQ/Slow-climbing	*Nycticebus, Perodicticus, Loris*
	AQ/Suspension	*Alouatta, Lagothrix*
Terrestrial Quadrupedalism		*Papio, Mandrillus, Erythrocebus*
	TQ/Knuckle-walking	*Pan, Gorilla*
	TQ/AQ	*Chlorocebus*, *Macaca mulatta*
Vertical Clinging and Leaping		*Propithecus, Galago, Hapalemur, Tarsius*
Suspensory		*Ateles, Hylobates, Symphalangus, Pongo*
Bipedalism		*Homo*

EVOLUTION OF PRIMATE LOCOMOTION

As a group, living and extinct primates inhabit and have inhabited a diverse array of ecological niches. Primates are arboreal, terrestrial, nocturnal, diurnal, and cathemeral, and live in biomes ranging from rainforest to desert (e.g., Napier and Napier, 1967; Strier, 2006). As a result of the widely varying mechanical demands and constraints of these various ecological niches, primate locomotor and postural behaviors are correspondingly complex and diverse (Napier and Napier, 1967; Strier, 2006). Among mammalian orders, primates are arguably the most diverse in their locomotor behaviors (except perhaps for the marsupial Order Diprotodontia, which has arboreal, terrestrial, fossorial, leaping, and gliding taxa). Because of this wide variation in locomotor niches that primates exhibit, the primate order is an ideal taxon to study form-function relationships between anatomy and locomotion.

Arboreal habitats, which comprise uneven substrates of varying diameters, stiffness, and orientation, are mechanically challenging to maneuver. Primates exhibit a suite of gait characteristics that are unique among mammals (see below), and it has been suggested that this set of features constituted an adaptation in early primates to a terminal branch environment (Cartmill et al., 2002). A brief review of unique gait characteristics in extant primates is offered here to provide a general background to the study of primate locomotion and its adaptations.

While most mammals utilize a lateral sequence gait in which the touchdown of the hindlimb is followed by that of the ipsilateral forelimb (Hildebrand, 1967; Rollinson and Martin, 1981; Vilensky and Larson, 1989), primates are relatively peculiar among mammals in preferring a diagonal sequence gait in which hindlimb touchdown is followed by that of the contralateral forelimb (e.g., Muybridge, 1957; Hildebrand, 1967; Prost, 1969; Rollinson and Martin, 1981; Vilensky and Larson, 1989; Larson, 1998). In addition to preferring a diagonal sequence gait, primate quadrupeds differ from other mammals by using more protracted forelimbs at touchdown (Reynolds, 1987; Larson, 1998) and having greater angular limb excursions (Larson et al., 2000; Larson et al., 2001). The combination of these factors produces the long stride that is characteristic of primates (Reynolds, 1987; Larson, 1998). In addition, primates experience greater vertical forces on their hindlimbs (Kimura, 1985; Reynolds, 1985; Demes et al., 1994; Schmitt and Hanna, 2004; Schmidt, 2005; Hanna et al., 2006; Kivell et al., 2010), which provide propulsion, and lesser on their forelimbs, which perform steering and braking functions (Demes et

al., 1994). This pattern is opposite to that found in other mammals (reviewed in Larson, 1998; Schmitt, 2003b), in which the forelimbs experience higher substrate reaction forces than the hindlimbs. Some strepsirrhines, however, have been found to occasionally experience higher forelimb than hindlimb vertical forces in laboratory settings (Schmitt and Lemelin, 2004; Demes et al., 2005; Franz et al., 2005), which may be related to a decreased reliance on forelimb manipulatory capabilities in these taxa (Franz et al., 2005). Reynolds (1985) proposed that the forelimb-hindlimb force differential is caused by an active posterior weight shift to the hindlimb (brought about by hindlimb retractors) that increases forelimb mobility (Larson, 1998; Larney and Larson, 2004; Larson and Stern, 2009; Kivell et al., 2010), while others have suggested that increased hindlimb vertical forces may be a result of increased forelimb compliance, which shifts weight to the stiffer hindlimbs (Schmitt, 1999), that limb weight support is a product of the position of the body's center of mass (Gray, 1944; Raichlen et al., 2009), or that hindlimb weight support may be a by-product of other kinematic requirements of diagonal sequence-diagonal couplet gait (Raichlen et al., 2009).

As mentioned above, all of these gait characteristics (limb protraction, diagonal sequence gait, greater limb angular excursions, hindlimb weight support, and long stride lengths) have been proposed to be part of an adaptive suite in early primates to maintaining stability in a mechanically demanding thin, flexible branch environment (Vilensky and Larson, 1989; Larson, 1998; Larson et al., 2001; Cartmill et al., 2002; Schmitt and Lemelin, 2002; Lemelin et al., 2003; Larney and Larson, 2004; Schmitt et al., 2010). Cartmill et al. (2002) suggested

that diagonal sequence gait may ensure that a grasping hindfoot is in contact with the substrate when the forefoot touches down—if the foothold of the forelimb is unsteady, the hindfoot can act to stabilize the body (Cartmill et al., 2002). Support for this hypothesis was offered by Lemelin et al. (2003), who found that in two species of didelphid marsupials that differ in use of arboreality and grasping abilities, diagonal sequence gait only occurs in the arboreal marsupial that has grasping extremities (like primates), and does *not* occur in the terrestrial marsupial that does not have grasping extremities.

However, an alternative hypothesis of the evolutionary significance of primate gait is that plasticity in primate use of gait types and characteristics—not reliance on a particular gait—allowed early primates to flourish (Nyakatura et al., 2008). Recent primatological work has shown support for this hypothesis; the primates studied used a variety of gaits, showing flexibility in the types of gaits used in small, flexible branch environments (Stevens, 2008; Wallace and Demes, 2008; Nyakatura and Heymann, 2010).

The rest of this chapter will focus on the theoretical framework for this project; a discussion of biomechanics of various systems is followed by an overview of comparative morphology of the primate pelvis. Although presented in two major parts, the experimental biomechanics and comparative morphometrics components of this project are not separable, but instead are interconnected through their shared utility in answering evolutionary questions of primate pelvic shape.

THEORETICAL BIOMECHANICS

Complex systems can be better understood by constructing and testing simplified models of those systems. Biomechanical models of different locomotor modes explain the forces that act on the skeleton (and how the skeletal system reacts to applied loads) during locomotion, while biomechanical models of the pelvis explain how it, specifically, reacts to applied forces. Because the forces on the pelvis are a result of the overall mechanics of the behaviors an animal engages in, it is necessary to take locomotor biomechanics into account when generating and testing hypotheses of pelvic adaptation to locomotion. Biomechanical models typically conceptualize bones as levers or struts, muscles as force vectors, and joints as pivots or fulcra (Hildebrand, 1985). The biomechanical differences among locomotor groups are outlined below, and the differences in pelvic shape among locomotor modes are explored later in the chapter.

Biomechanics of primate locomotion

General quadrupedalism. Quadrupedalism is a simple system; with the trunk approximately horizontal, four limbs move parasagittally in either a lateral or diagonal gait. The motion of the limbs in quadrupedalism is often modeled as an inverted pendulum—body mass is vaulted over stiff limbs in an exchange of potential and kinetic energy (Biewener, 2006). Predictions of this model have been tested and have been found to match the behavior of quadrupeds (Cavagna et al., 1977; Griffin et al., 2004). In a quadrupedal posture, compression is the dominant form of load applied to the limbs (Tuttle, 1969; Whitehead, 1993).

Because velocity is the product of stride length and stride frequency, as the stride length and/or frequency increases, speed will increase (Preuschoft et al., 1996). To optimize a quadruped for high velocity motion, stride length is increased via limb elongation and increased angular excursion of the limbs, and stride frequency is increased. To decrease the amount of muscle force required to maintain quadrupedal posture, the limb joints become more extended, which decreases joint moments by aligning joints with ground reaction forces (Polk, 2002; Polk, 2004). Because there is a negatively allometric relationship between muscle force and body size (as body size increases, muscle force relative to mass decreases, Schmidt-Nielsen, 1984; Biewener, 1990), larger bodied primates use more extended limb postures than smaller bodied primates (Polk, 2002; Polk, 2004).

Arboreal quadrupedalism. Arboreal quadrupeds must maintain balance in an irregular environment (Preuschoft et al., 1996; Biewener, 2003). Adaptations to arboreal instability include a long tail that is used to counterbalance the body (Rollinson and Martin, 1981; Larson and Stern, 2006), strong, grasping digits (e.g., Cartmill, 1972; Cartmill, 1974; Schmitt and Lemelin, 2002), limbs that are approximately equal in length (e.g., Napier and Napier, 1967; Cartmill, 1974), and a low body center of mass (Jenkins, 1974; Hildebrand, 1985; Schmitt, 1998, 1999). Although shortening the limbs is one method of achieving a low center of mass, arboreal primates primarily accomplish this by using flexed and abducted limb joint postures (Jenkins, 1974; Schmitt, 1998, 1999; Polk, 2002; Polk, 2004).

Terrestrial quadrupedalism. Terrestrial quadrupeds must solve two mechanical issues; one related to speed, and the other related to increased substrate reaction forces. Terrestrial quadrupeds must be prepared for encounters with cursorial predators—consequently, many terrestrial primates exhibit adaptations for speed. The mechanical demands on cursorial animals differ from those on non-cursorial taxa; cursoriality requires the ability to maneuver rapidly, which is achieved by elevating the body's center of mass, having relatively small body mass, and having a small center of support (Hildebrand, 1985). Elevating the limb center of mass decreases the mass moment of inertia, which increases speed while decreasing muscular work during swing phase (Wood, 1973). Some cursorial animals may employ a gallop (*e.g.*, within primates, *Erythrocebus*), a high-speed gait that entails moving the hind- and forelimb pairs simultaneously. During galloping, stride length (and ultimately, speed) is increased by rapid flexion and extension of the thoracic and lumbar vertebrae and by the bounding nature of the limb pairs (Biewener, 2003). In some species, tendons act like springs and store elastic energy during galloping (Biewener, 2003). All of these characteristics work to increase speed.

The other problem related to terrestrial quadrupedalism is that substrate reaction forces are greater terrestrially than arboreally (e.g., Schmitt, 1998; Schmitt, 2003; Schmitt and Hanna, 2004; Carlson et al., 2005; Franz et al., 2005). Although it has been widely thought that digitigrade terrestrial quadrupeds (*e.g.*, papionins) use extended hand and wrist postures instead of palmigrady to lengthen the limb to increase speed, recent work has questioned this assumption

(Patel, 2009; Patel, 2010; Patel and Wunderlich, 2010). As speed increases, terrestrial primates adopt more palmigrade forelimb hand postures (even in those taxa that are digitigrade at slow speeds) with less wrist extension because the wrist and hand joints collapse with the increased substrate reaction forces (Patel, 2010; Patel and Polk, 2010).

Vertical clinging and leaping. Vertical clinging and leaping (VCL) involves clinging to arboreal vertical supports during resting postures and moving between vertical supports by leaping with the trunk in an orthograde position; the hindlimbs provide the propulsive force in takeoff and land first (Napier and Walker, 1967; Preuschoft et al., 1996; Biewener, 2003). Vertical clingers and leapers have three main objectives: to achieve an appropriate height, to leap a particular distance, and to land on a vertical support. These goals occur respectively during three phases of motion: the takeoff, airborne, and landing phases.

The takeoff phase is critical because it is there that the power require for the leap is generated (Biewener, 2003). Kinetic energy (and subsequently, velocity) must be maximized in order to attain maximal jump height and/or distance, and this is usually supplied by muscle force or elastic energy stored in tendons (Aerts, 1998; Biewener, 2003). When primates leap, kinetic energy and velocity are provided by rapid extension of the hindlimbs (Preuschoft et al., 1996). The horizontal distance of a leap is determined by the velocity takeoff, leap height, limb length, and muscle force (Biewener, 2003); as any of these quantities increase, so, too, will leap distance. As mentioned above, limb length is

the distance over which acceleration occurs; longer limbs allow more time and distance over which to accelerate for takeoff (Peters and Preuschoft, 1984; Preuschoft et al., 1995; Demes et al., 1996; Biewener, 2003). Accordingly, VCL taxa do have relatively long limbs that increase the distance over which acceleration occurs (Demes et al., 1996), and large hindlimb angular excursions that they achieve through maintaining a range of hindlimb postures in preparation for the leap, from deeply flexed (during clinging) to fully extended (mid-leap). The mathematically-derived optimum takeoff angle is 45° (Marsh, 1994; Sellers and Crompton, 1994), but this may vary depending on body size and leap distance (Crompton et al., 1993; Marsh, 1994; Sellers and Crompton, 1994); larger-bodied animals will use a smaller-than-optimum takeoff angle because they have relatively less muscle force available than smaller-bodied animals (Biewener, 2003). Body size also has considerable effects on velocity and takeoff forces; small-bodied animals have absolutely short hindlimbs that reduce the distance over which acceleration is attained (Alexander, 1995; Preuschoft et al., 1996) and experience relatively larger substrate reaction forces (Demes et al., 1995; Demes et al., 1999), while large-bodied animals have less muscle force available for acceleration (Preuschoft et al., 1996) and experience relatively lower substrate reaction forces (Demes et al., 1995; Demes et al., 1999).

The airborne phase of leaping is governed by the law of conservation of angular momentum, which dictates that in the absence of external forces, angular momentum of a projectile will not change, and will continue along a certain parabolic trajectory (Freedman and Young, 2003). After takeoff, however, the

animal must accomplish mid-air rotations to correctly position the body for landing, and these rotations, then, must occur via movement of the body about three principal axes: mediolateral, anteroposterior, and craniocaudal (Peters and Preuschoft, 1984; Dunbar, 1988; Preuschoft et al., 1995; Demes et al., 1996). Because angular momentum is the product of moment of inertia and angular velocity, an animal may change its momentum by altering its moment of inertia (Dunbar, 1988), which is accomplished by moving the limbs and/or tail.

During the landing phase, the lower limb causes deceleration of the body. Because hindlimb length is directly proportional to the time required for landing, longer limbs provide more time for deceleration and consequently act to prevent injury from landing with high velocity (Peters and Preuschoft, 1984). Landing forces are somewhat smaller than takeoff forces (Demes et al., 1995; Demes et al., 1999), but both are an order of magnitude larger than reaction forces in quadrupedal or suspensory taxa.

Suspension. Although all suspensory behaviors require the ability to maintain grip on the superstrate (Preuschoft and Demes, 1985) and the ability to resolve tensile forces on the limbs through muscular forces acting in compression (Swartz, 1988), they each involve quite different biomechanical demands. In brachiation, the body is swung from support to support beneath a rigid link system (*i.e.*, the forelimb) in a pendular motion (Preuschoft and Demes, 1984, 1985; Bertram et al., 1999; Bertram and Chang, 2001; Usherwood and Bertram, 2003; Usherwood et al., 2003). Perhaps the most important aspect of brachiation is maintenance of an adequate grip on a support; the manus must provide enough

friction and maintain a hook-like grip so that it does not slip off the support. Bimanual suspension may be either locomotor or postural in nature (Hunt et al., 1996), and it differs from brachiation in the form of the movement; bimanual suspension is more varied and less pendular, and does not involve trunk rotation (Cant et al., 2003). In tail-assisted suspension, the tail acts as a fifth extremity, and the body weight is suspended from all five "extremities" (Hunt et al., 1996). Finally, quadrumanous suspension is not very different from tail-assisted suspension; the body hangs beneath the forelimbs and hindlimbs in both forms of suspension (Hunt et al., 1996). In all forms of suspension, the extremities are loaded in tension (Hollihn, 1984; Swartz, 1988; Swartz et al., 1989), and it is likely that the pelvic girdle is also subjected to tensile stresses. While the role of the hindlimb in mechanics of suspension is unknown, it may be used to regain kinetic energy during forelimb brachiation by lifting it towards the torso (Usherwood et al., 2003).

Biomechanics of the primate pelvis

There are both theoretical and methodological reasons to use a biomechanical model to identify pelvic adaptations to locomotion. Support for an hypothesis of adaptation requires both a correlation between the pelvic trait and the function (*i.e.*, locomotion) and a demonstration that the trait *performs* the function (Kay and Cartmill, 1977). In this case, it is challenging to demonstrate that a trait performs a function because there is no pragmatic way to directly observe whether a particular trait of the pelvis functions to allow a specific locomotor behavior. Besides direct observation, another way to show that a trait

performs a function is to build a biomechanical model of the system and to use optimality criteria (that are based on the expectations of optimal performance, however that may be defined for a given system) to generate predictions of adaptive morphology based on the mechanical requirements of the system (Rudwick, 1964). If mechanical predictions of morphology based on function are borne out via hypothesis-testing, then it can be concluded that the morphological trait performs the locomotor function.

Methodologically, the first step of using a biomechanical model to identify pelvic adaptations is to understand how the pelvis responds to applied load. This step will identify potential adaptive regions of the pelvis that function to resist applied load and eliminate those regions that do not resist load that results from substrate reaction forces. Then, regions that function to resist load can be further tested to identify specific features as adaptations to locomotion.

Applied load (external forces; from muscular contraction or substrate reaction forces) causes stress (internal forces; force per area) within bone, and it is this stress that bones must resist to prevent structural failure. During the stance phase of locomotion (*i.e.*, the locomotor period when the limb is in contact with the substrate), it is expected that load is transmitted from the hindlimb to the acetabulum, to the sacroiliac joint via the lower ilium, and finally to the vertebral column (as is the case with humans, e.g., Jacob et al., 1976; Goel et al., 1978; Dalstra and Huiskes, 1995). This scenario of load transmission emphasizes the role of the ilium, but does not address the function of the ischium and pubis; it is unclear whether these regions resist stresses resulting from substrate reaction

forces, or if they simply act as levers that provide anchorage for the extensor and adductor hindlimb musculature.

The effect of stress resistance on skeletal morphology is likely to be particularly important because loading regimes characteristic of locomotor categories will produce stereotypic stress in bone, which is expected to produce adaptive variation in bony anatomy. However, internal forces have been largely overlooked in previous work on the pelvis, most likely because the pelvis is complex and a general mechanical model of its structure has not been constructed. Instead, some studies have explored the importance of external forces in pelvic biomechanics. The lengths of several pelvic features have been related to muscle moment arms (*i.e.*, mechanical advantage of a muscle) and correlations between locomotor behavior and muscle morphology and positioning have been identified (e.g., Waterman, 1929; Stern, 1971; Jouffroy, 1975; Sigmon, 1975; Fleagle, 1976; McArdle, 1981; Sigmon and Farslow, 1986; Anemone, 1993). Testing formal models of pelvic stress resistance will elucidate the trait-function relationship between pelvic morphology and locomotion.

General models of pelvic stress resistance

Only two models of pelvic stress resistance have been previously proposed. Kummer (1975) modeled the pelvis as a two-armed lever in the sagittal plane, with the ilium and ischium constituting the two arms of the lever (Fig. 2-1). When unfixed by ischiosacral and abdominal muscles, this model predicted ventral rotation of the sacrum at the sacroiliac joints, as well as of the pelvis as a whole at the hip joints, caused by the force of body weight at the sacroiliac joints

and the tendency toward lordosis in the lumbar vertebral region. Kummer (1975) hypothesized that these rotatory tendencies are counteracted by the muscles and ligaments originating on the sacrum and ischium, and by the abdominal muscles, respectively. However, this model is incomplete because it did not incorporate forces in other planes besides the sagittal.

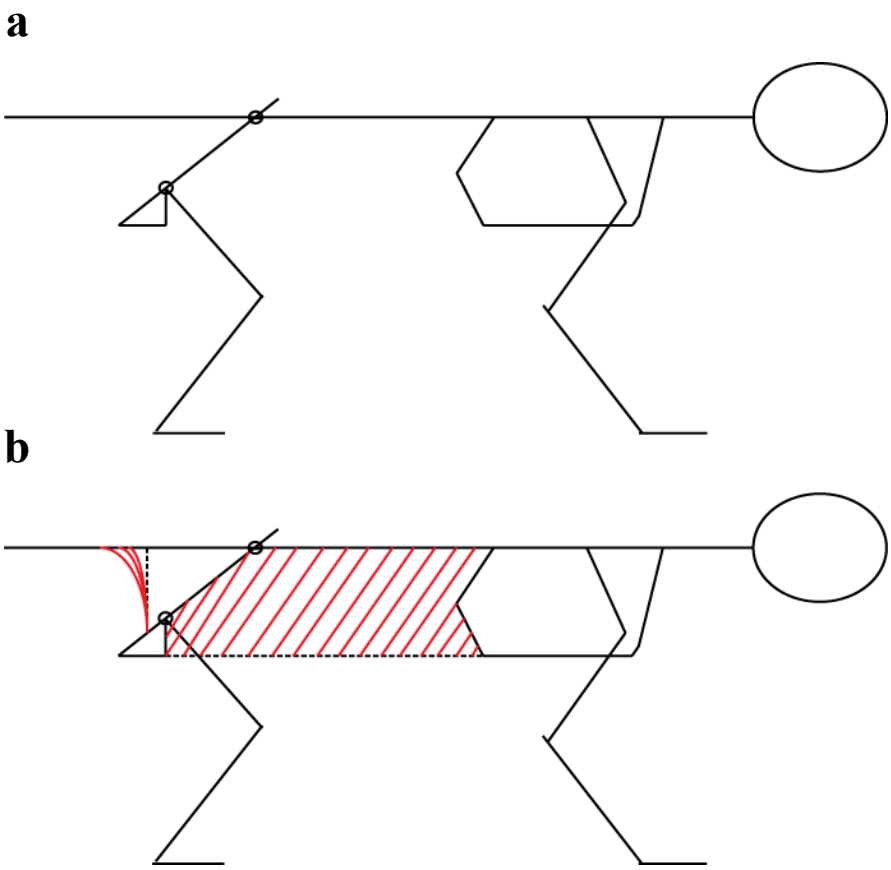

Fig. 2-1. Representation of Kummer's (1975) two-armed lever model of the pelvis. The hip and sacroiliac joints (small circles in the models) act as fulcra, and the ilium and ischium are the two arms of the lever. In (**a**) the pelvic girdle is unfixed, and as a result, the force of body weight on the sacroiliac joint causes ventral rotation of the entire structure. When the abdominal musculature (diagonal stripes) and the ischiosacral/ischiocaudal ligaments (dotted vertical line) and musculature (curved lines towards the "tail") are added to the model (**b**), the pelvic structure becomes fixed. Figure adapted from Kummer (1975).

Several workers have suggested another model in which the pelvis, essentially a ring of bones attached to each other at dorsal and ventral joints, acts as a cylinder (Badoux, 1974; Kummer, 1975; Pauwels, 1980). In this model, the diameter of the cylinder is the diameter of the pelvis in the transverse plane, while the height of the cylinder is the total length of the pelvis, from the superior-most point on the ilium to the inferior-most point on the ischium. Several predictions can be derived from this cylinder model regarding the locations and types of pelvic stresses experienced during loading, but previous efforts either focused on only a particular aspect of primate pelvic morphology (*e.g.*, the pubic symphysis should encounter tensile stress during typical quadrupedal stance [Badoux, 1974; Kummer, 1975]), or were only applied to the human pelvis (Pauwels, 1980). However, understanding patterns of stress resistance in non-human primate pelves is essential to interpreting variation (due to locomotion) in morphology among primates. As it is the most complete model put forward to date, this study will focus on testing the cylinder model of pelvic biomechanics. Several testable predictions can be derived from this model; three loading regimes (torsion, dorsoventral compression, and dorsoventral bending) will be tested here. These predictions are thoroughly presented in Chapter 3.

COMPARATIVE PRIMATE PELVIC MORPHOLOGY

As mentioned in Chapter 1, although there have been many studies on various aspects of primate pelvic morphology, few have focused specifically on the adaptive relationship between bony structure and locomotion. General

differences in pelvic shape among primates that are related to locomotion are grouped here by each bone of the pelvis for the sake of convenience.

Pelvic correlates of locomotor behavior

Ilium. The ilium of primates is generally long in quadrupeds, though shorter in terrestrial than arboreal taxa, and short in suspensory taxa. It generally forms a blade shape, except in small-bodied VCL taxa (*e.g.*, *Galago*, *Tarsius*) and slow-climbing quadrupeds, which have long, narrow, rod-like ilia (Jouffroy, 1975). There is considerable variation in the orientation of the faces of the ilium; the gluteal plane, which gives rise to the gluteal musculature, faces dorsolaterally and is large and concave in quadrupeds, while it is more laterally-facing and flatter in VCL and slow-climbing quadrupeds (Straus, 1929; Waterman, 1929; Stevens et al., 1981; Sigmon and Farslow, 1986). The gluteal plane is wider in suspensory taxa, perhaps to increase the area of attachment of the *mm. erector spinae* (Waterman, 1929), which support the pelvis and hindlimbs during suspension, and the *m. latissimus dorsi*, which facilitates forelimb retraction and adduction during brachiation. The iliac plane, which gives attachment to *m. iliopsoas*, is oriented ventrally in all quadrupeds, suspensory taxa, and large-bodied VCL, and laterally in small-bodied VCL (pers. obs. and Stevens et al., 1981). The iliac plane is narrow in TQ and VCL, and wider in suspensory taxa. The anterior superior iliac spine, which is the point of attachment for *m. sartorius* and the inguinal ligament, is small in quadrupeds (and virtually absent in slow-climbers in particular), but very prominent in VCL (Walker, 1974; Jouffroy, 1975; Jungers, 1976; Sigmon and Farslow, 1986), active quadrupeds like *Saimiri* (Straus, 1929),

and bipeds. The anterior inferior iliac spine is small or absent in quadrupeds (Straus, 1929), rugose in active quadrupeds, and prominent in VCL (Jouffroy, 1975) and bipeds (e.g., Stern and Susman, 1983).

Ischium. In general, quadrupeds have longer ischia than non-quadrupeds, with terrestrial taxa having the longest (Waterman, 1929). In addition, quadrupedal leapers (in this case, colobines) have shorter ischia than nonleaping quadrupeds (in this case, cercopithecines) (Steudel, 1981a). Vertical clingers and leapers have short ischia (Walker, 1974; McArdle, 1981; Yirga, 1987; Fleagle and Anapol, 1992; Anemone, 1993), and many of them have dorsally projecting ischia to increase hip extensor leverage during hindlimb extension (Fleagle and Anapol, 1992). Ischial tuberosities, which give rise to the hip and leg extensor musculature, are small in arboreal quadrupeds and larger in terrestrial quadrupeds (Mivart, 1867; Waterman, 1929), bipeds, and suspensory taxa, with VCL being intermediate in ischium length. Some taxa (cercopithecoids and *Hylobates*) have ischial callosities—fatty pads on the distal surface of the ischium with a discoid fibrous pad deep to the fat deposit—but the functional significance of these structures is unknown (but see the following for hypotheses, Waterman, 1929; Elftman, 1932; Washburn, 1957; Rose, 1974b). Ischial callosities result in expanded and everted ischial tuberosities (Mivart, 1867; Waterman, 1929; Sigmon and Farslow, 1986), and this relationship makes it difficult to determine whether ischial tuberosity size is a correlate of ischial callosity presence in cercopithecoid taxa. Bipeds and VCL have prominent ischial spines (bipeds:

Waterman, 1929; Abitbol, 1988, VCL: pers. obs.), while other locomotor groups have small to absent spines (Waterman, 1929).

Pubis. Surprisingly, there have been no studies specifically on the comparative morphology of the extant primate pubis (Sigmon and Farslow, 1986); previous work has focused on human evolution (e.g., Stewart, 1960; Trinkaus, 1976; Rosenberg, 1986; Hager, 1989; Rak, 1990; Rosenberg, 1992; Bondioli et al., 2006) or on very limited taxonomic groups (Tague, 1993). The studies that have commented on pubic morphology have concentrated on pelvic sexual dimorphism (e.g., Mobb and Wood, 1977; Steudel, 1981b; Leutenegger and Larson, 1985; Pissinatti et al., 1992; Tague, 1993; Arsuaga and Carretero, 1994). However, a few studies have mentioned observed differences in pubic morphology specifically related to locomotion. Terrestrial quadrupeds have short (Mivart, 1867; Schultz, 1930; Howell, 1944) and transversely-oriented pubes (pers. obs.), while the pubic rami are long in arboreal quadrupeds (especially in slow-climbers, Mivart, 1867) and small-bodied vertical clingers and leapers (Anemone, 1993). Howell (1944) remarks that pubis length (presumably, both the rami and the symphysis) is reduced in cursorial animals because they do not heavily rely on hip adductor musculature (also in Anemone, 1993). The craniocaudal length of the pubic symphysis, which may be related to forces encountered at the joint (Tague, 1993), is shorter in arboreal than terrestrial quadrupeds (Mivart, 1867), and longer in vertical clingers and leapers (Jouffroy, 1975).

Acetabulum. The acetabulum is an important part of the pelvis because it transmits load from the hindlimb to the rest of the pelvis and trunk. Among

features of pelvic structure, acetabular morphology has been relatively well-studied, and several aspects of shape related to locomotion have been identified. Articular lunate surface distribution of the acetabulum, which affects load transmission during locomotion (Jenkins and Camazine, 1977), differs between pronograde and orthograde taxa—quadrupedal taxa have expanded dorsal aspects of the lunate surface (MacLatchy, 1998), while vertical clinging and leaping and suspensory taxa have larger cranial aspects of the lunate surface (Ward, 1991; Ward et al., 1993; MacLatchy and Bossert, 1996; MacLatchy, 1998). Compared to suspensory taxa, the acetabulum of quadrupeds has thicker walls and is deeper; these traits seem to be related to increased load resistance (Schultz, 1969). The thickness of the acetabular margins, which may reflect loading history, is thickest in the dorsal aspect in quadrupeds (Schultz, 1969). The diameter of the acetabulum scales with slight positive allometry in catarrhines (Steudel, 1982; Ward, 1991; MacLatchy, 1995).

Sacrum. The sacrum is variable in width, the number of vertebrae it comprises, and the amount of ventral curvature it possesses (Schultz, 1930, 1961; Leutenegger, 1977). The number of sacral vertebrae varies among primates from two in some small strepsirrhines and platyrrhines to six or seven in lorids (Schultz, 1961). The width and curvature are less variable among taxa, with most primates having long, narrow, and relatively straight sacra (Schultz, 1930). Hominins are unique in this respect because they have short, ventrally curved, and wide sacra (Schultz, 1930; Elftman, 1932; Leutenegger, 1977). The sacroiliac joint is small in quadrupeds and VCL, and large in suspensory taxa (Ankel-

Simons, 2000), which may indicate that greater surface area is needed in suspensory taxa to relieve tension on the trunk from the suspended pelvic girdle and hindlimbs.

Pelvic traits likely to reflect loading

There are several pelvic features that are likely strongly correlated with loading regime that have not been studied in detail. Specifically, cross-sectional dimensions of pelvic struts and the morphology of the acetabular, pubic, and sacroiliac joints are expected to be functionally important load-bearing elements of the pelvis. Below is a review of relevant previous work on pelvic struts and joints.

Struts. Although some linear measures of bony struts of the pelvis (measures of the superior and inferior pubic rami, the ischium, and the lower ilium) seem to vary according to locomotor mode, the biomechanical relevance of these measures to stress resistance is unclear. The cross-sectional area of these bony supports may be more informative than linear dimensions because it should reflect differences in loading regime (as has been demonstrated with humeral and femoral cross-sectional geometry [e.g., Demes and Jungers, 1993; Jungers et al., 1998; Ruff, 2002; Ruff, 2003]). However, the cross-sectional area of bony struts of the pelvis has not been thoroughly investigated, and thus the relationships between this morphology and locomotor behavior are unknown.

Pubic symphysis length seems to vary among locomotor groups (*e.g.*, TQ taxa have longer pubic symphyses than AQ taxa [Mivart, 1867] and VCL strepsirrhines have longer pubic symphyses than non-leaping strepsirrhines

[Jouffroy, 1975]), but the functional significance of this variation has not been examined in a locomotor context (although it has been studied in the context of sexual dimorphism and obstetrics, (Leutenegger, 1974; Mobb and Wood, 1977; Steudel, 1981b; Leutenegger and Larson, 1985; Tague, 1991; Ward et al., 1993).

Joints. Joint surfaces must be able to accommodate both mobility and load requirements. There is a range of substrate reaction forces that are typical of different locomotor modes, and variability is expected in pelvic joint (acetabulofemoral, pubic symphysis, and sacroiliac) surfaces in accordance with differing locomotor behaviors and loading regimes. Among features of pelvic structure, acetabular morphology has been relatively well-studied, and several aspects of shape related to locomotion have been identified. Articular lunate surface distribution of the acetabulum, which affects load transmission during locomotion (Jenkins and Camazine, 1977), differs between pronograde and orthograde taxa—quadrupedal taxa have expanded dorsal aspects of the lunate surface (MacLatchy, 1998), while vertical clinging and leaping, suspensory, and knuckle-walking taxa have larger cranial aspects of the lunate surface (Ward, 1991; Ward et al., 1993; MacLatchy and Bossert, 1996; MacLatchy, 1998). Compared to suspensory taxa, the acetabulum of quadrupeds has thicker walls and is deeper; these traits seem to be related to increased load resistance (Schultz, 1969).

As with the acetabulum, the surface area of the pubic symphysis should be related to load distribution (some have proposed that increased pubic symphysis

length serves to guard against increased forces encountered during locomotion [Tague, 1993]), but this feature has not been broadly quantified.

The auricular surface has a highly variable shape and linear breadth dimensions do not adequately capture the shape differences among taxa. However, the *area* of the auricular surface (the articular surface that constitutes part of the sacroiliac joint) does differ between monkeys and apes (Ward, 1991)—apes have larger surface areas than monkeys. Because apes are larger than monkeys and need increased joint surface areas to accommodate larger forces resulting from body size, differences in auricular surface area may be related to differences in body size (but see Godfrey et al., 1991).

Effects of body size on pelvic parameters

Large animals encounter larger loads than small animals due to the effects of gravity and increasing mass on anatomical structure, and thus, body size produces differences in loading (Hildebrand, 1985; Biewener, 2003). Previous work on primate postcranial scaling has shown that features related to limb strength (*e.g.*, diaphyseal cross-sectional cortical area) scale with slight positive allometry, but do not achieve functional/dynamic similarity (e.g., Schaffler et al., 1985; Demes and Jungers, 1993; Jungers and Burr, 1994). Instead of increasing bone strength, larger animals compensate for increased forces by altering other correlates of locomotor behavior, such as joint posture and limb angular excursion (Schmidt-Nielsen, 1984; Biewener, 1990; Polk, 2004). While scaling analysis of pelvic traits has not been a focus of research (although some studies have included data on scaling [e.g., Mobb and Wood, 1977; Steudel, 1982;

Leutenegger and Larson, 1985; Ward, 1991; MacLatchy, 1995]), size-related differences in loading seem to be reflected in some aspects of pelvic bony morphology. It appears that regions of the pelvis that must resist stress scale with positive allometry (Ward, 1991; MacLatchy, 1995), which is in accord with studies on other hindlimb joints (e.g., Jungers, 1988). However, the hypothesis that regions of the pelvis that must resist stress scale with positive allometry has not been extensively tested.

The discussion of locomotor adaptations of the pelvis in this chapter is not meant to imply that all pelvic traits are adaptations to locomotion. Of course, postcranial anatomy has other functions besides locomotion and posture (*e.g.*, parturition), but these other functions are outside the scope of this dissertation. Furthermore, it is recognized that some traits may not be adaptations at all (*sensu* Bock and von Wahlert [1965]), but may instead be nonaptations (Ross et al., 2002) that are maintained passively. This project, however, seeks to identify those features that are adaptations to locomotion.

SUMMARY AND PROJECT OVERVIEW

This chapter outlines the feedback between biomechanical and adaptive questions concerning the causes of variation in primate pelvic morphology and has argued for the importance of approaching a study of pelvic adaptation with both types of questions in mind. Many studies have identified skeletal correlates of locomotor behavior in the pelvis, but answering evolutionary questions about pelvic shape—that is, accurately identifying which morphologies are adaptations—requires both a trait-function correlation and evidence that the trait

performs the function. To demonstrate that pelvic traits are functionally related to locomotion requires the use of a biomechanical model. While a model of primate pelvic mechanics has been proposed, it has not been examined in detail, and predictions from it have not been tested experimentally. Furthermore, certain aspects of pelvic anatomy that are likely to reflect habitual loading due to locomotion (*e.g.*, strut and joint dimensions) have not been documented in a large and diverse sample of taxa.

The field of pelvic functional morphology currently lacks a general theoretical model of pelvic stress resistance and *in vitro* determination of pelvic strain patterns to validate it. These data are necessary to improve existing adaptive hypotheses regarding pelvic morphology and will expand our understanding of the influences of applied load on pelvic anatomy. In addition, a primate-wide comparative study of pelvic bony morphology has not been conducted, but larger and more phylogenetically diverse samples than have been used in previous work should allow clearer differentiation in pelvic anatomy among all locomotor groups. This study will ameliorate these shortcomings by collecting experimental strain data during loading on cadaver specimens to test the cylinder model of pelvic biomechanics outlined in this chapter. These data are used to validate and/or refine existing hypotheses of pelvic adaptation to locomotion, and new hypotheses are proposed, based on those regions of the pelvis that appear to be functionally related to experimental loading. Adaptive hypotheses are tested using a comparative approach and a large, taxonomically diverse sample of primate species that exhibits variation in locomotor mode and body size. The experimental

and comparative data, and the results obtained from analyses of each, combine to form the basis of a general model of pelvic stress resistance and to elucidate the form-function interface between pelvic morphology and locomotion.

CHAPTER 3: PATTERNS OF STRAIN IN THE PRIMATE PELVIS

Knowledge of pelvic stress resistance is necessary for understanding both pelvic biomechanics in general, and the form-function relationship between bony structure and locomotion in particular, but surprisingly little is known about pelvic structural mechanics in non-human primates. Most studies of human pelvic mechanics have been clinical in nature and have focused on improving prosthetic devices and surgical repairs of injuries (e.g., Carter et al., 1982; Lionberger et al., 1985; Finlay et al., 1986; Huiskes, 1987; Ries et al., 1989a; Shim et al., 2007; Linstrom et al., 2009). As a result, studies of stress resistance during loading in normal, healthy human pelves is less well understood than in pathological or injured pelves (but see the following articles, reviewed below, Goel et al., 1978; Ries et al., 1989b; Dalstra and Huiskes, 1995; Dalstra et al., 1995; Anderson et al., 2005; Leung et al., 2009). Furthermore, the effects of loading on non-human primate pelves are completely unknown.

Nevertheless, some expectations about the patterns of stress resistance during loading in the primate pelvis can be reasonably derived from previous work on stress resistance in human pelves. This work has found that during loading through the hindlimbs in finite element pelvic models, forces are transmitted to the acetabulum and on to the sacroiliac joint via the lower ilium, as well as to the pubic symphysis via the superior pubic ramus (Dalstra and Huiskes, 1995). Given this pattern of load transmission, large magnitude strains (the deformation of bone in response to applied load) are expected to occur in the vicinity of the superior aspect of the acetabulum and the lower ilium, near the

sacroiliac joint, and near the pubic symphysis. Several studies have confirmed this expectation for humans, indicating that during experimental loading the human pelvis experiences relatively large magnitude strains in the superior aspect of the acetabulum, the lower ilium (between the acetabulum and the sacroiliac joint), the greater sciatic notch, in the ilium adjacent to the sacroiliac joint, and in the superior pubic ramus (Goel et al., 1978; Dalstra and Huiskes, 1995; Anderson et al., 2005; Leung et al., 2009).

The purpose of this study is to examine strain patterns during loading in non-human primate pelves in order to generate information that can be used to investigate the relationship between pelvic biomechanics and locomotor adaptation. Before continuing with a discussion of interpretation of experimental strain analyses and a description of the methods used herein, it is helpful to review the concepts of stress and strain. In the context of bone biology, strain is a measure of the deformation that occurs when a load is applied to bone (*i.e.*, it is a result of stress, which is force per area; $\sigma = F/A$). Strain is the change in length of an object divided by its original length ($\Delta L/\ell$, a dimensionless value). There are several methods to measure the deformative response of bone to applied load (e.g., photoelastic coatings, brittle coatings, thermal emission methods, Little and Finlay, 1992), but the most common method is by means of a strain gauge. The gauge, which is placed on the bone, consists of: 1) a backing that deforms as the bone is deformed and 2) one or more metallic foil grids that change in electrical resistance when deformed.

Changes in electrical resistance result directly from changes in length of the foil grid:

$$R = \frac{\rho L}{A}$$

where R is the electrical resistance, measured in ohms, ρ is the resistivity of the foil grid (a known factor), L is the length of the foil grid, and A is the cross-sectional area of the foil grid (Szivek and Gharpuray, 2000). For example, when tension is applied to the foil, its length increases and its cross-sectional area decreases, resulting in an increase of its electrical resistance. Thus, as a bone is loaded and deforms, so too does the applied strain gauge, thereby changing its electrical resistance. These electrical resistances are relayed as voltages via leadwires connecting the gauges to a signal conditioning system, and the eventual data output is in the form of microstrain (by convention, με, 1 x 10^{-6}).

INTERPRETATION OF STRAIN PATTERNS

A fundamental question arises in the process of studying bone functional adaptation to loading: what is the meaning of high strain observed during experimental loading? Does high strain indicate adaptation to applied loading, or not? One might intuitively expect that if a bone is adapted to mechanical loading, it would exhibit small strains (e.g., see Ruff et al., 2006; Grine et al., 2010), and conversely, if bone were not adapted to an applied loading regime, it would experience large strain (e.g., Hylander et al., 1991b; Hylander and Johnson, 1997). This question has not been satisfactorily answered.

Strain induces bone modeling and remodeling in a process now called "functional adaptation." This mechanobiological process (first proposed by Roux [1881] and Wolff [1892]) has been vigorously explored and experimentally-validated in many studies (e.g., Chamay and Tschantz, 1972; Hert et al., 1972; Goodship et al., 1979; Woo et al., 1981; Lanyon et al., 1982; Lanyon and Rubin, 1984; Burr et al., 1985; Biewener et al., 1986; Burr, 1993; Judex et al., 1997; Lieberman and Crompton, 1998; Hsieh et al., 2001; Lieberman and Pearson, 2001; Burr et al., 2002; Lieberman et al., 2003). While the exact mechanisms of bony response to mechanical stimuli are still not fully understood (Currey, 2002), it is generally apparent that increases and decreases in stress and strain cause an osteoblastic or osteoclastic response; bones model and remodel in response to strain caused by increased loading, and resorb when loading is decreased (Fig. 3-1). Modeling involves deposition of bone during growth, while Haversian remodeling involves osteoclastic activity of damaged bone followed by formation of new lamellar bone around the internal perimeter of Haversian canals by osteoblasts (Currey, 2002). The knowledge that bone remodels and functionally adapts to stress has led to a great many studies on the effects of mechanical loading on the skeleton, and specifically on how aspects of skeletal morphology, such as long bone cross-sectional geometry, are related to load (e.g., in anthropology, Bouvier and Hylander, 1981; Ruff and Hayes, 1983; Schaffler and Burr, 1984; Schaffler et al., 1985; Burr et al., 1989; Demes and Jungers, 1989, 1993; Runestad, 1994; Terranova, 1995; Runestad, 1997; Demes et al., 1998b; Demes et al., 2000; Polk et al., 2000; Demes et al., 2001; Lieberman and Pearson,

2001; Ruff, 2002; Kimura, 2003; Lieberman et al., 2003; Lieberman et al., 2004; Carlson, 2005; Carlson et al., 2006; Marchi, 2007).

Although bone modeling is a response to mechanical loading, there is a limit on the amount of bone that is metabolically feasible to maintain; bone is dense and consequently, heavy, requiring an increase in muscle mass to move it. Because bone tissue is metabolically expensive to maintain, bone modeling and remodeling is thought to be optimized for the trade-off between strength and bone mass; the optimal state is characterized by maximum bone strength for a minimum of bone mass (e.g., Martin et al., 1998). This optimization theory forms the general theoretical framework for biomechanical studies of the skeleton (e.g., Lanyon and Rubin, 1985; Hylander et al., 1991b; Hylander and Johnson, 1997; Lieberman and Crompton, 1998; Ravosa et al., 2000; Witzel and Preuschoft, 2002; Lieberman et al., 2003; Ross and Metzger, 2004; Dumont et al., 2005). The criterion of optimality of bone strength applies within an individual in response to mechanical loading, as well as evolutionarily; natural selection favors structures that are optimal in terms of mechanical performance (Wainwright et al., 1982). This is not to say that it is thought that the skeleton is perfectly adapted to biomechanical requirements; many workers recognize the genetic, developmental, and phylogenetic constraints on optimality.

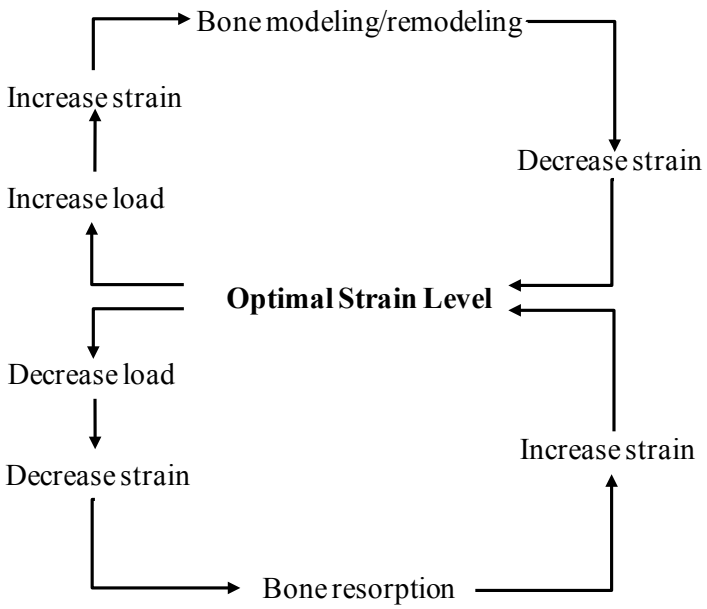

Fig. 3-1. Feedback loop demonstrating the processes by which bone maintains optimal strain levels. Adapted from Lanyon (1982) and Rubin (1984).

The interpretation of many workers is that optimality of bone strength predicts high strain in regions that resist stress (e.g., Hylander and Johnson, 1997). This trade-off model suggests that an observation of low strain indicates a large safety factor (the ratio of failure or yield strain to observed strain) and thus, overdesign, or excessive bone mass for the amount of stress that it must resist. Thus, large strains *should* be expected during loading in bones that are adapted to that loading regime, and small strains during loading indicate the functional importance of that bone for something other than routine mechanical loading. For example, in the facial skeleton, relatively large strains have been observed during *in vivo* masticatory loading in the zygomatic and mandible, and relatively small strains occur in the supraorbital margin (Hylander et al., 1991a,b; Hylander and Johnson, 1997; Ravosa et al., 2000; and in finite element analysis, Kupczik et al., 2009). This pattern has been interpreted to mean that the zygomatic and mandible

resist stress during mastication, but that the supraorbital region does not, leading Hylander and Johnson (1997) and others (Hylander et al., 1991b; Ravosa et al., 2000) to suggest that supraorbital tori have high margins of safety to protect against infrequent traumatic injury.

However, Ruff et al. (2006) caution that "strain gauges measure deformations in bones that have *already* adapted to mechanical loading…Thus, one must be careful in extrapolating from *strains* to *loads*" (Ruff et al., 2006, p. 489). Grine et al. (2010) suggest that high stresses resulting from a particular loading regime could be interpreted as evidence that the bone is *not* adapted to that loading regime (Grine et al., 2010, p. 300). According to these workers, bony adaptations exist to modulate forces resulting from loading and are, therefore, expected to exhibit low stresses and strains. This strain-reduction model is supported by the work of Dumont et al. (2005); they examined routine and atypical loading patterns in finite element models of the skulls of bats and found that the routine loading regimes generated lower strains than the atypical loading regimes (Dumont et al., 2005). Furthermore, several studies have shown that simple optimization models do not characterize bone functional adaptation and that the conventional idea that bone reacts to loading by minimizing mass and/or strain is not well supported (e.g., Rubin et al., 1990; Demes et al., 1998b; Demes et al., 2001)

A further question that the study of adaptation to load generates is, what levels of strain constitute "low" and "high" strain (Ross and Hylander, 1996)? Whether "large" strains are indicative, or not, of adaptation to loading will remain

unresolved until we have an idea of the magnitude of strain that is considered high and low, and until more research like that of Dumont et al. (2005) is done on the effects of alternative loading regimes on strain patterns. While I appreciate the theoretical issues raised by proponents of the strain-reduction model, and while these questions merit much more attention and research, I use the optimization/trade-off approach, here, to contextualize the results of this project because of its foundation in biomechanical theory and the greater abundance of support it has received from previous studies. This study, then, assumes that high strain is an indication of functional and evolutionary adaptation to load-bearing.

Strain gauge methods are used here to measure strain *in vitro* in a sample of non-human primate pelves. These data contribute to the two theoretical bases of this study; the information on stress resistance is used to evaluate the accuracy of the cylinder model of pelvic biomechanics, and it is also used to inform the adaptive hypotheses in the comparative component of this project. These biomechanical data, then, link the experimental and comparative aspects of this project, and are critical to the overall goal of understanding primate pelvic functional morphology.

BIOMECHANICAL HYPOTHESES

The cylinder model of pelvic mechanics generates several predictions regarding the magnitude and orientation of stresses in pelvic struts during specific loading regimes. Load is applied to the pelvis via the hip joints (through both unilateral and bilateral loading, depending on the gait phase of locomotion) and the sacroiliac joints (as a result of the forces of body weight bearing down on the

hindlimbs); load applied in this manner is likely to produce torsion, dorsoventral compression, and dorsoventral bending, and it is hypothesized here that these are important regimes during pelvic loading. To evaluate the validity of the cylinder model, the following predictions of strain patterns (strain type and location) for torsion, dorsoventral compression, and dorsoventral bending will be compared to data acquired from *in vitro* cadaver pelves.

Prediction A: Torsion

Torsion (twisting) occurs when a torque is applied to an object (Timoshenko and Gere, 1972). In a cylinder, this would occur from twisting the ends in opposite directions. In a pelvis, torsion should result from unilateral loading (*i.e.*, during stance phase) and will cause substrate reaction forces on one side of the pelvis to be resisted by joint reaction forces from the ipsilateral sacroiliac joint (Fig. 3-2). When a torque is applied to a cylinder, shear stresses are produced about two helical axes that are oriented 45° relative to the long axis of the cylinder, and perpendicular to each other (Timoshenko and Gere, 1972). The surface along one helical axis experiences tension, while the other experiences compression. The direction of principal stress will also be oriented 45° relative to the long axis of the cylinder. In a pelvis, tension is expected along the lower ilium of a given side, through the superior pubic ramus of that side, crossing the pubic symphysis to the contralateral side, and continuing along the inferior pubis and inferior pubic ramus of the contralateral side. Similarly, compression is expected along the lower ilium of the other side of the pelvis, through the superior pubic ramus of that side, crossing the pubic symphysis, and

continuing along the inferior pubis and inferior pubic ramus of the opposite side of the pelvis (Fig. 3-2). This pattern of strain approximates an “X” shape along the longitudinal axis of the pelvis, with one diagonal of the “X” experiencing tension, while the other experiences compression.

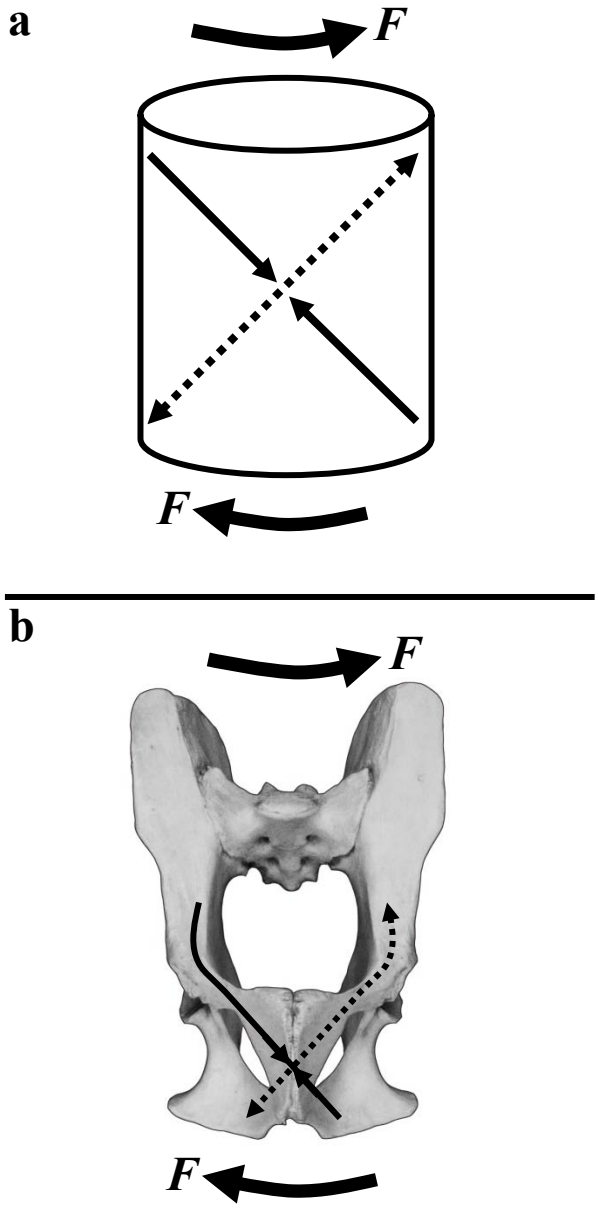

Fig. 3-2. Predictions of compressive and tensile strains during torsion of (**a**) a generalized cylinder or beam and (**b**) a primate pelvis in ventral view. *F* denotes the opposing forces applied to each end of the structure (applied torque) that create twisting of the structure. Force vectors are not drawn to represent force magnitude. The arrows within the structure indicate the type of stress predicted to occur along the length of the object; dotted lines indicate tensile stress, while the two solid arrows pointing towards each other indicate compressive stress. Compressive and tensile stresses are oriented 45° to each other and are helical in pattern (Timoshenko and Gere, 1972).

Prediction B: Dorsoventral compression

Dorsoventral (DV) compression of a cylinder occurs when axial load is applied dorsoventrally to the external walls of the object in transverse view. In a pelvis, DV compression should result from unilateral and bilateral stance, wherein the forces of either or both hindlimbs are counteracted by the force of body weight that travels through the sacroiliac joints. Viewed in a transverse plane, DV compression should result in two patterns of stress—one along the external aspect of the pelvic ring, and one along the internal aspect of the pelvic ring. The strain patterns along the external pelvic ring should demonstrate compression along its dorsal and ventral aspects, and tension along its lateral aspects. Similarly, the strain patterns along the internal pelvic ring should demonstrate tension along its dorsal and ventral aspects, and compression along its lateral aspects (Fig. 3-3). In the pubis, this mode of loading causes "wishboning" of the pubic symphysis (tension on the internal aspect of the symphysis and compression on the external aspect of the symphysis), a phenomenon that also occurs in the mandibular symphysis (Hylander et al., 1998).

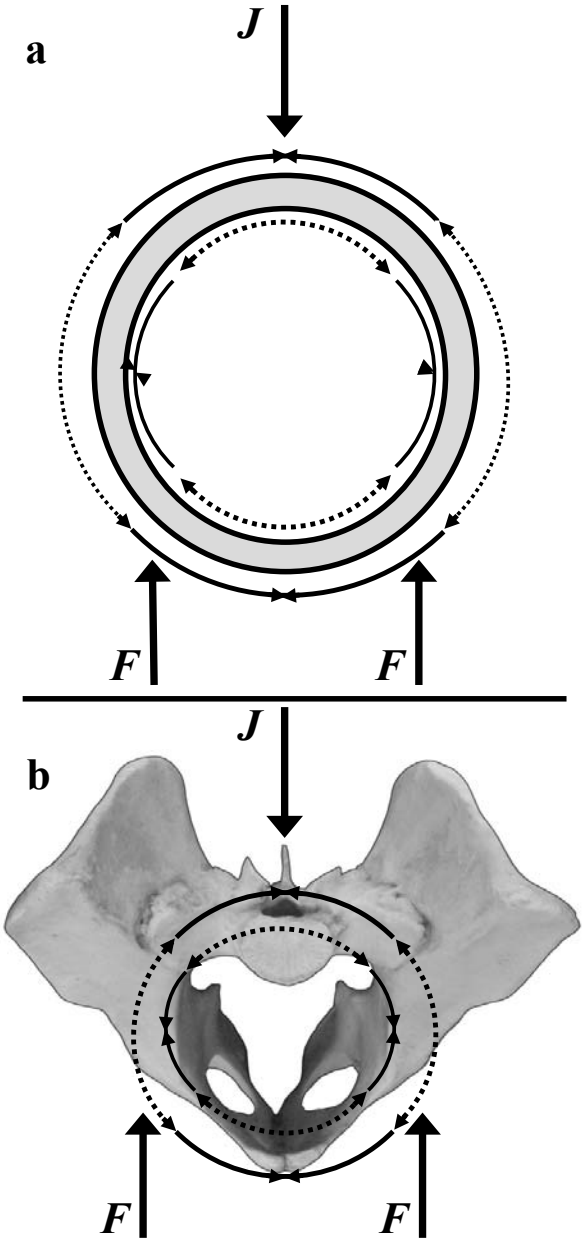

Fig. 3-3. Predictions of compressive and tensile strains during dorsoventral compression of (**a**) a generalized cylinder or beam and (**b**) a primate pelvis in transverse view. *F* is the ground reaction force, which travels to the pelvis via the hip joints, while *J* is the sacroiliac joint reaction force. Force vectors are not drawn to represent force magnitude. The inner circle of curved lines indicates the type of stress predicted to occur in the internal pelvic ring; dotted lines indicate tensile stress, while the two solid arrows pointing towards each other indicate compressive stress; the same pattern applies to the outer circle of curved lines.

Prediction C: Dorsoventral bending

Dorsoventral bending of a cylindrical beam occurs when load is applied latitudinally (*i.e.*, normal to the longitudinal axis of the beam) to either or both end(s). This pattern of loading results in compression along one of the longitudinal aspects of the beam, and tension along the other. In a pelvis, DV bending in the sagittal plane may occur during unilateral or bilateral stance, in which the forces delivered to the pelvis via the hindlimb are counteracted by the force of body weight applied to the opposing end of the pelvic beam (Fig. 3-4). This loading regime would result in compression along the dorsal aspect of the pelvis (in sagittal view) and tension along its ventral aspect.

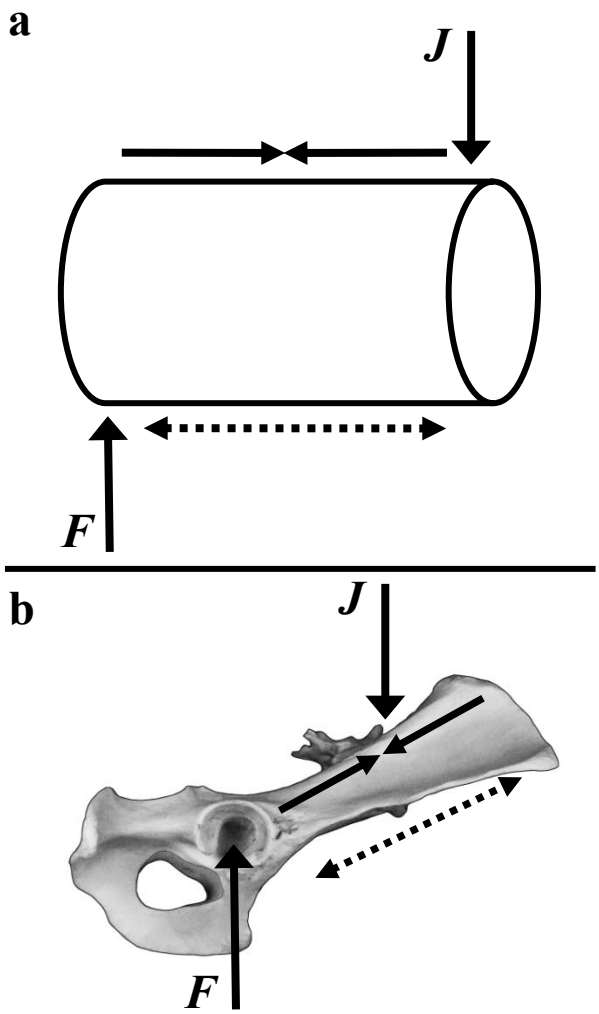

Fig. 3-4. Predictions of compressive and tensile strains during dorsoventral bending of (**a**) a generalized cylinder or beam and (**b**) a primate pelvis in sagittal/lateral view. *F* is the ground reaction force, which travels to the pelvis via the hip joint, while *J* is the sacroiliac joint reaction force. Force vectors are not drawn to represent force magnitude. Dotted line indicates tensile stress on the ventral aspect of the pelvis, while the two solid arrows pointing towards each other indicate compressive stress along the dorsal aspect of the pelvis.

MATERIALS AND METHODS

Sample

Although obtaining primate cadaver specimens can be logistically difficult, an effort was made to include specimens that differ in locomotor

behavior and exhibit a range of body sizes. Animals at the extreme ends of the body size spectrum were not appropriate for analysis because 1) small pelves cannot support a large number of strain gauges and 2) large pelves exceed the spatial capacity of the materials testing system. Therefore, this study examined three monkeys (*Ateles geoffroyi* [n=1], *Macaca mulatta* [n=2], and *Papio sp.* [n=1]) and one ape (*Hylobates lar* [n=1]) of medium body sizes that represent suspensory, terrestrial quadrupedal, and some arboreal quadrupedal locomotion (Table 3-1). Specimens were obtained from zoos and national primate research centers.

TABLE 3-1. Cadaver specimens used in bone strain analysis.

Species	Sex	Weight (kg)[a]	Age (years)	Peak force (bw)[b]	Load (N)[c]
Macaca mulatta					
a	F	5.6	13	0.745-1.697[d]	40
b	F	6.35	9	0.745-1.697[d]	20, 40, 65
Papio	M	25.1	7	0.564-0.907[d]	40, 80, 120
Ateles geoffroyi	-	7.535	-	0.67[e]	20, 40, 60
Hylobates lar	M	5.9	-	1.43[f]	40, 60, 80

[a] Specimen-specific weights were unknown for all specimens except the macaques; values represent species- and sex-specific average body masses, except for the *Ateles* specimen, which used a pooled-sex body mass (Smith and Jungers, 1997).
[b] Forces are in multiples of body weight and are derived from *in vivo* force-plate studies.
[c] Loads were applied such that each trial consisted of each of the three listed values being applied and held for 30 s each.
[d] from Schmitt and Hanna, 2004 and Hanna et al., 2006.
[e] from Schmitt and Hanna, 2004.
[f] from Vereecke et al., 2005.

Specimen preparation

Cadaver specimens were thoroughly dissected and muscle origins and insertions were recorded. Skeletal elements were removed such that each specimen consisted of an entire pelvis, both femora, and a short portion of the lumbar spine. Caudal vertebrae, if present, were removed. All muscular tissue was removed from bony attachment sites and only ligamentous tissue and joint capsules were left on the bone. Strain gauge sites were prepared according to standard protocol (Vishay Micro-Measurements Instruction Bulletins B-127-14 and B-129-8; all products used were manufactured by Vishay Micro-Measurements, Inc). Gauge sites were degreased using a degreasing agent (CSM-2 degreaser), the periosteum was removed via sandpaper abrasion, and a conditioner (M-prep Conditioner A) was applied via cotton swab, followed by a neutralizing solution (M-prep Neutralizer 5A). The bone was allowed to dry, and if it became contaminated, the conditioning and neutralizing process was repeated.

Gauge selection and application

In order to describe the state of stress at each gauge location, the maximum and minimum principal strains and their orientations must be calculated, which, when the orientation of load transmission is unknown, requires the use of rosette strain gauges (Chalmers, 1992; Murray and Miller, 1992). This study used stacked rectangular rosette strain gauges (C2A-13-031WW-120: Preattached leadwires, 120 Ohm resistance). These gauges each comprise three separate strain-recording grids oriented at 0°, 45°, and 90° (grids A, B, and C,

respectively), which allows the computation of the principal strains and their directions. A wide variety of rosette strain gauges are applicable to measuring bone strain, and these particular gauges were chosen for the advantages offered by their small size, foil alloy type, and backing material, described below.

The gauges used here measure approximately 7 mm by 8 mm, including the backing of the gauge. A constraint of working with relatively small bones is the limited space available on which to place gauges; using gauges with stacked grids reduces the overall size of the gauge. In addition, small gauges minimize the error associated with curved bone geometry and strain gradients (Chalmers, 1992; Murray and Miller, 1992). The foil grids on the C2A line of gauges are made of constantan, a copper-nickel alloy robust to changes in temperature and strain level (Murray and Miller, 1992). There are a variety of backings for strain gauges, each suited to a different test material; the gauges used here have a polyimide backing, which is flexible and ideal for use on curved surfaces.

A catalyst to aid adhesion of the gauges to bone was applied to the back of each gauge and allowed to dry (M-Bond 200 catalyst). Gauges were then glued to 19 prepared locations on the ilium, ischium, and pubis (see Mordan, 1992) using cyanoacrylate (M-Bond 200 adhesive) (Fig. 3-5). Thumb pressure was applied for 60 seconds after application of each gauge to ensure proper adhesion. Mylar tape (PCT-2M), which does not adhere to cyanoacrylate, was placed over each gauge prior to the application of thumb pressure. Following gauge placement, each gauge was coated with a thin film of waterproof silicone rubber (M-Coat C) to protect it from moisture and from changes in ambient temperature during testing.

Specimens were stored in a 0° F freezer when not in use. Low temperatures have little to no effect on bone mechanical properties (Evans, 1973; Dabestani, 1992), and these gauges are approved for use at -60° F to +150° F.

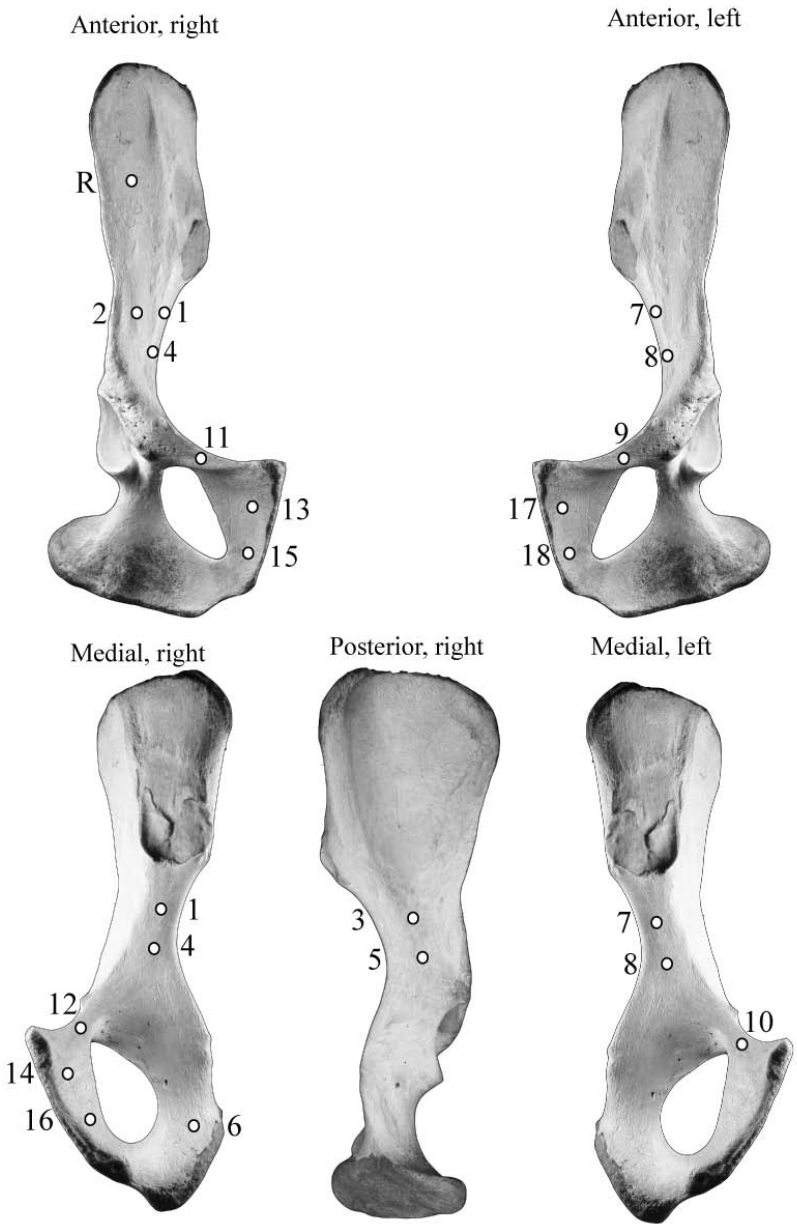

Fig. 3-5. Gauge locations ("R" represents the reference gauge).

In vitro strain data collection

To secure pelves to the materials testing system without restricting the natural movement of the sacroiliac and pubic symphysis joints, two threaded rods were inserted through holes drilled through the bodies of sacral vertebrae and secured on both the ventral and dorsal sides of the sacrum with nuts and washers, which were covered in marine epoxy to prevent loosening. The dorsally projecting rods were then embedded in a block of Bondo resin. The distal end of the right femur, to which the load would be applied, was also embedded in Bondo resin. Specimens were positioned within a servohydraulic materials testing system (MTS 858 MiniBionix, Minnesota) as shown in Figure 3-6. The distal end of the right femur was placed in a metal cap that was affixed to the MTS load cell via a ½-inch bolt. A guiding rod was placed first through the femoral cap and then passed through a hole drilled mediolaterally through the femoral condyles. This stabilization of the femur prevented binding of the femoral head on the acetabulum, which results from torque, by allowing the femur minimal mediolateral and rotational movement. The resin block (to which the sacrum was attached) was placed in a movable vise and positioned such that the femur was oriented vertically and loaded axially.

Static loads were applied in multiples of body weight over a range based on the average minimum and maximum substrate reaction forces encountered during experimental force-plate studies (Schmitt and Hanna, 2004; Vereecke et al., 2005; Hanna et al., 2006). For example, during *in vivo* experiments of arboreal and terrestrial walking and terrestrial galloping, *Macaca mulatta* experiences

forces ranging from 74.5% - 169.7% body weight (Schmitt and Hanna, 2004; Hanna et al., 2006). One *Macaca mulatta* cadaver used here weighed 6.35 kg during life, which translates to average substrate reaction forces of 46-106N at 0.745-1.697 times body weight.

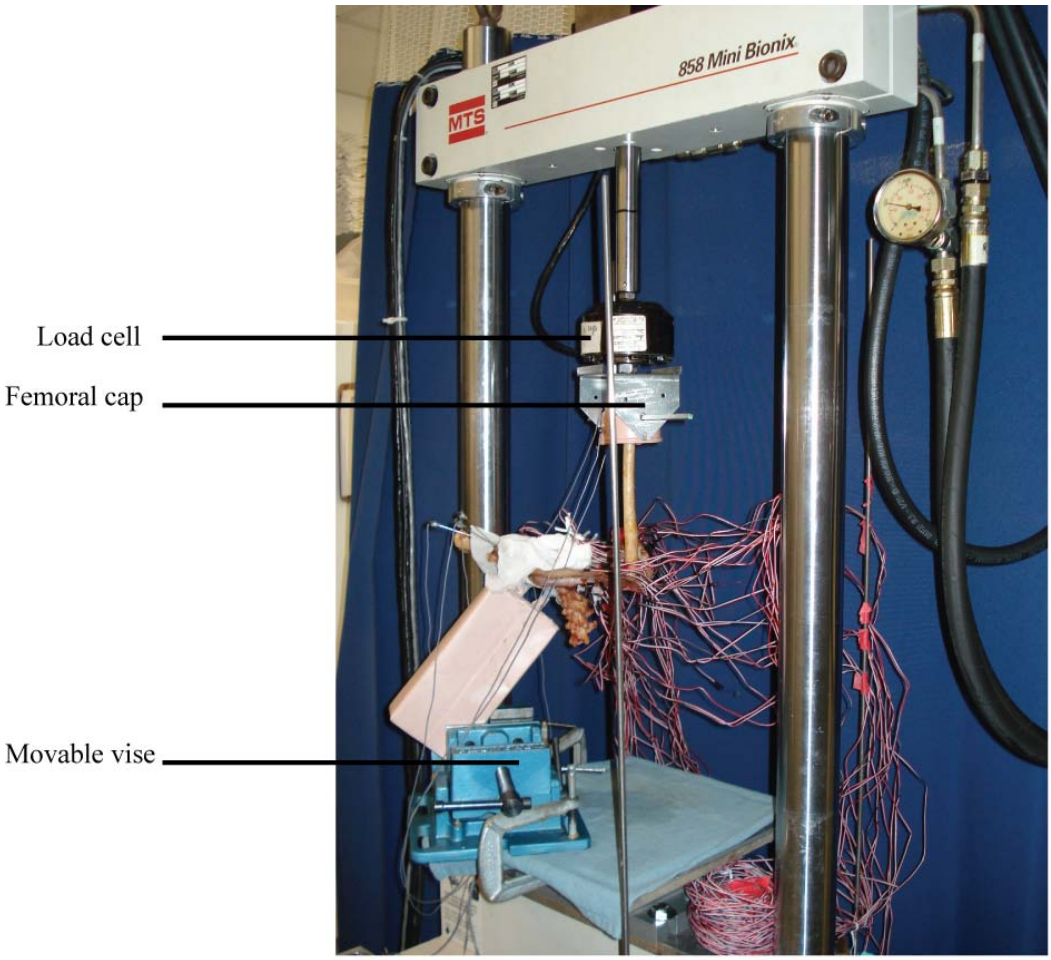

Fig. 3-6. Materials testing system with the *Ateles* specimen in the 90° limb position.

Specified loads were applied at five joint angular positions: 45° of hip flexion, 60° of hip flexion, 90° (an approximation of mid-stance), 105° of hip extension, and 120° of hip extension. Limb angles were measured from the long axis of the pelvis (Fig. 3-7). Each loading trial consisted of the application of

three sequentially increasing loads (minimum, medium, and maximum) at a given joint angular position, with each load held for 30 seconds (Fig. 3-8). This pattern was repeated for a total of two trials per limb angular position per specimen. Angular limb positions were determined using an Optotrak 3020 infrared motion analysis system (Northern Digital, Waterloo, Ontario, Canada) and via digital protractor on a digital photograph. Applied load was recorded simultaneously with strain data.

Strain gauges were calibrated and the analog signal converted to digital using a 20-channel data acquisition system (System 5000, Model 5100B scanner, Vishay Micro-Measurements, Inc.) via StrainSmart software (Vishay Micro-Measurements, Inc.). This amplifier uses a built-in Wheatstone bridge completion for 120 Ohm gauges, which records the electrical resistance of each deforming gauge. A 20-channel scanner can only accommodate six rosette gauges at a time because each rosette gauge has three data collection grids and uses three channels on the scanner. Therefore, data from the 18 gauges were collected in three groups—gauges 1-6, 7-12, and 13-18. Because data from all strain gauges were not collected during the same trials, a reference gauge was added. Data from two grids of gauge 19 were collected in every trial to allow assessment of reliability across trials. Because gauge 19 was used only as a reference to evaluate consistency across trails and was placed in a region of the ilium that likely does not resist stress, only data for gauges 1-18 are reported here.

Gauge outputs were monitored for signs of failure during testing. Signs of gauge failure include absence of data, atypical noise in the data, or drift in the

signal. Any gauges that exhibited signs of failure during testing were replaced and testing for that trial was repeated.

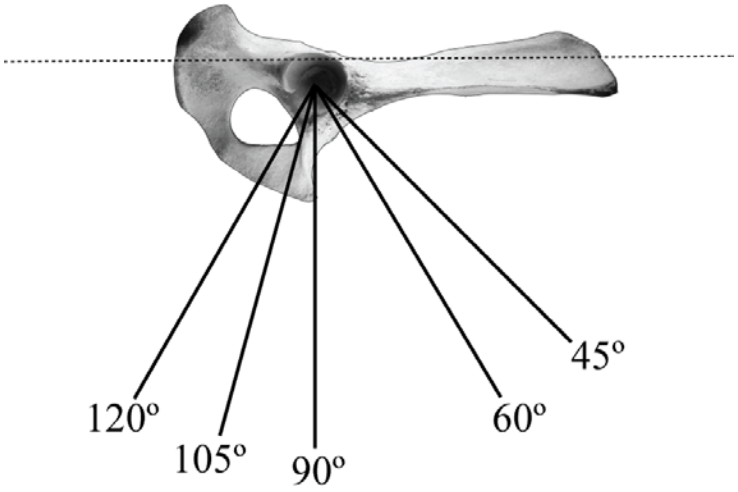

Fig. 3-7. Angular limb positions during hindlimb loading by the materials testing system.

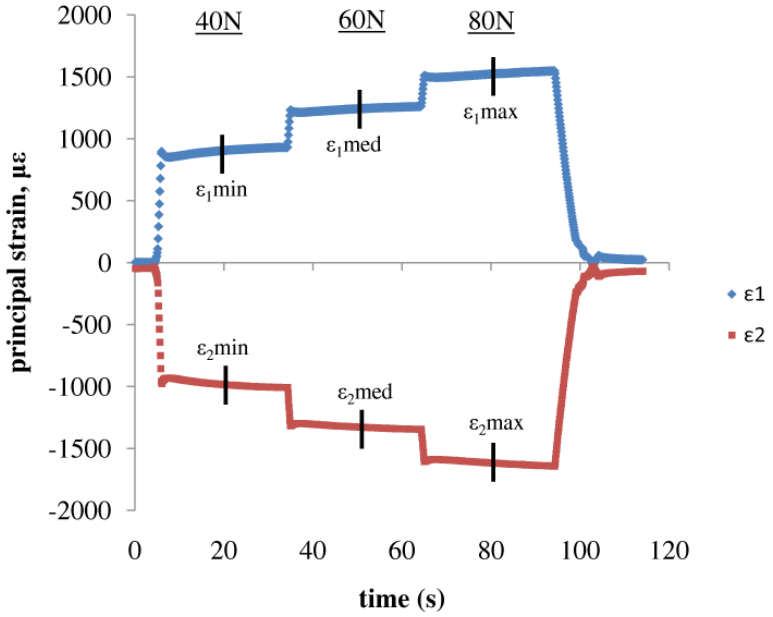

Fig. 3-8. Raw strain data plotted against time, ε_1 is positive, ε_2 is negative. Values of ε_1 and ε_2 were determined at the temporal midpoint of the minimum (40N), medium (60N), and maximum (80N) load applications. Average values of ε_1 and ε_2 were determined by averaging $\varepsilon_1$min, $\varepsilon_1$med, and $\varepsilon_1$max, and $\varepsilon_2$min, $\varepsilon_2$med, and $\varepsilon_2$max, respectively. Angle of maximum principal strain (α) and shear strain (γ) were also determined this way.

Strain data analysis

At the termination of testing, StrainSmart software calculated the maximum principal strain (ε_1), minimum principal strain (ε_2), angle of maximum principal strain (α), and shear strain (γ) for each gauge in 1 ms increments for the duration of each trial. Although the computer software automatically calculated these measures, they were double-checked manually using the following equations (in Perry, 1989; Dally and Riley, 1991).

Maximum and minimum principal strains are calculated from the strain recordings of each of the three grids on a gauge:

$$\varepsilon_{1,2} = \frac{\varepsilon_a + \varepsilon_c}{2} \pm \frac{1}{2}\sqrt{(\varepsilon_a - \varepsilon_c)^2 + (2\varepsilon_b - \varepsilon_a - \varepsilon_c)^2}$$

where ε_a, ε_b, and ε_c are the strains recorded by grids A, B, and C, respectively. Shear strain, which is often used as an indicator of overall strain, is merely the difference between the maximum and minimum principal strains:

$$\gamma = \varepsilon_1 - \varepsilon_2$$

The orientation of principal strain is also derived from the strains recorded by each grid and is measured from grid A to the principal axis:

$$\theta = \frac{1}{2}\tan^{-1}\frac{2\varepsilon_b - \varepsilon_a - \varepsilon_c}{\varepsilon_a - \varepsilon_c}$$

The sign of the angle between grid A and the principal axis determines whether it is measured clockwise or counterclockwise from grid A; if the angle is positive, it is measured counterclockwise from grid A. Conversely, if the angle is negative, it is measured clockwise from grid A. Because this calculated angle can represent the direction of either the maximum or minimum principal strain, the

strains from the recording grids must be examined: if the strain recorded from grid A is *larger* than that from grid C, then the calculated angle is to the *maximum* principal axis (α). If the strain recorded from grid A is *smaller* than that from grid C, then the calculated angle is to the *minimum* principal axis. Because the principal axes are perpendicular to each other, once one of the principal axes is determined, the other is also known.

In general, maximum principal strain is positive (*i.e.*, represents tension) and minimum principal strain is negative (*i.e.*, represents compression), but this is not always the case; occasionally maximum and minimum principal strain are of the same sign. When both values are positive, the largest positive strain is ε_1, and when both values are negative, the largest negative strain is ε_1 (*i.e.*, the absolute smallest ε_1).

Recall that each loading trial consists of the application of three different loads (minimum, medium, and maximum) at a particular joint angular position. The data were plotted against time and the values of maximum principal strain (ε_1), minimum principal strain (ε_2), angle of maximum principal strain (α), and shear strain (γ) were determined at the temporal midpoint of the minimum, medium, and maximum loads. These three sets of strain parameters were averaged within and across trials to derive mean values of ε_1, ε_2, α, and γ trials (Fig. 3-8).

The angles of maximum and minimum principal strain were superimposed onto digital photographs of the strain gauges (using ImageJ) to visualize principal strain orientation relative to bony anatomy.

To evaluate the predictions of the cylinder model (*i.e.*, torsion, dorsoventral compression, and dorsoventral bending), both average and peak values of maximum principal strain, minimum principal strain, shear strain, and angles of maximum and minimum principal strain were examined among: 1) gauge locations, 2) angular limb positions, and 3) species. Observed strain locations and types (*i.e.*, tensile or compressive) were compared to the predictions of the cylinder model (Figs. 3-2 to 3-4).

RESULTS

Most strain gauges that were observed to fail during data recording were replaced. However, a few gauges were impossible to replace without disturbing other gauges. Therefore, the *Papio* specimen is missing data from gauge 10, and the *Ateles* specimen from gauges 7, 8, and 14, and from the 45° limb position trial for gauges 13 and 18.

Average and peak values of ε_1, ε_2, angle of orientation of ε_1, and shear strain across limb positions are reported in Table 3-2. Average and peak values of ε_1, ε_2, angle of orientation of ε_1, and shear strain at each limb position are reported in Tables 3-3 and 3-4.

TABLE 3-2. Average and absolute maximum values of ε_1, ε_2, α, and γ across angular limb positions.

		ε_1			ε_2			α			γ		
Specimen	Gauge	Mean	SD	|Max|	Mean	SD	|Max|	Mean	SD	Anatomical direction	Mean	SD	Max
Macaca	1	5	15	26	-429	145	-557	30	6	CC[a]	434	151	573
	2	13	62	-88	-148	55	-223	25	7	CC	161	96	295
	3	205	76	298	-61	14	-74	-21	15	CC	266	69	346
	4	33	103	-129	-590	181	-743	22	6	CC	623	204	852
	5	340	136	483	-184	115	-389	-41	10	CC	524	185	747
	6	67	52	129	-308	124	-501	-54	7	DV	376	98	534
	7	549	62	630	-365	36	-414	39	25	DV	914	95	1044
	8	484	54	567	-331	36	-382	-78	11	CC	815	82	949
	9	105	67	162	-264	74	-350	73	12	ML	369	140	507
	10	897	340	1186	-387	44	-449	-66	6	ML	1284	354	1635
	11	160	117	234	-223	24	-249	49	68	CC	383	124	480
	12	85	72	184	-2221	138	-2339	28	3	ML	2305	155	2523
	13	-141	252	-521	-582	191	-826	-48	14	OB	441	87	527
	14	-282	426	-958	-1068	605	-1936	-13	19	OB	787	257	1129
	15	-52	239	-455	-812	420	-1468	-75	6	CC	761	188	1013
	16	877	160	1038	-1239	113	-1328	-47	3	OB	2115	250	2341
	17	44	189	291	-353	218	-638	-9	76	OB	397	87	529
	18	69	70	140	-303	115	-456	76	4	OB	373	108	524
Papio	1	582	59	639	-496	44	-543	60	6	DV	1078	99	1161
	2	220	30	256	-168	65	-243	75	6	CC	388	93	499
	3	-133	128	-237	-844	212	-1006	-66	4	DV	711	84	781
	4	15	26	49	-323	35	-354	-72	6	DV	339	56	392
	5	11	28	40	-545	88	-616	-75	4	DV	556	63	615
	6	88	26	116	-241	11	-253	-65	1	DV	329	36	366
	7	259	29	293	-312	53	-364	-74	3	CC	571	76	657
	8	170	70	214	-316	45	-371	-75	1	CC	487	53	552
	9	53	144	-195	-124	79	-263	-49	18	CC	177	67	232
	10	.	.	.	.	.	.	.	.	.	.	.	.
	11	-349	723	-1508	-1434	1010	-3068	-17	2	CC	1085	295	1560
	12	-6	248	-415	-872	106	-1019	42	11	ML	866	174	1021
	13	-215	292	-597	-516	276	-891	-68	9	OB	301	23	334
	14	51	25	83	-88	29	-128	46	28	DV	139	54	210
	15	121	34	154	-484	157	-639	-62	3	OB	605	147	708
	16	84	34	116	-165	36	-195	-67	2	CC	249	64	310
	17	102	29	127	-271	85	-353	-21	24	DV	373	66	424
	18	-217	309	-663	-472	323	-926	28	52	CC	255	43	299

TABLE 3-2. Continued.

Specimen	Gauge	ε_1			ε_2			α			γ		
		Mean	SD	|Max|	Mean	SD	|Max|	Mean	SD	Anatomical direction	Mean	SD	Max
Ateles	1	32	105	-145	-401	214	-662	33	39	CC	433	163	610
	2	312	256	693	-857	646	-1726	-39	21	ML	1168	829	2419
	3	-132	190	-355	-712	230	-973	19	52	CC	580	126	785
	4	-161	81	-258	-402	180	-683	-16	30	DV	242	210	600
	5	-41	115	-160	-589	218	-841	-70	14	CC	548	127	733
	6	-143	137	-290	-465	185	-643	22	27	DV	321	64	403
	7	.	.	.	.	.	.	.	.	.	.	.	.
	8	.	.	.	.	.	.	.	.	.	.	.	.
	9	-44	74	-170	-358	170	-534	26	20	ML	313	149	543
	10	107	77	177	-207	98	-333	-37	11	CC	314	37	365
	11	74	55	121	-369	217	-645	-49	13	CC	443	179	705
	12	-231	136	-419	-618	177	-871	18	18	ML	387	155	591
	13	-85	115	-209	-276	142	-471	-11	16	ML/DV	191	54	263
	14	.	.	.	.	.	.	.	.	.	.	.	.
	15	-23	80	-154	-422	144	-657	-63	7	ML/DV	399	66	503
	16	12	31	55	-171	112	-322	19	21	ML/DV	182	104	340
	17	-108	114	-299	-467	235	-827	-20	76	ML/DV	359	138	528
	18	34	28	65	-226	76	-333	-36	71	ML/DV	260	52	328
Hylobates	1	43	148	245	-314	176	-471	31	14	CC	357	280	691
	2	324	211	558	-302	250	-597	-57	13	ML	626	457	1141
	3	26	77	114	-356	52	-428	31	23	CC	381	54	469
	4	127	152	327	-233	147	-384	1	5	CC	361	291	711
	5	30	58	100	-227	45	-297	59	29	CC	257	41	307
	6	361	92	490	-367	118	-500	-66	2	DV	728	202	990
	7	963	284	1212	-1041	309	-1300	-83	0	CC	2003	592	2510
	8	984	309	1258	-970	284	-1203	-75	0	DV	1954	592	2461
	9	73	299	450	-604	207	-804	-60	2	CC	677	482	1171
	10	232	269	559	-1342	315	-1647	78	6	OB	1574	559	2079
	11	1408	543	1936	-1219	370	-1558	5	1	OB	2627	912	3494
	12	821	434	1291	-1129	359	-1452	-25	4	OB	1950	791	2734
	13	237	375	528	-973	282	-1296	61	9	OB	1210	580	1632
	14	125	322	-404	-1084	464	-1569	-12	3	OB	1209	427	1701
	15	254	192	426	-961	372	-1395	-73	7	OB	1215	341	1540
	16	1043	409	1387	-1062	301	-1370	-49	2	ML/DV	2105	695	2677
	17	-449	336	-990	-1165	1139	-3066	-27	32	ML/DV	716	805	2076
	18	-193	243	-530	-982	514	-1637	-17	9	ML/DV	789	367	1106

[a] CC: craniocaudal, DV: dorsoventral, ML: mediolateral, OB: oblique

TABLE 3-3. ε_1, ε_2, *angle of* ε_1, *and shear strains for each limb angular position.*[a]

		45°				60°				90°				105°				120°			
Specimen	Gauge	ε_1	ε_2	α	γ	ε_1	ε_2	α	γ	ε_1	ε_2	α	γ	ε_1	ε_2	α	γ	ε_1	ε_2	α	γ
Macaca	1	-10	-195	38	185	26	-389	29	415	-4	-486	23	482	16	-557	30	573	-3	-520	27	517
	2	22	-70	25	93	6	-132	34	138	-88	-147	26	59	53	-167	26	220	72	-223	15	295
	3	94	-74	-45	168	198	-45	-21	243	188	-71	-21	258	298	-48	-10	346	246	-67	-7	313
	4	19	-309	31	328	31	-518	18	549	-129	-743	19	614	129	-642	16	771	116	-737	24	852
	5	126	-124	-57	249	420	-143	-41	563	359	-389	-40	747	483	-118	-33	601	311	-148	-33	459
	6	45	-221	-65	266	129	-212	-53	341	34	-501	-51	534	118	-240	-52	358	12	-368	-47	379
	7	551	-387	84	938	529	-337	28	866	630	-414	26	1044	576	-360	28	936	461	-327	30	788
	8	449	-354	-87	803	462	-305	-82	767	567	-382	-83	949	508	-311	-59	819	435	-301	-79	736
	9	-3	-153	72	150	93	-248	79	340	116	-262	54	379	162	-308	83	469	156	-350	79	507
	10	332	-389	-57	720	886	-327	-69	1213	949	-393	-73	1342	1134	-375	-68	1509	1186	-449	-64	1635
	11	-45	-221	-73	176	166	-198	82	363	234	-201	79	435	232	-248	78	480	212	-249	78	460
	12	184	-2339	23	2523	101	-2011	29	2112	49	-2163	29	2212	101	-2252	31	2352	-10	-2338	29	2327
	13	121	-377	-61	498	-37	-564	-61	527	-11	-424	-45	413	-521	-826	-29	305	-258	-721	-42	463
	14	37	-518	-29	555	-303	-865	-14	562	124	-587	-30	710	-958	-1936	16	978	-308	-1436	-6	1129
	15	152	-374	-70	526	28	-713	-78	741	84	-573	-70	657	-455	-1468	-83	1013	-68	-935	-76	867
	16	647	-1048	-50	1695	778	-1328	-47	2106	1038	-1303	-46	2341	958	-1231	-42	2190	961	-1285	-49	2247
	17	291	-125	71	415	91	-213	78	304	70	-265	-65	334	-234	-638	-57	404	4	-526	-71	529
	18	94	-181	73	275	4	-277	81	281	123	-218	71	341	-13	-456	78	443	140	-384	75	524
Papio	1	508	-446	67	954	532	-457	66	989	607	-543	58	1150	626	-536	56	1161	639	-498	53	1138
	2	243	-234	81	477	256	-243	82	499	215	-120	71	335	205	-123	72	328	181	-119	71	300
	3	14	-592	-71	606	-1	-634	-70	632	-219	-985	-66	766	-224	-1006	-64	781	-237	-1004	-60	767
	4	49	-338	-65	387	38	-354	-65	392	2	-343	-78	344	-2	-315	-77	313	-9	-266	-74	257
	5	40	-435	-79	475	40	-465	-80	504	3	-612	-74	615	-6	-616	-73	611	-22	-596	-71	573
	6	116	-248	-64	364	113	-253	-64	366	82	-244	-65	325	73	-235	-66	308	57	-225	-66	282
	7	224	-227	-80	451	279	-306	-72	585	293	-364	-72	657	265	-342	-72	606	235	-323	-73	558
	8	47	-371	-74	418	188	-322	-74	510	214	-338	-74	552	204	-299	-75	503	198	-252	-76	450
	9	-195	-263	-21	68	56	-104	-45	159	107	-97	-56	204	145	-87	-58	232	153	-69	-66	222
	10	.	.	.	.	.	.	.	.	.	.	.	.	.	.	.	.	.	.	.	.
	11	-1508	-3068	-20	1560	-499	-1540	-16	1041	-130	-1250	-17	1119	-14	-936	-16	922	404	-377	-20	781
	12	-415	-1019	60	604	-43	-818	42	775	80	-941	37	1021	114	-827	36	942	232	-756	33	988
	13	143	-192	-69	334	-24	-325	-75	301	-204	-508	-78	305	-393	-663	-63	271	-597	-891	-56	294
	14	32	-56	15	88	24	-71	37	95	48	-75	69	123	71	-109	80	180	83	-128	27	210
	15	119	-240	-58	360	151	-426	-61	577	154	-533	-64	687	114	-580	-65	694	69	-639	-64	708
	16	74	-110	-69	184	97	-195	-68	292	116	-194	-67	310	104	-178	-64	282	30	-146	-68	176
	17	127	-142	-61	269	115	-230	-22	345	121	-303	-13	424	94	-326	-8	420	55	-353	1	408
	18	124	-161	26	285	-20	-209	61	189	-157	-395	25	239	-370	-669	84	299	-663	-926	-54	263

TABLE 3-3. Continued.

Specimen	Gauge	45°				60°				90°				105°				120°			
		ε_1	ε_2	α	γ	ε_1	ε_2	α	γ	ε_1	ε_2	α	γ	ε_1	ε_2	α	γ	ε_1	ε_2	α	γ
Ateles	1	-145	-662	29	518	49	-466	29	515	95	-515	-29	610	124	-175	70	299	37	-188	64	225
	2	693	-1726	-45	2419	374	-1193	-47	1567	-7	-903	-46	896	289	-139	-2	427	209	-323	-56	532
	3	-187	-973	-70	785	-241	-718	23	477	-355	-906	29	551	110	-492	56	602	13	-471	56	483
	4	-83	-683	-44	600	-219	-469	-45	250	-258	-334	-6	76	-75	-226	28	151	-169	-300	-13	131
	5	-160	-768	-49	608	-95	-592	-68	496	-109	-841	-65	733	110	-397	-82	507	49	-350	-85	399
	6	-290	-643	6	353	-193	-479	6	287	-236	-639	-2	403	13	-221	58	234	-11	-341	44	330
	7	.	.	.	.	.	.	.	.	.	.	.	.	.	.	.	.	.	.	.	.
	8	.	.	.	.	.	.	.	.	.	.	.	.	.	.	.	.	.	.	.	.
	9	10	-533	8	543	-15	-168	11	153	4	-228	53	231	-50	-325	40	275	-170	-534	19	364
	10	32	-333	-25	365	177	-129	-44	306	176	-150	-46	325	133	-131	-46	263	17	-293	-26	310
	11	-16	-533	-60	517	121	-104	-28	226	104	-262	-47	366	100	-302	-51	402	59	-645	-60	705
	12	-324	-530	-8	206	-137	-398	24	262	-180	-604	29	424	-95	-686	36	591	-419	-871	9	452
	13	.	.	.	.	59	-136	-31	194	-135	-268	-6	133	-209	-471	7	263	-53	-229	-12	176
	14	.	.	.	.	.	.	.	.	.	.	.	.	.	.	.	.	.	.	.	.
	15	15	-386	-59	401	15	-327	-57	342	-40	-448	-64	408	-154	-657	-60	503	51	-293	-74	344
	16	-21	-257	43	236	20	-87	31	107	-15	-119	2	104	19	-322	25	340	55	-70	-8	125
	17	-68	-456	69	387	-62	-220	57	158	-112	-528	-59	416	-299	-827	-85	528	1	-304	-80	304
	18	.	.	.	.	39	-163	69	202	37	-227	-57	264	-4	-333	-78	328	65	-184	-79	248
Hylobates	1	-2	-70	51	68	-47	-188	40	141	-123	-395	27	273	245	-446	18	691	142	-471	19	612
	2	209	-110	-64	319	197	-102	-70	299	111	-149	-65	259	558	-554	-44	1112	544	-597	-43	1141
	3	58	-282	50	341	18	-371	47	388	-95	-428	46	333	114	-354	7	469	33	-344	5	377
	4	18	-52	-1	70	-3	-125	2	122	40	-238	9	278	327	-384	-5	711	254	-369	-2	622
	5	100	-183	83	283	72	-236	80	307	-35	-297	77	262	34	-195	26	229	-19	-224	28	205
	6	284	-207	-69	490	334	-309	-64	643	277	-361	-68	638	490	-500	-64	990	420	-460	-65	880
	7	619	-635	-83	1254	699	-789	-83	1488	1080	-1180	-84	2260	1212	-1299	-83	2510	1204	-1300	-84	2505
	8	617	-583	-74	1200	692	-754	-75	1445	1097	-1111	-75	2207	1258	-1203	-75	2461	1257	-1200	-76	2458
	9	-150	-322	-58	172	-273	-449	-59	176	52	-723	-64	775	285	-804	-61	1090	450	-721	-61	1171
	10	-31	-920	83	890	-39	-1102	84	1063	240	-1566	76	1805	432	-1647	74	2079	559	-1476	71	2034
	11	735	-773	6	1508	959	-881	4	1840	1515	-1340	5	2855	1893	-1543	4	3436	1936	-1558	4	3494
	12	321	-691	-30	1011	429	-805	-28	1234	889	-1254	-25	2143	1174	-1452	-22	2626	1291	-1444	-21	2734
	13	268	-630	68	898	-396	-728	45	332	508	-1123	64	1632	276	-1296	67	1572	528	-1090	61	1617
	14	132	-426	-14	558	-404	-1481	-7	1078	363	-1044	-13	1407	132	-1569	-14	1701	403	-897	-13	1300
	15	188	-449	-75	637	-44	-1395	-63	1351	426	-873	-76	1299	294	-1245	-70	1540	407	-842	-81	1249
	16	642	-648	-46	1290	554	-851	-51	1405	1387	-1247	-49	2634	1308	-1370	-49	2677	1324	-1193	-50	2517
	17	-298	-588	-51	291	-990	-3066	-54	2076	-260	-501	13	241	-550	-1374	-44	824	-148	-297	1	150
	18	-211	-465	-25	254	-530	-1637	-28	1106	53	-880	-8	933	-303	-1382	-12	1079	28	-545	-12	573

[a] Data are averages of two trials, except: *Papio* 60° gauges 13-18 are from trial 2, *Hylobates* 105° gauges 13-18 are from trial 1.

TABLE 3-4. Results from Macaca mulatta *-a pilot specimen. ε_1, ε_2, angle of $\varepsilon_{1/2}$, and shear strains for each limb angular position.*

	45°				60°				75°				90°				105°				120°			
Gauge	ε_1	ε_2	α	γ	ε_1	ε_2	α	γ	ε_1	ε_2	α	γ	ε_1	ε_2	α	γ	ε_1	ε_2	α	γ	ε_1	ε_2	α	γ
1	49	-256	44	306	51	-291	42	341	50	-313	35	364	49	-317	34	366	34	-289	35	323	18	-255	37	273
2	-23	-428	-30[a]	405	-29	-478	-32	448	-63	-478	-33	414	-66	-483	-31	417	-67	-453	-28	387	-67	-414	-25	347
3	-1578	-6692	37[a]	5114	-1985	-6425	34	4440	-2221	-6196	31	3975	-2296	-6024	30	3728	-2227	-5849	30	3623	-2058	-5646	32	3588
4	770	-4974	-11	5744	1153	-4776	-11	5929	1410	-4588	-11	5999	1505	-4443	-11	5948	1458	-4314	-11	5772	1292	-4187	-11	5480
5	-1301	-7433	-28	6132	-1159	-7216	-28	6057	-1053	-6957	-27	5904	-1016	-6775	-28	5758	-1017	-6563	-28	5547	-1054	-6346	-29	5293
6	-506	-3646	20[a]	3140	-501	-3404	23	2902	-461	-3205	25	2744	-440	-3082	26	2642	-429	-2998	26	2569	-435	-2940	24	2505

[a]All angular values for gauges 2, 3, and 6 are given in degrees to the axis of minimum principal strain (ε_2).

Macaca mulatta - **a**

This specimen was tested as part of a preliminary study; the data are not compared directly to those from the other specimens because of differences in mechanical testing circumstances, but these data are included here to contribute to general results regarding magnitudes and directions of strain during pelvic loading. Six gauges were placed on the loaded-side ilium and pubis (corresponding approximately to current gauge locations 1, 4, 11, 12, 13, and 15, Fig. 3-9) and an extra hindlimb position at 75° hip flexion was examined. In addition, the sacroiliac joint exhibited visible mobility during loading. All results from this specimen are in Table 3-4.

Regional effects. Comparison of average peak ε_1 and ε_2 across gauge locations reveals that absolute values of ε_2 are consistently greater than those of ε_1, which is indicative of compressive stresses. The ilium (gauges 1 and 2) exhibits small average peak shear strains (273-448 με) compared to the pubis (2505-6132 με). Average peak shear strains in the superior pubic ramus are quite high (3588-5998 με), and average values of ε_1 and ε_2 indicate compression on both the ventral and dorsal aspects of the superior pubic ramus (gauges 3 and 4). Strain at the pubic symphysis is also high; the superior aspect of the symphysis registers strains ranging from 5293-6132 με (gauge 5), while the inferior aspect of the symphysis encounters strains ranging from 2505-3140 με (gauge 6).

Strain orientation. Peak strain in the ilium is oriented along the long axis of the bone, from the hip to the sacroiliac joint. In the superior pubic ramus, strain on the ventral aspect is oriented along the length of the bone (*i.e.*, mediolaterally), while

strain on the dorsal aspect of the ramus is oriented orthogonal to the length of the bone (*i.e.*, craniocaudally). The superior aspect of the pubic symphysis indicates mediolaterally-oriented strain (*i.e.*, in the same direction as the gauge on the ventral aspect of the superior pubic ramus), while the inferior aspect of the symphysis registers strain oriented obliquely (oriented approximately 45° to the parasagittal plane).

Effects of angular limb position. Shear strain is larger during more flexed limb postures. Of the six gauges, three (gauges 3, 5, 6) recorded largest strain at the 45° limb position, gauge 2 recorded largest strain at the 60° limb position, gauge 4 recorded largest strain at the 75° limb position, and gauge 1 recorded largest strain at the 90° limb position.

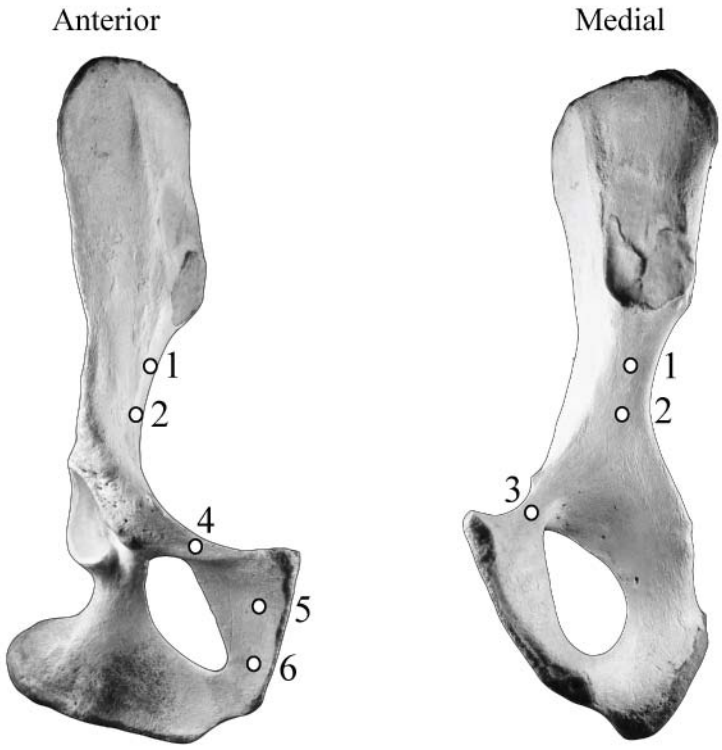

Fig. 3-9. Gauge locations for the *Macaca mulatta* –a specimen.

Macaca mulatta - b

During testing, mobility of the sacroiliac joint was observed that did not seem to be in excess compared to the other *Macaca* specimen. However, visual inspection after testing began revealed partial disarticulation of a 1-2 cm portion of the right sacroiliac joint. However, the results from this specimen are not obviously unusual; there are no major differences in strain patterns among trials and data from reference gauge 19 were consistent. Therefore, this partial disarticulation did not appear to impact the results.

Regional effects. Comparison of average absolute maximum values of ε_1 and ε_2 across gauge locations reveals that compression dominates (Table 3-2, Fig. 3-10). The loading-side ilium exhibits compression medially (gauges 1 and 4) and tension laterally (gauges 3 and 5). The unloaded-side ilium exhibits the opposite pattern, with tension medially (gauges 7 and 8). Except for gauge 10, all gauges in the pubis are characterized by compression. The ischium (gauge 6) registers larger compressive than tensile strains.

Average peak shear strains are largest in the pubis (gauges 10, 12, 14, 15, 16) and range from 1013-2523 με (Fig. 3-11). The unloaded side of the pubic symphysis registers relatively low peak shear strains (524-529 με). The loaded-side ilium exhibits lower peak strains than the unloaded-side ilium (loaded-side 295-852 με vs. unloaded-side 949-1044 με). The ischium also experiences relatively low peak shear (534 με) compared to other gauges.

Strain orientation. Maximum and minimum principal strain orientations are shown in Figure 3-12. The direction of absolute maximum principal strain

(averaged across limb angular positions) for gauges 1-5 on the loaded-side ilium is along the length of the bone from the hip joint to the sacroiliac joint (Table 3-2, Fig. 3-12). On the unloaded ilium, peak strain recorded by gauge 7 was oriented dorsoventrally, while peak strain recorded by gauge 8 was oriented along the axis between the hip and sacroiliac joints, as in the loaded-side ilium. Strain in the ischium is oriented dorsoventrally. Of the four gauges on the superior pubic rami, three recorded peak strain along the length of the ramus (gauges 9, 10, and 12); peak strain on gauge 11 was oriented craniocaudally. Of the six gauges located alongside the pubic symphysis, five recorded peak strains oriented obliquely (at ~45° angles to the midsagittal plane); gauge 15 showed strain oriented craniocaudally.

Effects of angular limb position. In general, peak shear strain magnitudes increase from maximum hip flexion (45°) to maximum hip extension (120°) (Table 3-3, Fig. 3-11). Only one gauge (gauge 12) registers larger strain in the 45° limb position than in all the other limb positions. The same finding is true for gauge 13 in the 60° limb position. Five gauges (5-8, 16) register largest strain in the 90° limb position, four gauges (1, 3, 11, 15) register largest strain in the 105° limb position, and seven gauges (2, 4, 9, 10, 14, 17, 18) register largest strain in the 120° limb position.

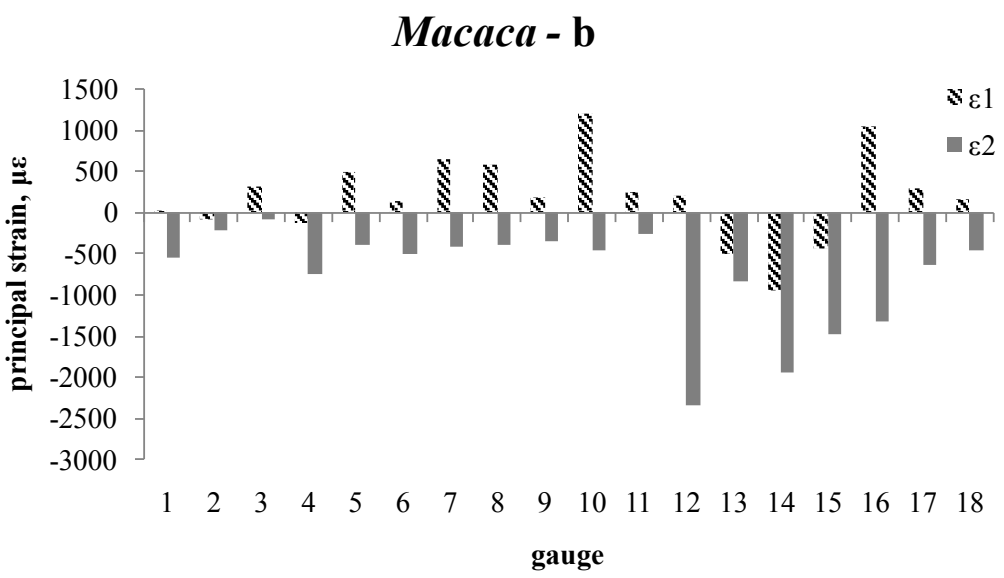

Fig. 3-10. Average absolute maximum values of maximum (ε_1) and minimum (ε_2) principal strains across limb positions for *Macaca mulatta* –b.

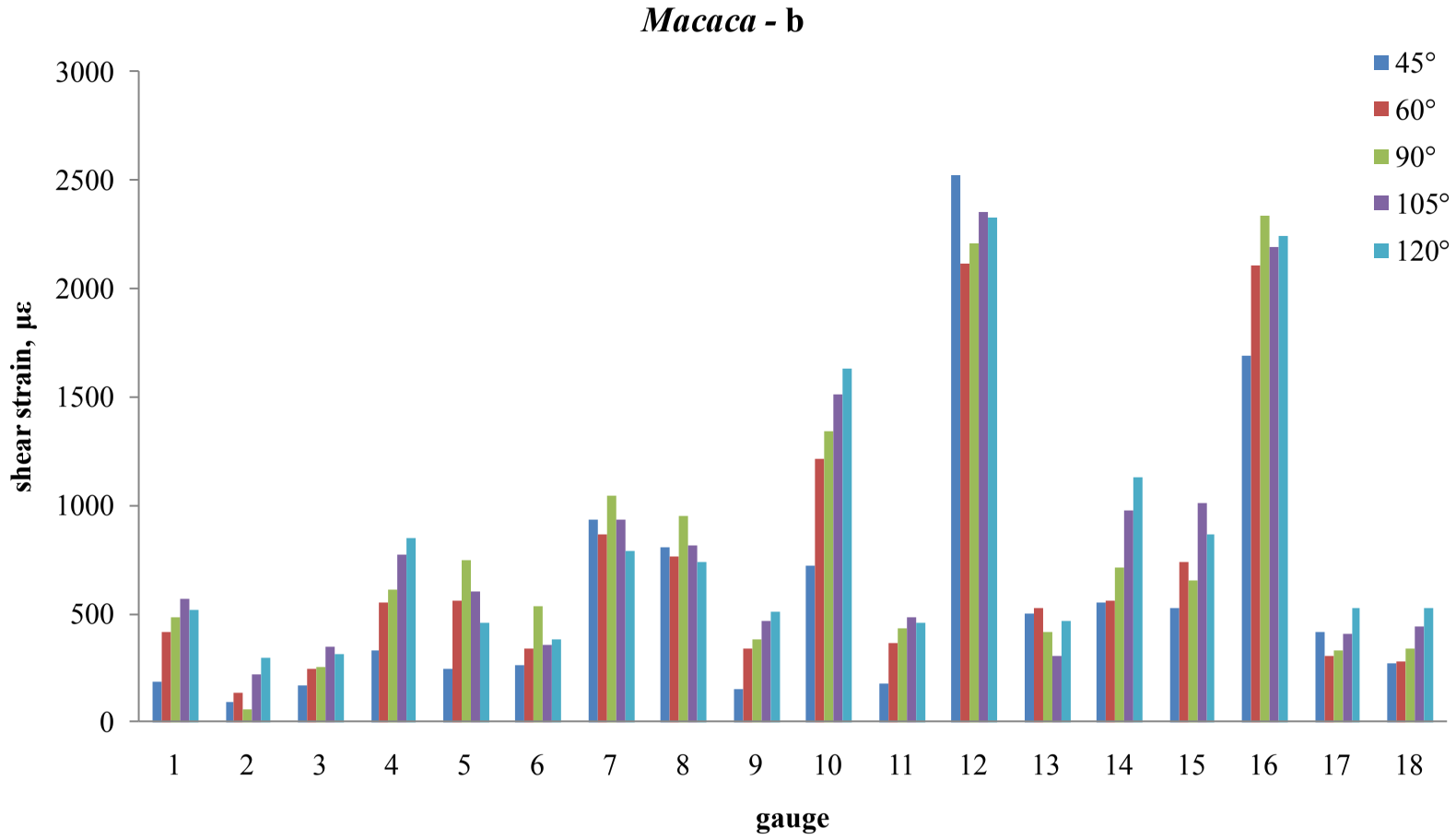

Fig. 3-11. Maximum shear strain for each limb position, by gauge, for *Macaca mulatta* –b.

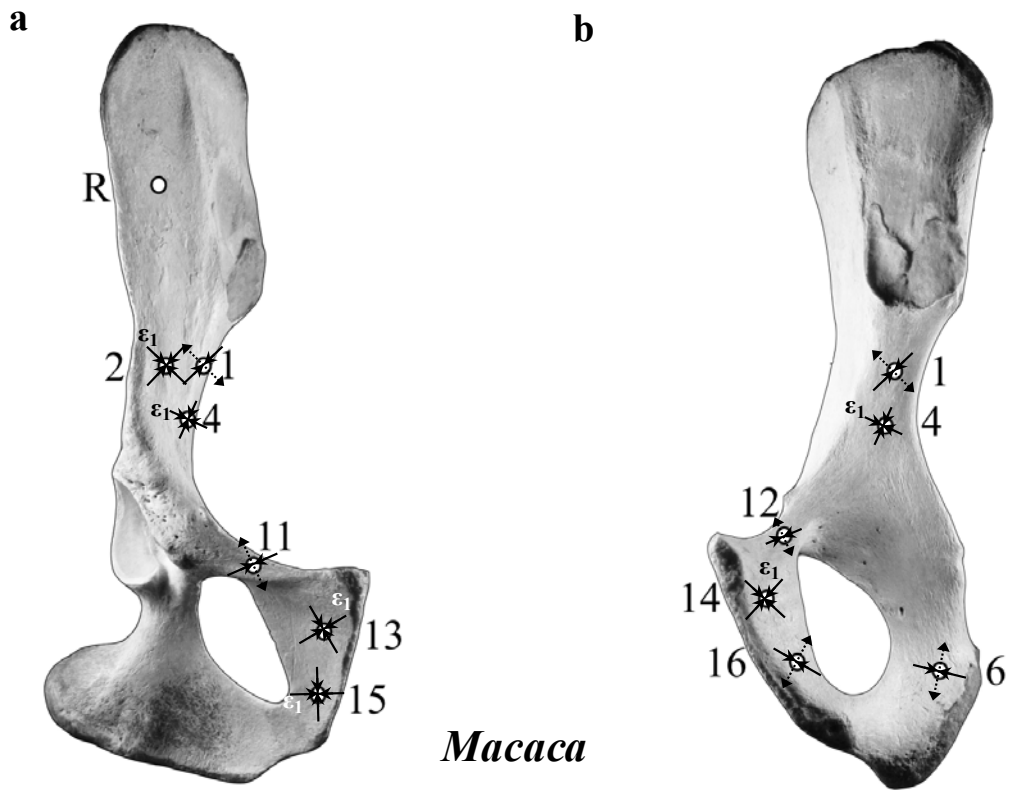

Fig. 3-12. Right anterior (**a**) and right medial (**b**) views of a pelvis depicting the angular orientation of the average maximum principal strains (ε_1) recorded by each strain gauge on the *Macaca* specimen (minimum principal strains—ε_2– are, by definition, the axes that are perpendicular to the axis of the maximum principal strain). Maximum principal strains were averaged across limb positions. Dotted lines with outward-facing arrows indicate tension, while solid lines with inward-facing arrows indicate compression. Note: the photograph on which the strain orientations are drawn is that of a baboon, not a macaque.

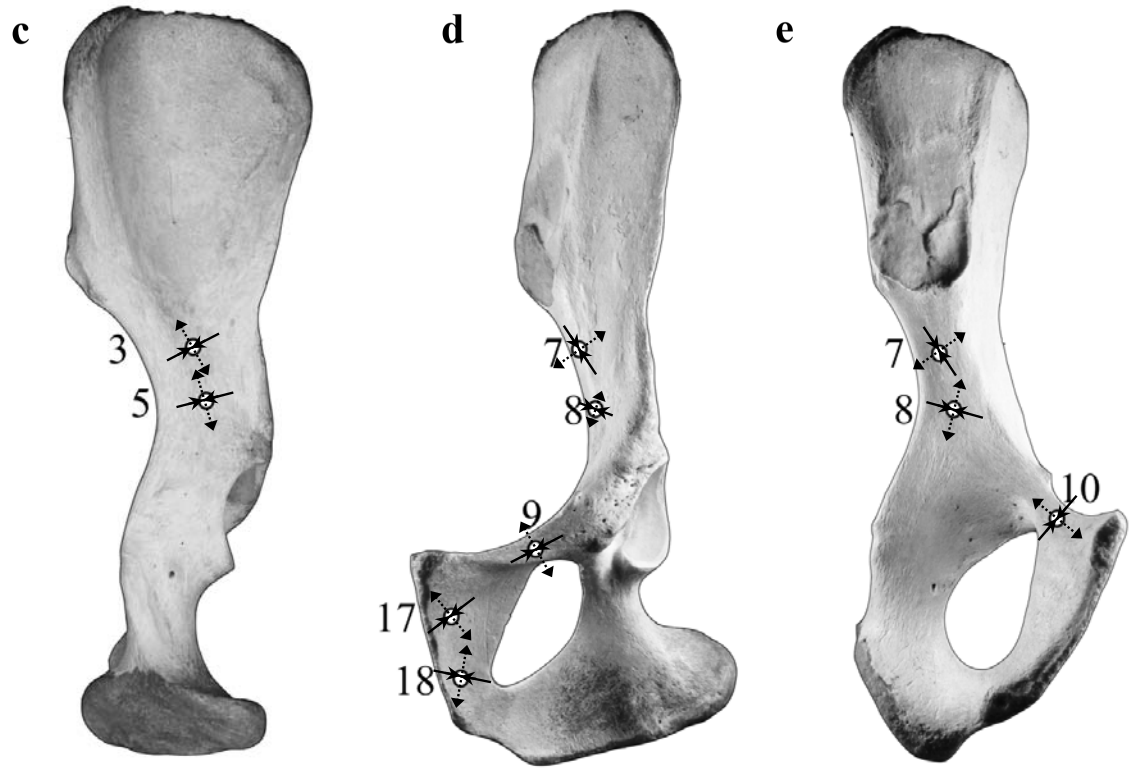

Fig. 3-12, continued. Posterior (**c**), left anterior (**d**), and left medial (**e**) views of a pelvis depicting the angular orientation of the average maximum principal strains (ε_1) recorded by each strain gauge on the *Macaca* specimen (minimum principal strains—ε_2– are, by definition, the axes that are perpendicular to the axis of the maximum principal strain). Maximum principal strains were averaged across limb positions. Dotted lines with outward-facing arrows indicate tension, while solid lines with inward-facing arrows indicate compression. Data from gauge ten are missing due to gauge failure. Note: the photograph on which the strain orientations are drawn is that of a baboon, not a macaque.

Papio

Regional effects. This pelvis is characterized by a remarkable amount of compression (Table 3-2). Absolute maximum principal strains were tensile in only two gauges (on the ilium, gauges 1 and 2); the rest of the gauges exhibited larger compressive than tensile strains, and many gauges showed compressive strains for both ε_1 and ε_2 (gauges 3, 9, 11, 12, 13, and 18, Fig. 3-13). Average peak shear strains were largest in gauges 1 and 3 on the ilium and gauges 11 and 12 on the loaded-side superior pubic ramus; these peak shear strains ranged from 781-1560 με (Fig. 3-14).

Strain orientation. Maximum and minimum principal strain orientations are shown in Figure 3-15. Absolute maximum principal strain in the loaded-side ilium is oriented dorsoventrally except for gauge 2, which exhibits peak strain oriented along the long axis of the ilium (Table 3-2). Like gauge 2, peak strains on the unloaded side ilium are oriented along the axis connecting the hip and sacroiliac joints. Ischial peak strain is oriented dorsoventrally. Strains in the ventral aspect of the superior pubic rami are craniocaudally-oriented (gauges 9 and 11). Peak strain recorded by gauge 12 on the dorsal aspect of the loaded-side superior pubic ramus is oriented along the length of the bone. Peak strains along the pubic symphysis are mostly obliquely-oriented (relative to the midsagittal plane). Gauges 13 and 15 are nearly identical in their strain orientations, which lie approximately 45° away from the midsagittal plane and are directed toward the cranial aspect of the loaded side. Peak strains of gauges 14 and 17 are directed dorsoventrally, and peak strains on 16 and 18 are oriented craniocaudally.

Effects of angular limb position. Peak shear strain magnitudes were largest in the 90° limb position, with five gauges (7, 8, 12, 16, 17) registering larger magnitude strains here than in other limb positions (Table 3-3, Fig. 3-14). Only two gauges (11 and 13) recorded largest strain at the 45° limb position, three gauges (2, 4, 6) recorded largest strain at the 60° limb position, four gauges (1, 3, 5, 18) recorded largest strain at the 105° limb position, and two gauges (14 and 15) recorded largest strain at the 120° limb position.

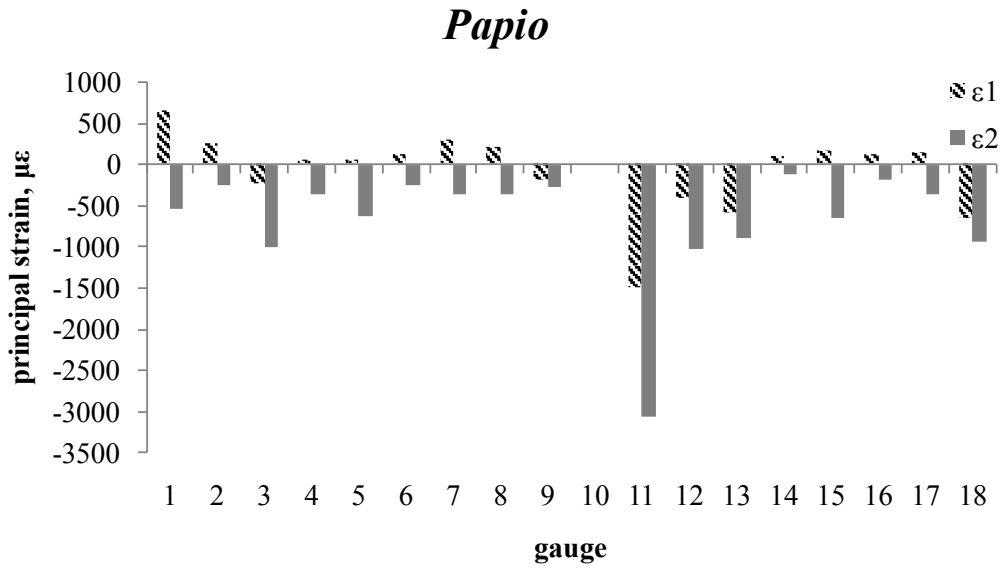

Fig. 3-13. Average absolute maximum values of maximum (ε_1) and minimum (ε_2) principal strains across limb positions for *Papio*.

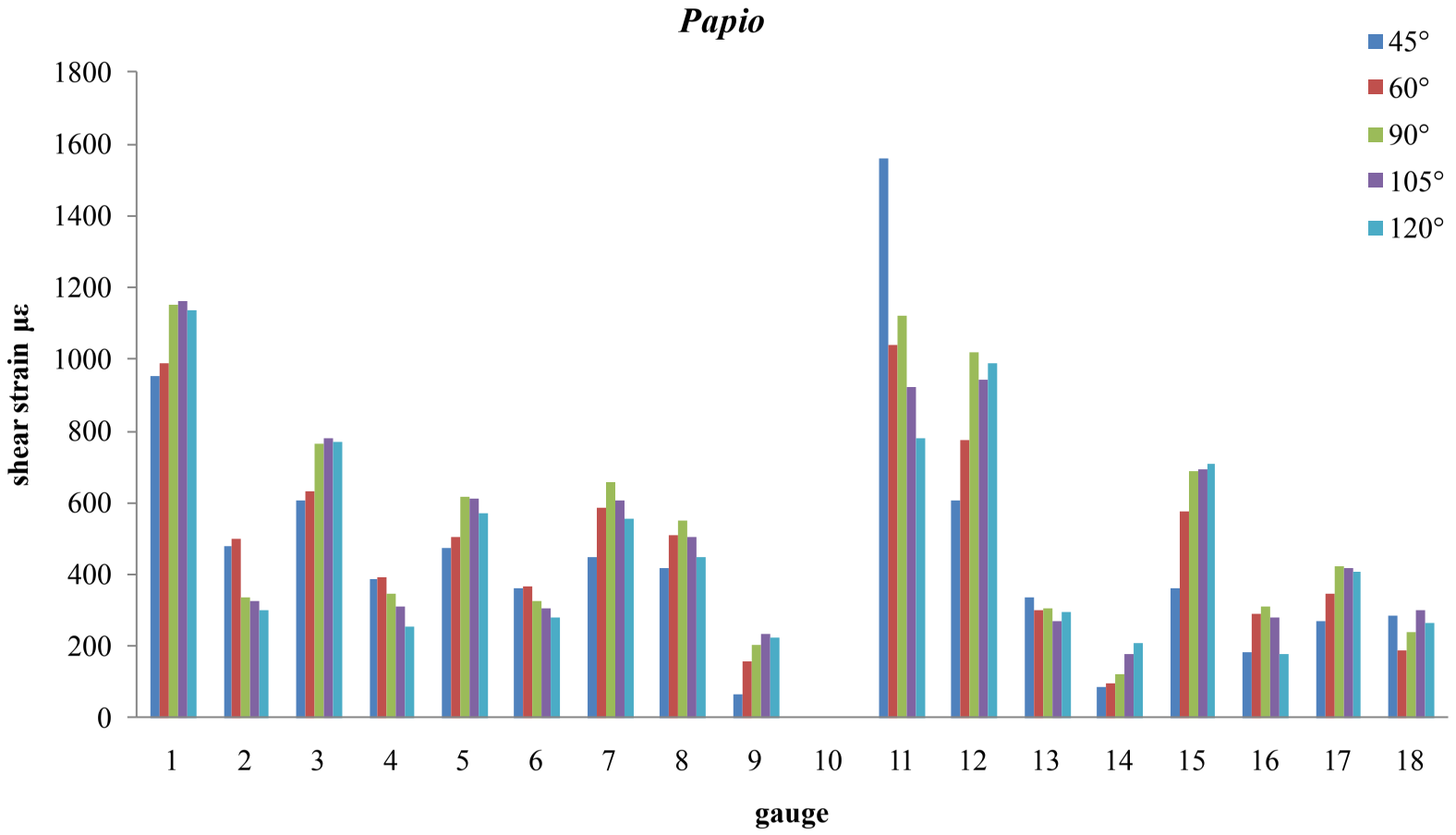

Fig. 3-14. Maximum shear strain for each limb position, by gauge, for *Papio*.

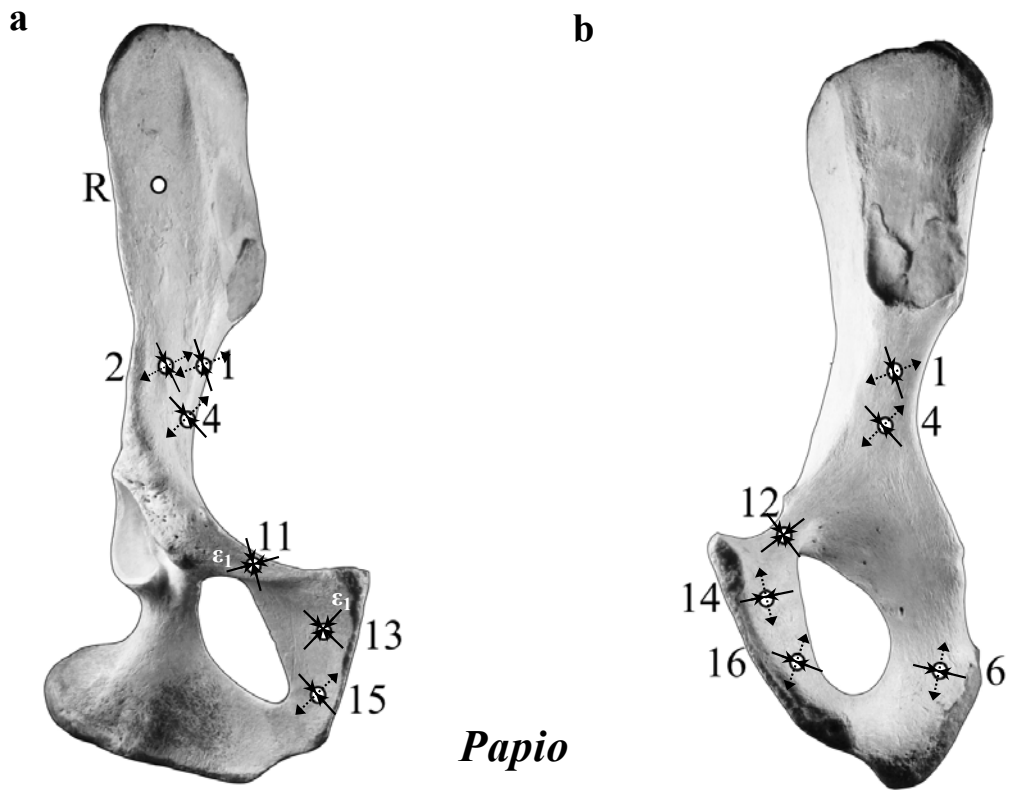

Fig. 3-15. Right anterior (**a**) and right medial (**b**) views of a pelvis depicting the angular orientation of the average maximum principal strains (ε_1) recorded by each strain gauge on the *Papio* specimen (minimum principal strains—ε_2– are, by definition, the axes that are perpendicular to the axis of the maximum principal strain). Maximum principal strains were averaged across limb positions. Dotted lines with outward-facing arrows indicate tension, while solid lines with inward-facing arrows indicate compression.

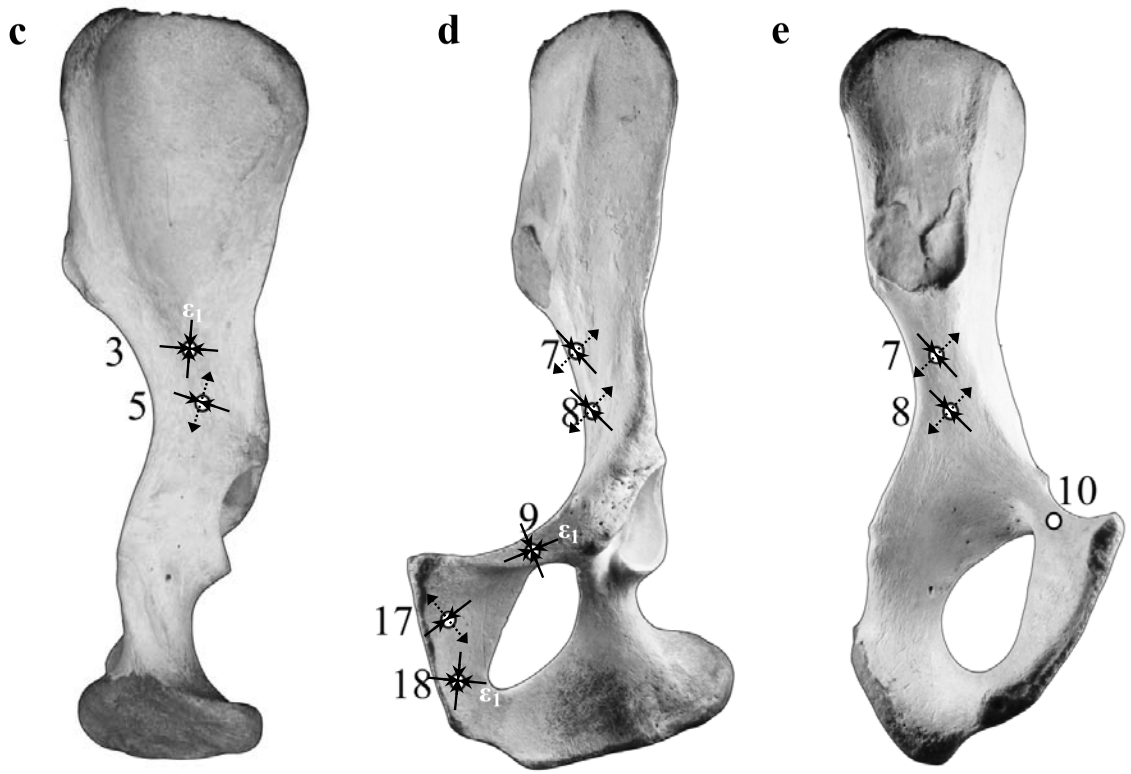

Fig. 3-15, continued. Posterior (**c**), left anterior (**d**), and left medial (**e**) views of a pelvis depicting the angular orientation of the average maximum principal strains (ε_1) recorded by each strain gauge on the *Papio* specimen (minimum principal strains—ε_2– are, by definition, the axes that are perpendicular to the axis of the maximum principal strain). Maximum principal strains were averaged across limb positions. Dotted lines with outward-facing arrows indicate tension, while solid lines with inward-facing arrows indicate compression. Data from gauge ten are missing due to gauge failure.

Ateles geoffroyi

Regional effects. Comparison of absolute maximum values of ε_1 and ε_2 across gauge locations demonstrates that in each location, the absolute maximum strain exhibited is compressive (Table 3-2, Fig. 3-16). Overall strain levels are low, with average peak shear strains ranging from 263-785 με, except for gauge 2 (2419 με, Fig. 3-17).

Strain orientation. Maximum and minimum principal strain orientations are shown in Figure 3-18. Average absolute maximum principal strain in the ilium is oriented along the length of the bone from the hip joint to the sacroiliac joint (gauges 1, 3, and 5), mediolaterally (gauge 2), and dorsoventrally (gauge 4). Peak strain is also directed dorsoventrally in the ischium (gauge 6). Peak strain in the superior pubic rami is oriented along the length of the bone (gauges 9 and 12), or craniocaudally (gauges 10 and 11). Peak strains along the pubic symphysis are oriented dorsoventrally/mediolaterally (these anatomical directions combine when the pubic rami project ventrally because the rami are oriented in neither a frontal nor a sagittal plane, but are instead oriented obliquely).

Effects of angular limb position. Peak shear strain magnitudes were largest in the 45° and 105° limb positions (Table 3-3, Fig. 3-17). In the 105° limb position, six gauges (12, 13, 15, 16, 17, 18) registered strains that were larger than in the other limb positions. Five gauges (2, 3, 4, 9, 10) recorded largest strain at the 45° limb position, none recorded largest strain at the 60° limb position, three gauges (1, 5, 6) recorded largest strain at the 90° limb position, and one gauge (11) recorded largest strain at the 120° limb position.

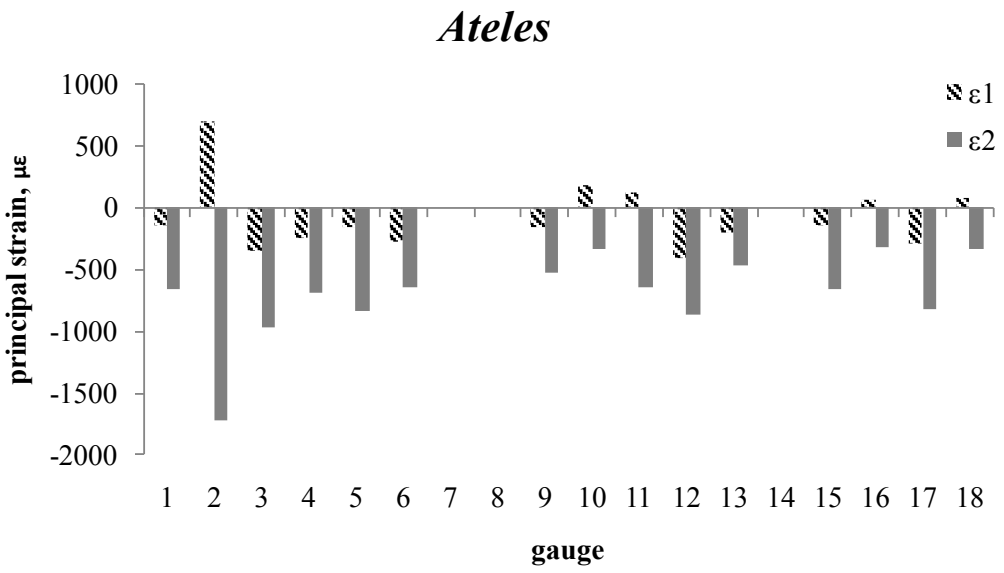

Fig. 3-16. Average absolute maximum values of maximum (ε_1) and minimum (ε_2) principal strains across limb positions for *Ateles*.

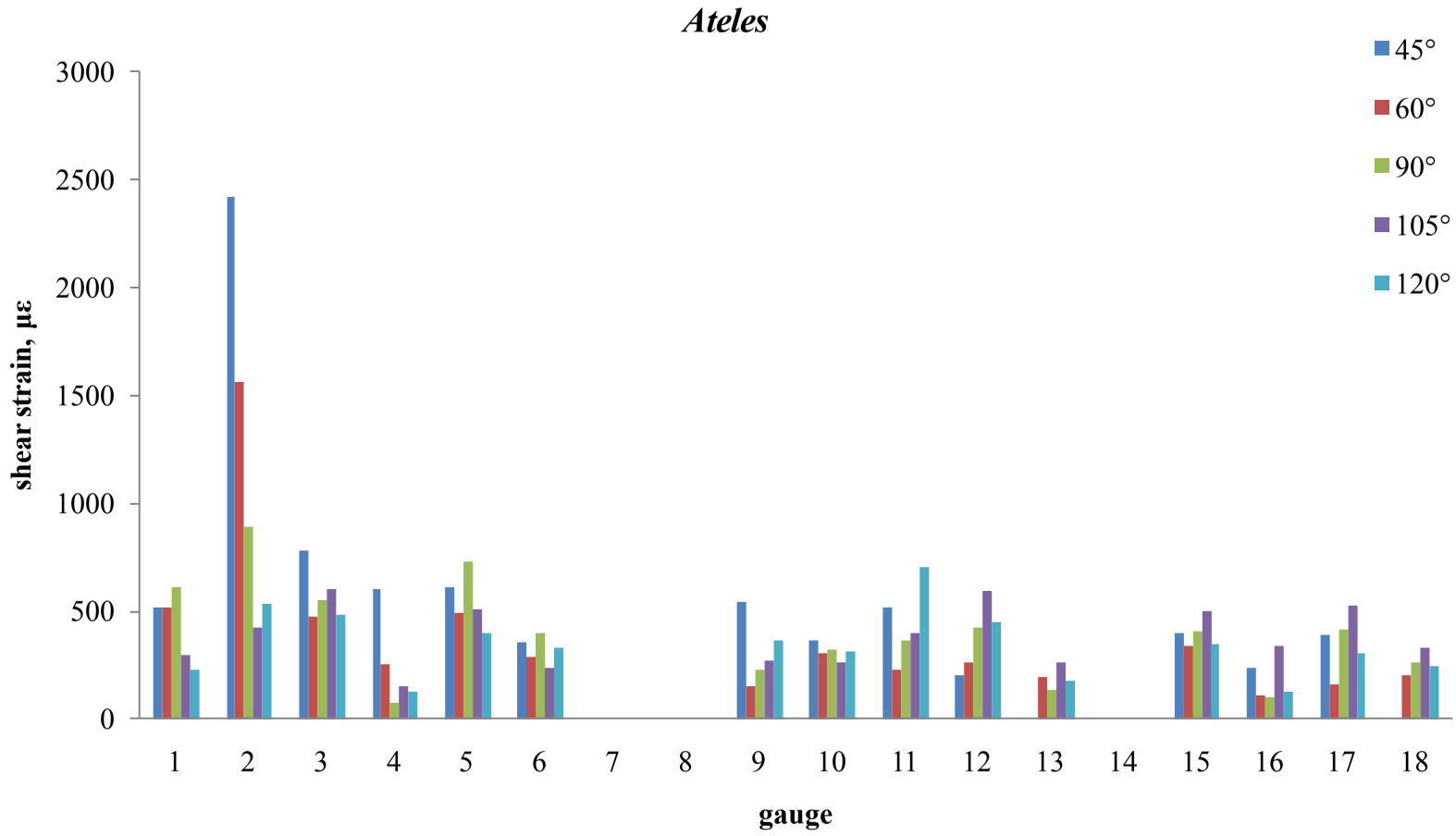

Fig. 3-17. Maximum shear strain for each limb position, by gauge, for *Ateles*.

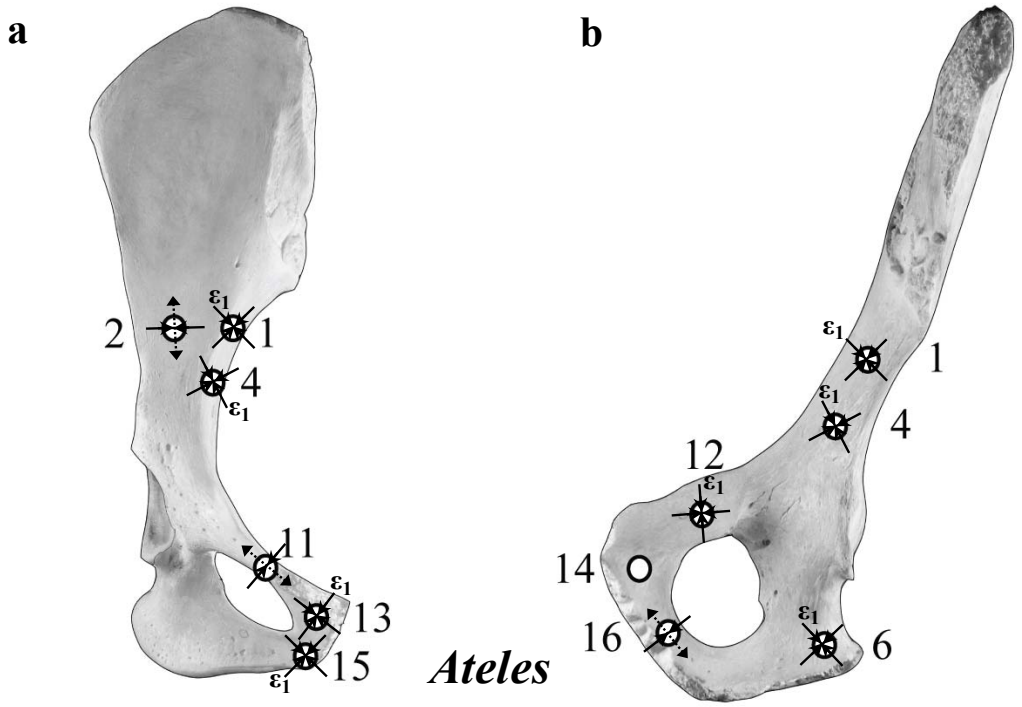

Fig. 3-18. Right anterior (**a**) and right medial (**b**) views of a pelvis depicting the angular orientation of the average maximum principal strains (ε_1) recorded by each strain gauge on the *Ateles* specimen (minimum principal strains—ε_2– are, by definition, the axes that are perpendicular to the axis of the maximum principal strain). Maximum principal strains were averaged across limb positions. Dotted lines with outward-facing arrows indicate tension, while solid lines with inward-facing arrows indicate compression. Note: the photograph on which the strain orientations are drawn is that of a gibbon, not a spider monkey.

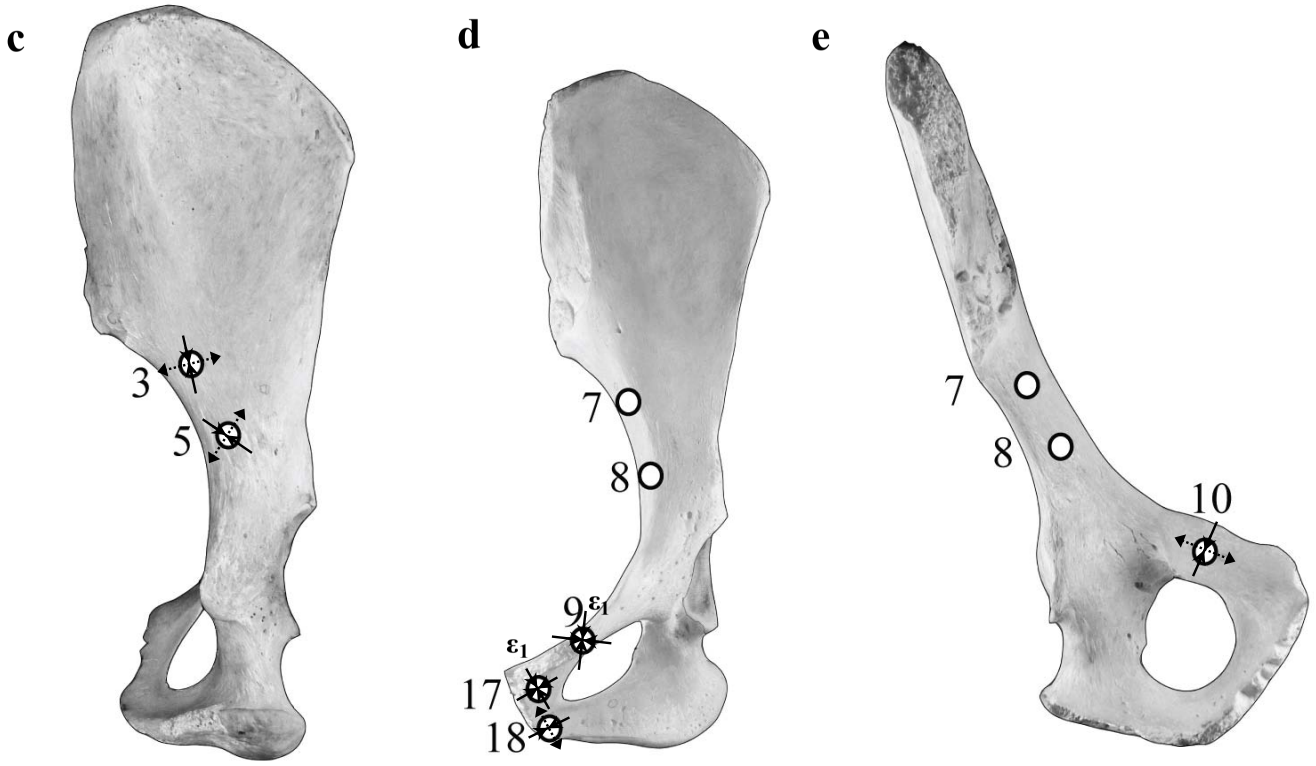

Fig. 3-18, continued. Posterior (**c**), left anterior (**d**), and left medial (**e**) views of a pelvis depicting the angular orientation of the average maximum principal strains (ε_1) recorded by each strain gauge on the *Ateles* specimen (minimum principal strains—ε_2– are, by definition, the axes that are perpendicular to the axis of the maximum principal strain). Maximum principal strains were averaged across limb positions. Dotted lines with outward-facing arrows indicate tension, while solid lines with inward-facing arrows indicate compression. Data from gauge ten are missing due to gauge failure. Note: the photograph on which the strain orientations are drawn is that of a gibbon, not a spider monkey.

Hylobates lar

This specimen exhibited considerable mobility of the sacroiliac joint and pubic symphysis during loading, but neither of the joints was structurally compromised.

Regional effects. This pelvis is predominantly characterized by compression. Comparisons of absolute maximum values of ε_1 and ε_2 across gauge locations illustrate that only three gauges exhibit larger tensile than compressive strains (gauge 8 on the unloaded-side ilium, and gauges 11 and 16 on the pubis), but only by a very small margin (Table 3-2, Fig. 3-19). Overall strain levels are high; peak shear strains from gauges 2 and 7-18 (the gauges with the largest strains) range from 1106-3494 με (Fig. 3-20).

Strain orientation. Maximum and minimum principal strain orientations are shown in Figure 3-21. In general, average absolute maximum strain in the ilium is oriented along its length between the hip and sacroiliac joints (Table 3-2). The only gauge on the ilium that does not follow this pattern is gauge 2 on the ventral aspect of the iliac blade of the loaded-side ilium, which exhibits relatively high peak strain (1141 με) oriented mediolaterally, and gauge 8 on the medial aspect of the unloaded side ilium, which exhibits high peak strain (2461 με) oriented dorsoventrally. Peak strain in the ischium is also oriented dorsoventrally, while peak strains in the pubis are generally oriented obliquely. Strains in the unloaded-side superior pubic ramus (gauges 9 and 10) are both compressive and are oriented orthogonally to each other. The gauges on the loaded-side superior pubic ramus (gauges 11 and 12) register the highest peak strains of all gauges (3494 με

and 2734 με, respectively) and are oriented in the same oblique direction. Gauges alongside the pubic symphysis record compressive strains (except for gauge 16 on the dorsal aspect). Gauges 13 and 14 exhibit peak strains that are oriented obliquely, approximately 45° to the long axis of the pelvis, directed cranially on the loaded side. Gauge 15 also shows obliquely-oriented principal strain, but it is directed cranially towards the unloaded side. Gauges 16-18 exhibit principal strains that are more mediolaterally/dorsoventrally-oriented than obliquely-oriented.

Effects of angular limb position. Ten out of 18 gauges (2-3, 6-8, 14-16) exhibited the largest peak shear strain during the 105° limb position (Table 3-3, Fig. 3-20). The 45° limb position did not generate the largest strains in any of the gauges. Three gauges (5, 17, 18) exhibited largest strains at the 60° limb position, gauge 13 recorded largest strain at the 90° limb position, and four gauges (2, 9, 11, 12) recorded largest strains at the 120° limb position.

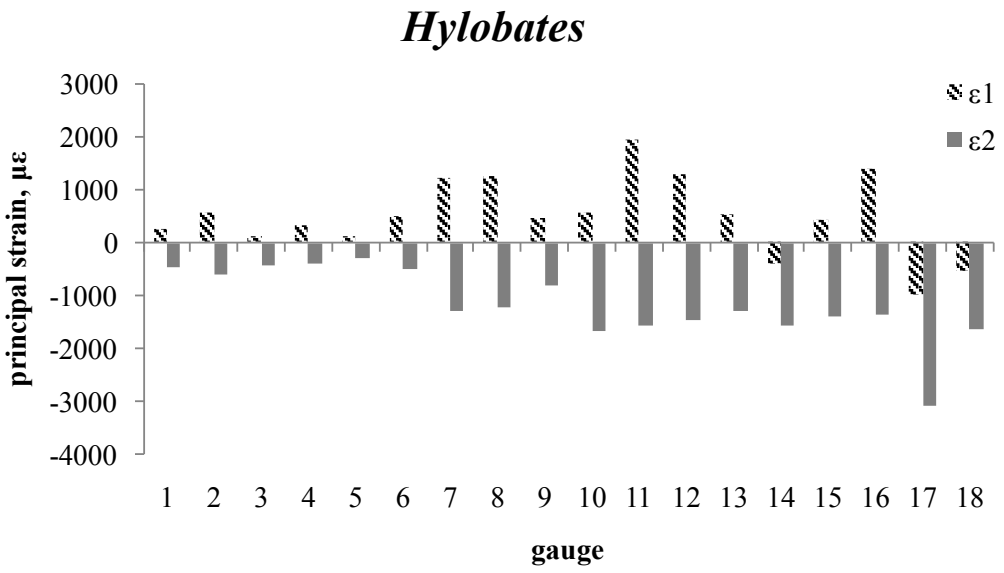

Fig. 3-19. Average absolute maximum values of maximum (ε_1) and minimum (ε_2) principal strains across limb positions for *Hylobates*.

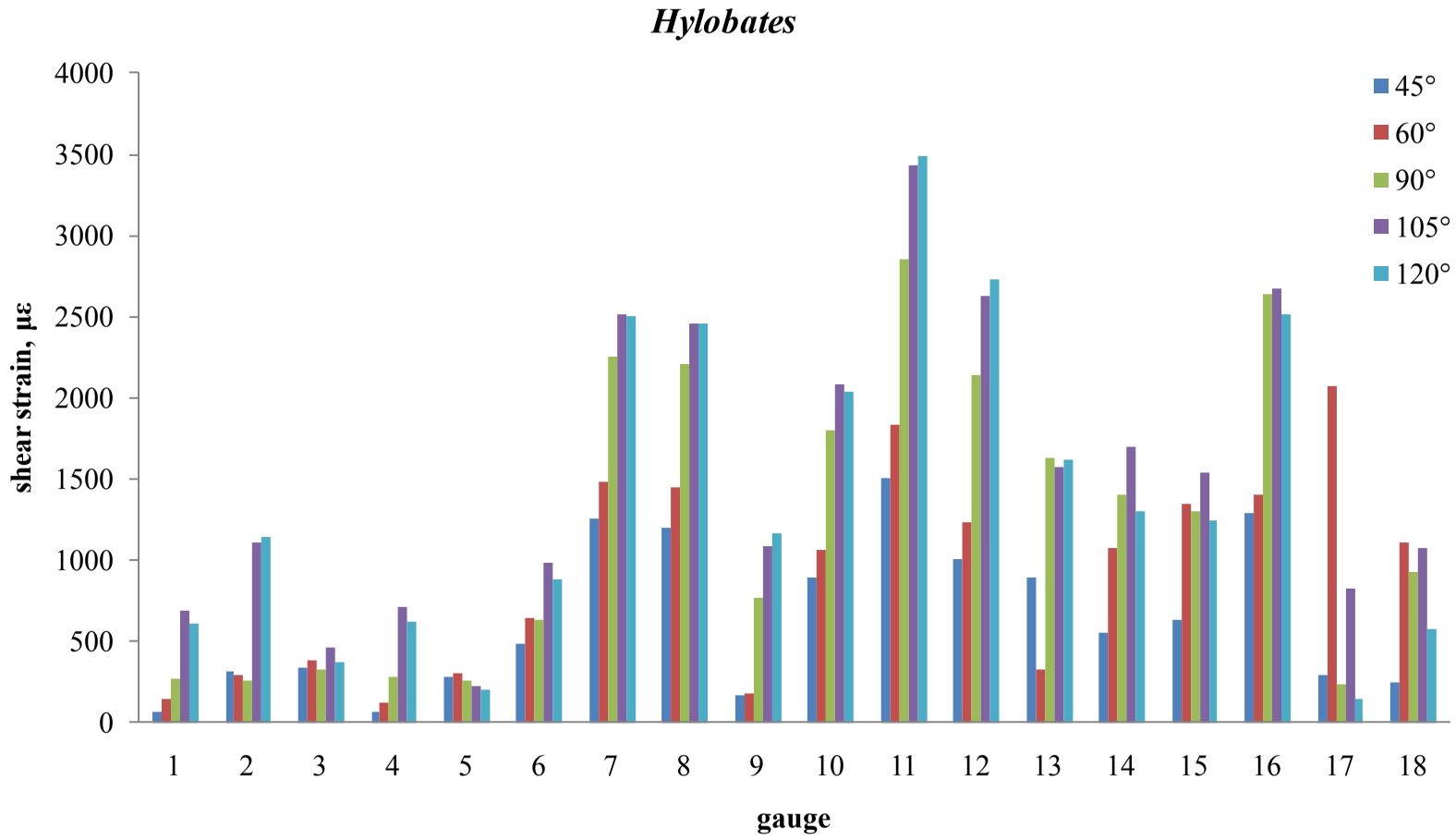

Fig. 3-20. Maximum shear strain for each limb position, by gauge, for *Hylobates*.

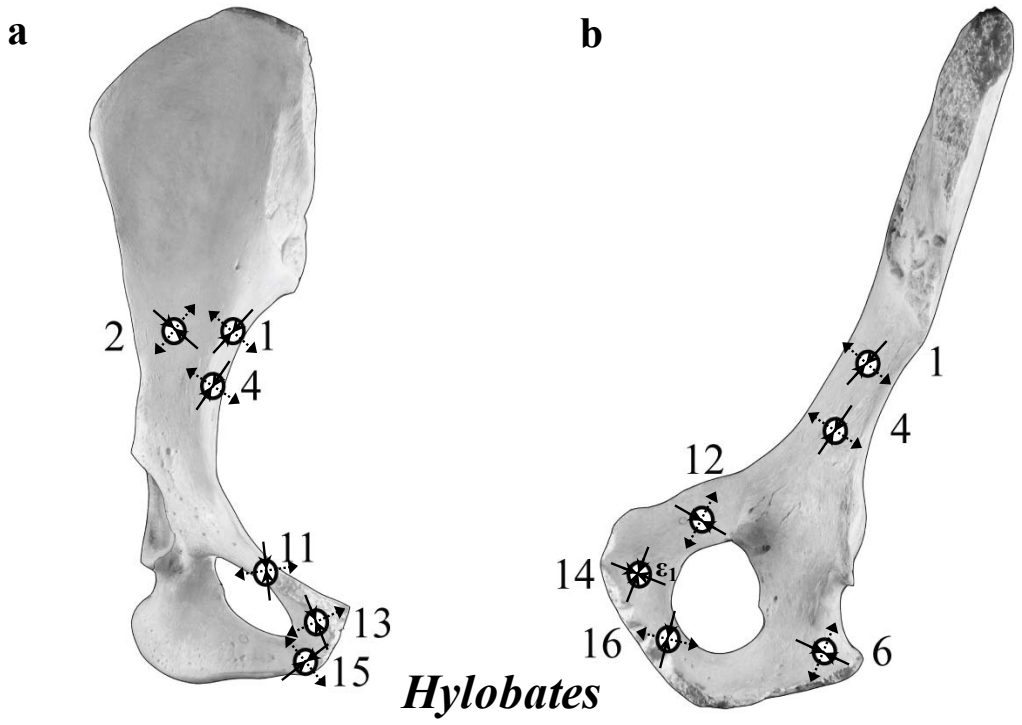

Fig. 3-21. Right anterior (**a**) and right medial (**b**) views of a pelvis depicting the angular orientation of the average maximum principal strains (ε_1) recorded by each strain gauge on the *Hylobates* specimen (minimum principal strains—ε_2– are, by definition, the axes that are perpendicular to the axis of the maximum principal strain). Maximum principal strains were averaged across limb positions. Dotted lines with outward-facing arrows indicate tension, while solid lines with inward-facing arrows indicate compression.

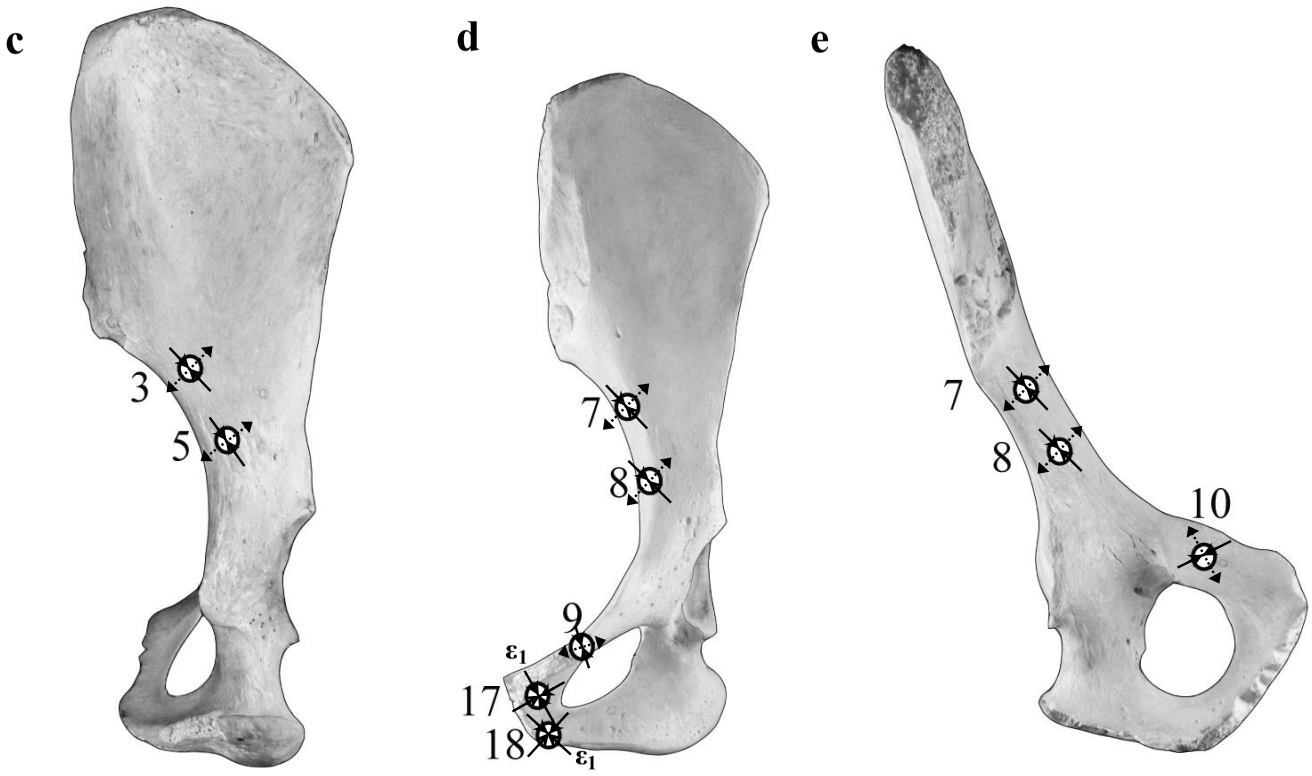

Fig. 3-21, continued. Posterior (**c**), left anterior (**d**), and left medial (**e**) views of a pelvis depicting the angular orientation of the average maximum principal strains (ε_1) recorded by each strain gauge on the *Hylobates* specimen (minimum principal strains—ε_2– are, by definition, the axes that are perpendicular to the axis of the maximum principal strain). Maximum principal strains were averaged across limb positions. Dotted lines with outward-facing arrows indicate tension, while solid lines with inward-facing arrows indicate compression. Data from gauge ten are missing due to gauge failure.

DISCUSSION

This study yields several interesting results regarding regions of the pelvis that experience large magnitude strain, the effects of limb position on strain distribution, and the utility of the cylinder model to predict pelvic stress resistance. First, the regional and positional differences in observed strain patterns will be examined. Then, the cylinder model tested here will be evaluated in relation to predictions of strain patterns derived from loading regimes.

Regional and positional differences in strain patterns

A summary of the predicted and observed strain patterns for each loading regime is shown in Table 3-5. In addition, a summary figure of the differences in shear strain amongst angular positions and taxa is shown in Figure 3-22.

Ilium. Results from this study indicate only low to moderate strain levels in the ilium relative to other pelvic regions (absolute strains generally ~300 με – 1000 με), with the exception of two gauges on the *Papio* and *Ateles* specimens (Table 3-2). Both compressive and tensile strains were observed, with a higher incidence of compression than tension. In general, the observed strain orientation was as predicted for most trials (except in *Papio*). These results reject dorsoventral bending as a dominant loading regime (Table 3-5), and provide partial support for dorsoventral compression (only in the *Macaca* specimen) and torsion (strain type is partially consistent with torsion, but strain orientations are not). Furthermore, these results support the hypothesis that load is transmitted through the long axis of the ilium.

Ischium. The ischium experienced dorsoventrally-oriented low strains (absolute strains generally 200 με – 600 με) relative to the rest of the pelvis. Peak strains were compressive. *A priori* strain predictions during torsion and dorsoventral bending were not made, thus these results can neither reject nor support these two loading regimes. However, these results do support the presence of dorsoventral compression during pelvic loading.

Pubis. In general, the pubis experienced large-magnitude compressive strains (absolute strains ~200 με – 3000 με). Peak pubic strains were on its loaded side, but some strains on its unloaded side were also large (gauge 17 in *Hylobates* and gauge 10 in *Macaca*-b). In *Macaca*-b, *Papio*, and *Ateles*, all pubic strains were compressive, even on dorsal and ventral sides of the superior pubic rami where compression and tension are expected based on beam theory. The observed pattern of strain orientation was variable, with many instances of craniocaudally-, mediolaterally-, and obliquely-oriented strain. These patterns of compressive versus tensile strain reject the hypotheses of torsion, dorsoventral compression, and dorsoventral bending. The orientations of these strains, however, provide some support for torsion (*i.e.*, many strains were oriented ~45° to the long axis of the pelvis) and dorsoventral compression (mediolaterally-oriented strains). Furthermore, from the perspective of the trade-off model, these data, uninformed by the morphometric data, suggest that the pubic region functions to resist stress and its morphology may be adaptive (however, see Chapter 5).

Effects of limb angular position on strain patterns. In addition to differences in strain patterns among pelvic regions, there were also differences in strain

magnitude among limb angular positions. Average peak shear strain was largest during hip extension (from 90° ["mid-stance"] to 120° of limb extension, Figure 3-22). The *Ateles* specimen also exhibited large peak strains during 45° of hip flexion in addition to 120° hip extension.

TABLE 3-5. Predicted and observed average peak principal strains.[a]

	Cylinder model predictions			Observed average peak principal strain patterns			
Gauge	Torsion	DV Compression	DV Bending	*Macaca*	*Papio*	*Ateles*	*Hylobates*
1	+/-[b]	-	+	-	+	-	-
2	+/-	*	*	-	+	-	-
3	+/-	+	-	+	-	-	-
4	+/-	-	+	-	-	-	-
5	+/-	+	-	+	-	-	-
6	*	-	*	-	-	-	-
7	+/-	-	+	+	-	x	-
8	+/-	-	+	+	x	x	≈
9	+	-	*	-	-	-	-
10	-	+	*	+	-	-	-
11	-	-	*	≈	-	-	+
12	+	+	*	-	-	-	-
13	+	-	*	-	-	-	-
14	-	+	*	-	-	x	-
15	+	-	*	-	-	-	-
16	-	+	*	-	-	-	≈
17	-	-	*	-	-	-	-
18	-	-	*	-	-	-	-

[a]Asterisks indicate no prediction based on loading regime. Peak principal strains are averaged across all angular limb positions for each species. Sign represents the sign of the absolute maximum strain (either ε_1 or ε_2); + is tension, - is compression, ≈ indicates approximately equal ε_1 and ε_2, x indicates missing data.

[b]Ilium predictions for torsion were that all gauges on one ilium would exhibit the same type of strain (*i.e.*, all + or all -), while all gauges on the opposite ilium would exhibit the opposite sign.

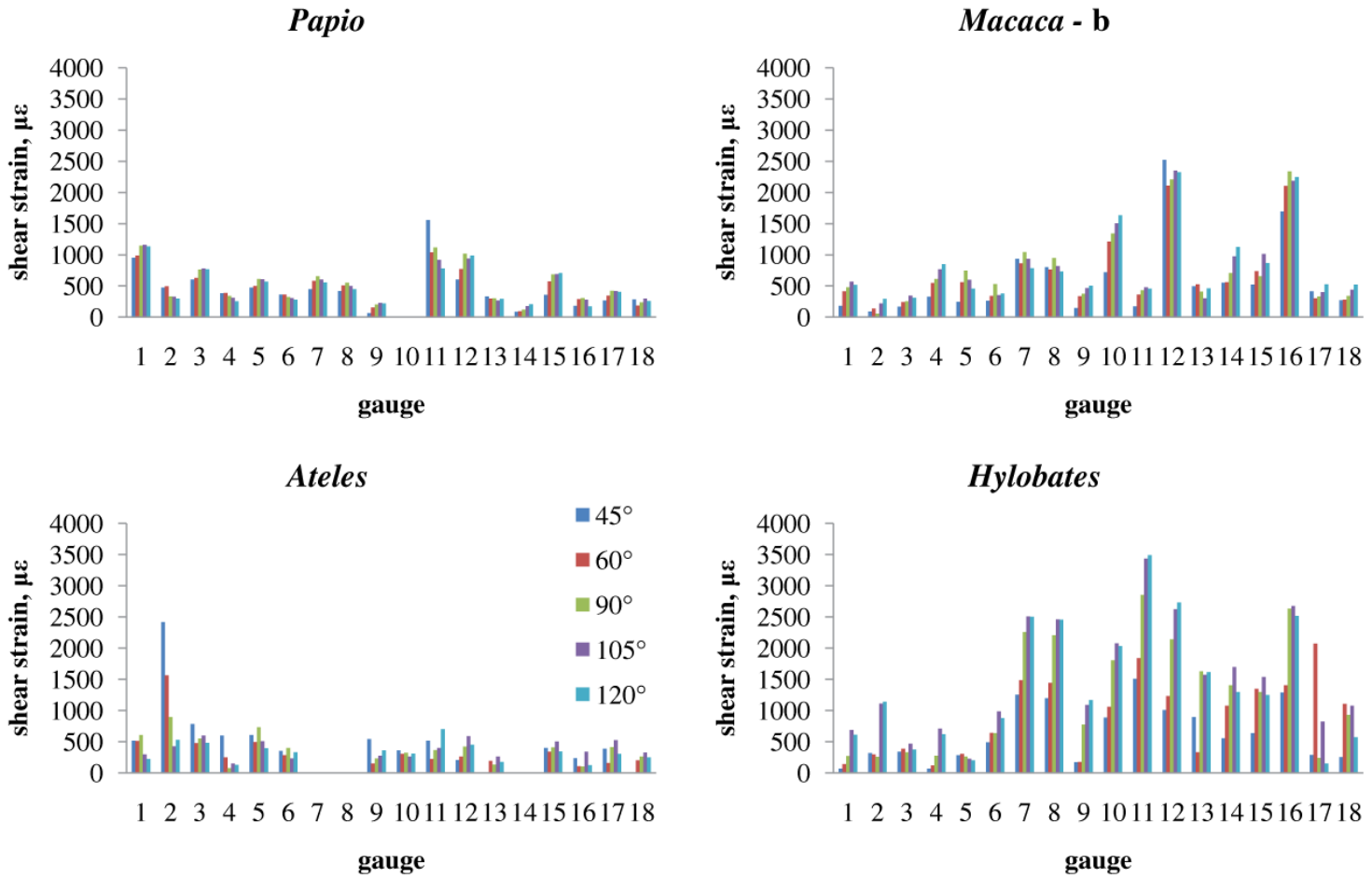

Fig. 3-22. Maximum shear strain for each limb angular position, by gauge and specimen.

Cylinder model of pelvic biomechanics

To better understand pelvic biomechanics, this study sought to determine whether the pelvis can be explained by a mechanical model that is generalizable to all primate taxa. A cylinder model was chosen here because previous work (Badoux, 1974; Kummer, 1975; Pauwels, 1980) suggested that this was a plausible mechanical description of a pelvis. Loading regimes that seem likely to occur during hindlimb force application—torsion, dorsoventral compression, and dorsoventral bending—were proposed, and predictions were made regarding the locations and types of strains that would occur in a cylinder under those loading regimes. The cylinder model was tested by comparing observed strain patterns to those predicted by the model.

Predicted strain patterns are compared to observed patterns in Table 3-5. While the orientations of observed strains provide partial support for torsion and dorsoventral bending, the types of strains that the pelves experienced reject these hypotheses; based on the data collected here, these loading regimes do not occur singly (see below for a discussion of this issue). However, the hypothesis of dorsoventral compression was not wholly rejected; partial support was obtained from the ilium in the *Macaca*-b specimen, and among all specimens, the compressive strains in the ischium and the orientation of some strains in the pubis provide some support for this hypothesis. Therefore, these data provide some support for dorsoventral compression of the pelvis, but reject the hypothesis that torsion or dorsoventral bending occur individually.

Although the majority of the data do not support the model predictions, outright rejection of the hypothetical cylinder model is premature. The model predictions as formulated here were generated under the assumption that evidence of each loading regime could be distinguished from evidence of the others. However, when multiple loading regimes occur simultaneously, it is possible that the "layering" of loading regimes masks evidence of individual regimes in such a way that it is impossible to identify a specific loading regime. Having multiple loading regimes that occur simultaneously is not incompatible with the cylinder model. In fact, loading regimes often occur together (e.g., torsion and dorsoventral bending frequently occur simultaneously, Timoshenko and Gere, 1972), and this is likely the case for the pelvis. The patterns of strain that would be expected during multiple, simultaneous loading regimes are unclear and were not tested here (although some stress states can be calculated, for example, with dorsoventral bending and torsion, Timoshenko and Gere, 1972). Therefore, although the data from this study generally reject the cylinder model as formulated here, future work may find support for the model if predictions of strain patterns are generated that account for the effects of multiple, simultaneous loading regimes.

An alternative model based on local loading environments may more accurately describe strain patterns encountered during *in vitro* loading. A conceptualization of the pelvis as a singular structure that likely experiences layered loading regimes—for example, a cylinder—may be inaccurate; it might be better envisioned as separate structures connected at pelvic joints. While there

are different ways of compartmentalizing a structure, the most obvious and perhaps most successful in this case would be to model the ilium, ischium, and pubis separately. Each of these bony regions may act as beams; the ilium is a beam that is secured at the hip and sacroiliac joints, the ischium is a cantilevered beam that is secured at the hip joint and is acted upon by musculature on its caudal end, and the pubic rami are secured at both medial and lateral ends (*i.e.*, struts).

The loading regime acting on the ilium, which is generally long and blade- or rod-like, is likely bending. This study found that dorsoventral bending does *not* characterize the ilium; instead, perhaps mediolateral bending occurs. Because the sacroiliac joint is medial to the hip joint, forces applied through both hips would cause compression on the medial aspect of the iliac beam and tension on its lateral aspect. This hypothesis is supported by the results of the *Macaca* specimen, but not by the other specimens, and the work of Pauwels (1980) suggests that this may be the case[1].

The loading regime acting on the cantilevered ischial beam would be dorsoventral bending. Substrate reaction forces acting on the hip joint would be countered by the ventral pull of the hamstring musculature, resulting in tension on the dorsal aspect of the ischium and compression on its ventral aspect. This hypothesis cannot be examined using the data here because only one gauge collected ischial data.

[1] Pauwels (1980) did not comment on the stresses in the iliac beam, but focused instead on the stresses in the sacroiliac and pubic symphysis joints. Examination of his Fig. 6 (p. 141) appears to illustrate mediolateral bending of the ilium.

There are several loading regimes that might characterize the pubic struts, which are secured at medial and lateral ends by the pubic symphysis and hip joints. The data here show that torsion and dorsoventral compression do not characterize the pubis singly, although there is some evidence of each, and it is possible that they act together. Given the compressive strains that were found to characterize both the internal and external aspects of the pubis, and the general lack of tension, it seems likely that the pubic struts are at least loaded in axial compression, and are likely loaded in additional ways.

Finite element analysis may contribute to building this hypothesized model of pelvic mechanics. One of the disadvantages of the present study is the absence of muscle forces acting on the pelvis during *in vitro* loading, which may result in erroneous high strains. For example, a study comparing results of finite element models that include and exclude the contribution of muscle forces found that applying muscle forces to a model decreased the magnitude of strains as compared to a model that did not factor in the role of hip musculature in force modulation (Dalstra and Huiskes, 1995). Thus, a finite element model that includes the musculature acting on the pelvis may generate more accurate hypotheses of loading.

CONCLUSION

This study is the first to collect *in vitro* strain data on a sample of primate pelvic cadavers to test a general, mechanical model of pelvic stress resistance. The predicted loading regimes of the cylinder model of pelvic mechanics were

compared to observed strain patterns at 18 sites on the ilium, ischium, and pubis during a range of hindlimb angular excursions.

The pelvis undergoes significant compression during loading, especially in the pubic region. High compressive strains in the pubis suggest that this region may be functionally significant during hindlimb loading, and may differ in taxa that differ in locomotor behavior. Because *in vivo* strain data collection would be logistically difficult on the pelvis due to the large thigh musculature that attach to it, finite element analysis incorporating muscle forces would be a worthwhile avenue of future research to determine the role of muscles in modulating forces on the pelvis. Use of finite element models would also allow the investigation of the effects of sacroiliac and pubic symphysis joint mobility on force modulation.

These data do not provide support for torsion or dorsoventral bending as dominant loading regimes for the entire pelvis, and only partial support is given for dorsoventral compression. Although these data can neither confirm nor reject the cylinder model, it will likely not be useful in the pursuit of understanding the mechanics and functional morphology of the pelvis. Instead, local loading environments of functional subunits of the pelvis (*i.e.*, ilium, ischium, and pubis) may better explain pelvic stress resistance, and future work should model each of these elements separately.

CHAPTER 4: PELVIC ADAPTATIONS TO LOCOMOTION IN PRIMATES

Identification of locomotor adaptations of the primate pelvis requires a verified relationship between pelvic form and its locomotor function. Ideally, this functional association should be demonstrated in a comparative context that accounts for sharing of traits among taxa due to homology. The study presented in this chapter focuses on testing univariate adaptive hypotheses of pelvic shape in a taxonomically broad comparative sample of primate species. Some of these hypotheses are derived from existing knowledge of primate pelvic functional morphology (see Chapter 2), while novel hypotheses of pelvic adaptation to locomotion are introduced that are founded on the experimental biomechanical modeling component of this dissertation described in Chapter 3. In addition, an exploration of multivariate pelvic shape using geometric morphometrics is used to visualize and enhance understanding of overall pelvic anatomy.

ADAPTIVE HYPOTHESES

The goal of the comparative morphometric component of this project is to determine how pelvic shape is related to locomotor behavior. As stated in Chapter 2, the general hypothesis is that differences in pelvic morphology reflect loading regimes associated with differing locomotor behaviors. First, the general hypotheses are described, followed by a rationale for the specific predictions for each hypothesis.

Linear dimensions of the pelvis

Linear measures of pelvic morphology, such as length and width of the ilium, should vary with locomotion. As explained in Chapter 2, the relationship between linear dimensions of the pelvis and stress resistance is uncertain. However, it is clear that bony levers act as sites of muscle attachment and thus are directly related to muscle moment arms. The lengths of these levers, then, should vary according to the mechanical requirements of each locomotor mode. Lever lengths should increase to facilitate behaviors that must generate or sustain large forces.

Traits related to pelvic stress resistance

Among locomotor categories, pelvic struts that are exposed to large loads during locomotion should have relatively larger cross-sectional areas than those that are not. This expectation is related to the necessity of bones to resist stresses incurred during locomotion; large forces require a larger area to provide resistance to stress, among other things (including the optimal arrangement of internal trabecular architecture). Studies of long bone cross-sectional geometry have shown that bone strength is related to typical load[2] (*i.e.*, bone shaft diameter and/or cortical thickness increases in relation to applied load) (e.g., Schaffler et al., 1985; Demes and Jungers, 1993; Carlson, 2005; Shaw and Stock, 2009). While *in vivo* data on directions and magnitudes of forces on the pelvis during primate locomotion do not exist, information on *in vitro* pelvic stress resistance

[2] However, some work has shown that largest loads do not always occur in the plane in which bending strength is largest (Demes et al., 2001; Lieberman et al., 2004).

(Chapter 3) may provide sufficient information to investigate this specific phenomenon in pelvic struts.

The acetabular, pubic symphysis, and sacroiliac joints should be larger in taxa that experience large hindlimb loads, and should differ accordingly among locomotor categories. These expectations are based on the same biomechanical principles as those of the strut cross-sectional areas.

Allometric scaling of pelvic traits

Common to all of these hypotheses of univariate measures is the expectation that patterns of scaling in pelvic dimensions among primates should reflect those in other hindlimb measures. Pelvic traits that are functionally related to stress resistance (especially pelvic strut cross-sections and joint surfaces) are expected to scale with slight positive allometry, as is found in parameters relating to hindlimb long bone strength (e.g., Demes and Jungers, 1993; Jungers and Burr, 1994; Ruff, 2000).

Overall pelvic shape

Overall three-dimensional pelvic shape should vary in a consistent way among locomotor categories. This broad hypothesis assumes that variation in pelvic shape due to locomotion will reflect pelvic morphotypes for each locomotor category. While phylogenetic and developmental constraints make identification of clearly defined morphotypes unlikely, the mechanical requirements of locomotion do vary among locomotor categories, and general pelvic shape should also vary. This hypothesis will be rejected if differentiation among locomotor categories is not detected. It is likely that some locomotor

categories will result in pelvic shape differentiation and that others will overlap. If this is the case, tests of the following hypotheses will be able to demonstrate differences, if they exist, among taxa in the shape of specific components of pelvic morphology.

Specific predictions for locomotor categories

Specific predictions for each of the preceding hypotheses are listed and justified in Table 4-1. The general approach taken here is to characterize the biomechanical profile of each of the major locomotor groups and generate predictions of pelvic shape for them based on known kinematics and kinetics. Specific predictions are laid out for arboreal quadrupeds, terrestrial quadrupeds, and vertical clinger and leapers. Suspensory and bipedal taxa are excluded from specific hypothesis-testing because of a lack of *a priori* hypotheses regarding how the pelvis responds to loading (for suspensory taxa) or because of a lack of other taxa within the same locomotor category for use of the comparative method (for bipedal humans).

Each prediction is based on biomechanical assumptions of how the bony pelvis should be structured to withstand both substrate reaction and muscle forces associated with a given locomotor behavior. These inferences of skeletal biomechanics are derived from the literature on primate locomotor mechanics detailed in Chapter 2. Briefly, the typical substrate reaction forces encountered by each locomotor group, and the requirements of muscular force generation for each locomotor group, are considered simultaneously with typical postural features of

locomotor (*e.g.*, pronogrady versus orthogrady) to derive predictions of how various aspects of the pelvis should react to biomechanical pressures.

TABLE 4-1. Predictions of univariate pelvic dimensions based on biomechanical requirements of locomotion. [a]

Pelvic measure	Prediction[b]	Basis
Ilium length	TQ < AQ < VCL	SRF, resistance to bending
Upper iliac height	AQ = TQ = VCL	Muscle attachment
Lower iliac height	TQ < AQ < VCL	SRF, resistance to bending
AIIS to hip joint	AQ = TQ < VCL	Leverage of *m. rectus femoris*
Ilium width	AQ = VCL < TQ	Muscle attachment
Lower ilium cross-sectional area	AQ < TQ < VCL	SRF, resistance to bending
Auricular surface area	AQ < TQ < VCL	SRF
Ischium length	AQ = TQ < VCL	Leverage of hip extensors
Ischium dorsal projection	AQ = TQ < VCL	Leverage of hip extensors
Ischium cross-sectional area	AQ < TQ < VCL	Resistance to bending
Acetabulum diameter	AQ < TQ < VCL	SRF, required range of motion
Superior pubic ramus length	TQ < VCL < AQ	Use of hip adductor musculature
Superior pubic ramus cross-sectional area	AQ < TQ < VCL	SRF, resistance to bending, strain results
Inferior pubic ramus length	TQ < VCL < AQ	Use of hip adductor musculature
Inferior pubic ramus cross-sectional area	AQ < TQ < VCL	SRF, resistance to bending, strain results
Pubic symphysis length	AQ < TQ < VCL	SRF, resistance to tension
Pubic symphysis area	AQ < TQ < VCL	SRF, resistance to tension, strain results

[a] Predictions for each locomotor mode are based on known differences in substrate reaction forces (SRF) during experimental studies of locomotion. Because experimental data do not exist for suspensory taxa, *a priori* predictions of pelvic shape in suspensory taxa are not tenable.

[b] Average peak vertical forces encountered during locomotion: AQ, 0.5-0.8 times body weight (Schmitt and Hanna, 2004); TQ, 0.6-1.0 times body weight (Kimura, 1985; Schmitt and Hanna, 2004, Hanna et al., 2006); VCL, 6.0-14.0 times body weight (Demes et al., 1999).

MORPHOMETRIC SAMPLE

The comparative morphometric sample consists of complete pelves of 885 adult individuals from 67 primate species (42 genera) derived from several osteological collections held at the: American Museum of Natural History (NY), National Museum of Natural History (WA, DC), Field Museum (Chicago, IL), Museum of Comparative Zoology (Cambridge, MA), Cleveland Museum of Natural History, Natural History Museum (London, UK), Muséum national d'Histoire naturelle (Paris, France), Beza Mahafaly Osteological Collection (Madagascar) (the full list of taxa is in Appendix A, while Table 4-2, below, provides a summary). Chosen taxa represent a broad cross-section of primate genera for which corresponding data on locomotor behavior are available, and have been selected to facilitate comparisons between closely related species that differ in locomotor behavior to control for phylogeny.

Adult age was determined based on fusion of pelvic epiphyseal caps. While many studies of postcranial morphology use epiphyseal fusion of long bones to estimate age, this method was not appropriate here because pelvic epiphyses ossify later in ontogeny than limb bone epiphyses (Scheuer and Black, 2000; Baker et al., 2005). Because some of the landmarks investigated here were located on epiphyseal caps (*e.g.*, on the ischial tuberosity), it was necessary that all specimens exhibited fusion of pertinent epiphyses. This stringent requirement had a major effect of decreasing available sample size because museum specimens that were deemed "adult" by limb bone epiphyseal fusion and third molar development were still juvenile in their pelvic development.

While pelvic ossification patterns have not generally been studied in non-human primates (but see Barham, 1970; Coleman, 1970), it is known that the epiphyses of the pelvis are variable in humans (Scheuer and Black, 2000). Of the pelvic epiphyses—the anterior inferior iliac spine (AIIS), iliac crest, ischial tuberosity, and ischial spine—the AIIS and ischial spine are not always present as separate centers of ossification (Scheuer and Black, 2000). Thus, age determination was based on epiphyseal fusion of the iliac crest and ischial tuberosity; specimens with unfused ischial tuberosity caps were not used. However, specimens with unfused iliac crests were used on a case by case basis—if the anterior and posterior superior iliac spines were fully formed, the specimen was used.

Ideal sample size for those taxa included in pairwise comparisons is 20 individuals of each sex per taxon, while ideal sample size for those taxa that are only included as species means in the general analyses is ten individuals of each sex per taxon. Constraints on sample size due to museum collection specimen availability resulted in less than ideal sample sizes for some taxa.

While it is preferable to include only wild-shot specimens in morphometric studies due to possible differences in morphology caused by a captive environment, specimens obtained from zoos and other captive situations are included here to bolster sample sizes (163 zoo specimens, see Appendix A). Nonparametric analyses of variance (Kruskal-Wallis tests) were conducted to test for differences due to rearing (wild vs. captive), and in general, the results indicate that differences between wild-shot and captive specimens are not

statistically detectable at the 0.05 significance level. Only three taxa exhibited differences between captive-reared and wild-caught specimens, and none of these taxa demonstrated differences in more than three pelvic measures. Thus, captive-bred and wild-caught specimens were combined to increase sample sizes. Appendix A lists the numbers of wild and captive specimens used for each taxon.

TABLE 4-2. Comparative morphometric osteological sample.[a]

Species	n	Locomotion
Alouatta caraya	20	AQ/Suspensory
Ateles belzebuth	2	Suspensory
Ateles fusciceps	13	Suspensory
Ateles geoffroyi	3	Suspensory
Ateles paniscus	2	Suspensory
Ateles sp.	1	Suspensory
Cebuella pygmaea	12	AQ/Leaping
Cebus albifrons	15	AQ
Cebus apella	22	AQ
Cebus olivaceus	3	AQ
Cercocebus torquatus	11	AQ/TQ
Cercopithecus ascanius	3	AQ
Cercopithecus mitis	24	AQ
Cercopithecus mona	5	AQ
Cercopithecus neglectus	4	AQ
Cercopithecus nictitans	5	AQ
Chlorocebus aethiops	20	AQ/TQ
Colobus angolensis	7	AQ/Leaping
Colobus guereza	23	AQ/Leaping
Daubentonia madagascariensis	8	AQ
Erythrocebus patas	6	TQ
Eulemur fulvus	22	AQ
Eulemur mongoz	3	AQ
Galago senegalensis	32	VCL
Gorilla gorilla	21	TQ
Hapalemur griseus	14	VCL
Hapalemur simus	1	VCL
Hapalemur sp.	1	VCL
Homo sapiens	40	Bipedal
Hylobates agilis	2	Suspensory
Hylobates concolor	3	Suspensory
Hylobates hoolock	13	Suspensory
Hylobates klossi	2	Suspensory
Hylobates lar	24	Suspensory
Indri indri	8	VCL
Lagothrix lagotricha	10	AQ/Suspensory
Lemur catta	24	AQ/TQ
Leontopithecus chrysomelas	3	AQ/Leaping
Leontopithecus rosalia	17	AQ/Leaping
Lepilemur mustelinus	19	VCL
Lepilemur sp.	1	VCL
Lophocebus albigena	3	AQ
Loris tardigradus	3	AQ/Slow climbing
Macaca fascicularis	39	AQ
Macaca mulatta	6	AQ/TQ
Macaca nemestrina	13	TQ
Mandrillus leucophaeus	5	TQ
Mandrillus sphinx	8	TQ
Miopithecus talapoin	16	AQ

TABLE 4-2. Continued.

Nasalis larvatus	20	AQ/Leaping
Nycticebus coucang	16	AQ/Slow climbing
Nycticebus sp.	2	AQ/Slow climbing
Nycticebus pygmaeus	2	AQ/Slow climbing
Otolemur crassicaudatus	29	AQ
Pan troglodytes	41	TQ
Papio hamadryas anubis	20	TQ
Papio hamadryas cynocephalus	10	TQ
Papio hamadryas hamadryas	5	TQ
Papio hamadryas papio	3	TQ
Papio hamadryas sp.	2	TQ
Papio hamadryas ursinus	5	TQ
Perodicticus potto	26	AQ/Slow climbing
Pithecia monachus	3	AQ/Leaping
Pithecia pithecia	6	AQ/Leaping
Pithecia sp.	1	AQ/Leaping
Pongo pygmaeus	20	Suspensory
Procolobus badius	10	AQ/Leaping
Propithecus diadema	4	VCL
Propithecus sp.	1	VCL
Propithecus verreauxi	34	VCL
Saimiri boliviensis	16	AQ
Saimiri sciureus	2	AQ
Saimiri sp.	2	AQ
Semnopithecus entellus	5	AQ/TQ
Symphalangus syndactylus	10	Suspensory
Tarsius bancanus	4	VCL
Tarsius syrichta	4	VCL
Theropithecus gelada	6	TQ
Varecia variegata	14	AQ
Total sample size	885	

[a]Total numbers of individuals for each species. Locomotor categories are derived from Rowe's (1996) compilation.

MORPHOMETRIC DATA COLLECTION

Landmarks

Unlike the cranium, for example, there is a paucity of recognized landmarks on the pelvis. As this study is the first to use three-dimensional landmark-based data collection on the pelvis, some of the landmarks used here are novel. While type I landmarks—based on locations where separate structures meet (for example, the intersection of cranial vault sutures, Bookstein, 1991)—are preferable to use in geometric morphometrics, there are few such structures in the

pelvis. Instead, type II landmarks, which are defined by maxima and minima (Bookstein, 1991), are more common in the pelvis (*e.g.*, the most dorsal point on the ischial tuberosity). Type III landmarks, those whose identification depends on the location of another landmark (Bookstein, 1991), are least desirable because of difficulties in establishing homology, but some of the landmarks used here are type III out of necessity.

Because the aim of this study is to understand the functional relationship between pelvic morphology and locomotion, landmarks were chosen to facilitate univariate measures of biomechanical relevance (*e.g.*, ischium length). In addition, it is necessary that landmarks are homologous across taxa, and this was accomplished through verification of similarity in muscle and ligament attachment sites. Because the other aim of this study is to examine the three-dimensional morphology of the pelvis, chosen landmarks cover all major regions of the pelvis in order to capture an accurate representation of overall pelvic shape. In all, 27 landmarks were collected on the os coxa and sacrum. Definitions of landmarks are in Table 4-3, and Figure 4-1 illustrates them.

TABLE 4-3. Three-dimensional pelvic landmarks.

No.	Landmark	Definition	Type[a]
1	Lateral extent of iliac crest	The lateral-most extent of the iliac crest. In most cases this is the same as ASIS	II
2	Anterior Superior Iliac Spine (ASIS)	The anterior-most point on the lateral extent of the iliac crest (ASIS); site of attachment for *m. sartorius*	II
3	Anterior Inferior Iliac Spine (AIIS)	The anterior-most point on the AIIS. If only a bony roughening, the point in the center of the AIIS rugosity; site of attachment for *m. rectus femoris*	II
4	Lateral ilium	The lateral-most point on the lateral aspect of the iliac margin, above the AIIS, where the cross-section of the lower ilium is smallest	III
5	Posterior superior iliac spine	The superomedial-most point on the posterior iliac crest	II
6	Inferior extent of auricular surface	The inferior-most extent of the auricular surface, on the dorsal aspect of the pelvis	II
7	Dorsal ilium	The dorsal-most point on the dorsal aspect of the lower ilium, where the cross-section of the lower ilium is smallest. Taken directly across from Landmark 4	III
8	Ischial spine	The dorsal-most projection of the spine located on the posterior ischium, medial to the acetabulum	II
9	Ischial tuberosity	The dorsal-most point on the ischial tuberosity	II
10	Acetabulum 1	The point on the superior rim of the acetabulum that marks the intersection of the iliac margin and acetabulum, which is defined as the extension of the line connecting ASIS and AIIS	III
11	Acetabulum 2	The point on the inferior rim of the acetabulum directly across from Landmark 10, along the long axis of the ischium	III
12	Acetabulum 3	The medial-most point on the cranial horn of the lunate surface	II
13	Acetabulum 4	The medial-most point on the caudal horn of the lunate surface	II
14	Acetabulum 5	The center of the acetabulum; defined as the midpoint of the line between Landmarks 10 and 11	III
15	Acetabulum 6	The point on the inner rim of the cranial lunate surface that is across from Landmark 10 and in line with Landmarks 10 and 14	III
16	Acetabulum 7	The point on the internal rim of the dorsal lunate surface that is in line with Landmark 14 and perpendicular to the line between Landmarks 10 and 11	III
17	Acetabulum 8	The point on the outer rim of the dorsal lunate surface that is across from Landmark 16 and is in line with Landmarks 16 and 14	III
18	Acetabulum 9	The point on the inner rim of the caudal lunate surface that is in line with Landmarks 10 and 11	III
19	Acetabulum 10	The point on the outer rim of the caudal lunate surface at its maximum width; taken across from Landmark 18	III
20	Ischium	The distal-most point on the ischium that forms a line with the center of the acetabulum (Landmark 14) that is parallel to the long axis of the ischium	III
21	Superior pubic symphysis	The superior-most point on the pubic symphysis, taken on the most medial point of the pubis	II
22	Inferior pubic symphysis	The inferior-most point on the pubic symphysis, taken on the most medial point of the pubis	II
23	Superior promontory - ventral	The ventral-most point on the midline of the sacral promontory	II
24	Inferior tip of sacrum	The caudal-most point on the midline of the last sacral vertebra	II
25	Lateral sacrum[b]	The point that marks the intersection of the arcuate line of the ilium and the sacrum	I
26	Transverse diameter of pelvis[b]	The point on the arcuate line that constitutes the maximum distance between the arcuate line of the opposing os coxa	II
27	Medial ilium	The medial-most point on the medial aspect of the lower ilium, where the cross-section of the ilium is the smallest. Taken directly across from Landmarks 7 and 4	III

[a]As in Bookstein, 1991.

[b]From Tague, 2005.

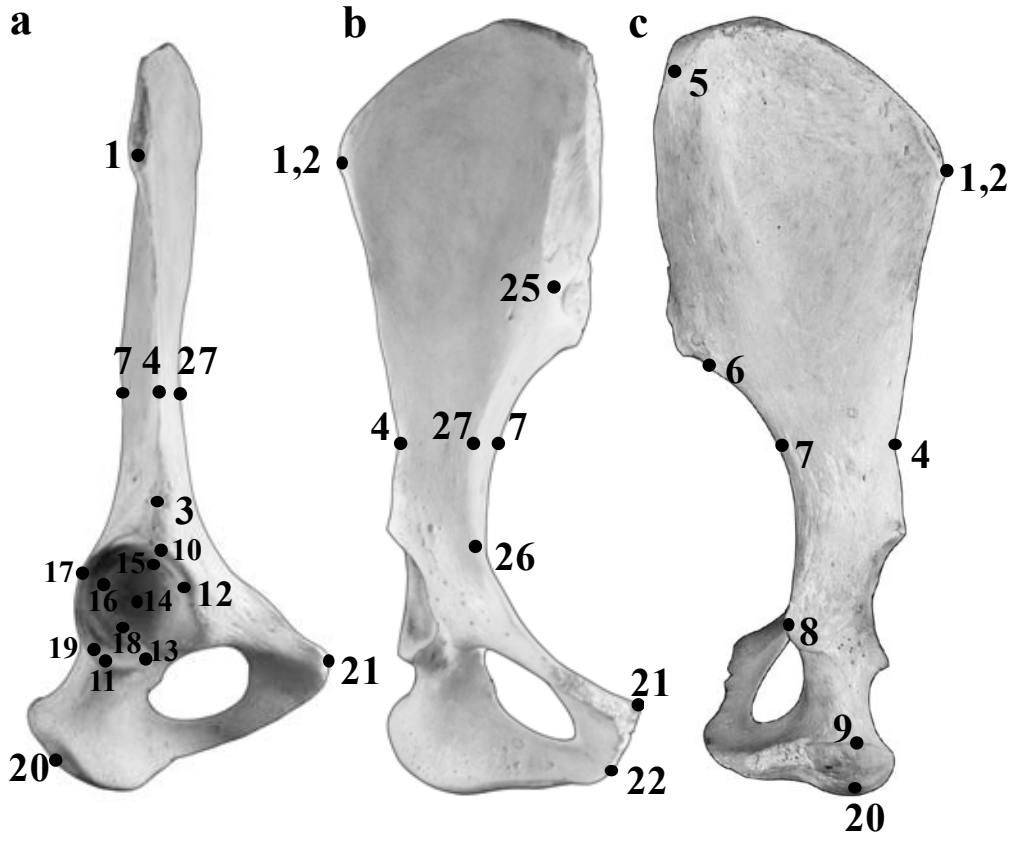

Fig. 4-1. Lateral (**a**), anterior (**b**), and posterior (**c**) views of a pelvis depicting the three-dimensional landmarks used in this study. Some landmarks are shown in multiple views. Landmarks 23 and 24 (superior promontory and inferior tip of sacrum) are not shown here. See Table 4-3 for landmark definitions.

Data acquisition

This study aims to quantify the three-dimensional shape of the pelvis using landmark data, and consequently, it requires that the pelvis be articulated for data collection. Some pelves were articulated at the pubic symphysis and/or sacroiliac joint—either by osteological fusion or by remnants of ligamentous tissue—but for those specimens that were disarticulated, Sculpey was placed on adjoining articular surfaces of the os coxa and sacrum and they were articulated using rubber bands (as in Hager, 1989; Tague, 2005). As landmarks were only

collected on one os coxa, it was only necessary to articulate one os coxa with the sacrum. Both os coxae were articulated with the sacrum only when lack of doing so created instability and mobility between the os coxa and sacrum, or when the proper orientation of the sacrum on the os coxa was uncertain.

The articulated pelvic bones were mounted on a custom-built adjustable, raised square platform so that landmarks could be collected on both the ventral and dorsal sides without re-positioning. The base of the platform is constructed of differing lengths of polyvinyl chloride pipe (PVC)—to achieve differently sized bases—and two-way 90° connectors. Four vertical PVC supports, one in each corner of the base, serve to create the elevated platform. Slats cut into the four vertical supports accommodated two pieces of reinforcing bar, upon which two wooden dowels were placed in an orthogonal direction. Thus, each pelvis rested on a smooth wooden surface. Contact between the bone and the wooden dowels was reinforced with Sculpey and/or Scotch adhesive putty (neither of which adhere to nor leave a residue on bone) to eliminate movement.

Landmarks were collected using a Microscribe G2X digitizer (Immersion Corp.). Twelve linear measures were also collected using calipers and, when the femur was available, two caliper measures of femoral head diameter were also collected. Landmarks were evaluated on their own using geometric morphometrics, and were also used to calculate a series of univariate measures of pelvic morphology that are comparable to previous studies (e.g., Steudel, 1981a; Ward, 1991; Fleagle and Anapol, 1992; Tague, 2005). Table 4-4 lists all linear and area measures that were calculated from the landmarks and caliper measures.

Interlandmark distances, strut cross-sectional areas, and joint surface areas were calculated using formulae in an Excel spreadsheet (see below for equations).

TABLE 4-4. Univariate measures of the pelvis.

Pelvic measure	Method	Definition
Ilium length	Landmark	Distance between Landmarks 2 and 10
Upper iliac height	Landmark	Distance between Landmarks 5 and 6
Lower iliac height	Landmark	Distance between Landmarks 6 and 14
AIIS to hip joint	Landmark	Distance between Landmarks 3 and 14
Ilium width	Landmark	Distance between Landmarks 2 and 5
Lower ilium cross-sectional area	Landmark	Area of the triangle formed by Landmarks 4, 7, and 27
Auricular surface height[a]	Caliper	Maximum superoinferior height of the auricular surface
Auricular surface width[a]	Caliper	Maximum mediolateral width of the auricular surface, measured perpendicular to auricular surface height
Auricular surface area	Caliper	Estimated by multiplying auricular surface height by its width
Ischium length	Landmark	Distance between Landmarks 14 and 20
Ischium dorsal projection	Landmark	Distance from ischial tuberosity (Landmark 9) to a plane defined by the center of the acetabulum (Landmark 14), the lateral side of the sacrum (Landmark 25), and the ASIS (Landmark 2)
Ischium width[a]	Caliper	The mediolateral dimension of the ischium measured at the midpoint of ischial length (from Landmarks 14-20)
Ischium depth[a]	Caliper	The anteroposterior dimension of the ischium measured at the midpoint of ischial length (from Landmarks 14-20)
Ischium cross-sectional area	Caliper	Estimated by multiplying ischium width by ischium depth
Pelvis length	Landmark	Ilium length + ischium length
Acetabulum diameter	Landmark	Distance between Landmarks 10 and 11
Superior pubic ramus length	Landmark	Distance between Landmarks 14 and 21
Superior pubic ramus height[a]	Caliper	Superoinferior height of the superior pubic ramus, taken at the midpoint of the line between the center of the acetabulum (Landmark 14) and the superior aspect of the pubic symphysis (Landmark 21)

TABLE 4-4, Continued.

Pelvic measure	Method	Definition
Superior pubic ramus width[a]	Caliper	Anteroposterior width of the superior pubic ramus, taken at the midpoint of the line between the center of the acetabulum (Landmark 14) and the superior aspect of the pubic symphysis (Landmark 21)
Superior pubic ramus cross-sectional area	Caliper	Estimated by multiplying superior pubic ramus height by its width
Inferior pubic ramus length	Landmark	Distance between Landmarks 20 and 22
Inferior pubic ramus height[a]	Caliper	Superoinferior height of the inferior pubic ramus, taken at the midpoint of the line between the distal aspect of the ischium (Landmark 20) and the inferior aspect of the pubic symphysis (Landmark 22)
Inferior pubic ramus width[a]	Caliper	Anteroposterior width of the inferior pubic ramus, taken at the midpoint of the line between the distal aspect of the ischium (Landmark 20) and the inferior aspect of the pubic symphysis (Landmark 22)
Inferior pubic ramus cross-sectional area	Caliper	Estimated by multiplying inferior pubic ramus height by its width
Pubic symphysis length	Landmark and caliper	Distance between Landmarks 21 and 22
Pubic symphysis width	Caliper	Anteroposterior width of the face of the pubic symphysis, taken at the midpoint of the length of the symphysis
Pubic symphysis area	Caliper	Estimated by multiplying pubic symphysis length by its width
Obturator foramen height[a]	Caliper	The superoinferior dimension of the obturator foramen measured between the midpoints of the superior and inferior pubic rami
Obturator foramen width[a]	Caliper	The mediolateral dimension of the obturator foramen measured perpendicular to the height of the foramen
Obturator foramen area	Caliper	Estimated by multiplying obturator foramen height by width
Sacrum length[b]	Landmark	Distance between Landmarks 23 and 24
Sacrum width[c]	Landmark	Twice the perpendicular distance from the sagittal plane to Landmark 25
Anteroposterior diameter	Landmark	Distance between Landmarks 23 and 21

TABLE 4-4, Continued.

Pelvic measure	Method	Definition
Bi-iliac breadth	Landmark	Twice the perpendicular distance from the sagittal plane to Landmark 2 (ASIS)
Biacetabular distance	Landmark	Twice the perpendicular distance from the sagittal plane to Landmark 14 (center of the acetabulum)
Maximum transverse diameter	Landmark	Twice the perpendicular distance from the sagittal plane to Landmark 26 on the arcuate line
Femoral head height	Caliper	Superoinferior dimension of the femoral head, measured perpendicular to the long axis of the femoral neck
Femoral head width	Caliper	Anteroposterior dimension of the femoral head, measured perpendicular to the long axis of the femoral neck

[a]Measure was used to calculate an area and was not analyzed singly.

[b]Sacrum length was not analyzed because many specimens had damaged sacra that were missing the caudal-most sacral vertebrae.

[c]The sagittal plane is determined by Landmarks 21, 22, and 23. To measure dimensions that require antimeres (e.g., transverse diameter), pelvic symmetry is assumed and the distance from a point to the sagittal plane was determined and multiplied by two.

Measurement error

Landmark measurement error was determined in two ways. First, the data collection spreadsheet was configured to calculate landmark precision automatically following input of three-dimensional landmarks. The vast majority of specimens were measured twice and an estimate of error was calculated as the difference between the XYZ coordinates of the first and second trials, measured as the Euclidean distance between (x_1, y_1, z_1) and (x_2 ,y_2, z_2):

$$d = \sqrt{(x_2 - x_1)^2 + (y_2 - y_1)^2 + (z_2 - z_1)^2}$$

In general, errors for each landmark were found to be acceptable if they were ≤ 1.0 mm, although for very large taxa (*e.g.*, *Gorilla*), errors up to 2 mm were common.

Second, measurement error was also estimated in a more traditional manner (McNulty, 2003, 2005) by collecting 10 complete landmark configurations for a single medium-sized *Alouatta* sp. pelvis. Mean values were calculated for each landmark (the mean of the 10 replicates) and the deviations from individual landmark replicates to the mean landmark were recorded (in the form of Euclidean distance). The mean deviation of the 10 replicate landmark deviations was then calculated and scaled by the Euclidean distance from the landmark mean to the centroid and multiplied by 100 to derive a percent error (Table 4-5).

TABLE 4-5. Measurement error represented by minimum, maximum, and mean landmark deviations derived from data collection of ten replicate landmark configurations on one Alouatta *pelvis.*

Landmark	Minimum (mm)	Maximum (mm)	Mean (mm)	Consensus to centroid (mm)	Percent error (%)
Lateral extent of iliac crest	0.13	0.43	0.27	62.68	0.43
Anterior Superior Iliac Spine	0.10	0.47	0.24	62.55	0.38
Anterior Inferior Iliac Spine	0.12	0.53	0.28	16.80	1.67
Lateral ilium	0.09	0.66	0.32	20.72	1.54
Posterior superior iliac spine	0.15	0.54	0.29	69.11	0.41
Inferior extent of auricular surface	0.08	0.21	0.14	23.56	0.58
Dorsal ilium	0.12	0.34	0.20	17.04	1.16
Ischial spine	0.06	0.37	0.20	29.88	0.65
Ischial tuberosity	0.06	0.33	0.21	40.45	0.51
Acetabulum 1	0.07	0.33	0.17	11.64	1.42
Acetabulum 2	0.05	0.44	0.25	25.92	0.95
Acetabulum 3	0.06	0.41	0.22	18.81	1.19
Acetabulum 4	0.13	0.44	0.27	24.50	1.12
Acetabulum 5	0.07	0.25	0.18	17.54	1.04
Acetabulum 6	0.07	0.34	0.19	11.53	1.61
Acetabulum 7	0.12	0.35	0.23	16.24	1.42
Acetabulum 8	0.09	0.41	0.25	17.26	1.44
Acetabulum 9	0.07	0.37	0.22	21.56	1.01
Acetabulum 10	0.08	0.34	0.22	25.56	0.88
Ischium	0.12	0.49	0.27	46.44	0.58
Superior pubic symphysis	0.16	0.61	0.29	49.77	0.59
Inferior pubic symphysis	0.10	0.36	0.20	56.81	0.34
Superior promontory - ventral	0.04	0.29	0.14	52.26	0.26
Inferior tip of sacrum	0.04	0.20	0.11	27.13	0.42
Sacral width	0.10	0.60	0.27	37.79	0.70
Transverse diameter of pelvis	0.11	0.65	0.28	6.71	4.18
Medial ilium	0.02	0.39	0.21	16.98	1.25
Grand Mean			0.23		1.03

The shaded value for transverse pelvic diameter percent error is large compared to the other landmarks. This is an artifact of the fact that this landmark is near the specimen centroid (which is reflected by the relatively small centroid to mean landmark distance) and thus the value in the denominator of the percent error equation is small.

Missing landmarks

As is often the case in osteological collections, some specimens were damaged or not fully cleaned of soft tissue, so some landmarks were occasionally

inaccessible. Thus, some specimens are missing landmarks and any univariate measures that are based on those missing landmarks. These specimens with missing data are removed from analyses of relevant individual variables. Additionally, because the phenomenon of missing data is problematic for geometric morphometric methods (analyses cannot be performed using individuals that have missing data, and the only way to estimate missing data is by substituting values of the Procrustes mean shape for that taxon [Bastir et al., 2005]), those specimens with any missing landmarks were excluded from geometric morphometrics analyses. Thus, the sample sizes differ markedly between the univariate and geometric morphometric analyses.

Calculation of univariate measures

Interlandmark distances. Distances between landmarks (*e.g.*, superior pubic ramus length) were calculated using the formula for the Euclidean distance between two sets of XYZ coordinates:

$$d = \sqrt{(x_2 - x_1)^2 + (y_2 - y_1)^2 + (z_2 - z_1)^2}$$

where (x_1, y_1, z_1) and (x_2, y_2, z_2) are the three-dimensional points of interest.

Pelvic diameters. Pelvic diameters are estimated by calculating the distance from a point to the sagittal plane and multiplying that distance by two. The sagittal plane was defined by the ventral promontory of the sacrum (Landmark 23), the superior aspect of the pubic symphysis (Landmark 21), and the inferior aspect of the pubic symphysis (Landmark 22). Given the plane:

$$ax + by + cz + d = 0$$

formed by the points (x_1, y_1, z_1), (x_2, y_2, z_2), and (x_3, y_3, z_3),

where $a = y_1(z_2 - z_3) + y_2(z_3 - z_1) + y_3(z_1 - z_2)$,

and $b = z_1(x_2 - x_3) + z_2(x_3 - x_1) + z_3(x_1 - x_2)$,

and $c = x_1(y_2 - y_3) + x_2(y_3 - y_1) + x_3(y_1 - y_2)$,

and

$$d = -1\Big(x_1\big((y_2 \times z_3) - (y_3 \times z_2)\big) + x_2\big((y_3 \times z_1) - (y_1 \times z_3)\big) + x_3\big((y_1 \times z_2) - (y_2 \times z_1)\big)\Big)$$

then the distance from a point (x_4, y_4, z_4) to the plane is given by the equation:

$$\left|\frac{(a \times x_4) + (b \times y_4) + (c \times z_4) + d}{\sqrt{a^2 + b^2 + c^2}}\right|$$

Areal measures. Although computed tomography (CT) is better suited to obtaining cross-sectional data, it is not feasible to collect CT data for a sample of this magnitude. Additionally, digitizing the surface contour of pelvic struts using the auto-plot feature of the Microscribe was found to be unreliable in many specimens. For these reasons,

strut cross-sectional areas and joint surface areas were estimated by multiplying the major and minor dimensions of the surface. For struts, the cross-sectional area was estimated in the following ways: the cross-sectional areas of the pubic rami were estimated as the product of the superoinferior and anteroposterior dimensions; the cross-sectional area of the ischium was estimated as the product of the mediolateral and anteroposterior dimensions; the cross-sectional area of the lower ilium was estimated as the area of the triangle formed by the most medial, lateral, and dorsal points on the narrowest aspect of the bone (Landmarks 4, 7, and 27). Given the points (x_1, y_1, z_1), (x_2, y_2, z_2), and (x_3, y_3, z_3), and the distances

between each set of points—*a*, *b*, and *c*—the area of the triangle formed by them is:

$$\sqrt{s(s-a)(s-b)(s-c)}$$

where *s* is $(a+b+c)/2$.

The area of the auricular surface was estimated as the product of the maximum superoinferior dimension and the maximum mediolateral dimension. The area of the pubic symphysis was estimated as the product of the maximum superoinferior dimension and the dorsoventral dimension taken at the midpoint of the superoinferior dimension.

MORPHOMETRIC DATA ANALYSIS

Geometric morphometric data

The sample used in the geometric morphometric data analysis is listed in Table 4-6.

TABLE 4-6. List of taxa used in geometric morphometric analysis.

Taxon	N	Locomotion
Alouatta caraya	19	AQ/Suspensory
Ateles spp.	20	Suspensory
Cebuella pygmaea	12	AQ/Leaping
Cebus spp.	39	AQ
Cercocebus torquatus	10	AQ/TQ
Cercopithecus spp.	41	AQ
Chlorocebus aethiops	20	AQ/TQ
Colobus guereza	29	AQ/Leaping
Daubentonia madagascariensis	8	AQ
Erythrocebus patas	5	TQ
Eulemur spp.	25	AQ
Galago senegalensis	30	VCL
Gorilla gorilla	20	TQ
Hapalemur spp.	16	VCL
Homo sapiens	35	Bipedal
Hylobates spp.	40	Suspensory
Indri indri	7	VCL
Lagothrix lagotricha	10	AQ/Suspensory
Lemur catta	23	AQ/TQ
Leontopithecus spp.	18	AQ/Leaping
Lepilemur spp.	20	VCL
Lophocebus albigena	3	AQ
Loris tardigradus	2	AQ/Slow climbing
Macaca fascicularis	37	AQ
Macaca mulatta	6	AQ/TQ
Macaca nemestrina	13	TQ
Mandrillus spp.	12	TQ
Miopithecus talapoin	15	AQ
Nasalis larvatus	20	AQ/Leaping
Nycticebus coucang	14	AQ/Slow climbing
Nycticebus pygmaeus	2	AQ/Slow climbing
Otolemur crassicaudatus	26	AQ
Pan troglodytes	37	TQ
Papio hamadryas	43	TQ
Perodicticus potto	24	AQ/Slow climbing
Pithecia spp.	9	AQ/Leaping
Pongo pygmaeus	16	Suspensory
Procolobus badius	8	AQ/Leaping
Propithecus spp.	33	VCL
Saimiri spp.	20	AQ
Semnopithecus spp.	5	AQ/TQ
Symphalangus syndactylus	9	Suspensory
Tarsius spp.	8	VCL
Theropithecus gelada	6	TQ
Varecia variegata	14	AQ
Total specimens	829	

Generalized Procrustes Analysis. Landmark data were rotated, translated, and scaled to remove the effects of non-shape parameters (*e.g.*, size) using Generalized Procrustes Analysis (GPA) in *morphologika2* (Rohlf and Slice, 1990; Goodall, 1991; Dryden and Mardia, 1998; O'Higgins and Jones, 2006). First, the centroid of each landmark dataset (*i.e.*, each specimen) was determined and translated to the origin. Then, the specimens were rotated such that the sum of the squared Procrustes distances among all homologous landmarks was minimized. Lastly, each shape was scaled to the centroid size of the mean shape configuration. Because some landmark datasets were collected variably on left and right os coxae, the GPA enabled reflections of landmark coordinates such that all of the Procrustes-aligned coordinates are of the same side and in the same orientation.

Principal Component Analysis. Procrustes-aligned coordinates were then used in a Principal Component Analysis (PCA) to identify the primary variables that influence differences in pelvic shape and to visualize differences among locomotor groups. Because Procrustes coordinates are in Kendall's shape space, which is non-Euclidean and consequently, nonlinear (Kendall, 1984), the Procrustes-aligned coordinates were projected into the plane tangent to the shape space (*i.e.* Kendall's tangent space), and the PCA was performed on these tangent space coordinates.

Principal component scores (eigenvalues) were examined to investigate the proportion of shape variance described by each. Variation in shape was assessed by bivariate plots of principal component scores on each other for the

entire sample, and for taxon means and landmark subsets. Scaling of principal component scores was examined by plotting each PC score on ln-centroid size for the entire sample and for taxon means.

Geometric morphometric analysis was performed on several subsets of the data: all landmarks, ilium landmarks only, and ischiopubic landmarks only (Tables 4-7 and 4-8). Because the pelvic shape of *Homo sapiens* is unique, the inclusion of humans in these samples resulted in a swamping effect wherein variation between humans and other primates was so great that variation within nonhuman primates was decreased. Therefore, humans were removed from the general primate dataset and were instead examined within a subset of data that included only extant hominoid taxa.

TABLE 4-7. Ilium and acetabulum subset of landmarks.

No.	Landmark
1	Lateral extent of iliac crest
2	Anterior Superior Iliac Spine
3	Anterior Inferior Iliac Spine
4	Lateral ilium
5	Posterior superior iliac spine
6	Inferior extent of auricular surface
7	Dorsal ilium
10	Acetabulum 1
11	Acetabulum 2
12	Acetabulum 3
13	Acetabulum 4
14	Acetabulum 5
15	Acetabulum 6
16	Acetabulum 7
17	Acetabulum 8
18	Acetabulum 9
19	Acetabulum 10
26	Lateral sacrum
27	Transverse diameter of pelvis
28	Medial ilium

TABLE 4-8. Ischiopubic and acetabulum subset of landmarks.

No.	Landmark
8	Ischial spine
9	Ischial tuberosity
10	Acetabulum 1
11	Acetabulum 2
12	Acetabulum 3
13	Acetabulum 4
14	Acetabulum 5
15	Acetabulum 6
16	Acetabulum 7
17	Acetabulum 8
18	Acetabulum 9
19	Acetabulum 10
20	Ischium
21	Superior pubic symphysis
22	Inferior pubic symphysis

Phylogenetic analysis. Because species are descended from a common ancestor, they are, as observations in a statistical analysis, non-independent. However, independence of observations is an assumption of common statistical methods, and therefore, an adjustment to the data must be considered to take phylogenetic relatedness into account (Felsenstein, 1985; Harvey and Pagel, 1991).

To investigate the effect of phylogeny on the geometric morphometric data, a primate consensus phylogeny for the taxa studied here was obtained from the *10kTrees* website (Arnold et al., 2010). The topology and branch lengths of trees available for download are determined using Bayesian Markov chain Monte Carlo methods. A patristic distance matrix, describing the distances among phylogenetic nodes, was then derived from this tree using Mesquite (Maddison and Maddison, 2009). To determine whether overall 3D pelvic shape is correlated with phylogeny, the patristic distance matrix (Appendix B) was compared to a matrix of Procrustes distances among each pair of taxa (Appendix B). The matrix correlation was calculated and a randomization test (performed at 1000 iterations)

was used to determine the significance of the correlation statistic using a Mantel test conducted in the PopTools add-in for Microsoft Excel 2007. The matrix correlation was statistically significant ($r = 0.462$, $p = 0.001$), indicating that pelvic shape is correlated with phylogeny. This correlation between morphology and phylogeny can be addressed by using a comparative method, such as pairwise comparisons between closely related taxa that differ in behavior (see below).

Univariate data

The univariate data were collected on the taxa listed in Table 4-9. Raw univariate data were examined for violations of the assumptions of parametric statistics; normal probability plots indicated a violation of the assumption of normality, and this was corrected using a ln-transformation. Data were examined for outliers, which were determined as those individuals with deleted studentized residuals greater than 3 (or less than -3), and when found, were removed from analyses. Error variances were examined for patterns that might signal inconstancy, and were found to be homoscedastic. However, due to unequal sample sizes per taxon, and especially between males and females within a taxon, nonparametric tests were used for all statistical analyses.

TABLE 4-9. List of taxa used in univariate analyses.

Taxon	N	Locomotion
Alouatta caraya	20	AQ/Suspensory
Ateles spp.	21	Suspensory
Cebuella pygmaea	12	AQ/Leaping
Cebus spp.	40	AQ
Cercocebus torquatus	11	AQ/TQ
Cercopithecus spp.	41	AQ
Chlorocebus aethiops	20	AQ/TQ
Colobus spp.	30	AQ/Leaping
Daubentonia madagascariensis	8	AQ
Erythrocebus patas	6	TQ
Eulemur fulvus	22	AQ
Eulemur mongoz	3	AQ
Galago senegalensis	31	VCL
Gorilla gorilla	21	TQ
Hapalemur spp.	16	VCL
Homo sapiens	40	Bipedal
Hylobates spp.	44	Suspensory
Indri indri	7	VCL
Lagothrix lagotricha	10	AQ/Suspensory
Lemur catta	23	AQ/TQ
Leontopithecus spp.	19	AQ/Leaping
Lepilemur spp.	20	VCL
Lophocebus albigena	3	AQ
Loris tardigradus	2	AQ/Slow climbing
Macaca fascicularis	39	AQ
Macaca mulatta	6	AQ/TQ
Macaca nemestrina	13	TQ
Mandrillus leucophaeus	5	TQ
Mandrillus sphinx	8	TQ
Miopithecus talapoin	15	AQ
Nasalis larvatus	20	AQ/Leaping
Nycticebus coucang	15	AQ/Slow climbing
Nycticebus pygmaeus	2	AQ/Slow climbing
Otolemur crassicaudatus	29	AQ
Pan troglodytes	41	TQ
Papio hamadryas	45	TQ
Perodicticus potto	24	AQ/Slow climbing
Pithecia spp.	10	AQ/Leaping
Pongo pygmaeus	19	Suspensory
Procolobus badius	10	AQ/Leaping
Propithecus spp.	38	VCL
Saimiri spp.	20	AQ
Semnopithecus entellus	5	AQ/TQ
Symphalangus syndactylus	10	Suspensory
Tarsius spp.	8	VCL
Theropithecus gelada	6	TQ
Varecia variegata	14	AQ
Total specimens	872	

Calculation of shape variables. After the data were examined for violations of assumptions of parametric statistics, morphometric dimensions were corrected to account for differences in body size among taxa. The most common way of achieving a size-correction is to define a Mosimann shape variable (Mosimann, 1970; Darroch and Mosimann, 1985; Jungers et al., 1995), which is the variable of interest divided by a measure of size. While some have argued against the use of ratios as data because of their supposed tendency toward non-normality (Albrecht, 1978; Atchley, 1978; Atchley and Anderson, 1978; Albrecht et al., 1993, 1995), ratios are a favorable form of data because they retain important information about allometry and are readily interpretable (Jungers et al., 1995).

Although body mass is the most intuitive measure of overall body size, these data are not available for the majority of museum specimens. Instead, a proxy for overall body size can be found in the geometric mean of pelvic measures. A geometric mean is the *n*th root of the product of *n* variables. In this case, the geometric mean was chosen to represent overall pelvic size and is the third root of the product of pelvis length, width (bi-iliac breadth), and depth (anteroposterior diameter). To ensure that the shape variables are dimensionless, the square-root of those pelvic traits that were measured in units of mm^2 (*i.e.*, areal measures) was first taken before standardizing the measure by the geometric mean. Thus, shape variables were created by standardizing linear and areal measures by the geometric mean of these three measures of overall pelvis size.

The use of the geometric mean as a size proxy was investigated by regressing the average geometric mean on the average body mass (raised to the

one-third power) for each taxon (body mass data are derived mostly from Smith and Jungers (1997) and Smith and Cheverud (2002) [see Appendix A for a complete list of body mass sources]). This regression yielded an R^2 of 0.97 and a slope of 1.14 with 95% confidence limits of 1.09 to 1.20. This preliminary analysis shows that the geometric mean scales with positive allometry relative to body size. Thus, in large-bodied animals, the geometric mean will be relatively larger than in small-bodied animals. Because the geometric mean is the denominator of the shape variable, large-bodied animals will have relatively smaller values for shape variables than small-bodied taxa.

Effects of phylogeny. In addition to the preliminary examination of phylogenetic signal in the three-dimensional landmark dataset, the effects of phylogeny on pelvic shape were also investigated using the univariate dataset. The term "phylogenetic signal" is used here according to Blomberg et al.'s definition: "a tendency (pattern) for evolutionarily related organisms to resemble each other, with no implication as to the mechanism that might cause such resemblance (process)" (Blomberg et al., 2003, p. 717). The amount of phylogenetic signal exhibited by each shape variable was examined using both Pagel's lambda (Pagel, 1997; Freckleton et al., 2002) and Blomberg's K statistics (Blomberg et al., 2003). Given a phylogeny and accompanying characters for tip taxa, the lambda test transforms the internal branch lengths by multiplying by lambda (which is between 0 and 1). The maximum likelihood estimate of lambda is then calculated and compared to lambda equals 0 (no phylogenetic structure) and lambda equals 1 (total phylogenetic data structuring) using a chi-squared test.

Blomberg's K statistic measures the observed phylogenetic signal and compares it to the expected phylogenetic signal under an evolutionary model of Brownian motion. Phylogenetic independent contrasts are computed and the observed variance of contrasts is compared to a random distribution of contrasts obtained by randomly shuffling the tip taxa. Like lambda, a K value of 1 or greater indicates phylogenetic signal, while a K value of 0 indicates an absence of phylogenetic signal.

Both Pagel's lambda and Blomberg's K indicated strong phylogenetic signal in the univariate dataset (Table 4-10). Locomotor category, as its own variable, was found to be significantly correlated with phylogeny (*i.e.*, all terrestrial quadrupeds are catarrhines, etc Fig. 4-2). Furthermore, linear dimensions of the pelvis were also strongly significantly correlated with phylogeny. Therefore, because locomotion and pelvic shape are patterned phylogenetically within primates, it makes little sense to "control" for phylogeny when analyzing the relationship between locomotion and pelvic morphology—it is not possible to account for phylogeny when the characters of interest map almost perfectly onto it. Instead the data must be interpreted with this phylogenetic signal in mind.

One approach that is used to minimize the overall effect of phylogeny on the functional signal is pairwise comparisons between closely related species that differ in locomotor category (Felsenstein, 1985; Harvey and Pagel, 1991). However, this method was not widely used across the primate order because sample sizes were small for many of the relevant taxa. Thus, for those taxon-pairs

that had large enough samples, separate tests were performed for each taxon-sex pair unless sex-specific means were not statistically different (see Table 4-11 for the list of taxa used in comparisons). These comparisons test the specific predictions of the adaptive hypotheses outlined at the beginning of this chapter (Table 4-1) for each shape variable using Mann-Whitney U tests (the nonparametric equivalent of a *t* test) with locomotion as the categorical variable. Because statistical power is already compromised by using nonparametric tests, the alpha-level for statistical significance was not adjusted for the number of tests performed.

TABLE 4-10. Estimates of λ- and K-statistics for phylogenetic signal in a subset of univariate measures.

Variable	Maximum Likelihood Estimate of λ	*p* for λ = 0	*p* for λ = 1	K-statistic	*p*
Locomotor category	1	<<0.001	~1	0.946	0.001
Body mass	1	<<0.001	~1	0.575	0.001
Superior pubic ramus length/GM[a]	0.983	<<0.001	0.196	1.152	0.001
Inferior pubic ramus length/GM	0.989	<<0.001	1	1.097	0.001
Pubic symphysis length/GM	0.921	<<0.001	0.036	0.875	0.001
Ilium length/GM	0.995	<<0.001	0.686	1.013	0.001
Upper iliac height/GM	1	<<0.001	1	0.357	0.003
Lower iliac height/GM	1	<<0.001	1.000	1.073	0.001
AIIS to hip/GM	0.409	<0.001	<<0.001	0.271	0.003
Ischium length/GM	0.998	<<0.001	0.711	1.006	0.001
Acetabulum diam/GM	0.788	<<0.001	0.198	0.635	0.001
Ilium width/GM	0.922	<<0.001	0.026	0.618	0.001
Lower ilium cross-sectional area/GM	0.674	<0.001	0.004	0.383	0.001
Ischium cross-sectional area/GM	0.738	<<0.001	0.006	0.369	0.001
Superior pubic ramus cross-sectional area/GM	0.411	0.015	<<0.001	0.195	0.064[b]
Inferior pubic ramus cross-sectional area/GM	0.867	<<0.001	<<0.001	0.922	0.001
Pelvis length/GM	0.995	<<0.001	0.486	0.927	0.001

[a]GM = geometric mean

[b]The λ- and K-statistics for superior pubic ramus cross-sectional area are not in agreement; the λ-statistic shows phylogenetic signal while the K-statistic does not. Additionally, the phylogenetic signal of the areal measures is generally lower than that of the linear measures. All other measures show statistically significant correspondence with phylogeny.

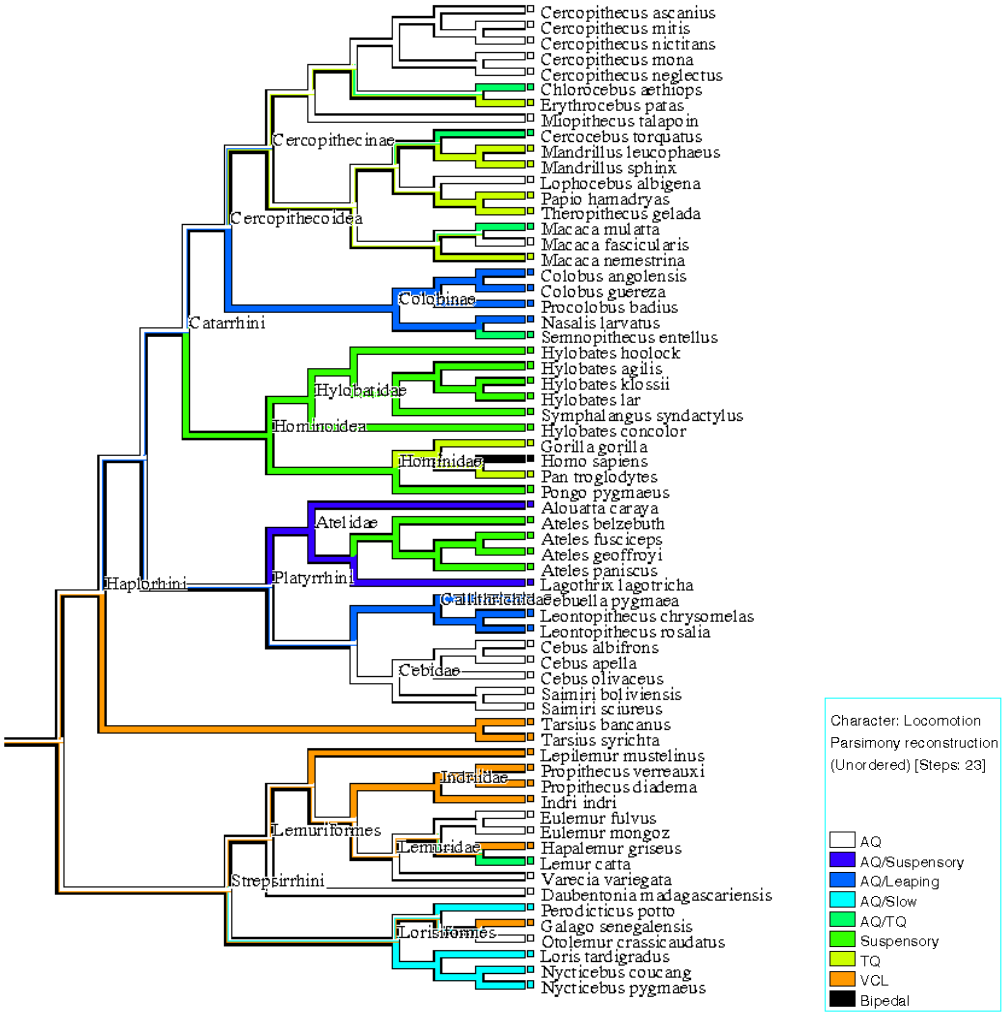

Fig. 4-2. A consensus phylogeny of the taxa used in this study derived from GenBank data (from the 10kTrees website, Arnold et al., 2010). The topology and branch lengths are determined using Bayesian Markov chain Monte Carlo methods. Locomotor behavior as a character has been mapped onto the tree to demonstrate the strong correlation between phylogeny and locomotion.

TABLE 4-11. Taxa used in pairwise comparisons.[a]

Locomotion	Species	Male n	Female n	Unknown n	Combined n
AQ	*Eulemur fulvus*	4	12	6	-
VCL	*Propithecus verreauxi*	9	6	16	-
	Otolemur				
AQ	*crassicaudatus*	23	-	-	-
VCL	*Galago senegalensis*	15	-	-	-
AQ	*Varecia variegata*	-	-	-	14
VCL	*Propithecus verreauxi*	-	-	-	31
AQ	*Macaca fascicularis*	23	12	-	-
TQ	*Papio hamadryas*	23	14	-	-
AQ	*Macaca fascicularis*	23	-	-	-
TQ	*Macaca nemestrina*	9	-	-	-

[a]Males, females, and individuals of unknown sex were tested separately, except in the *Varecia* vs. *Propithecus* comparison. No differences were found among the sex categories, thus they were combined to increase total sample size.

Primate-wide analyses. In addition to the targeted pairwise comparisons, adaptive hypotheses were examined among the entire sample of primates using Kruskal-Wallis tests, the nonparametric equivalent of a one-way analysis of variance (ANOVA). Locomotor category was used as the factor, and separate tests were performed for each pelvic shape variable (defined as a univariate measure divided by the geometric mean). Separate tests were performed for a sample containing combined sexes, a sample of males only, and a sample of females only. There were only very minor differences among the males and females, and in the interest of increasing sample size, the results will be presented here for the combined sex sample only. When differences due to locomotion were found, multiple *post hoc* nonparametric comparisons were performed for each pair of locomotor groups to determine which group medians were significantly different from others.

Regression analysis. To test whether taxa that differ in locomotor behavior also differ predictably in pelvic morphology among the entire primate sample, each univariate measure was natural-logged and regressed on the species- and sex-specific average body mass (raised to the one-third power and natural-logged to simplify the comparison of slopes) using reduced major axis (RMA) regression (see Appendix A for a list of body masses used). Combined-sex taxon means were used as the unit of analysis (as opposed to separate male and female taxon means) because preliminary analyses found that the regression results for separate male and female analyses were nearly identical, and pooling the sexes increased the sample sizes of taxon means. Because the bipedal locomotor group consists of only one taxon, and the AQ/suspensory group comprises only two taxa, these two locomotor groups were excluded from regression analyses; the total number of taxa used in these regressions is 47.

Reduced major axis was chosen over the more traditional ordinary least squares (OLS) regression model because it is a more appropriate method when the aim of the study is to address the allometric relationship between the Y- and X-variables, and specifically when it is necessary to test the similarity of the slopes and elevations of multiple regression fits (Warton et al., 2006; Smith, 2009). In addition to using bivariate line-fitting to examine the relationship among taxa for each pelvic measure, allometric scaling was also investigated using these regressions. For linear measures, the slope of the isometric line is 1.0, while for areal measures the isometric slope is 2.0. Significant departures from isometry were determined by comparison to 95% confidence intervals for each slope.

When comparing slopes of lines among locomotor groups, the equivalence of slopes was tested using a likelihood ratio, and the test statistic was compared to a chi-squared distribution to obtain a *p*-value for the test (Warton et al., 2006).

Statistical software. The test statistics for phylogenetic signal were calculated using R (R Development Core Team, 2010); the "ape" and "geiger" packages were used to calculate Pagel's lambda, and the "picante" package was used to calculate Blomberg's K. Mann-Whitney U tests, Kruskal-Wallis tests, and bivariate plots were performed in both JMP version 8 (SAS Institute, Inc.) and Statistica 7 (StatSoft). Reduced major axis regressions were performed using the free Java program RMA (Bohonak and van der Linde, 2004) and tests concerning the slopes and elevations of regression lines were performed using the "smatr" package in R (R Development Core Team, 2010).

Hypothesis-rejection. As described in the beginning of this chapter, the adaptive hypotheses of pelvic shape and their relationships to locomotion are derived from expectations based on theoretical biomechanics and on previous experimental work on kinetics and kinematics of primate locomotion (see Chapter 2). The specific predictions of these hypotheses are relative; expectations of arboreal quadrupeds are relative to those of terrestrial quadrupeds, which are themselves relative to those of vertical clingers and leapers. Therefore, to accept a functional hypothesis, each relationship of the three-part chain must be upheld. While this may be considered an overly conservative approach, it is based on the logic behind each hypothesis. If only part of an hypothesis is upheld (for example, the relationship between arboreal and terrestrial quadrupeds is as predicted, but one or

both of them do not relate to vertical clingers and leapers as expected), then the theory upon which the prediction is based is incorrect; if the theory were correct, it would be true for all taxa. In this example, the functional hypothesis would be rejected.

UNIVARIATE RESULTS

Here, the results for the hypothesis-testing components of the study—comparisons of arboreal quadrupeds, terrestrial quadrupeds, and vertical clingers and leapers—will first be reported. Then, an exploratory analysis of univariate measures in all locomotor groups will be described. Both sections include the results of Kruskal-Wallis/Mann-Whitney U tests for differences among/between locomotor groups, a description of box plots of locomotor-group and taxon-group medians for each shape variable, and the results of scaling analyses for each univariate pelvic measure. Results of scaling analyses presented use a combined-sex sample because separate analyses of females and males showed negligible sex differences in scaling (see above).

Pairwise comparisons

Pairwise comparisons of univariate pelvic dimensions were performed between AQ and TQ taxa, and AQ and VCL taxa. The specific, directional hypotheses tested are found in Table 4-1.

Macaca fascicularis *(AQ) v.* Macaca nemestrina *(TQ).* Preliminary testing revealed a statistically significant sex-difference in many of the traits of interest for *Macaca fascicularis*. Because the female sample for *M. nemestrina* is too small to allow for a separate pairwise comparison of females, the statistical tests

presented here include only males. However, females have been included in the box plots for visual comparison. Descriptive statistics and results of the Mann-Whitney U test are in Table 4-12.

The hypothesized relationship between the arboreal and terrestrial quadrupedal taxa was upheld for the following pelvic traits: upper iliac height, lower iliac height, ischium length and dorsal projection, lower ilium cross-sectional area, ischium cross-sectional area, and pubic symphysis area (Table 4-12 and Appendix C). Accordingly, the hypothesized association between locomotion and pelvic morphology was rejected for the remaining pelvic traits: ilium length and width, distance from AIIS to hip, acetabulum diameter, lengths of the pubic rami and symphysis, cross-sectional areas of the pubic rami, and area of the auricular surface (Table 4-12 and Appendix C).

Sexual dimorphism was assessed qualitatively using box plots. With regard to traits that are hypothesized to be related to pelvic stress resistance and load transmission, males possess forms that seem to act to decrease biomechanical stress. Males appear to have shorter lower iliac heights, longer pubic symphyses (but the samples are quite small for verification of this pattern), larger lower ilium, ischium, and inferior pubic ramus cross-sectional areas, and larger pubic symphysis areas (Appendix C). All of these traits seem to be related to resisting stress related to increasing reaction forces due to large body size, which suggests that the body size dimorphism within these taxa may have effects on pelvic morphology similar to those resulting from variation in mechanical pressures associated with locomotion. Similarly, males also seem to differ in traits that may

be related to muscle leverage: they have longer and more dorsally-projecting ischia than females, which would act to increase the moment arm of hip extensor musculature (Appendix C).

TABLE 4-12. Descriptive statistics and Mann-Whitney U results of comparison between Macaca fascicularis *and* Macaca nemestrina *males*[a]

	Macaca fascicularis				*Macaca nemestrina*				Mann-Whitney U	
Pelvic shape variable	Mean	St. Dev.	n	Rank Sum	Mean	St. Dev.	n	Rank Sum	U	*p*
Ilium length/GM	0.878	0.043	23	333	0.911	0.032	9	195	57	0.053
Upper iliac height/GM	0.423	0.051	23	341	0.461	0.058	9	187	65	0.112
Lower iliac height/GM	0.544	0.033	23	434	0.512	0.032	9	94	49	0.022
AIIS to hip joint/GM	0.278	0.020	23	321	0.354	0.099	9	207	45	0.013
Ilium width/GM	0.387	0.029	23	343	0.412	0.048	9	185	67	0.133
Lower ilium cross-sectional area/GM	0.088	0.010	23	305	0.103	0.010	9	223	29	0.001
Auricular surface area/GM	0.233	0.039	21	282	0.245	0.019	8	153	51	0.114
Ischium length/GM	0.453	0.027	23	376	0.455	0.016	9	152	100	0.902
Dorsal projection of ischium/GM	0.228	0.041	23	376	0.231	0.019	9	152	100	0.902
Ischium cross-sectional area/GM	0.134	0.011	21	245	0.153	0.010	9	220	14	< 0.0001
Acetabulum diameter/GM	0.217	0.010	23	343	0.224	0.011	9	185	67	0.133
Superior pubic ramus length/GM	0.416	0.028	23	349	0.429	0.027	9	179	73	0.213
Superior pubic ramus cross-sectional area/GM	0.066	0.007	23	393	0.065	0.005	9	135	90	0.592
Inferior pubic ramus length/GM	0.407	0.040	23	343	0.443	0.044	9	185	67	0.133
Inferior pubic ramus cross-sectional area/GM	0.143	0.038	23	377	0.148	0.039	9	151	101	0.934
Pubic symphysis length/GM	0.428	0.045	23	346	0.454	0.049	9	182	70	0.170
Pubic symphysis area/GM	0.110	0.018	18	191	0.138	0.026	7	134	20	0.008

[a]GM = geometric mean

Macaca fascicularis *(AQ)* v. Papio hamadryas *(TQ).* Preliminary testing revealed a statistically significant sex-difference in many of the traits of interest in *Papio hamadryas*. Therefore, the comparisons of arboreal quadrupedal *Macaca fascicularis* and terrestrial quadrupedal *Papio hamadryas* were performed separately for males and females. Results are depicted together on the box plots. Descriptive statistics and results of the Mann-Whitney U tests are in Tables 4-13 for males and 4-14 for females.

The results of Mann-Whitney U tests support the hypothesized relationships between locomotion and morphology in: ilium length and width, lower iliac height and cross-sectional area, ischium length and cross-sectional area, and acetabulum diameter (Appendix C). Hypothesized relationships between locomotion and morphology in upper iliac height, pubic rami and symphysis lengths, pubic rami cross-sectional areas, auricular and pubic symphysis areas, ischium dorsal projection, and the distance of the AIIS to the hip were rejected (Appendix C). The relationships between locomotion and upper iliac height, pubic symphysis length, and inferior pubic ramus cross-sectional area differ by sex. For upper iliac height, there is no effect of locomotion for males ($p = 0.2$), but within females, the TQ baboons have longer upper iliac regions than the AQ macaques ($p = 0.02$, Appendix C). The opposite pattern is found in the length of the pubic symphysis (females $p = 0.32$, males $p = 0.009$, Appendix C). Finally, there is a significant effect of locomotion on the cross-sectional area of the inferior pubic ramus (females, $p = 0.18$, males, $p = 0.001$, Appendix C).

The boxplots comparing these two taxa demonstrate that many pelvic traits appear to be sexually dimorphic in both species. For traits that are hypothesized to relate to pelvic stress resistance—acetabulum diameter, pubic symphysis length, cross-sectional areas of the lower ilium and inferior pubic ramus—males are larger than females (Appendix C). In addition, males have longer ischia than females, a trait hypothesized to be related to muscle leverage (Appendix C).

TABLE 4-13. Descriptive statistics and Mann-Whitney U results of comparison between Macaca fascicularis *and* Papio hamadryas *males*[a]

	Macaca fascicularis				*Papio hamadryas*				Mann-Whitney U	
Pelvic shape variable	Mean	St. Dev.	n	Rank Sum	Mean	St. Dev.	n	Rank Sum	U	*p*
Ilium length/GM	0.878	0.043	23	750	0.800	0.054	23	331	55	< 0.0001
Upper iliac height/GM	0.423	0.051	23	482	0.439	0.046	23	599	206	0.205
Lower iliac height/GM	0.544	0.033	23	656	0.513	0.033	23	425	149	0.011
AIIS to hip joint/GM	0.278	0.020	23	347	0.346	0.054	23	734	71	< 0.0001
Ilium width/GM	0.387	0.029	23	277	0.516	0.044	23	804	1	< 0.0001
Lower ilium cross-sectional area/GM	0.088	0.010	23	326	0.107	0.010	23	755	50	< 0.0001
Auricular surface area/GM	0.233	0.039	21	427	0.227	0.015	20	434	196	0.728
Ischium length/GM	0.453	0.027	23	570	0.450	0.025	23	511	235	0.528
Dorsal projection of ischium/GM	0.228	0.041	23	326	0.296	0.033	23	755	50	< 0.0001
Ischium cross-sectional area/GM	0.134	0.011	21	250	0.161	0.013	23	740	19	< 0.0001
Acetabulum diameter/GM	0.217	0.010	23	372	0.233	0.016	23	709	96	0.0001
Superior pubic ramus length/GM	0.416	0.028	23	497	0.424	0.024	23	584	221	0.348
Superior pubic ramus cross-sectional area/GM	0.066	0.007	23	466	0.070	0.010	23	615	190	0.104
Inferior pubic ramus length/GM	0.407	0.040	23	563	0.404	0.043	22	472	219	0.451
Inferior pubic ramus cross-sectional area/GM	0.143	0.038	23	397	0.173	0.027	23	684	121	0.001
Pubic symphysis length/GM	0.428	0.045	23	415	0.464	0.054	22	620	139	0.009
Pubic symphysis area/GM	0.110	0.018	18	328	0.108	0.015	17	302	149	0.909

[a]GM = geometric mean

TABLE 4-14. Descriptive statistics and Mann-Whitney U results of comparison between Macaca fascicularis *and* Papio hamadryas *females*[a]

	Macaca fascicularis				*Papio hamadryas*				Mann-Whitney U	
Pelvic shape variable	Mean	St. Dev.	n	Rank Sum	Mean	St. Dev.	n	Rank Sum	U	*p*
Ilium length/GM	0.862	0.048	12	217	0.794	0.056	14	134	29	0.004
Upper iliac height/GM	0.358	0.035	12	115	0.401	0.041	14	236	37	0.015
Lower iliac height/GM	0.570	0.028	12	218	0.531	0.036	14	133	28	0.003
AIIS to hip joint/GM	0.251	0.026	12	89	0.320	0.043	14	262	11	< 0.0001
Ilium width/GM	0.362	0.035	12	81	0.461	0.038	14	270	3	< 0.0001
Lower ilium cross-sectional area/GM	0.079	0.007	12	97	0.096	0.013	14	254	19	0.0004
Auricular surface area/GM	0.226	0.073	11	133	0.210	0.018	12	143	65	0.976
Ischium length/GM	0.411	0.018	12	148	0.420	0.026	14	203	70	0.494
Dorsal projection of ischium/GM	0.203	0.025	12	80	0.285	0.037	14	271	2	< 0.0001
Ischium cross-sectional area/GM	0.134	0.035	11	89	0.147	0.013	14	236	23	0.002
Acetabulum diameter/GM	0.201	0.012	12	101	0.220	0.010	14	250	23	0.001
Superior pubic ramus length/GM	0.472	0.040	12	227	0.419	0.021	14	124	19	0.0004
Superior pubic ramus cross-sectional area/GM	0.064	0.013	12	134	0.069	0.008	14	217	56	0.160
Inferior pubic ramus length/GM	0.433	0.111	12	160	0.438	0.069	14	191	82	0.940
Inferior pubic ramus cross-sectional area/GM	0.099	0.069	12	135	0.107	0.041	14	216	57	0.176
Pubic symphysis length/GM	0.320	0.089	12	142	0.360	0.098	14	209	64	0.322
Pubic symphysis area/GM	0.093	0.042	10	89	0.105	0.013	12	164	34	0.093

[a]GM = geometric mean

Otolemur crassicaudatus *(AQ)* *v.* Galago senegalensis *(VCL).* Because of small sample sizes for females, the statistical tests presented here include only males. However, females have been included in the box plots for visual comparison. Sample sizes were dramatically reduced for the areas of the auricular surface and the pubic symphysis because many specimens had fused sacroiliac and pubic symphysis joints. Descriptive statistics and results of the Mann-Whitney U tests are in Table 4-15.

Results of the Mann-Whitney U tests for each pelvic measure indicate that the hypothesized association between locomotion and morphology is supported for only the upper iliac height and the width of the ilium (Table 4-15). However, these two hypotheses are not particularly informative regarding the relationship between locomotor function and pelvic morphology, as neither trait was predicted to differ between locomotor groups (Appendix C). The hypotheses for all other pelvic traits are rejected (Appendix C). There *were* statistically significant differences between *Otolemur* and *Galago* in some pelvic traits (lower iliac height, lower ilium cross-sectional area, ischium length and dorsal projection, superior pubic ramus cross-sectional area, and pubic symphysis length, Table 4-15), but they were not in the predicted direction. The almost complete lack of support for hypothesized differences between these two taxa that differ dramatically in locomotor behavior is puzzling, but may be due to differences in body size that may confound the comparison; the average combined-sex body mass for *Otolemur crassicaudatus* is 1.2 kg, while that for *Galago senegalensis* is 0.2 kg.

In general, the box plots do not indicate sexual dimorphism in pelvic traits in either of these taxa. The only pelvic measure that exhibited a difference between the sexes was the upper iliac height, in which males had slightly longer upper ilia than females (Appendix C).

TABLE 4-15. Descriptive statistics and Mann-Whitney U results of comparison between Galago senegalensis *and* Otolemur crassicaudatus *males*[a]

	Galago senegalensis				*Otolemur crassicaudatus*				Mann-Whitney U	
Pelvic shape variable	Mean	St. Dev.	n	Rank Sum	Mean	St. Dev.	n	Rank Sum	U	p
Ilium length/GM	1.018	0.059	15	351	0.989	0.039	23	390	114	0.083
Upper iliac height/GM	0.475	0.043	15	332	0.872	2.018	23	409	133	0.248
Lower iliac height/GM	0.741	0.065	15	398	1.121	2.170	23	343	67	0.001
AIIS to hip joint/GM	0.369	0.023	15	282	0.371	0.024	23	459	162	0.768
Ilium width/GM	0.330	0.034	15	284	0.332	0.037	23	457	164	0.813
Lower ilium cross-sectional area/GM	0.067	0.015	15	220	0.077	0.008	23	521	100	0.030
Auricular surface area/GM	0.228	0.028	4	34	0.229	0.018	14	137	24	0.721
Ischium length/GM	0.107	0.045	15	160	0.138	0.046	23	581	40	< 0.0001
Dorsal projection of ischium/GM	0.225	0.041	15	225	0.157	0.073	23	516	105	0.044
Ischium cross-sectional area/GM	0.147	0.017	15	318	0.144	0.007	23	423	147	0.460
Acetabulum diameter/GM	0.325	0.040	15	349	0.308	0.017	23	392	116	0.095
Superior pubic ramus length/GM	0.501	0.051	15	259	0.509	0.024	23	482	139	0.329
Superior pubic ramus cross-sectional area/GM	0.083	0.011	15	205	0.092	0.006	23	536	85	0.008
Inferior pubic ramus length/GM	0.562	0.060	15	270	0.572	0.055	23	471	150	0.516
Inferior pubic ramus cross-sectional area/GM	0.060	0.014	15	283	0.059	0.008	22	420	163	0.963
Pubic symphysis length/GM	0.224	0.036	15	163	0.278	0.036	23	578	43	< 0.0001
Pubic symphysis area/GM	0.142	0.021	3	17	0.143	0.025	6	28	7	0.714

[a]GM = geometric mean

Eulemur fulvus *(AQ)* v. Propithecus verreauxi *(VCL).* Preliminary testing revealed some sex differences in a few pelvic traits for both *Eulemur* and *Propithecus*. A large number of samples for these species were of unknown sex; therefore, pairwise comparisons for these taxa were performed separately for males, females, and individuals of unknown sex. Results of all sex subsamples are shown in the box plots. Descriptive statistics and results of the Mann-Whitney U tests are in Tables 4-16 to 4-18.

Results of the Mann-Whitney U tests support the hypothesized relationship between morphology and locomotion in: ilium length, lower iliac height, the distance from the AIIS to the hip, acetabulum diameter, inferior pubic ramus length, and lower ilium cross-sectional area (Appendix C). The hypothesized relationship between morphology and locomotion was rejected for: upper iliac height, ilium width, ischium length and dorsal projection, superior pubic ramus length, pubic symphysis length, the cross-sectional areas of the ischium and pubic rami, the auricular surface area, and the pubic symphysis area (Appendix C).

Ischium dorsal projection, superior pubic ramus length, pubic symphysis length, ischium cross-sectional area, superior pubic ramus cross-sectional area, and auricular surface area showed no significant differences between taxa. Upper iliac height, ilium width, and ischium length *did* differ significantly between taxa, but the difference was not in the predicted direction. Finally, for pubic symphysis length, inferior pubic ramus cross-sectional area, and pubic symphysis area, significant differences between locomotor groups were found only in one sex.

The only pelvic trait that shows signs of sexual dimorphism is the dorsal projection of the ischium, which appears to be more dorsally-projecting in females than in males for both *Eulemur fulvus* and *Propithecus verreauxi* (Appendix C). This pattern is more pronounced in *Eulemur*, in which, except for a single outlying female, there is no overlap between males and females.

TABLE 4-16. Descriptive statistics and Mann-Whitney U results of comparison between Eulemur fulvus *and* Propithecus verreauxi *males*[a]

	Eulemur fulvus				*Propithecus verreauxi*				Mann-Whitney U	
Pelvic shape variable	Mean	St. Dev.	n	Rank Sum	Mean	St. Dev.	n	Rank Sum	U	*p*
Ilium length/GM	0.876	0.049	4	42	0.800	0.035	9	49	4	0.034
Upper iliac height/GM	0.408	0.021	4	12	0.490	0.052	9	79	2	0.011
Lower iliac height/GM	0.578	0.020	4	46	0.478	0.027	9	45	0	0.003
AIIS to hip joint/GM	0.316	0.015	4	10	0.458	0.035	9	81	0	0.003
Ilium width/GM	0.342	0.037	4	10	0.438	0.024	9	81	0	0.003
Lower ilium cross-sectional area/GM	0.079	0.006	4	12	0.108	0.017	9	79	2	0.011
Auricular surface area/GM	0.181	0.020	4	24	0.193	0.007	8	54	14	0.808
Ischium length/GM	0.424	0.017	4	46	0.373	0.014	9	45	0	0.003
Dorsal projection of ischium/GM	0.146	0.011	4	31	0.136	0.032	9	60	15	0.710
Ischium cross-sectional area/GM	0.103	0.005	4	23	0.107	0.009	9	68	13	0.503
Acetabulum diameter/GM	0.232	0.015	4	10	0.271	0.016	9	81	0	0.003
Superior pubic ramus length/GM	0.415	0.014	4	40	0.387	0.030	9	51	6	0.076
Superior pubic ramus cross-sectional area/GM	0.066	0.007	4	29	0.063	0.003	9	62	17	0.940
Inferior pubic ramus length/GM	0.458	0.027	4	46	0.339	0.059	9	45	0	0.003
Inferior pubic ramus cross-sectional area/GM	0.040	0.006	4	12	0.054	0.008	9	79	2	0.011
Pubic symphysis length/GM	0.228	0.030	4	14	0.280	0.050	9	77	4	0.034
Pubic symphysis area/GM	0.104	0.006	3	20	0.096	0.010	6	25	4	0.262

[a]GM = geometric mean

TABLE 4-17. Descriptive statistics and Mann-Whitney U results of comparison between Eulemur fulvus *and* Propithecus verreauxi *females*[a]

	Eulemur fulvus				*Propithecus verreauxi*				Mann-Whitney U	
Pelvic shape variable	Mean	St. Dev.	n	Rank Sum	Mean	St. Dev.	n	Rank Sum	U	*p*
Ilium length/GM	0.854	0.033	12	146	0.771	0.041	6	25	4	0.001
Upper iliac height/GM	0.382	0.029	12	78	0.501	0.040	6	93	0	0.0001
Lower iliac height/GM	0.580	0.031	12	147	0.482	0.045	6	24	3	0.001
AIIS to hip joint/GM	0.323	0.012	12	78	0.458	0.025	6	93	0	0.0001
Ilium width/GM	0.338	0.024	12	78	0.449	0.041	6	93	0	0.0001
Lower ilium cross-sectional area/GM	0.071	0.005	12	78	0.103	0.017	6	93	0	0.0001
Auricular surface area/GM	0.192	0.014	12	114	0.194	0.019	6	57	36	1.000
Ischium length/GM	0.415	0.022	12	147	0.361	0.015	6	24	3	0.001
Dorsal projection of ischium/GM	0.173	0.018	12	128	0.163	0.020	6	43	22	0.213
Ischium cross-sectional area/GM	0.103	0.010	12	111	0.104	0.011	6	60	33	0.820
Acetabulum diameter/GM	0.237	0.013	12	88	0.269	0.026	6	83	10	0.013
Superior pubic ramus length/GM	0.412	0.017	12	113	0.409	0.030	6	58	35	0.964
Superior pubic ramus cross-sectional area/GM	0.069	0.009	12	113	0.069	0.007	6	58	35	0.964
Inferior pubic ramus length/GM	0.434	0.036	12	145	0.328	0.054	6	26	5	0.002
Inferior pubic ramus cross-sectional area/GM	0.042	0.007	12	100	0.048	0.011	6	71	22	0.213
Pubic symphysis length/GM	0.276	0.025	12	96	0.315	0.054	6	75	18	0.102
Pubic symphysis area/GM	0.095	0.006	7	28	0.121	0.009	4	38	0	0.006

[a]GM = geometric mean

TABLE 4-18. Descriptive statistics and Mann-Whitney U results of comparison between Eulemur fulvus *and* Propithecus verreauxi *unknown sex*[a]

	Eulemur fulvus				*Propithecus verreauxi*				Mann-Whitney U	
Pelvic shape variable	Mean	St. Dev.	n	Rank Sum	Mean	St. Dev.	n	Rank Sum	U	*p*
Ilium length/GM	0.878	0.016	6	117	0.777609	0.019	16	136	0	< 0.0001
Upper iliac height/GM	0.429	0.030	6	32	0.489722	0.042	16	221	11	0.005
Lower iliac height/GM	0.538	0.019	6	116	0.465117	0.027	16	137	1	< 0.0001
AIIS to hip joint/GM	0.310	0.011	6	21	0.419739	0.030	16	232	0	< 0.0001
Ilium width/GM	0.329	0.022	6	21	0.450847	0.027	16	232	0	< 0.0001
Lower ilium cross-sectional area/GM	0.070	0.005	6	21	0.107623	0.010	16	232	0	< 0.0001
Auricular surface area/GM	0.188	0.014	6	66	0.186924	0.017	14	144	39	0.841
Ischium length/GM	0.423	0.016	6	116	0.366680	0.018	16	137	1	< 0.0001
Dorsal projection of ischium/GM	0.141	0.038	6	66	0.151256	0.024	16	187	45	0.858
Ischium cross-sectional area/GM	0.107	0.006	6	79	0.105394	0.006	16	174	38	0.494
Acetabulum diameter/GM	0.230	0.010	6	23	0.272097	0.020	16	230	2	0.0001
Superior pubic ramus length/GM	0.409	0.018	6	82	0.403374	0.011	16	171	35	0.367
Superior pubic ramus cross-sectional area/GM	0.068	0.012	6	77	0.063395	0.006	16	176	40	0.590
Inferior pubic ramus length/GM	0.467	0.048	6	116	0.348979	0.055	16	137	1	< 0.0001
Inferior pubic ramus cross-sectional area/GM	0.043	0.005	6	36	0.051833	0.006	16	217	15	0.013
Pubic symphysis length/GM	0.244	0.027	6	48	0.274512	0.045	16	205	27	0.134
Pubic symphysis area/GM	0.092	0.009	6	45	0.101213	0.013	13	145	24	0.210

[a]GM = geometric mean

Varecia variegata *(AQ)* v. Propithecus verreauxi *(VCL).* Sample sizes for these taxa were too small to allow for testing of intraspecific sex differences or for sex-segregated pairwise comparisons. Therefore, all individuals (males, females, and individuals of unknown sex) were pooled for this comparison. However, samples are depicted separately by sex category in the box plots. Descriptive statistics and results of the Mann-Whitney U tests are in Table 4-19.

The results of the Mann-Whitney U tests support the predicted associations between locomotion and pelvic morphology in: the distance from the AIIS to the hip, the lengths of the superior and inferior pubic rami, the length of the pubic symphysis, and the cross-sectional area of the lower ilium (Appendix C). The hypothesized relationships between locomotion and pelvic morphology are rejected in: ilium length and width, lower iliac height, ischium length and dorsal projection, acetabulum diameter, superior pubic ramus length, the cross-sectional areas of the pubic rami and ischium, the auricular surface area, and the pubic symphysis area (Appendix C).

Dorsal projection of the ischium, acetabulum diameter, and inferior pubic ramus cross-sectional area did not differ significantly between taxa (Appendix C), while ilium length and width, upper and lower iliac height, ischium length, cross-sectional area of the ischium, and auricular surface area differed significantly, but in the direction opposite from predicted (Appendix C).

Sexual dimorphism in pelvic traits is only apparent in the dorsal projection of the ischium in *Propithecus verreauxi*, which is greater in females than males, but which does not differ between the sexes in *Varecia variegata* (Appendix C).

TABLE 4-19. Descriptive statistics and Mann-Whitney U results of comparison between Varecia variegata *and* Propithecus verreauxi *combined sexes*[a]

	Varecia variegata				*Propithecus verreauxi*				Mann-Whitney U	
Pelvic shape variable	Mean	St. Dev.	n	Rank Sum	Mean	St. Dev.	n	Rank Sum	U	*p*
Ilium length/GM	0.923	0.037	14	539	0.783	0.030	31	496	0	< 0.0001
Upper iliac height/GM	0.438	0.029	14	174	0.492	0.044	31	861	69	0.0001
Lower iliac height/GM	0.600	0.054	14	534	0.472	0.031	31	501	5	< 0.0001
AIIS to hip joint/GM	0.347	0.025	14	111	0.438	0.035	31	924	6	< 0.0001
Ilium width/GM	0.309	0.026	14	105	0.447	0.029	31	930	0	< 0.0001
Lower ilium cross-sectional area/GM	0.075	0.006	14	109	0.107	0.013	31	926	4	< 0.0001
Auricular surface area/GM	0.206	0.008	7	191	0.190	0.015	28	439	33	0.006
Ischium length/GM	0.430	0.015	14	539	0.367	0.017	31	496	0	< 0.0001
Dorsal projection of ischium/GM	0.162	0.032	14	363	0.149	0.027	31	672	176	0.325
Ischium cross-sectional area/GM	0.119	0.009	14	485	0.106	0.008	31	550	54	< 0.0001
Acetabulum diameter/GM	0.273	0.029	14	348	0.271	0.019	31	687	191	0.536
Superior pubic ramus length/GM	0.414	0.016	14	411	0.400	0.023	31	624	128	0.029
Inferior pubic ramus length/GM	0.492	0.035	14	539	0.342	0.055	31	496	0	< 0.0001
Inferior pubic ramus cross-sectional area/GM	0.052	0.006	14	327	0.052	0.008	31	708	212	0.913
Pubic symphysis length/GM	0.232	0.025	14	193	0.284	0.049	31	842	88	0.001

[a]GM = geometric mean

Summary of pairwise comparisons

The goal of the targeted pairwise comparisons was to test the biomechanically-based adaptive hypotheses of pelvic shape using a phylogenetic comparative method, in order to rule out the possibility of shared traits among taxa due to shared ancestry. Unfortunately, the sample sizes for many of the planned comparisons were too small to achieve statistical power sufficient to discriminate between taxa, and only those comparisons that were feasible in terms of sample size were performed here. In general, the results of the pairwise tests among groups were uninformative. The two comparisons of arboreal and terrestrial quadrupeds yielded internally inconsistent results. Similarly, the results of the three comparisons of arboreal quadrupeds and vertical clingers and leapers conflicted with each other. Because the pairwise tests did not reliably support the hypotheses proposed here, the majority of the hypotheses must be rejected based on a strict criterion of concordance.

Several hypotheses were rejected in every instance—those regarding the cross-sectional areas of both the superior and inferior pubic rami, and the area of the auricular surface. According to the data presented here, these pelvic traits do not differ predictably according to locomotion. Additionally, two traits were rejected in all but one test: superior pubic ramus length and pubic symphysis length. These results are particularly interesting because all but one of these measures is an aspect of pubic morphology, which, based on the results of the experimental strain tests presented in Chapter 3, was hypothesized to play a critical role in pelvic stress resistance and to differ in taxa that differ in habitual

loading regimes. The contrasting results of the experimental and comparative morphometric data hinder interpretation of the functional significance of primate pubic morphology.

The one pelvic trait that seems best correlated with locomotor behavior is the cross-sectional area of the lower ilium. The prediction that this measure would be greater in those taxa that experience larger substrate reaction forces during locomotion was supported in four out of five comparisons. The one test in which the hypothesis was not supported was the comparison of *Otolemur crassicaudatus* with *Galago senegalensis*. As was suggested above, this particular comparison may not adequately control for differences in body size; the results demonstrate that the larger-bodied, but arboreal quadrupedal *Otolemur* possesses strut cross-sectional and joint surface areas that are approximately equal to those of the small-bodied vertical clinging and leaping *Galago*, as well as relatively longer linear measures. However, it is quite plausible that it is the large difference in body size that is driving the differences between these two taxa, and that this body size difference swamps any morphological effects of locomotion that may be present. Although the samples here are insufficient to investigate the hypothesis that body size differences within locomotor groups affect pelvic functional morphology, the implications of this issue for the interpretation of these results will be discussed later in the Discussion of this chapter.

Finally, lower iliac height may also be related to differing loading regimes associated with locomotor behaviors. While the hypothesis that this measure is related to resisting bending of the ilium is not strictly supported, predictions

regarding its morphology were upheld in three of the five tests (it was rejected in the *Otolemur* v. *Galago* and *Varecia* v. *Propithecus* comparisons).

Primate-wide analyses

Although samples per taxon are not large enough to perform more pairwise comparisons than already presented, an investigation of the primate-wide patterns of pelvic morphology may fill in remaining gaps by generating a more complete picture of the diversity of pelvic shapes that result from locomotion. This section examines the same biomechanical predictions of pelvic shape as above using a broader sample of primates. This analysis follows the same logic of the pairwise comparisons, but is instead open to the entire sample of AQ, TQ, and VCL primates. The format of this section follows that of the pairwise comparison section, but also includes results of primate-wide scaling analyses for each pelvic measure. Results of examinations of locomotor differences in shape variables among AQ, TQ, and VCL taxa using Kruskal-Wallis tests are presented first, followed by *post hoc* multiple comparisons to determine which groups differed significantly. Then, box plots of median values and ranges for each locomotor group and taxon are qualitatively examined for patterns among taxa that may not be captured by the analyses presented here. The results of reduced major axis (RMA) scaling analyses on the entire primate sample are then presented, including presentation of the slopes of multiple regressions fit to each locomotor group (including all the locomotor groups, not just AQ, TQ, and VCL taxa). Finally, the bivariate scaling plots are examined qualitatively for differences among taxa.

As stated at the outset of this chapter, predictions for the scaling tests were that linear dimensions should scale with isometry while areal measures should scale with slight positive allometry. Results of *post hoc* multiple comparisons tests are in Appendix D.

Ilium length. Prediction: TQ < AQ < VCL. There is a significant effect of locomotor behavior on ilium length (H = 6.44, $p = 0.04$). *Post hoc* multiple comparisons indicate that, as predicted, arboreal quadrupeds have significantly longer ilia than terrestrial quadrupeds ($p = 0.04$, Fig. 4-3), but contrary to the predictions, VCL taxa do not have the longest ilia (Fig. 4-3). Therefore, these results do not support the specific hypothesis relating ilium length to locomotion.

Qualitatively, slow climbers have the longest ilia of all locomotor groups, while the suspensory and AQ/suspensory taxa have the shortest ilia (Fig. 4-3). All other locomotor groups are intermediate in ilium length and their ranges overlap each other (Fig. 4-3). In addition to the differences apparent in the box plots of locomotor groups, the box plots of taxa indicate that the terrestrial quadrupedal apes (*Gorilla gorilla* and *Pan troglodytes*) have relatively shorter ilia than the terrestrial quadrupedal monkeys (Fig. 4-4). In addition, a bivariate plot of ln-ilium length on ln-body mass$^{1/3}$ for the entire primate sample reveals that small-bodied AQ/leapers have relatively short ilia for their body size (Fig. 4-5).

Results of the reduced major axis scaling analysis of ilium length using the combined-sex sample (taxon means) indicates isometry (slope = 0.92, 95% confidence interval 0.83 – 1.00). However, the locomotor groups do not all exhibit the same scaling relationships. An examination of the slopes and

confidence intervals for each group reveals that terrestrial quadrupeds and vertical clingers and leapers exhibit negative allometry in ilium length (TQ slope = 0.68, VCL slope = 0.86, Table 4-20), while the other locomotor groups demonstrate isometry in ilium length relative to body size (Table 4-20). The prediction of isometry in this measure is supported in the overall primate sample, but within locomotor categories it is rejected for terrestrial quadrupeds and vertical clingers and leapers.

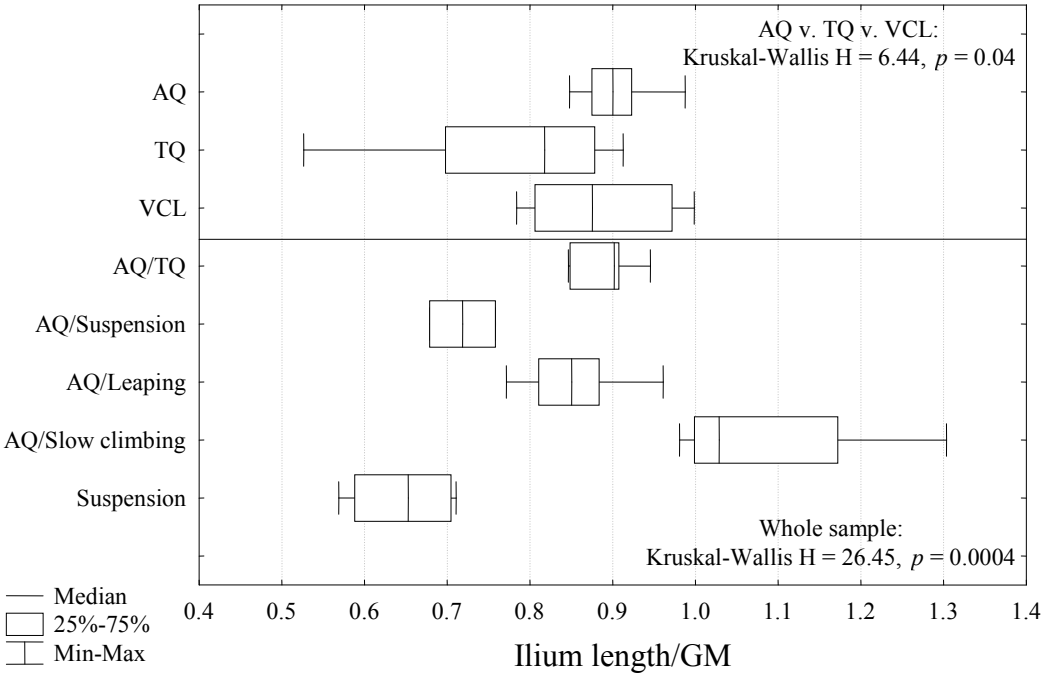

Fig. 4-3. Box-and-whiskers plots comparing the medians and ranges of the ilium length shape variable for each locomotor group. The three boxes above the horizontal line were used in hypothesis-testing, while the box plots below the horizontal line were not included in *a priori* hypothesis-testing. Kruskal-Wallis tests were performed on both samples, and the *p*-values are listed accordingly.

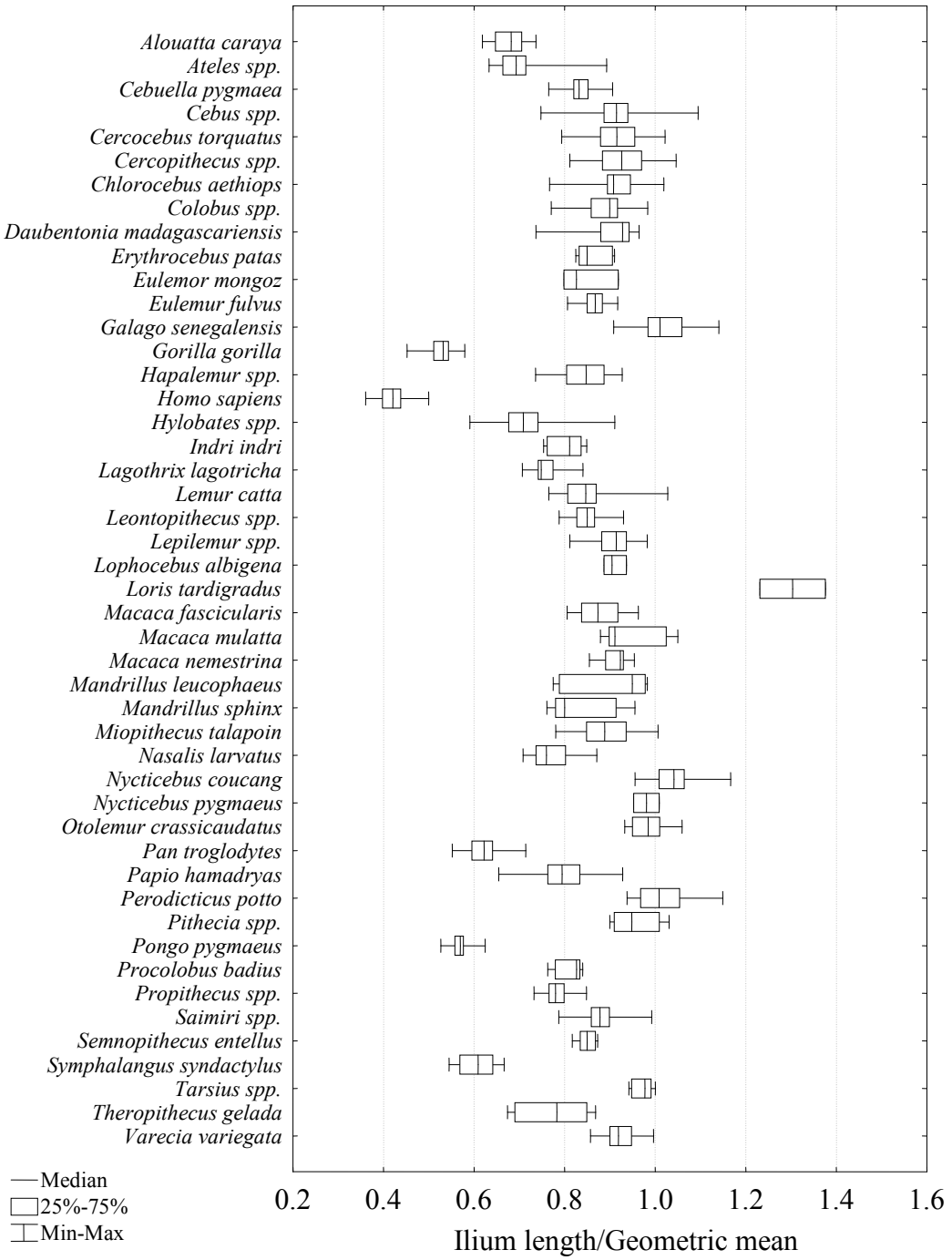

Fig. 4-4. Box-and-whiskers plots of medians and ranges of the ilium length shape variable for each taxon.

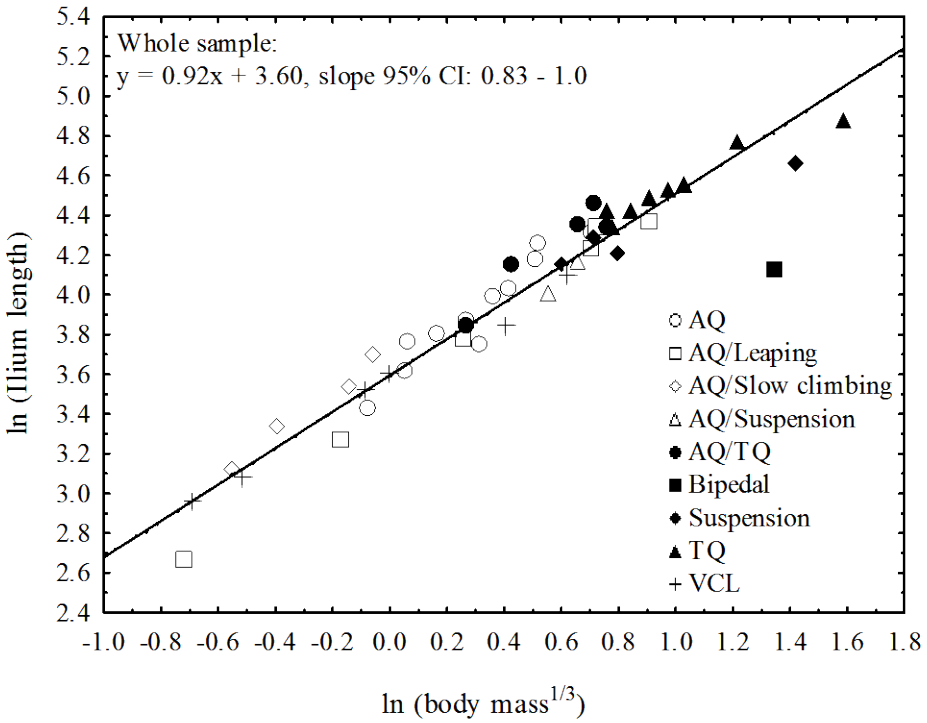

Fig. 4-5. Bivariate plot of ln-ilium length on ln-body mass$^{1/3}$.

Upper iliac height. Prediction AQ = TQ = VCL. Upper iliac height does not differ among taxa according to locomotor behavior (H = 1.13, p = 0.57). These results support the prediction that upper iliac height would not differ according to locomotor category.

Qualitatively, there is extensive overlap in the ranges of the AQ, TQ, and VCL taxa (Fig. 4-6), and across all taxa (Fig. 4-7). A bivariate plot of ln-upper iliac height on ln-body mass$^{1/3}$ demonstrates a low level of deviations from the regression line (Fig. 4-8), and the taxa that have large regression residuals do not appear to be patterned. As has been noted previously, *Homo sapiens* has a short upper ilium for its body size (Fig. 4-8).

Upper iliac height scales with positive allometry within the primate-wide sample (slope = 1.18, 95% confidence interval 1.08 - 1.27, Table 4-20). Based on

the slopes and 95% confidence intervals for each locomotor category, four groups demonstrate isometry in upper iliac height relative to body size (AQ, slow climbers, AQ/TQ, and suspensory taxa) and three groups exhibit positive allometry in upper iliac height (AQ/leapers, TQ, VCL). The prediction that upper iliac height would scale isometrically with body size is rejected for the primate-wide sample and AQ/leapers, TQ, and VCL taxa, but isometry cannot be rejected for the other four locomotor groups.

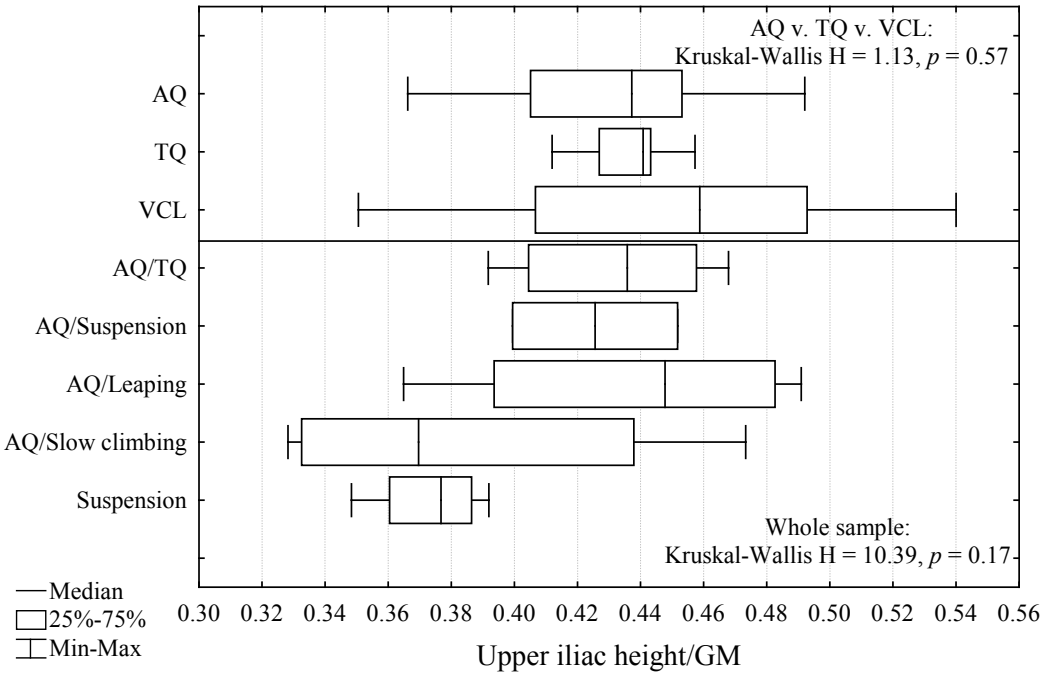

Fig. 4-6. Box-and-whiskers plots comparing the medians and ranges of the upper iliac height shape variable for each locomotor group. The three boxes above the horizontal line were used in hypothesis-testing, while the box plots below the horizontal line were not included in *a priori* hypothesis-testing. Kruskal-Wallis tests were performed on both samples, and the *p*-values are listed accordingly.

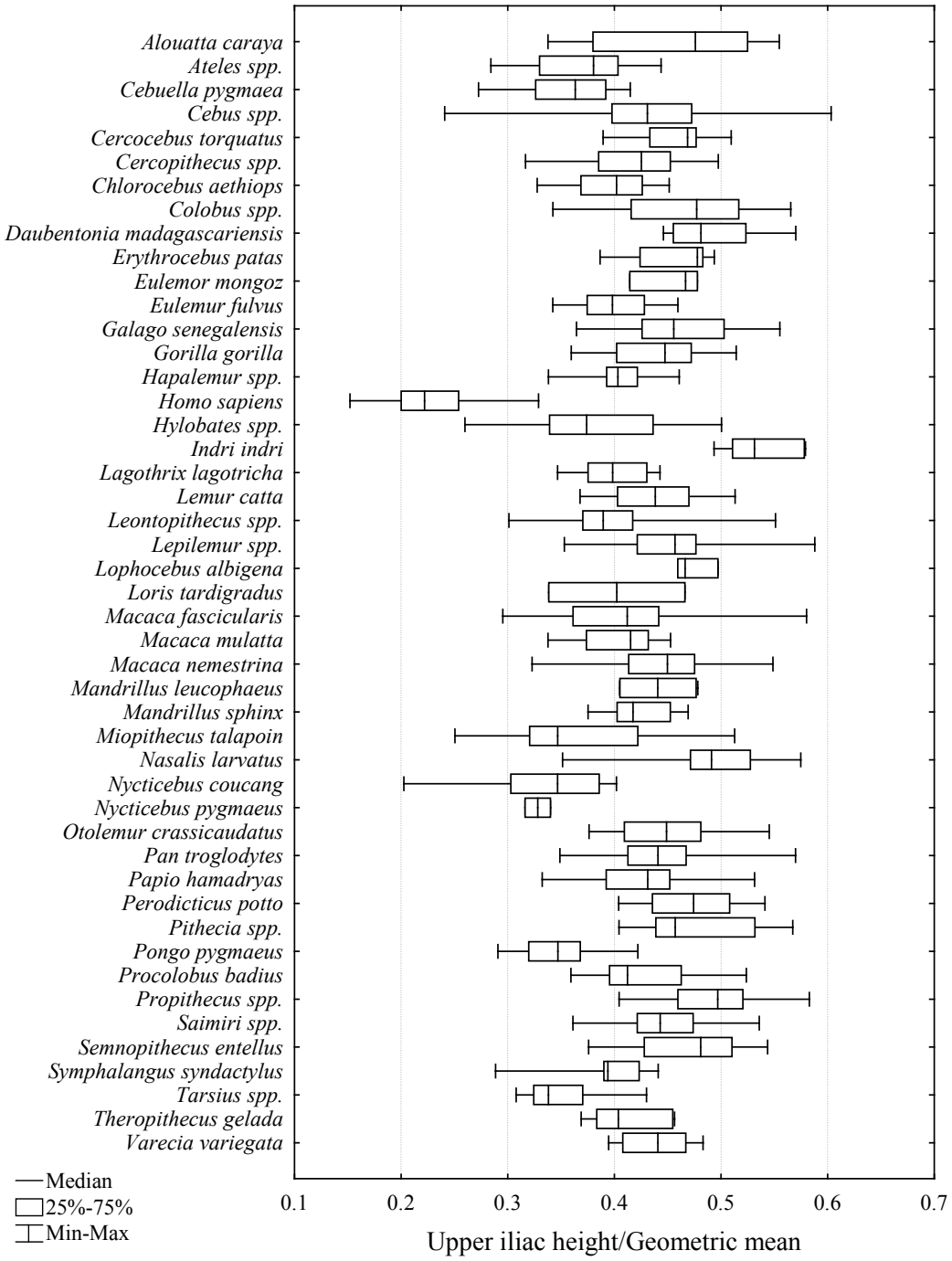

Fig. 4-7. Box-and-whiskers plots of medians and ranges of the upper iliac height shape variable for each taxon.

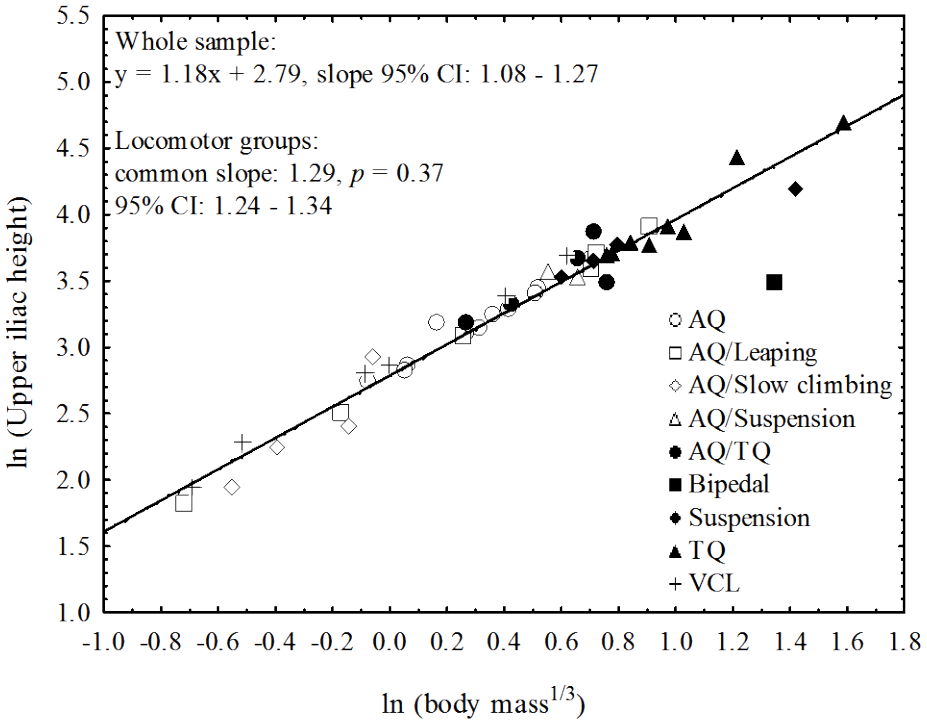

Fig. 4-8. Bivariate plot of ln-upper iliac height on ln-body mass$^{1/3}$.

Lower iliac height. Prediction TQ < AQ < VCL. There is a significant effect of locomotor behavior on lower iliac height (H = 10.13, p = 0.006). *Post hoc* comparisons reveal that arboreal quadrupeds have significantly longer lower iliac regions than their terrestrial counterparts (p = 0.006), but contrary to predictions, VCL taxa do not have the longest lower iliac region (Fig. 4-9). Therefore, these results do not support the specific hypothesis relating lower iliac height to locomotion.

A qualitative examination of the box plots of all locomotor groups shows that slow climbers have the longest lower iliac region, while terrestrial quadrupeds have the shortest (Fig. 4-9). Vertical clingers and leapers have a wide range of variation that overlaps with all other locomotor groups (Fig. 4-9). An examination of box plots for all taxa demonstrates that this large range in VCL

taxa corresponds to variation in body size—small-bodied VCL taxa have quite long lower iliac regions, while the larger-bodied VCL taxa have shorter lower iliac regions, and even overlap with some terrestrial quadruped taxa (Fig. 4-10). Specifically, *Galago senegalensis* and *Tarsius* spp. have the long lower iliac regions, overlapping only with the arboreal quadruped *Otolemur crassicaudatus*, while *Indri indri* and *Propithecus* spp. plot have the short lower iliac regions and overlap with large-bodied terrestrial quadrupeds (Fig. 4-10). In addition, a bivariate plot of ln-lower iliac height on ln-body mass$^{1/3}$ indicates that AQ/leapers have short lower iliac regions relative to body size, while three out of four suspensory taxa have relatively long lower iliac regions (the fourth, *Pongo*, has a relatively short lower iliac region) (Fig. 4-11).

In the primate-wide sample, lower iliac height scales with slight negative allometry relative to body size (slope = 0.91, 95% confidence interval 0.84 – 0.98, Table 4-20). However, the locomotor groups do not share the same scaling relationship. The hypothesis of isometry cannot be rejected for five groups, in fact, it is only the suspensory and VCL taxa that are characterized by negative allometry (suspensory slope = 0.58, VCL slope = 0.62, Table 4-20). These results do not support the prediction of isometry in lower iliac height relative to body size in the primate-wide sample, but among locomotor groups, isometry is rejected only for suspensory and VCL taxa.

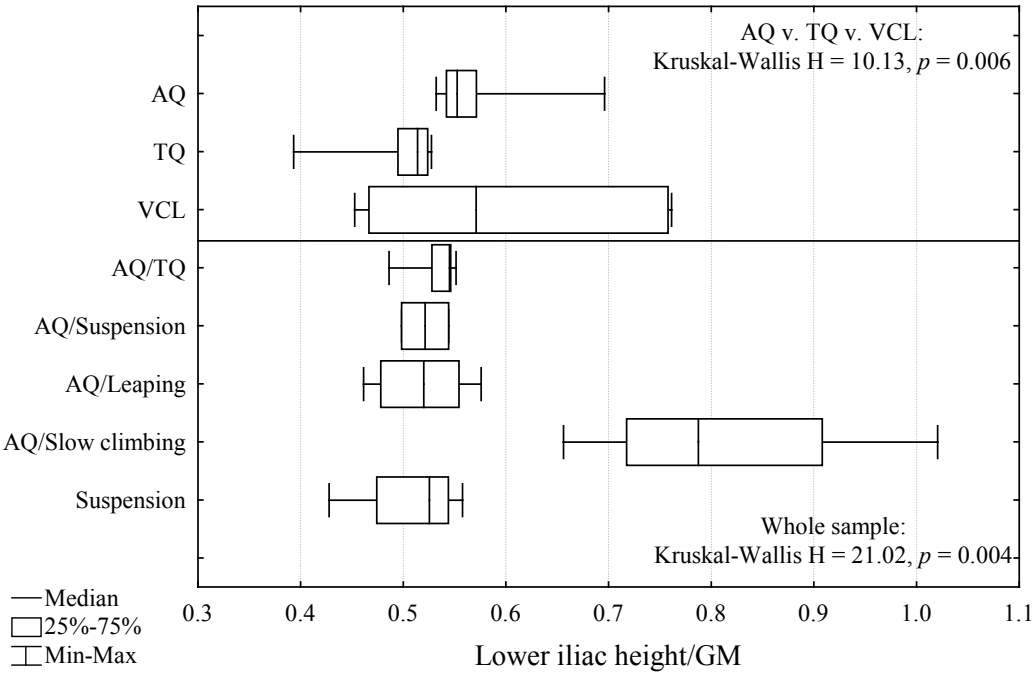

Fig. 4-9. Box-and-whiskers plots comparing the medians and ranges of the lower iliac height shape variable for each locomotor group. The three boxes above the horizontal line were used in hypothesis-testing, while the box plots below the horizontal line were not included in *a priori* hypothesis-testing. Kruskal-Wallis tests were performed on both samples, and the *p*-values are listed accordingly.

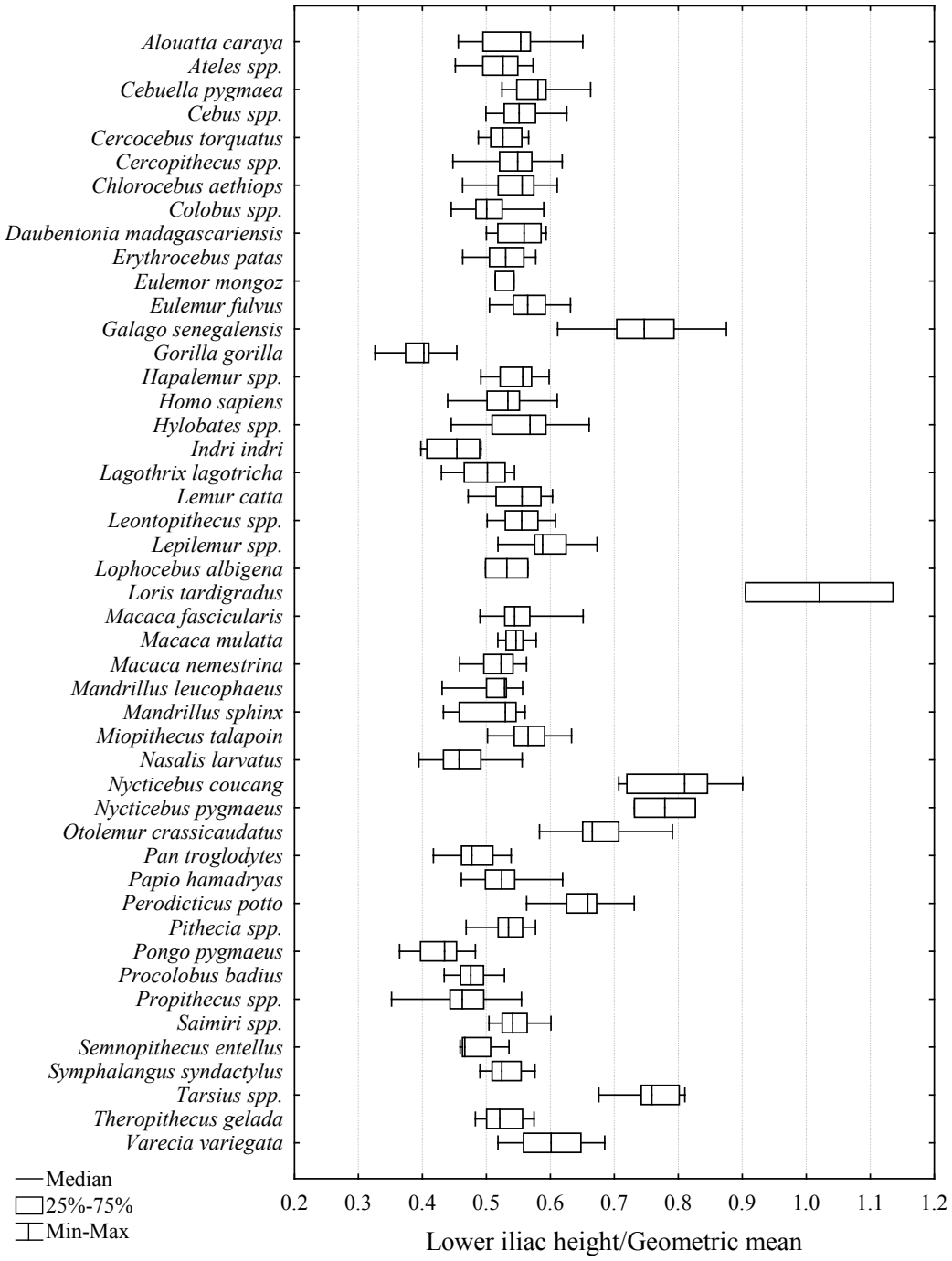

Fig. 4-10. Box-and-whiskers plots of medians and ranges of the lower iliac height shape variable for each taxon.

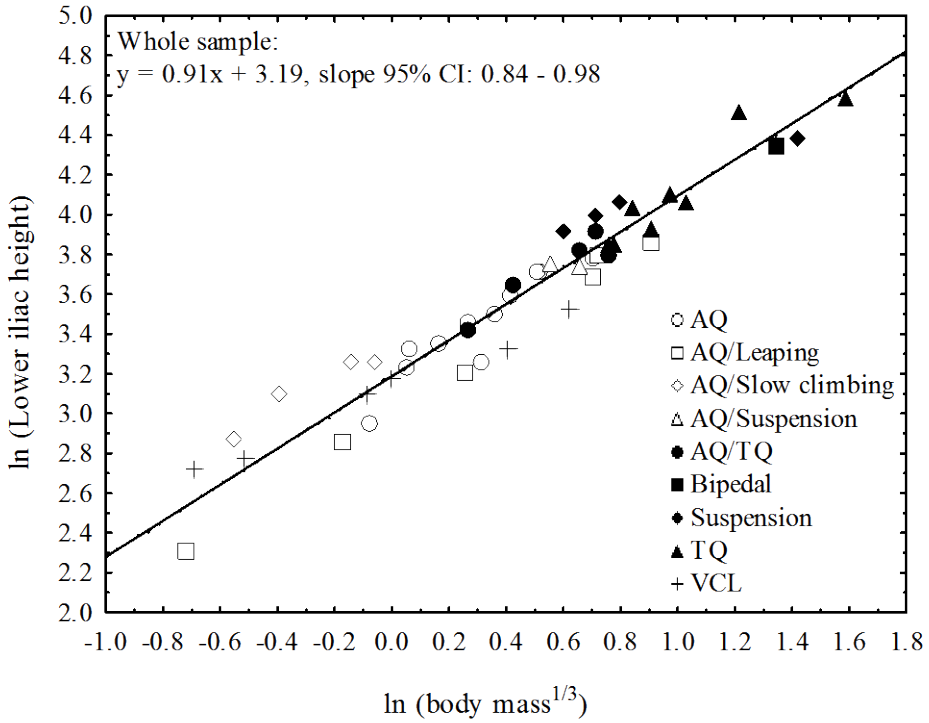

Fig. 4-11. Bivariate plot of ln-lower iliac height on ln-body mass$^{1/3}$.

AIIS to hip joint. Prediction AQ = TQ < VCL. There is no effect of locomotion on the placement of the AIIS in relation to the hip joint (H = 4.18, p = 0.12). A box plot of median values for locomotor groups demonstrates extensive overlap among AQ and TQ taxa, as predicted, but contrary to predictions, the vertical clingers and leapers overlap with the two quadrupedal groups (Fig. 4-12). Furthermore, a box plot of median values for each taxon does not demonstrate any locomotor patterns in this pelvic measure (Fig. 4-13). Therefore, these results do not support the specific hypothesis relating locomotion to the distance from the AIIS to the hip.

The distance between the AIIS and the hip joint is isometric with body size (slope = 1.02, 95% confidence interval 0.95 – 1.09, Table 4-20). An examination of locomotor-group slope confidence intervals demonstrates

isometry in all but vertical clinging and leaping taxa, which demonstrate positive allometry (slope = 1.24, Table 4-20). The prediction that this dimension scales with isometry relative to body size is supported in the primate-wide regression, but is rejected within vertical clingers and leapers.

This scaling pattern in vertical clingers and leapers suggests that relative to body size, VCL taxa have a greater AIIS to hip joint distance compared to other taxa. This pattern is also evident in a bivariate plot of ln-AIIS to hip joint on ln-body mass$^{1/3}$ (Fig. 4-14). This result only partially supports the prediction that VCL taxa would have a greater AIIS-to-hip joint dimension relative to other taxa because it occurs in large-bodied, but not small-bodied, VCL taxa.

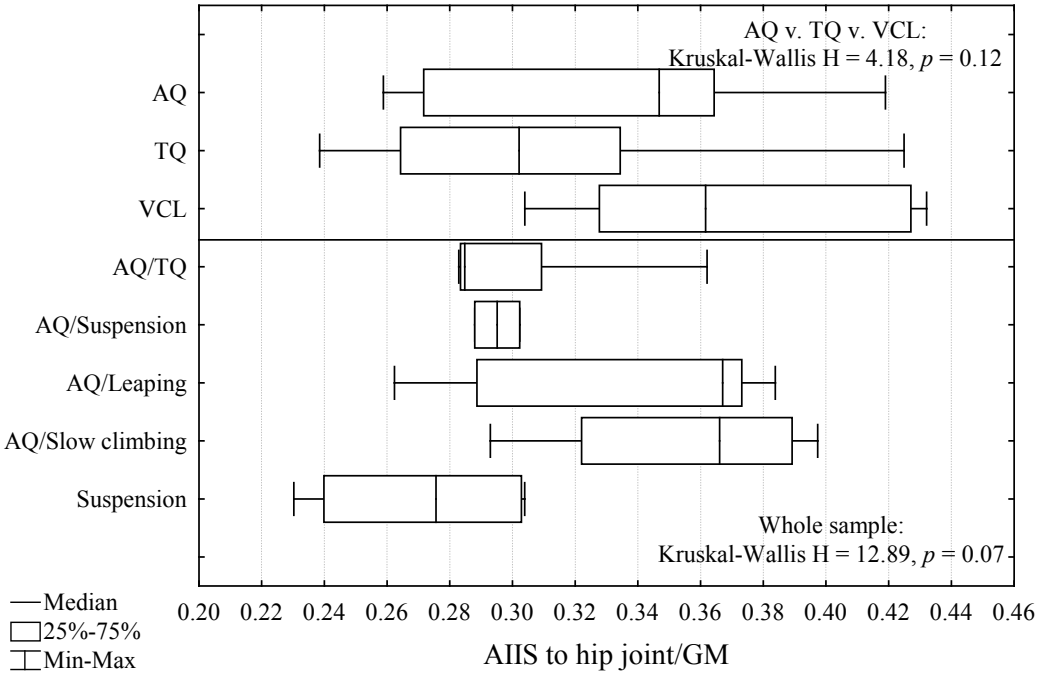

Fig. 4-12. Box-and-whiskers plots comparing the medians and ranges of the AIIS-to-hip joint shape variable for each locomotor group. The three boxes above the horizontal line were used in hypothesis-testing, while the box plots below the horizontal line were not included in *a priori* hypothesis-testing. Kruskal-Wallis tests were performed on both samples, and the *p*-values are listed accordingly.

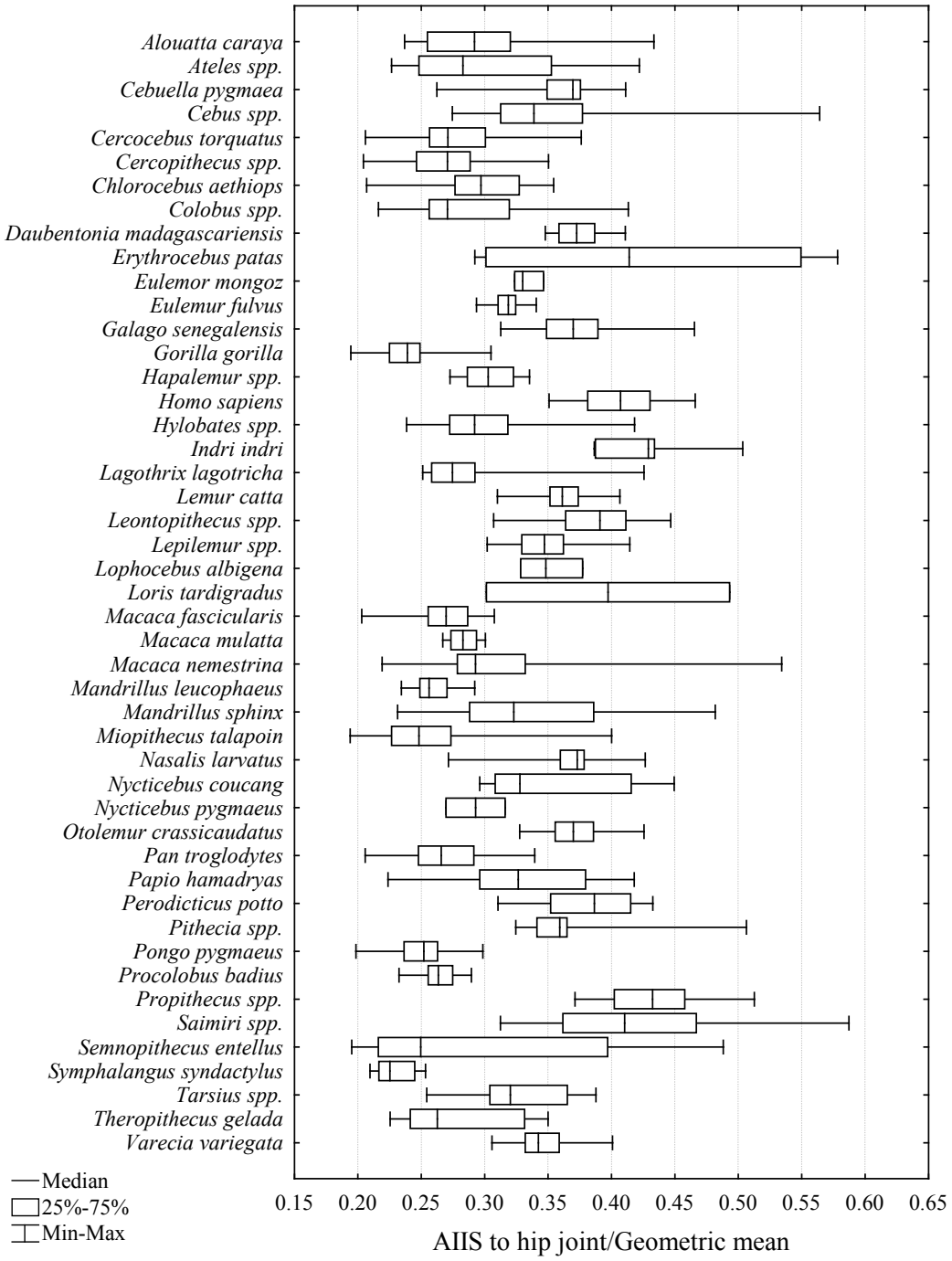

Fig. 4-13. Box-and-whiskers plots of medians and ranges of the AIIS-to-hip joint shape variable for each taxon.

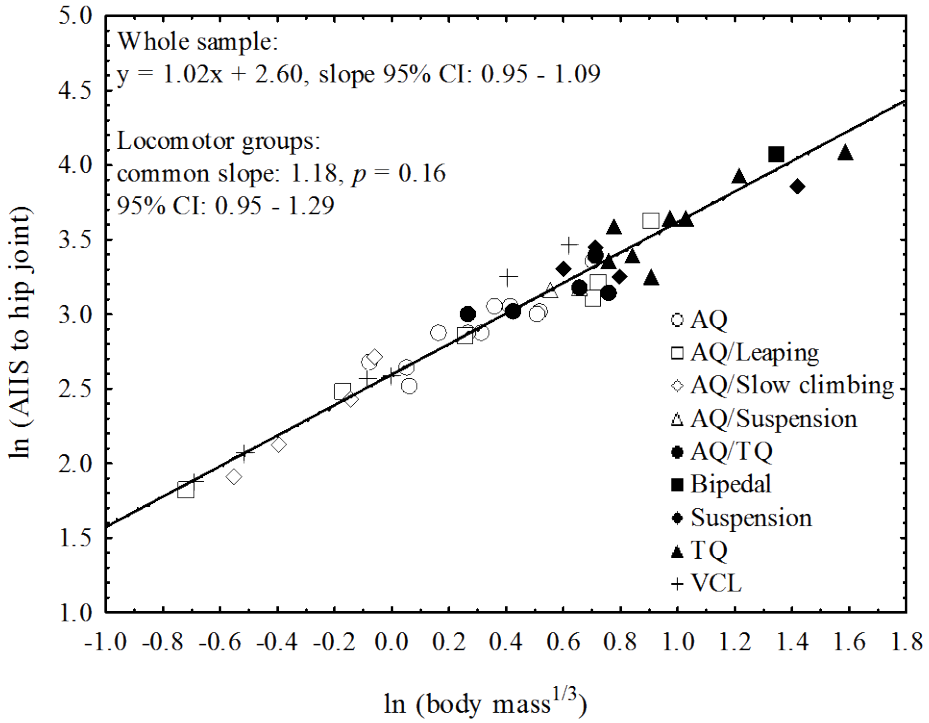

Fig. 4-14. Bivariate plot of ln-AIIS-to-hip joint on ln-body mass$^{1/3}$.

Ilium width. Prediction AQ = VCL < TQ. There is a significant effect of locomotion on the width of the ilium (H = 12.64, p = 0.002). *Post hoc* multiple comparisons show that, as predicted, terrestrial quadrupeds have significantly wider ilia than arboreal quadrupeds (p = 0.003) and vertical clinger and leapers (p = 0.02, Fig. 4-15). These results support the hypothesis relating ilium width to locomotion.

A qualitative examination of ilium width across primate locomotor groups indicates that slow climbers have narrow ilia, arboreal and VCL taxa are intermediate in ilium width, and suspensory and TQ taxa have the widest ilia (Fig. 4-15). A box plot of median values for each taxon shows a large range for TQ taxa, with *Gorilla gorilla* at the extreme end of ilium width. Terrestrial monkeys do overlap with arboreal monkeys and with large-bodied VCL taxa (Fig. 4-16).

There are also qualitative differences within locomotor categories apparently related to body size; small-bodied suspensory taxa (*i.e.*, *Ateles*) have narrower ilia than large-bodied suspensory taxa (*e.g.*, *Symphalangus* and *Pongo*), and the same pattern is found within vertical clingers and leapers (Fig. 4-16). Furthermore, a bivariate plot of ln-ilium width on ln-body mass$^{1/3}$ indicates that large-bodied TQ taxa (*Pan* and *Gorilla*) have wide ilia relative to body size (Fig. 4-17).

The width of the ilium scales with positive allometry in the primate-wide sample (slope = 1.57, 95% confidence interval 1.48 – 1.67, Table 4-20). A comparison of the slopes and confidence intervals for each locomotor group reveals that approximately half of the locomotor groups have confidence intervals that include isometry, while the other half are positively allometric. Ilium width in arboreal quadrupeds, slow climbers, semi-terrestrial taxa, and suspensory taxa is isometric relative to body size, whereas it is positively allometric with body size in AQ/leapers, terrestrial quadrupeds, and vertical clingers and leapers (Table 4-20). Therefore, the positively allometric locomotor subgroups affect the regression of the entire sample, effectively "pulling" the slope of the regression towards them. Thus, the hypothesis of isometry in ilium width relative to body size is rejected for the primate-wide sample, but cannot be rejected for AQ, AQ/slow climbers, AQ/TQ, and suspensory taxa.

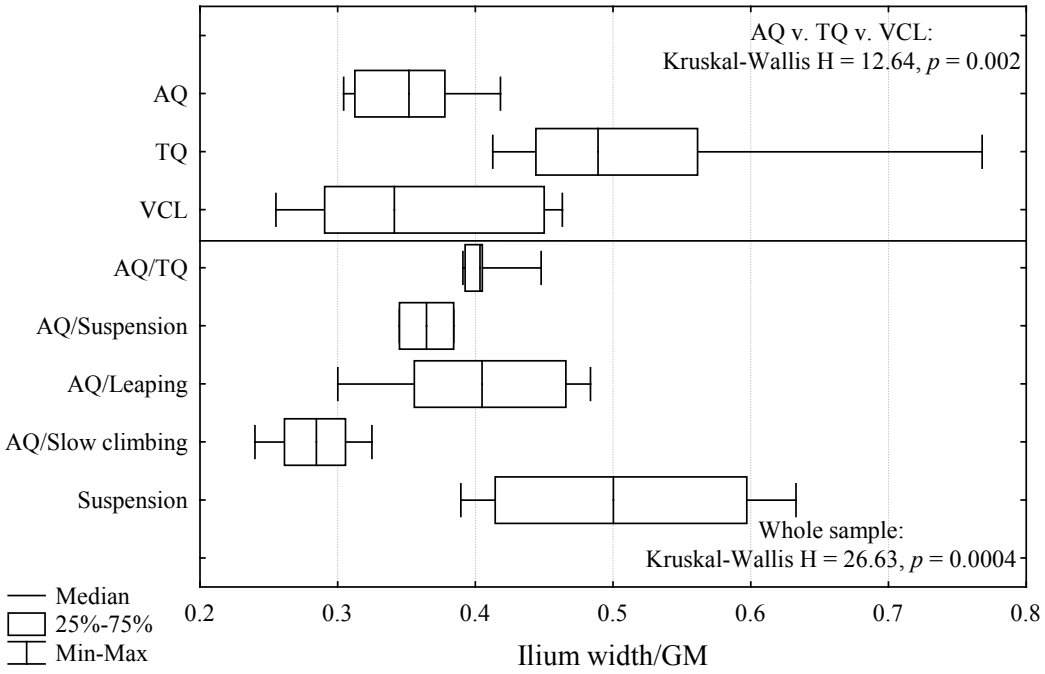

Fig. 4-15. Box-and-whiskers plots comparing the medians and ranges of the ilium width shape variable for each locomotor group. The three boxes above the horizontal line were used in hypothesis-testing, while the box plots below the horizontal line were not included in *a priori* hypothesis-testing. Kruskal-Wallis tests were performed on both samples, and the *p*-values are listed accordingly.

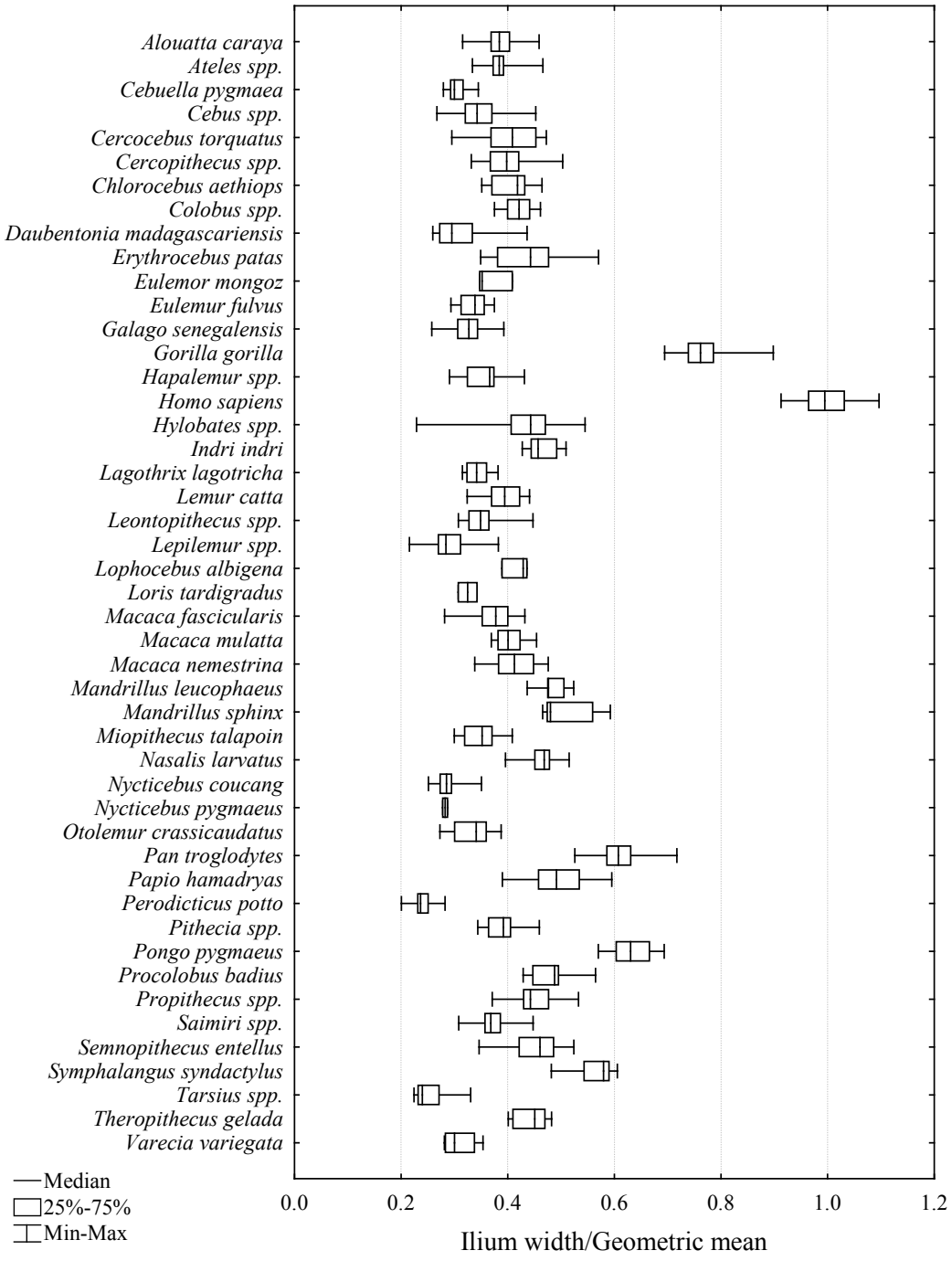

Fig. 4-16. Box-and-whiskers plots of medians and ranges of the ilium width shape variable for each taxon.

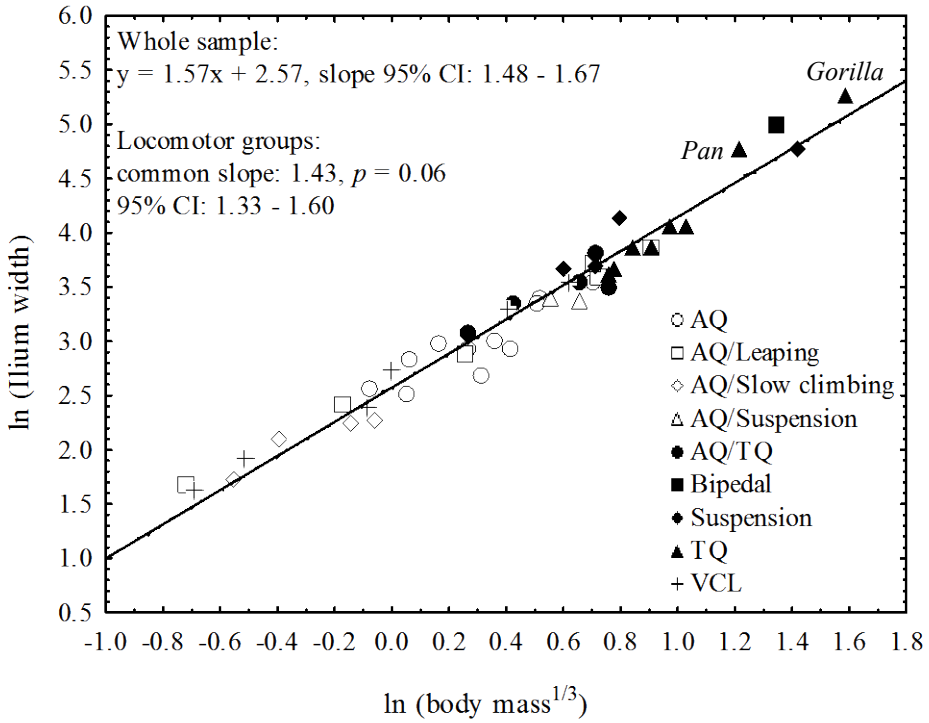

Fig. 4-17. Bivariate plot of ln-ilium width on ln-body mass$^{1/3}$.

Ischium length. Prediction AQ = TQ < VCL. There is a significant effect of locomotion on ischium length (H = 11.81, p = 0.003). However, contrary to predictions, *post hoc* multiple comparisons indicate that VCL taxa have significantly *shorter* ischia than both AQ (p = 0.004) and TQ taxa (p = 0.009). Visual inspection of the box plot of locomotor category medians for ischium length reveals that the range for arboreal quadrupeds is broad, and the lower whisker overlaps the box of the VCL group (Fig. 4-18). Thus, these results do not support the specific hypothesis of the relationship between ischium length and locomotion.

A qualitative inspection of all locomotor groups suggests that suspensory, slow climbing, and VCL taxa have similar ischia lengths that are all shorter than the other locomotor groups (Fig. 4-18). All the quadrupedal groups have long

ischia (Fig. 4-18). The box plot of taxon medians for all primates indicates a body size difference within VCL taxa; small-bodied leapers have shorter ischia than large-bodied leapers (Fig. 4-19), and this pattern is also demonstrated in the bivariate plot of ln-ischium length on ln-body mass$^{1/3}$ (Fig. 4-20).

The length of the ischium scales with positive allometry in the primate-wide sample (slope = 1.18, 95% confidence interval 1.11 – 1.26, Table 4-20). However, all but one group includes isometry in the 95% confidence interval of its slope; slow climbers are actually the only taxa that have ischia that scale with positive allometry relative to body size (slope = 1.23, Table 4-20). This suggests that slow climbers drive the primate-wide pattern of positive allometry relative to body size in ischium length. These scaling results reject the hypothesis of isometry in ischium length relative to body size in the entire primate sample, but among locomotor categories, it can only be rejected for slow climbers.

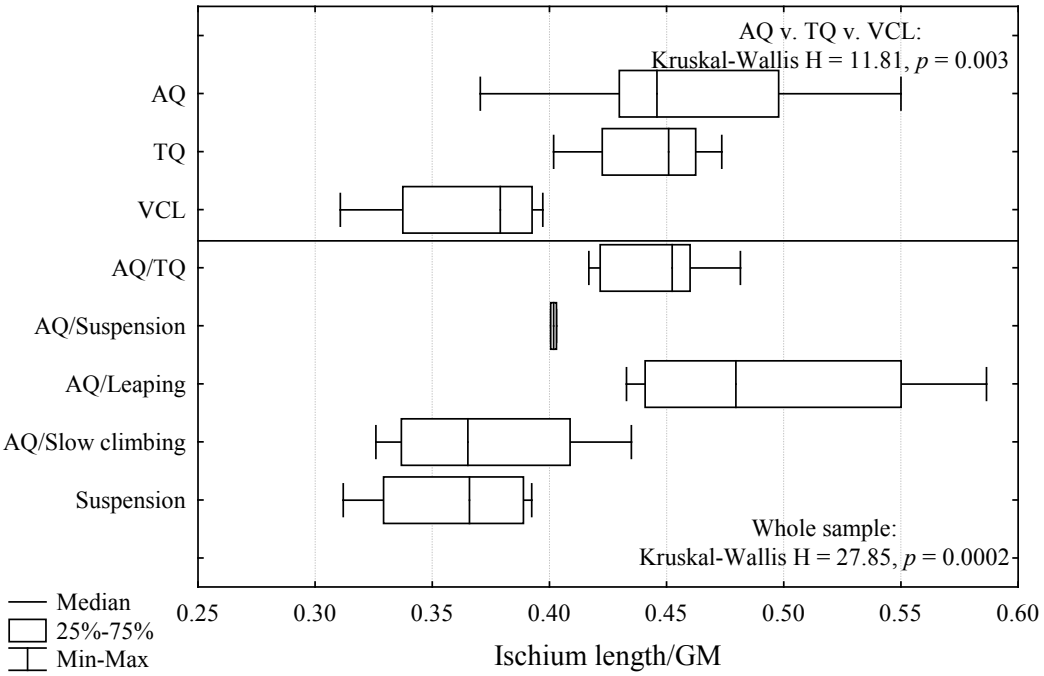

Fig. 4-18. Box-and-whiskers plots comparing the medians and ranges of the ischium length shape variable for each locomotor group. The three boxes above the horizontal line were used in hypothesis-testing, while the box plots below the horizontal line were not included in *a priori* hypothesis-testing. Kruskal-Wallis tests were performed on both samples, and the *p*-values are listed accordingly.

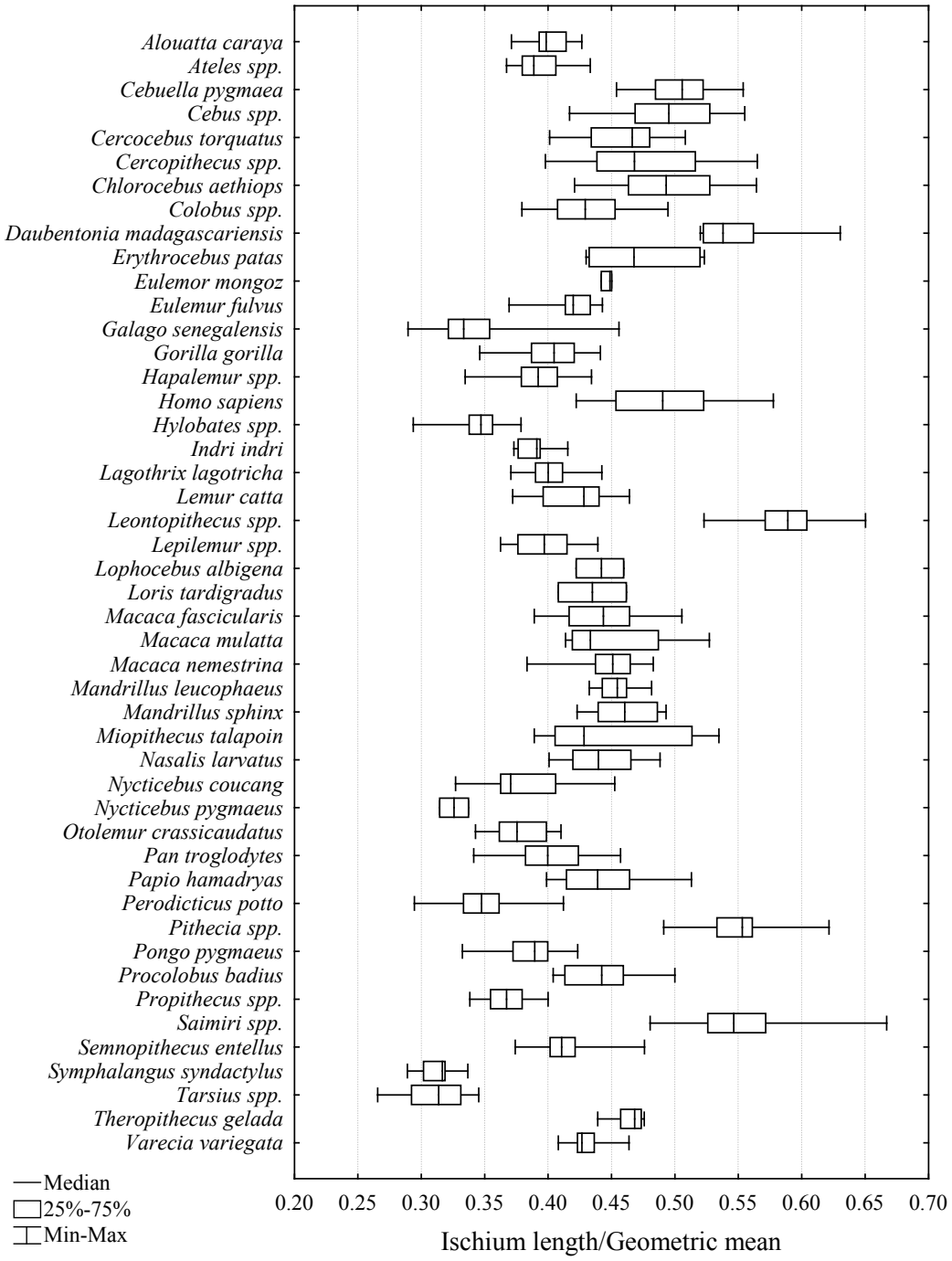

Fig. 4-19. Box-and-whiskers plots of medians and ranges of the ischium length shape variable for each taxon.

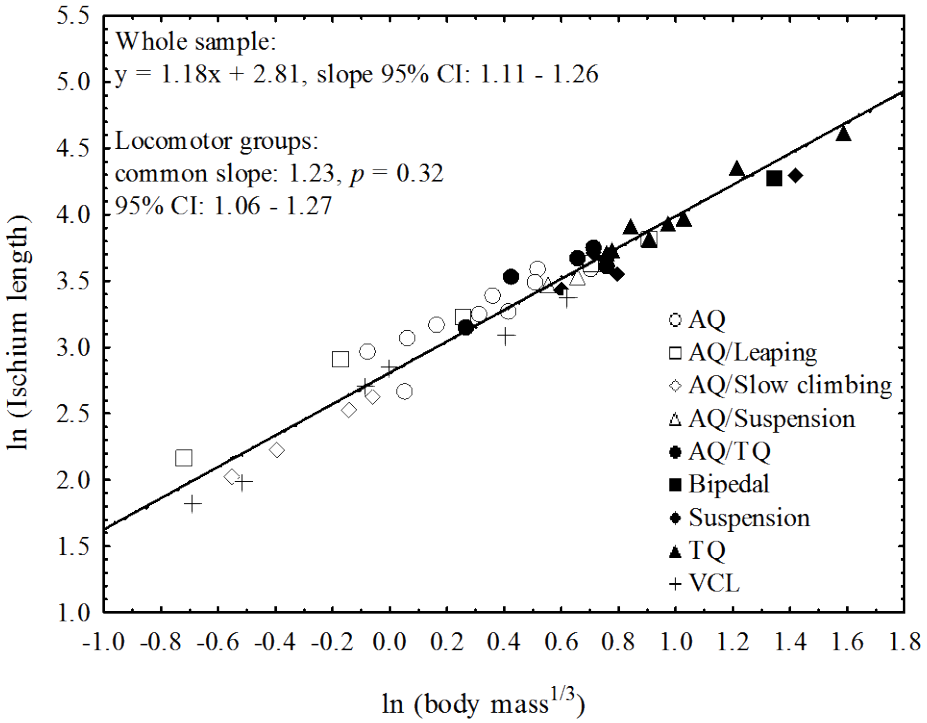

Fig. 4-20. Bivariate plot of ln-ischium length on ln-body mass$^{1/3}$.

Ischium dorsal projection. Prediction AQ = TQ < VCL. There is a significant effect of locomotion on the dorsal projection of the ischium (H = 14.59, p = 0.0007). However, contrary to predictions, *post hoc* multiple comparisons demonstrate that TQ taxa have significantly more dorsally-projecting ischia than both AQ (p = 0.03) and VCL taxa (p = 0.0005). In addition, a box plot of locomotor group medians indicates that VCL taxa have the least dorsally projecting ischia (Fig. 4-21). These results do not support the hypothesized relationship between ischium dorsal projection and locomotion.

A qualitative examination of all locomotor groups demonstrates that slow climbers have the least dorsally-projecting ischia, while VCL, AQ, suspensory, and AQ/suspensory taxa are intermediate in ischium dorsal projection, and semi-terrestrial and TQ taxa have the most dorsally-projecting ischia (Fig. 4-21). The

box plot of taxon medians indicates that the TQ cercopithecines have the most dorsally projecting ischia and appear to be driving the trend seen in terrestrial quadrupeds in general (Fig. 4-22). Among VCL taxa, small-bodied leapers have less dorsally projecting ischia than large-bodied leapers (Fig. 4-22). In addition, the variation within taxa is quite large (Figs. 4-21 and 4-22) and suggests that there is no relationship between ischial dorsal projection and locomotion.

The dorsal projection of the ischium scales with positive allometry in the primate-wide sample (slope = 1.87, 95% confidence interval 1.67 – 2.07, Table 4-20, Fig. 4-23). However, the 95% confidence intervals of the slopes of three out of the seven locomotor groups are so broad that they also include isometry (AQ/TQ, suspensory, and TQ taxa, Table 4-20). This variation in confidence intervals—like the variation seen in the boxplots—also suggests that this trait is highly variable and may not be related to locomotion. Therefore, the prediction of isometry in ischium dorsal projection relative to body size is rejected for the primate-wide sample, but cannot be rejected for AQ/TQ, suspensory, and TQ taxa.

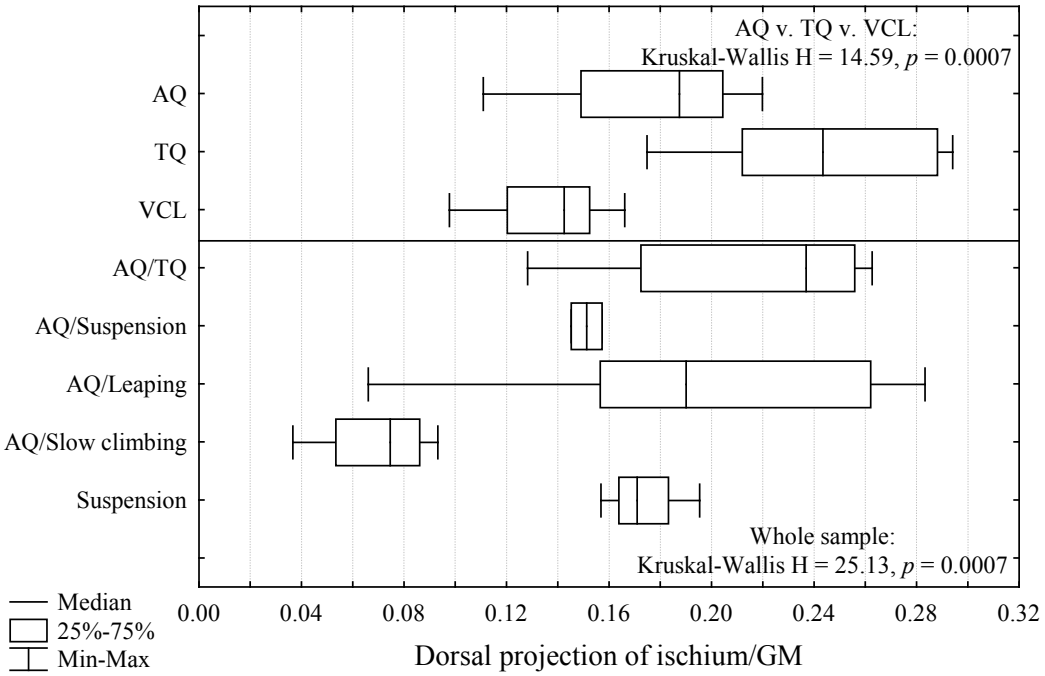

Fig. 4-21. Box-and-whiskers plots comparing the medians and ranges of the ischium dorsal projection shape variable for each locomotor group. The three boxes above the horizontal line were used in hypothesis-testing, while the box plots below the horizontal line were not included in *a priori* hypothesis-testing. Kruskal-Wallis tests were performed on both samples, and the *p*-values are listed accordingly.

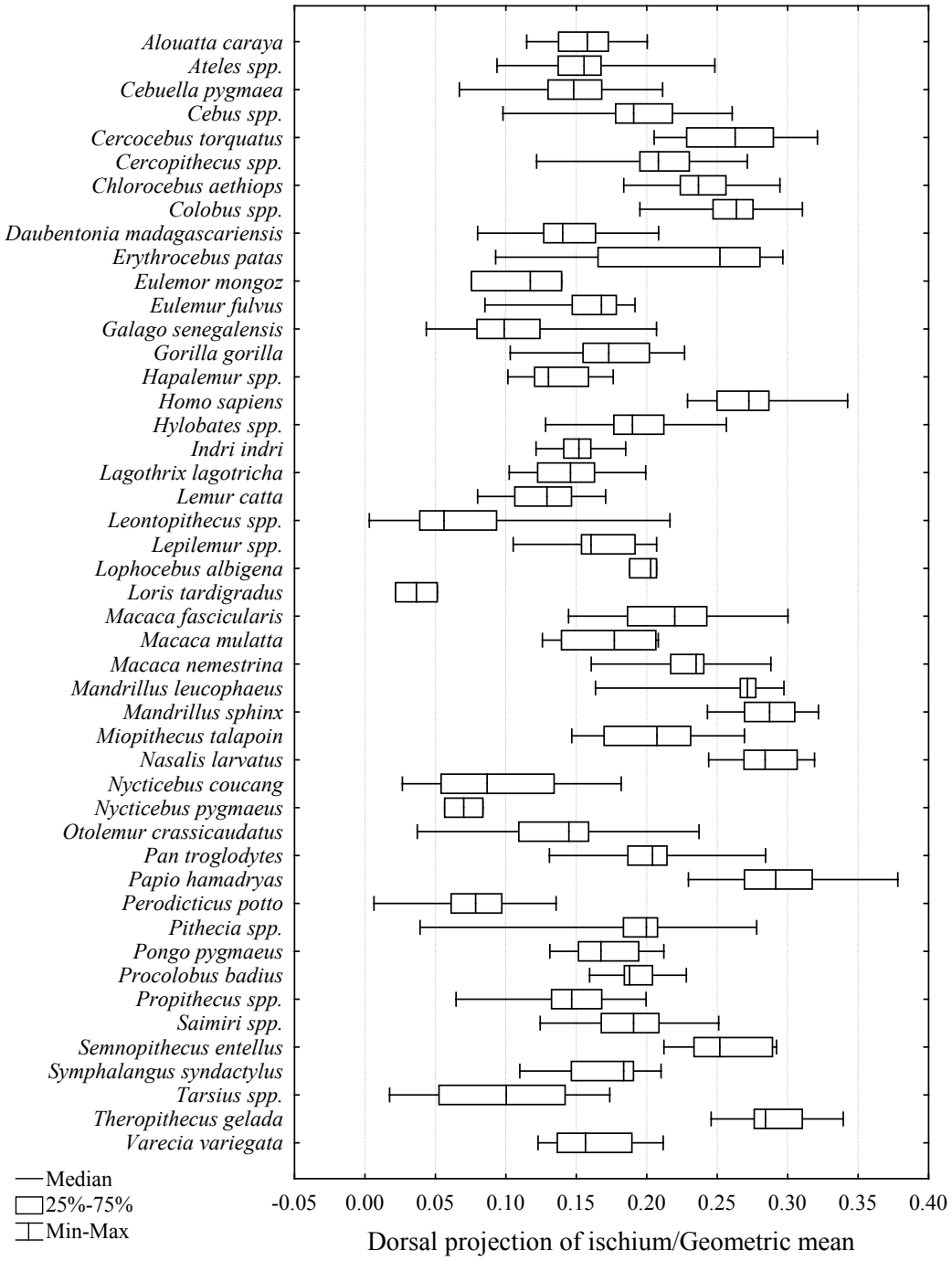

Fig. 4-22. Box-and-whiskers plots of medians and ranges of the ischium dorsal projection shape variable for each taxon.

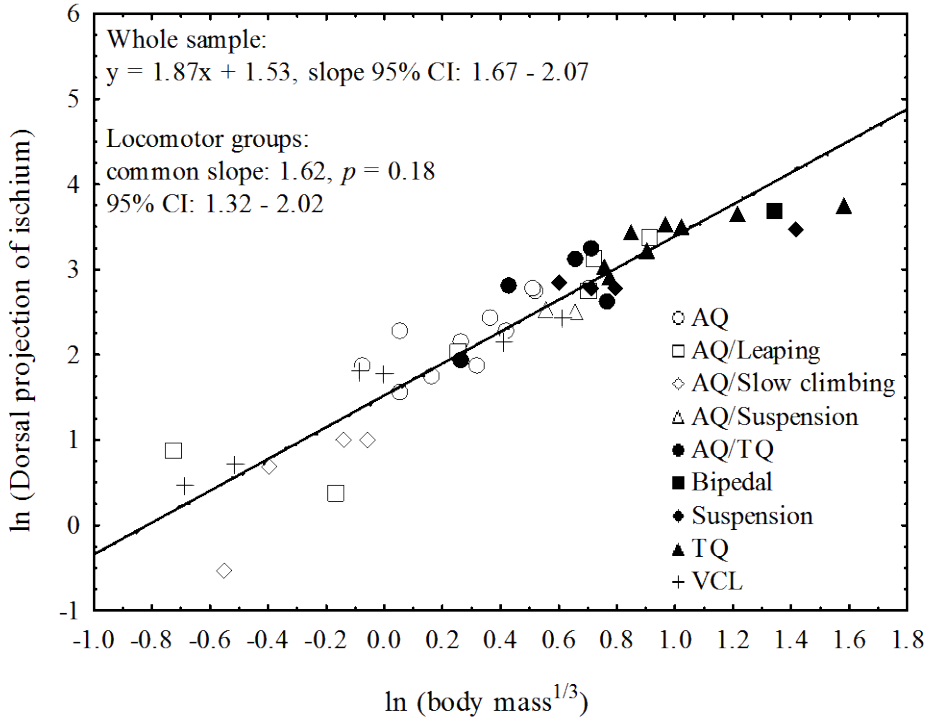

Fig. 4-23. Bivariate plot of ln-ischium dorsal projection on ln-body mass$^{1/3}$.

Acetabulum diameter. Prediction AQ < TQ < VCL. Locomotor behavior does not have an effect on the diameter of the acetabulum (H = 5.66, p = 0.06). The box plot of locomotor group medians confirms overlap of all three locomotor group boxes (Fig. 4-24). These results do not support the hypothesis of locomotor effect on acetabulum diameter.

A qualitative examination of all locomotor groups indicates that slow climbers and VCL taxa have the largest acetabulae, suspensory taxa are intermediate in acetabulum size, and the remaining quadrupeds have the smallest acetabulae relative to body size (Fig. 4-24). Furthermore, the box plot of taxon group medians shows that the largest acetabulae belong specifically to AQ and VCL strepsirrhines and *Homo sapiens* (Fig. 4-25).

In the primate-wide regression, acetabulum diameter scales with isometry (slope = 1.05, 95% confidence interval 0.99 – 1.10, Table 4-20, Fig. 4-26). An examination of the slopes and 95% confidence intervals for each locomotor group individually shows that two groups (AQ/leapers and terrestrial quadrupeds) exhibit positive allometry relative to body size (slopes = 1.09 and 1.24, respectively, Table 4-20). Within the primate-wide sample, these results support the hypothesis that acetabulum diameter scales with isometry relative to body size, while this hypothesis is rejected for AQ/leapers and terrestrial quadrupeds.

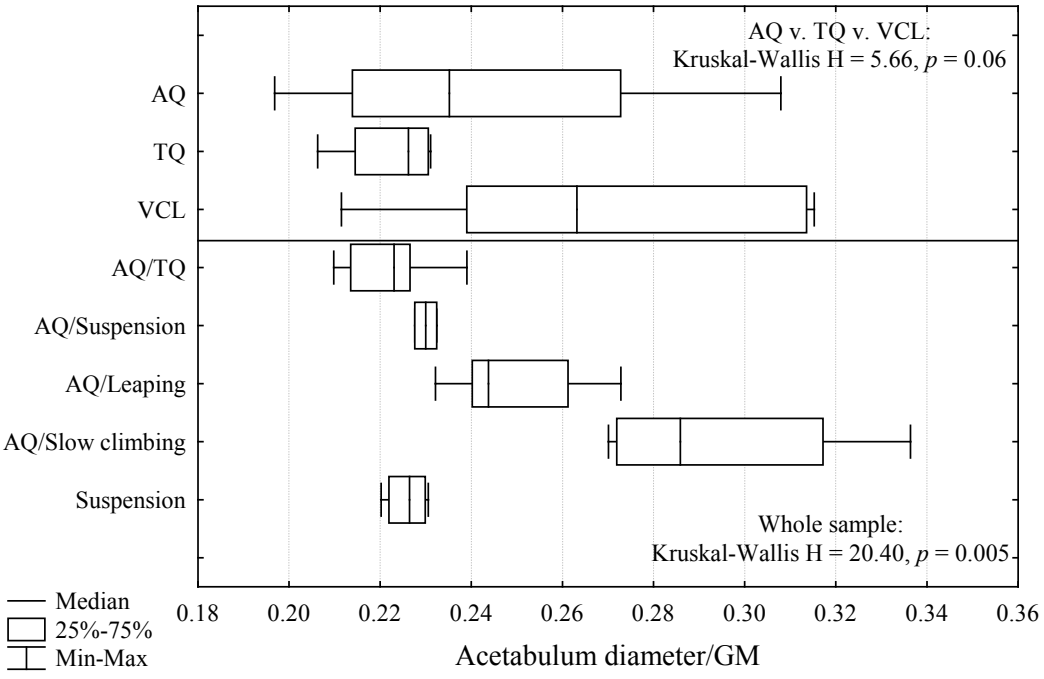

Fig. 4-24. Box-and-whiskers plots comparing the medians and ranges of the acetabulum diameter shape variable for each locomotor group. The three boxes above the horizontal line were used in hypothesis-testing, while the box plots below the horizontal line were not included in *a priori* hypothesis-testing. Kruskal-Wallis tests were performed on both samples, and the *p*-values are listed accordingly.

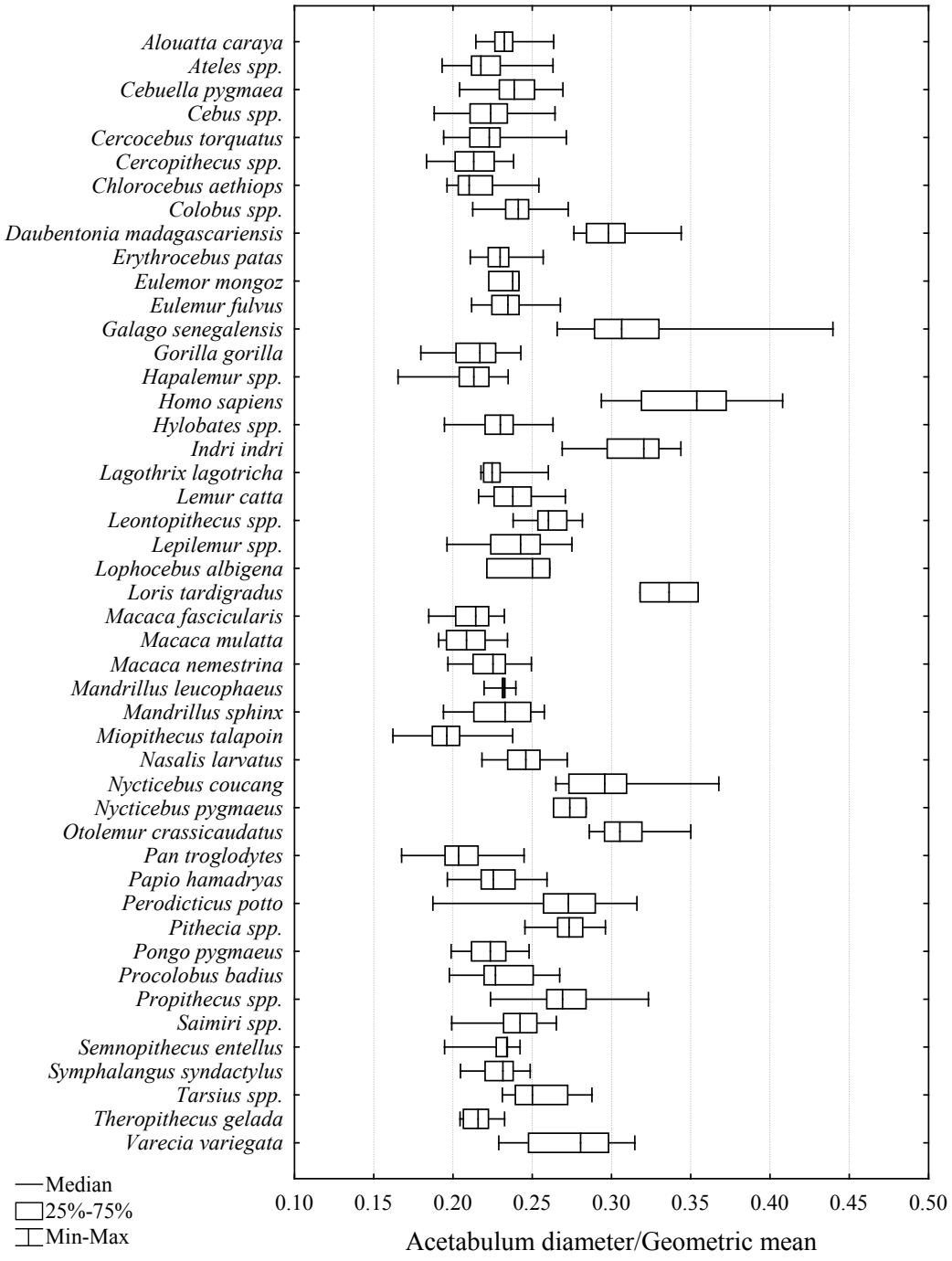

Fig. 4-25. Box-and-whiskers plots of medians and ranges of the acetabulum diameter shape variable for each taxon.

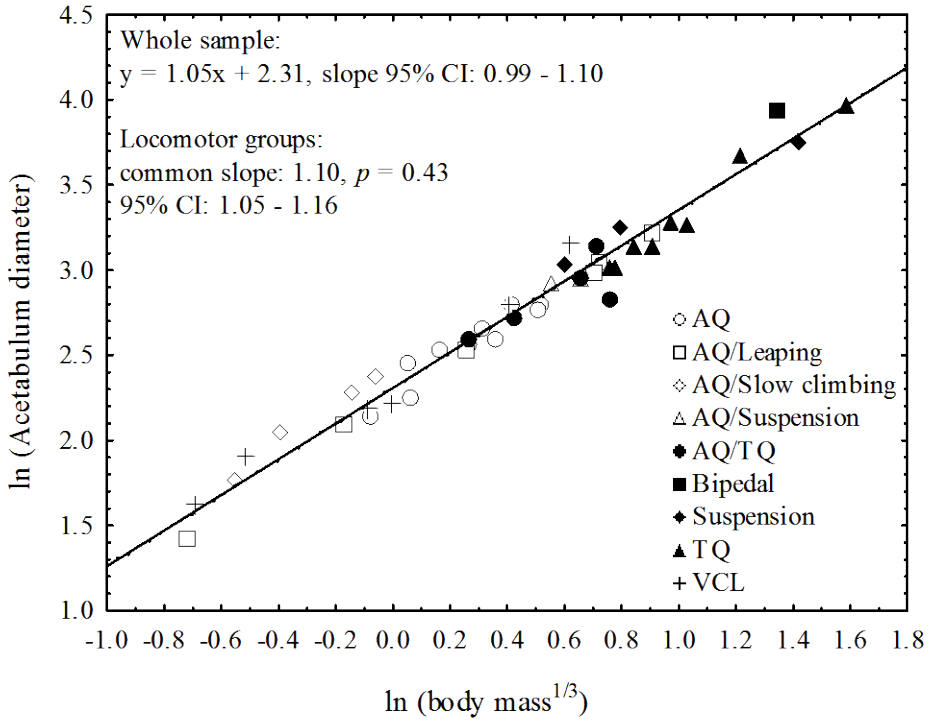

Fig. 4-26. Bivariate plot of ln-acetabulum diameter on ln-body mass$^{1/3}$.

Superior pubic ramus length. Prediction TQ < VCL < AQ. There is no differentiation among taxa in the length of the superior pubic ramus (H = 1.95, p = 0.38); a box plot of locomotor group medians demonstrates overlap among AQ, TQ, and VCL taxa (Fig. 4-27). These results do not support the hypothesized relationship between superior pubic ramus length and locomotor mode.

Qualitatively, slow climbers have much longer superior pubic rami than all other locomotor groups (Fig. 4-27). Suspensory taxa appear to have the shortest superior pubic rami, while all other taxa are intermediate in the length of this trait (Fig. 4-27). The box plot of taxon medians shows that the longest superior pubic rami are those of all four slow climbing taxa (Fig. 4-28). A bivariate plot of ln-superior pubic ramus length on ln-body mass$^{1/3}$ confirms the qualitative results of box plots; slow climbers have very long superior pubic rami

relative to their body size, while most VCL and AQ/leaping taxa have short superior pubic rami relative to body size (Fig. 4-29).

The length of the superior pubic ramus scales with isometry in the primate-wide sample (slope = 0.97, 95% confidence interval 0.89 – 1.06, Table 4-20). Furthermore, an examination of the slopes and 95% confidence intervals of each locomotor group shows no deviations from this overall pattern, with all locomotor groups indicating isometry of superior pubic ramus length (Table 4-20). This result supports the hypothesized isometry in superior pubic ramus length relative to body size in all primates.

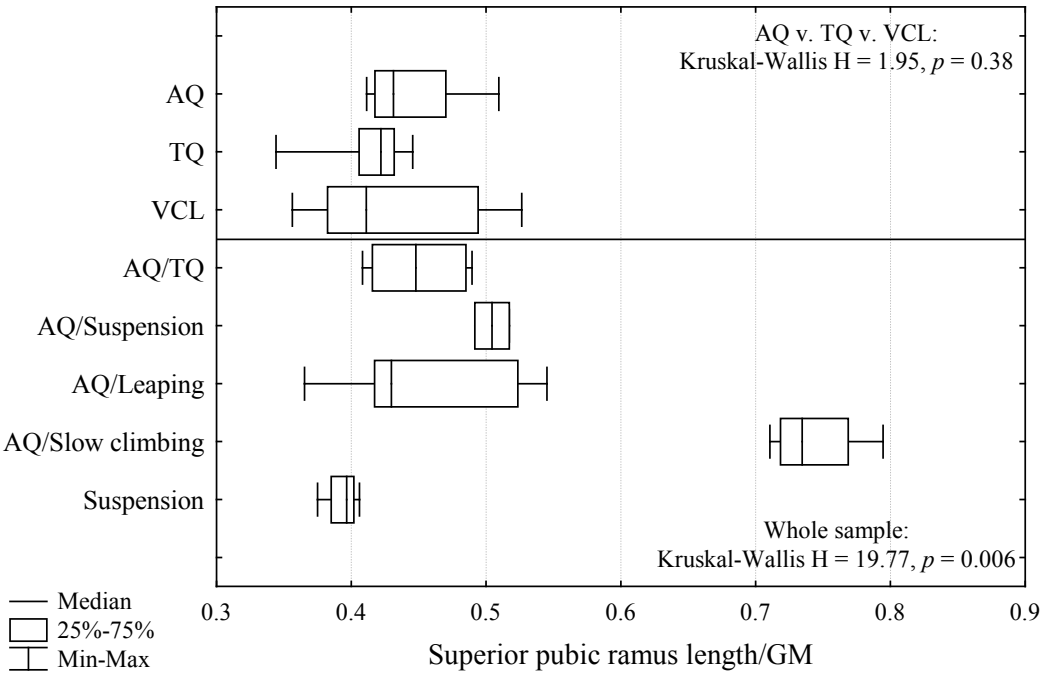

Fig. 4-27. Box-and-whiskers plots comparing the medians and ranges of the superior pubic ramus length shape variable for each locomotor group. The three boxes above the horizontal line were used in hypothesis-testing, while the box plots below the horizontal line were not included in *a priori* hypothesis-testing. Kruskal-Wallis tests were performed on both samples, and the *p*-values are listed accordingly.

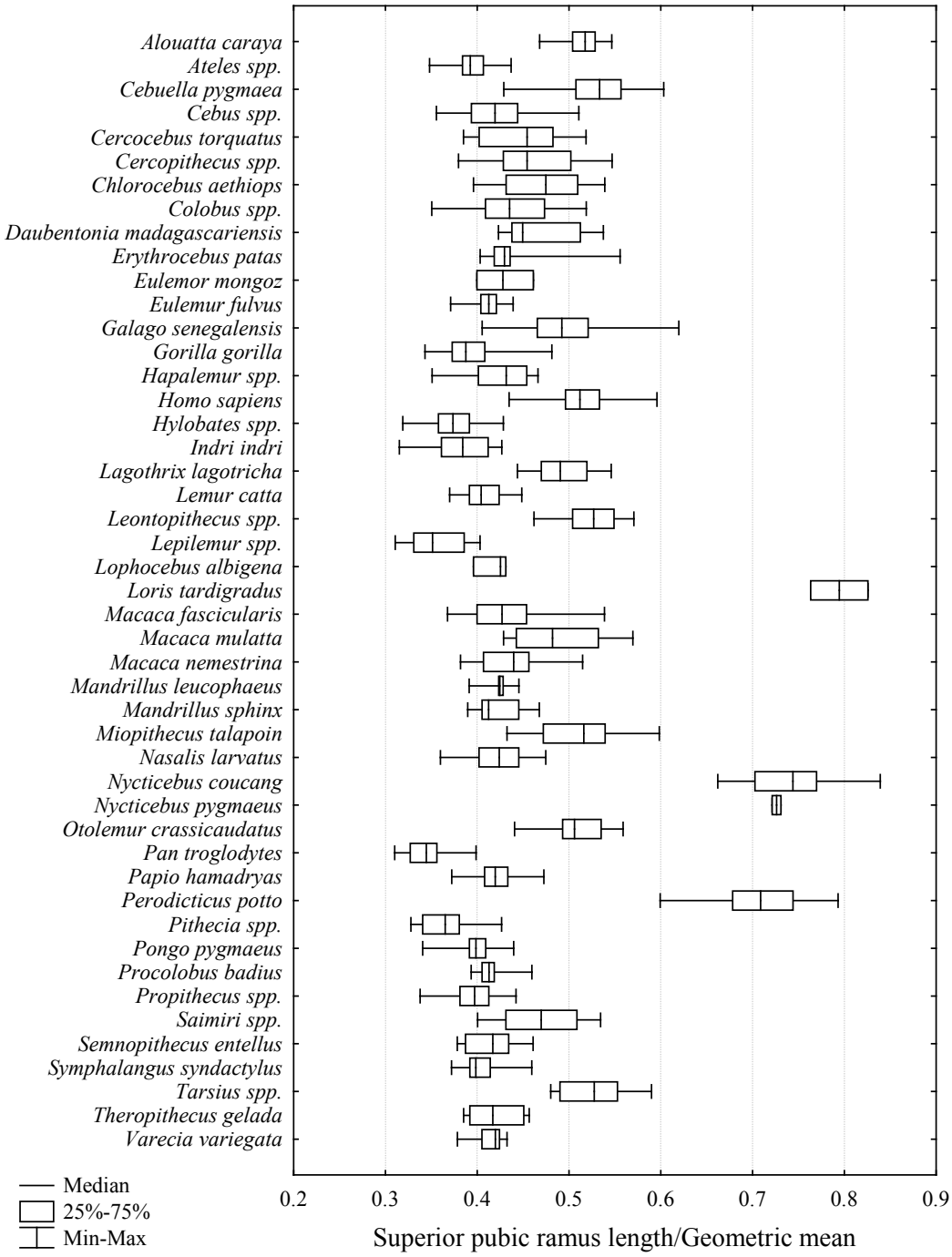

Fig. 4-28. Box-and-whiskers plots of medians and ranges of the superior pubic ramus length shape variable for each taxon.

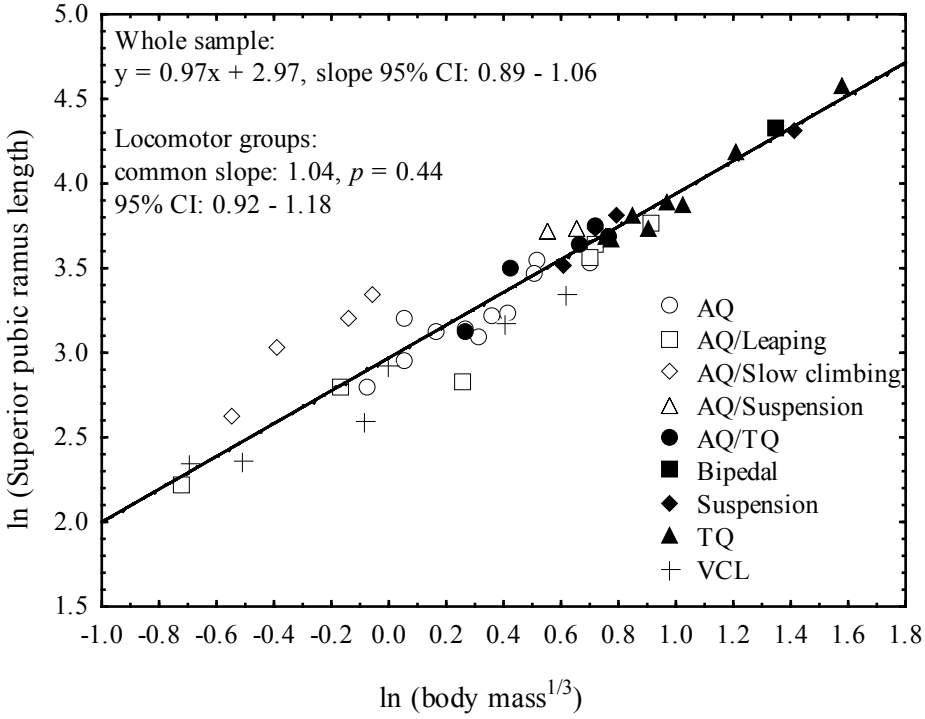

Fig. 4-29. Bivariate plot of ln-superior pubic ramus length on ln-body mass$^{1/3}$.

Inferior pubic ramus length. Prediction TQ < VCL < AQ. There is a significant effect of locomotion on the length of the inferior pubic ramus (H = 8.05, p = 0.02). As predicted, *post hoc* multiple comparisons indicate that arboreal quadrupeds have significantly longer inferior pubic rami than terrestrial quadrupeds (p = 0.01), but contrary to predictions, VCL taxa have a wide range that encompasses both AQ and TQ taxa and are not differentiated from either taxon (Fig. 4-30). These results do not support the specific hypothesis regarding the relationship between inferior pubic ramus length and locomotor mode.

Qualitatively, slow climbers have the longest inferior pubic ramus of all locomotor groups, while suspensory taxa have the shortest; all other locomotor groups are intermediate in inferior pubic ramus length (Fig. 4-30). In addition to suspensory hylobatids, *Indri indri* also has very short inferior pubic ramus lengths

(Fig. 4-31). Interestingly, the large-bodied VCL taxa have shorter inferior pubic rami than the small-bodied taxa (Figs. 4-31 and 4-32). The bivariate plot of ln-inferior pubic ramus length on ln-body mass$^{1/3}$ indicates results similar to those for the superior pubic ramus: slow climbers have longer inferior pubic rami relative to body size, while VCL and AQ/leaping taxa have relatively short inferior pubic rami for their size (Fig. 4-32). In addition, the largest bodied-TQ taxa have relatively long inferior pubic rami for their size (Fig. 4-32).

The length of the inferior pubic ramus scales with isometry in the primate-wide sample (slope = 0.90, 95% confidence interval 0.80 – 1.01, Table 4-20). An examination of the slopes and 95% confidence intervals of each locomotor group shows that only two out of the seven groups are negatively allometric (AQ and VCL taxa), while the rest are isometric relative to body size (Table 4-20). These scaling analyses support the hypothesis of isometry in inferior pubic ramus length relative to body size in the primate-wide sample, but the hypothesis is not upheld within the AQ and VCL locomotor groups.

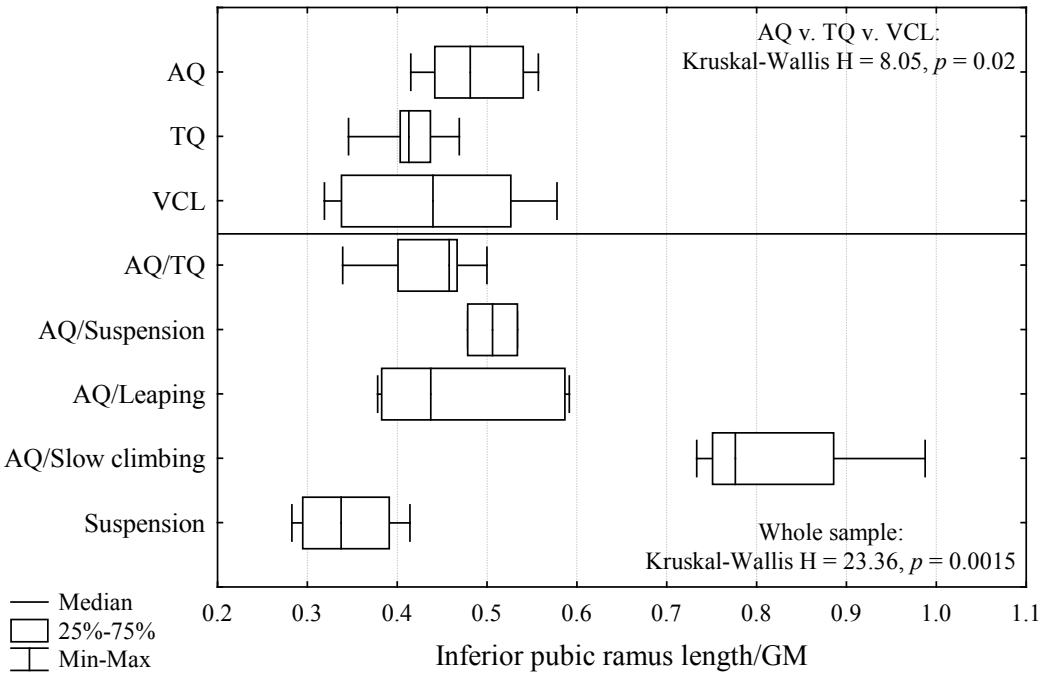

Fig. 4-30. Box-and-whiskers plots comparing the medians and ranges of the inferior pubic ramus length shape variable for each locomotor group. The three boxes above the horizontal line were used in hypothesis-testing, while the box plots below the horizontal line were not included in *a priori* hypothesis-testing. Kruskal-Wallis tests were performed on both samples, and the *p*-values are listed accordingly.

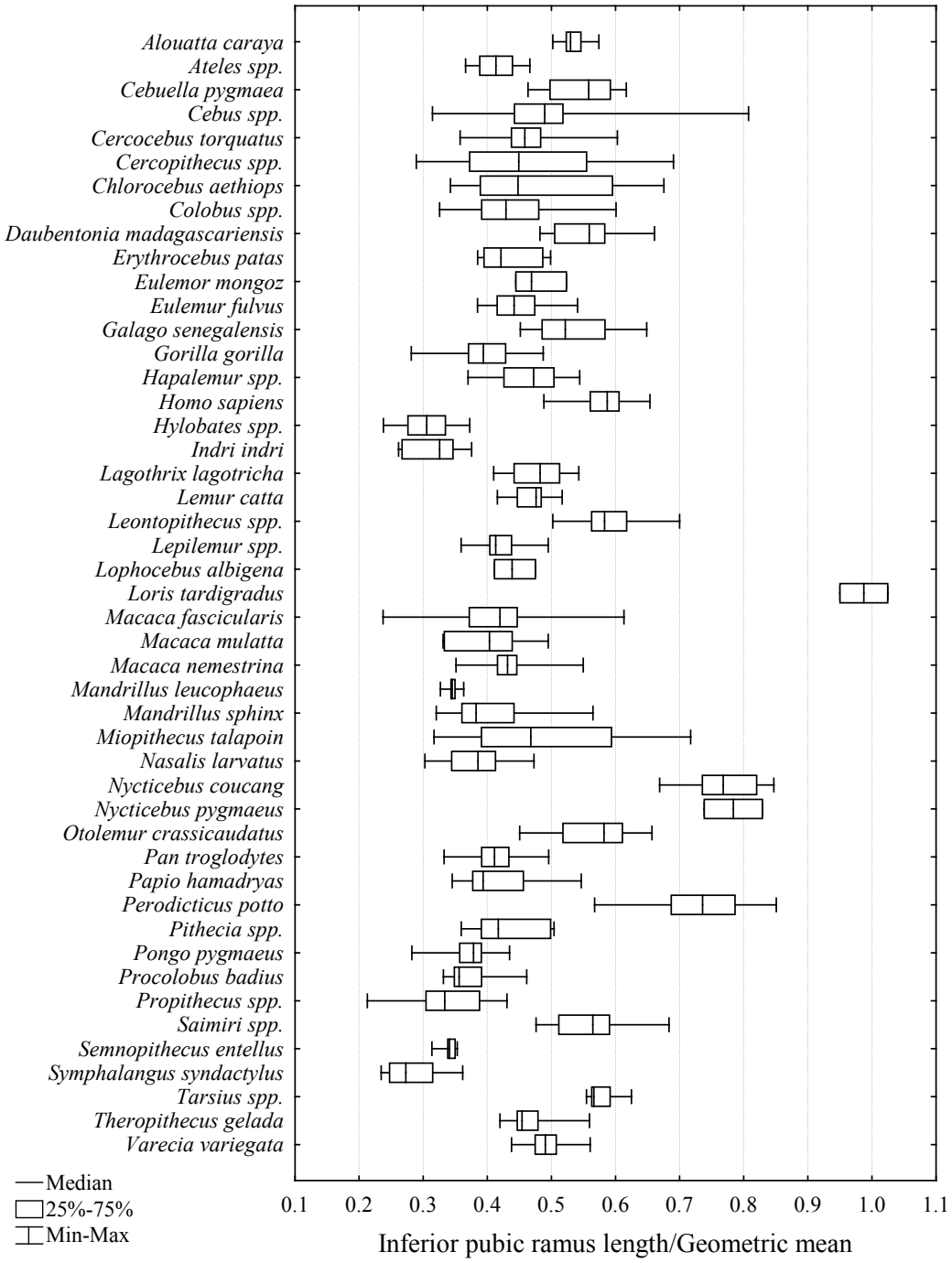

Fig. 4-31. Box-and-whiskers plots of medians and ranges of the inferior pubic ramus length shape variable for each taxon.

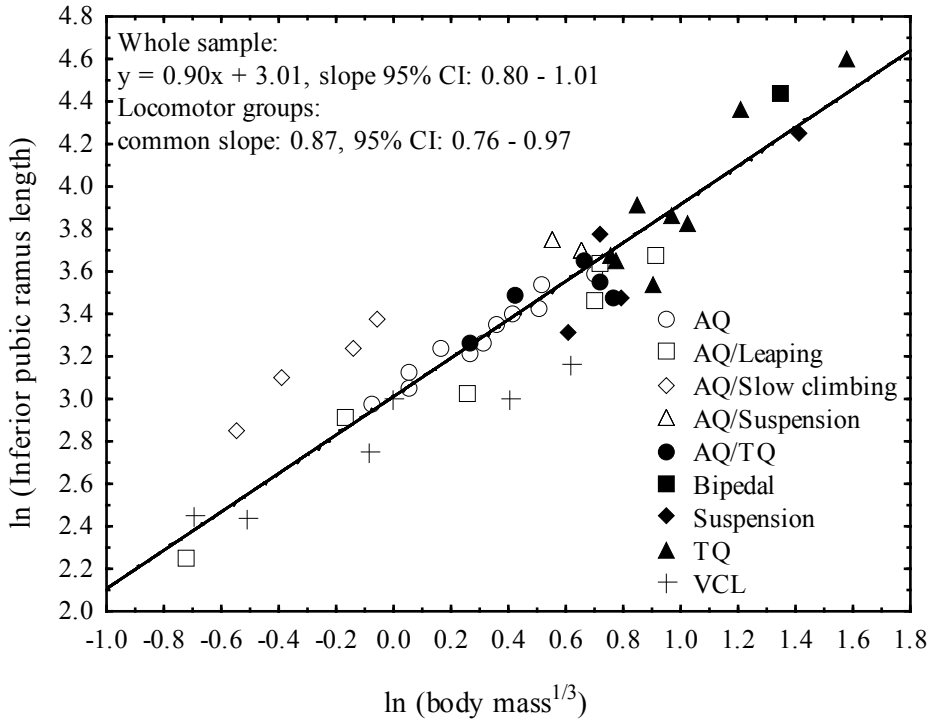

Fig. 4-32. Bivariate plot of ln-inferior pubic ramus length on ln-body mass$^{1/3}$.

Pubic symphysis length. Prediction AQ < TQ < VCL. There is a significant effect of locomotion on the length of the pubic symphysis (H = 7.44, $p = 0.024$), but contrary to predictions, *post hoc* multiple comparisons indicate that terrestrial quadrupeds have significantly longer pubic symphyses than vertical clingers and leapers ($p = 0.02$), and there is no difference between AQ and VCL taxa (Fig. 4-33). These results do not support the specific hypothesis regarding the relationship between pubic symphysis length and locomotion.

Qualitatively, slow climbers have the shortest pubic symphyses among all locomotor groups, while TQ, AQ/TQ, and AQ/leapers have the longest pubic symphyses (Fig. 4-33). A box plot by species shows that there is considerable diversity in pubic symphysis length within terrestrial taxa; large-bodied hominoids have very short symphyses, while smaller-bodied cercopithecines have

some of the longest pubic symphyses of all taxa (Figs. 4-34). In addition, cercopithecines, as a group, have the longest pubic symphyses (Fig. 4-34).

Pubic symphysis length scales with positive allometry in the primate-wide sample (slope = 1.52, 95% confidence interval 1.35 – 1.70, Table 4-20, Fig. 4-35). Among locomotor groups, four out of seven groups exhibit positive allometry in pubic symphysis length (AQ, AQ/leapers, AQ/TQ, and VCL taxa), two groups demonstrate isometry in pubic symphysis length (slow climbers and suspensory taxa), and terrestrial quadrupeds exhibit negative allometry of pubic symphysis length (Table 4-20). The prediction of isometry in this measure is rejected in the overall primate sample, as well as within all locomotor groups except slow climbers and suspensory taxa.

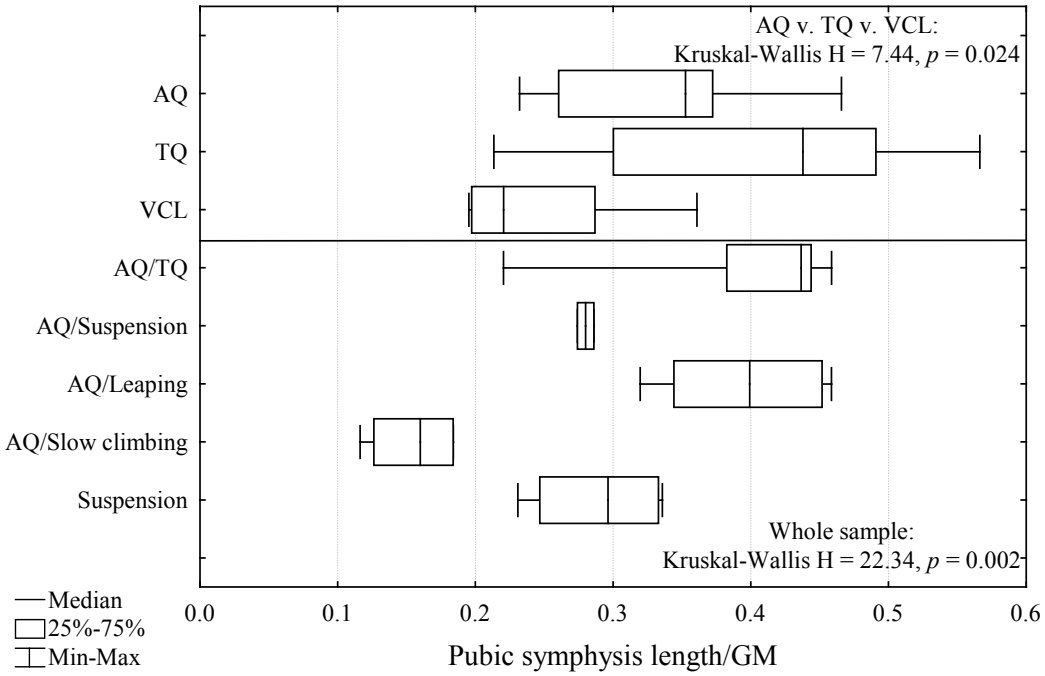

Fig. 4-33. Box-and-whiskers plots comparing the medians and ranges of the pubic symphysis length shape variable for each locomotor group. The three boxes above the horizontal line were used in hypothesis-testing, while the box plots below the horizontal line were not included in *a priori* hypothesis-testing. Kruskal-Wallis tests were performed on both samples, and the *p*-values are listed accordingly.

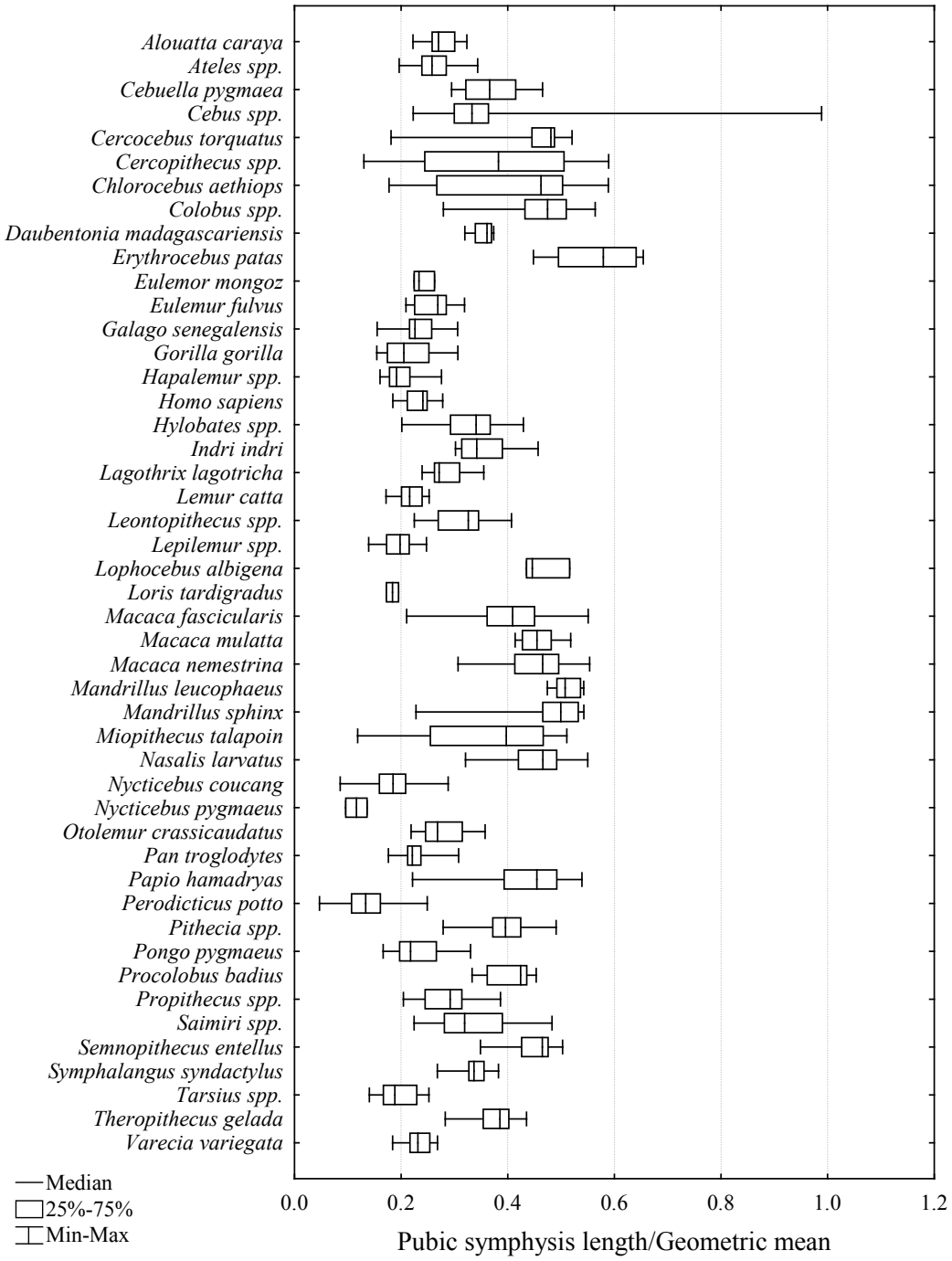

Fig. 4-34. Box-and-whiskers plots of medians and ranges of the pubic symphysis length shape variable for each taxon.

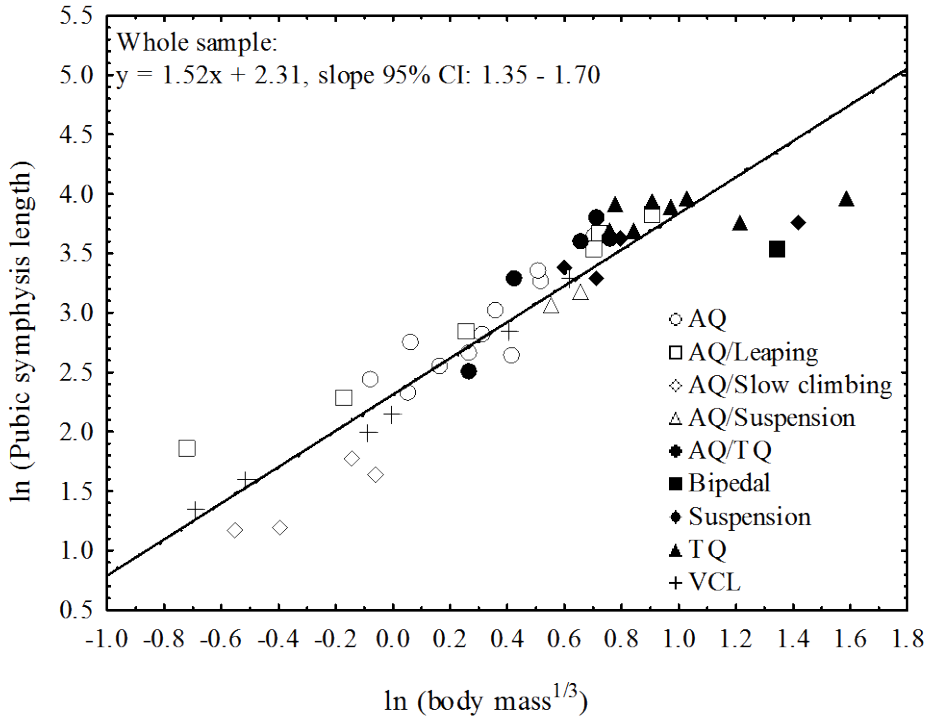

Fig. 4-35. Bivariate plot of ln-pubic symphysis length on ln-body mass$^{1/3}$.

Lower ilium cross-sectional area. Prediction AQ < TQ < VCL. There is a significant effect of locomotion on the cross-sectional area of the lower ilium ($H = 6.31$, $p = 0.04$), but *post hoc* multiple comparisons show that none of the differences among AQ, TQ, and VCL taxa are statistically significant. The box plot of locomotor groups shows that only the whiskers of the AQ and TQ groups overlap (TQ having a larger group median than AQ taxa), while the range of the VCL group is so large that it spans the ranges of both AQ and TQ taxa (Fig. 4-36). These results do not support the specific hypothesis relating lower ilium cross-sectional area to locomotion.

Qualitatively, the box plots of each taxon show that there is a difference due to body size dimorphism within VCL taxa; large-bodied VCL taxa have larger cross-sectional areas of the lower ilium, while the small-bodied taxa have

smaller lower ilium areas (Fig. 4-36). When considering all locomotor groups, the substantial range of the VCL taxa is even more apparent—the range of vertical clingers and leapers encompasses the range of variation among all locomotor groups (Fig. 4-37). The largest ilium cross-sectional areas belong to TQ, AQ/suspensory, and AQ/leaping taxa, while the smallest values belong to slow climbers (Fig. 4-37). Interestingly, a bivariate plot of ln-lower ilium cross-sectional area on ln-body mass$^{1/3}$ demonstrates that terrestrial quadrupeds plot on the regression line (except for *Gorilla*), indicating that they have cross-sectional areas of the lower ilium that are as expected for their size (Fig. 4-38).

The cross-sectional area of the lower ilium scales with positive allometry in the primate-wide sample (slope = 2.75, 95% confidence interval 2.60 – 2.89, Table 4-20). An examination of the slopes and 95% confidence intervals of each locomotor group indicates that three out of seven groups demonstrate isometry in lower ilium cross-sectional area relative to body size (slow climbers, AQ/TQ, and suspensory taxa), while the other four groups all demonstrate positive allometry of lower ilium cross-sectional area (Table 4-20). The hypothesis of positive allometry in this measure is supported in the overall primate sample, and within some locomotor groups. However, this hypothesis is rejected in slow climbers, semi-terrestrial taxa, and suspensory taxa.

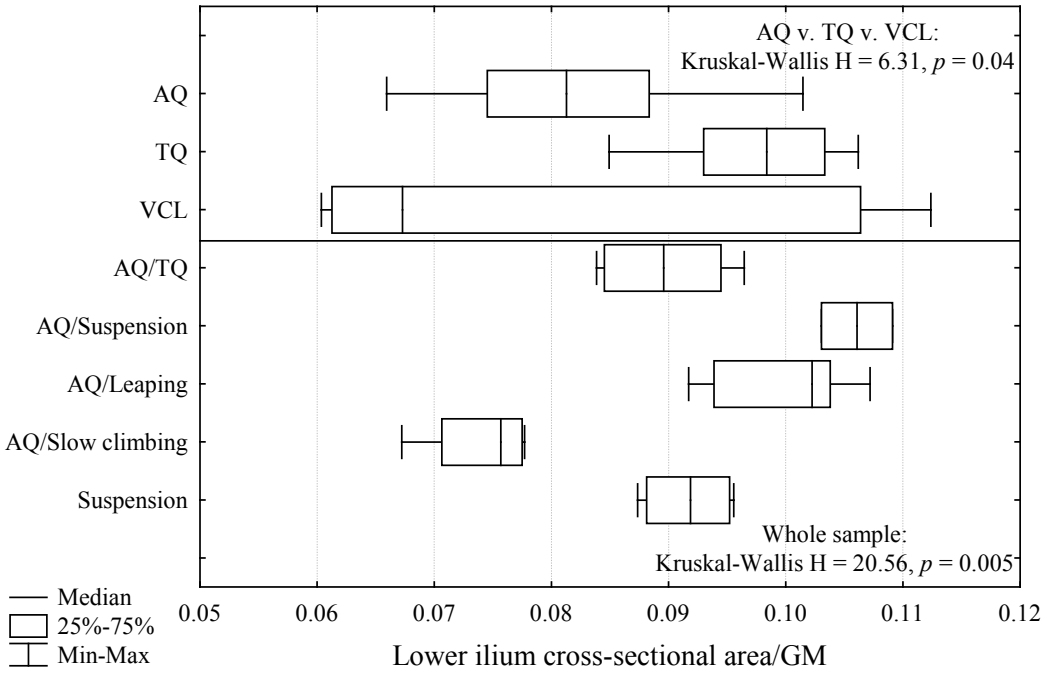

Fig. 4-36. Box-and-whiskers plots comparing the medians and ranges of the lower ilium cross-sectional area shape variable for each locomotor group. The three boxes above the horizontal line were used in hypothesis-testing, while the box plots below the horizontal line were not included in *a priori* hypothesis-testing. Kruskal-Wallis tests were performed on both samples, and the *p*-values are listed accordingly.

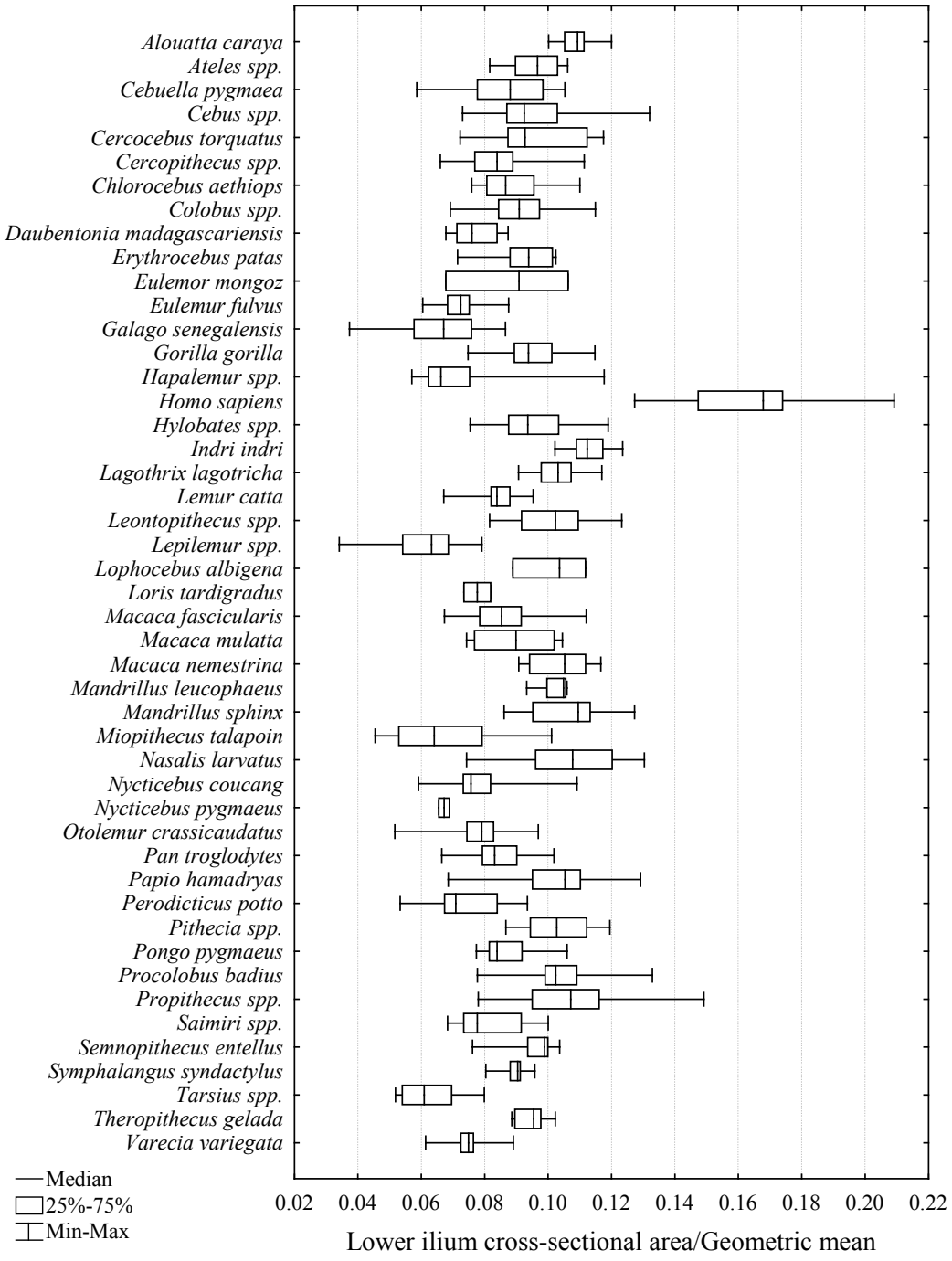

Fig. 4-37. Box-and-whiskers plots of medians and ranges of the lower ilium cross-sectional area shape variable for each taxon.

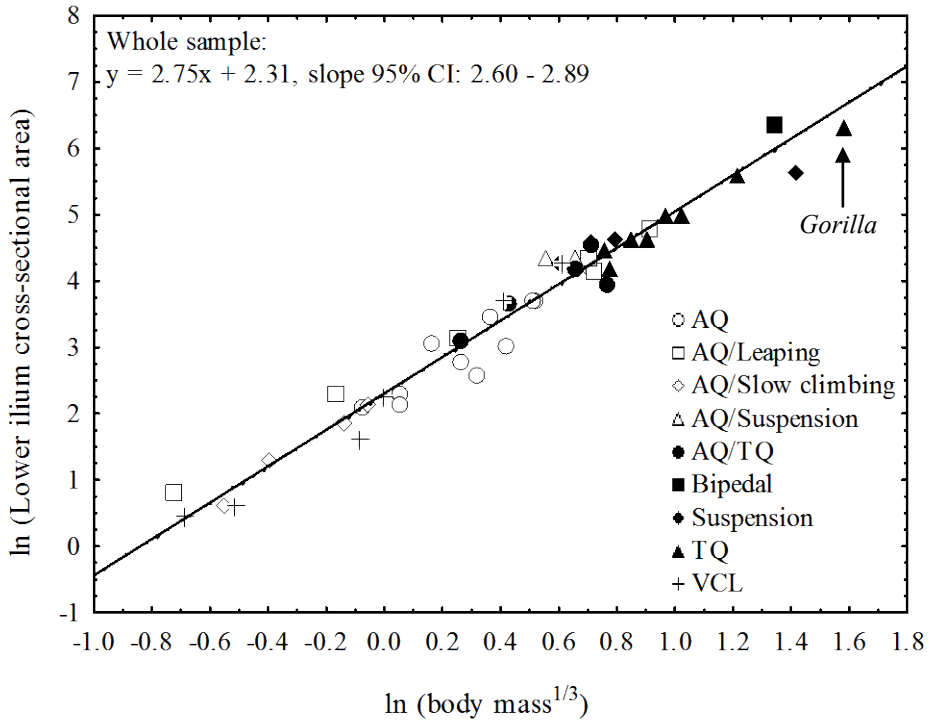

Fig. 4-38. Bivariate plot of ln-lower ilium cross-sectional area on ln-body mass$^{1/3}$.

Ischium cross-sectional area. Prediction: AQ < TQ < VCL. There is a significant effect of locomotion on the cross-sectional area of the ischium (H = 12.79, p = 0.002). Contrary to the predictions, *post hoc* comparisons demonstrate that terrestrial quadrupeds have significantly larger ischium cross-sectional areas than both AQ (p = 0.04) and VCL taxa (p = 0.002), and there is no difference between AQ and VCL taxa (Fig. 4-39). These results do not support the specific hypothesis of the relationship between ischium cross-sectional area and locomotion.

Qualitatively, the box plot of locomotor groups demonstrates that in general, the ranges of the locomotor groups are wide and there is extensive overlap among groups (Fig. 4-39). Among all locomotor categories, vertical clingers and leapers have the smallest ischium cross-sectional areas while

terrestrial quadrupeds have the largest median values for this trait (Fig. 4-39). The box plots by species and the bivariate plot indicate that *Homo sapiens*, large-bodied cercopithecines, and, surprisingly, *Loris tardigradus* have large ischium cross-sectional areas relative to body size, while most VCL taxa have relatively small ischium cross-sectional areas (Figs. 4-40 and 4-41).

The cross-sectional area of the ischium scales with positive allometry relative to body size in the primate-wide sample (slope = 2.51, 95% confidence interval 2.37 – 2.65, Table 4-20). Regressions for each of the individual locomotor groups indicate that they do not share the same scaling relationship; five of the groups demonstrate isometry relative to body size, while two (AQ and AQ/leapers) have ischium cross-sectional areas that are positively allometric relative to body size (Table 4-20). The hypothesis that ischium cross-sectional area scales with positive allometry relative to body size is upheld in the primate-wide sample, and within AQ and AQ/leaping taxa, but it is rejected for the other five locomotor groups.

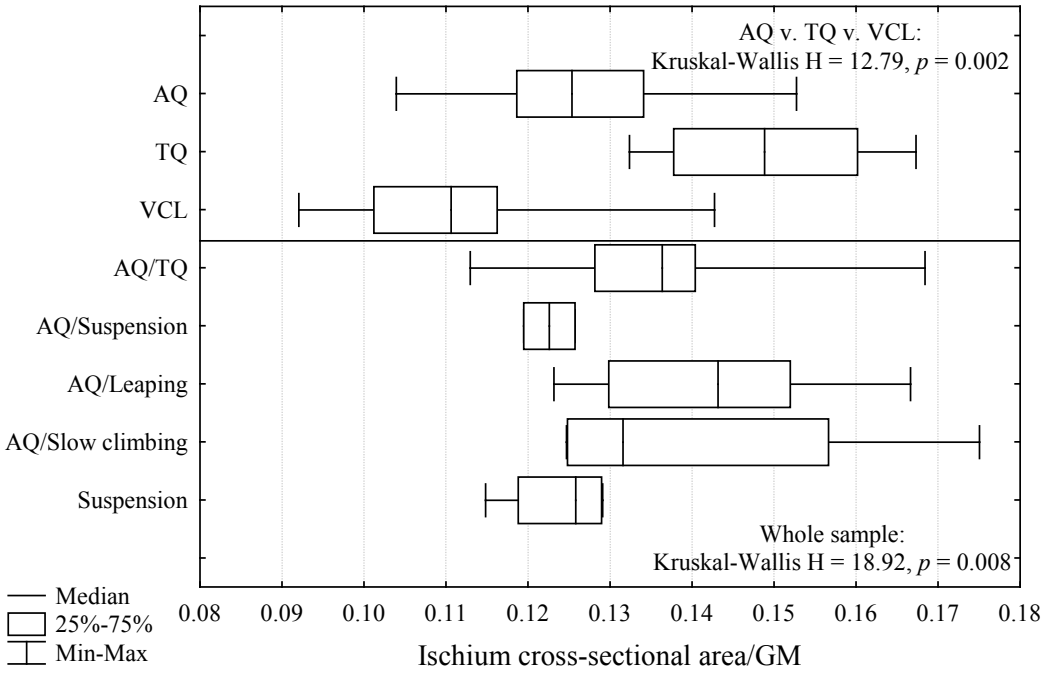

Fig. 4-39. Box-and-whiskers plots comparing the medians and ranges of the ischium cross-sectional area shape variable for each locomotor group. The three boxes above the horizontal line were used in hypothesis-testing, while the box plots below the horizontal line were not included in *a priori* hypothesis-testing. Kruskal-Wallis tests were performed on both samples, and the *p*-values are listed accordingly.

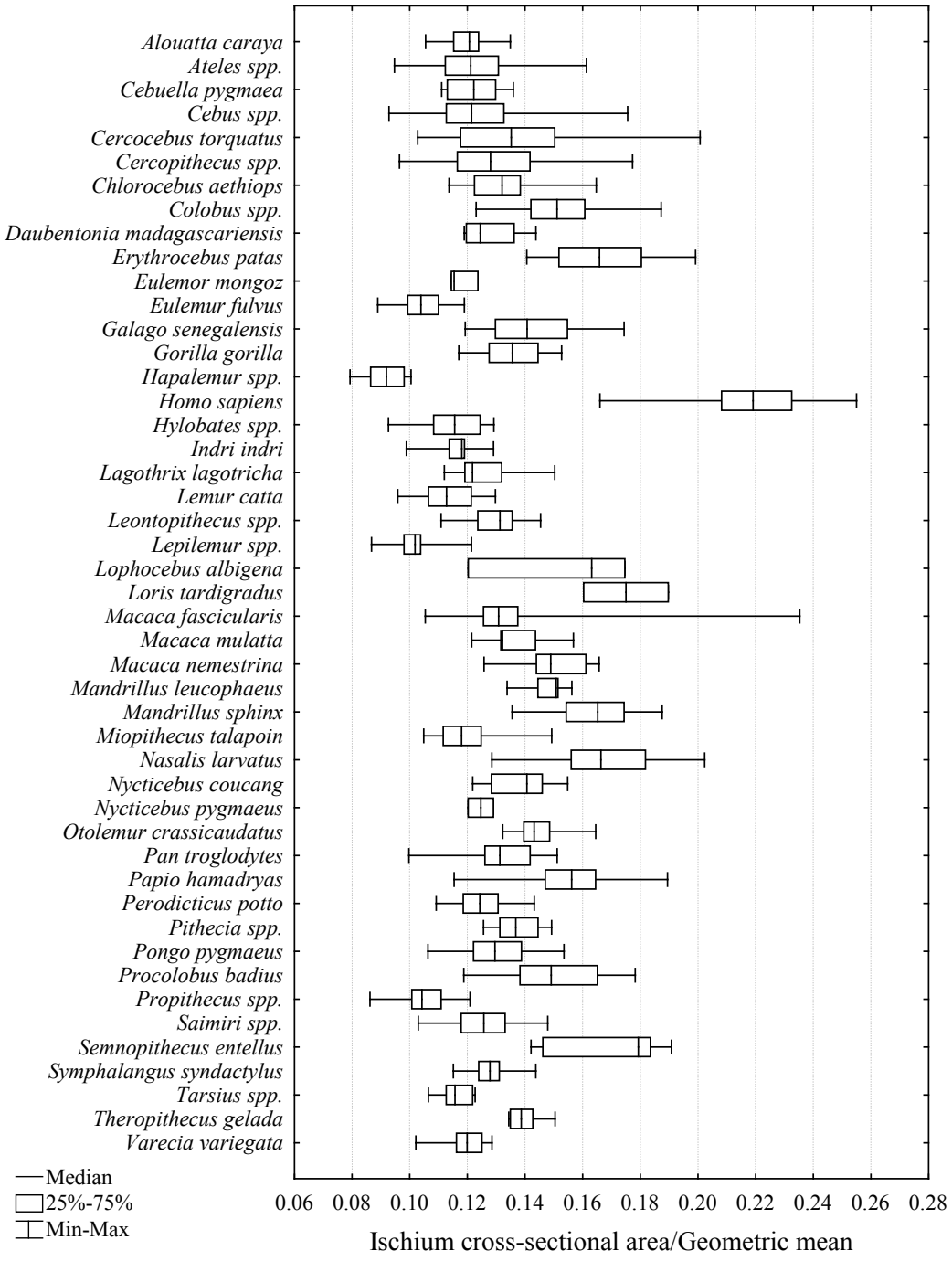

Fig. 4-40. Box-and-whiskers plots of medians and ranges of the ischium cross-sectional area shape variable for each taxon.

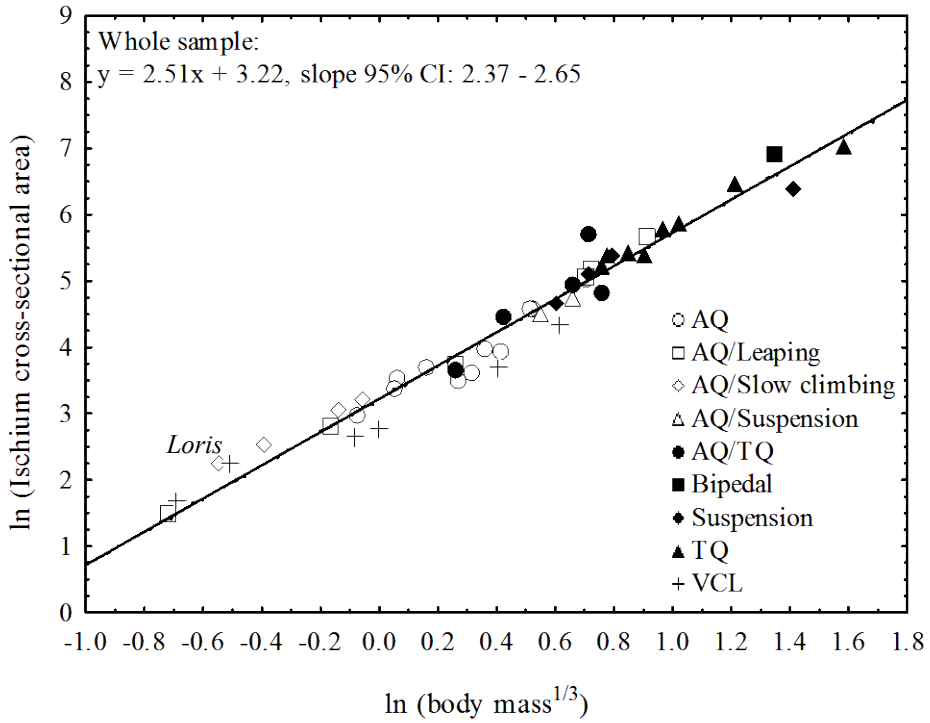

Fig. 4-41. Bivariate plot of ln-ischium cross-sectional area on ln-body mass$^{1/3}$.

Superior pubic ramus cross-sectional area. Prediction: AQ < TQ < VCL. There is no effect of locomotion on the cross-sectional area of the superior pubic ramus ($H = 1.97$, $p = 0.37$). The box plot of locomotor group medians shows that arboreal and terrestrial quadrupeds have the same median, and these two groups have somewhat larger superior pubic ramus cross-sectional areas than vertical clingers and leapers (Fig. 4-42). These results do not support the hypothesis that superior pubic ramus cross-sectional area differs according to locomotion.

Qualitatively, a comparison of all locomotor categories reveals that slow climbers and *Homo sapiens* have the largest superior pubic ramus cross-sectional area relative to body size, while suspensory, VCL, and large-bodied TQ taxa have the smallest (Figs. 4-42 and 4-43). A bivariate plot of ln-superior pubic ramus cross-sectional area on ln-body mass$^{1/3}$ confirms this finding and also

demonstrates AQ/leapers have smaller superior pubic ramus cross-sectional areas than expected for their size (Fig. 4-44).

The cross-sectional area of the superior pubic ramus scales with positive allometry relative to body size in the primate-wide sample (slope = 2.17, 95% confidence interval 2.03 – 2.30, Table 4-20). However, an examination of the individual slopes and 95% confidence intervals for each locomotor group indicates that only *one* group demonstrates positive allometry of the superior pubic ramus cross-sectional area (AQ/leapers, slope = 2.43), while all other locomotor groups exhibit isometry relative to body size in this measure (Table 4-20). The prediction of positive allometry in this measure is supported in the overall primate sample, but within locomotor categories, is rejected for all groups except for AQ/leapers.

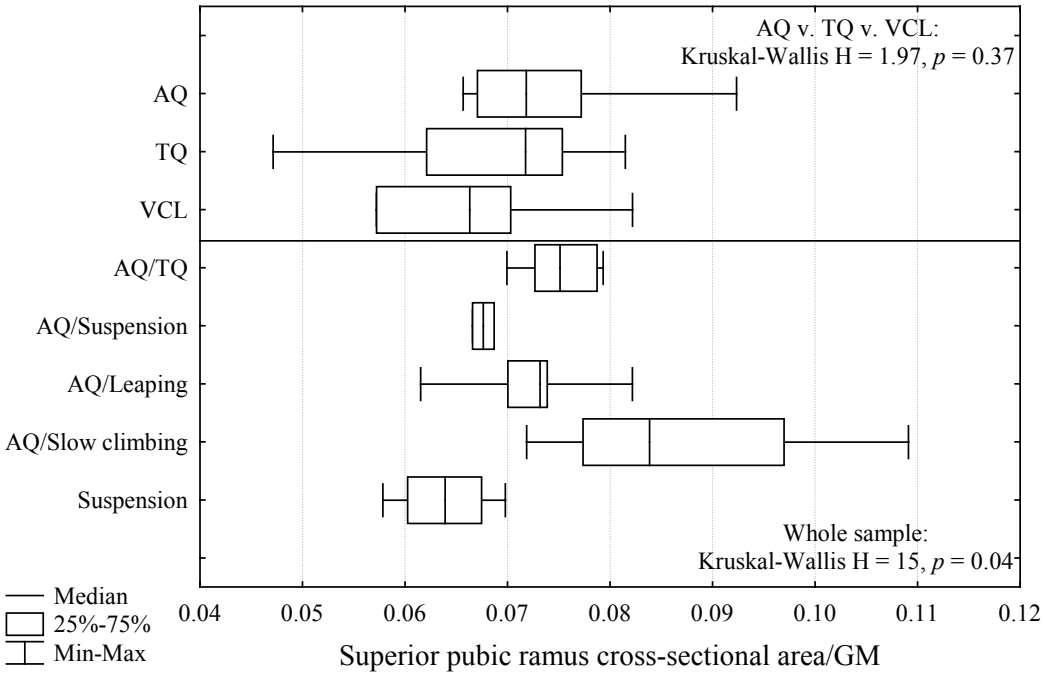

Fig. 4-42. Box-and-whiskers plots comparing the medians and ranges of the superior pubic ramus cross-sectional area shape variable for each locomotor group. The three boxes above the horizontal line were used in hypothesis-testing, while the box plots below the horizontal line were not included in *a priori* hypothesis-testing. Kruskal-Wallis tests were performed on both samples, and the *p*-values are listed accordingly.

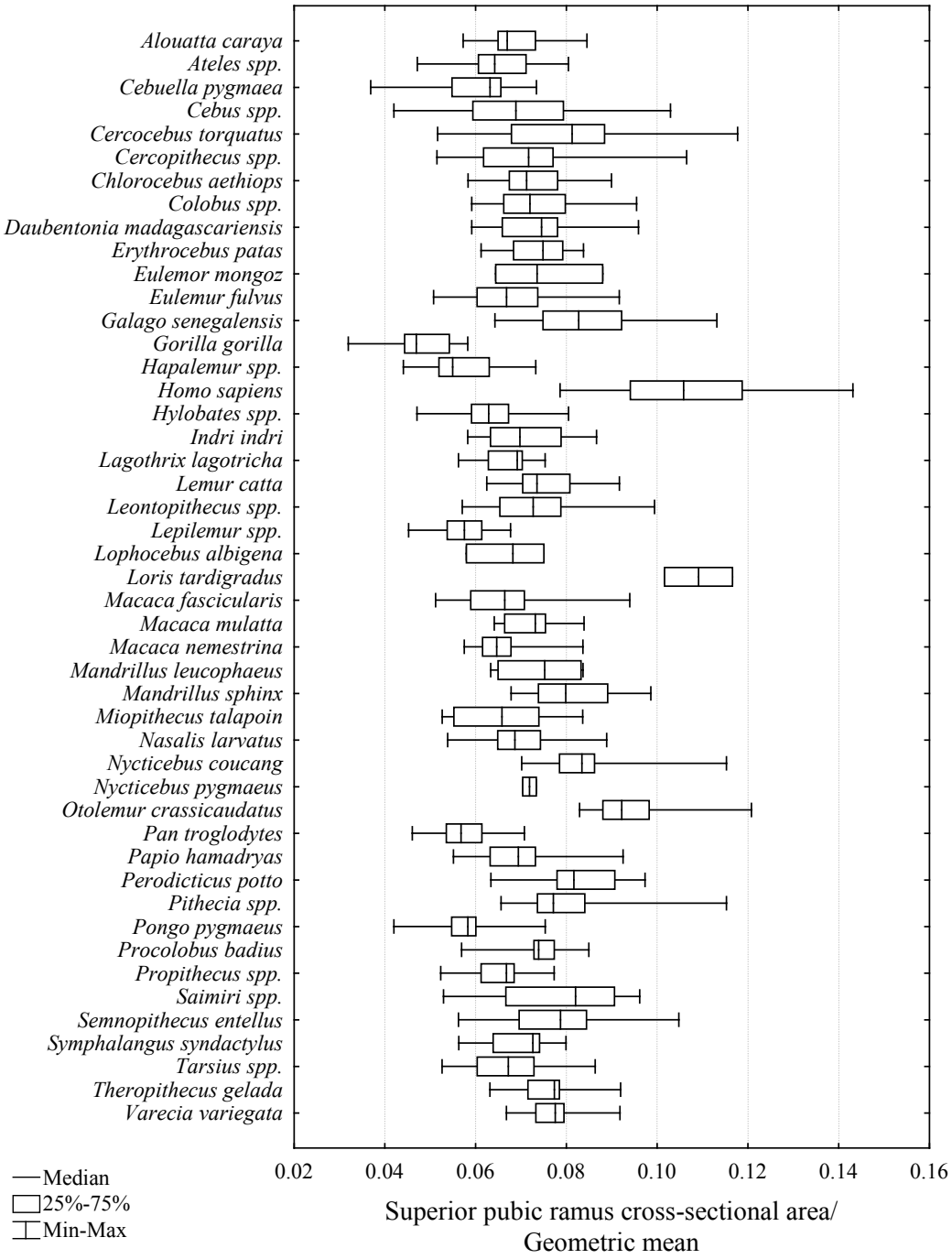

Fig. 4-43. Box-and-whiskers plots of medians and ranges of the superior pubic ramus cross-sectional area shape variable for each taxon.

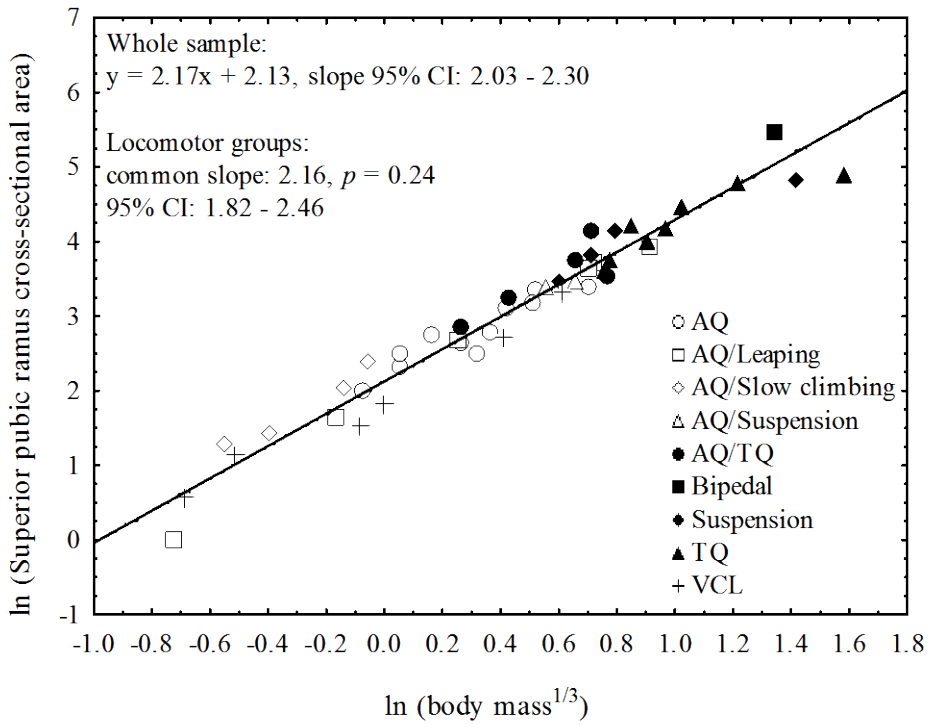

Fig. 4-44. Bivariate plot of ln-superior pubic ramus cross-sectional area on ln-body mass$^{1/3}$.

Inferior pubic ramus cross-sectional area. Prediction: AQ < TQ < VCL. There is a significant effect of locomotion on the cross-sectional area of the inferior pubic ramus (H = 14.21, p = 0.0008). However, contrary to the predictions, *post hoc* comparisons demonstrate that terrestrial quadrupeds have significantly larger cross-sectional areas of the inferior pubic ramus compared to vertical clingers and leapers (p = 0.0006), and there is no difference between terrestrial and arboreal quadrupeds or between arboreal quadrupeds and vertical clingers and leapers (Fig. 4-45). These results do not support the specific hypothesis relating inferior pubic ramus cross-sectional area to locomotion.

Qualitatively, among all locomotor categories, it is apparent that there is substantial variation within the AQ, AQ/TQ, and AQ/leaping locomotor groups,

which have the largest inferior pubic ramus cross-sectional areas (Fig. 4-45). A box plot of taxon medians reveals considerable spread within specific AQ taxa (especially *Cercopithecus* spp., *Macaca fascicularis*, and *Miopithecus talapoin*) and TQ taxa (*Macaca nemestrina, Mandrillus sphinx*, and *Papio hamadryas*, Fig. 4-46). Both AQ and VCL strepsirrhines, on the other hand, have narrow ranges and have the smallest cross-sectional areas of the inferior pubic ramus (Figs. 4-45 and 4-46). These differences are also demonstrated in a bivariate plot of ln-inferior pubic ramus cross-sectional area on ln-body mass$^{1/3}$ (Fig. 4-47).

This substantial variation within locomotor groups appears to be driven by cercopithecids. These monkeys have wide ranges of variation, as well as relatively large cross-sectional areas. While the large range of variation may be due to sexual dimorphism within these taxa, it is quite likely that the relatively large inferior pubic ramus cross-sectional areas—as compared to other taxa—may be related to the presence of ischial callosities in these taxa. Ischial callosities (Washburn, 1957; Rose, 1974a; Vilensky, 1978) result in large, flaring ischial tuberosities (Rose, 1974a), which, upon visual examination, appear to also result in craniocaudally deep inferior pubic rami, which would increase the cross-sectional area of the rami. The hominoids, in comparison, also share a large range of variation with the cercopithecids, but they do not have large cross-sectional areas; instead, the apes (which, besides *Hylobates*, do not possess ischial callosities) demonstrate relatively smaller cross-sectional areas of the inferior pubic ramus, which supports the hypothesis that inferior pubic ramus cross-

sectional area is relatively large in cercopithecids as a result of the presence of ischial callosities.

The cross-sectional area of the inferior pubic ramus scales with strong positive allometry in the primate-wide sample (slope = 3.60, 95% confidence interval 3.22 – 3.98, Table 4-20). The locomotor groups do not share a common scaling relationship; three out of the seven locomotor groups demonstrate isometry of inferior pubic ramus cross-sectional area (slow climbers, suspensory, and terrestrial quadrupedal taxa), while the other four locomotor groups demonstrate strong positive allometry (Table 4-19). The relatively large slopes and/or confidence intervals for AQ, AQ/slow, AQ/TQ, and suspensory taxa (Table 4-20) suggest that this trait is highly variable within and among locomotor groups and may not be particularly informative regarding its relationship to locomotor function. In summary, the prediction of positive allometry in this measure is supported for the entire primate sample, but within locomotor categories, the prediction is rejected for slow climbers, suspensory taxa, and terrestrial quadrupeds.

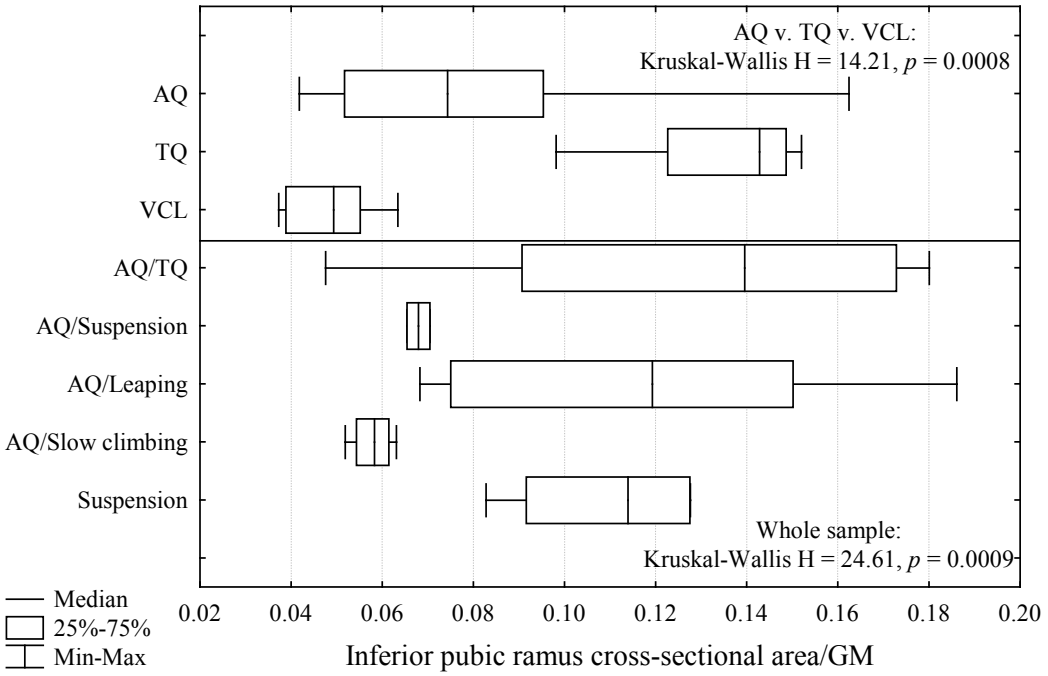

Fig. 4-45. Box-and-whiskers plots comparing the medians and ranges of the inferior pubic ramus cross-sectional area shape variable for each locomotor group. The three boxes above the horizontal line were used in hypothesis-testing, while the box plots below the horizontal line were not included in *a priori* hypothesis-testing. Kruskal-Wallis tests were performed on both samples, and the *p*-values are listed accordingly.

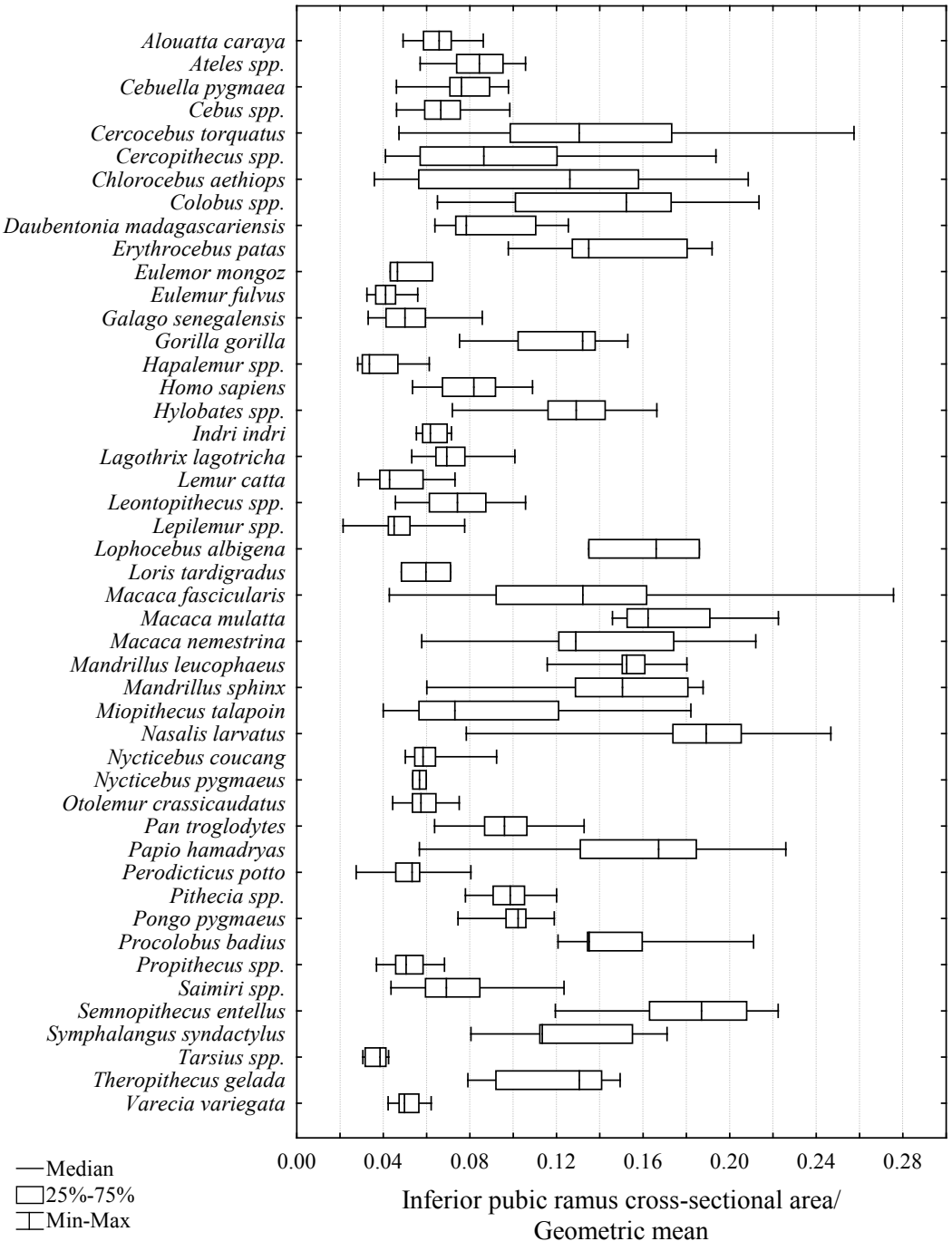

Fig. 4-46. Box-and-whiskers plots of medians and ranges of the inferior pubic ramus cross-sectional area shape variable for each taxon.

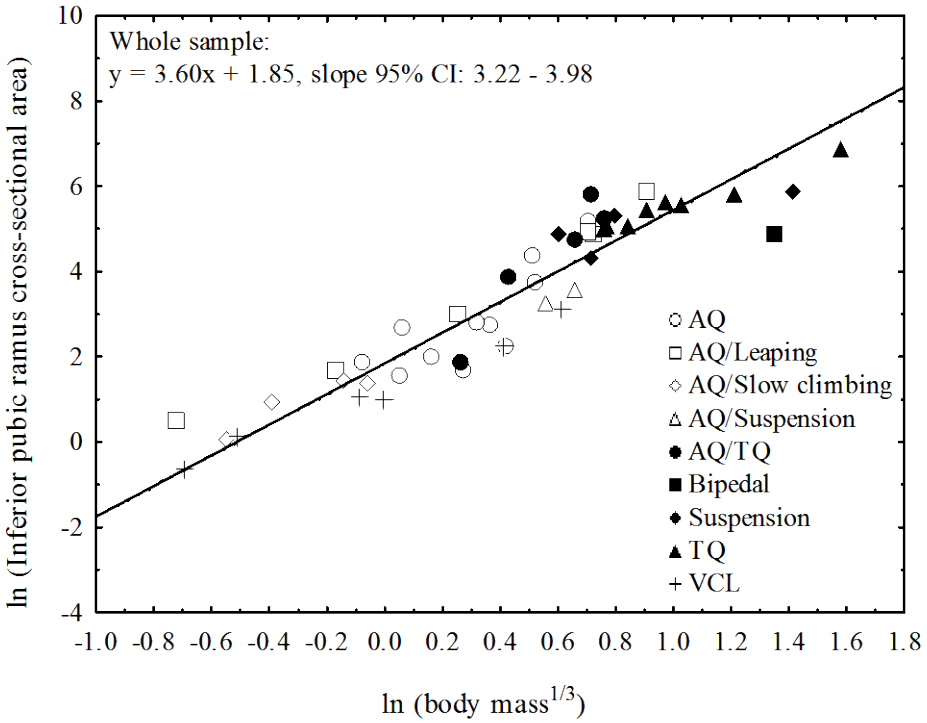

Fig. 4-47. Bivariate plot of ln-inferior pubic ramus cross-sectional area on ln-body mass$^{1/3}$.

Auricular surface area. Prediction: AQ < TQ < VCL. There is no effect of locomotion on the area of the auricular surface (H = 4.42, p = 0.11). The box plot of locomotor groups indicates that quadrupeds have very similar medians and that vertical clingers and leapers have slightly smaller auricular surfaces (Fig. 4-48). These results do not support the hypothesis that auricular surface area differs according to locomotion.

Qualitatively, a box plot of taxa confirms these findings. Among all locomotor categories, slow climbers, AQ/leaping, and AQ/suspensory taxa have the largest auricular surfaces relative to body size, while the remaining locomotor groups all overlap in the auricular surface area (Figs. 4-48 and 4-49). A bivariate plot of ln-auricular surface area on ln-body mass$^{1/3}$ demonstrates that slow

climbers and bipeds have large auricular surfaces for their size, and vertical clingers and leapers have small auricular surfaces for their size (Fig. 4-50).

The area of the auricular surface scales with positive allometry in the primate-wide sample (slope = 2.27, 95% confidence interval 2.12 – 2.43, Table 4-20). Individually, the slopes and 95% confidence intervals of each locomotor group demonstrate isometry relative to body size in the area of the auricular surface (Table 4-20). Therefore, the prediction that auricular surface scales with positive allometry is upheld in the primate-wide sample, but is rejected within each locomotor subgroup.

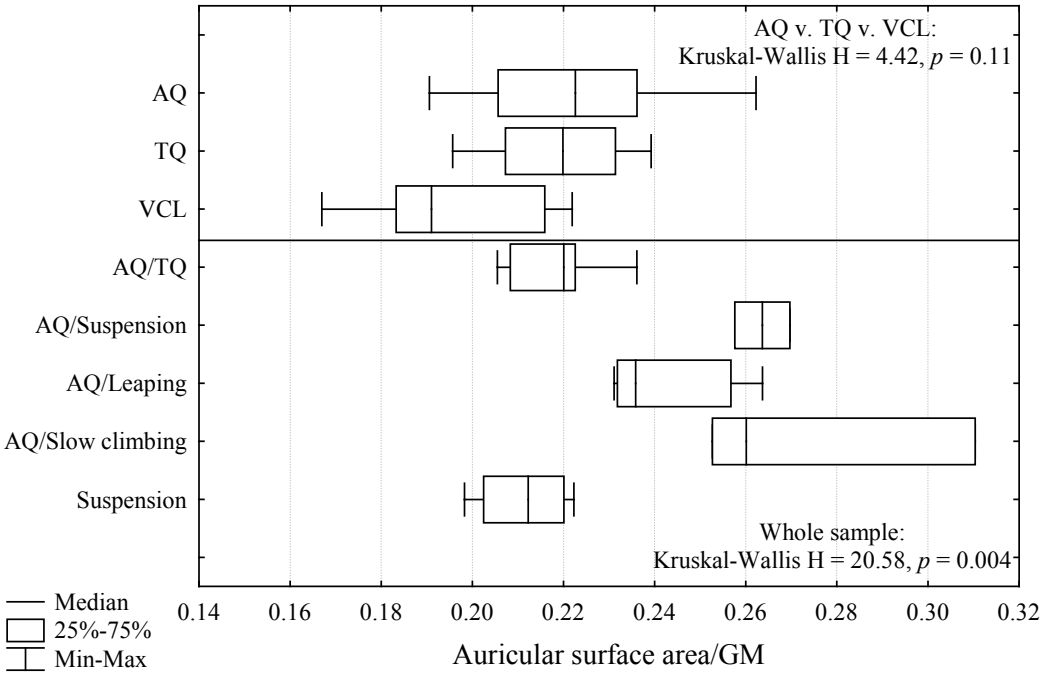

Fig. 4-48. Box-and-whiskers plots comparing the medians and ranges of the auricular surface area shape variable for each locomotor group. The three boxes above the horizontal line were used in hypothesis-testing, while the box plots below the horizontal line were not included in *a priori* hypothesis-testing. Kruskal-Wallis tests were performed on both samples, and the *p*-values are listed accordingly.

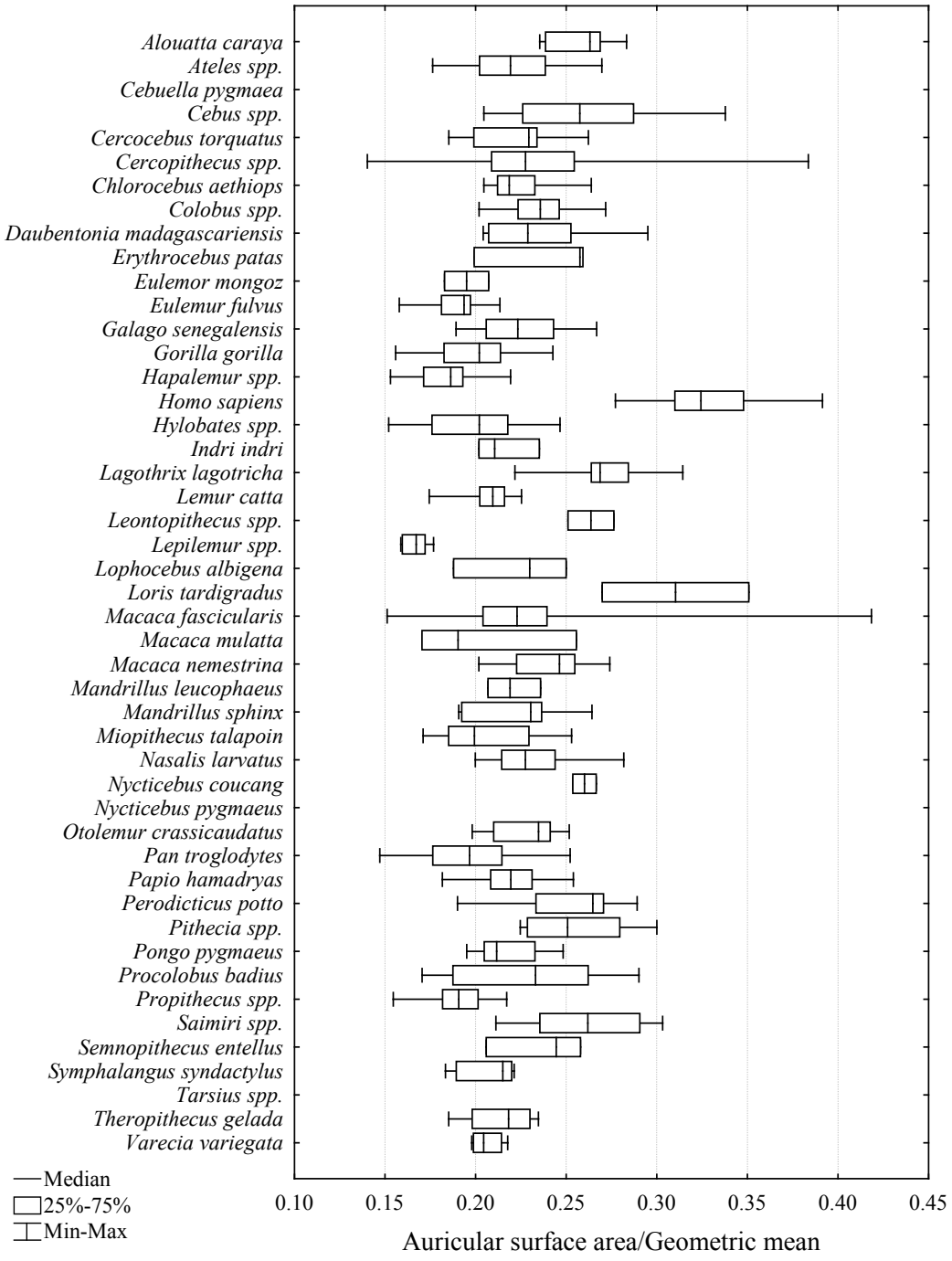

Fig. 4-49. Box-and-whiskers plots of medians and ranges of the auricular surface area shape variable for each taxon.

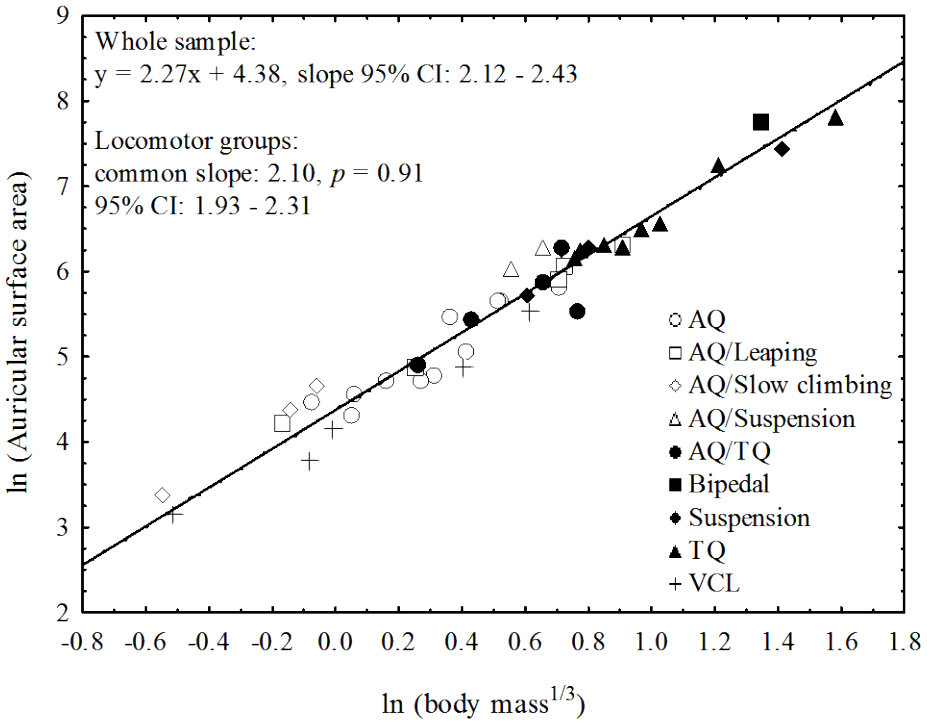

Fig. 4-50. Bivariate plot of ln-auricular surface area on ln-body mass$^{1/3}$.

Pubic symphysis area. Prediction: AQ < TQ < VCL. There is no effect of locomotion on the area of the pubic symphysis (H = 0.035, p = 0.98). This result does not support the hypothesis that pubic symphysis area differs according to locomotor mode. Box plots of locomotor groups and taxon medians indicate total overlap (Figs. 4-51 and 4-52), and a bivariate plot of ln-pubic symphysis area on ln-body mass$^{1/3}$ for the entire primate sample indicates an even scatter of points within each locomotor group around the regression line (Fig. 4-53). Qualitatively, AQ/leapers have the largest area of the pubic symphysis and AQ/suspensory taxa have the smallest (Fig. 4-51).

The area of the pubic symphysis scales with positive allometry in the primate-wide sample (slope = 2.31, 95% confidence interval 2.16 – 2.46, Table 4-20). An examination of the slopes and 95% confidence intervals for each group

demonstrates that the only locomotor group that exhibits allometry is terrestrial quadrupeds (positively allometric slope = 2.74, Table 4-20). The prediction of positive allometry in pubic symphysis area is supported in the primate-wide sample, but within locomotor categories, it is rejected in all groups except for terrestrial quadrupeds.

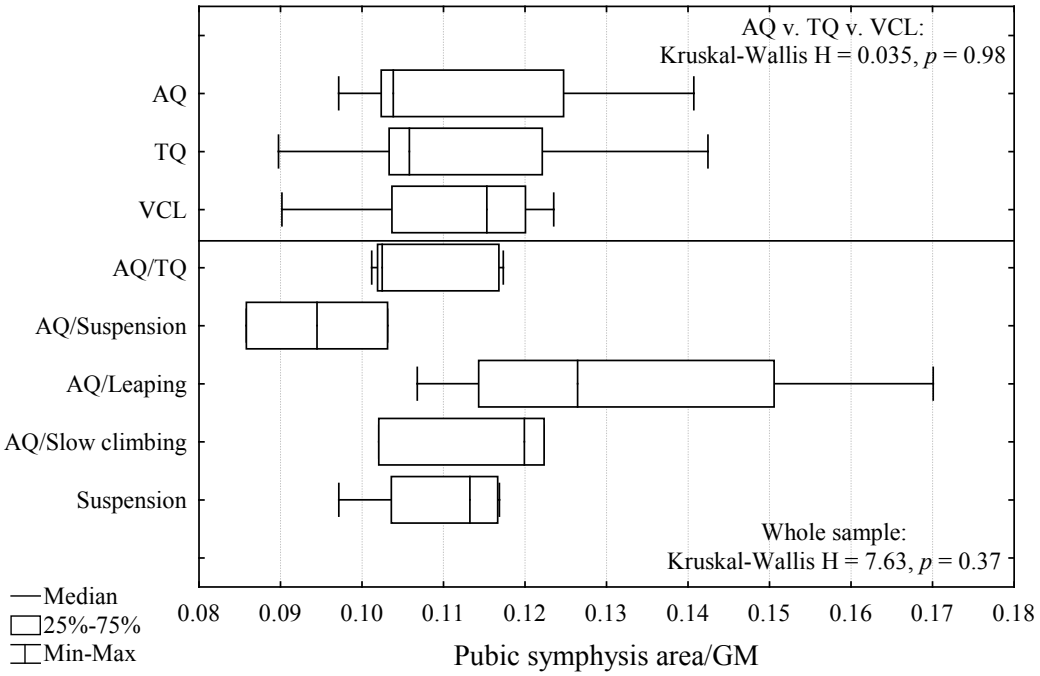

Fig. 4-51. Box-and-whiskers plots comparing the medians and ranges of the pubic symphysis area shape variable for each locomotor group. The three boxes above the horizontal line were used in hypothesis-testing, while the box plots below the horizontal line were not included in *a priori* hypothesis-testing. Kruskal-Wallis tests were performed on both samples, and the *p*-values are listed accordingly.

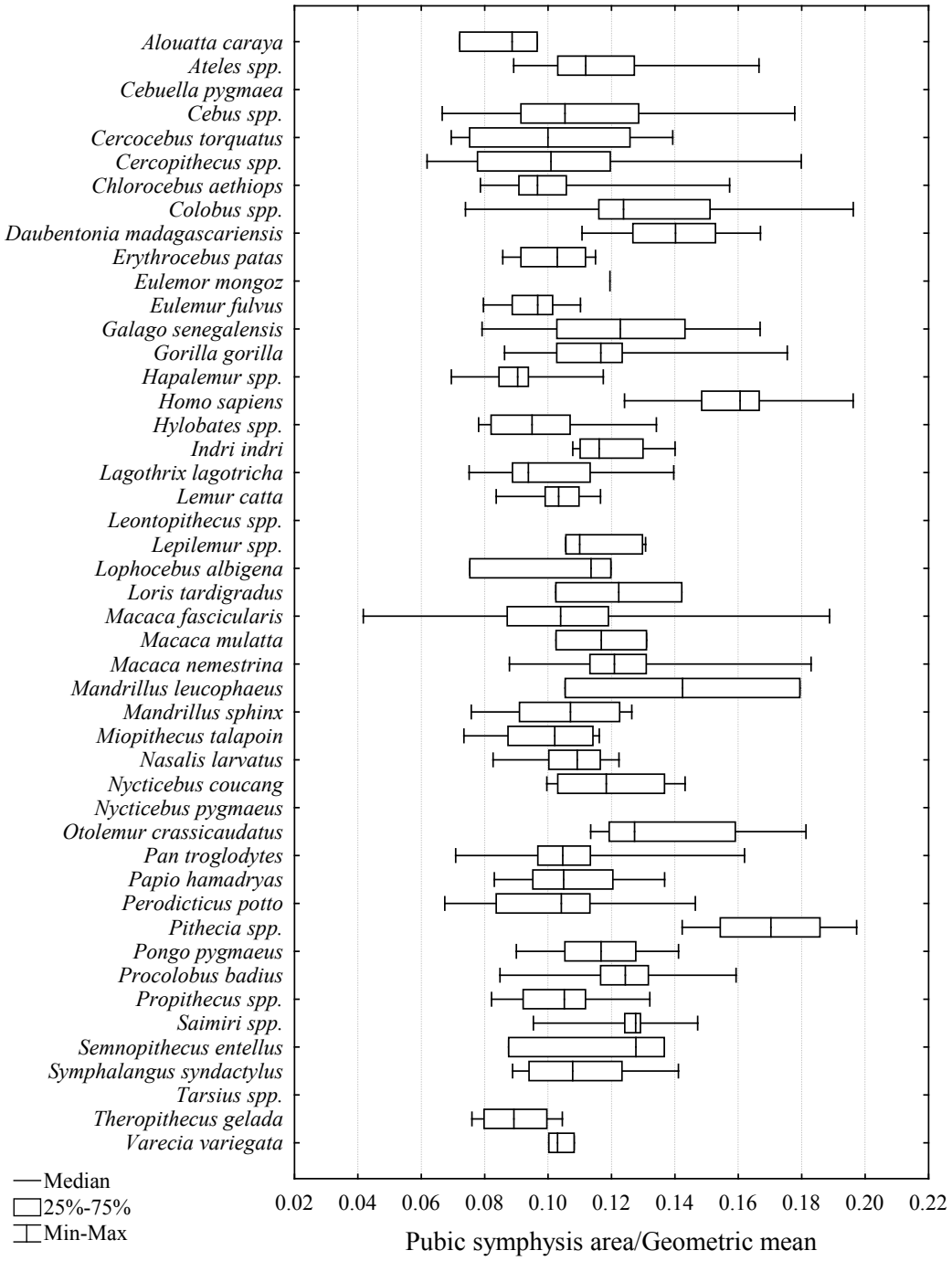

Fig. 4-52. Box-and-whiskers plots of medians and ranges of the pubic symphysis area shape variable for each taxon.

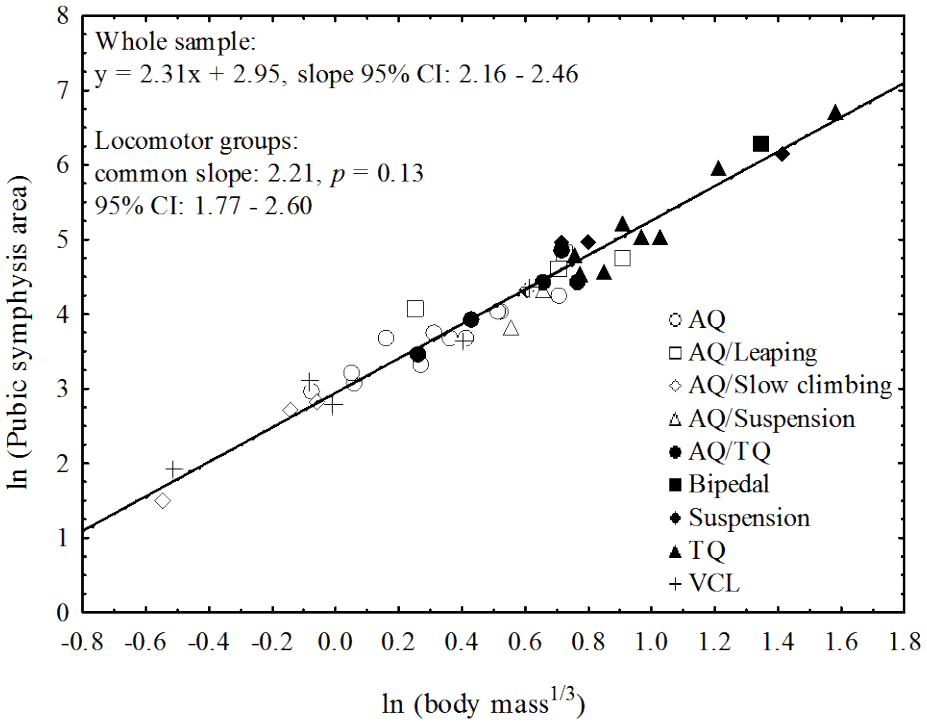

Fig. 4-53. Bivariate plot of ln-pubic symphysis area on ln-body mass$^{1/3}$.

The following pelvic traits did not have *a priori* hypotheses of locomotor adaptation, but are included here to increase overall understanding of primate pelvic morphology and its relationship to locomotion. Predictions for hypotheses relating to scaling analyses are as in the previous section.

Anteroposterior diameter. There is a significant effect of locomotion on the anteroposterior diameter of the pelvis (H = 25.42, $p = 0.0006$). *Post hoc* comparisons show that slow climbers have the widest pelvic inlet relative to pelvis size and are significantly different from AQ/leapers ($p = 0.04$) and TQ taxa ($p = 0.0005$). A box plot of locomotor groups shows that AQ/suspensory, suspensory, and VCL taxa overlap and all share intermediate anteroposterior pelvic diameters. The narrowest pelvic inlets belong to terrestrial quadrupeds (Fig. 4-54), and AQ/TQ, AQ, and AQ/leaper taxa overlap and also have narrow

pelvic inlets (Fig. 4-54). A box plot of taxon medians again demonstrates the large anteroposterior diameter of slow climbing lorises, and also shows that the small-bodied VCL taxa (*Galago senegalensis* and *Tarsius* spp.) have the second largest pelvic inlets among primates (Fig. 4-55).

The anteroposterior diameter of the pelvis scales isometrically with body size in the primate-wide sample (slope = 0.99, 95% confidence interval 0.90 – 1.08, Table 4-20, Fig. 4-56). An examination of slopes and 95% confidence intervals for each locomotor group indicates that terrestrial quadrupeds and vertical clingers and leapers differ significantly from isometry in different directions. The anteroposterior diameter in TQ taxa scales with positive allometry relative to body size (slope = 1.41, Table 4-19), and in VCL taxa it scales with negative allometry (slope = 0.75, Table 4-20). The hypothesis of isometry is not rejected for the overall primate sample, but is rejected for TQ and VCL taxa.

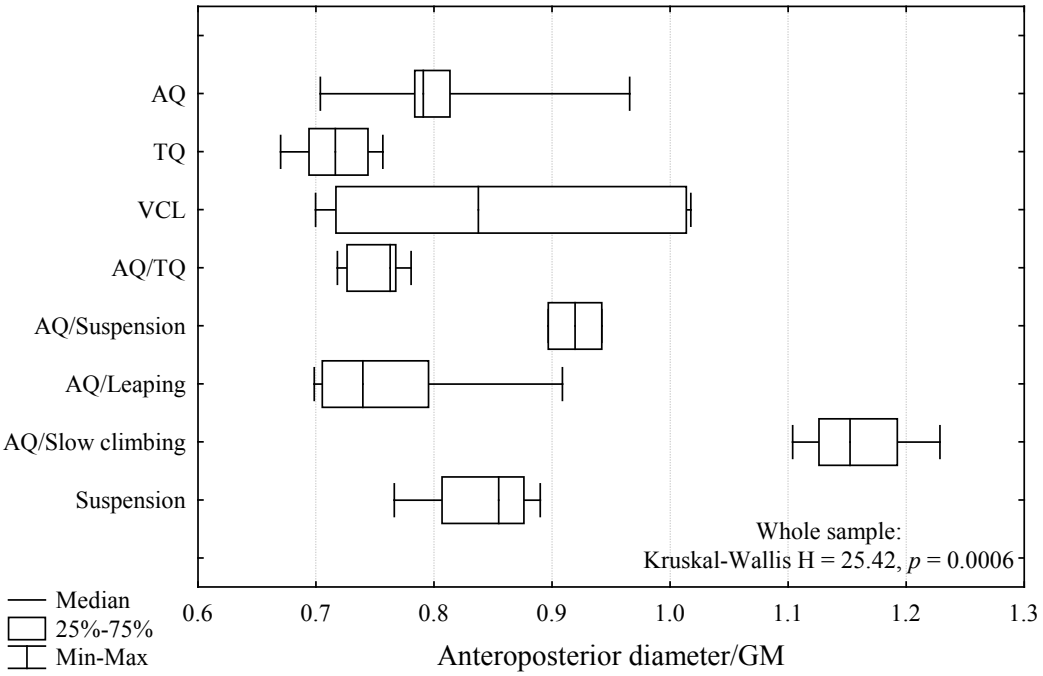

Fig. 4-54. Box-and-whiskers plots comparing the medians and ranges of the anteroposterior pelvic diameter shape variable for each locomotor group. These are the results of an exploratory examination of pelvic diameter, and were not a result of *a priori* hypothesis-testing.

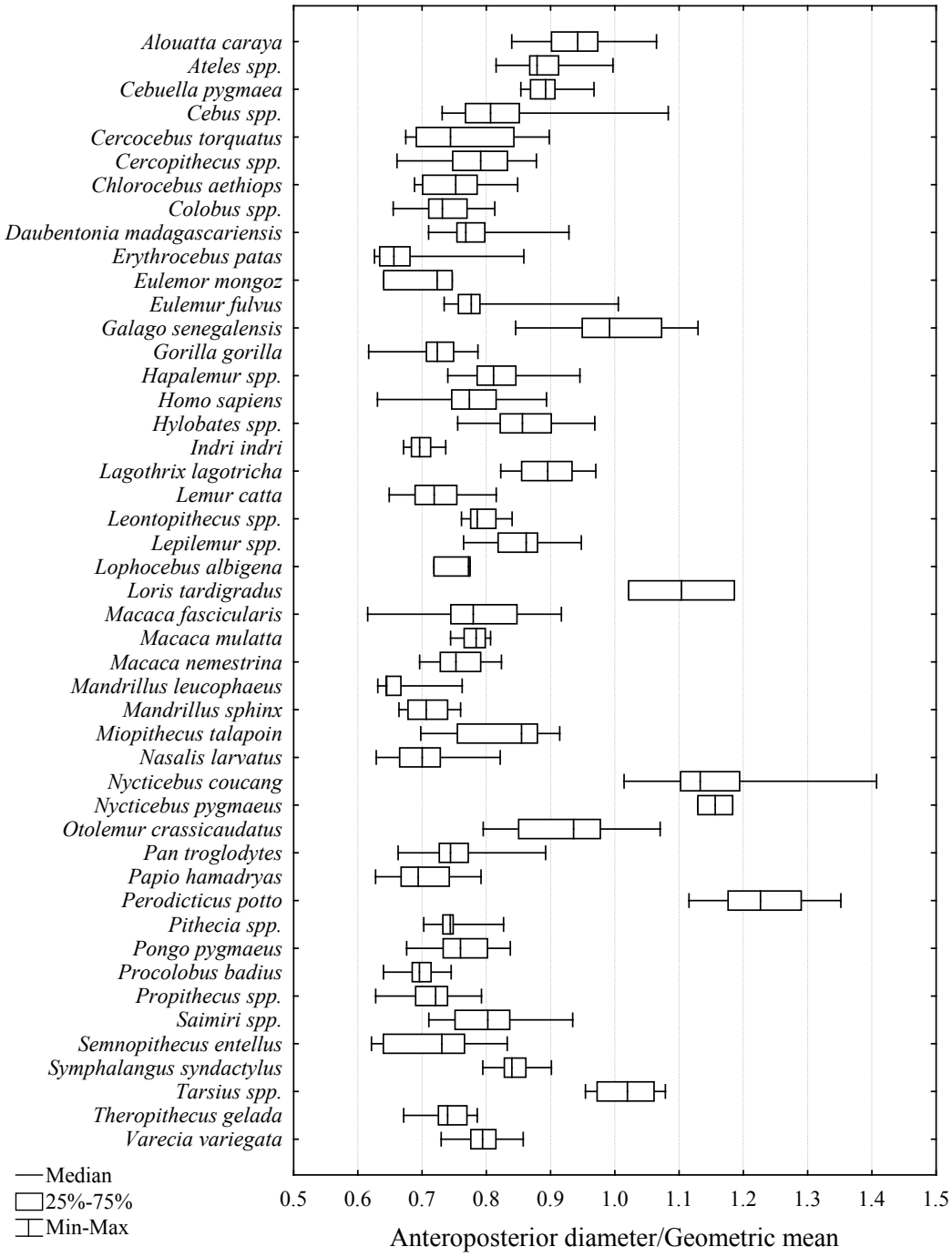

Fig. 4-55. Box-and-whiskers plots of medians and ranges of the anteroposterior pelvic diameter shape variable for each taxon.

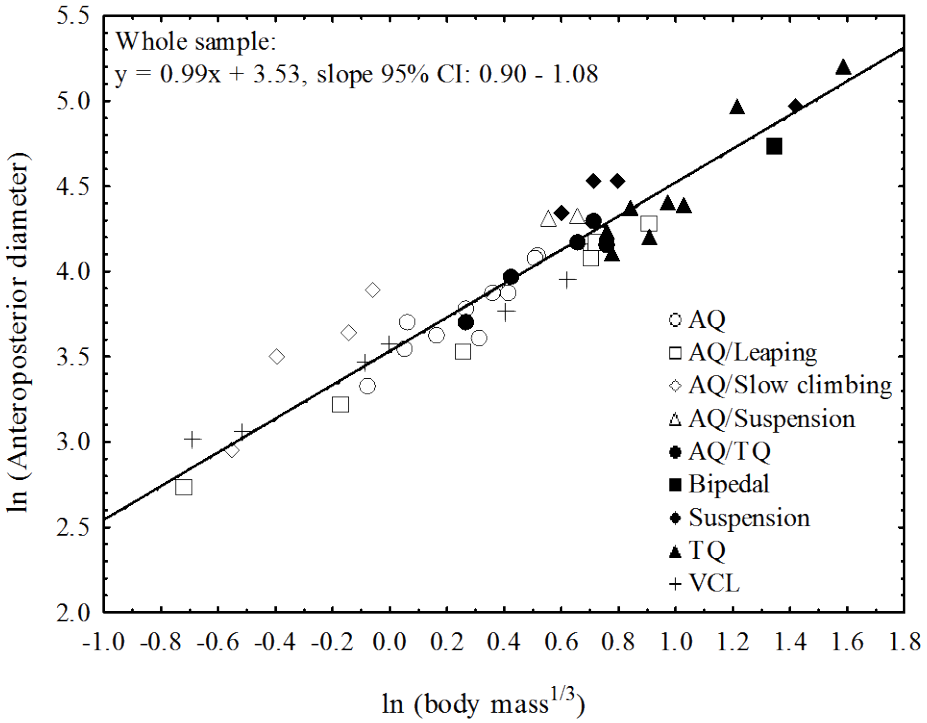

Fig. 4-56. Bivariate plot of ln-anteroposterior pelvic diameter on ln-body mass$^{1/3}$.

Bi-iliac breadth. There is a significant effect of locomotion on bi-iliac breadth ($H = 22.63$, $p = 0.002$). *Post hoc* multiple comparisons indicate that slow climbers have significantly narrower bi-iliac breadths than suspensory ($p = 0.007$) and TQ taxa ($p = 0.002$). A box plot of locomotor groups and a bivariate plot of ln-bi-iliac breadth on ln-body mass$^{1/3}$of all taxa demonstrates the narrow bi-iliac breadth of slow climbers, the intermediate breadth of various forms of arboreal quadrupedalism, and the wider bi-iliac distance of suspensory and terrestrial quadrupedal taxa relative to body size (Fig. 4-57). A box plot of all taxa reveals that the largest bi-iliac breadths belong to all hominoids except *Hylobates* spp., while lorisiformes and tarsiers have the narrowest bi-iliac breadths (Fig. 4-58). Focusing on the taxa in the mid-region of the plot indicates that taxa seem to be ordered somewhat according to body size, with larger-bodied taxa exhibiting

wider bi-iliac breadths, and smaller-bodied taxa displaying relatively narrower bi-iliac breadths (Fig. 4-58). These results suggest that there is an interaction between locomotion and body size in the bi-iliac breadth of the pelvis.

Bi-iliac breadth scales with positive allometry relative to body size in the primate-wide sample (slope = 1.49, 95% confidence interval 1.39 – 1.59, Table 4-20, Fig. 4-59). However, four of the seven locomotor groups are characterized by isometry in bi-iliac breadth relative to body size (AQ, slow climbers, AQ/TQ, and suspensory taxa), while the other three locomotor groups exhibit positive allometry (Table 4-20). The hypothesis of isometry in this pelvic measure relative to body size is rejected for the primate-wide sample, and for TQ, VCL, and AQ/leaping taxa.

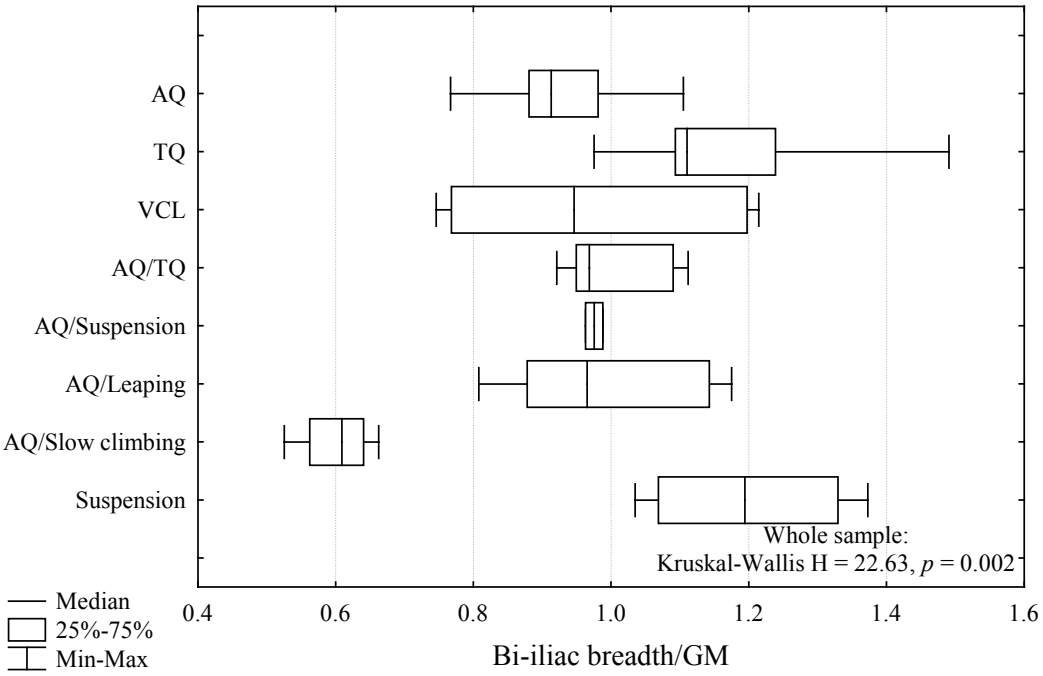

Fig. 4-57. Box-and-whiskers plots comparing the medians and ranges of the bi-iliac breadth shape variable for each locomotor group. These are the results of an exploratory examination of pelvic diameter, and were not a result of *a priori* hypothesis-testing.

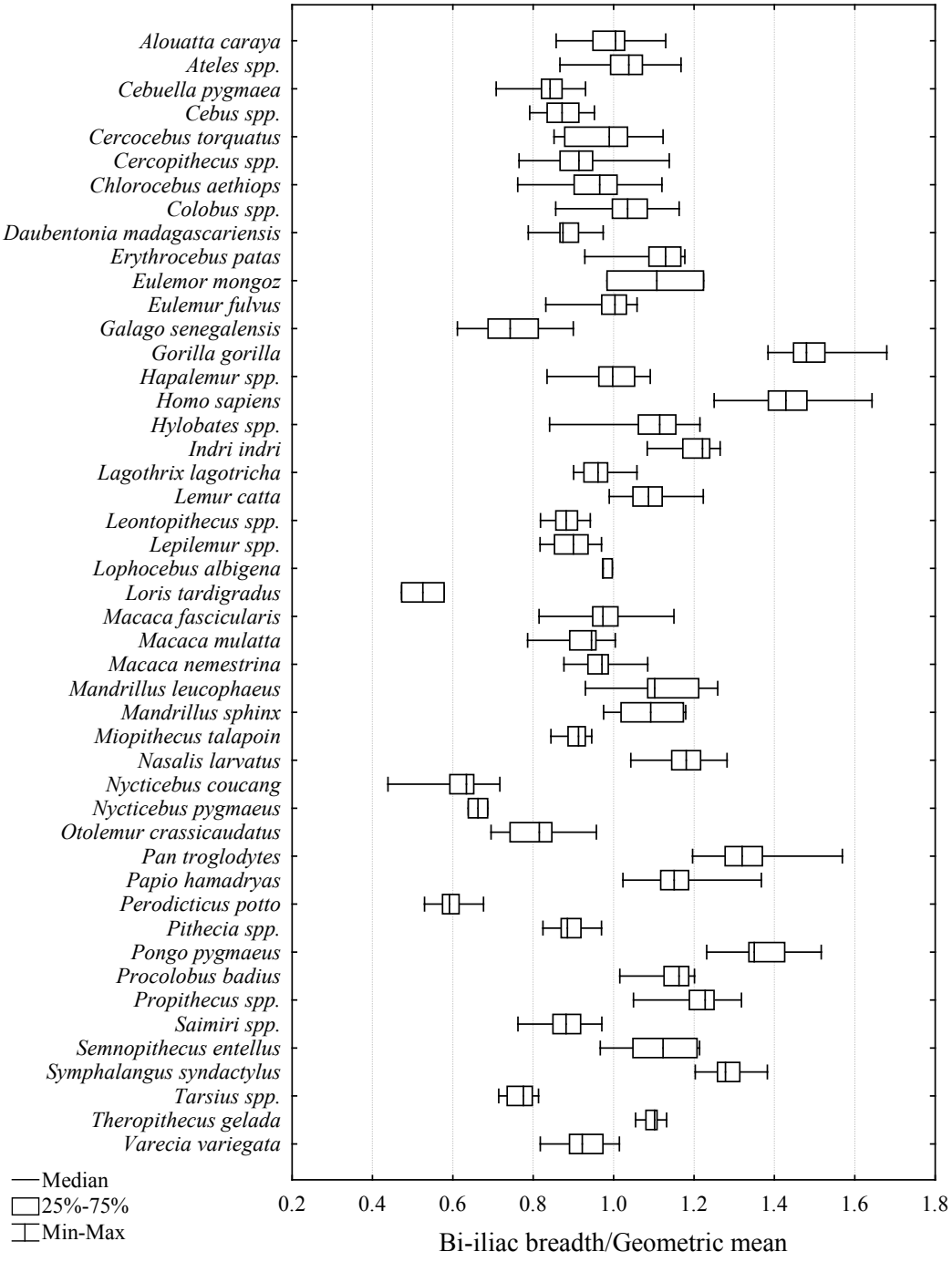

Fig. 4-58. Box-and-whiskers plots of medians and ranges of the bi-iliac breadth shape variable for each taxon.

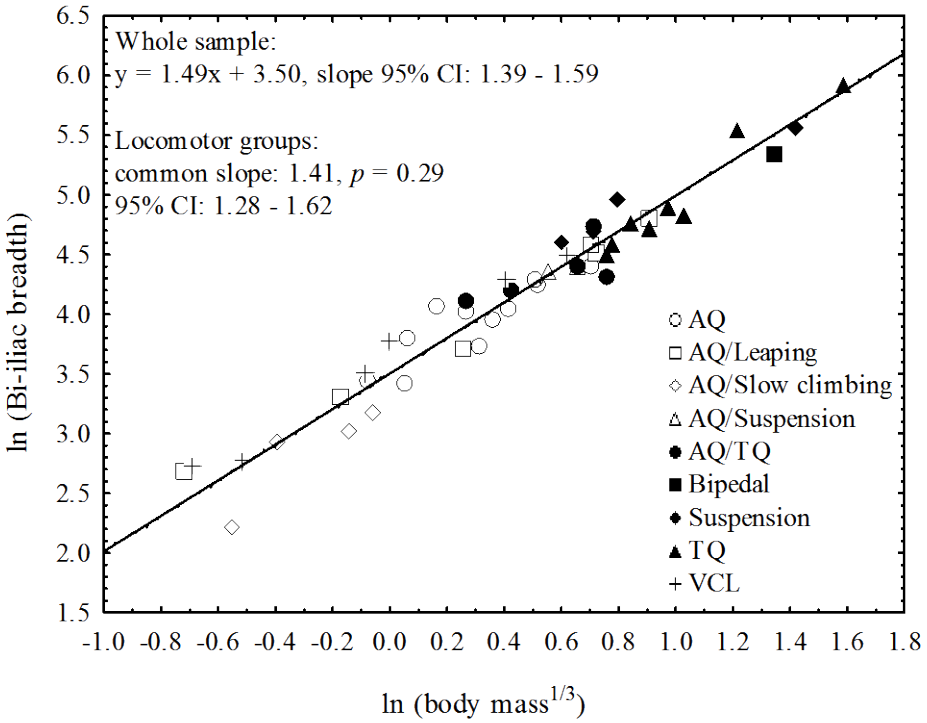

Fig. 4-59. Bivariate plot of ln-bi-iliac breadth on ln-body mass$^{1/3}$.

Biacetabular distance. There is a significant locomotor effect on biacetabular distance (H = 21.3, p = 0.003). Vertical clingers and leapers have the narrowest biacetabular distance and are significantly different from AQ/leapers (p = 0.038). A box plot of locomotor group medians demonstrates that although there is no significant difference among other locomotor categories, AQ/leapers, AQ/TQ taxa, and suspensory taxa have larger biacetabular distances than AQ, AQ/suspensory, and slow climbing taxa (Fig. 4-60). A plot of biacetabular distance by taxa shows that the four loris species have disproportionately large ranges that span the entire range of biacetabular distance values (Fig. 4-61).

Biacetabular distance scales with positive allometry relative to body size (slope = 1.31, 95% confidence interval 1.21 – 1.41, Table 4-20, Fig. 4-62). However, an examination of slopes and 95% confidence intervals for each

locomotor group indicates that all but one group exhibits isometry in biacetabular distance relative to body size; terrestrial quadrupeds are characterized by slight positive allometry (slope = 1.40, Table 4-20). The hypothesis of isometry for this pelvic measure is rejected for the entire primate sample and for the terrestrial quadrupeds.

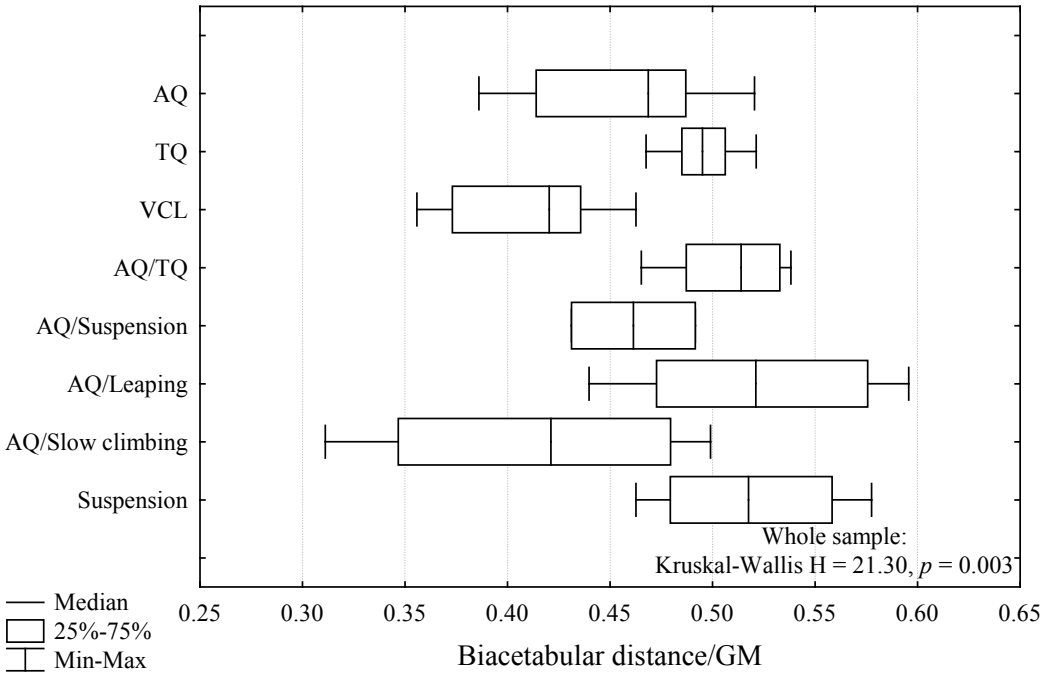

Fig. 4-60. Box-and-whiskers plots comparing the medians and ranges of the biacetabular diameter shape variable for each locomotor group. These are the results of an exploratory examination of pelvic diameter, and were not a result of *a priori* hypothesis-testing.

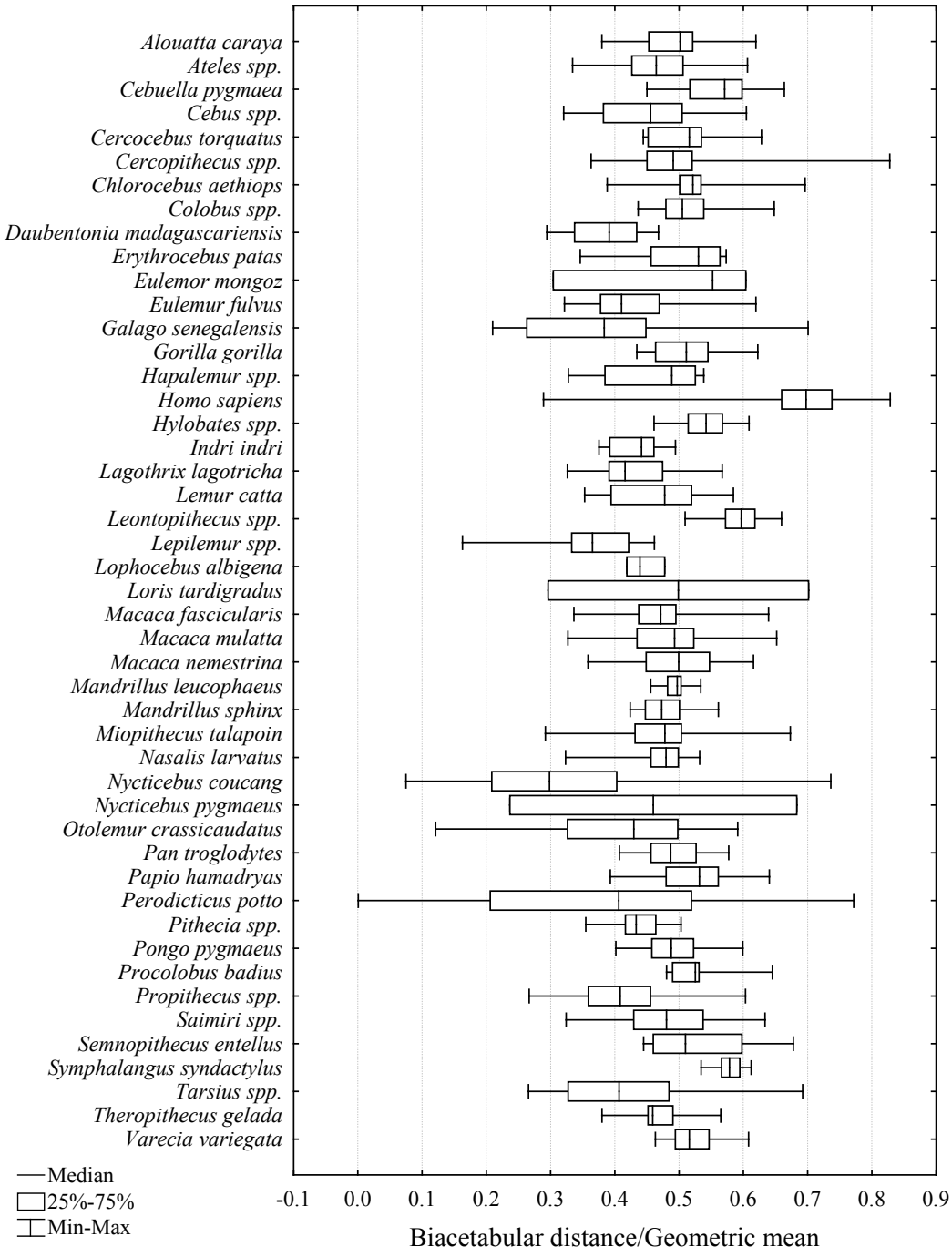

Fig. 4-61. Box-and-whiskers plots of medians and ranges of the biacetabular diameter shape variable for each taxon.

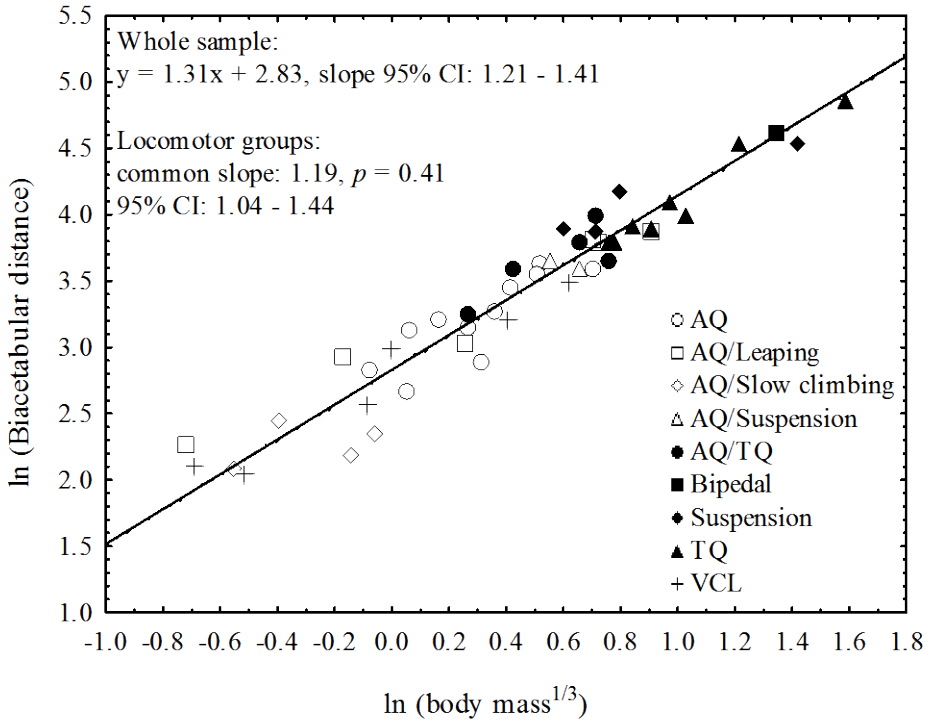

Fig. 4-62. Bivariate plot of ln-biacetabular diameter on ln-body mass$^{1/3}$.

Transverse diameter. There is no difference among locomotor groups in the maximum transverse diameter of the pelvis (H = 8.47, p = 0.293). Qualitatively, the box plots demonstrate that vertical clingers and leapers and slow climbers have the narrowest transverse diameter of the pelvis relative to body size, while the other locomotor groups show no differentiation (Figs. 4-63 and 4-64).

Transverse diameter scales with positive allometry relative to body size in the primate-wide sample (slope = 1.17, 95% confidence interval 1.10 – 1.24, Table 4-20, Fig. 4-65). However, an examination of the slopes and 95% confidence intervals for each locomotor group indicates isometry of transverse diameter relative to body size for each group (Table 4-20). The hypothesis that this pelvic trait scales with isometry is rejected for the primate-wide sample, but not for each individual locomotor group.

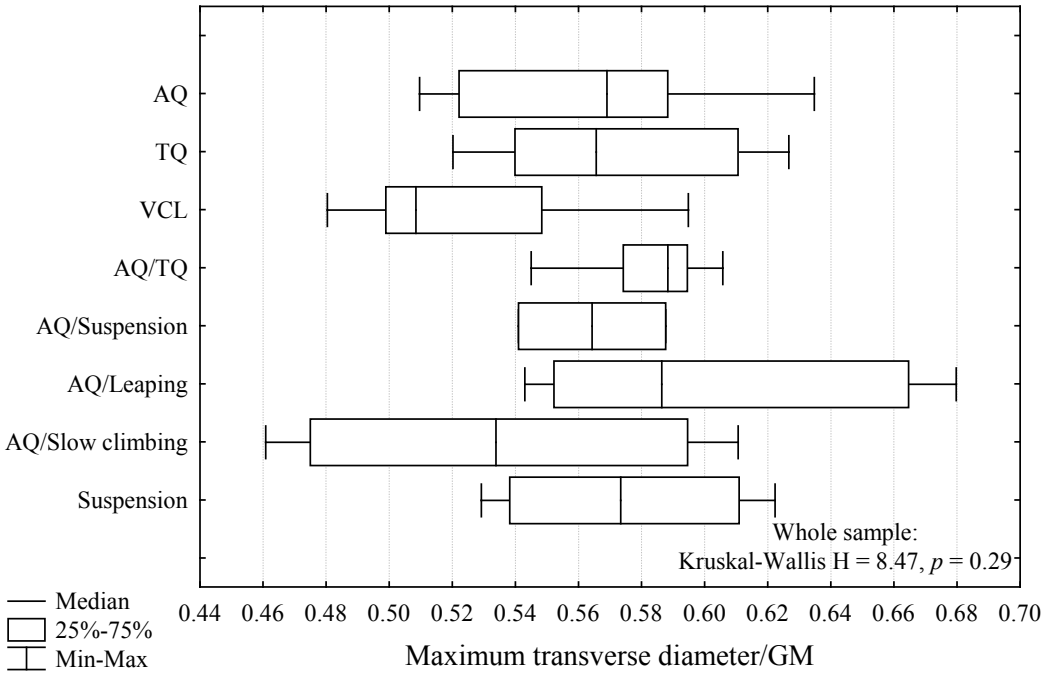

Fig. 4-63. Box-and-whiskers plots comparing the medians and ranges of the maximum transverse diameter shape variable for each locomotor group. These are the results of an exploratory examination of pelvic diameter, and were not a result of *a priori* hypothesis-testing.

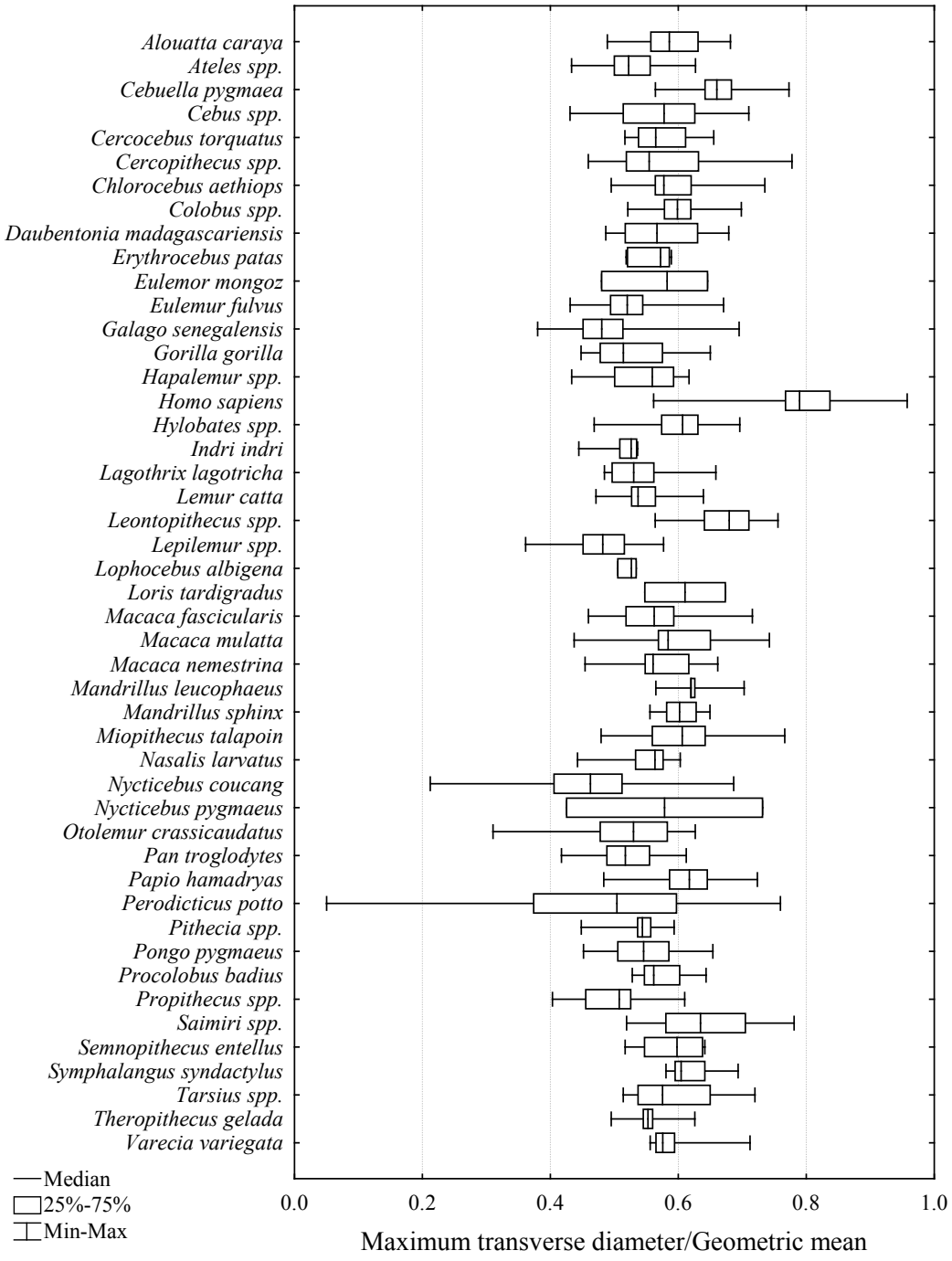

Fig. 4-64. Box-and-whiskers plots of medians and ranges of the maximum transverse diameter shape variable for each taxon.

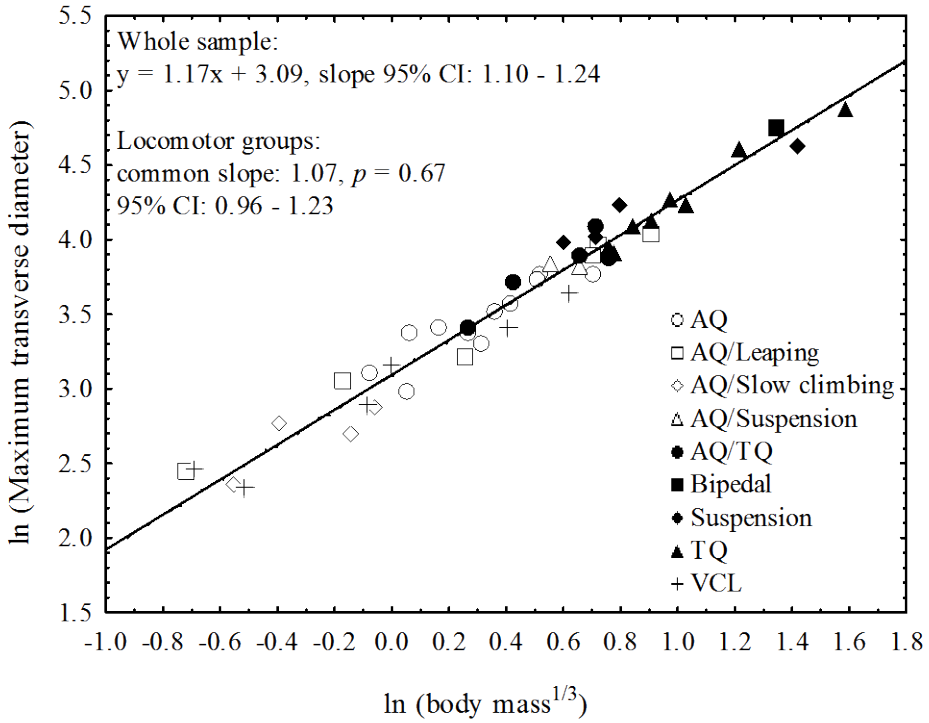

Fig. 4-65. Bivariate plot of ln-maximum transverse diameter on ln-body mass$^{1/3}$.

Sacrum width. There is a significant locomotor effect on sacrum width (H = 18.53, p = 0.0098). *Post hoc* multiple comparisons indicate that AQ/leapers have the widest sacra, and are significantly different from slow climbers (p = 0.045), which have the narrowest sacra. The other quadrupedal groups (both arboreal and terrestrial) have similar sacrum widths, while suspensory and VCL taxa have slightly narrower sacra (Fig. 4-66). A box plot of sacrum width by taxon and a bivariate plot of ln-sacrum width on ln-body mass$^{1/3}$ shows that small-bodied AQ/leapers and *Homo sapiens* have the widest sacra, while the narrowest sacra belong to all three great ape species and some lorises (Figs. 4-67 and 4-68).

The width of the sacrum scales with slight positive allometry in the primate-wide sample (slope = 1.12, 95% confidence interval 1.03 – 1.21, Table 4-20). However, an examination of slopes and 95% confidence intervals of each

locomotion group indicates that all but one of the groups exhibit isometry in sacrum width—terrestrial quadrupeds are characterized by negative allometry (slope = 0.70, Table 4-20). The hypothesis that sacrum width scales with isometry is rejected for the primate-wide sample, but among locomotor categories, it is only rejected for the terrestrial quadrupeds.

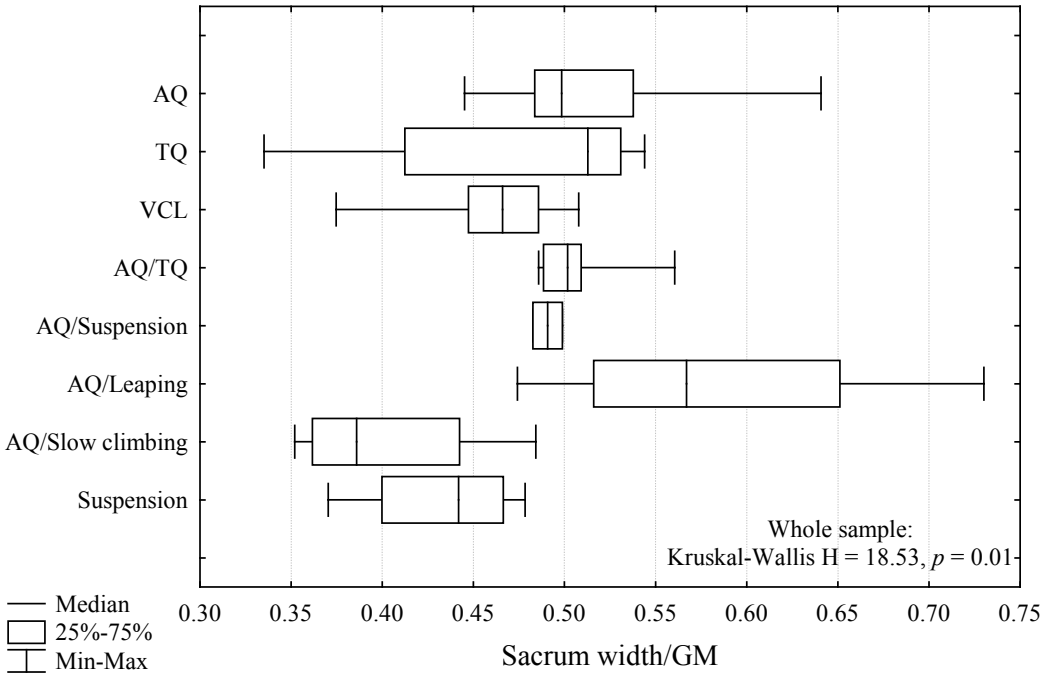

Fig. 4-66. Box-and-whiskers plots comparing the medians and ranges of the sacrum width shape variable for each locomotor group. These are the results of an exploratory examination of pelvic diameter, and were not a result of *a priori* hypothesis-testing.

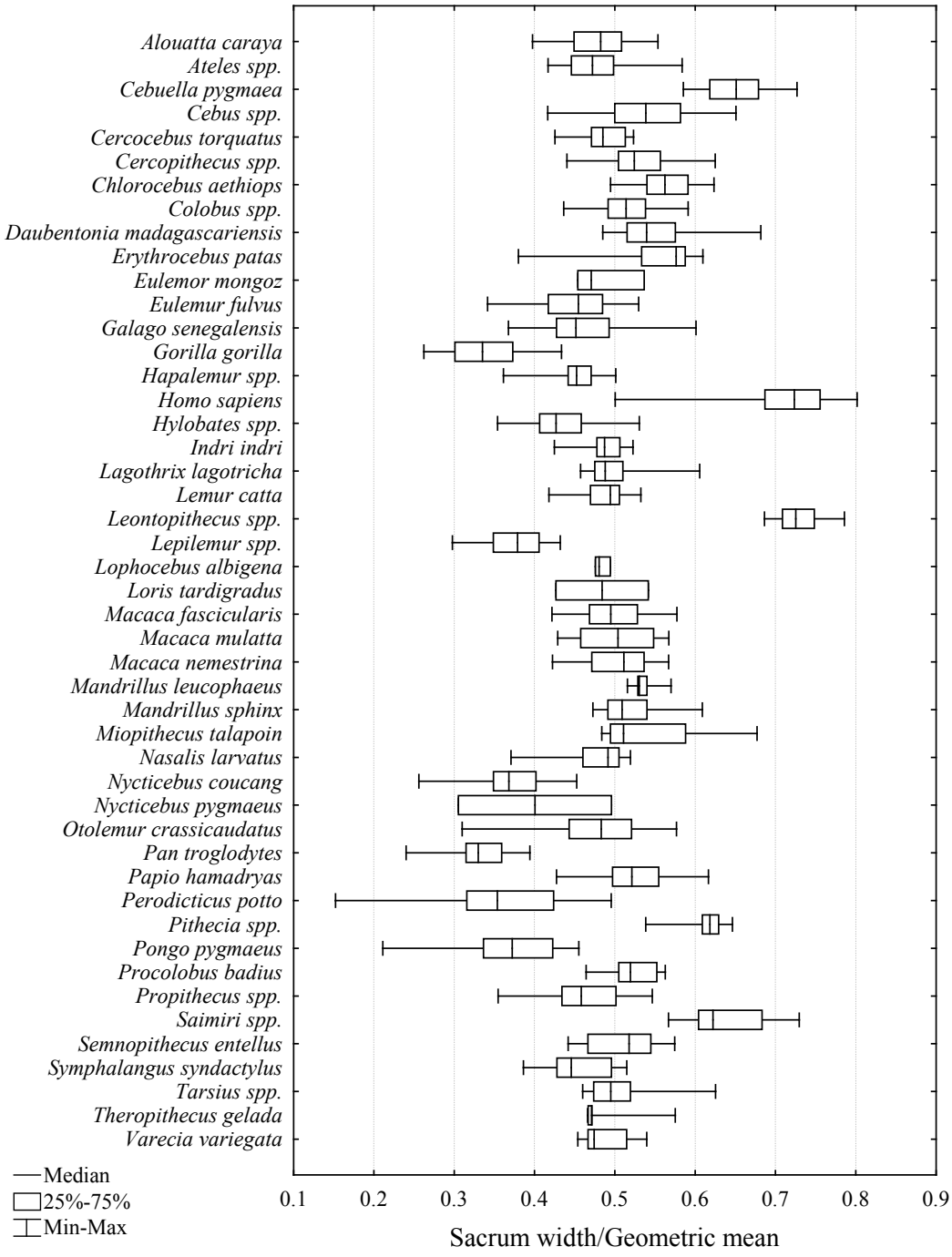

Fig. 4-67. Box-and-whiskers plots of medians and ranges of the sacrum width shape variable for each taxon.

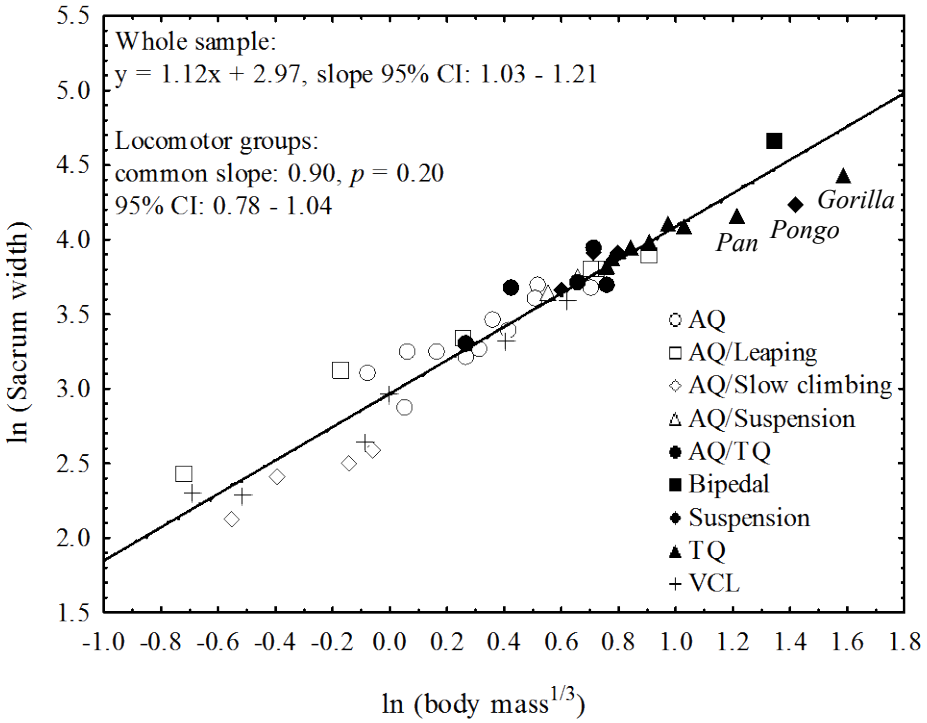

Fig. 4-68. Bivariate plot of ln-sacrum width on ln-body mass$^{1/3}$.

Pelvis length. There is a significant effect of locomotion on overall pelvis length (H = 23.44, p = 0.001). *Post hoc* comparisons indicate that suspensory taxa have the shortest pelves and are significantly different from AQ (p = 0.013) and slow climbing taxa (p = 0.021). A box plot of pelvis length by locomotor group and a bivariate plot of ln-pelvis length on ln-body mass$^{1/3}$ indicate that suspensory taxa (both AQ/suspensory and suspensory) have the shortest pelves, TQ and VCL taxa are intermediate in pelvic length, and all other forms of arboreal quadrupedalism have the longest pelves (Fig. 4-69). All hominoids have the shortest pelves, as do atelids and indriids (Fig. 4-70).

Total pelvis length scales with isometry in the primate-wide sample (slope = 0.99, 95% confidence interval 0.93 – 1.05, Table 4-20, Fig. 4-71). An examination of slopes and 95% confidence intervals for each locomotor group

demonstrates that they are all characterized by isometry in pelvis length relative to body size (Table 4-20). The hypothesis that pelvis length scales with isometry relative to body size is not rejected in neither the primate-wide sample, nor the individual locomotor groups.

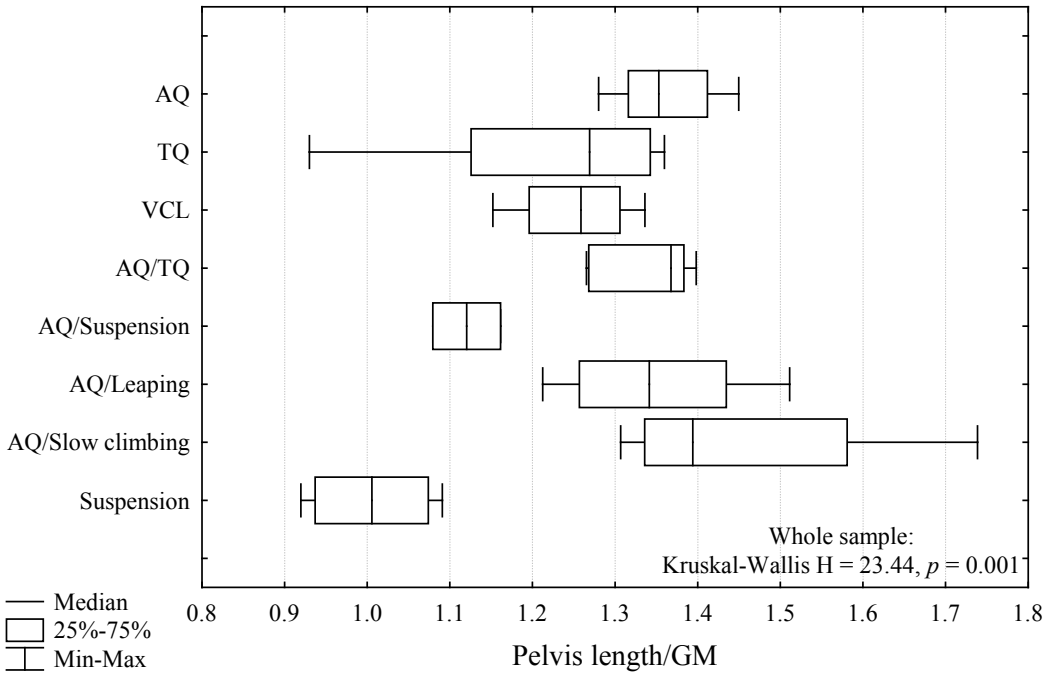

Fig. 4-69. Box-and-whiskers plots comparing the medians and ranges of the pelvic length shape variable for each locomotor group. These are the results of an exploratory examination of pelvic diameter, and were not a result of *a priori* hypothesis-testing.

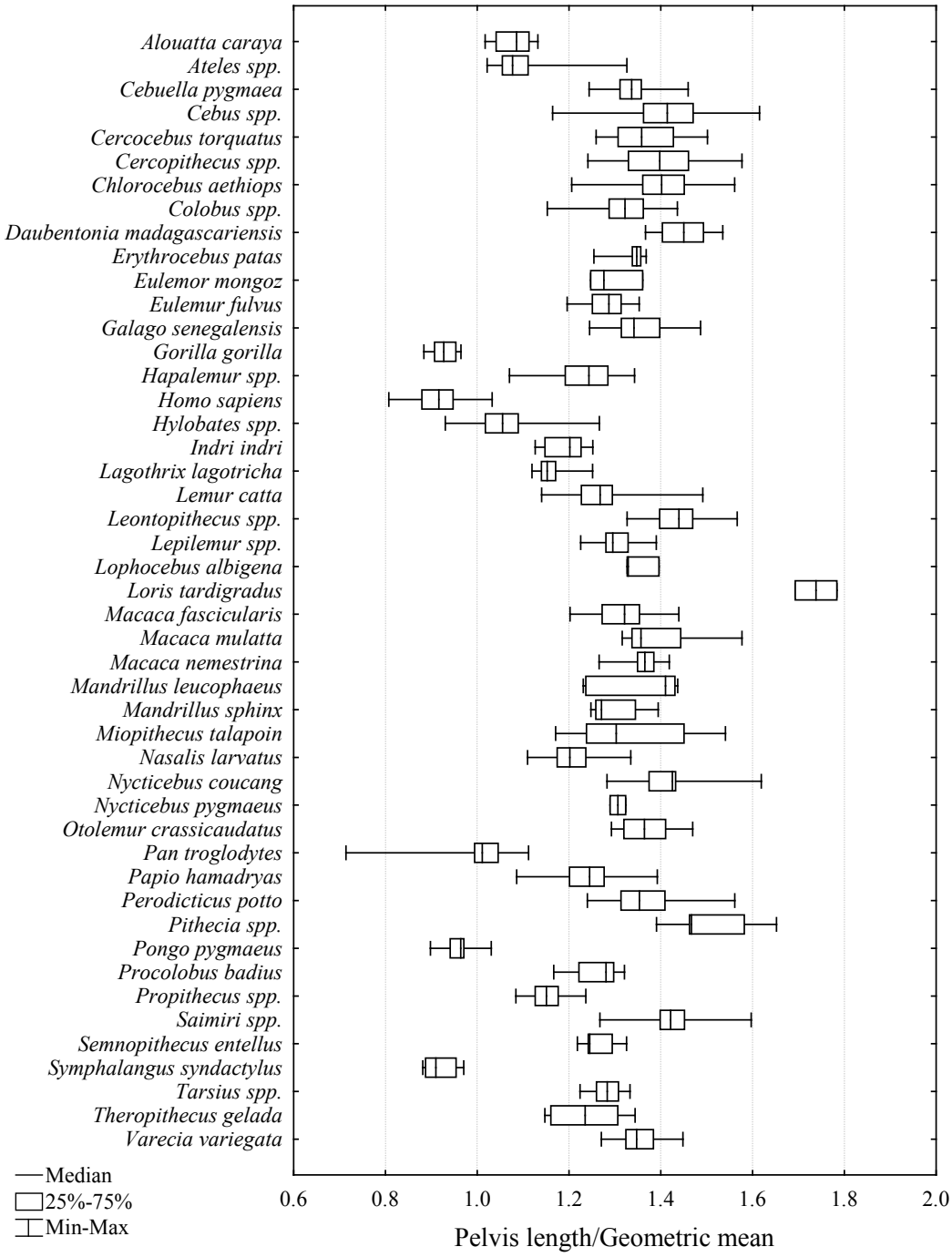

Fig. 4-70. Box-and-whiskers plots of medians and ranges of the pelvic length shape variable for each taxon.

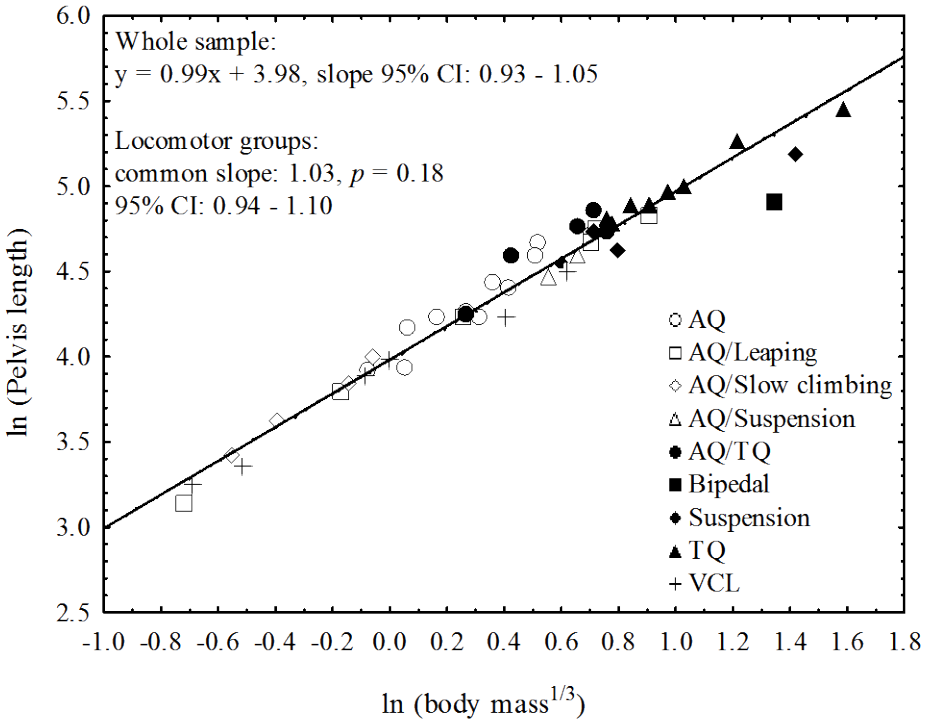

Fig. 4-71. Bivariate plot of ln-pelvis length on ln-body mass$^{1/3}$.

TABLE 4-20. Results of reduced major axis scaling analyses for the primate-wide and individual locomotor group samples.[a]

Measure	Primate-wide	AQ	AQ/Leap	AQ/Slow	AQ/TQ	Suspensory	TQ	VCL
Ilium length								
Prediction	Iso.							
β	0.92	1.16	1.09	1.11	1.13	0.64	0.68	0.86
95% CI	0.83-1.00	0.93-1.45	0.97-1.23	0.72-1.71	0.64-2.01	0.33-1.24	0.53-0.87	0.76-0.99
Result	Iso.	Iso.	Iso.	Iso.	Iso.	Iso.	-	-
Upper iliac height								
Prediction	Iso.							
β	1.18	1.19	1.29	1.86	1.27	0.79	1.36	1.3
95% CI	1.08-1.27	1.01-1.41	1.23-1.36	0.68-5.09	0.51-3.18	0.54-1.16	1.07-1.72	1.19-1.42
Result	+	+	+	Iso.	Iso.	Iso.	+	+
Lower iliac height								
Prediction	Iso.							
β	0.91	1.07	0.98	0.82	0.9	0.58	1.04	0.62
95% CI	0.84-0.98	0.81-1.40	0.88-1.08	0.39-1.72	0.50-1.61	0.43-0.76	0.74-1.48	0.52-0.73
Result	-	Iso.	Iso.	Iso.	Iso.	-	Iso.	-
AIIS to hip joint								
Prediction	Iso.							
β	1.02	0.99	1.01	1.58	0.74	0.74	1.04	1.24
95% CI	0.95-1.09	0.74-1.33	0.79-1.28	0.92-2.71	0.26-2.08	0.27-2.05	0.65-1.67	1.10-1.41
Result	Iso.	Iso.	Iso.	Iso.	Iso.	Iso.	Iso.	+
Ilium width								
Prediction	Iso.							
β	1.57	1.42	1.38	1.08	1.27	1.43	2.09	1.49
95% CI	1.48-1.67	1.00-2.02	1.24-1.54	0.42-2.76	0.55-2.93	0.71-2.86	1.77-2.46	1.28-1.74
Result	+	Iso.	+	Iso.	Iso.	Iso.	+	+

TABLE 4-20, Continued.

Measure	Primate-wide	AQ	AQ/Leap	AQ/Slow	AQ/TQ	Suspensory	TQ	VCL
Lower ilium cross-sectional area								
Prediction	+							
β	2.75	3.01	2.39	3	2.58	1.61	2.48	3.12
95% CI	2.60-2.89	2.29-3.97	2.18-2.61	1.94-4.66	1.19-5.61	1.17-2.21	2.10-2.93	2.53-3.85
Result	+	+	+	Iso.	Iso.	Iso.	+	+
Auricular surface area								
Prediction	+							
β	2.27	2.28	2.03	2.59	2.41	1.97	2.11	2.09
95% CI	2.12-2.43	1.72-3.02	1.67-2.48	1.21-5.54	0.93-6.25	1.16-3.37	1.75-2.55	1.63-2.67
Result	+	Iso.	Iso.	Iso.	Iso.	Iso.	Iso.	Iso.
Ischium length								
Prediction	Iso.							
β	1.18	1.19	0.98	1.23	1.09	1.04	1.15	1.22
95% CI	1.11-1.26	0.84-1.68	0.84-1.14	1.17-1.30	0.49-2.43	0.50-2.18	0.94-1.42	0.96-1.55
Result	+	Iso.	Iso.	+	Iso.	Iso.	Iso.	Iso.
Ischium dorsal projection								
Prediction	Iso.							
β	1.87	1.84	1.96	3.23	2.43	0.92	1.07	1.56
95% CI	1.67-2.07	1.20-2.83	1.14-3.38	1.04-10.10	0.85-6.93	0.41-2.02	0.63-1.82	1.13-2.16
Result	+	+	+	+	Iso.	Iso.	Iso.	+
Ischium cross-sectional area								
Prediction	+							
β	2.51	2.61	2.58	2.01	3.46	2.00	2.28	1.91
95% CI	2.37-2.65	2.05-3.34	2.36-2.82	1.95-2.06	1.49-8.02	1.15-3.48	1.88-2.76	1.49-2.43
Result	+	+	+	Iso.	Iso.	Iso.	Iso.	Iso.

TABLE 4-20, Continued.

Measure	Primate-wide	AQ	AQ/Leap	AQ/Slow	AQ/TQ	Suspensory	TQ	VCL
Acetabulum diameter								
Prediction	Iso.							
β	1.05	1.06	1.09	1.20	1.01	0.87	1.24	1.12
95% CI	0.99-1.10	0.86-1.31	1.03-1.15	0.75-1.89	0.40-2.55	0.67-1.14	1.05-1.46	0.88-1.43
Result	Iso.	Iso.	+	Iso.	Iso.	Iso.	+	Iso.
Superior pubic ramus length								
Prediction	Iso.							
β	0.97	1.00	0.98	1.37	1.18	0.93	1.13	0.84
95% CI	0.89-1.06	0.72-1.39	0.72-1.33	0.64-2.93	0.66-2.09	0.58-1.50	0.97-1.31	0.61-1.15
Result	Iso.	Iso.	Iso.	Iso.	Iso.	Iso.	Iso.	Iso.
Superior pubic ramus cross-sectional area								
Prediction	+							
β	2.17	1.91	2.43	2.29	2.29	1.57	1.70	2.00
95% CI	2.03-2.30	1.45-2.51	2.14-2.76	1.26-4.15	1.00-5.25	0.72-3.43	1.12-2.57	1.58-2.53
Result	+	Iso.	+	Iso.	Iso.	Iso.	Iso.	Iso.
Inferior pubic ramus length								
Prediction	Iso.							
β	0.90	0.83	0.87	0.99	0.69	1.12	1.33	0.61
95% CI	0.80-1.01	0.71-0.97	0.67-1.12	0.51-1.92	0.24-1.94	0.38-3.28	0.90-1.98	0.40-0.92
Result	Iso.	-	Iso.	Iso.	Iso.	Iso.	Iso.	-
Inferior pubic ramus cross-sectional area								
Prediction	+							
β	3.60	4.97	3.34	2.87	7.21	1.85	2.21	2.68
95% CI	3.22-3.98	3.29-7.51	2.73-4.10	1.13-7.32	4.28-12.13	0.50-6.88	1.86-2.63	2.23-3.23
Result	+	+	+	Iso.	+	Iso.	Iso.	+

TABLE 4-20, Continued.

Measure	Primate-wide	AQ	AQ/Leap	AQ/Slow	AQ/TQ	Suspensory	TQ	VCL
Pubic symphysis length								
Prediction	Iso.							
β	1.52	1.75	1.29	1.38	2.43	0.61	0.42	1.46
95% CI	1.35-1.70	1.23-2.48	1.06-1.57	0.48-3.92	1.31-4.52	0.17-2.25	0.19-0.96	1.19-1.80
Result	+	+	+	Iso.	Iso.	Iso.	-	+
Pubic symphysis area								
Prediction	+							
β	2.31	1.73	1.24	2.80	2.52	2.11	2.74	2.07
95% CI	2.16-2.46	1.35-2.23	0.46-3.31	1.01-7.77	1.39-4.58	1.12-3.98	2.10-3.58	1.39-3.09
Result	+	Iso.	Iso.	Iso.	Iso.	Iso.	+	Iso.
Anteroposterior diameter								
Prediction	Iso.							
β	0.99	1.07	0.97	1.75	1.09	0.72	1.41	0.75
95% CI	0.90-1.08	0.81-1.41	0.85-1.12	0.72-4.25	0.61-1.95	0.44-1.17	1.04-1.92	0.62-0.90
Result	Iso.	Iso.	Iso.	Iso.	Iso.	Iso.	+	-
Bi-iliac breadth								
Prediction	Iso.							
β	1.49	1.38	1.33	1.89	1.14	1.19	1.81	1.47
95% CI	1.39-1.59	0.94-1.97	1.13-1.56	0.60-5.95	0.40-3.26	0.71-2.00	1.45-2.28	1.23-1.76
Result	+	Iso.	+	Iso.	Iso.	Iso.	+	+
Biacetabular distance								
Prediction	Iso.							
β	1.31	1.38	1.04	0.71	1.31	0.85	1.40	1.17
95% CI	1.21-1.41	0.93-2.04	0.79-1.36	0.12-4.21	0.54-3.17	0.37-1.97	1.12-1.74	0.85-1.61
Result	+	Iso.	Iso.	Iso.	Iso.	Iso.	+	Iso.

TABLE 4-20, Continued.

Measure	Primate-wide	AQ	AQ/Leap	AQ/Slow	AQ/TQ	Suspensory	TQ	VCL
Transverse diameter								
Prediction	Iso.							
β	1.17	1.11	1.01	0.99	1.20	0.82	1.20	1.03
95% CI	1.10-1.24	0.79-1.56	0.81-1.26	0.26-3.8	0.58-2.48	0.44-1.50	1.00-1.44	0.75-1.42
Result	+	Iso.	Iso.	Iso.	Iso.	Iso.	Iso.	Iso.
Sacral width								
Prediction	Iso.							
β	1.12	1.06	0.90	0.90	1.10	0.65	0.70	1.06
95% CI	1.03-1.21	0.75-1.51	0.74-1.09	0.38-2.08	0.45-2.72	0.26-1.61	0.56-0.87	0.80-1.41
Result	+	Iso.	Iso.	Iso.	Iso.	Iso.	-	Iso.
Pelvis length								
Prediction	Iso.							
β	0.99	1.13	1.05	1.14	1.12	0.79	0.85	0.96
95% CI	0.93-1.05	0.91-1.41	0.95-1.16	0.84-1.55	0.58-2.13	0.39-1.59	0.71-1.01	0.82-1.14
Result	Iso.	Iso.	Iso.	Iso.	Iso.	Iso.	Iso.	Iso.

[a]Positive allometry is denoted by +, negative allometry is denoted by -.

Summary of primate-wide analyses

The goal of the primate-wide investigation of univariate pelvic shape was to examine pelvic variation from the same perspective as the pairwise comparisons, but within a taxonomically broad sample of primate species. Variability in pelvic shape and its relationship to locomotion was also explored qualitatively among taxa in other locomotor categories for which *a priori* functional predictions were not feasible due to a lack of knowledge of locomotor group kinematics and kinetics (these include subgroups of arboreal quadrupedalism). Among the three locomotor groups for which there were shape predictions (AQ, TQ, and VCL), differences due to locomotion were found for ten of the 17 univariate measures. However, the specific predictions were supported for only two measures: the upper iliac height and the width of the ilium; all other hypotheses were rejected.

Both upper iliac height and ilium width were hypothesized to relate to increasing the area of muscular attachment. The height of the upper ilium was not predicted to differ among locomotor categories, and this was supported by statistical analyses. In addition, the prediction that the width of the ilium would be the same in arboreal quadrupeds and vertical clingers and leapers, and that terrestrial quadrupeds would have significantly wider ilia than these two groups was supported.

Additional differences according to locomotion were found in the length of the ilium, lower iliac height, ischium length and dorsal projection, inferior pubic ramus length and cross-sectional area, pubic symphysis length, and the

cross-sectional areas of the lower ilium and ischium. However, none of these differences were in the predicted direction. For many of these hypotheses the prediction was partially borne out; for example, for both ilium length and lower iliac height, the prediction was that TQ < AQ < VCL, but the results demonstrated that while terrestrial quadrupeds had shorter iliac lengths than arboreal quadrupeds, vertical clingers and leapers did not have longer iliac lengths than the other two groups of taxa. In many instances vertical clingers and leapers exhibit a wide range of variation, which is likely related to body size dimorphism within the locomotor group; although previous work has shown clear differences in muscle morphology (Demes et al., 1998a) and locomotor kinetics and kinematics (Dunbar, 1988; Demes et al., 1995; Demes et al., 1996; Demes et al., 1999) between small- and large-bodied vertical clingers and leapers, this study did not differentiate between the differing leaping mechanics of small- and large-bodied VCL taxa (this is discussed in more detail in the Discussion of this chapter).

It is worth mentioning here that the results of the investigation of the dorsal projection of the ischium and the dimensions of the inferior pubic rami may be skewed by the inclusion of cercopithecoids, a group that demonstrates larger values of both of these pelvic traits compared to other taxa (Figs. 4-22, 4-31, 4-46). It is likely that these results are influenced by the presence of ischial callosities in these taxa, which increase the size and prominence of the ischiopubis. Future work may benefit from excluding cercopithecoids and hylobatids (the only taxa that have ischial callosities) from primate-wide analyses.

The scaling relationships between pelvic traits and body size were also investigated in the primate-wide sample, and scaling hypotheses were supported in 13 out of 23 tests. In all but two cases (pelvis length and superior pubic ramus length), the analyses of individual locomotor groups demonstrated different scaling relationships than the primate-wide analyses. For example, joint and strut cross-sectional areas were found to support the prediction of positive allometry in the primate-wide sample, but there was substantial variation in the scaling relationships among locomotor groups, with many groups exhibiting isometry instead of positive allometry in this feature (Table 4-20). In fact, no locomotor group exhibited positive allometry in more than half of the areal measures, and some groups (slow climbers and suspensory taxa) only exhibit isometry in areal measures (Table 4-20). Therefore, in both linear and areal measures, isometry relative to body size is a common scaling relationship among functional locomotor groups. As far as areal measures are concerned, positive allometry occurs in some taxa, but does not appear to be the norm; thus the scaling hypotheses for areal measures are generally rejected.

GEOMETRIC MORPHOMETRIC RESULTS

All pelvic landmarks

The following set of results examines variation in overall three-dimensional pelvic shape using geometric morphometric methods. This exploration also allows an examination of the influences of size and locomotion on morphology. The first 20 principal components account for 93.4% of the variation in pelvic shape (Table 4-21). The first four PCs account for 66.1% of the

variation: principal component 1 accounts for 32.8% of the variation, PC2 accounts for 13%, PC3 accounts for 12%, and PC4 accounts for 8.2%. Bivariate plots of principal components are useful for interpretation of shape variation among taxa. The sign of principal component loadings is arbitrary; the relative values of each loading compared to others are the relevant data. However, positive and negative loadings in bivariate plots of pairs of principal components will be examined here to simplify discussion.

Locomotor group patterns: PCs 1 and 2. A plot of PC1 on PC2 using individual specimens demonstrates differentiation among taxa in body size along PC1 (Fig. 4-72). Variation along PC2 also appears to be related to body size, with some differentiation within locomotor categories by size. A plot of PC1 on PC2 using taxon means shows slight differentiation based on locomotor category (Fig. 4-73); while different styles of arboreal quadrupedalism overlap in the center of the plot, there is minimal overlap on the periphery by suspensory, terrestrial quadrupedal, and slow climbing taxa.

Generalized arboreal quadrupeds exhibit a large spread, with *Daubentonia* somewhat separate from the rest of the group (Fig. 4-73). Interestingly, the often-suspensory AQ taxa *Lagothrix* and *Alouatta* group closer to the suspensory taxa than with other AQ, supporting the hypothesis that these taxa share suspensory adaptations with *Ateles* and *Hylobates*. Of the wholly suspensory taxa, three out of four group very close to each other, with the exception of *Pongo*, which is situated closer to the larger-bodied apes. The AQ/Leapers overlap entirely with the other AQ, with the exception of *Cebuella*. Slow climbers group together and

show a clear distinction along PC2 between the small- and large-bodied taxa. Semi-terrestrial taxa overlap with both AQ and TQ, and one of the taxa, *Lemur catta*, groups with the medium-sized strepsirrhines (both VCL and AQ). Cercopithecine terrestrial quadrupeds group together and away from the ape terrestrial quadrupeds *Gorilla* and *Pan*, which may be a result of both body size and/or phylogeny. Finally, the VCL taxa are quite spread out, with the larger-bodied taxa lying on the negative end of PC2 and the small-bodied *Tarsius* and *Galago* on the positive end of PC2.

Locomotor group patterns: PCs 3 and 4. Plots of PC3 on PC4 of both individual specimens (Fig. 4-74) and taxon means (Fig. 4-75) do not show clear differentiation among taxonomic, locomotor, body size, or sex groups. Taxa within the slow climbing and suspensory locomotor groups are clustered, while the rest are more spread out (generalized AQ, AQ/Leapers, AQ/Suspensory, AQ/TQ, TQ, and VCL, Fig. 4-75). Similar to the pattern observed in the PC1 and PC2 data, spread within locomotor categories on PCs 3 and 4 seems to be related to body size differences.

Morphological patterns: PC 1. Principal component 1 sorts specimens by size and relates most notably to ilium dimensions, but also to pubis shape, ischium orientation, and acetabulum size (Fig. 4-73). Positive loadings on PC1 demonstrate a shorter distance between the ASIS and PSIS, a more anteriorly-oriented ASIS, and a longer iliac blade. These three traits result in a long, narrow, anteriorly-oriented iliac blade. Pubis shape becomes mediolaterally longer and craniocaudally narrower (owing to a shorter pubic symphysis) towards the

positive side of PC1, which results in a rectangular or somewhat triangular pubis. Positive loadings on PC1 also illustrate a short ischium that is parallel to the long axis of the pelvis, and a small acetabulum. Locomotor categories that are on the positive end of PC1 are arboreal quadrupeds, slow climbers, and some vertical clingers and leapers.

Moving from the positive end to the negative end of PC1, the ASIS becomes more laterally-oriented, the PSIS more posteriorly-oriented, and the iliac blade shorter and wider. The pubis becomes mediolaterally shorter and the pubic symphysis longer, resulting in a square—short and stout—shape. The ischium elongates and projects dorsally and the acetabulum increases in diameter. The negative morphospace of PC1 is inhabited by suspensory, TQ, and some semi-terrestrial taxa.

Morphological patterns: PC 2. Principal component 2 also differentiates among iliac blade, pubic, and ischium dimensions, but it also differentiates the shape of the AIIS (Fig. 4-73). The positive loadings on PC2 indicate a narrow iliac blade with a long lower iliac region. The pubis is characterized by a short symphysis and long rami, resulting in a mediolaterally long and craniocaudally short pubis, much like the positive loadings on PC1. Additionally, the ischium is short and the AIIS does not project from the lateral iliac margin. Suspensory, slow climbing, and some VCL taxa are located on the positive morphospace of PC2.

The negative loadings on PC2 indicate a wider iliac blade and a shorter lower iliac region. The pubis has short rami and a long symphysis, which results in a mediolaterally short and craniocaudally deep pubis. The AIIS becomes large

and protrudes anteriorly from the lateral margin of the iliac blade. Most of the VCL, AQ/leapers, and AQ taxa are located in the negative portion of PC2. Terrestrial quadrupeds span both sides of PC2.

Morphological patterns: PC 3. Positive loadings on principal component 3 are associated with a longer lower iliac region, a more inferiorly-placed ASIS, long pubic rami, a short pubic symphysis, a short ischium that is parallel to the long axis of the ilium, and a large acetabulum (Fig. 4-75). Taxa that are positioned along the positive portion of PC3 include some of the arboreal quadrupeds, most terrestrial quadrupeds, some of the VCL, and all of the AQ/leapers and semi-terrestrial taxa.

Negative loadings on PC3 indicate a shorter lower iliac region and a more superiorly-oriented ASIS, shorter pubic rami with a long pubic symphysis, a longer more dorsally-projecting ischium, and a relatively small acetabulum. Suspensory and slow climbing taxa are located on the negative end of PC3, as well as some of the VCL and AQ taxa.

Morphological patterns: PC 4. Positive loadings on PC4 are associated with a anterolaterally-oriented ASIS, somewhat shorter pubic rami and symphysis, and an ischium that is parallel to the long axis of the ilium (Fig. 4-75). The only locomotor group whose taxa are all located on the positive side of PC4 is slow climbers. Negative loadings on PC4 are associated with a more laterally-oriented ASIS, longer pubic rami and symphysis, and a slightly dorsally-projecting ischium. All remaining locomotor groups are randomly positioned on both the negative and positive ends of PC4.

Allometric scaling. To investigate whether any of the principal components are correlated with size, each principal component was regressed on ln centroid size (Table 4-22). Of the first ten principal components, two are statistically correlated with size at the 0.05 significance level: PC1 (Pearson r = -0.85, $p < 0.0001$) and PC 4 (Pearson r = -0.41, p = 0.006).

As ln centroid size increases, the scores of PCs 1 and 4 become negative (Figs. 4-76 and 4-77). Negative loadings on PC1 indicate a short, wide iliac blade with a laterally-oriented ASIS, a square pubis (with short pubic rami and a long pubic symphysis), a long and more dorsally-projecting ischium, and a larger acetabulum. Negative loadings on PC4 also indicate a laterally-oriented ASIS, a long pubic symphysis, and a dorsally-projecting ischium, but also a slightly conflicting result with that of PC1—slightly longer pubic rami.

The scaling results from PCs 1 and 4 suggest that as size increases, the pelvis becomes shorter and wider, likely as a response to the biomechanical requirements of increased loads that accompany large body size. The results of PCs 1 and 4 are largely in agreement, except for a slight difference in the lengths of the pubic rami.

TABLE 4-21. PCA results for all landmarks; Homo sapiens *excluded*

PC	Eigenvalue	Proportion of variance (%)	Cumulative variance (%)
1	0.01136	32.8	32.8
2	0.00451	13.0	45.9
3	0.00416	12.0	57.9
4	0.00282	8.2	66.1
5	0.00177	5.1	71.2
6	0.00118	3.4	74.6
7	0.00095	2.7	77.4
8	0.00081	2.3	79.7
9	0.00069	2.0	81.7
10	0.00061	1.8	83.5
11	0.00054	1.6	85.0
12	0.00047	1.3	86.4
13	0.00040	1.2	87.5
14	0.00038	1.1	88.6
15	0.00035	1.0	89.6
16	0.00032	0.9	90.5
17	0.00028	0.8	91.4
18	0.00025	0.7	92.1
19	0.00023	0.7	92.7
20	0.00021	0.6	93.4

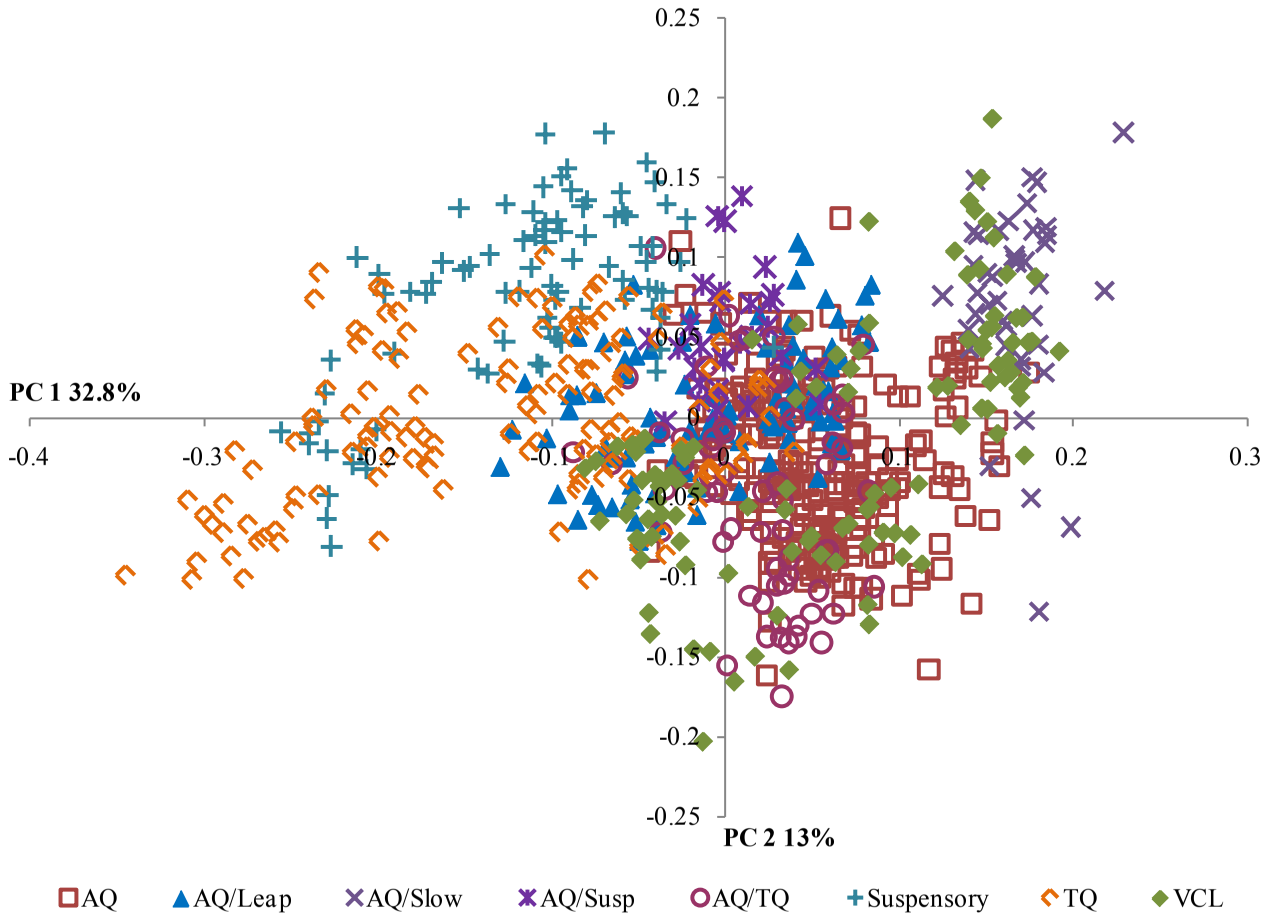

Fig. 4-72. Bivariate plot of principal component 1 on principal component 2 for the dataset containing all landmarks. Individuals are plotted (n = 794).

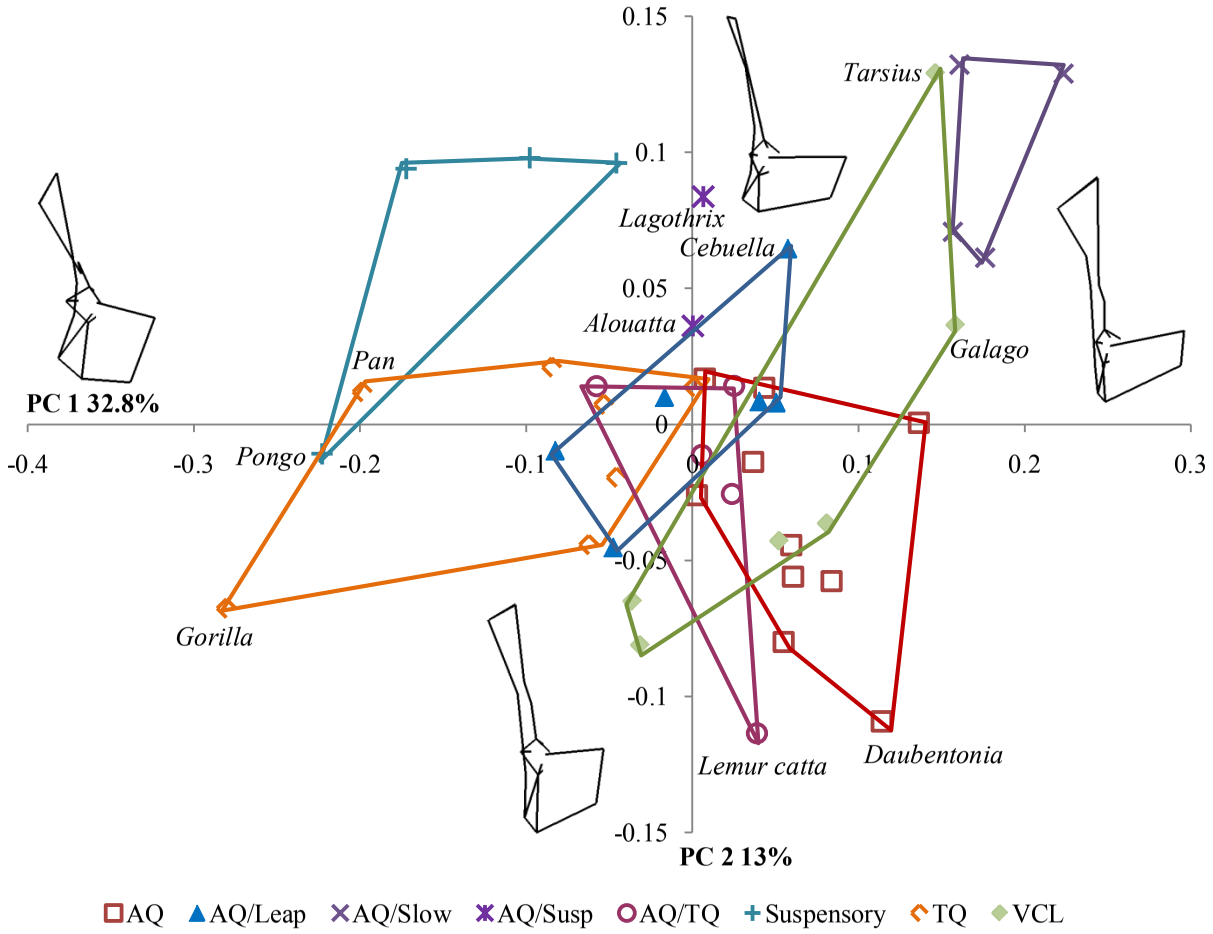

Fig. 4-73. Bivariate plot of principal component 1 on principal component 2 for the dataset containing all landmarks. Taxon means are plotted (n = 44). Wireframes of the consensus pelvic shape at the ends of the principal component axes are shown.

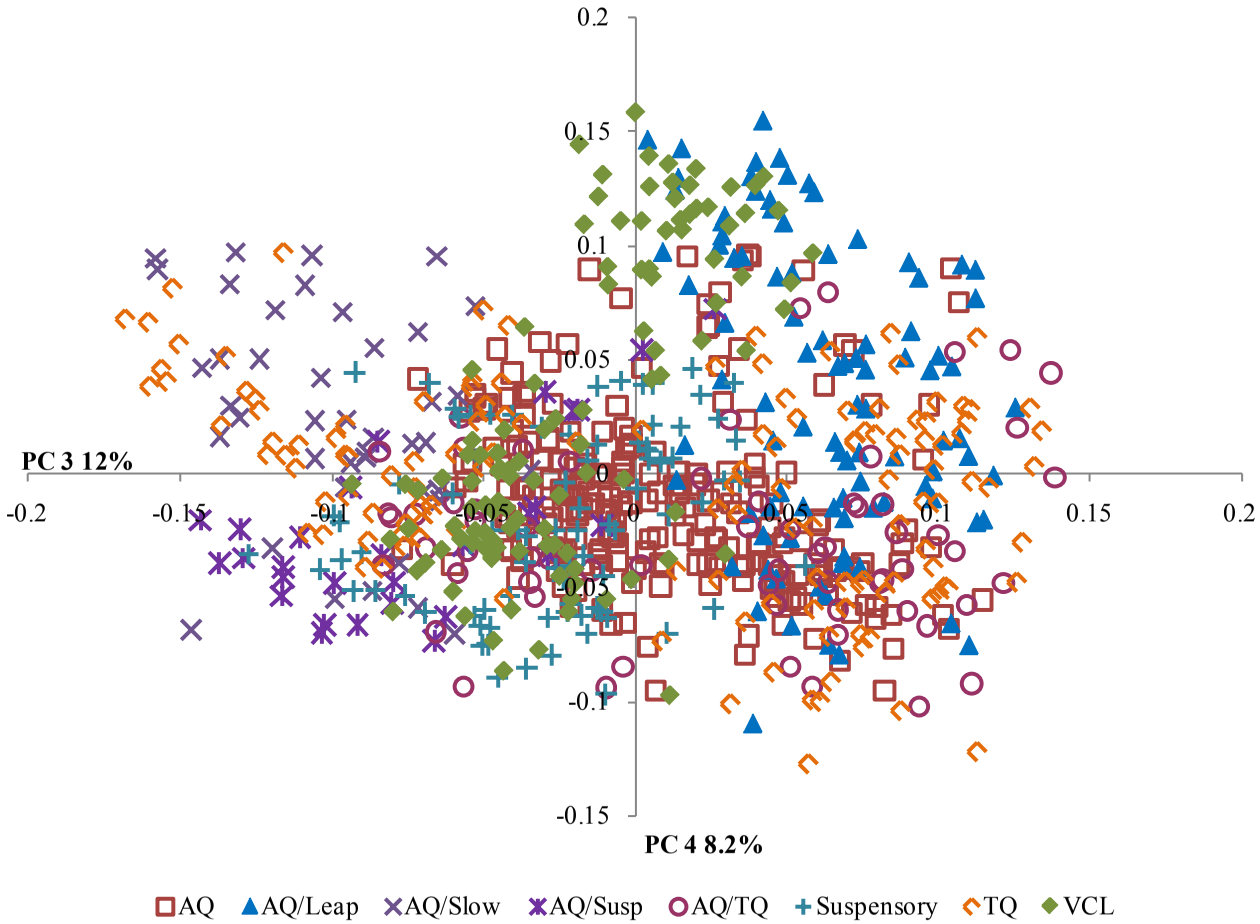

Fig. 4-74. Bivariate plot of principal component 3 on principal component 4 for the dataset containing all landmarks. Individuals are plotted (n = 794).

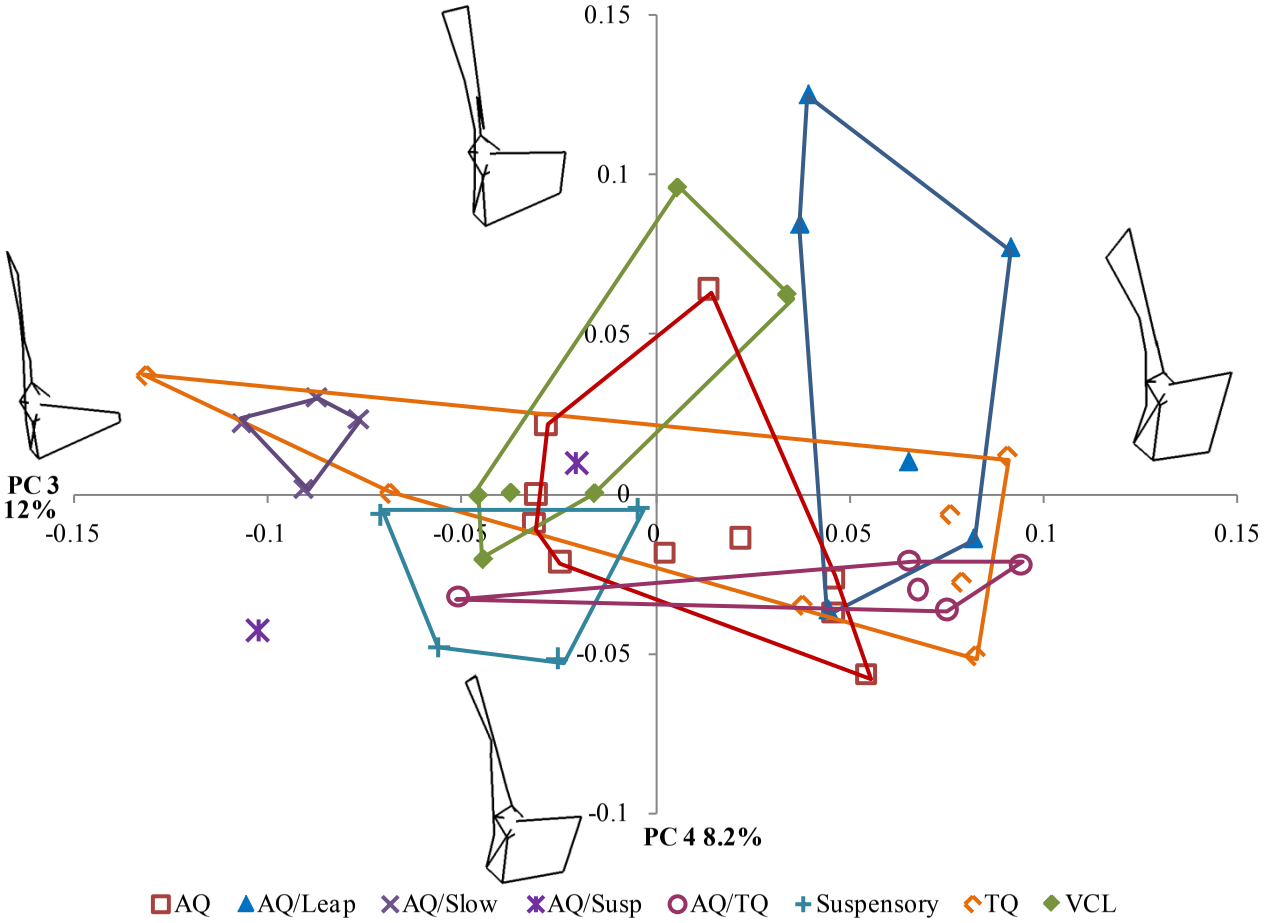

Fig. 4-75. Bivariate plot of principal component 3 on principal component 4 for the dataset containing all landmarks. Taxon means are plotted (n = 44). Wireframes of the consensus pelvic shape at the ends of the principal component axes are shown.

TABLE 4-22. Results of least squares regression of principal component scores on ln centroid size

PC	All landmarks[a,b]		Ilium and acetabulum subset[a,b]		Ischiopubis and acetabulum subset[a,b]		All landmarks, hominoids only[a]	
	Correlation (Pearson's *r*)	*p*	Correlation (Pearson's *r*)	*p*	Correlation (Pearson's *r*)	*p*	Correlation (Pearson's *r*)	*p*
1	**-0.8505**	**<0.0001**	**0.7942**	**<0.0001**	**0.5862**	**<0.0001**	**0.3255**	**<0.0001**
2	-0.2729	0.0731	**-0.4158**	**0.0050**	**0.4238**	**0.0041**	**0.8591**	**<0.0001**
3	0.1632	0.2897	0.2673	0.0794	0.1286	0.4053	-0.0671	0.4039
4	**-0.4060**	**0.0063**	**0.3187**	**0.0350**	**-0.3246**	**0.0316**	**-0.1700**	**0.0333**
5	0.0223	0.8857	-0.1051	0.4973	**-0.3616**	**0.0159**	-0.0011	0.9890
6	0.1551	0.3147	-0.2393	0.1177	-0.2172	0.1568	-0.0154	0.8482
7	0.0439	0.7772	-0.1763	0.2523	0.0974	0.5292	0.1432	0.0736
8	-0.2387	0.1186	0.1198	0.4385	-0.0853	0.5819	-0.0800	0.3193
9	-0.2106	0.1700	-0.2765	0.0692	0.1961	0.2021	-0.0528	0.5116
10	0.0452	0.7706	0.1119	0.4697	0.1377	0.3727	0.0117	0.8842

[a]Using taxon means for PC scores and ln centroid size, n = 44; bold denotes statistical significance at the 0.05 level

[b]*Homo sapiens* excluded

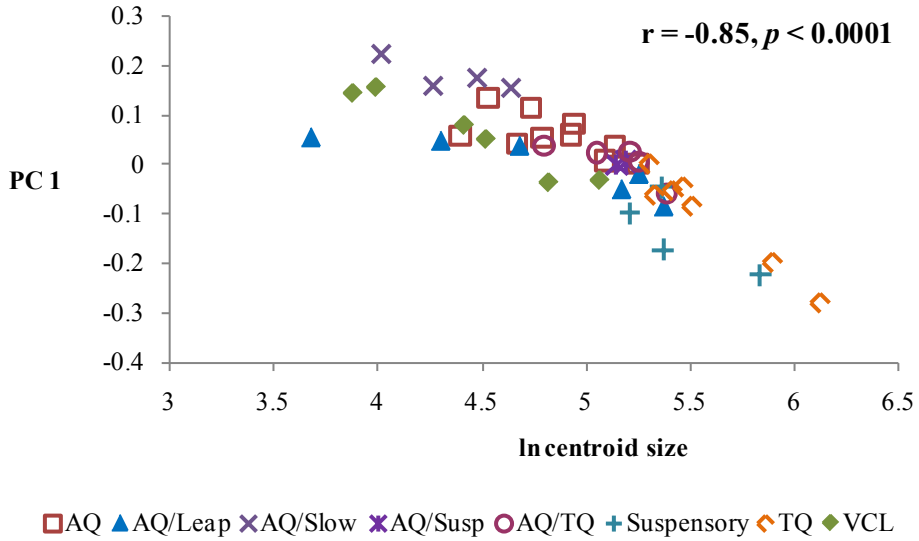

Fig. 4-76. Bivariate plot of principal component 1 on ln centroid size for the dataset containing all landmarks. Results of the Pearson's correlation are included. Points are taxon means (n = 44).

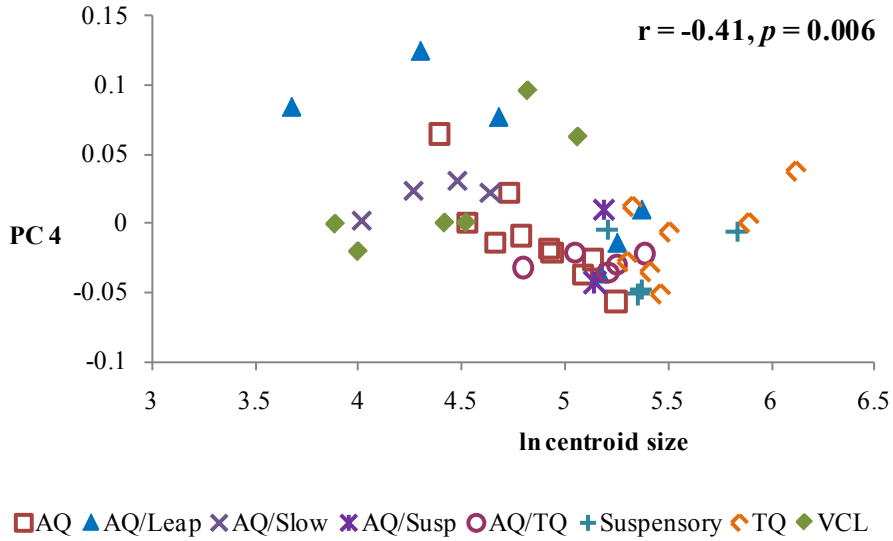

Fig. 4-77. Bivariate plot of principal component 4 on ln centroid size for the dataset containing all landmarks. Results of the Pearson's correlation are included. Points are taxon means (n = 44).

Ilium landmarks

The first 20 principal components derived from the data subset containing the ilium and acetabulum landmarks account for 96.6% of the variation in shape (Table 4-23). The first four components alone account for 78% (PC1 44.1%, PC2 18.5%, PC3 9.5%, and PC4 5.9%).

Locomotor group patterns: PCs 1 and 2. A plot of PC1 on PC2 using individual specimens demonstrates differentiation among taxa in body size along PC1 (Fig. 4-78), and a lack of differentiation in taxa along PC2. A plot of PC1 on PC2 using taxon means demonstrates slight differentiation based on locomotor category (Fig. 4-79), but like the data for the entire pelvis, the locomotor groups overlap extensively in the middle of the plot.

General AQ taxa are clustered together and partially overlap other groups (Fig. 4-79). The AQ/Suspensory taxa are not clustered closely, but are located between the AQ and the suspensory groups. The suspensory taxa overlap slightly with the TQ and AQ/leapers. Interestingly, there is strong phylogenetic differentiation within AQ/Leapers between the platyrrhines and catarrhines that is not influenced by body size, as the small-bodied *Leontopithecus* and *Cebuella* group with the relatively larger-bodied *Pithecia*. The slow climbers only overlap slightly with the VCL group. The semi-terrestrial taxa overlap with both the AQ and TQ taxa, as might be expected, but also slightly with the VCL group. The TQ taxa are clustered into two subgroups, with the cercopithecines forming a dense group and the large-bodied apes spread out both from each other and from the cercopithecines. Finally, the VCL taxa overlap with several groups, and exhibit a

possible size difference in shape, with the small-bodied *Tarsius* and *Galago* clustering away from the rest of the VCLs.

Locomotor group patterns: PCs 3 and 4. Plots of PC3 on PC4 on both individual specimens (Fig. 4-80) and taxon means (Fig. 4-81) show no differentiation among taxonomic, locomotor groups, body size, or sex groups.

General AQ taxa are spread out along PC4, with the platyrrhines and strepsirrhines located on one end and the cercopithecines on the other. The cercopithecine AQ taxa cluster with the other cercopithecines (AQ/TQ and TQ), again indicating that phylogeny may result in differences in pelvic shape. The AQ/Suspensory taxa are spread out, as in the plots of PCs 1 and 2. The suspensory taxa are near each other, but appear to separate slightly based on body size: the smaller-bodied *Hylobates* and *Ateles* are located close to each other, while the larger-bodied *Symphalangus* and *Pongo* are in proximity to each other. The AQ/Leapers are somewhat spread out and overlap with both AQ and TQ taxa. Three of the four slow climbing taxa cluster together, while *Nycticebus pygmaeus* is slightly distanced. The semi-terrestrial taxa overlap with other cercopithecines, but form a dense group. The TQ taxa form a large group, once again, but the spread of variation is less than that for PCs 1 and 2. Finally, VCL taxa form two separate groups, with indriids (*Indri* and *Propithecus*) grouping together and away from the rest of the taxa.

Morphological patterns: PC 1. Positive loadings on PC1 are associated with an increased distance between the ASIS and PSIS, which widens the iliac blade, which is oriented laterally (Fig. 4-79). The AIIS is more anterior compared to the

ASIS, and the lower iliac region is shorter. The acetabulum is slightly larger in diameter. The terrestrial quadrupeds and suspensory taxa are positioned along the positive end of PC1.

Negative loadings on PC1 are associated with a narrow iliac blade that is oriented slightly anteriorly, with an anteriorly placed ASIS. The ASIS and AIIS lie in the same frontal plane. The lower iliac region is longer and the acetabulum smaller. The remaining locomotor groups are located on the negative side of PC1.

Morphological patterns: PC 2. PC2 reflects minimal shape differences among taxa. The only morphology that changes along the axis of PC2 is the location of the narrowest part of the lower ilium, which is near the acetabulum on the positive end of PC2, and nearer the sacrum on the negative end (Fig. 4-79).

The taxa located on the positive side of PC2 are the slow climbers, most of the AQ/Leapers and suspensory taxa. Most of the AQ taxa are on the negative end of PC2, and the rest of the locomotor categories are distributed somewhat evenly on both the positive and negative ends.

Morphological patterns: PC 3. The morphologies loading on PC3 are the height and width of the iliac blade, the length of the lower ilium, and the size of the AIIS. Positive loadings on PC1 are associated with an ASIS located superior to the PSIS, a wide blade with a short lower ilium, and a larger AIIS (Fig. 4-81). The taxa on the positive end of PC3 are the large-bodied VCL taxa, most of the terrestrial quadrupeds, the semi-terrestrial quadrupeds, the AQ/Leapers, and most of the arboreal quadrupeds.

Negative loadings on PC3 are associated with an ASIS located inferior to the PSIS, a narrow blade with a longer lower ilium, and a smaller AIIS. The taxa on the negative end of PC3 include the suspensory taxa, slow climbers, and smaller-bodied VCL.

Morphological patterns: PC 4. Like principal component 3, PC4 reflects blade dimensions and the size of the AIIS (Fig. 4-81). Positive loadings on PC4 are associated with a wide iliac blade, a longer lower iliac region, and a small AIIS. Negative loadings on PC4 are associated with a narrower iliac blade, a shorter lower iliac region, and a larger AIIS. Members of locomotor categories are spread between both the positive and negative ends of PC4.

Allometric scaling. Of the first ten principal components, three are significantly correlated with ln centroid size at the 0.05 level: PC 1 (Pearson $r = 0.79$, $p < 0.0001$), PC 2 (Pearson $r = -0.41$, $p = 0.006$), and PC4 (Pearson $r = 0.32$, $p = 0.035$) (Table 4-22).

As size increases, the loadings on PC1 become positive, which is associated with a wide iliac blade with a short lower iliac region, and a more anteriorly-positioned AIIS and a larger acetabulum. The loadings on PC2 become negative, resulting in a superior position of the narrowest part of the lower ilium. The loadings on PC4 become positive, which relates to a wide iliac blade, a longer lower iliac region, and a small AIIS. It is clear that iliac blade width and acetabulum diameter increase as size increases, but the results of the size correlations among PCs 1 and 4 conflict regarding the length of the lower iliac region (Figs. 4-82 to 4-84).

TABLE 4-23. PCA results for ilium and acetabulum landmarks; Homo sapiens *excluded*

PC	Eigenvalue	Proportion of variance (%)	Cumulative variance (%)
1	0.01411	44.1	44.1
2	0.00593	18.5	62.6
3	0.00303	9.5	72.1
4	0.00189	5.9	78.0
5	0.00099	3.1	81.0
6	0.00088	2.7	83.8
7	0.00070	2.2	86.0
8	0.00065	2.0	88.0
9	0.00053	1.6	89.7
10	0.00041	1.3	90.9
11	0.00032	1.0	91.9
12	0.00029	0.9	92.9
13	0.00024	0.8	93.6
14	0.00017	0.5	94.1
15	0.00016	0.5	94.6
16	0.00016	0.5	95.1
17	0.00014	0.4	95.6
18	0.00012	0.4	95.9
19	0.00010	0.3	96.3
20	0.00010	0.3	96.6

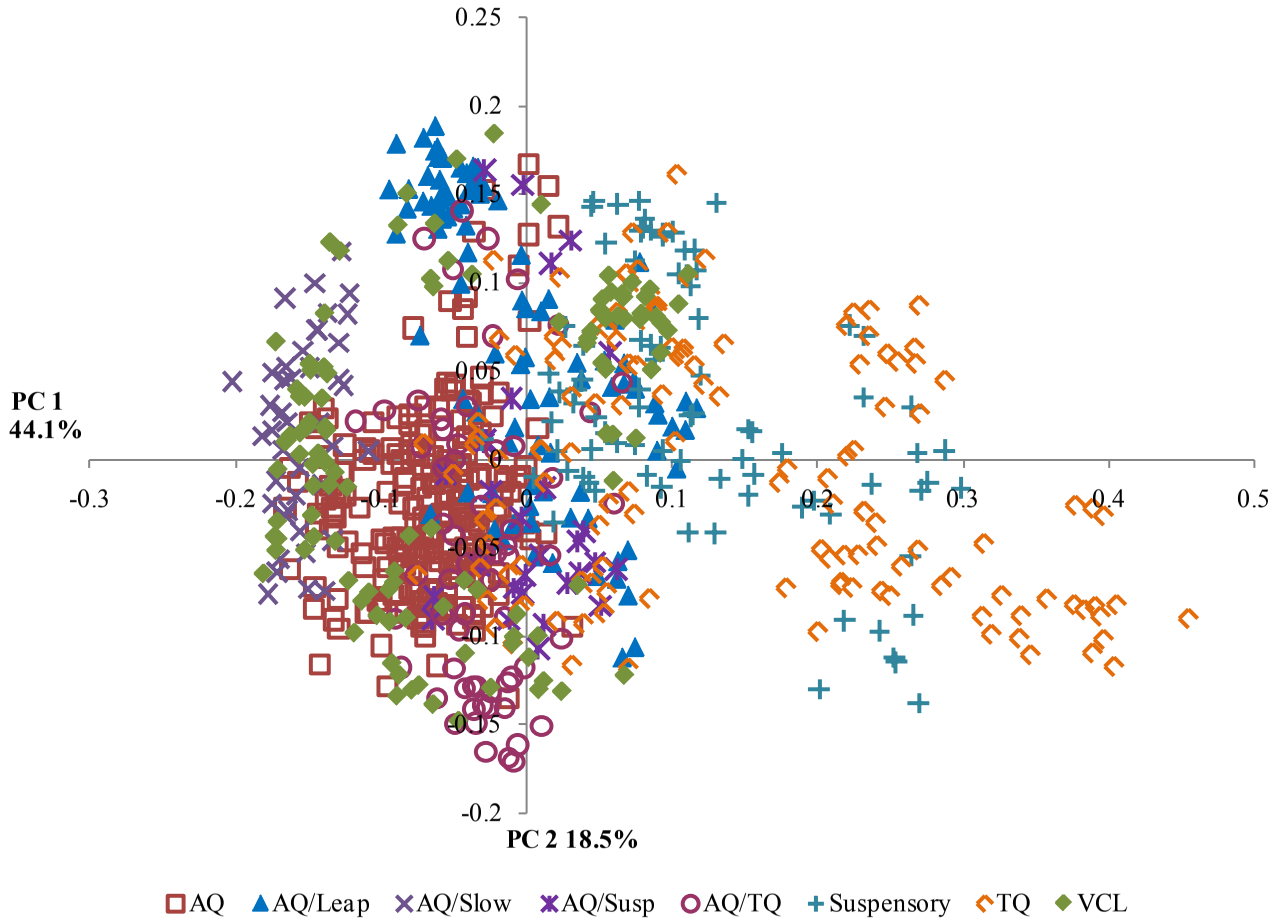

Fig. 4-78. Bivariate plot of principal component 1 on principal component 2 for the dataset containing ilium landmarks. Individuals are plotted (n = 794).

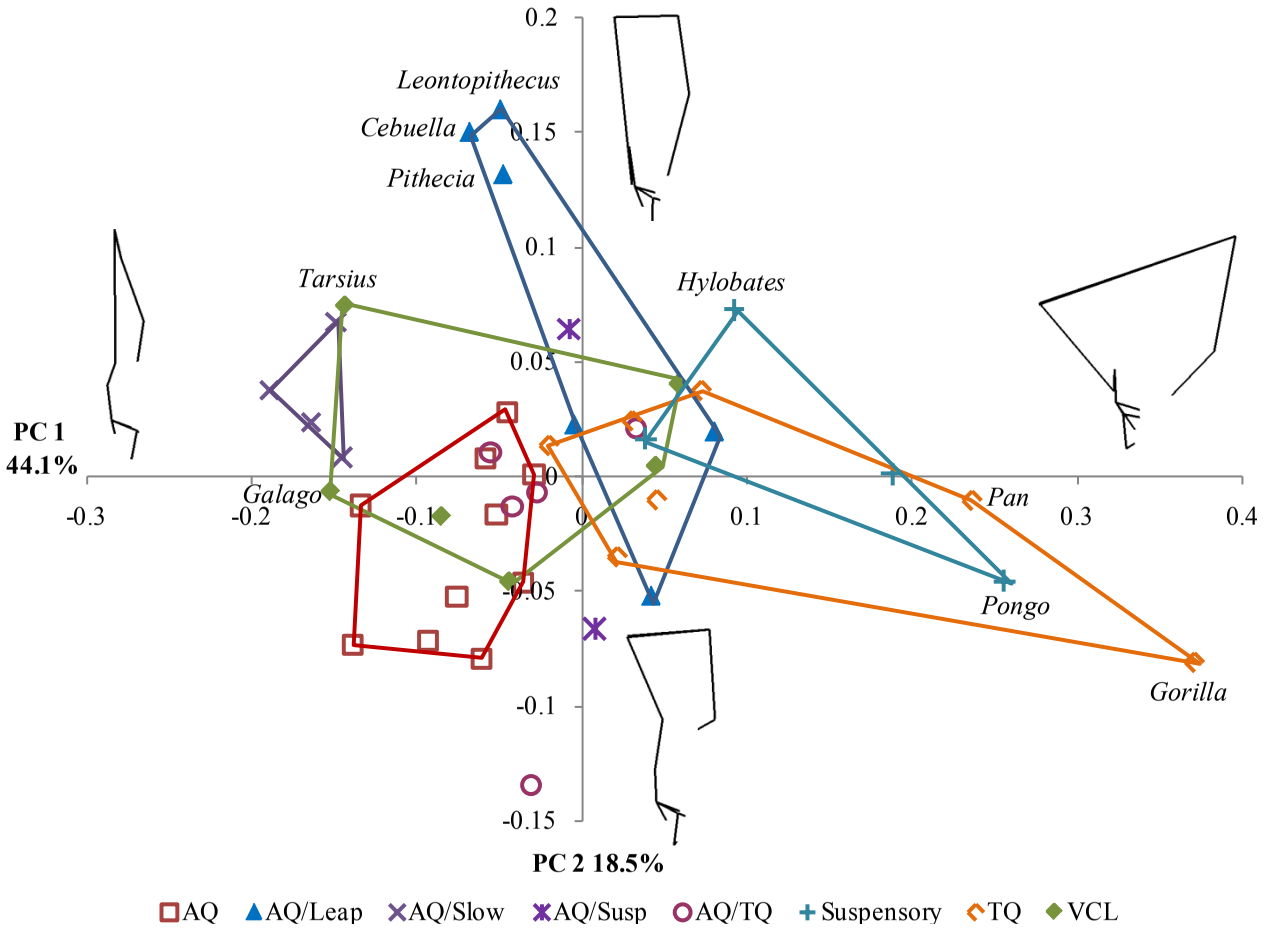

Fig. 4-79. Bivariate plot of principal component 1 on principal component 2 for the dataset containing ilium landmarks. Taxon means are plotted (n = 44). Wireframes of the consensus ilium shape at the ends of the principal component axes are shown.

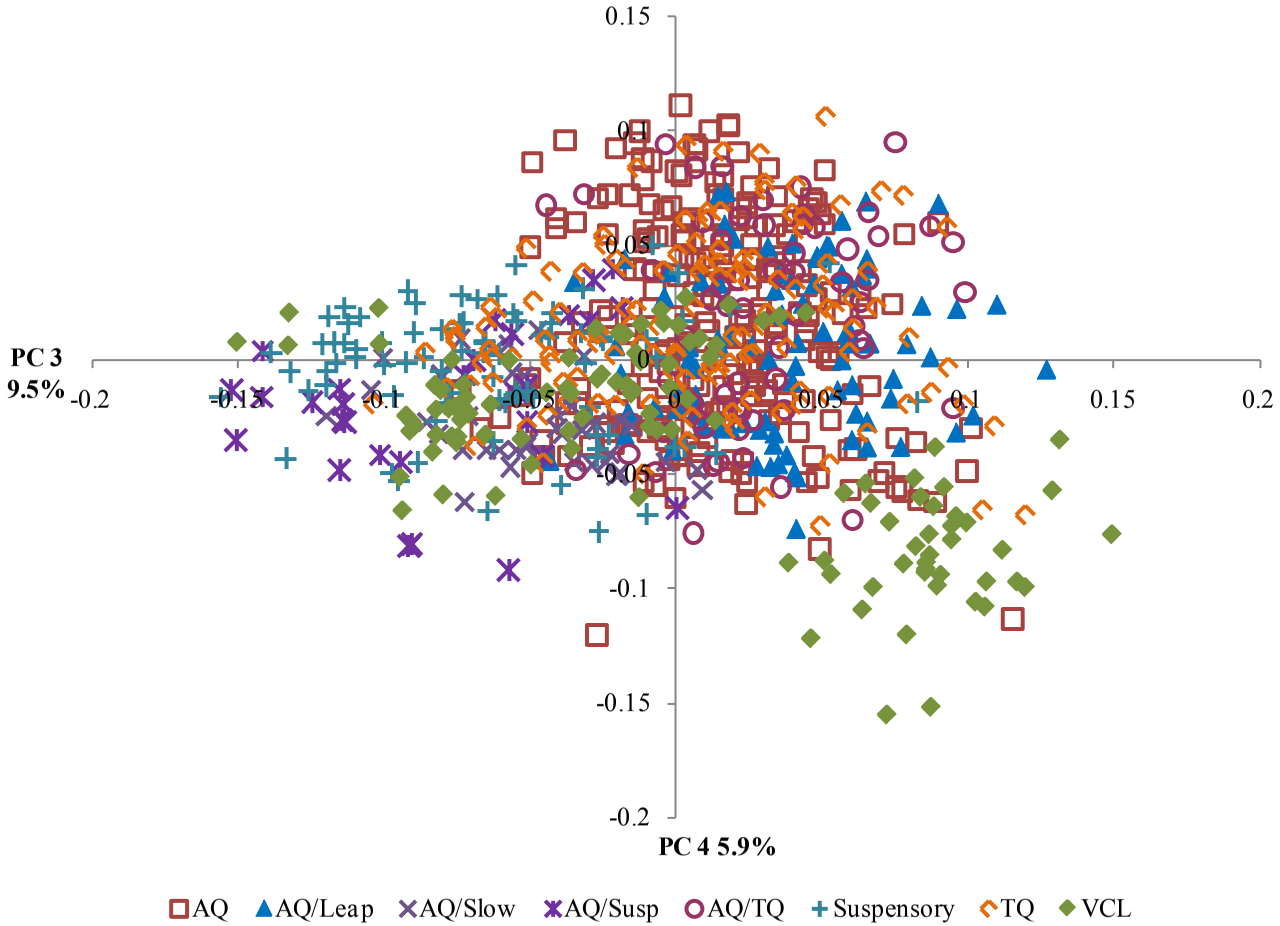

Fig. 4-80. Bivariate plot of principal component 3 on principal component 4 for the dataset containing ilium landmarks. Individuals are plotted (n = 794).

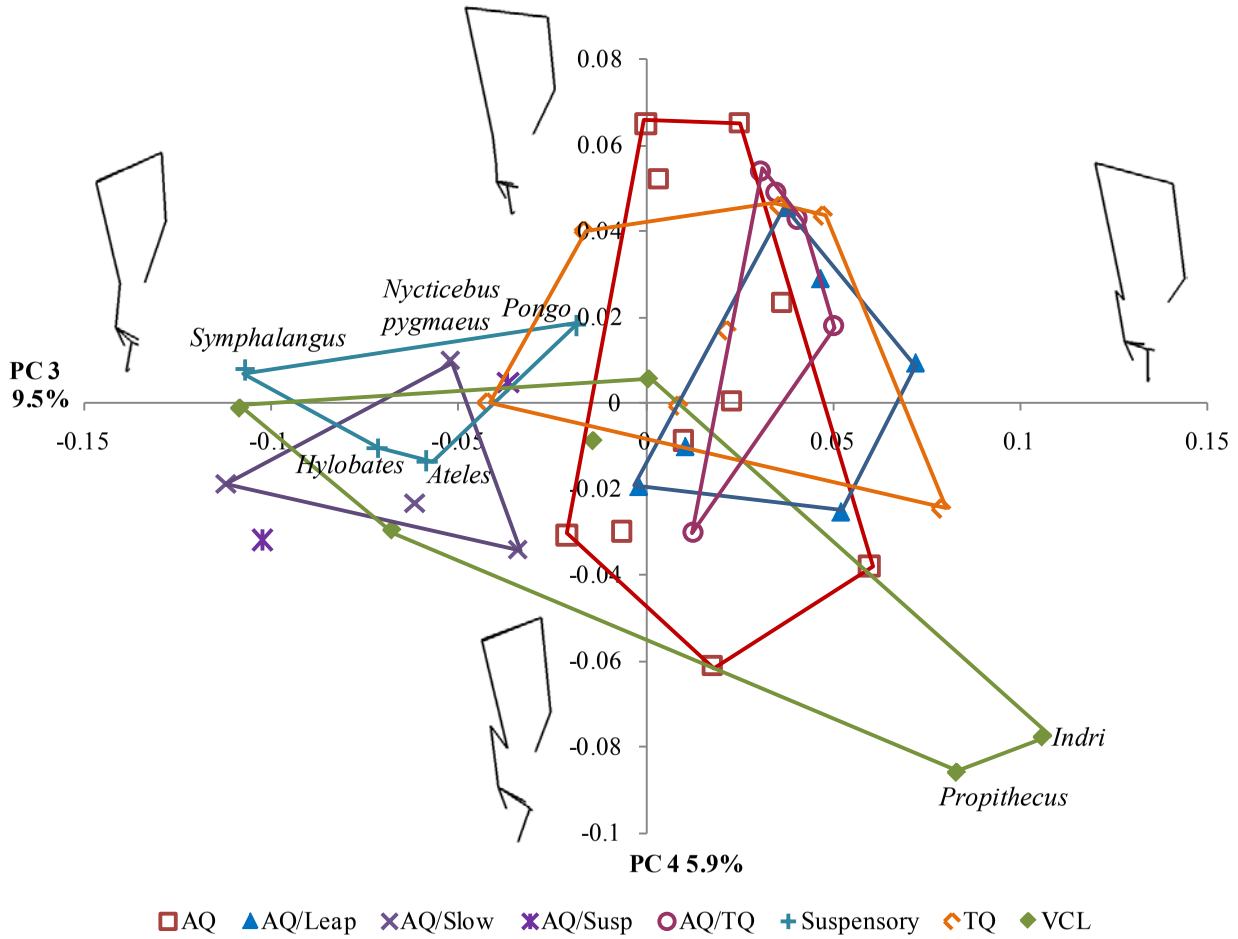

Fig. 4-81. Bivariate plot of principal component 3 on principal component 4 for the dataset containing ilium landmarks. Taxon means are plotted (n = 44). Wireframes of the consensus ilium shape at the ends of the principal component axes are shown.

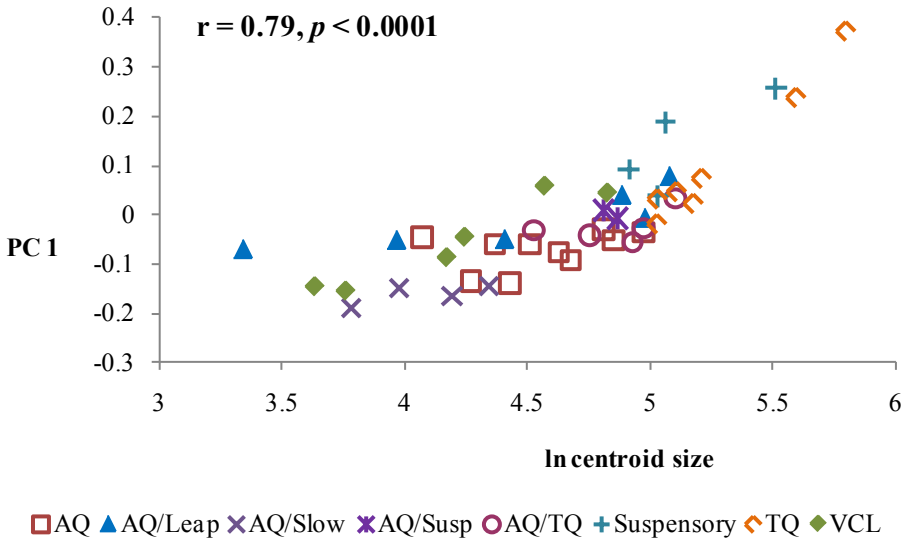

Fig. 4-82. Bivariate plot of principal component 1 on ln centroid size for the dataset containing ilium landmarks. Results of the Pearson's correlation are included. Points are taxon means (n = 44).

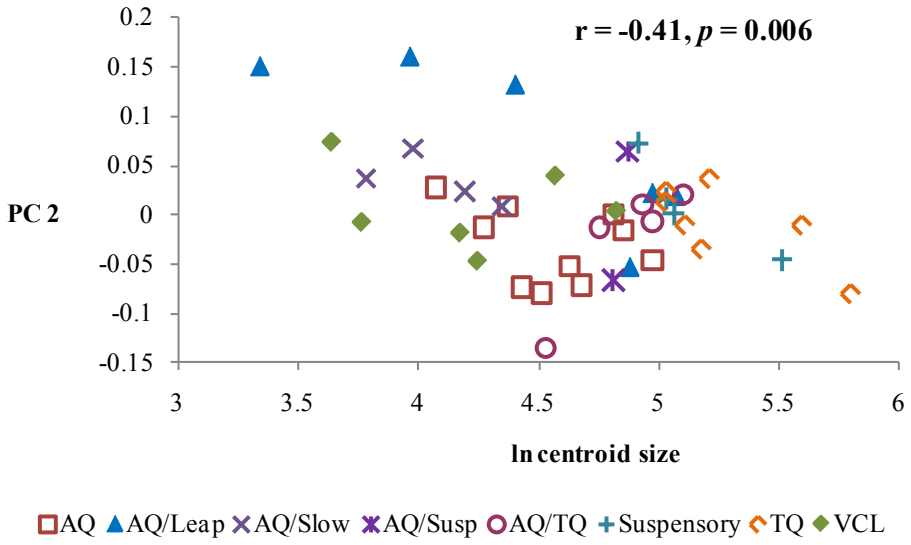

Fig. 4-83. Bivariate plot of principal component 2 on ln centroid size for the dataset containing ilium landmarks. Results of the Pearson's correlation are included. Points are taxon means (n = 44).

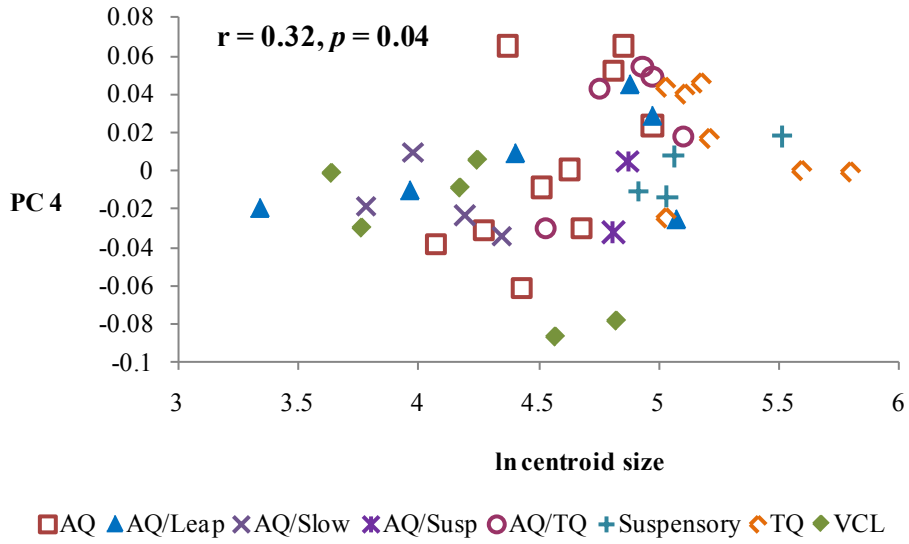

Fig. 4-84. Bivariate plot of principal component 4 on ln centroid size for the dataset containing ilium landmarks. Results of the Pearson's correlation are included. Points are taxon means (n = 44).

Ischiopubic landmarks

The first 20 principal components in the ischiopubis subset account for 96.7% of the variation in the sample. The first four principal components account for a total of 67.7% of the variation: PC1 37.8%, PC2 11.9%, PC3 10.4%, and PC4 7.6% (Table 4-24).

Locomotor group patterns: PCs 1 and 2. A plot of PC1 on PC2 using individual specimens demonstrates differentiation among taxa in body size along PC1 (Fig. 4-85), and no differentiation in taxa along PC2 in body size, locomotion, or phylogeny. A plot of PC1 on PC2 using taxon means demonstrates slight differentiation based on locomotor category (Fig. 4-86).

General AQ taxa overlap with several other groups (Fig. 4-86). Again, AQ/Suspensory taxa are not grouped with either the AQ or the suspensory groups. The suspensory, AQ/TQ, TQ, and AQ/Leapers generally overlap with each other.

Semi-terrestrial taxa partially overlap with AQ. The slow climbers do not overlap with other locomotor groups. The VCL taxa form a large group that overlaps the AQ group.

Locomotor group patterns: PCs 3 and 4. Plots of PC3 on PC4 for both individuals and taxon means do not show patterned differences in shape along either of the principal components (Figs. 4-87 and 4-88).

Morphological patterns: PC 1. The morphologies loading on PC1 are the lengths of the pubic rami, pubic symphysis, and ischium, the size of the ischial spine, and the shape of the acetabulum (Fig. 4-86). Positive loadings on PC1 are associated with a long pubic symphysis, shorter pubic rami, a long ischium with a larger spine, and an acetabulum characterized by a longer dorsoventral than craniocaudal diameter. In general, terrestrial and semi-terrestrial quadrupeds, AQ/Leapers, and most of the suspensory taxa fall on the positive side of PC1.

Negative loadings on PC1 indicate a shorter pubic symphysis, longer pubic rami, a short ischium with a small spine, and an acetabulum that is craniocaudally long. The mean ischiopubic shape along PC1 varies from triangular on the negative end to square on the positive end. The VCL and AQ taxa span both sides, while the slow climbers fall far on the negative end of the axis.

Morphological patterns: PC 2. Principal component 2 relates to ischium and pubic symphysis length (Fig. 4-86). Positive loadings on PC2 indicate a short ischium that does not project dorsally, and a long pubic symphysis, while negative loadings indicate a long, dorsally-projecting ischium and a short pubic symphysis.

Slow climbers and suspensory taxa plot on the positive side of PC2, while the rest of the locomotor groups span both the negative and positive ends of the PC2 axis.

Morphological patterns: PC 3. The shapes loading on PC3 are the lengths of the pubic rami, symphysis, and ischium (Fig. 4-88). Positive loadings on PC3 indicate slightly shorter rami, a short symphysis, and a long ischium, while negative loadings demonstrate longer rami, a longer symphysis, and a shorter, dorsally-projecting ischium.

Most of the locomotor groups span the negative and positive sides of PC3, except for the suspensory taxa, which fall on the positive end of the axis, and the slow climbers, which plot on the negative end.

Morphological patterns: PC 4. The morphologies loading on PC4 are pubic rami length, ischium length, ischial spine size, and acetabulum diameter (Fig. 4-88). Positive loadings on PC4 indicate shorter pubic rami, a short ischium with a small spine, and a large acetabulum. Negative loadings on PC4 indicate longer pubic rami, a long ischium with a larger spine, and a smaller acetabulum. The mean shape on the positive end of PC4 can be visualized as a rectangle that is craniocaudally long, while the shape on the negative end of PC4 is a rectangle that is mediolaterally or dorsoventrally long.

All of the locomotor groups but the slow climbers span both ends of the axis of PC4; the slow climbers plot on the negative end.

Allometric scaling. Four of the first ten principal components are significantly correlated with ln centroid size at the 0.05 level: PC1 (Pearson $r = 0.59$, $p <$

0.0001), PC2 (Pearson r = 0.43, p = 0.003), PC4 (Pearson r = -0.33, p = 0.03), and PC5 (Pearson r = -0.37, p = 0.01, Table 4-22). Principal component 5 is associated with the orientations of the pubic symphysis and ischium.

Because PC5 is significantly correlated with centroid size, a brief summary of its representative shape variation is necessary. Negative loadings on PC5 are associated with a more laterally-positioned superior pubic symphysis (Landmark 21, relative to the inferior aspect of the pubic symphysis), which results in a longer inferior pubic ramus, and an ischium that is oriented towards the sagittal plane (medially-flaring) and projects somewhat dorsally.

As size increases, principal components 1 and 2 become positive while PCs 4 and 5 become negative (Figs. 4-89 to 4-92). The pelvic shapes that are correlated with ln centroid size on these principal components are: a long pubic symphysis, a long ischium with a larger spine that is oriented dorsomedially, and an acetabulum with a shorter craniocaudal diameter (but a larger mediolateral diameter). There is a conflict between the loadings on PCs 1 and 4: PC1 indicates that pubic rami shorten with increasing size, while PC4 indicates that pubic rami lengthen with increasing size. In general, however, increasing centroid size is correlated with a deeper pubis and a larger pubic symphysis, perhaps to withstand the demands of increasing forces on pelvic structure that result from increasing body size.

TABLE 4-24. PCA results for ischiopubis and acetabulum landmarks; Homo sapiens *excluded*

PC	Eigenvalue	Proportion of variance (%)	Cumulative variance (%)
1	0.01425	37.8	37.8
2	0.00451	11.9	49.7
3	0.00391	10.4	60.1
4	0.00288	7.6	67.7
5	0.00212	5.6	73.3
6	0.00169	4.5	77.8
7	0.00121	3.2	81.0
8	0.00087	2.3	83.3
9	0.00085	2.3	85.6
10	0.00067	1.8	87.4
11	0.00065	1.7	89.1
12	0.00056	1.5	90.6
13	0.00041	1.1	91.7
14	0.00039	1.0	92.7
15	0.00036	1.0	93.7
16	0.00030	0.8	94.4
17	0.00026	0.7	95.1
18	0.00022	0.6	95.7
19	0.00019	0.5	96.2
20	0.00017	0.4	96.7

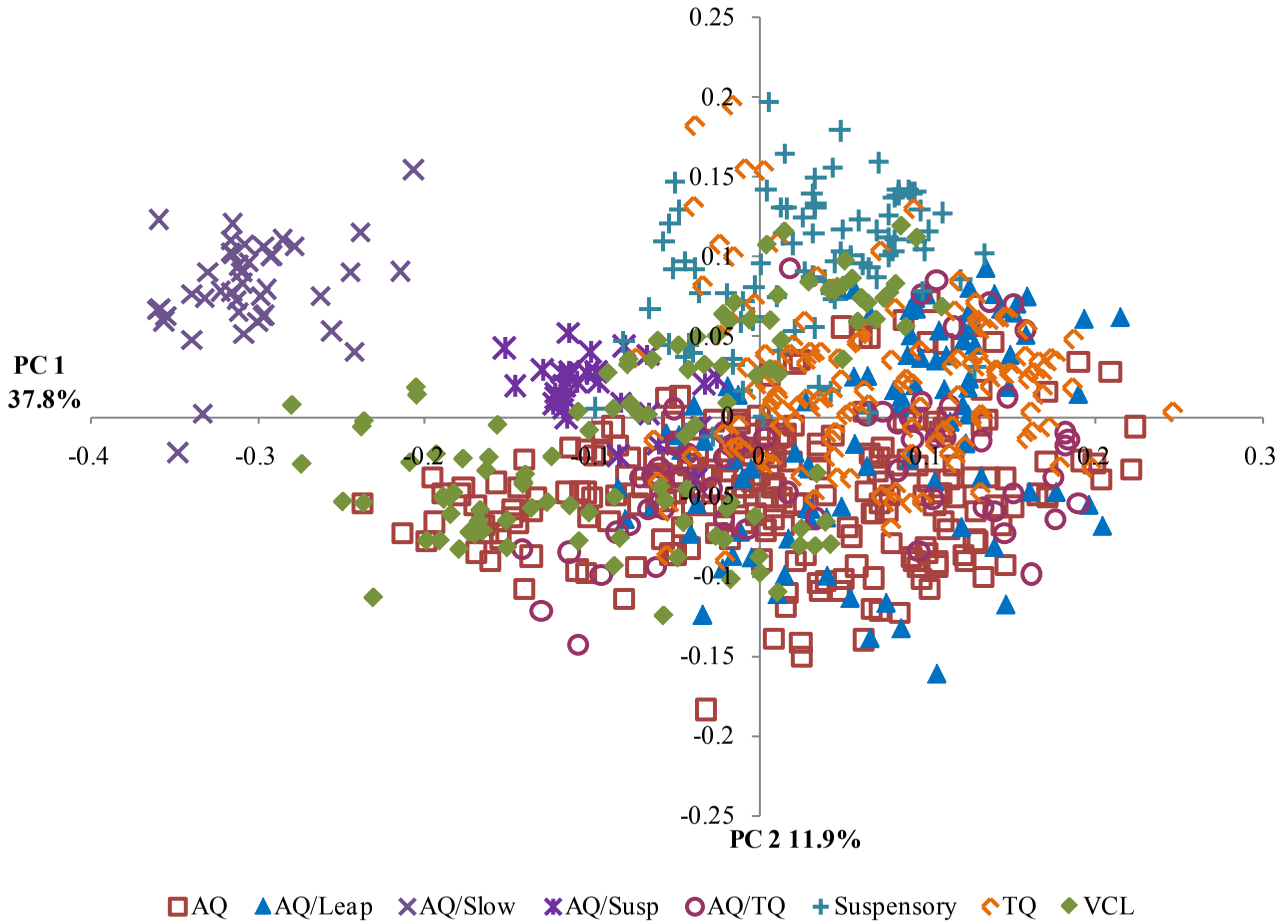

Fig. 4-85. Bivariate plot of principal component 1 on principal component 2 for the dataset containing ischiopubic landmarks. Individuals are plotted (n = 794).

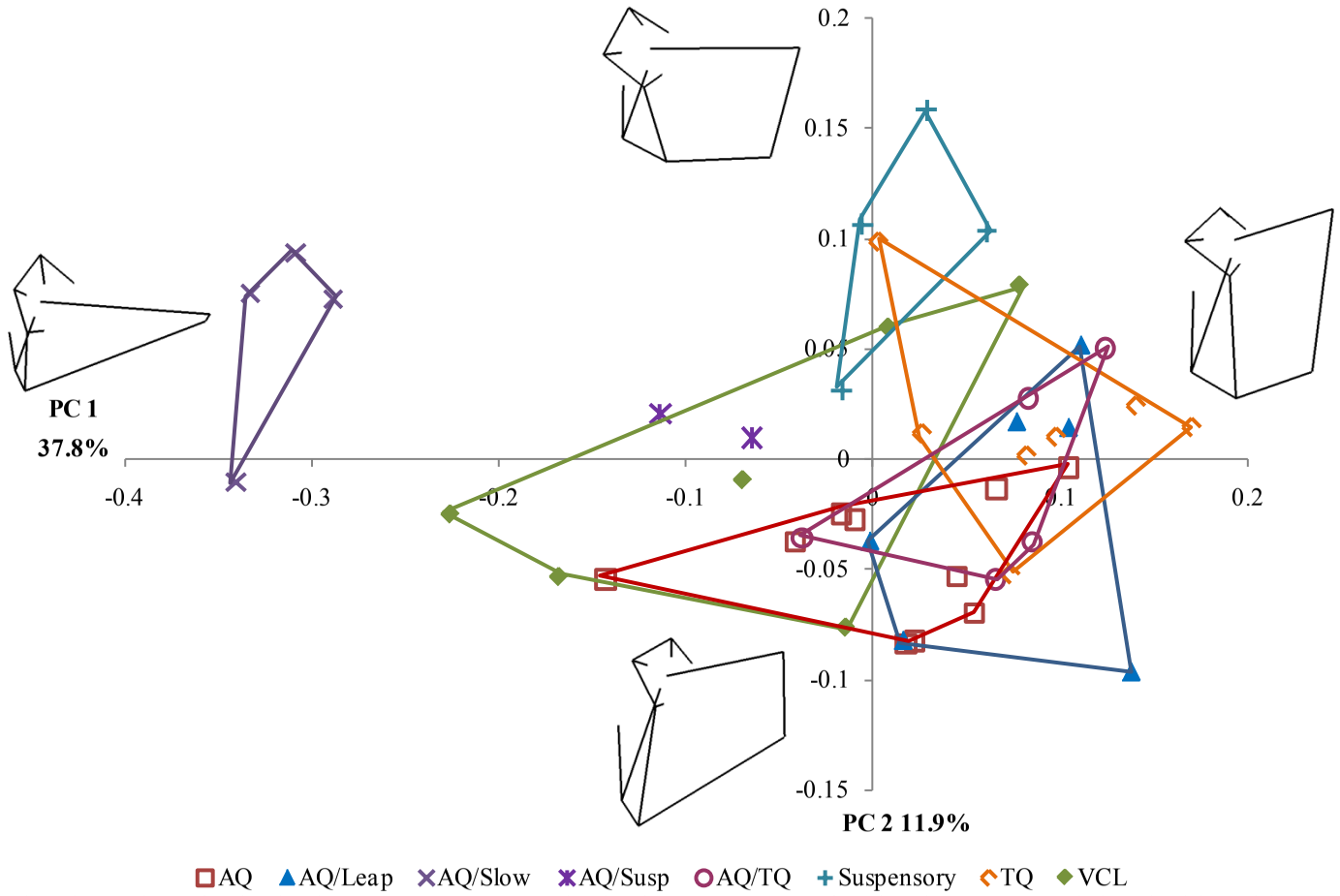

Fig. 4-86. Bivariate plot of principal component 1 on principal component 2 for the dataset containing ischiopubic landmarks. Taxon means are plotted (n = 44). Wireframes of the consensus ischiopubic shape at the ends of the principal component axes are shown.

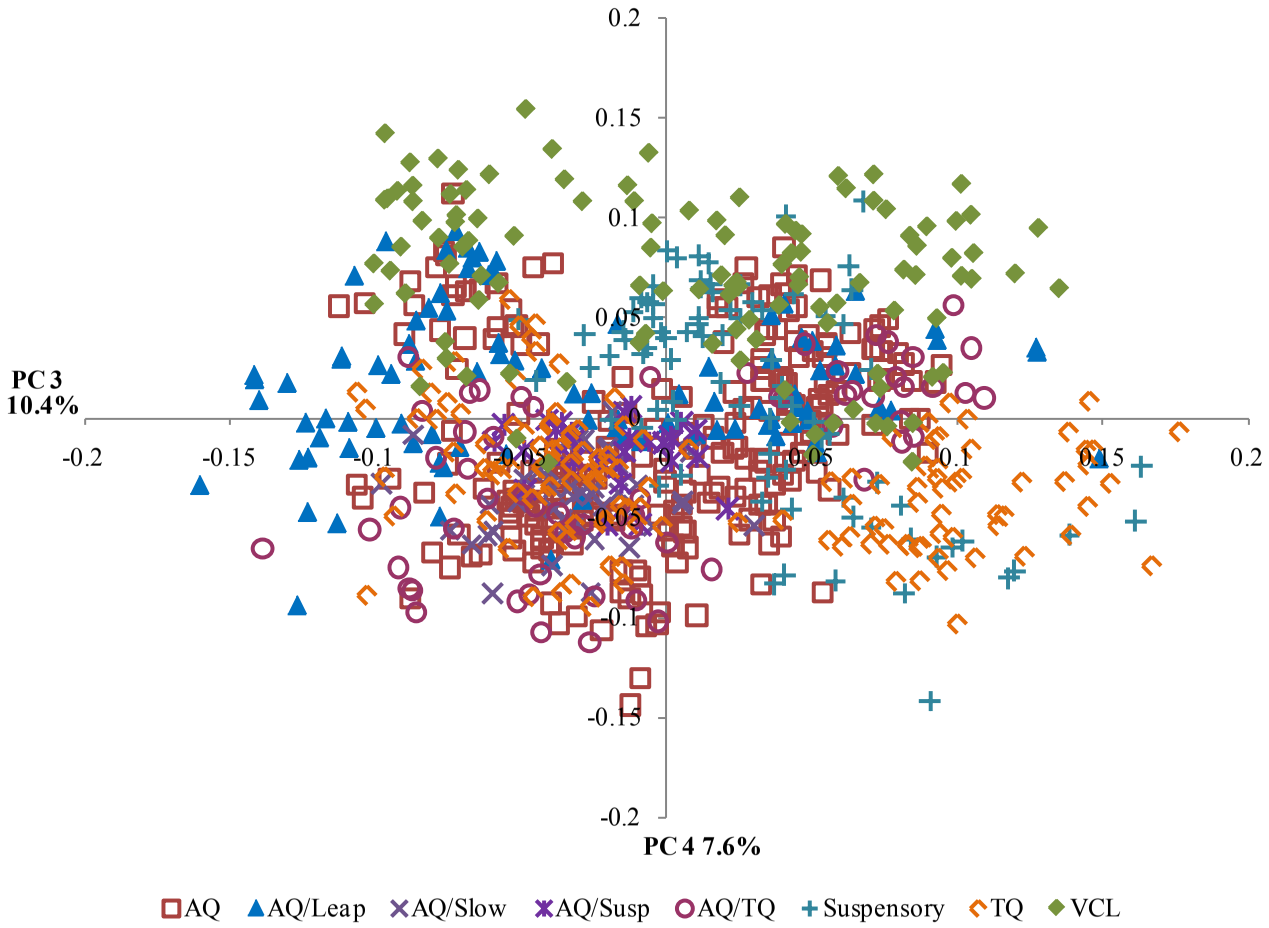

Fig. 4-87. Bivariate plot of principal component 3 on principal component 4 for the dataset containing ischiopubic landmarks. Individuals are plotted (n = 794).

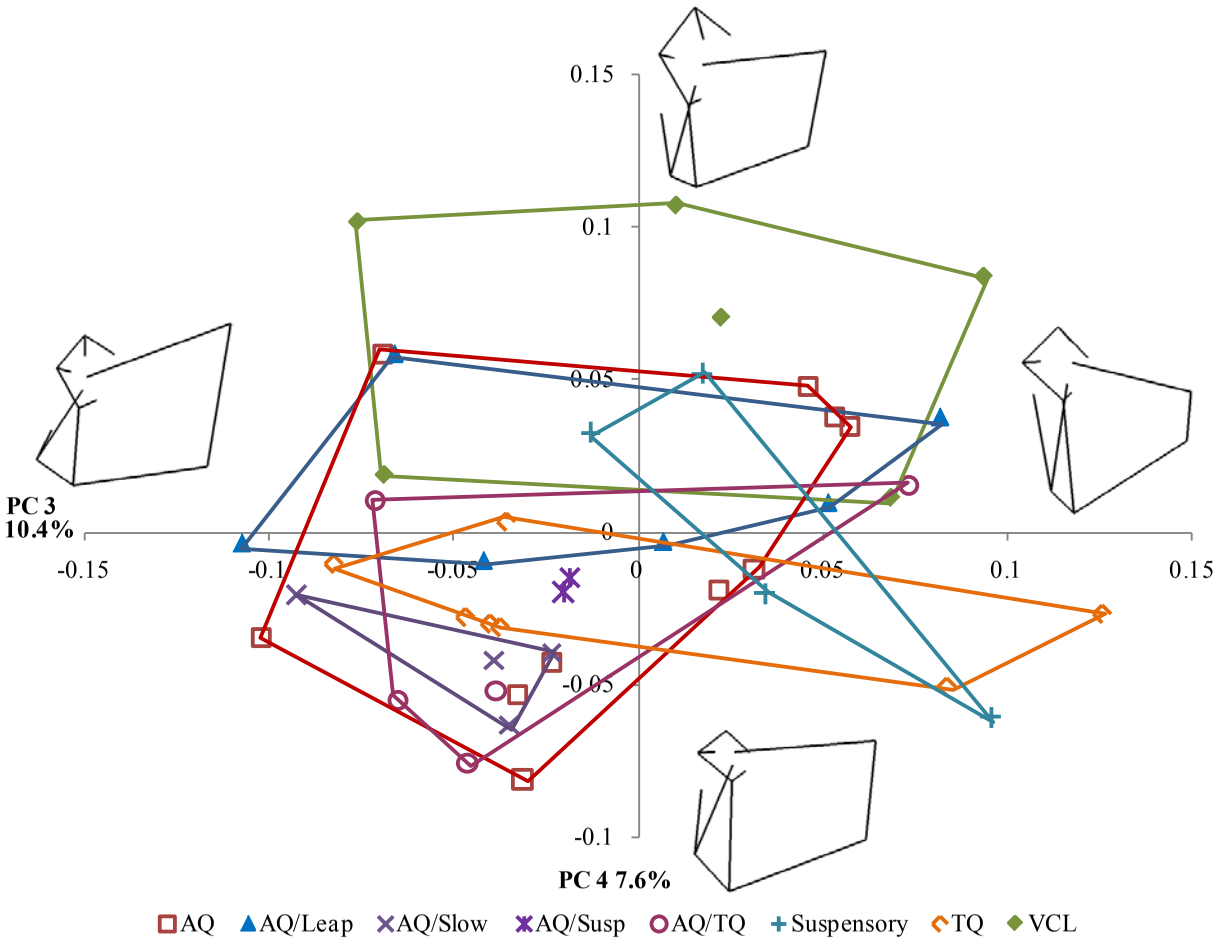

Fig. 4-88. Bivariate plot of principal component 3 on principal component 4 for the dataset containing ischiopubic landmarks. Taxon means are plotted (n = 44). Wireframes of the consensus ischiopubic shape at the ends of the principal component axes are shown.

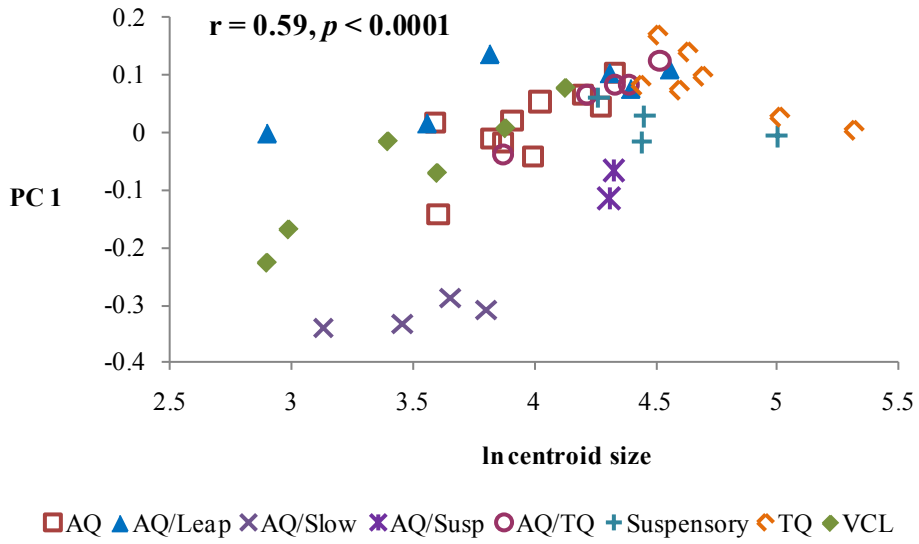

Fig. 4-89. Bivariate plot of principal component 1 on ln centroid size for the dataset containing ischiopubic landmarks. Results of the Pearson's correlation are included. Points are taxon means (n = 44).

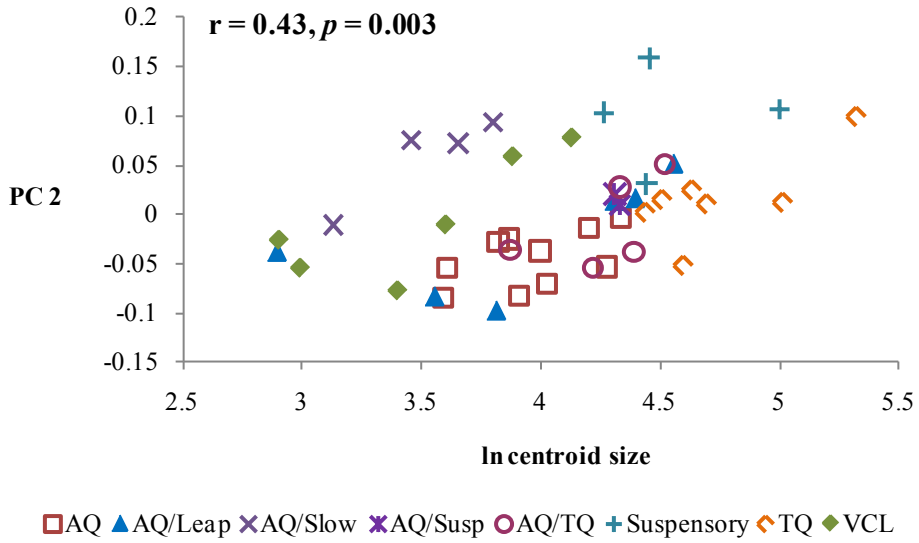

Fig. 4-90. Bivariate plot of principal component 2 on ln centroid size for the dataset containing ischiopubic landmarks. Results of the Pearson's correlation are included. Points are taxon means (n = 44).

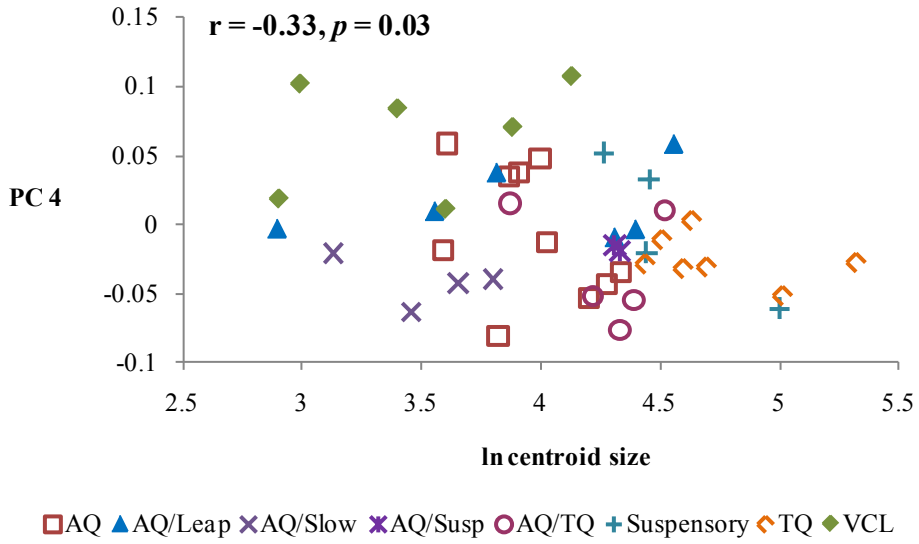

Fig. 4-91. Bivariate plot of principal component 4 on ln centroid size for the dataset containing ischiopubic landmarks. Results of the Pearson's correlation are included. Points are taxon means (n = 44).

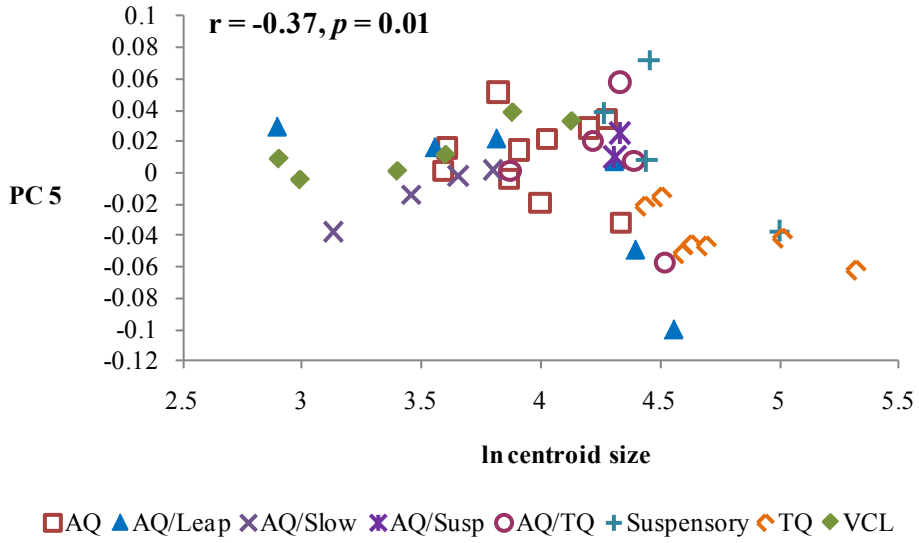

Fig. 4-92. Bivariate plot of principal component 5 on ln centroid size for the dataset containing ischiopubic landmarks. Results of the Pearson's correlation are included. Points are taxon means (n = 44).

Hominoids

The first 20 principal components in the hominoid sample account for 97.1% of the variation; the first four principal components account for 85.4%: PC1 66.8%, PC2 13.7%, PC3 2.5%, and PC4 2.4% (Table 4-25).

Locomotor group patterns: PCs 1 and 2. A plot of PC1 on PC2 using individual specimens demonstrates differentiation along PC1 between humans and the other apes, as well as differentiation within non-human apes by body size (Fig. 4-93). Variation on PC2 is ordered by body size. While the suspensory hylobatids are separate from the other apes, the more terrestrial African apes overlap with the more suspensory *Pongo*. Thus, differentiation among locomotor categories is affected by phylogeny and body size.

Locomotor group patterns: PCs 3 and 4. A plot of PC3 on PC4 of individual specimens does not differentiate among hominoid taxa (Fig. 4-94).

Morphological patterns: PC 1. Principal component 1 separates humans from the other apes, and only separates the non-human apes from each other (Fig. 4-93). Positive loadings on PC1 are associated with human-like pelvic morphology: 1) a short, broad, anteriorly-curved ilium that results from increasing the distance between ASIS and PSIS and decreasing the height of both the lower ilium and the iliac blade, 2) a large AIIS, 3) a short pubic symphysis with long pubic rami, 4) a large acetabulum, 5) a dorsally-projecting ischium, and 6) a large ischial spine. Negative loadings on PC1 generally reflect non-human ape-like morphology: 1) a longer and narrower laterally-oriented ilium that results primarily from decreasing the distance between ASIS and PSIS and increasing the height of the lower iliac

region, 2) a more superiorly positioned PSIS relative to the ASIS, 3) a small, non-protruding AIIS, 4) a long pubic symphysis and short pubic rami, 5) a smaller acetabulum, 6) an ischium that does not project dorsally, and 7) a small-to-absent ischial spine.

The bipedal humans fall on the positive end of PC1, while the suspensory and terrestrial taxa plot on the negative side (*Gorilla gorilla* spans both the positive and negative ends of PC1).

Morphological patterns: PC 2. Principal component 2 separates all ape taxa by size, with *Hylobates* on the negative end of the axis and *Gorilla gorilla* on the positive end (Fig. 4-93). Positive loadings on PC2 are associated with an ilium that is longer and wider. Interestingly, the length of the ilium is achieved in the blade and not in the height of the lower ilium; the lower ilium shortens as PC2 becomes positive. The width of the blade is achieved by moving the ASIS more laterally and by displacing the PSIS more superomedially, such that the ASIS is inferior to the PSIS. The AIIS becomes smaller and the acetabulum becomes relatively smaller. The ischium elongates and flares laterally, which contributes to a deepening of the body of the pubis without increasing the length of the pubic symphysis. Negative loadings on PC2 are associated with a narrower and more medially-oriented iliac blade, with a longer lower ilium region and a shorter blade. The ASIS is more medially-located and is superior to the PSIS. The AIIS and acetabulum are larger. The ischium is shorter and deviates slightly towards the sagittal plane. The pubic symphysis is longer, with the superior aspect of the

symphysis located more medially than its inferior aspect, resulting in a longer superior than inferior pubic ramus.

The terrestrial apes and the suspensory *Pongo* plot on the positive end of PC2, while bipeds and the suspensory hylobatids plot on the negative side.

Morphological patterns: PC 3. Principal component 3 does not separate taxa according to size, locomotion, or phylogeny (Fig. 4-94). Shape variation along PC3 is in the width of the ilium, length of the ischium, and length and depth of the pubis. Positive loadings on PC3 result in a narrower iliac blade, slightly shorter pubic rami, and a slightly longer ischium. Negative loadings on PC4 are associated with a wider iliac blade, achieved by displacing the PSIS medially, slightly longer pubic rami that result from minimal shortening of the pubic symphysis, and a somewhat shorter ischium. PC3 does not differentiate among locomotor categories.

Morphological patterns: PC 4. Shape variation along PC4 is differentiated by the length of the iliac blade, the length and orientation of the ischium, and the length and depth of the pubis (Fig. 4-94). Positive loadings on PC4 are associated with a shorter iliac blade (but not a shorter lower ilium), a shorter ischium with a small-to-absent ischial spine, and a longer pubic symphysis. Negative loadings on PC4 are associated with a longer iliac blade, a longer, slightly dorsolaterally-oriented ischium with a larger ischial spine, and a shorter pubic symphysis that results in a longer inferior pubic ramus. PC4 does not differentiate among locomotor categories.

Allometric scaling. Of the first ten principal components, three are significantly correlated with ln centroid size: PC1 (Pearson $r = 0.33$, $p < 0.0001$), PC2 (Pearson $r = 0.86$, $p < 0.0001$), and PC4 (Pearson $r = -0.17$, $p = 0.03$, Table 4-22).

As size increases, loadings on PCs 1 and 2 become positive, while those on PC4 become negative. There is a slight conflict between the scaling results of PCs 1 and 2. As size increases, PC1 becomes positive, which is associated with a shortening and widening of the iliac blade. However, PC2 also becomes positive with increasing size, and this is associated with a lengthening and widening of the iliac blade. PC4 becomes negative as size increases, which is associated with lengthening the iliac blade, shortening the pubic symphysis, and lengthening the pubic rami.

TABLE 4-25. PCA results for all landmarks; hominoids only

PC	Eigenvalue	Proportion of variance (%)	Cumulative variance (%)
1	0.03858	66.8	66.8
2	0.00791	13.7	80.5
3	0.00145	2.5	83.0
4	0.00136	2.4	85.4
5	0.00104	1.8	87.2
6	0.00089	1.5	88.7
7	0.00069	1.2	89.9
8	0.00065	1.1	91.0
9	0.00054	0.9	92.0
10	0.00050	0.9	92.8
11	0.00044	0.8	93.6
12	0.00035	0.6	94.2
13	0.00030	0.5	94.7
14	0.00025	0.4	95.2
15	0.00023	0.4	95.5
16	0.00021	0.4	95.9
17	0.00019	0.3	96.2
18	0.00018	0.3	96.6
19	0.00016	0.3	96.8
20	0.00015	0.3	97.1

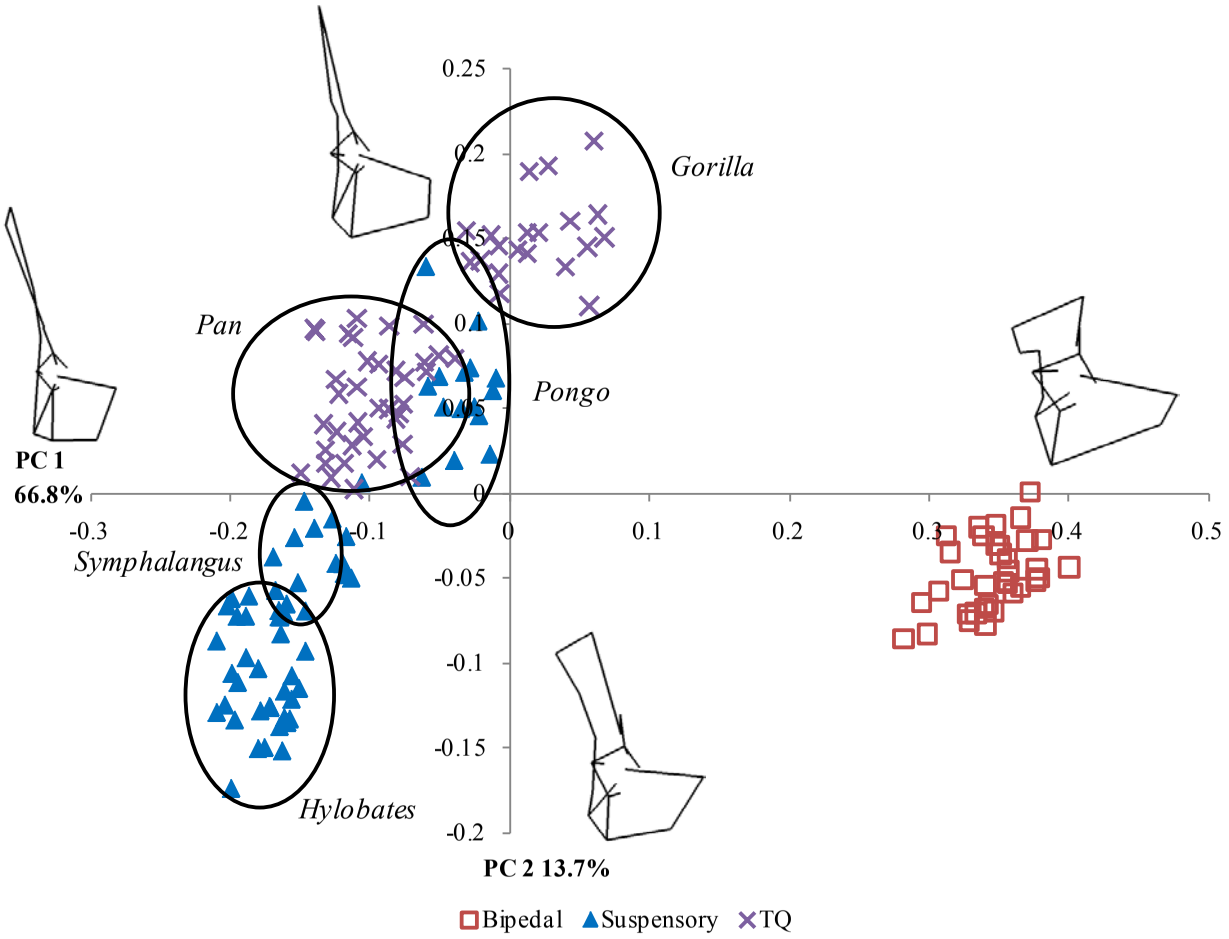

Fig. 4-93. Bivariate plot of principal component 1 on principal component 2 for the dataset containing hominoid taxa only. Individuals are plotted (n = 157). Wireframes of the consensus pelvic shape at the ends of the principal component axes are shown.

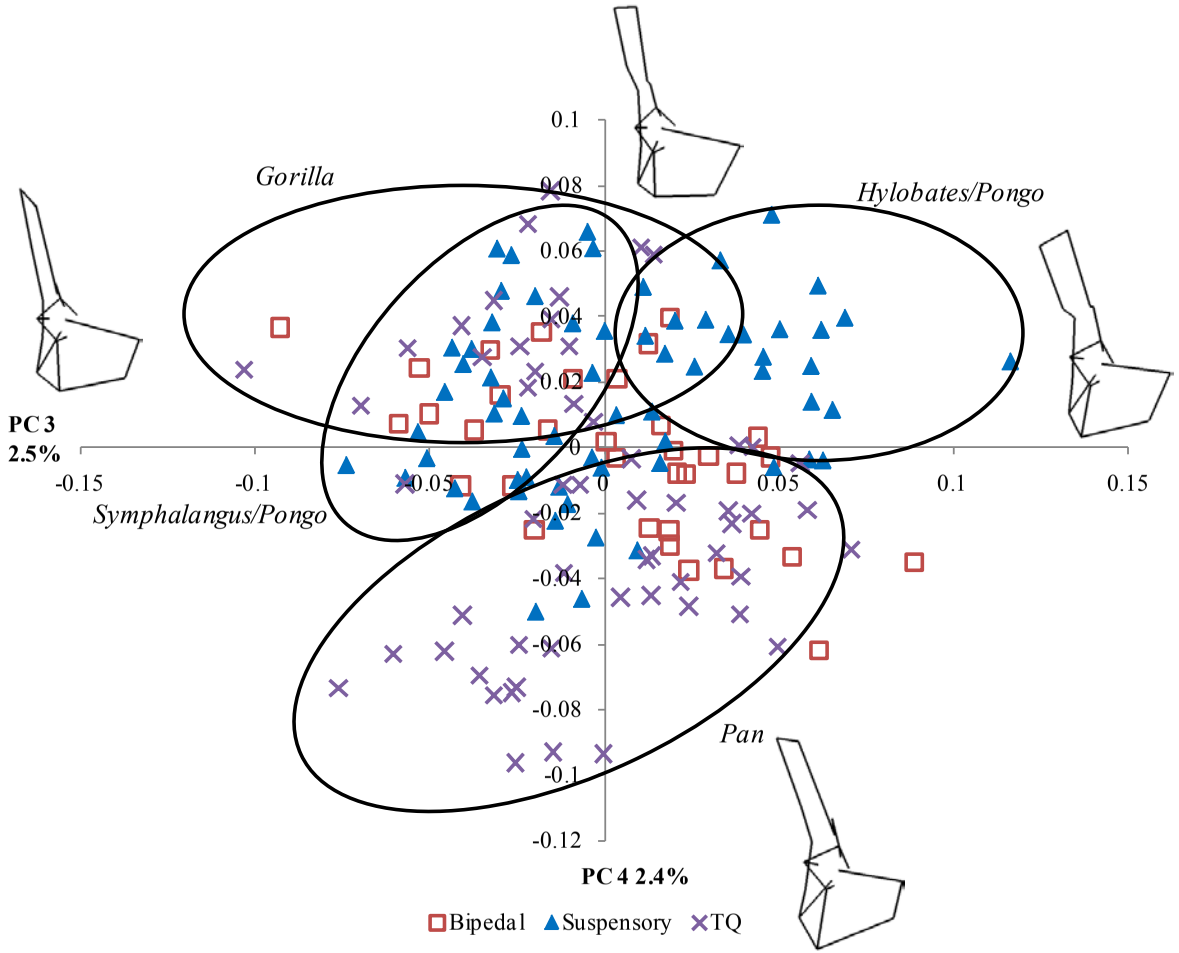

Fig. 4-94. Bivariate plot of principal component 3 on principal component 4 for the dataset containing hominoid taxa only. Individuals are plotted (n = 157). Wireframes of the consensus pelvic shape at the ends of the principal component axes are shown.

Summary of geometric morphometric results

Although pelvic shape is widely variable among primates, there are a few combinations of traits that frequently occur together and vary according to locomotor category and size. These are the shape and orientation of the ilium (blade length and width, lower ilium length, and blade orientation), the length and orientation of the ischium (dorsally-projecting versus parallel to the long axis of the pelvis, and medially- versus laterally-inclined), and the shape of the pubis (lengths of the pubic rami and symphysis). The acetabulum and the anterior projection of the ASIS also vary in shape.

The dataset that includes all of the landmarks separates taxa according to locomotor category better than either of the subsets of landmarks. While there are occasional exceptions to the "mean" shapes that categorize locomotor groups, in general, locomotor categories can be summarized as follows.

Arboreal quadruped. These taxa are characterized by a long, narrow iliac blade. Lengths of various bony struts (including the lower ilium, pubic rami and symphysis, and ischium length) and the diameter of the acetabulum are all moderate.

Semi-terrestrial quadruped. These taxa are described here by a long, narrow iliac blade and a long lower ilium, moderate-to-long pubic rami with a short pubic symphysis, an ischium of moderate length, and a large-diameter acetabulum.

Terrestrial quadruped. In general, terrestrial quadrupeds have a short, wide iliac blade, along with a short lower ilium, and short pubic rami. In addition, they have a long pubic symphysis, a long ischium, and a large acetabulum.

AQ/Slow climber. Slow climbers have a long, narrow iliac blade. These taxa have very long pubic rami and a short pubic symphysis. In addition, the ischium is short and the acetabulum is small.

AQ/Leaper. These taxa are characterized by an iliac blade that is short and wider than other arboreal quadrupeds. The factors loading on differing principal components are somewhat contradictory, but in general it appears that AQ/Leapers have a short lower ilium, short pubic rami, a long pubic symphysis, and a short ischium.

Suspensory. In general, suspensory taxa have a short, wide iliac blade and a short lower ilium. The short pubic rami end in a long pubic symphysis. In addition, the ischium is long and the acetabulum is large.

Vertical clinger and leaper. These taxa have a long, moderate-width blade and a lower ilium that is also moderate in length. The pubic rami and pubic symphysis are also of moderate length, but the ischium is relatively short.

Biped. Compared to other primates, humans have a shorter, wider iliac blade and a short lower ilium. The pubic rami are long, while the pubic symphysis is short. The ischium is short and somewhat dorsally-projecting and the acetabulum is large.

DISCUSSION

The overarching goal of this chapter is to identify pelvic adaptations to locomotion in primates. Determining adaptation requires both evidence that a trait performs a function, and an association between the trait and function. In Chapter 3, the results of experimental testing demonstrated an association between

functional loading of the pelvis and stress resistance in particular aspects of its morphology, particularly the pubis—suggesting that these features may be adaptations to resisting stress due to locomotor loading (*i.e.*, that the pelvic traits perform the function of stress resistance during hindlimb loading). In this chapter, hypotheses relating pelvic bony anatomy to the mechanical requirements of locomotion were tested to demonstrate a correlation between pelvic traits and their locomotor functions.

Pairwise comparisons and primate-wide analyses were conducted in tandem to achieve the goals of this study. Considering these results together, it is apparent that none of the functional hypotheses proposed here are supported in all instances. Predictions of shape for the lengths of the superior pubic ramus and pubic symphysis, and the areas of both pubic rami cross-sections and the auricular surface were consistently rejected. Furthermore, while some pairwise tests produced support for some hypotheses, only two of the primate-wide analyses provided support for those hypotheses.

The only pelvic trait that is likely related to locomotion as predicted is the cross-sectional area of the lower ilium. It was hypothesized that this feature serves to strengthen the ilium against bending, and that it would be relatively larger in those taxa that experience large substrate reaction forces (SRF). Because arboreal quadrupeds experience low SRF, terrestrial quadrupeds experience larger SRF, and vertical clingers and leapers experience SRF many times that of either AQ or TQ taxa, the specific prediction of lower ilium cross-sectional size was AQ < TQ < VCL. This prediction was supported in four out of five pairwise comparisons,

but not in the overall primate-wide sample. The support for this hypothesis in the pairwise comparisons, on the one hand, and the lack of support in the primate-wide sample on the other, may indicate that other factors, such as phylogeny and body size, also affect pelvic morphology (see below for discussion of these factors). While the null hypothesis of no difference among locomotor groups cannot strictly be rejected because total agreement across statistical tests was not achieved, it does appear that the cross-sectional area of the ilium is functionally related to loading regimes that result from locomotion and that it varies predictably across taxa.

Some predictions of pelvic traits received only partial support, and this may indicate that the biomechanical assumptions upon which these hypotheses rely are incorrect, or that there is no predictable functional relationship between these measures and locomotor behavior. These other pelvic traits (lower iliac height, ischium length, ischium cross-sectional area, and ilium width) do seem to be functionally related to locomotor biomechanics, but not in the manner predicted here. The hypotheses proposed here for these measures were partially supported among both the five pairwise comparisons and the primate-wide analysis. The prediction for lower iliac height was TQ < AQ < VCL; primate-wide analyses demonstrate that arboreal quadrupeds have longer lower iliac regions than terrestrial quadrupeds, as predicted, but vertical clingers and leapers are not significantly different from either group. Similarly, the prediction for ischium length was AQ = TQ < VCL; primate-wide analyses showed that while the quadrupeds have the same length ischia, the VCL taxa actually have shorter

ischia than the other two groups, instead of the reverse. The prediction for ischium cross-sectional area was AQ < TQ < VCL, and primate-wide examination indicated that terrestrial quadrupeds have larger cross-sectional areas than arboreal quadrupeds, as predicted, but that there is no difference among vertical clingers and leapers and the other taxa. Finally, the prediction for ilium width was AQ = VCL < TQ, and this was supported in two of the five pairwise comparisons (but completely rejected in the remaining three tests), as well as in the primate-wide analysis. In the majority of these analyses, the predictions were upheld for the relationship between arboreal and terrestrial quadrupeds, but the vertical clingers and leapers did not match the expected pattern. It was the vertical clingers and leapers, then, that resulted in lack of support for these specific predictions. As mentioned earlier in this chapter, the vertical clingers and leapers, as a group, have been shown to differ in both muscle morphology (Demes et al., 1998a) and locomotor kinetics and kinematics (Dunbar, 1988; Demes et al., 1995; Demes et al., 1996). Small-bodied VCLs are ankle-powered "tarsifulcrumators" that use the foot in propulsion (Demes et al., 1998a), while large-bodied VCLs are thigh-powered "tarsirotators" that use the foot in grasping (Demes et al., 1998a). Accordingly, the sizes of muscle groups differ between size classes: small-bodied VCLs have relatively large lateral hip rotators, ankle plantarflexors, and larger leg than hip muscles (Demes et al., 1998a), while large-bodied VCLs have relatively large medial hip rotators, hip extensors, and larger hip than leg muscles (Demes et al., 1998a). In addition to myological differences between these two size classes, there are mechanical differences in preparatory movements such as crouch

posture (Demes et al., 1996), hindlimb excursion (Demes et al., 1996), and body positioning and mid-air rotation (Dunbar, 1988; Demes et al., 1996). Thus, a variety of data indicates morphological and mechanical differences between the small- and large-bodied vertical clingers and leapers. However, the predictions formulated here did not account for these mechanical differences and as a result, these predictions may have been based on an inaccurate representation of the locomotor biomechanics of vertical clinging and leaping.

Therefore, while the pelvic traits listed above do not correlate with locomotion as predicted partly because the vertical clingers and leapers do not conform to predictions, they do suggest that they are features of the pelvis that are functionally related to locomotion, but in ways that are presently unclear.

Of the four pelvic traits listed above that seem to vary according to locomotion, three were also found to show some differences among locomotor groups in the exploratory geometric morphometric analysis of pelvic shape. Geometric morphometric analyses indicate that lower iliac height, ischium length, and ilium width differ among locomotor groups. These analyses also suggest that the overall length and orientation of the ilium and the orientation of the ischium and pubis vary with locomotion. That both the univariate and geometric morphometric analyses demonstrated differences among groups in the same pelvic characters is further support for the hypothesis that those characters are functionally related to locomotion, even though the specific biomechanical relevance of these features are not elucidated by this study. Furthermore, the geometric morphometric analyses suggested differences among locomotor groups

in pelvic traits that are *not* indicated by the univariate tests to be related to locomotion, which may be useful for generating hypotheses about other facets of shape—for example, three-dimensional orientation of bony elements to one another—that may be tested in future work.

To facilitate understanding of primate pelvic adaptation to locomotion, it is also necessary to consider the effects of body size and phylogeny on anatomy. In addition, the locomotor categorization used is also relevant to interpretation of these results. A discussion of these factors follows.

Effects of allometry on pelvic shape

An understanding of pelvic adaptation to locomotion requires complementary understanding of allometry in pelvic traits because both body size and locomotor adaptation may produce shape changes. This is especially relevant to studies of locomotion because locomotor behavior and body size are correlated (Preuschoft et al., 1996). As a result, it can be difficult to discern whether morphological patterns that differ among locomotor groups (whose members tend to be similarly sized) are due to the effects of locomotion on skeletal anatomy, or to the effect of body size on anatomy (*i.e.*, the changes in shape that maintain functional equivalence at different body sizes) Moreover, the effects of size and locomotor function on skeletal anatomy often interact.

The results of the allometric studies presented herein are not immediately clear. In the majority of the tests presented in this chapter, the primate-wide analysis yields different results than the analyses of each locomotor group individually. For example, while positive allometry in areal measures of pelvic

morphology was predicted and observed for the primate-wide sample, further testing of individual locomotor groups indicated a much higher incidence of isometry than allometry. This difference in scaling relationship between the primate-wide sample and the locomotor subsamples is probably a result of differences in locomotor function among taxa. When an allometric study includes taxa that differ in locomotor function, the possibility exists that one might obtain a significant allometric result as an artifact of functional differences embedded in the dataset that are correlated with body size (*i.e.*, a Type I error). For example, in a study of anthropoid limb joint surface areas, Godfrey et al. (1991) described the finding of sample-wide positive allometry as a "spurious consequence of functional differences between taxonomic subgroups that also happen to differ in body size" (p. 622). In order to appropriately quantify skeletal allometry among taxa, it is necessary to remove the possible confounding effect of function from allometric analyses, and *vice versa*. This can only be achieved by examining allometry within functional subgroups, and in this case, results from the primate-wide allometric analyses should not be considered.

It was predicted that linear measures of pelvic morphology would scale with isometry and areal measures would scale with slight positive allometry relative to body size, due to the increased forces associated with increased body size. Across locomotor groups, these predictions are rejected. Instead, there is a wide range of variation in the scaling relationships of most linear and areal pelvic traits; for a given trait, the different locomotor groups often exhibit different scaling relationships. This difference in scaling of pelvic straits among locomotor

groups is interesting because it reveals an interaction between scaling and locomotor function; the effects of increasing body size are not the same for each type of locomotion. For traits that serve no biomechanical function, the effect of increasing body size should not be influenced by different mechanical demands of differing locomotor behaviors. Therefore, for a given trait, an interaction between scaling and locomotor category can be interpreted as a signal of functional relevance that merits further investigation.

In addition to differences in scaling relationships among locomotor groups, inter- and intra-specific body size dimorphism *within* locomotor and taxonomic groupings was also an important factor affecting the interpretation of pelvic variation. Within locomotor groups, large-bodied taxa were qualitatively found to exhibit morphologies that are hypothesized to strengthen the bony structure of the pelvis (lower ilium cross-sectional area, inferior pubic ramus length) or increase muscle leverage (ilium width, ischium length and dorsal projection). For example, the vertical clingers and leapers, a group that spans a range of body sizes from 0.12 – 6.84 kg in this sample, exhibited different lower iliac heights at small and large sizes; the small-bodied taxa have long lower ilia, while the large-bodied taxa have shorter lower iliac regions. Lower ilium cross-sectional area, ilium width, ischium length and dorsal projection, inferior pubic ramus length, and pubic symphysis length were also found to differ similarly according to body size within vertical clingers and leapers. In addition, similar pelvic differences due to body size were also found within terrestrial quadrupeds and suspensory taxa.

Additionally, within species, body size dimorphism (*i.e.*, sexual size dimorphism) in some taxa results in features that apparently serve to increase strength in the larger-bodied males. In other words, intraspecific differences between the sexes mirror those that are expected among groups that differ in magnitude of substrate reaction forces encountered during locomotion. For example, in the comparison of *Macaca fascicularis* with *Papio hamadryas*, for traits that were hypothesized to relate to pelvic stress resistance and muscle leverage, males were relatively larger than females. The finding of sexual size dimorphism in pelvic traits that are hypothesized to be related to stress resistance bolsters the hypothesis that these traits function to resist increased stress associated with larger substrate reaction forces.

Thus, both inter- and intra-specific patterns of body size dimorphism in pelvic morphology support the hypotheses that 1) areal measures increase in size relative to body size to strengthen the pelvis against increased substrate reaction forces, and 2) pelvic struts lengthen to increase muscle leverage when more power is necessary.

Effects of phylogeny on pelvic shape

Preliminary testing for the effects of phylogeny on behavioral and morphological traits demonstrated that locomotion—as a trait—and features of the pelvis that are believed to be related to locomotion, are highly correlated with phylogeny. This strong correlation raises an interesting conundrum; there is an implicit assumption in studies of adaptation that the processes that generate both phylogeny and adaptation are not the same and thus, that one can "control" for the

effects of phylogeny on observed characters, but that is not necessarily so. Theoretically, we expect phylogenetic change in response to environmental change or niche differentiation (Fleagle and Reed, 1996, 1999). Because locomotion is the conduit through which animals interact with their environmental space, locomotion is also expected to change in response to environmental change or niche differentiation. Phylogenetic change and locomotor adaptation, then, may often result simultaneously from the same evolutionary pressures. In those cases, phylogenetic patterns and patterns of locomotor variation will mirror each other, because, as Fleagle and Reed (1996) note in regard to dietary and locomotor adaptations of primate clades, "it is these basic adaptations that have permitted (or driven) the adaptive radiations of these groups" (p. 505). An additional side to this problem is that locomotor behaviors do not seem to have evolved repeatedly in extant primates, but instead only arose a handful of times. Thus, the tight correlation between phylogeny and locomotion makes it difficult to disentangle one from the other in an effort to "control" for phylogenetic effects, and therefore impossible to determine whether observed trait-function associations between pelvic morphology and locomotion are due to adaptation or to shared ancestry. There are no immediate solutions to this epistemological problem. However, instead of an unrealistic endeavor to render minimal the effects of phylogeny on pelvic variation, it may be more useful in this case to conceive of the strong correlation between phylogeny and locomotion not as a confound, but perhaps as evidence of the importance of locomotion in driving primate evolution.

Regardless of one's interpretation of the meaning of strong phylogenetic correlation with locomotion and its anatomical correlates, the objective is to determine whether specific morphologies are locomotor adaptations or not. Within primates, this task will not be easily achieved, if at all, simply because the correlation between locomotion and phylogeny is so strong. To further address this question, it may be more helpful to investigate adaptation to locomotion across a broader mammalian context, of which primates constitute only a part. While primates arguably exhibit the most diverse locomotor behavior of any mammalian order, a comparison of multiple clades of mammals may be able to identify common adaptations due to locomotion that are definitively not resultant from phylogenetic inertia or constraint. Such a study would require a large sample of taxa and would also benefit from a simultaneous pairwise "narrow phylogeny" (Ross et al., 2002) approach within taxonomic groups as was used here.

Effects of locomotor classification on interpretation of pelvic shape

A final consideration in the interpretation of these results is the issue of locomotor categorization. The process of assigning taxa to locomotor groups forces categorization of what is essentially a continuous trait. The broad spectrum of locomotor behaviors that individuals and species use cannot fully be described by a discrete categorization. Assigning an entire species to a discrete locomotor category discards real variation that does not fit within it, oversimplifying (albeit necessarily) species-typical locomotor repertoires and the designation of their biomechanical requirements. For example, while a generalized arboreal quadruped like *Cebus* may be more or less accurately categorized as such, an

animal with more variability in its locomotor repertoire, like the AQ/leaper *Pithecia*, will not be as well described by its singular locomotor assignment. This problem of uncertain boundaries between some locomotor categories may result in "noise" in the data that can obscure real functional signals in pelvic variation. This difficulty in appropriately categorizing taxa was most acute for species in the AQ/Leaping, AQ/Suspensory, and AQ/TQ locomotor groups. These were also the groups that consistently showed the least differentiation and repeatedly overlapped with the general AQ group. This may indicate that these animals are not functionally different from generalized arboreal quadrupeds. Alternatively, it may indicate that the functional signal among these groups was obfuscated by a locomotor categorization that did not accurately describe their locomotor behavior and that a finer-grained approach to qualifying their locomotor behavior is needed.

CONCLUSION

While it is necessary to remain cognizant of the effects of body size and phylogeny on these results, there are several conclusions that can be drawn from this study of comparative morphometrics of the primate pelvis. In general, the biomechanical predictions of adaptive hypotheses relating pelvic shape to locomotion are rejected. But, the cross-sectional area of the lower ilium, a trait that was hypothesized to strengthen the ilium via increasing resistance to bending at large substrate reaction forces, does appear to be an adaptation to locomotion. Other traits may be locomotor adaptations—the lower iliac height, ischium length, ischium cross-sectional area, and ilium width—but their specific biomechanical

function is still uncertain because some tests rejected the hypothesis of adaptation. All other pelvic traits do not differentiate taxa based on the differing loading regimes of alternate locomotor behaviors, and the results of this study contradict the hypothesis that they constitute locomotor adaptation to stress resistance or muscle leverage.

Measures of strut cross-sectional and joint surface areas do not appear to differentiate locomotor groups better than linear measures. In general, the hypothesis that cross-sectional and surface areas of pelvic features are related to stress resistance is not supported. The exception to this is the lower ilium cross-sectional area, as mentioned above.

The results of univariate analyses and geometric morphometrics both yield the same regions/traits of the pelvis as possible adaptations to locomotion. Geometric morphometric investigation of pelvic morphology may also help to generate new hypotheses of pelvic shape and its relationship to locomotion.

In summary, singular biomechanical predictions of each aspect of the pelvis that do not consider the varied non-locomotor functions of the pelvis are unlikely to be unanimously upheld. While mechanical optimization for locomotion is one (perhaps the major) function of the pelvis, it must also allow for obstetrical and visceral functions. In other words, adaptation to biomechanical pelvic function is likely to be constrained by non-locomotor requirements of the pelvis. Therefore, even though the results of this study were not exactly as expected based on biomechanical predictions, a number of features do seem to be biomechanically relevant. Future work should consider whether the strict criteria

for hypothesis-rejection used here is actually reasonable given the complex and multifaceted nature of pelvic function.

CHAPTER 5: DISSERTATION DISCUSSION AND CONCLUSION

The aim of this project was to identify pelvic adaptations to locomotion using an integrated experimental and comparative framework. The specific research questions that guided this study were: How does the primate pelvis respond to loading? And, how does pelvic shape reflect locomotion within primates? The former question is biomechanical in nature and addresses the proximate causes of pelvic shape, while the latter question is evolutionary in nature and addresses the ultimate causes of pelvic morphology. These questions are complementary and the approach taken here uses the interplay between them to gain a clearer understanding of the proximate and ultimate causes of morphology. The research design implemented here considered these questions together by incorporating an experimental study of *in vitro* pelvic strain in response to applied loading with a primate-wide analysis of pelvic morphometry. The findings of each aspect of this study are discussed in Chapters 3 and 4, respectively; here, the results of the experimental and comparative components of the project are unified and a summary of the current state of understanding of primate pelvic functional morphology is given.

EVOLUTION OF THE PRIMATE PELVIS

Functional and evolutionary adaptation

One issue clarified by the simultaneous consideration of the experimental and morphometric data generated here is the unresolved debate regarding how to interpret patterns of strain from an evolutionary perspective. The experimental data presented in Chapter 3 demonstrated differential strain magnitudes and

orientations throughout the pelvis, which suggests that certain parts of the pelvis resist stress during loading, while others may not. Specifically, the pubis exhibited high strains, while the ilium and ischium demonstrated low strains.

There are two theoretical positions regarding the inference of adaptation to stress resistance based on patterns of strain, dubbed here the strain-reduction model and the trade-off model (see Chapter 3). The strain-reduction model asserts that adult bones have already adapted to typical loading, and thus, when subjected to stress analysis, observed strains should be low in bony regions that are adapted to resist stress resulting from applied load and high in regions that are not adapted to resist stress resulting from applied load, probably because they do not actually experience those stresses in reality (Ruff et al., 2006; Grine et al., 2010). From this perspective, the strain data collected here suggest that the ilium and ischium, which exhibit low strains, are adapted to resist stress due to habitual loading, while the pubis, which exhibits high strains, is not. The trade-off model states that bone is optimized to maximize strength while minimizing mass, which results in an appearance of relatively high and nearly uniform levels of strain in bones that are functionally adapted to stress resistance (e.g., Hylander et al., 1991b; Hylander et al., 1991a; Hylander and Johnson, 1997; Ravosa et al., 2000). What constitutes "high" strain is still a matter of debate (see Chapter 3), but from this perspective, the strain data observed here suggest that the ilium and ischium are not adapted to stress resistance resulting from loading, while the pubis is.

Pelvic adaptations to resist stress associated with habitual loading are expected to vary according to locomotor mode. At the outset of this study,

observed high strain was taken as evidence of adaptation to stress resistance; thus, measures of the pubis were hypothesized to be adaptive and were expected to differ according to the typical forces associated with differing locomotor modes. However, the comparative morphometric results demonstrate that the pubic measures did not seem to relate to locomotion in any patterned way. Instead, only the cross-sectional area of the lower ilium differed reliably according to locomotion, and a few other measures of the ilium and ischium (lower iliac height, ilium width, and ischium length and cross-sectional area) were found to probably be related to locomotion (recall that the criteria for rejection of functional hypotheses in the morphometric study may have been unrealistically strict). The morphometric measures that were hypothesized to be related solely to stress resistance—strut cross-sectional areas—also differed according to locomotion in both the ilium and ischium, but not in the pubis.

From the perspective of the strain-reduction model, the experimental and morphometric data are consistent with a scenario of adaptation to stress resistance in the ilium and ischium, and not in the pubis. However, from the perspective of the trade-off model, the experimental and morphometric data lead to opposite conclusions regarding the importance of stress resistance resulting from locomotion for the three pelvic elements—the morphometric data are in direct conflict with this interpretation of the strain data. According to the trade-off model, the low strains in the ilium and ischium reflect overdesign of these skeletal elements for locomotor stress resistance and suggest that these regions exhibit increased strength for some other, non-locomotor function (as suggested for the

supraorbital region of primates, Hylander et al., 1991b). The contradictory results of the strain data according to the trade-off model and the conclusions from the morphometric data indicate that either the assumptions underlying the interpretation of strain based on the trade-off model or the assumptions underlying the interpretation of the morphometric data presented here is incorrect.

The morphometric study operates under three general assumptions: 1) that joint areas and strut cross-sectional areas are related to stress resistance, 2) that the lengths of bony elements act as levers to maximize muscle leverage according to the biomechanical requirements of each locomotor mode, and 3) that the basic biomechanical characterization of each locomotor mode is correct (see Chapter 2). If the assumptions of the morphometric study are valid, then the optimization assumption of the trade-off model—that observed high strain is indicative of adaptation or functional relevance to stress resistance—is falsified. Conversely, if the assumptions of the strain study are valid, then one or more of the three morphometric assumptions is/are falsified.

While aspects of the trade-off model have been shown experimentally (for example, optimization for bone strength relative to mass in cross-sectional geometry of long bones, Lieberman et al., 2003), the model cannot predict strain patterns in bones that likely perform other functions in addition to stress resistance (*e.g.*, the pelvis). Furthermore, the acceptable (*i.e.*, optimized) level of stress in a bone that is adapted to stress resistance is ambiguous. Surveys of *in vivo* strain in animal limb bones (mammals, birds, and fish) demonstrate that, on average, the peak strains experienced during loading are between 2000-3000 με

(e.g., Rubin and Lanyon, 1984), resulting in average safety factors of ~2-3. The safety factors observed in this study, however, range from 2-3 in the pubis of the *Hylobates* specimen to upwards of 20-30 in the monkeys. These large safety factors are further evidence that the varied functions of the pelvis preclude predictions of what an "acceptable" level of strain would be.

The assumptions of the morphometric study are well-supported by other lines of evidence. First, the cross-sectional geometry of other skeletal elements (*e.g.*, long bones) is related to typical loading patterns (e.g., Burr et al., 1989), and this should be the case with the pelvis as well. Second, other skeletal elements are shown to act as levers, the lengths of which optimize muscular force output (e.g., Spencer and Demes, 1993), and this is also expected in the pelvis. Third, while the basic biomechanical characterizations of the locomotor modes here are simplifications of functional models, they are based on accepted principles of theoretical biomechanics.

The most parsimonious conclusion is one of concordance between the experimental strain and morphometric datasets. Here, results of the morphometric portion of the study are in accord with the strain-reduction model of bone adaptation to loading, indicating that elements of the ilium and ischium are adaptations to stress resistance resulting from hindlimb loading, and that the pubis is relatively unimportant in this regard. Incidentally, morphometric work in other taxa on the masticatory system is also consistent with the strain-reduction model of adaptation to loading. Observed cranial strain in two species of Chiroptera is higher under atypical loading regimes that are not experienced during normal

masticatory behavior than under typical loading regimes that reflect loading during normal mastication (Dumont et al., 2005).

However, there are other issues that almost certainly affect the interpretation of the strain results. The *in vitro* data may not be representative of *in vivo* strain because the experimental design did not include the effects of muscle forces on the pelvis, and, although the forces that were applied to the pelvis via hindlimb loading were chosen based on forces encountered during *in vivo* force-plate studies, the loads may not actually be similar to those incurred in a non-experimental setting. Regarding muscle forces, it is possible that observed high strain (for example, in the pubic region) may result from a lack of muscle forces which might function to modulate load *in vivo*. In life, the hip adductor musculature takes origin from the pubis and exerts forces on it. Data derived from *in vivo* loading is needed to resolve this issue, but the pelvis is heavily covered by musculature and collection of bone strain *in vivo* is virtually impossible. Finite element analysis, however, that simultaneously models forces due to locomotion and those due to muscles may help to clarify this issue.

This study is the first to integrate experimentally-derived data on pelvis biomechanics with comparative morphometric data on locomotor adaptations, and in the process it highlights an important issue in evolutionary biological studies that seek to understand adaptation to loading; while functional adaptation to *in vivo* loading (epigenetic change that occurs during an individual's lifecycle) is relatively well understood (i.e., that bone responds to increased loading by depositing or remodeling tissue: Jones et al., 1977; Goodship et al., 1979; Woo et

al., 1981; Lanyon et al., 1982; Lanyon and Rubin, 1984; Lanyon and Rubin, 1985), how this phenomenon translates to evolutionary adaptation remains unclear. Although the debate surrounding the identification of bony adaptation to stress is not resolved, and while the strain data presented here are inadequate to definitively come to a conclusion regarding this issue (due to the absence of *in vivo* muscle forces), this study does provide data that supports the strain-reduction model, and it clarifies the types of studies that are necessary to make progress on this issue.

General biomechanical model of the primate pelvis

The cylinder model of pelvic biomechanics was generally not supported by the data presented here, either because the test design was incapable of differentiating among overlapping loading regimes, or because the pelvis is not accurately represented by a cylinder. Based on the cylinder model, the pelvis was expected to exhibit torsion, dorsoventral bending, and dorsoventral compression during loading. Using cadaver specimens of *Papio*, *Macaca*, *Ateles*, and *Hylobates*, typical loads were applied to the pelvis via the hindlimb at a range of limb angular positions. Predictions of these loading regimes were tested using these experimental strain data. Expectations of strain during loading included predictions of both the types (compressive or tensile) and orientations of observed strains. While the orientations of observed strains were as predicted for torsion and dorsoventral bending, the types of strains observed at specific locations in the pelvic structure do not support the presence of these loading regimes. While dorsoventral compression was not wholly supported by the strain data, the

majority of the results seem to suggest that dorsoventral compression does occur during pelvic loading via the hindlimb, as supposed by Pauwels (1980).

Therefore, partial support was found for dorsoventral compression, but the predictions of strain patterns for dorsoventral bending and torsion were generally not supported. It is likely that during loading, the pelvic structure actually encounters multiple loading regimes simultaneously, but this study did not test predictions based on hypotheses of overlapping loading regimes. Furthermore, the resultant patterns of strain from partially or fully overlapping loading regimes are unclear, and thus, this study was unable to differentiate among them. In sum, although the cylinder model was not supported, the potential complexities of it have not been sufficiently tested here to confidently reject it. If it can be shown that these loading regimes (overlapping or otherwise) do not characterize the pelvis, then the cylinder model as formulated here will be rejected.

Alternatively, using a local modeling approach (as opposed to the global model used here), in which functional subunits of the pelvis (*i.e.*, ilium, ischium, pubis) are modeled as separate structures (*e.g.*, different types of beams and struts), may better explain pelvic response to loading. In this model, the ilium would act as a beam that is fixed at the hip and sacroiliac joints, the ischium would act as a cantilevered beam that is fixed at the acetabulum and acted upon by hip extensor musculature on its caudal end, and the pubic rami would act as struts that are fixed at their medial and lateral ends. Finite element analysis may also prove to be a useful approach to generate biomechanical hypotheses of stress resistance during pelvic loading. Because this study did not include effects of

musculature on force modulation of the pelvic structure—and because *in vivo* strain analysis is not feasible due to the large musculature that originates from the pelvis—future finite element modeling should include the actions of muscles, which is likely to be more accurate in generating hypotheses of pelvic stress resistance than models that exclude the effects of musculature. Experimental strain data, such as those presented here, can then be used to validate future finite element models.

Morphological integration and modularity

Ultimately, this study seeks to shed light on primate evolution by providing a functional basis for answering questions regarding how the primate pelvis evolved and to use information derived from data on extant primate pelves to infer locomotor function in fossil taxa. To understand the evolution of the pelvis, it is necessary to gain an understanding of the selection pressures on, constraints on (developmental, functional, and genetic), and the evolvability (the reduction of constraint that allows adaptation; the ability to evolve, Kirschner and Gerhart, 1998; Hansen and Houle, 2004; Futuyma, 2010) of the pelvic structure.

While the overall shape of the pelvis suggests patterned morphological differences according to locomotion (see geometric morphometric analyses in Chapter 4), the discrete pelvic traits that were analyzed separately did not vary as predicted according to locomotion. Morphological integration (Olson and Miller, 1958) of pelvic morphology may be responsible for this disjunct between the univariate and geometric morphometric analyses. It would be useful to document morphological integration of suites of discrete pelvic features (*e.g.*, the anterior

superior iliac spine) to determine whether pelvic traits are functionally and developmentally independent, or whether they evolve together and should be considered as functional subunits. If pelvic features are morphologically integrated, then they will evolve together. In that case, examining individual pelvic traits as functionally independent structures, as was done in the univariate analyses presented here, may obscure interpretation of both the functional significance and the evolutionary history of pelvic shape among primates.

In the study of adaptation, the proximate causes of morphological integration (*i.e.,* covariation among morphological traits) include genetic and/or developmental constraint, while the ultimate causes are selective processes. Previous studies of morphological integration in mammals have focused on both levels of causation in crania (e.g., Cheverud, 1982; Ackermann and Cheverud, 2000; Lieberman et al., 2000; Marroig and Cheverud, 2001; Klingenberg et al., 2002; Hallgrimsson et al., 2004; Monteiro et al., 2005; Goswami, 2006a,b; Wroe and Milne, 2007; Mitteroecker and Bookstein, 2008; Bastir and Rosas, 2009; Hlusko and Mahaney, 2009; Willmore et al., 2009; Goswami and Polly, 2010) and limbs (e.g., Chiu and Hamrick, 2002; Young and Hallgrimsson, 2005; Young, 2006; Lawler, 2008; Rolian, 2009; Young et al., 2010). Pelvic traits have only been investigated independently, and covariance patterns have not been examined. It is likely, however, that many pelvic traits are *not* independent and are, instead, morphologically integrated (*i.e.*, they covary) as a result of shared function and development from the same cartilaginous anlagen (Malashichev et al., 2005; Weisbecker et al., 2008; Pomikal and Streicher, 2010). Furthermore,

embryological data on developmental heterochrony suggest that the ilium and the ischiopubis may form separate modules (Weisbecker et al., 2008), which are suites of morphologically integrated traits. If so, studying individual aspects of the ilium, for example, is inappropriate because those traits will covary with others on the ilium.

The rearrangement of the pelvic girdle to accommodate different modes of locomotion is one of the most notable features of primate variation—especially in human evolution—but our understanding of its adaptive features, and how those features developed, is limited. If modularity describes pelvic morphology, then small genetic change (*e.g.*, through regulatory mutations) could effect large phenotypic change (Chan et al., 2010). Understanding the extent of morphological integration and modularity of the pelvis is the first step to understanding its constraints, evolvability, and the selective pressures that shaped it.

CONCLUSION

This study of the biomechanical function and adaptation of the primate pelvis contributes data to several realms within the field of pelvic functional morphology. This study was primarily concerned with determining how the pelvis responds to applied loading and how the bony structure of the pelvis varies with locomotor behavior among primates. The experimental strain data indicate that during *in vitro* loading, the ilium and ischium encounter small to moderate strains, while the pubis experiences high strains. Overall, the pelvis predominately encounters compressive strains, and the tensile strains that are documented are small in magnitude. The orientation of typical strains is variable; the ilium

generally exhibits strains that are oriented along the length of the bone, from the hip joint to the sacroiliac joint, which suggests that load is transmitted along this path. The orientations of strain in the pubis are generally craniocaudally-, mediolaterally-, or obliquely-oriented. In many cases, load seemed to be transmitted along the length of the superior pubic ramus, but this was not always the case. Strain data were compared to a theoretical cylinder model of pelvic stress resistance and the model was generally not supported. Predictions of loading regimes were not supported, except in the case of dorsoventral compression, which was partially supported by these results. These results suggest that a global model of pelvic stress resistance may not accurately describe the mechanics of the pelvis (or may be so complex as to be of little utility), and that a local model that considers functional subunits separately may be more successful.

The comparative morphometric data demonstrated that the cross-sectional area of the lower ilium varies predictably with locomotion; the area of the lower ilium strut increases as the forces associated with locomotion increase. Other dimensions of the ilium and ischium (lower iliac height, ilium width, ischium length, and ischium cross-sectional area) may differ according to locomotion, but not all of the predictions concerning these measures were supported. The remaining measures of the pelvis, including all of the measures of the pubis, did not differ according to the differing mechanical demands of alternate locomotor modes. Other factors, including the effects of body size and phylogeny on pelvic morphology, are also relevant to interpretation of these results. Observed differences due to body size support the adaptive hypotheses concerning the

relationship between loading regimes and pelvic morphology. In addition, the strong correlation between phylogeny and locomotor behavior—and purported locomotor adaptations—suggests that selective pressures on locomotion and its anatomical correlates may have been influential in driving primate evolution. Finally, the lack of support for many of the adaptive hypotheses proposed here suggests that pelvic function and morphology is likely constrained by the other non-locomotor requirements of the pelvic girdle.

In summary, while the relationship between pelvic morphology and function is complex, it is clear that the pelvic structure exhibits adaptations to resisting stresses associated with loading regimes typical of locomotor modes and with the effects of increasing body size. In response to these factors, the ilium and ischium exhibit adaptations to increase strength; the ilium becomes shorter and wider in cross-section, which reduces the bending moment and allows greater resistance of force per area. The ischium also increases in cross-sectional area in response to increasing stress that results from these factors. The pubis does not vary predictably according to locomotion, and the functional relevance of its structure remains unclear. These results form the basis of a preliminary model of primate pelvic stress resistance.

LITERATURE CITED

Abitbol MM. 1988. Evolution of the ischial spine and of the pelvic floor in the Hominoidea. Am J Phys Anthropol 75:53-67.

Abitbol MM. 1991. Ontogeny and evolution of pelvic diameters in anthropoid primates and in *Australopithecus afarensis* (AL-288-1). Am J Phys Anthropol 85:135-148.

Ackermann RR, Cheverud JM. 2000. Phenotypic covariance structure in tamarins (genus *Saguinus*): a comparison of variation patterns using matrix correlation and common principal component analysis. Am J Phys Anthropol 111:489-501.

Aerts P. 1998. Vertical Jumping in *Galago senegalensis*: The Quest for an Obligate Mechanical Power Amplifier. Philos Trans R Soc Lond 353:1607-1620.

Albrecht GH. 1978. Some comments on the use of ratios. Syst Zool 27:67-71.

Albrecht GH, Gelvin BR, Hartman SE. 1993. Ratios as a size adjustment in morphometrics. Am J Phys Anthropol 91:441-468.

Albrecht GH, Gelvin BR, Hartman SE. 1995. Ratio adjustments in morphometrics: a reply to Dr. Corruccini. Am J Phys Anthropol 96:193-197.

Alexander RM. 1995. Leg Design and Jumping Technique for Humans, other Vertebrates and Insects. Philos Trans R Soc Lond 347:235-248.

Anderson AE, Peters CL, Tuttle BD, Weiss JA. 2005. Subject-specific finite element model of the pelvis: development, validation and sensitivity studies. J Biomech Eng 127:364-373.

Anemone RL. 1993. The functional anatomy of the hip and thigh in primates. In: Gebo DL, editor. Postcranial adaptation in nonhuman primates. DeKalb, IL: Northern Illinois University Press. p 150-174.

Anemone RL, Covert HH. 2000. New skeletal remains of Omomys (Primates, Omomyidae): functional morphology of the hindlimb and locomotor behavior of a Middle Eocene primate. J Hum Evol 38:607-633.

Ankel-Simons F. 2000. Primate Anatomy. New York: Academic Press.

Arnold C, Matthews LJ, Nunn CL. 2010. The 10kTrees website: a new online resource for primate phylogeny. Evol Anthropol 19:114-118.

Arsuaga JL, Carretero JM. 1994. Multivariate analysis of the sexual dimorphism of the hip bone in a modern human population and in early hominids. Am J Phys Anthropol 93:241-257.

Ashton EH, Flinn RM, Moore WJ, Oxnard CE, Spence TF. 1981. Further quantitative studies of form and function in the primate pelvis with special reference to *Australopithecus*. Trans Zool Soc Lond 36:1-98.

Atchley WR. 1978. Ratios, regression intercepts, and the scaling of data. Syst Zool 27:78-83.

Atchley WR, Anderson D. 1978. Ratios and the statistical analysis of biological data. Syst Zool 27:71-78.

Autumn K, Ryan MJ, Wake DB. 2002. Integrating historical and mechanistic biology enhances the study of adaptation. Q Rev Biol 77:383-408.

Badoux DM. 1974. An introduction to biomechanical principles in primate locomotion and structure. In: Jenkins FA, editor. Primate locomotion. New York: Academic Press. p 1-43.

Baker BJ, Dupras TL, Tocheri MW. 2005. The osteology of infants and children. College Station: Texas A&M University Press.

Barham WW. 1970. A longitudinal study of the growth of the chimpanzee bony pelvis. Basel: Karger. p 169-175.

Bastir M, Rosas A. 2009. Mosaic evolution of the basicranium in *Homo* and its relation to modular development. Evol Biol 36:57-70.

Bastir M, Rosas A, Sheets HD. 2005. The morphological integration of the hominoid skull: a partial least squares and PC analysis with implications for European Middle Pleistocene mandibular variation. In: Slice DE, editor. Modern morphometrics in Physical Anthropology. New York: Plenum Publishers. p 265-284.

Baum DA, Larson A. 1991. Adaptation reviewed: a phylogenetic methodology for studying character macroevolution. Syst Zool 40:1-18.

Berge C. 1984. Multivariate analysis of the pelvis for hominids and other extant primates: implications for the locomotion and systematics of the different species of australopithecines. J Hum Evol 13:555-562.

Berge C. 1991. Size- and locomotion-related aspects of hominid and anthropoid pelves: an osteometrical multivariate analysis. Hum Evol 6:365-376.

Berge C. 1994. How did the australopithecines walk? A biomechanical study of the hip and thigh of *Australopithecus afarensis*. J Hum Evol 26:259-273.

Berge C, Kazmierczak JB. 1986. Effects of size and locomotor adaptations on the hominid pelvis: evaluation of australopithecine bipedality with a new multivariate method. Folia Primatol 46:185-204.

Berger LR, de Ruiter DJ, Churchill SE, Schmid P, Carlson KJ, Dirks PHGM, Kibii JM. 2010. *Australopithecus sediba*: a new species of *Homo*-like australopith from South Africa. Science 328:195-204.

Bertram JEA, Chang Y-H. 2001. Mechanical energy oscillations of two brachiation gaits: measurement and simulation. Am J Phys Anthropol 115:319-326.

Bertram JEA, Ruina A, Cannon CE, Chang Y-H, Coleman MJ. 1999. A point-mass model of gibbon locomotion. J Exp Biol 202:2609-2617.

Bezanson M. 2009. Life history and locomotion in *Cebus capucinus* and *Alouatta palliata*. Am J Phys Anthropol 140:508-517.

Biewener AA. 1990. Biomechanics of mammalian terrestrial locomotion. Science 250:1097-1103.

Biewener AA. 2003. Animal locomotion. Willmer P, Norman D, editors. Oxford: Oxford University Press.

Biewener AA. 2006. Patterns of mechanical energy change in tetrapod gait: pendula, springs and work. J Exp Zool 305A:899-911.

Biewener AA, Swartz SM, Bertram JEA. 1986. Bone modeling during growth: dynamic strain equilibrium in the chick tibiotarsus. Calcif Tissue Int 39:390-395.

Bitty EA, McGraw WS. 2007. Locomotion and habitat use of Stampflii's putty-nosed monkey (*Cercopithecus nictitans stampflii*) in the Tai National Park, Ivory Coast. Am J Phys Anthropol 134:383-391.

Black ES. 1970. Sexual dimorphism in the ischium and pubis of three species of South American monkeys. J Mammal 51:794-796.

Blomberg SP, Garland T, Jr., Ives AR. 2003. Testing for phylogenetic signal in comparative data: behavioral traits are more labile. Evolution 57:717-745.

Bock WJ. 1980. The definition and recognition of biological adaptation. Amer Zool 20:217-227.

Bock WJ, von Wahlert G. 1965. Adaptation and the form-function complex. Evolution 19:269-299.

Bohonak AJ, van der Linde K. 2004. RMA: software for reduced major axis regression, Java version.

Boinski S. 1989. The positional behavior and substrate use of squirrel monkeys: ecological implications. J Hum Evol 18:659-677.

Bondioli L, Coppa A, Frayer DW, Libsekal Y, Rook L, Macchiarelli R. 2006. A one-million-year-old human pubic symphysis. J Hum Evol 50:479-483.

Bookstein FL. 1991. Morphometric tools for landmark data: geometry and biology. New York: Cambridge University Press.

Bouhallier J, Berge C, Penin X. 2004. Procrustes analysis of the pelvic cavity in australopithecines (AL 288, Sts 14), humans and chimpanzees: obstetrical consequences. Comptes Rendus Palevol 3:295-304.

Bouvier M, Hylander WL. 1981. Effect of bone strain on cortical bone structure in macaques (*Macaca mulatta*). J Morphol 167:1-12.

Brain CK, Vrba ES. 1974. A new hominid innominate bone from Swartkrans. Annls Transv Mus 29:55-63.

Burr DB. 1993. Remodeling and the repair of fatigue damage. Calcif Tissue Int 53:S75-S81.

Burr DB, Martin RB, Schaffler MB, Radin EL. 1985. Bone remodeling in response to in vivo fatigue microdamage. J Biomech 18:189-200.

Burr DB, Robling AG, Turner CH. 2002. Effects of biomechanical stress on bones in animals. Bone 30:781-786.

Burr DB, Ruff CB, Johnson C. 1989. Structural adaptations of the femur and humerus to arboreal and terrestrial environments in three species of macaque. Am J Phys Anthropol 79:357-367.

Cant JGH. 1986. Locomotion and feeding postures of spider and howling monkeys: field study and evolutionary interpretation. Folia Primatol 46:1-14.

Cant JGH, Youlatos D, Rose MD. 2003. Suspensory locomotion of *Lagothrix lagothricha* and *Ateles belzebuth* in Yasuni National Park, Ecuador. J Hum Evol 44:685-699.

Carleton A. 1937. On the osteology of certain extinct lemurids of Madagascar. Proc Zool Soc Lond 107:551-556.

Carlson KJ. 2005. Investigating the form-function interface in African apes: Relationships between principal moments of area and positional behaviors in femoral and humeral diaphyses. Am J Phys Anthropol 127:312-334.

Carlson KJ, Demes B, Franz TM. 2005. Mediolateral forces associated with quadrupedal gaits of lemurids. J Zool 266:261-273.

Carlson KJ, Doran-Sheehy DM, Hunt KD, Nishida T, Yamanaka A, Boesch C. 2006. Locomotor behavior and long bone morphology in individual free-ranging chimpanzees. J Hum Evol 50:394-404.

Carter D, Vasu R, Harris WH. 1982. Stress distributions in the acetabular region--II. Effects of cement thickness and metal backing of the total hip acetabular component. J Biomech 15:165-170.

Cartmill M. 1972. Arboreal adaptations and the origin of the order primates. In: Tuttle RH, editor. The functional and evolutionary biology of primates. Chicago: Aldine. p 97-122.

Cartmill M. 1974. Pads and claws in arboreal locomotion. In: Jenkins FA, editor. Primate locomotion. New York: Academic Press. p 45-83.

Cartmill M, Lemelin P, Schmitt D. 2002. Support polygons and symmetrical gaits in mammals. Zool J Linn Soc 136:401-420.

Cavagna GA, Heglund NC, Taylor CR. 1977. Mechanical work in terrestrial locomotion: two basic mechanisms for minimizing energy expenditure. Am J Physiol Regul Integr Comp Physiol 2:R243-R261.

Chalmers GF. 1992. Materials, construction, performance and characteristics. In: Window AL, editor. Strain gauge technology. 2nd ed. New York: Elsevier Science Publishers. p 1-38.

Chamay A, Tschantz P. 1972. Mechanical influences in bone remodeling. Experimental research on Wolff's law. J Biomech 5:173-180.

Chan YF, Marks ME, Jones FC, Villareal G, Jr., Shapiro MD, Brady SD, Southwick AM, Absher DM, Grimwood J, Schmutz J, Myers RM, Petrov D, Jonsson B, Schluter D, Bell MA, Kingsley DM. 2010. Adaptive evolution of pelvic reduction in sticklebacks by recurrent deletion of a *Pitx1* enhancer. Science 327:302-305.

Cheverud JM. 1982. Phenotypic, genetic, and environmental morphological integration in the cranium. Evolution 36:499-516.

Chiu C-h, Hamrick MW. 2002. Evolution and development of the primate limb skeleton. Evol Anthropol 11:94-107.

Coddington JA. 1994. The roles of homology and convergence in studies of adaptation. In: Eggleton P, Vane-Wright RI, editors. Phylogenetics and Ecology. London: Academic Press. p 55-78.

Coleman H. 1970. Comparison of the pelvic growth patterns of chimpanzee and man. Zurich: Karger. p 176-182.

Crompton RH, Sellers WI, Gunther MM. 1993. Energetic efficiency and ecology as selective factors in the saltatory adaptation of prosimian primates. Proc R Soc Lond B 254:41-45.

Currey J. 2002. Bones: structure and mechanics. Princeton: Princeton University Press.

Dabestani M. 1992. *In vitro* strain measurement in bone. In: Miles AW, Tanner KE, editors. Strain measurement in biomechanics. New York: Chapman & Hall. p 58-69.

Dagosto M. 1995. Seasonal variation in positional behavior of Malagasy lemurs. Int J Primatol 16:807-833.

Dally JW, Riley WF. 1991. Experimental stress analysis. New York: McGraw-Hill.

Dalstra M, Huiskes R. 1995. Load transfer across the pelvic bone. J Biomech 28:715-724.

Dalstra M, Huiskes R, van Erning L. 1995. Development and validation of a three-dimensional finite element model of the pelvic bone. J Biomech Eng 117:272-278.

Darroch JN, Mosimann JE. 1985. Canonical and principal components of shape. Biometrika 72:241-252.

Dart RA. 1949. Innominate fragments of *Australopithecus prometheus*. Am J Phys Anthropol 7:301-334.

Day MH. 1973. Locomotor features of the lower limb in hominids. Symp Zool Soc Lond 33:29-51.

Demes B, Fleagle JG, Jungers WL. 1999. Takeoff and landing forces of leaping strepsirhine primates. J Hum Evol 37:279-292.

Demes B, Fleagle JG, Lemelin P. 1998a. Myological correlates of prosimian leaping. J Hum Evol 34:385-399.

Demes B, Franz TM, Carlson KJ. 2005. External forces on the limbs of jumping lemurs at takeoff and landing. Am J Phys Anthropol 128:348-358.

Demes B, Jungers WL. 1989. Functional differentiation of long bones in lorises. Folia Primatol 52:58-69.

Demes B, Jungers WL. 1993. Long bone cross-sectional dimensions, locomotor adaptations and body size in prosimian primates. J Hum Evol 25:57-74.

Demes B, Jungers WL, Fleagle JG, Wunderlich RE, Richmond BG, Lemelin P. 1996. Body size and leaping kinematics in Malagasy vertical clingers and leapers. J Hum Evol 31:367-388.

Demes B, Jungers WL, Gross TS, Fleagle JG. 1995. Kinetics of leaping primates: influence of substrate orientation and compliance. Am J Phys Anthropol 96:419-429.

Demes B, Jungers WL, Walker C. 2000. Cortical bone distribution in the femoral neck of strepsirhine primates. J Hum Evol 39:367-379.

Demes B, Larson SG, Stern JT, Jungers WL, Biknevicius AR, Schmitt D. 1994. The kinetics of primate quadrupedalism: "hindlimb drive" reconsidered. J Hum Evol 26:353-374.

Demes B, Qin Y-X, Stern JT, Larson SG, Rubin CT. 2001. Patterns of strain in the macaque tibia during functional activity. Am J Phys Anthropol 116:257-265.

Demes B, Stern JT, Hausman MR, Larson SG, McLeod KJ, Rubin CT. 1998b. Patterns of strain in the macaque ulna during functional activity. Am J Phys Anthropol 106:87-100.

Doran DM. 1996. Comparative positional behavior of the African apes. In: McGrew WC, Marchant LF, Nishida T, editors. Great Ape Societies. New York: Cambridge University Press. p 213-224.

Dryden IL, Mardia KV. 1998. Statistical shape analysis. New York: John Wiley & Sons.

Dumont ER, Piccirillo J, Grosse IR. 2005. Finite-element analysis of biting behavior and bone stress in the facial skeletons of bats. Anat Rec 283A:319-330.

Dunbar DC. 1988. Aerial maneuvers of leaping lemurs: the physics of whole-body rotations while airborne. Am J Primatol 16:291-303.

Elftman HO. 1932. The evolution of the pelvic floor of primates. Am J Anat 51:307-346.

Evans FG. 1973. The mechanical properties of bone. Springfield: C.C. Thomas.

Felsenstein J. 1985. Phylogenies and the comparative method. Amer Nat 125:1-15.

Finlay JB, Bourne RB, Landsberg RPD, Andreae P. 1986. Pelvic stresses *in vitro*--I. Malsizing of endoprostheses. J Biomech 19:703-714.

Fleagle JG. 1976. Locomotor behavior and skeletal anatomy of sympatric Malaysian leaf-monkeys (*Presbytis obscura* and *Presbytis melalophos*). Yearb Phys Anthropol 20:440-453.

Fleagle JG. 1999. Primate adaptation and evolution. San Diego: Academic Press.

Fleagle JG, Anapol FC. 1992. The indriid ischium and the hominid hip. J Hum Evol 22:285-305.

Fleagle JG, Meldrum DJ. 1988. Locomotor behavior and skeletal morphology of two pitheciine monkeys, *Pithecia pithecia* and *Chiropotes satanas*. Am J Primatol 16:227-249.

Fleagle JG, Mittermeier RA. 1980. Locomotor behavior, body size, and comparative ecology of seven Surinam monkeys. Am J Phys Anthropol 52:301-314.

Fleagle JG, Reed KE. 1996. Comparing primate communities: a multivariate approach. J Hum Evol 30:489-510.

Fleagle JG, Reed KE. 1999. Phylogenetic and temporal perspectives on primate ecology. In: Fleagle JG, Janson CH, Reed KE, editors. Primate communities. Cambridge: Cambridge University Press. p 92-115.

Fleagle JG, Simons EL. 1995. Limb skeleton and locomotor adaptations of *Apidium phiomense*, an Oligocene anthropoid from Egypt. Am J Phys Anthropol 97:235-289.

Franz TM, Demes B, Carlson KJ. 2005. Gait mechanics of lemurid primates on terrestrial and arboreal substrates. J Hum Evol 48:199-217.

Freckleton RP, Harvey PH, Pagel M. 2002. Phylogenetic analysis and comparative data: a test and review of evidence. Amer Nat 160:712-726.

Freedman RA, Young HD. 2003. University physics. Pearson: Addison-Wesley.

Futuyma DJ. 2010. Evolutionary constraint and ecological consequences. Evolution 64:1865-1884.

Garber PA, Preutz JD. 1995. Positional behavior in moustached tamarin monkeys: effects f habitat on locomotor variability and locomotor stability. J Hum Evol 28:411-426.

Gingerich PD. 1972. The development of sexual dimorphism in the bony pelvis of the squirrel monkey. Anat Rec 172:589-595.

Godfrey LR, Sutherland MR, Boy DS, Gomberg N. 1991. Scaling of limb joint surface areas in anthropoid primates and other mammals. J Zool 223:603-625.

Goel VK, Valliappan S, Svensson NL. 1978. Stresses in the normal pelvis. Comp Biol Med 8:91-104.

Goodall C. 1991. Procrustes methods in the statistical analysis of shape. J R Stat Soc Series B (Method) 53:285-339.

Goodship AE, Lanyon LE, McFie H. 1979. Functional adaptation of bone to increased stress: an experimental study. J Bone Joint Surg 61-A:539-546.

Goswami A. 2006a. Cranial modularity shifts during mammalian evolution. Amer Nat 168:270-280.

Goswami A. 2006b. Morphological integration in the carnivoran skull. Evolution 60:169-183.

Goswami A, Polly PD. 2010. The influence of modularity on cranial morphological disparity in Carnivora and Primates (Mammalia). PLoS ONE 5:e9517.

Gould SJ, Lewontin RC. 1979. The spandrels of San Marco and the Panglossian paradigm: a critique of the adaptationist programme. Proc R Soc Lond B 205:581-598.

Gould SJ, Vrba E. 1982. Exaptation: a missing term in the science of form. Paleobiol 8:4-15.

Gray H. 1918. Anatomy of the human body. Philadelphia: Lea & Febiger.

Gray J. 1944. Studies in the mechanics of the tetrapod skeleton. J Exp Biol 20:88-116.

Griffin TM, Main RP, Farley CT. 2004. Biomechanics of quadrupedal walking: how do four-legged animals achieve inverted pendulum-like movements? J Exp Biol 207:3545-3558.

Grine FE, Judex S, Daegling DJ, Ozcivici E, Ungar PS, Teaford MF, Sponheimer M, Scott J, Scott RS, Walker A. 2010. Craniofacial biomechanics and functional and dietary inferences in hominin paleontology. J Hum Evol 58:293-308.

Haeusler M. 2002. New insights into the locomotion of *Australopithecus africanus* based on the pelvis. Evol Anthropol 11:53-57.

Hager LD. 1989. The evolution of sex differences in the hominid bony pelvis [Ph.D.]. Berkeley: University of California. 288 p.

Hager LD. 1996. Sex differences in the sciatic notch of great apes and modern humans. Am J Phys Anthropol 99:287-300.

Hallgrimsson B, Willmore K, Dorval C, Cooper DML. 2004. Craniofacial Variability and Modularity in Macaques and Mice. J Exp Zool 302B:207-225.

Hanna JB, Polk JD, Schmitt D. 2006. Forelimb and hindlimb forces in walking and galloping primates. Am J Phys Anthropol 130:529-535.

Hansen TF, Houle D. 2004. Evolvability, stabilizing selection, and the problem of stasis. In: Pigliucci M, Preston K, editors. Phenotypic integration: studying the ecology and evolution of complex phenotypes. Cary: Oxford University Press. p 130-153.

Harvey PH, Pagel MD. 1991. The comparative method in evolutionary biology. Oxford: Oxford University Press.

Hert J, Pribylova E, Liskova M. 1972. Reaction of bone to mechanical stimuli: part 3: microstructure of compact bone of rabbit tibia after intermittent loading. Acta Anat 82:218-230.

Hildebrand M. 1967. Symmetrical gaits of primates. Am J Phys Anthropol 26:119-130.

Hildebrand M. 1985. Walking and running. In: Hildebrand M, Bramble DM, Liem KF, Wake DB, editors. Functional vertebrate morphology. Cambridge: Harvard University Press. p 38-57.

Hlusko LJ, Mahaney MC. 2009. Quantitative genetics, pleiotropy, and morphological integration in the dentition of *Papio hamadryas*. Evol Biol 36:5-18.

Hollihn U. 1984. Bimanual suspensory behaviour: morphology, selective advantages and phylogeny. In: Preuschoft H, Chivers DJ, Brockelman WY, Creel N, editors. The lesser apes: evolutionary and behavioural biology. Edinburgh: Edinburgh University Press. p 85-95.

Howell AB. 1944. Speed in animals: their specialization for running and leaping. New York: Hafner Publishing Company.

Hsieh Y-F, Robling AG, Ambrosius WT, Burr DB, Turner CH. 2001. Mechanical loading of diaphyseal bone *in vivo*: the strain threshold for an osteogenic response varies with location. J Bone Miner Res 16:2291-2297.

Huiskes R. 1987. Finite element analysis of acetabular reconstruction. Acta Orthop Scand 58:620-625.

Hunt KD, Cant JGH, Gebo DL, Rose MD, Walker SE, Youlatos D. 1996. Standardized descriptions of primate locomotor and postural modes. Primates 37:363-387.

Hylander WL, Johnson KR. 1997. In vivo bone strain patterns in the zygomatic arch of macaques and the significance of these patterns for functional interpretations of craniofacial form. Am J Phys Anthropol 102:203-232.

Hylander WL, Picq PG, Johnson KR. 1991a. Function of the supraorbital region of primates. Arch Oral Biol 36:273-281.

Hylander WL, Picq PG, Johnson KR. 1991b. Masticatory-stress hypotheses and the supraorbital region of primates. Am J Phys Anthropol 86:1-36.

Hylander WL, Ravosa MJ, Ross CF, Johnson KR. 1998. Mandibular corpus strain in primate: further evidence for a functional link between symphyseal fusion and jaw-adductor muscle force. Am J Phys Anthropol 107:257-271.

Jacob HAC, Huggler AH, Dietschi C, Schreiber A. 1976. Mechanical function of subchondral bone as experimentally determined on the acetabulum of the human pelvis. J Biomech 9:625-627.

Jenkins FA. 1974. Tree shrew locomotion and the origins of primate arborealism. In: Jenkins FA, editor. Primate locomotion. New York: Academic Press. p 85-115.

Jenkins FA, Camazine SM. 1977. Hip structure and locomotion in ambulatory and cursorial carnivores. J Zool 181:351-370.

Jones HH, Priest JD, Hayes WC, Tickenor CC, Nagel DA. 1977. Humeral hypertrophy in response to exercise. J Bone Joint Surg 59A:204-208.

Jouffroy FK. 1975. Osteology and myology of the lemuriform postcranial skeleton. In: Tattersall I, Sussman RW, editors. Lemur biology. New York: Plenum Press. p 149-192.

Judex S, Gross TS, Zernicke RF. 1997. Strain gradients correlate with sites of exercise-induced bone-forming surfaces in the adult skeleton. J Bone Miner Res 12:1737-1745.

Jungers WL. 1976. Hindlimb and pelvic adaptations to vertical climbing and clinging in *Megaladapis*, a giant subfossil prosimian from Madagascar. Yearb Phys Anthropol 20:508-524.

Jungers WL. 1988. Relative joint size and hominoid locomotor adaptations with implications for the evolution of hominid bipedalism. J Hum Evol 17:247-265.

Jungers WL, Burr DB. 1994. Body size, long bone geometry, and locomotion in quadrupedal monkeys. Zeitschrift fuer Morphologie und Anthropologie 80:89-97.

Jungers WL, Burr DB, Cole MS. 1998. Body size and scaling of long bone geometry, bone strength, and positional behavior in cercopithecoid primates. In: Strasser E, Fleagle JG, Rosenberger A, McHenry HM, editors. Primate locomotion: recent advances. New York: Plenum Press.

Jungers WL, Falsetti AB, Wall CE. 1995. Shape, relative size, and size-adjustments in morphometrics. Yearb Phys Anthropol 38:137-161.

Kay RF, Cartmill M. 1977. Cranial morphology and adaptations of *Palaechthon naeimienti* and other Paromomyidae (Plesiadapoidea, ? Primates), with a description of a new genus and species. J Hum Evol 6:19-53.

Kendall DG. 1984. Shape manifolds, procrustean metrics, and complex projective spaces. Bull Lond Math Soc 16:81-121.

Kimura T. 1985. Bipedal and quadrupedal walking of primates: comparative dynamics. In: Kondo S, editor. Primate morphophysiology, locomotor analyses and human bipedalism. Tokyo: University of Tokyo Press. p 81-104.

Kimura T. 2003. Differentiation between fore- and hindlimb bones and locomotor behaviour in primates. Folia Primatol 74:17-32.

Kirschner M, Gerhart J. 1998. Evolvability. Proceedings of the National Academy of Sciences 95:8420-8427.

Kivell TL, Schmitt D, Wunderlich RE. 2010. Hand and foot pressures in the aye-aye (Daubentonia madagascariensis) reveal novel biomechanical trade-offs required for walking on gracile digits. J Exp Biol 213:1549-1557.

Klingenberg CP, Barluenga M, Meyer A. 2002. Shape analysis of symmetric structures: quantifying variation among individuals and asymmetry. Evolution 56:1909-1920.

Kummer B. 1975. Functional adaptation to posture in the pelvis of man and other primates. In: Tuttle RH, editor. Primate functional morphology and evolution. Chicago: Aldine. p 281-290.

Kupczik K, Dobson CA, Crompton RH, Phillips R, Oxnard CE, Fagan MJ, O'Higgins P. 2009. Masticatory loading and bone adaptation in the supraorbital torus of developing macaques. Am J Phys Anthropol 139:193-203.

Lanyon LE, Goodship AE, Pye CJ, MacFie JH. 1982. Mechanically adaptive bone remodelling. J Biomech 15:141-154.

Lanyon LE, Rubin CT. 1984. Static vs. dynamic loads as an influence on bone remodelling. J Biomech 17:897-905.

Lanyon LE, Rubin CT. 1985. Functional adaptation in skeletal structures. In: Hildebrand M, Bramble DM, Liem KF, Wake DB, editors. Functional Vertebrate Morphology. Cambridge: Harvard University Press. p 1-25.

Larney E, Larson SG. 2004. Compliant walking in primates: elbow and knee yield in primates compared to other mammals. Am J Phys Anthropol 125:42-50.

Larson SG. 1998. Unique aspects of quadrupedal locomotion in nonhuman primates. In: Strasser E, Fleagle JG, Rosenberger A, McHenry HM, editors. Primate locomotion: recent advances. New York: Plenum Press. p 157-173.

Larson SG, Schmitt D, Lemelin P, Hamrick M. 2000. Uniqueness of primate forelimb posture during quadrupedal locomotion. Am J Phys Anthropol 112:87-101.

Larson SG, Schmitt D, Lemelin P, Hamrick MW. 2001. Limb excursion during quadrupedal walking: how do primates compare to other mammals? J Zool 255:353-365.

Larson SG, Stern JT. 2006. Maintenance of above-branch balance during primate arboreal quadrupedalism: coordinated use of forearm rotators and tail motion. Am J Phys Anthropol 129:71-81.

Larson SG, Stern JT, Jr. 2009. Hip extensor EMG and forelimb/hind limb weight support asymmetry in primate quadrupeds. Am J Phys Anthropol 138:343-355.

Lauder GV. 1995. On the inference of function from structure. In: Thomason JJ, editor. Functional morphology in vertebrate paleontology. Cambridge: Cambridge University Press. p 1-18.

Lawler RR. 2008. Morphological integration and natural selection in the postcranium of wild Verreaux's sifaka (*Propithecus verreauxi verreauxi*). Am J Phys Anthropol 136:204-213.

Le Gros Clark WE. 1955. The os innominatum of the recent ponginae with special reference to that of the australopithecinae. Am J Phys Anthropol 13:19-28.

Lemelin P, Schmitt D, Cartmill M. 2003. Footfall patterns and interlimb co-ordination in opossums (Family Didelphidae): evidence for the evolution of diagonal-sequence walking gaits in primates. J Zool 260:423-429.

Leung ASO, Gordon LM, Skrinskas T, Szwedowski T, Whyne CM. 2009. Effects of bone density alterations on strain patterns in the pelvis: application of a finite element model. Proc Inst Mech Eng, Part H: J Eng Med 223:965-979.

Leutenegger W. 1973. Sexual dimorphism in pelves of African lorises. Am J Phys Anthropol 38:251-254.

Leutenegger W. 1974. Functional aspects of pelvic morphology in simian primates. J Hum Evol 3:207-222.

Leutenegger W. 1977. Functional interpretation of sacrum of *Australopithecus africanus*. S Afr J Sci 73:308-310.

Leutenegger W. 1982. Encephalization and obstetrics in primates with particular reference to human evolution. In: Armstrong E, Falk D, editors. Primate brain evolution: methods and concepts. New York: Plenum Press. p 85-95.

Leutenegger W, Larson S. 1985. Sexual dimorphism in the postcranial skeleton of new world primates. Folia Primatol 44:82-95.

Levangie PK, Norkin CC. 2001. Joint structure and function: a comprehensive analysis. Philadelphia: F.A. Davis Company.

Lieberman DE, Crompton AW. 1998. Responses of bone to stress: constraints on symmorphosis. In: Weibel ER, Taylor CR, Bolis L, editors. Principles of

animal design: the optimization and symmorphosis debate. New York: Cambridge University Press. p 78-86.

Lieberman DE, Pearson OM. 2001. Trade-off between modeling and remodeling responses to loading in the mammalian limb. Bull Mus Comp Zool 156:269-282.

Lieberman DE, Pearson OM, Mowbray KM. 2000. Basicranial influence on overall cranial shape. J Hum Evol 38:291-315.

Lieberman DE, Pearson OM, Polk JD, Demes B, Crompton AW. 2003. Optimization of bone growth and remodeling in response to loading in tapered mammalian limbs. J Exp Biol 206:3125-3138.

Lieberman DE, Polk JD, Demes B. 2004. Predicting long bone loading from cross-sectional geometry. Am J Phys Anthropol 123:156-171.

Linstrom NJ, Heiserman JE, Kortman KE, Crawford NR, Baek S, Anderson RL, Pitt AM, Karis JP, Ross JS, Lekovic GP, Dean BL. 2009. Anatomical and biomechanical analyses of the unique and consistent locations of sacral insufficiency fractures. Spine 34:309-315.

Lionberger D, Walker PS, Granholm J. 1985. Effects of prosthetic acetabular replacement on strains in the pelvis. J Orthop Res 3:372-379.

Little EG, Finlay JB. 1992. Perspectives of strain measurement techniques. In: Miles AW, Tanner KE, editors. Strain measurement in biomechanics. New York: Chapman & Hall. p 1-13.

Lockwood CA, Fleagle JG. 1999. The recognition and evaluation of homoplasy in primate and human evolution. Am J Phys Anthropol 42:189-232.

Lovejoy CO. 2005. The natural history of human gait and posture: Part 1. Spine and pelvis. Gait Posture 21:95-112.

Lovejoy CO, Heiple KG, Burstein AH. 1973. The gait of *Australopithecus*. Am J Phys Anthropol 38:757-780.

Lovejoy CO, Suwa G, Spurlock L, Asfaw B, White TD. 2009. The pelvis and femur of *Ardipithecus ramidus*: the emergence of upright walking. Science 326:71-77.

Macchiarelli R, Bondioli L, Galichon V, Tobias PV. 1999. Hip bone trabecular architecture shows uniquely distinctive locomotor behaviour in South African australopithecines. J Hum Evol 36:211-232.

MacLatchy L. 1998. Reconstruction of hip joint function in extant and extinct fossil primates. In: Strasser E, Fleagle JG, Rosenberger A, McHenry HM, editors. Primate locomotion: recent advances. New York: Plenum Press.

MacLatchy LM. 1995. A three-dimensional analysis of the functional morphology of the primate hip joint [Ph.D.]. Cambridge: Harvard University.

MacLatchy LM. 1996. Another look at the australopithecine hip. J Hum Evol 31:455-476.

MacLatchy LM, Bossert WH. 1996. An analysis of the articular surface distribution of the femoral head and acetabulum in anthropoids, with implications for hip function in Miocene hominoids. J Hum Evol 31:425-453.

Maddison WP, Maddison DR. 2009. Mesquite: a modular system for evolutionary analysis. Version 2.72.

Malashichev Y, Borkhvardt V, Christ B, Scaal M. 2005. Differential regulation of avian pelvic girdle development by the limb field ectoderm. Anat Embryol 210:187-197.

Marchal F. 2000. A new morphometric analysis of the hominid pelvic bone. J Hum Evol 38:347-365.

Marchi D. 2007. Relative strength of the tibia and fibula and locomotor behavior in hominoids. J Hum Evol 53:647-655.

Marivaux L, Beard KC, Chaimanee Y, Jaeger J-J, Marandat B, Soe AN, Tun ST, Aung HH, Htoon W. 2008. Anatomy of the bony pelvis of a relatively large-bodied strepsirrhine primate from the late middle Eocene Pondaung Formation (central Myanmar). J Hum Evol 54:391-404.

Marroig G, Cheverud JM. 2001. A comparison of phenotypic variation and covariation patterns and the role of phylogeny, ecology, and ontogeny during cranial evolution of new world monkeys. Evolution 55:2576-2600.

Marsh RL. 1994. Jumping ability of anuran amphibians. Adv Vet Sci Comp Med 38B:51-111.

Martin RB, Burr DB, Sharkey NA. 1998. Skeletal tissue mechanics. New York: Springer-Verlag.

McArdle JE. 1981. Functional morphology of the hip and thigh of the lorisiformes. Szalay FS, editor. New York: Basel.

McCrossin ML, Benefit BR. 1992. Comparative assessment of the ischial morphology of *Victoriapithecus macinnesi*. Am J Phys Anthropol 87:277-290.

McHenry HM. 1975. Biomechanical interpretation of the early hominid hip. J Hum Evol 4:343-355.

McNulty KP. 2003. Geometric morphometric analyses of extant and fossil hominoid craniofacial morphology [Ph.D.]. New York: The City University of New York.

McNulty KP. 2005. A geometric morphometric assessment of the hominoid supraorbital region: affinities of the Eurasian Miocene hominoids *Dryopithecus*, *Graecopithecus*, and *Sivapithecus*. In: Slice DE, editor. Modern morphometrics in physical anthropology. New York: Kluwer Academic Publishers. p 349-373.

Mittermeier RA. 1978. Locomotion and posture in *Ateles geoffroyi* and *Ateles paniscus*. Folia Primatol 30:161-193.

Mitteroecker P, Bookstein F. 2008. The evolutionary role of modularity and integration in the hominoid cranium. Evolution 62:943-958.

Mivart SG. 1867. On the appendicular skeleton of the primates. Philos Trans R Soc Lond 157:299-429.

Mobb GE, Wood BA. 1977. Allometry and sexual dimorphism in primate innominate bone. Am J Anat 150:531-537.

Monteiro LR, Bonato V, dos Reis SF. 2005. Evolutionary integration and morphological diversification in complex morphological structures: mandible shape divergence in spiny rats (Rodentia, Echimyidae). Evolution and Development 7:429-439.

Morbeck ME. 1976. Leaping, bounding and bipedalism in *Colobus guereza*: a spectrum of positional behavior. Yearb Phys Anthropol 20:408-420.

Mordan GC. 1992. Adhesives and installation techniques. In: Window AL, editor. Strain gauge technology. 2nd ed. New York: Elsevier Science Publishers. p 39-83.

Mosimann JE. 1970. Size allometry: size and shape variables with characterizations of the lognormal and generalized gamma distributions. J Amer Stat Assoc 65:930-945.

Murray WM, Miller WR. 1992. The bonded electrical resistance strain gage: an introduction. New York: Oxford University Press.

Muybridge E. 1957. Animals in motion. Brown LS, editor. New York: Dover Publications, Inc.

Napier JR, Napier PH. 1967. A handbook of living primates. London: Academic Press.

Napier JR, Walker AC. 1967. Vertical clinging and leaping - a newly recognized category of locomotor behaviour of primates. Folia Primatol 6:204-219.

Nekaris KAI. 2001. Activity budget and positional behavior of the Mysore slender loris (*Loris tardigradus lydekkerianus*): Implications for slow climbing locomotion. Folia Primatol 72:228-241.

Nyakatura JA, Fischer MS, Schmidt M. 2008. Gait parameter adjustments of cotton-top tamarins (*Saguinus oedipus*, Callitrichidae) to locomotion on inclined arboreal substrates. Am J Phys Anthropol 135:13-26.

Nyakatura JA, Heymann EW. 2010. Effects of support size and orientation on symmetric gaits in free-ranging tamarins of Amazonian Peru: implications for the functional significance of primate gait sequence patterns. J Hum Evol 58:242-251.

O'Higgins P, Jones N. 2006. Tools for statistical shape analysis. 2.3.1 ed: Hull York Medical School.

Olson EC, Miller RL. 1958. Morphological integration. Chicago: University of Chicago Press.

Orr CM, Delezene LK, Scott JE, Tocheri MW, Schwartz GT. 2007. The comparative method and the inference of venom-delivery systems in fossil mammals. J Vert Paleontol 27:541-546.

Oxnard CE. 1974. Primate locomotor classifications for evaluating fossils: their inutility and an alternative. Tokyo: Japan Science Press. p 269-286.

Oxnard CE, Crompton RH, Lieberman SS. 1990. Animal lifestyles and anatomies: the case of the prosimian primates. Seattle: University of Washington Press.

Pagel M. 1997. Inferring evolutionary processes from phylogenies. Zoologica Scripta 26:331-348.

Patel BA. 2009. Not so fast: speed effects on forelimb kinematics in cercopithecine monkeys and implications for digitigrade postures in primates. Am J Phys Anthropol 140:92-112.

Patel BA. 2010. The interplay between speed, kinetics, and hand postures during primate terrestrial locomotion. Am J Phys Anthropol 141:222-234.

Patel BA, Polk JD. 2010. Distal forelimb kinematics in *Erythrocebus patas* and *Papio anubis* during walking and galloping. Int J Primatol 31:191-207.

Patel BA, Wunderlich RE. 2010. Dynamic pressure patterns in the hands of olive baboons (*Papio anubis*) during terrestrial locomotion: implications for cercopithecoid primate hand morphology. Anat Rec 293:710-718.

Pauwels F. 1980. Biomechanics of the locomotor apparatus: Contributions on the functional anatomy of the locomotor apparatus. Maquet P, Furlong R, translator. New York: Springer-Verlag.

Perry CC. 1989. Data-reduction algorithms for strain-gage rosette measurements. Experimental Techniques 13:13-18.

Peters A, Preuschoft H. 1984. External biomechanics of leaping in *Tarsius* and its morphological and kinematic consequences. In: Niemitz C, editor. Biology of tarsiers. New York: Gustav Fischer Verlag. p 227-255.

Pissinatti A, da Silva J, Espedito C., Coimbra Filho AF, Bertolazzo W, Batista da Cruz J. 1992. Sexual dimorphism of the pelvis in *Leontopithecus* (Lesson, 1840). Folia Primatol 58:204-209.

Polk JD. 2002. Adaptive and phylogenetic influences on musculoskeletal design in cercopithecine primates. J Exp Biol 205:3399-3412.

Polk JD. 2004. Influences of limb proportions and body size on locomotor kinematics in terrestrial primates and fossil hominins. J Hum Evol 47:237-252.

Polk JD, Demes B, Jungers WL, Biknevicius AR, Heinrich RE, Runestad JA. 2000. A comparison of primate, carnivoran and rodent limb bone cross-sectional properties: are primates really unique? J Hum Evol 39:297-325.

Pomikal C, Streicher J. 2010. 4D-analysis of early pelvic girdle development in the mouse (*Mus musculus*). J Morphol 271:116-126.

Preuschoft H, Demes B. 1984. Biomechanics of brachiation. In: Preuschoft H, Chivers DJ, Brockelman WY, Creel N, editors. The lesser apes: evolutionary and behavioural biology. Edinburgh: Edinburgh University Press. p 96-118.

Preuschoft H, Demes B. 1985. Influence of size and proportions on the biomechanics of brachiation. In: Jungers WL, editor. Size and scaling in primate biology. New York: Plenum Press. p 383-399.

Preuschoft H, Witte H, Christian A, Fischer M. 1996. Size influences on primate locomotion and body shape, with special emphasis on the locomotion of "small mammals". Folia Primatol 66:93-112.

Preuschoft H, Witte H, Fischer M. 1995. Locomotion in nocturnal prosimians. In: Alterman L, Doyle GA, Izard MK, editors. Creatures of the dark: the nocturnal prosimians. New York: Plenum Press. p 453-472.

Prost JH. 1965. A definitional system for the classification of primate locomotion. Amer Anthropol 67:1198-1214.

Prost JH. 1969. A replication study on monkey gaits. Am J Phys Anthropol 30:203-208.

Raichlen DA, Pontzer H, Shapiro LJ, Sockol MD. 2009. Understanding hind limb weight support in chimpanzees with implications for the evolution of primate locomotion. Am J Phys Anthropol 138:395-402.

Rak Y. 1990. On the differences between two pelvises of Mousterian context from the Qafzeh and Kebara caves, Israel. Am J Phys Anthropol 81:323-332.

Rak Y. 1991. Lucy's pelvic anatomy: its role in bipedal gait. J Hum Evol 20:283-290.

Rak Y, Arensburg B. 1987. Kebara 2 neanderthal pelvis: first look at a complete inlet. Am J Phys Anthropol 73:227-231.

Ravosa MJ, Johnson KR, Hylander WL. 2000. Strain in the galago facial skull. J Morphol 245:51-66.

R Development Core Team. 2010. R: A Language and Environment for Statistical Computing. Vienna: R Foundation for Statistical Computing.

Reynolds E. 1931. The evolution of the human pelvis in relation to the mechanics of erect posture. Papers of the Peabody Museum of American Archaeology and Ethnology, Harvard University. Cambridge.

Reynolds TR. 1985. Stresses on the limbs of quadrupedal primates. Am J Phys Anthropol 67:351-362.

Reynolds TR. 1987. Stride length and its determinants in humans, early hominids, primates, and mammals. Am J Phys Anthropol 72:101-116.

Ries M, Pugh J, Choy Au J, Gurtowski J, Dee R. 1989a. Cortical pelvic strains with varying size hemiarthroplasty *in vitro*. J Biomech 22:775-780.

Ries M, Pugh J, Choy Au J, Gurtowski J, Dee R. 1989b. Normal pelvic strain pattern *in vitro*. J Biomed Eng 11:398-402.

Rohlf FJ, Slice D. 1990. Extensions of the Procrustes method for the optimal superimposition of landmarks. Syst Zool 39:40-59.

Rolian C. 2009. Integration and Evolvability in Primate Hands and Feet. Evol Biol 36:100-117.

Rollinson J, Martin RD. 1981. Comparative aspects of primate locomotion, with special reference to arboreal cercopithecines. Symp Zool Soc Lond 48:377-427.

Rose MD. 1974a. Ischial tuberosities and ischial callosities. Am J Phys Anthropol 40:375-384.

Rose MD. 1974b. Postural adaptations in new and old world monkeys. In: Jenkins FA, editor. Primate locomotion. New York: Academic Press. p 201-222.

Rose MD. 1977. Positional behavior of olive baboons (*Papio anubis*) and its relationship to maintenance and social activities. Primates 18:59-116.

Rosenberg KR. 1986. The functional significance of Neandertal pubic morphology [Ph.D.]: University of Michigan.

Rosenberg KR. 1992. The evolution of modern human childbirth. Yearb Phys Anthropol 35:89-124.

Ross CF, Hylander WL. 1996. *In vivo* and *in vitro* bone strain in the owl monkey circumorbital region and the function of the postorbital septum. Am J Phys Anthropol 101:183-215.

Ross CF, Lockwood CA, Fleagle JG, Jungers WL. 2002. Adaptation and behavior in the primate fossil record. In: Plavcan JM, editor. Reconstructing Behavior in the Primate Fossil Record. New York: Kluwer Academic/Plenum Publishers. p 1-41.

Ross CF, Metzger KA. 2004. Bone strain gradients and optimization in vertebrate skulls. Ann Anat 186:387-396.

Roux W. 1881. Der zuchtende Kampf der Teile, oder die 'Teilauslese' im Organismus. (Theorie der 'funktionellen Anpassung'). Leipzig: Wilhelm Engelmann.

Rowe N. 1996. The pictorial guide to the living primates. Charlestown: Pogonias Press.

Rubin CT. 1984. Skeletal strain and the functional significance of bone architecture. Calcif Tissue Int 36:S11-S18.

Rubin CT, Lanyon LE. 1984. Dynamic strain similarity in vertebrates; an alternative to allometric limb bone scaling. J Theor Biol 107:321-327.

Rubin CT, McLeod KJ, Bain SD. 1990. Functional strains and cortical bone adaptation: epigenetic assurance of skeletal integrity. J Biomech 23:43-54.

Rudwick MJS. 1964. The inference of function from structure in fossils. Brit J Philos Sci 15:27-40.

Ruff CB. 1995. Biomechanics of the hip and birth in early *Homo*. Am J Phys Anthropol 98:527-574.

Ruff CB. 2000. Body size, body shape, and long bone strength in modern humans. J Hum Evol 38:269-290.

Ruff CB. 2002. Long bone articular and diaphyseal structure in Old World monkeys and apes, I: Locomotor effects. Am J Phys Anthropol 119:305-342.

Ruff CB. 2003. Ontogenetic adaptation to bipedalism: age changes in femoral to humeral length and strength proportions in humans, with a comparison to baboons. J Hum Evol 45:317-349.

Ruff CB. 2010. Body size and body shape in early hominins - implications of the Gona pelvis. J Hum Evol 58:166-178.

Ruff CB, Hayes WC. 1983. Cross-sectional geometry of Pecos Pueblo femora and tibiae--a biomechanical investigation: I. Method and general patterns of variation. Am J Phys Anthropol 60:359-381.

Ruff CB, Holt B, Trinkaus E. 2006. Who's afraid of the big bad Wolff?: "Wolff's Law" and bone functional adaptation. Am J Phys Anthropol 129:484-498.

Ruff CB, Runestad JA. 1992. Primate limb bone structural adaptations. A Rev Anthropol 21:407-433.

Runestad JA. 1994. Humeral and femoral diaphyseal cross-sectional geometry and articular dimensions in Prosimii and Platyrrhini (Primates) with application for reconstruction of body mass and locomotor behavior in Adapidae (Primates: Eocene) [Ph.D.]: Johns Hopkins University.

Runestad JA. 1997. Postcranial adaptations for climbing in Loridae (Primates). J Zool 242:261-290.

Schaffler MB, Burr DB. 1984. Primate cortical bone microstructure: relationship to locomotion. Am J Phys Anthropol 65:191-197.

Schaffler MB, Burr DB, Jungers WL, Ruff CB. 1985. Structural and mechanical indicators of limb specialization in primates. Folia Primatol 45:61-75.

Scheuer L, Black S. 2000. Developmental juvenile osteology. New York: Academic Press.

Schmidt M. 2005. Quadrupedal locomotion in squirrel monkeys (Cebidar: *Saimiri sciureus*): a cineradiographic study of limb kinematics and related substrate reaction forces. Am J Phys Anthropol 128:359-370.

Schmidt-Nielsen K. 1984. Scaling: Why is animal size so important? Cambridge: Cambridge University Press.

Schmitt D. 1998. Forelimb mechanics during arboreal and terrestrial quadrupedalism in old world monkeys. In: Strasser E, Fleagle JG, Rosenberger A, McHenry HM, editors. Primate locomotion: recent advances. New York: Plenum Press. p 175-200.

Schmitt D. 1999. Compliant walking in primates. J Zool 248:149-160.

Schmitt D. 2003. Mediolateral reaction forces and forelimb anatomy in quadrupedal primates: implications for interpreting locomotor behavior in fossil primates. J Hum Evol 44:47-58.

Schmitt D, Gruss LT, Lemelin P. 2010. Brief communication: forelimb compliance in arboreal and terrestrial opossums. Am J Phys Anthropol 141:142-146.

Schmitt D, Hanna JB. 2004. Substrate alters forelimb to hindlimb peak force ratios in primates. J Hum Evol 46:239-254.

Schmitt D, Lemelin P. 2002. Origins of primate locomotion: gait mechanics of the woolly opossum. Am J Phys Anthropol 118:231-238.

Schmitt D, Lemelin P. 2004. Locomotor mechanics of the slender loris (*Loris tardigradus*). J Hum Evol 47:85-94.

Schultz AH. 1930. The skeleton of the trunk and limbs of higher primates. Hum Biol 2:303-438.

Schultz AH. 1936. Characters common to higher primates and characters specific to man (continued). Q Rev Biol 11:425-455.

Schultz AH. 1949. Sex differences in the pelves of primates. Am J Phys Anthropol 7:401-424.

Schultz AH. 1961. Vertebral column and thorax. New York: Karger.

Schultz AH. 1969. Observations on the acetabulum of primates. Folia Primatol 11:181-199.

Sellers WI, Crompton RH. 1994. A system for 2- and 3D kinematic and kinetic analysis of locomotion, and its application to analysis of the energetic efficiency of jumping locomotion. Zeitschrift fuer Morphologie und Anthropologie 80:99-108.

Shaw CN, Stock JT. 2009. Intensity, repetitiveness, and directionality of habitual adolescent mobility patterns influence the tibial diaphysis morphology of athletes. Am J Phys Anthropol 140:149-159.

Shim VB, Pitto RP, Streicher RM, Hunter PJ, Anderson IA. 2007. The use of sparse CT datasets for auto-generating accurate FE models of the femur and pelvis. J Biomech 40:26-35.

Sigmon BA. 1975. Functions and evolution of hominid hip and thigh musculature. In: Tuttle RH, editor. Primate functional morphology and evolution. Chicago: Aldine. p 235-252.

Sigmon BA, Farslow DL. 1986. The primate hindlimb. In: Swindler DR, Erwin J, editors. Comparative primate biology, volume 1: Systematics, evolution, and anatomy. New York: Alan R. Liss, Inc. p 671-718.

Smith RJ. 2009. Use and misuse of the reduced major axis for line-fitting. Am J Phys Anthropol 140:476-486.

Smith RJ, Cheverud JM. 2002. Scaling of sexual dimorphism in body mass: a phylogenetic analysis of Rensch's rule in primates. Int J Primatol 23:1095-1135.

Smith RJ, Jungers WL. 1997. Body mass in comparative primatology. J Hum Evol 32:523-559.

Spencer MA. 2003. Tooth-root form and function in platyrrhine seed-eaters. Am J Phys Anthropol 122:325-335.

Spencer MA, Demes B. 1993. Biomechanical analysis of masticatory system configuration in Neandertals and Inuits. Am J Phys Anthropol 91:1-20.

St. Clair EM. 2007. Sexual dimorphism in the pelvis of Microcebus. Int J Primatol 28:1109-1122.

Stern JT. 1971. Functional myology of the hip and thigh of cebid monkeys and its implications for the evolution of erect posture. Hofer H, Schultz AH, Starck D, editors. Chicago: Karger.

Stern JT, Susman RL. 1983. The locomotor anatomy of *Australopithecus afarensis*. Am J Phys Anthropol 60:279-312.

Steudel K. 1981a. Functional aspects of primate pelvic structure: a multivariate approach. Am J Phys Anthropol 55:399-410.

Steudel K. 1981b. Sexual dimorphism and allometry in primate ossa coxae. Am J Phys Anthropol 55:209-215.

Steudel K. 1982. Allometry and adaptation in the catarrhine postcranial skeleton. Am J Phys Anthropol 59:431-441.

Stevens JL, Edgerton VR, Haines DE, Meyer DM. 1981. An atlas and source book of the lesser bushbaby, *Galago senegalensis*. Boca Raton: CRC Press, Inc.

Stevens NJ. 2008. The effect of branch diameter on primate gait sequence pattern. Am J Primatol 70:356-362.

Stewart TD. 1960. Form of the pubic bone in Neanderthal man. Science 131:1437-1438.

Straus WL, Jr. 1929. Studies on primate ilia. Am J Anat 43:403-460.

Strier KB. 2006. Primate behavioral ecology. New York: Allyn & Bacon.

Swartz SM. 1988. The biomechanics and structural design of the forelimb of brachiating primates [Ph.D.]. Chicago: University of Chicago.

Swartz SM, Bertram JEA, Biewener AA. 1989. Telemetered *in vivo* strain analysis of locomotor mechanics of brachiating gibbons. Nature 342:270-271.

Szivek JA, Gharpuray VM. 2000. Strain gauge measurements from bone surfaces. In: An YH, Draughn RA, editors. Mechanical testing of bone and the bone-implant interface. New York: CRC Press. p 305-320.

Tague RG. 1991. Commonalities in dimorphism and variability in the anthropoid pelvis, with implications for the fossil record. J Hum Evol 21:153-176.

Tague RG. 1993. Pubic symphyseal synostosis and sexual dimorphism of the pelvis in *Presbytis cristata* and *Presbytis rubicunda*. Int J Primatol 14:637-654.

Tague RG. 1995. Variation in pelvic size between males and females in nonhuman anthropoids. Am J Phys Anthropol 97:213-233.

Tague RG. 2005. Big-bodied males help us recognize that females have big pelves. Am J Phys Anthropol 127:392-405.

Terranova CJ. 1995. Functional morphology of leaping behaviors in galagids: associations between landing limb use and diaphyseal geometry. In: Alterman L, Doyle GA, Izard MK, editors. Creatures of the dark: The nocturnal prosimians. New York: Plenum Press. p 473-493.

Timoshenko SP, Gere JM. 1972. Mechanics of materials. New York: D. Van Nostrand Company.

Trinkaus E. 1976. Morphology of European and Southwest Asian Neanderthal pubic bones. Am J Phys Anthropol 44:95-103.

Tuttle RH. 1969. Terrestrial trends in the hands of the anthropoidea. Basel: Karger. p 192-200.

Usherwood JR, Bertram JEA. 2003. Understanding brachiation: insight from a collisional perspective. J Exp Biol 206:1631-1642.

Usherwood JR, Larson SG, Bertram JEA. 2003. Mechanisms of force and power production in unsteady ricochetal brachiation. Am J Phys Anthropol 120:364-372.

Vereecke E, D'Aout K, Van Elsacker L, De Clercq D, Aerts P. 2005. Functional analysis of the gibbon foot during terrestrial bipedal walking: plantar pressure distributions and three-dimensional ground reaction forces. Am J Phys Anthropol 128:659-669.

Vilensky JA. 1978. The function of ischial callosities. Primates 19:363-369.

Vilensky JA, Larson SG. 1989. Primate locomotion: utilization and control of symmetrical gaits. A Rev Anthropol 18:17-35.

Wainwright SA, Biggs WD, Currey JD, Gosline JM. 1982. Mechanical design in organisms. Princeton: Princeton University Press.

Walker A. 1974. Locomotor adaptations in past and present prosimian primates. In: Jenkins FA, editor. Primate locomotion. New York: Academic Press. p 349-381.

Wallace IJ, Demes B. 2008. Symmetrical gaits of Cebus apella: implications for the functional significance of diagonal sequence gait in primates. J Hum Evol 54:783-794.

Ward CV. 1991. Functional anatomy of the lower back and pelvis of the Miocene hominoid *Proconsul nyanzae* from Mfangano Island, Kenya [Ph.D.]. Baltimore: The Johns Hopkins University.

Ward CV, Walker A, Teaford MF, Odhiambo I. 1993. Partial skeleton of *Proconsul nyanzae* from Mfangano Island, Kenya. Am J Phys Anthropol 90:77-111.

Warton DI, Wright IJ, Falster DS, Westoby M. 2006. Bivariate line-fitting methods for allometry. Biol Rev 81:259-291.

Washburn SL. 1942. Skeletal proportions of adult langurs and macaques. Hum Biol 14:444-472.

Washburn SL. 1957. Ischial callosities as sleeping adaptations. Am J Phys Anthropol 15:269-276.

Waterman HC. 1929. Studies on the evolution of the pelvis of man and other primates. Bull Brit Mus Nat Hist 58:585-642.

Weaver TD, Hublin J-J. 2009. Neandertal birth canal shape and the evolution of human childbirth. Proc Natl Acad Sci 106:8151-8156.

Weisbecker V, Goswami A, Wroe S, Sanchez-Villagra MR. 2008. Ossification heterochrony in the therian postcranial skeleton and the marsupial-placental dichotomy. Evolution 62:2027-2041.

Whitehead PF. 1993. Aspects of the anthropoid wrist and hand. In: Gebo DL, editor. Postcranial adaptation in nonhuman primates. DeKalb: Northern Illinois University Press. p 96-120.

Willmore KE, Roseman CC, Rogers J, Cheverud JM, Richtsmeier JT. 2009. Comparison of mandibular phenotypic and genetic integration between baboon and mouse. Evol Biol 36:19-36.

Witzel U, Preuschoft H. 2002. Function-dependent shape characteristics of the human skull. Anthropol Anz 60:113-135.

Wolff J. 1892. The Law of Bone Remodelling: Springer-Verlag.

Woo S, Kuei S, Amiel D, Gomez M, Hayes W, White F, Akeson W. 1981. The effect of prolonged physical training on the properties of long bone: a study of Wolff's Law. J Bone Joint Surg 63:780-787.

Wood CD. 1973. Morphology and biomechanical adaptations in the hindlimb of *Erythrocebus patas* for high speed terrestrial locomotion [Ph.D.]. Seattle: University of Washington.

Wroe S, Milne N. 2007. Convergence and remarkably consistent constraint in the evolution of carnivore skull shape. Evolution 61:1251-1260.

Yirga S. 1987. Interrelation between ischium, thigh extending muscles and locomotion in some primates. Primates 28:79-86.

Young NM. 2006. Function, ontogeny and canalization of shape variance in the primate scapula. J Anat 209:623-636.

Young NM, Hallgrimsson B. 2005. Serial homology and the evolution of mammalian limb covariation structure. Evolution 59:2691-2704.

Young NM, Wagner GP, Hallgrimsson B. 2010. Development and the evolvability of human limbs. Proc Natl Acad Sci 107:3400-3405.

Zuckerman S, Ashton EH, Flinn RM, Oxnard CE, Spence TF. 1973. Some locomotor features of the pelvic girdle in primates. Symp Zool Soc Lond 33:71-165.

APPENDIX A

OSTEOLOGICAL SAMPLE FOR COMPARATIVE MORPHOMETRICS

Species		Wild	Zoo	Unknown	W/Z	Total N	Body mass (kg)	Body mass source
Alouatta caraya , n=20								
	male	10				10	6.42	Smith and Jungers, 1997
	female	10				10	4.33	Smith and Jungers, 1997
	unknown sex							
Ateles belzebuth , n=2								
	male	1				1	8.29	Smith and Jungers, 1997
	female	1				1	7.85	Smith and Jungers, 1997
	unknown sex							
Ateles fusciceps , n=13								
	male	9				9	8.89	Smith and Jungers, 1997
	female	4				4	9.16	Smith and Jungers, 1997
	unknown sex							
Ateles geoffroyi , n=3								
	male	1				1	7.78	Smith and Jungers, 1997
	female	1	1			2	7.29	Smith and Jungers, 1997
	unknown sex							
Ateles paniscus , n=2								
	male							
	female	2				2	8.44	Smith and Jungers, 1997
	unknown sex							
Ateles sp., n=1								
	male							
	female							
	unknown sex		1			1	7.865	Species average from Fleagle, 1999
Cebuella pygmaea , n=12								
	male	4	3			7	0.11	Smith and Jungers, 1997
	female	2	3			5	0.122	Smith and Jungers, 1997
	unknown sex							
Cebus albifrons , n=15								
	male	7				7	3.18	Smith and Jungers, 1997
	female	8				8	2.29	Smith and Jungers, 1997
	unknown sex							
Cebus apella , n=22								
	male	14				14	3.65	Smith and Jungers, 1997
	female	8				8	2.52	Smith and Jungers, 1997
	unknown sex							
Cebus olivaceus , n=3								
	male	2				2	3.29	Smith and Jungers, 1997
	female	1				1	2.52	Smith and Jungers, 1997
	unknown sex							
Cercocebus torquatus , n=11								
	male	2	1	1	1	5	9.47	Smith and Jungers, 1997
	female	3	2			5	5.5	Smith and Jungers, 1997
	unknown sex	1				1	7.485	Smith and Jungers, 1997
Cercopithecus ascanius , n=3								
	male	2				2	3.7	Smith and Jungers, 1997
	female	1				1	2.92	Smith and Jungers, 1997
	unknown sex							
Cercopithecus mitis , n=24								
	male	10				10	5.85	Smith and Cheverud, 2002
	female	13				13	3.93	Smith and Cheverud, 2002
	unknown sex	1				1	4.89	Smith and Cheverud, 2002
Cercopithecus mona , n=5								
	male	4				4	5.1	Smith and Jungers, 1997
	female	1				1	5.1	Male average from Smith and Jungers, 1997
	unknown sex							
Cercopithecus neglectus , n=4								
	male	2				2	7.35	Smith and Jungers, 1997
	female	2				2	4.13	Smith and Jungers, 1997
	unknown sex							
Cercopithecus nictitans , n=5								
	male	2				2	6.67	Smith and Jungers, 1997
	female	2			1	3	4.26	Smith and Jungers, 1997
	unknown sex							

Species		Wild	Zoo	Unknown	W/Z	Total N	Body mass (kg)	Body mass source
Chlorocebus aethiops , n=20								
	male	5	5			10	4.26	Smith and Cheverud, 2002
	female	9				9	2.98	Smith and Cheverud, 2002
	unknown sex		1			1	3.62	Smith and Cheverud, 2002
Colobus angolensis , n=7								
	male	5				5	9.68	Smith and Jungers, 1997
	female	2				2	7.57	Smith and Jungers, 1997
	unknown sex							
Colobus guereza , n=23								
	male	7				7	9.89	Smith and Cheverud, 2002
	female	12				12	7.9	Smith and Cheverud, 2002
	unknown sex	4				4	8.895	Smith and Cheverud, 2002
Daubentonia madagascariensis , n=8								
	male	4				4	2.62	Smith and Jungers, 1997
	female	2				2	2.49	Smith and Jungers, 1997
	unknown sex	2				2	2.555	Smith and Jungers, 1997
Erythrocebus patas , n=6								
	male	2		1		3	12.4	Smith and Jungers, 1997
	female	1				1	6.5	Smith and Jungers, 1997
	unknown sex	1	1			2	9.45	Smith and Jungers, 1997
Eulemur fulvus , n=22								
	male	4				4	2.18	Smith and Cheverud, 2002
	female	11		1		12	2.25	Smith and Cheverud, 2002
	unknown sex	4			2	6	2.215	Smith and Cheverud, 2002
Eulemur mongoz , n=3								
	male		3			3	1.63	Smith and Cheverud, 2002
	female							
	unknown sex							
Galago senegalensis , n=32								
	male	9	7			16	0.227	Smith and Cheverud, 2002
	female	3	7			10	0.199	Smith and Cheverud, 2002
	unknown sex	5	1			6	0.213	Smith and Cheverud, 2002
Gorilla gorilla , n=21								
	male	10	1			11	169.3	Smith and Cheverud, 2002
	female	10				10	75.7	Smith and Cheverud, 2002
	unknown sex							
Hapalemur griseus , n=14								
	male	2				2	0.987	Smith and Cheverud, 2002
	female	5	1			6	0.903	Smith and Cheverud, 2002
	unknown sex	4		2		6	0.945	Smith and Cheverud, 2002
Hapalemur simus , n=1								
	male		1			1	2.15	Smith and Jungers, 1997
	female							
	unknown sex							
Hapalemur sp., n=1								
	male							
	female							
	unknown sex	1				1	0.945	Smith and Cheverud, 2002
Homo sapiens , n=40								
	male	20				20	60.2	Smith and Cheverud, 2002
	female	20				20	53.6	Smith and Cheverud, 2002
	unknown sex							
Hylobates agilis , n=2								
	male							
	female	2				2	5.82	Smith and Jungers, 1997
	unknown sex							
Hylobates concolor , n=3								
	male		2			2	7.79	Smith and Jungers, 1997
	female		1			1	7.62	Smith and Jungers, 1997
	unknown sex							
Hylobates hoolock , n=13								
	male	7				7	6.87	Smith and Jungers, 1997
	female	6				6	6.88	Smith and Jungers, 1997
	unknown sex							

Species		Wild	Zoo	Unknown	W/Z	Total N	Body mass (kg)	Body mass source
Hylobates klossi , n=2								
	male	1				1	5.67	Smith and Jungers, 1997
	female	1				1	5.92	Smith and Jungers, 1997
	unknown sex							
Hylobates lar , n=24								
	male	13				13	5.9	Smith and Jungers, 1997
	female	11				11	5.34	Smith and Jungers, 1997
	unknown sex					0		
Indri indri , n=8								
	male	2				2	5.83	Smith and Jungers, 1997
	female	2				2	6.84	Smith and Jungers, 1997
	unknown sex	3		1		4	6.335	Smith and Jungers, 1997
Lagothrix lagotricha , n=10								
	male	6				6	7.28	Smith and Jungers, 1997
	female	3				3	7.02	Smith and Jungers, 1997
	unknown sex	1				1	7.15	Smith and Jungers, 1997
Lemur catta , n=24								
	male	2	4			6	2.21	Smith and Jungers, 1997
	female	1	3			4	2.21	Smith and Jungers, 1997
	unknown sex	10	3	1		14	2.21	Smith and Jungers, 1997
Leontopithecus chrysomelas , n=3								
	male		2			2	0.62	Smith and Jungers, 1997
	female		1			1	0.535	Smith and Jungers, 1997
	unknown sex							
Leontopithecus rosalia , n=17								
	male		8			8	0.62	Smith and Jungers, 1997
	female		9			9	0.598	Smith and Jungers, 1997
	unknown sex							
Lepilemur mustelinus , n=19								
	male	7		1		8	0.77	Smith and Jungers, 1997
	female	11				11	0.77	Smith and Jungers, 1997
	unknown sex							
Lepilemur sp., n=1								
	male							
	female			1		1	0.76	Species average from Fleagle, 1999
	unknown sex							
Lophocebus albigena , n=3								
	male	3				3	8.25	Smith and Jungers, 1997
	female							
	unknown sex							
Loris tardigradus , n=3								
	male		1			1	0.192	Smith and Jungers, 1997
	female							
	unknown sex	2				2	0.1925	Smith and Jungers, 1997
Macaca fascicularis , n=39								
	male	21	2			23	5.36	Smith and Jungers, 1997
	female	13				13	3.59	Smith and Jungers, 1997
	unknown sex	2			1	3	4.475	Smith and Jungers, 1997
Macaca mulatta , n=6								
	male	1	2			3	11	Smith and Cheverud, 2002
	female	1	2			3	8.8	Smith and Cheverud, 2002
	unknown sex							
Macaca nemestrina , n=13								
	male	8	1			9	11.2	Smith and Cheverud, 2002
	female	2	1			3	6.5	Smith and Cheverud, 2002
	unknown sex	1				1	8.85	Smith and Cheverud, 2002
Mandrillus leucophaeus , n=5								
	male		2			2	20	Smith and Jungers, 1997
	female	2	1			3	12.5	Smith and Jungers, 1997
	unknown sex							
Mandrillus sphinx , n=8								
	male	1	2		1	4	31.6	Smith and Jungers, 1997
	female	1	2			3	12.9	Smith and Jungers, 1997
	unknown sex	1				1	22.25	Smith and Jungers, 1997

Species		Wild	Zoo	Unknown	W/Z	Total N	Body mass (kg)	Body mass source
Miopithecus talapoin , n=16								
	male	3	2			5	1.38	Smith and Cheverud, 2002
	female	6	1	3	1	11	1.12	Smith and Cheverud, 2002
	unknown sex							
Nasalis larvatus , n=20								
	male	11				11	20.4	Smith and Jungers, 1997
	female	7				7	9.82	Smith and Jungers, 1997
	unknown sex	2				2	15.11	Smith and Jungers, 1997
Nycticebus coucang , n=16								
	male	1			3	4	0.679	Smith and Jungers, 1997
	female	2	2			4	0.626	Smith and Jungers, 1997
	unknown sex	4	3		1	8	0.6525	Smith and Jungers, 1997
Nycticebus sp., n=2								
	male							
	female							
	unknown sex	2				2	0.8085	Species average from Fleagle, 1999
Nycticebus pygmaeus , n=2								
	male							
	female				1	1	0.307	Smith and Jungers, 1997
	unknown sex	1				1	0.307	Smith and Jungers, 1997
Otolemur crassicaudatus , n=29								
	male	11	12			23	1.19	Smith and Jungers, 1997
	female	3	3			6	1.11	Smith and Jungers, 1997
	unknown sex							
Pan troglodytes , n=41								
	male	20				20	42.7	Smith and Cheverud, 2002
	female	21				21	33.7	Smith and Cheverud, 2002
	unknown sex							
Papio hamadryas anubis , n=20								
	male	2	6	1		9	25.1	Smith and Jungers, 1997
	female	2	6			8	13.3	Smith and Jungers, 1997
	unknown sex	1	2			3	19.2	Smith and Jungers, 1997
Papio hamadryas cynocephalus , n=10								
	male	3	1			4	21.8	Smith and Jungers, 1997
	female	3			1	4	12.3	Smith and Jungers, 1997
	unknown sex		2			2	17.05	Smith and Jungers, 1997
Papio hamadryas hamadryas , n=5								
	male		4			4	16.9	Smith and Jungers, 1997
	female							
	unknown sex	1				1	13.4	Smith and Jungers, 1997
Papio hamadryas papio , n=3								
	male	1	2			3	17.596	Rowe, 1996
	female							
	unknown sex							
Papio hamadryas sp., n=2								
	male							
	female							
	unknown sex	1	1			2	19.85	Species average from Fleagle, 1999
Papio hamadryas ursinus , n=5								
	male	1	2			3	29.8	Smith and Jungers, 1997
	female	1	1			2	14.8	Smith and Jungers, 1997
	unknown sex							
Perodicticus potto , n=26								
	male	11		1		12	0.83	Smith and Cheverud, 2002
	female	3		1		4	0.836	Smith and Cheverud, 2002
	unknown sex	6	1	3		10	0.833	Smith and Cheverud, 2002
Pithecia monachus , n=3								
	male	3				3	2.61	Smith and Cheverud, 2002
	female							
	unknown sex							
Pithecia pithecia , n=6								
	male	5	1			6	1.94	Smith and Jungers, 1997
	female							
	unknown sex							

Species		Wild	Zoo	Unknown	W/Z	Total N	Body mass (kg)	Body mass source
Pithecia sp., n=1								
	male							
	female							
	unknown sex	1				1	2.29	Species average from Fleagle, 1999
Pongo pygmaeus, n=20								
	male	10	2	3	1	16	78.3	Smith and Cheverud, 2002
	female	1	1			2	35.8	Smith and Cheverud, 2002
	unknown sex			2		2	57.05	Smith and Cheverud, 2002
Procolobus badius, n=10								
	male	5				5	8.36	Smith and Cheverud, 2002
	female	5				5	8.21	Smith and Cheverud, 2002
	unknown sex							
Propithecus diadema, n=4								
	male	1				1	5.94	Smith and Jungers, 1997
	female	1				1	6.26	Smith and Jungers, 1997
	unknown sex	1		1		2	6.1	Smith and Jungers, 1997
Propithecus sp., n=1								
	male							
	female							
	unknown sex		1			1	4.605	Species average from Fleagle, 1999
Propithecus verreauxi, n=34								
	male	7			2	9	3.25	Smith and Jungers, 1997
	female	6				6	2.95	Smith and Jungers, 1997
	unknown sex	19				19	3.1	Smith and Jungers, 1997
Saimiri boliviensis, n=16								
	male	9				9	0.911	Smith and Cheverud, 2002
	female	7				7	0.711	Smith and Cheverud, 2002
	unknown sex							
Saimiri sciureus, n=2								
	male							
	female	2				2	0.662	Smith and Cheverud, 2002
	unknown sex							
Saimiri sp., n=2								
	male	1				1	0.845	Species average from Fleagle, 1999
	female	1				1	0.674	Species average from Fleagle, 1999
	unknown sex							
Semnopithecus entellus, n=5								
	male	1				1	11.4	Smith and Cheverud, 2002
	female	2				2	6.91	Smith and Cheverud, 2002
	unknown sex	2				2	9.155	Smith and Cheverud, 2002
Symphalangus syndactylus, n=10								
	male	2				2	11.9	Smith and Jungers, 1997
	female	6	2			8	10.7	Smith and Jungers, 1997
	unknown sex							
Tarsius bancanus, n=4								
	male	1				1	0.128	Smith and Jungers, 1997
	female	1	1			2	0.117	Smith and Jungers, 1997
	unknown sex	1				1	0.1225	Smith and Jungers, 1997
Tarsius syrichta, n=4								
	male	1	2			3	0.134	Smith and Jungers, 1997
	female		1			1	0.117	Smith and Jungers, 1997
	unknown sex							
Theropithecus gelada, n=6								
	male		1			1	19	Smith and Jungers, 1997
	female	1	4			5	11.7	Smith and Jungers, 1997
	unknown sex							
Varecia variegata, n=14								
	male	2	3			5	3.47	Smith and Cheverud, 2002
	female	1	1			2	3.51	Smith and Cheverud, 2002
	unknown sex	3	4			7	3.49	Smith and Cheverud, 2002
Total sample size		682	163	24	16	**885**		

Numbers of individuals per sex for each species. The majority of specimens were wild-caught, but some were obtained from zoos, have unknown rearing histories, or were wild-caught but zoo-raised. Body masses are sex-specific species means. Sex means were used for individuals of unknown sex.

APPENDIX B

DISTANCE MATRICES FOR GEOMETRIC MORPHOMETRIC AND PHYLOGENETIC DATA

PROCRUSTES DISTANCE MATRIX

	Alouatta caraya	*Ateles*	*Cebuella pygmaea*	*Cebus*	*Cercocebus torquatus*	*Cercopithecus*	*Chlorocebus aethiops*	*Colobus guereza*	*Daubentonia madagascariensis*	*Erythrocebus patas*	*Eulemur*	*Galago senegalensis*
Alouatta caraya	0	0.1389	0.2106	0.1717	0.2003	0.1892	0.2001	0.2127	0.2257	0.2572	0.1826	0.2173
Ateles	0.1389	0	0.2015	0.1985	0.1829	0.1875	0.1915	0.179	0.2838	0.2329	0.2245	0.2439
Cebuella pygmaea	0.2106	0.2015	0	0.1799	0.1838	0.169	0.166	0.1837	0.2189	0.2295	0.2066	0.2195
Cebus	0.1717	0.1985	0.1799	0	0.1314	0.1069	0.1122	0.1666	0.1266	0.1959	0.0998	0.1871
Cercocebus torquatus	0.2003	0.1829	0.1838	0.1314	0	0.0625	0.0541	0.0702	0.2096	0.1426	0.148	0.2145
Cercopithecus	0.1892	0.1875	0.169	0.1069	0.0625	0	0.0503	0.1033	0.1827	0.1724	0.1247	0.1906
Chlorocebus aethiops	0.2001	0.1915	0.166	0.1122	0.0541	0.0503	0	0.0903	0.1872	0.1505	0.1346	0.2112
Colobus guereza	0.2127	0.179	0.1837	0.1666	0.0702	0.1033	0.0903	0	0.2383	0.1341	0.1759	0.2319
Daubentonia madagascariensis	0.2257	0.2838	0.2189	0.1266	0.2096	0.1827	0.1872	0.2383	0	0.2625	0.1202	0.2007
Erythrocebus patas	0.2572	0.2329	0.2295	0.1959	0.1426	0.1724	0.1505	0.1341	0.2625	0	0.2101	0.1769
Eulemur	0.1826	0.2245	0.2066	0.0998	0.148	0.1247	0.1346	0.1759	0.1202	0.2101	0	0
Galago senegalensis	0.2173	0.2439	0.2195	0.1871	0.2145	0.1906	0.2112	0.2319	0.2007	0.2923	0.1769	0.4576
Gorilla gorilla	0.3115	0.3164	0.3948	0.3642	0.3493	0.3597	0.3553	0.3423	0.405	0.3305	0.346	0.4576
Hapalemur	0.1689	0.2016	0.1862	0.1115	0.1424	0.1172	0.1324	0.1675	0.1512	0.2135	0.0565	0.1636
Hylobates	0.2007	0.1365	0.2208	0.2423	0.196	0.2104	0.2169	0.1814	0.3139	0.2106	0.2417	0.2761
Indri indri	0.254	0.2469	0.2338	0.1876	0.1751	0.1865	0.1796	0.1648	0.2167	0.1737	0.1667	0.2682
Lagothrix lagothricha	0.1301	0.1059	0.1411	0.1684	0.1614	0.152	0.1625	0.1611	0.2395	0.2266	0.1994	0.2062
Lemur catta	0.193	0.2401	0.2489	0.1237	0.1783	0.1596	0.1623	0.2062	0.1455	0.2272	0.0681	0.21
Leontopithecus	0.2444	0.2523	0.1043	0.1883	0.2024	0.186	0.1811	0.2132	0.2122	0.2296	0.2093	0.2478
Lepilemur	0.2191	0.2368	0.2119	0.1446	0.1698	0.1498	0.1695	0.1947	0.1663	0.2261	0.1096	0.1459
Lophocebus albigena	0.201	0.1866	0.2184	0.1322	0.0769	0.0995	0.0999	0.1022	0.2164	0.1391	0.157	0.2171
Loris tardigradus	0.288	0.3167	0.2831	0.296	0.3243	0.2947	0.3142	0.3332	0.3003	0.4048	0.2977	0.185
Macaca fascicularis	0.1765	0.1489	0.1693	0.126	0.0551	0.0584	0.0698	0.0851	0.2112	0.1659	0.1465	0.2002
Macaca mulatta	0.2073	0.1771	0.1749	0.1379	0.0682	0.0725	0.0738	0.095	0.2149	0.1728	0.1647	0.2117
Macaca nemestrina	0.2014	0.166	0.1747	0.1447	0.0651	0.0816	0.0801	0.0681	0.2242	0.1522	0.1683	0.2235
Mandrillus	0.2148	0.1852	0.2142	0.168	0.0947	0.116	0.1027	0.0881	0.2405	0.1432	0.179	0.265
Miopithecus talapoin	0.17	0.1753	0.1473	0.1155	0.0913	0.059	0.0766	0.1221	0.1901	0.1924	0.1365	0.1869
Nasalis larvatus	0.2233	0.1922	0.215	0.2049	0.1399	0.168	0.1532	0.1011	0.2659	0.1156	0.2037	0.2832
Nycticebus coucang	0.2187	0.2703	0.2127	0.2229	0.2544	0.2259	0.2424	0.2672	0.2229	0.329	0.2142	0.1469
Nycticebus pygmaeus	0.24	0.2638	0.2242	0.2665	0.277	0.2514	0.2678	0.2793	0.2847	0.3542	0.2647	0.1913
Otolemur crassicaudatus	0.1961	0.232	0.1903	0.1461	0.179	0.1585	0.1716	0.2013	0.1586	0.2578	0.1347	0.0772
Pan troglodytes	0.2346	0.2108	0.3118	0.286	0.2505	0.2676	0.267	0.2444	0.3467	0.2374	0.2764	0.3589
Papio hamadryas	0.2162	0.167	0.199	0.2003	0.1167	0.1466	0.1284	0.0909	0.2743	0.1354	0.2114	0.2834
Perodicticus potto	0.2034	0.2574	0.2238	0.226	0.2596	0.2306	0.253	0.2697	0.2373	0.3295	0.2223	0.1619
Pithecia	0.2615	0.2265	0.1414	0.1656	0.1591	0.1532	0.1537	0.1659	0.2133	0.2025	0.1963	0.2345
Pongo pygmaeus	0.2536	0.2326	0.3304	0.3041	0.2709	0.2846	0.2822	0.2639	0.3633	0.2605	0.2924	0.3908
Procolobus badius	0.2012	0.19	0.2217	0.1554	0.0893	0.1077	0.1012	0.098	0.2266	0.1424	0.1501	0.2533
Propithecus	0.2443	0.2424	0.2186	0.1946	0.1861	0.195	0.1884	0.1777	0.2239	0.1803	0.1678	0.2637
Saimiri	0.2006	0.2248	0.1327	0.103	0.1651	0.143	0.1356	0.1799	0.1448	0.2032	0.1435	0.2175
Semnopithecus	0.2331	0.1802	0.2093	0.1975	0.1092	0.1393	0.1252	0.0643	0.2694	0.1337	0.203	0.2669
Symphalangus syndactylus	0.2247	0.1822	0.3052	0.3017	0.2576	0.2727	0.2783	0.2453	0.3705	0.2654	0.2938	0.3435
Tarsius	0.2208	0.2257	0.1969	0.2301	0.2397	0.2172	0.2378	0.249	0.2646	0.3234	0.2339	0.1176
Theropithecus gelada	0.1749	0.1519	0.1956	0.1661	0.0901	0.1141	0.1033	0.097	0.2423	0.147	0.1738	0.2465
Varecia variegata	0.1878	0.2218	0.2036	0.1066	0.1554	0.1316	0.1407	0.1801	0.1229	0.2284	0.0626	0.1456

	Gorilla gorilla	*Hapalemur*	*Hylobates*	*Indri indri*	*Lagothrix lagothricha*	*Lemur catta*	*Leontopithecus*	*Lepilemur*	*Lophocebus albigena*	*Loris tardigradus*	*Macaca fascicularis*	*Macaca mulatta*
Alouatta caraya	0.3115	0.1689	0.2007	0.254	0.1301	0.193	0.2444	0.2191	0.201	0.288	0.1765	0.2073
Ateles	0.3164	0.2016	0.1365	0.2469	0.1059	0.2401	0.2523	0.2368	0.1866	0.3167	0.1489	0.1771
Cebuella pygmaea	0.3948	0.1862	0.2208	0.2338	0.1411	0.2489	0.1043	0.2119	0.2184	0.2831	0.1693	0.1749
Cebus	0.3642	0.1115	0.2423	0.1876	0.1684	0.1237	0.1883	0.1446	0.1322	0.296	0.126	0.1379
Cercocebus torquatus	0.3493	0.1424	0.196	0.1751	0.1614	0.1783	0.2024	0.1698	0.0769	0.3243	0.0551	0.0682
Cercopithecus	0.3597	0.1172	0.2104	0.1865	0.152	0.1596	0.186	0.1498	0.0995	0.2947	0.0584	0.0725
Chlorocebus aethiops	0.3553	0.1324	0.2169	0.1796	0.1625	0.1623	0.1811	0.1695	0.0999	0.3142	0.0698	0.0738
Colobus guereza	0.3423	0.1675	0.1814	0.1648	0.1611	0.2062	0.2132	0.1947	0.1022	0.3332	0.0851	0.095
Daubentonia madagascariensis	0.405	0.1512	0.3139	0.2167	0.2395	0.1455	0.2122	0.1663	0.2164	0.3003	0.2112	0.2149
Erythrocebus patas	0.3305	0.2135	0.2106	0.1737	0.2266	0.2272	0.2296	0.2261	0.1391	0.4048	0.1659	0.1728
Eulemur	0.346	0.0565	0.2417	0.1667	0.1994	0.0681	0.2093	0.1096	0.157	0.2977	0.1465	0.1647
Galago senegalensis	0.4576	0.1636	0.2761	0.2682	0.2062	0.21	0.2478	0.1459	0.2171	0.185	0.2002	0.2117
Gorilla gorilla	0	0.34	0.2963	0.3139	0.3361	0.3352	0.39	0.3937	0.3544	0.5305	0.3438	0.3726
Hapalemur	0.34	0	0.2221	0.1722	0.1752	0.0969	0.1982	0.1039	0.161	0.282	0.1322	0.1552
Hylobates	0.2963	0.2221	0	0.2256	0.1703	0.267	0.2579	0.2377	0.2071	0.3591	0.1742	0.2005
Indri indri	0.3139	0.1722	0.2256	0	0.2285	0.182	0.2331	0.1913	0.1848	0.3792	0.1851	0.1918
Lagothrix lagothricha	0.3361	0.1752	0.1703	0.2285	0	0.229	0.1892	0.2138	0.1793	0.2724	0.1332	0.1546
Lemur catta	0.3352	0.0969	0.267	0.182	0.229	0	0.2434	0.1529	0.1754	0.3225	0.1785	0.1964
Leontopithecus	0.39	0.1982	0.2579	0.2331	0.1892	0.2434	0	0.2216	0.2317	0.3195	0.2016	0.2072
Lepilemur	0.3937	0.1039	0.2377	0.1913	0.2138	0.1529	0.2216	0	0.1808	0.2881	0.1612	0.1812
Lophocebus albigena	0.3544	0.161	0.2071	0.1848	0.1793	0.1754	0.2317	0.1808	0	0.3327	0.0946	0.1064
Loris tardigradus	0.5305	0.282	0.3591	0.3792	0.2724	0.3225	0.3195	0.2881	0.3327	0	0.303	0.3068
Macaca fascicularis	0.3438	0.1322	0.1742	0.1851	0.1332	0.1785	0.2016	0.1612	0.0946	0.303	0	0.0557
Macaca mulatta	0.3726	0.1552	0.2005	0.1918	0.1546	0.1964	0.2072	0.1812	0.1064	0.3068	0.0557	0
Macaca nemestrina	0.353	0.1588	0.1864	0.1758	0.1482	0.1986	0.2063	0.183	0.0996	0.3209	0.0603	0.0624
Mandrillus	0.3211	0.1804	0.1877	0.1796	0.187	0.1964	0.2349	0.2133	0.1132	0.3638	0.1038	0.1077
Miopithecus talapoin	0.358	0.1175	0.2077	0.2054	0.1297	0.1733	0.1795	0.1623	0.1319	0.2758	0.0691	0.0843
Nasalis larvatus	0.2902	0.1993	0.1687	0.1504	0.1924	0.2236	0.2306	0.225	0.1478	0.3848	0.1504	0.168
Nycticebus coucang	0.4596	0.1938	0.3113	0.3031	0.212	0.2482	0.2491	0.2179	0.2688	0.1644	0.237	0.2414
Nycticebus pygmaeus	0.472	0.2358	0.3117	0.3376	0.2124	0.3	0.279	0.2614	0.2967	0.1719	0.2535	0.2589
Otolemur crassicaudatus	0.4274	0.1252	0.2665	0.2314	0.1879	0.171	0.2116	0.1357	0.1887	0.213	0.1729	0.182
Pan troglodytes	0.1672	0.2661	0.1764	0.2551	0.243	0.277	0.317	0.2968	0.2524	0.4417	0.2411	0.275
Papio hamadryas	0.2932	0.2011	0.1538	0.185	0.1721	0.2286	0.2201	0.2356	0.1426	0.3735	0.1194	0.1349
Perodicticus potto	0.4482	0.1997	0.3014	0.3012	0.1999	0.2546	0.2641	0.2243	0.2663	0.1842	0.2408	0.2485
Pithecia	0.3952	0.1871	0.232	0.1857	0.1874	0.2354	0.1444	0.1862	0.1907	0.3245	0.1548	0.1555
Pongo pygmaeus	0.1334	0.2838	0.2081	0.2676	0.2612	0.2898	0.3348	0.33	0.2728	0.4744	0.2623	0.2902
Procolobus badius	0.2947	0.1508	0.1875	0.1551	0.1873	0.1612	0.2266	0.1956	0.1028	0.3613	0.1037	0.1234
Propithecus	0.2987	0.1643	0.2161	0.0678	0.217	0.1836	0.2113	0.1928	0.2005	0.3719	0.193	0.2063
Saimiri	0.3655	0.1424	0.2585	0.1858	0.1733	0.1714	0.1363	0.1818	0.1845	0.3009	0.1634	0.1718
Semnopithecus	0.3273	0.1961	0.165	0.1722	0.1847	0.2259	0.2364	0.2211	0.1264	0.3668	0.1169	0.1236
Symphalangus syndactylus	0.2523	0.2788	0.1109	0.28	0.2323	0.304	0.334	0.3071	0.2606	0.4164	0.2372	0.2654
Tarsius	0.4662	0.204	0.2598	0.3081	0.1867	0.2696	0.2494	0.2045	0.2563	0.1528	0.212	0.2243
Theropithecus gelada	0.2956	0.1646	0.1633	0.1969	0.1526	0.1923	0.2119	0.2007	0.1158	0.3459	0.0927	0.1258
Varecia variegata	0.3802	0.0841	0.2479	0.1859	0.1959	0.0908	0.2125	0.1131	0.1611	0.2635	0.1518	0.1641

	Macaca nemestrina	*Mandrillus*	*Miopithecus talapoin*	*Nasalis larvatus*	*Nycticebus coucang*	*Nycticebus pygmaeus*	*Otolemur crassicaudatus*	*Pan troglodytes*	*Papio hamadryas*	*Perodicticus potto*	*Pithecia*	*Pongo pygmaeus*
Alouatta caraya	0.2014	0.2148	0.17	0.2233	0.2187	0.24	0.1961	0.2346	0.2162	0.2034	0.2615	0.2536
Ateles	0.166	0.1852	0.1753	0.1922	0.2703	0.2638	0.232	0.2108	0.167	0.2574	0.2265	0.2326
Cebuella pygmaea	0.1747	0.2142	0.1473	0.215	0.2127	0.2242	0.1903	0.3118	0.199	0.2238	0.1414	0.3304
Cebus	0.1447	0.168	0.1155	0.2049	0.2229	0.2665	0.1461	0.286	0.2003	0.226	0.1656	0.3041
Cercocebus torquatus	0.0651	0.0947	0.0913	0.1399	0.2544	0.277	0.179	0.2505	0.1167	0.2596	0.1591	0.2709
Cercopithecus	0.0816	0.116	0.059	0.168	0.2259	0.2514	0.1585	0.2676	0.1466	0.2306	0.1532	0.2846
Chlorocebus aethiops	0.0801	0.1027	0.0766	0.1532	0.2424	0.2678	0.1716	0.267	0.1284	0.253	0.1537	0.2822
Colobus guereza	0.0681	0.0881	0.1221	0.1011	0.2672	0.2793	0.2013	0.2444	0.0909	0.2697	0.1659	0.2639
Daubentonia madagascariensis	0.2242	0.2405	0.1901	0.2659	0.2229	0.2847	0.1586	0.3467	0.2743	0.2373	0.2133	0.3633
Erythrocebus patas	0.1522	0.1432	0.1924	0.1156	0.329	0.3542	0.2578	0.2374	0.1354	0.3295	0.2025	0.2605
Eulemur	0.1683	0.179	0.1365	0.2037	0.2142	0.2647	0.1347	0.2764	0.2114	0.2223	0.1963	0.2924
Galago senegalensis	0.2235	0.265	0.1869	0.2832	0.1469	0.1913	0.0772	0.3589	0.2834	0.1619	0.2345	0.3908
Gorilla gorilla	0.353	0.3211	0.358	0.2902	0.4596	0.472	0.4274	0.1672	0.2932	0.4482	0.3952	0.1334
Hapalemur	0.1588	0.1804	0.1175	0.1993	0.1938	0.2358	0.1252	0.2661	0.2011	0.1997	0.1871	0.2838
Hylobates	0.1864	0.1877	0.2077	0.1687	0.3113	0.3117	0.2665	0.1764	0.1538	0.3014	0.232	0.2081
Indri indri	0.1758	0.1796	0.2054	0.1504	0.3031	0.3376	0.2314	0.2551	0.185	0.3012	0.1857	0.2676
Lagothrix lagothricha	0.1482	0.187	0.1297	0.1924	0.212	0.2124	0.1879	0.243	0.1721	0.1999	0.1874	0.2612
Lemur catta	0.1986	0.1964	0.1733	0.2236	0.2482	0.3	0.171	0.277	0.2286	0.2546	0.2354	0.2898
Leontopithecus	0.2063	0.2349	0.1795	0.2306	0.2491	0.279	0.2116	0.317	0.2201	0.2641	0.1444	0.3348
Lepilemur	0.183	0.2133	0.1623	0.225	0.2179	0.2614	0.1357	0.2968	0.2356	0.2243	0.1862	0.33
Lophocebus albigena	0.0996	0.1132	0.1319	0.1478	0.2688	0.2967	0.1887	0.2524	0.1426	0.2663	0.1907	0.2728
Loris tardigradus	0.3209	0.3638	0.2758	0.3848	0.1644	0.1719	0.213	0.4417	0.3735	0.1842	0.3245	0.4744
Macaca fascicularis	0.0603	0.1038	0.0691	0.1504	0.237	0.2535	0.1729	0.2411	0.1194	0.2408	0.1548	0.2623
Macaca mulatta	0.0624	0.1077	0.0843	0.168	0.2414	0.2589	0.182	0.275	0.1349	0.2485	0.1555	0.2902
Macaca nemestrina	0	0.08	0.1038	0.1284	0.256	0.2685	0.1929	0.2569	0.1059	0.2575	0.1478	0.2715
Mandrillus	0.08	0	0.1442	0.1107	0.3017	0.3181	0.2342	0.2385	0.0864	0.3052	0.191	0.2422
Miopithecus talapoin	0.1038	0.1442	0	0.187	0.197	0.2192	0.1543	0.2684	0.1578	0.2063	0.1636	0.2855
Nasalis larvatus	0.1284	0.1107	0.187	0	0.3154	0.3311	0.2533	0.2061	0.0913	0.3103	0.2018	0.2202
Nycticebus coucang	0.256	0.3017	0.197	0.3154	0	0.0999	0.1386	0.3832	0.3105	0.0818	0.2714	0.4024
Nycticebus pygmaeus	0.2685	0.3181	0.2192	0.3311	0.0999	0	0.1896	0.3912	0.3178	0.1173	0.2899	0.4129
Otolemur crassicaudatus	0.1929	0.2342	0.1543	0.2533	0.1386	0.1896	0	0.3379	0.2533	0.1587	0.2044	0.3647
Pan troglodytes	0.2569	0.2385	0.2684	0.2061	0.3832	0.3912	0.3379	0	0.1962	0.3714	0.3045	0.1062
Papio hamadryas	0.1059	0.0864	0.1578	0.0913	0.3105	0.3178	0.2533	0.1962	0	0.3135	0.1891	0.2118
Perodicticus potto	0.2575	0.3052	0.2063	0.3103	0.0818	0.1173	0.1587	0.3714	0.3135	0	0.282	0.3891
Pithecia	0.1478	0.191	0.1636	0.2018	0.2714	0.2899	0.2044	0.3045	0.1891	0.282	0	0.3334
Pongo pygmaeus	0.2715	0.2422	0.2855	0.2202	0.4024	0.4129	0.3647	0.1062	0.2118	0.3891	0.3334	0
Procolobus badius	0.1091	0.0853	0.1372	0.1167	0.2926	0.3189	0.2182	0.2139	0.1101	0.2939	0.1965	0.2215
Propithecus	0.1922	0.2013	0.2036	0.1611	0.2902	0.3252	0.2249	0.2387	0.1877	0.2898	0.1881	0.2544
Saimiri	0.1712	0.1986	0.137	0.205	0.2227	0.2612	0.1713	0.2993	0.2043	0.2281	0.1462	0.317
Semnopithecus	0.0952	0.0823	0.1623	0.085	0.3072	0.3141	0.2409	0.23	0.0728	0.3053	0.1872	0.2447
Symphalangus syndactylus	0.2554	0.2393	0.2688	0.2213	0.3718	0.3708	0.3332	0.1481	0.2075	0.3569	0.3184	0.1757
Tarsius	0.2367	0.2858	0.1915	0.3036	0.1418	0.1489	0.1483	0.3641	0.2865	0.1594	0.2454	0.3956
Theropithecus gelada	0.103	0.0931	0.1266	0.113	0.2812	0.2964	0.2171	0.1933	0.0787	0.2845	0.1951	0.2158
Varecia variegata	0.1727	0.1897	0.1444	0.2185	0.1983	0.2493	0.1129	0.2988	0.2216	0.2075	0.1984	0.3196

	Procolobus badius	*Propithecus*	*Saimiri*	*Semnopithecus*	*Symphalangus syndactylus*	*Tarsius*	*Theropithecus gelada*	*Varecia variegata*
Alouatta caraya	0.2012	0.2443	0.2006	0.2331	0.2247	0.2208	0.1749	0.1878
Ateles	0.19	0.2424	0.2248	0.1802	0.1822	0.2257	0.1519	0.2218
Cebuella pygmaea	0.2217	0.2186	0.1327	0.2093	0.3052	0.1969	0.1956	0.2036
Cebus	0.1554	0.1946	0.103	0.1975	0.3017	0.2301	0.1661	0.1066
Cercocebus torquatus	0.0893	0.1861	0.1651	0.1092	0.2576	0.2397	0.0901	0.1554
Cercopithecus	0.1077	0.195	0.143	0.1393	0.2727	0.2172	0.1141	0.1316
Chlorocebus aethiops	0.1012	0.1884	0.1356	0.1252	0.2783	0.2378	0.1033	0.1407
Colobus guereza	0.098	0.1777	0.1799	0.0643	0.2453	0.249	0.097	0.1801
Daubentonia madagascariensis	0.2266	0.2239	0.1448	0.2694	0.3705	0.2646	0.2423	0.1229
Erythrocebus patas	0.1424	0.1803	0.2032	0.1337	0.2654	0.3234	0.147	0.2284
Eulemur	0.1501	0.1678	0.1435	0.203	0.2938	0.2339	0.1738	0.0626
Galago senegalensis	0.2533	0.2637	0.2175	0.2669	0.3435	0.1176	0.2465	0.1456
Gorilla gorilla	0.2947	0.2987	0.3655	0.3273	0.2523	0.4662	0.2956	0.3802
Hapalemur	0.1508	0.1643	0.1424	0.1961	0.2788	0.204	0.1646	0.0841
Hylobates	0.1875	0.2161	0.2585	0.165	0.1109	0.2598	0.1633	0.2479
Indri indri	0.1551	0.0678	0.1858	0.1722	0.28	0.3081	0.1969	0.1859
Lagothrix lagothricha	0.1873	0.217	0.1733	0.1847	0.2323	0.1867	0.1526	0.1959
Lemur catta	0.1612	0.1836	0.1714	0.2259	0.304	0.2696	0.1923	0.0908
Leontopithecus	0.2266	0.2113	0.1363	0.2364	0.334	0.2494	0.2119	0.2125
Lepilemur	0.1956	0.1928	0.1818	0.2211	0.3071	0.2045	0.2007	0.1131
Lophocebus albigena	0.1028	0.2005	0.1845	0.1264	0.2606	0.2563	0.1158	0.1611
Loris tardigradus	0.3613	0.3719	0.3009	0.3668	0.4164	0.1528	0.3459	0.2635
Macaca fascicularis	0.1037	0.193	0.1634	0.1169	0.2372	0.212	0.0927	0.1518
Macaca mulatta	0.1234	0.2063	0.1718	0.1236	0.2654	0.2243	0.1258	0.1641
Macaca nemestrina	0.1091	0.1922	0.1712	0.0952	0.2554	0.2367	0.103	0.1727
Mandrillus	0.0853	0.2013	0.1986	0.0823	0.2393	0.2858	0.0931	0.1897
Miopithecus talapoin	0.1372	0.2036	0.137	0.1623	0.2688	0.1915	0.1266	0.1444
Nasalis larvatus	0.1167	0.1611	0.205	0.085	0.2213	0.3036	0.113	0.2185
Nycticebus coucang	0.2926	0.2902	0.2227	0.3072	0.3718	0.1418	0.2812	0.1983
Nycticebus pygmaeus	0.3189	0.3252	0.2612	0.3141	0.3708	0.1489	0.2964	0.2493
Otolemur crassicaudatus	0.2182	0.2249	0.1713	0.2409	0.3332	0.1483	0.2171	0.1129
Pan troglodytes	0.2139	0.2387	0.2993	0.23	0.1481	0.3641	0.1933	0.2988
Papio hamadryas	0.1101	0.1877	0.2043	0.0728	0.2075	0.2865	0.0787	0.2216
Perodicticus potto	0.2939	0.2898	0.2281	0.3053	0.3569	0.1594	0.2845	0.2075
Pithecia	0.1965	0.1881	0.1462	0.1872	0.3184	0.2454	0.1951	0.1984
Pongo pygmaeus	0.2215	0.2544	0.317	0.2447	0.1757	0.3956	0.2158	0.3196
Procolobus badius	0	0.1681	0.1889	0.1066	0.2255	0.2834	0.0917	0.1698
Propithecus	0.1681	0	0.1785	0.1871	0.2725	0.2953	0.1974	0.1899
Saimiri	0.1889	0.1785	0	0.2107	0.3256	0.2424	0.1883	0.1512
Semnopithecus	0.1066	0.1871	0.2107	0	0.2236	0.2822	0.1078	0.2075
Symphalangus syndactylus	0.2255	0.2725	0.3256	0.2236	0	0.3311	0.2106	0.3055
Tarsius	0.2834	0.2953	0.2424	0.2822	0.3311	0	0.2599	0.2084
Theropithecus gelada	0.0917	0.1974	0.1883	0.1078	0.2106	0.2599	0	0.1864
Varecia variegata	0.1698	0.1899	0.1512	0.2075	0.3055	0.2084	0.1864	0

PATRISTIC DISTANCE MATRIX

	Alouatta caraya	*Ateles*	*Cebuella pygmaea*	*Cebus*	*Cercocebus torquatus*	*Cercopithecus*	*Chlorocebus aethiops*	*Colobus guereza*	*Daubentonia madagascariensis*	*Erythrocebus patas*	*Eulemur*	*Galago senegalensis*	*Gorilla gorilla*
Alouatta caraya	0.00	31.10	45.55	45.55	99.31	99.31	99.31	99.31	144.57	99.31	144.57	144.57	99.31
Ateles	31.10	0.00	45.55	45.55	99.31	99.31	99.31	99.31	144.57	99.31	144.57	144.57	99.31
Cebuella pygmaea	45.55	45.55	0.00	42.16	99.31	99.31	99.31	99.31	144.57	99.31	144.57	144.57	99.31
Cebus	45.55	45.55	42.16	0.00	99.31	99.31	99.31	99.31	144.57	99.31	144.57	144.57	99.31
Cercocebus torquatus	99.31	99.31	99.31	99.31	0.00	34.11	34.11	43.75	144.57	34.11	144.57	144.57	60.00
Cercopithecus	99.31	99.31	99.31	99.31	34.11	0.00	22.13	43.75	144.57	22.13	144.57	144.57	60.00
Chlorocebus aethiops	99.31	99.31	99.31	99.31	34.11	22.13	0.00	43.75	144.57	20.73	144.57	144.57	60.00
Colobus guereza	99.31	99.31	99.31	99.31	43.75	43.75	43.75	0.00	144.57	43.75	144.57	144.57	60.00
Daubentonia madagascariensis	144.57	144.57	144.57	144.57	144.57	144.57	144.57	144.57	0.00	144.57	103.32	122.02	144.57
Erythrocebus patas	99.31	99.31	99.31	99.31	34.11	22.13	20.73	43.75	144.57	0.00	144.57	144.57	60.00
Eulemur	144.57	144.57	144.57	144.57	144.57	144.57	144.57	144.57	103.32	144.57	0.00	122.02	144.57
Galago senegalensis	144.57	144.57	144.57	144.57	144.57	144.57	144.57	144.57	122.02	144.57	122.02	0.00	144.57
Gorilla gorilla	99.31	99.31	99.31	99.31	60.00	60.00	60.00	60.00	144.57	60.00	144.57	144.57	0.00
Hapalemur	144.57	144.57	144.57	144.57	144.57	144.57	144.57	144.57	103.32	144.57	30.39	122.02	144.57
Hylobates	99.31	99.31	99.31	99.31	60.00	60.00	60.00	60.00	144.57	60.00	144.57	144.57	40.76
Indri indri	144.57	144.57	144.57	144.57	144.57	144.57	144.57	144.57	103.32	144.57	62.17	122.02	144.57
Lagothrix lagothricha	31.10	20.54	45.55	45.55	99.31	99.31	99.31	99.31	144.57	99.31	144.57	144.57	99.31
Lemur catta	144.57	144.57	144.57	144.57	144.57	144.57	144.57	144.57	103.32	144.57	30.39	122.02	144.57
Leontopithecus	45.55	45.55	31.69	42.16	99.31	99.31	99.31	99.31	144.57	99.31	144.57	144.57	99.31
Lepilemur	144.57	144.57	144.57	144.57	144.57	144.57	144.57	144.57	103.32	144.57	69.26	122.02	144.57
Lophocebus albigena	99.31	99.31	99.31	99.31	25.55	34.11	34.11	43.75	144.57	34.11	144.57	144.57	60.00
Loris tardigradus	144.57	144.57	144.57	144.57	144.57	144.57	144.57	144.57	122.02	144.57	122.02	76.00	144.57
Macaca fascicularis	99.31	99.31	99.31	99.31	28.52	34.11	34.11	43.75	144.57	34.11	144.57	144.57	60.00
Macaca mulatta	99.31	99.31	99.31	99.31	28.52	34.11	34.11	43.75	144.57	34.11	144.57	144.57	60.00
Macaca nemestrina	99.31	99.31	99.31	99.31	28.52	34.11	34.11	43.75	144.57	34.11	144.57	144.57	60.00
Mandrillus	99.31	99.31	99.31	99.31	16.07	34.11	34.11	43.75	144.57	34.11	144.57	144.57	60.00
Miopithecus talapoin	99.31	99.31	99.31	99.31	34.11	28.01	28.01	43.75	144.57	28.01	144.57	144.57	60.00
Nasalis larvatus	99.31	99.31	99.31	99.31	43.75	43.75	43.75	32.55	144.57	43.75	144.57	144.57	60.00
Nycticebus coucang	144.57	144.57	144.57	144.57	144.57	144.57	144.57	144.57	122.02	144.57	122.02	76.00	144.57
Nycticebus pygmaeus	144.57	144.57	144.57	144.57	144.57	144.57	144.57	144.57	122.02	144.57	122.02	76.00	144.57
Otolemur crassicaudatus	144.57	144.57	144.57	144.57	144.57	144.57	144.57	144.57	122.02	144.57	122.02	38.03	144.57
Pan troglodytes	99.31	99.31	99.31	99.31	60.00	60.00	60.00	60.00	144.57	60.00	144.57	144.57	20.25
Papio hamadryas	99.31	99.31	99.31	99.31	25.55	34.11	34.11	43.75	144.57	34.11	144.57	144.57	60.00
Perodicticus potto	146.03	146.03	146.03	146.03	146.03	146.03	146.03	146.03	123.47	146.03	123.47	77.45	146.03
Pithecia	99.31	99.31	99.31	99.31	43.75	43.75	43.75	24.23	144.57	43.75	144.57	144.57	60.00
Pongo pygmaeus	45.55	45.55	42.16	40.39	99.31	99.31	99.31	99.31	144.57	99.31	144.57	144.57	99.31
Procolobus badius	99.31	99.31	99.31	99.31	60.00	60.00	60.00	60.00	144.57	60.00	144.57	144.57	30.41
Propithecus	144.57	144.57	144.57	144.57	144.57	144.57	144.57	144.57	103.32	144.57	62.17	122.02	144.57
Saimiri	45.55	45.55	42.16	38.62	99.31	99.31	99.31	99.31	144.57	99.31	144.57	144.57	99.31
Semnopithecus	99.31	99.31	99.31	99.31	43.75	43.75	43.75	32.55	144.57	43.75	144.57	144.57	60.00
Symphalangus syndactylus	99.31	99.31	99.31	99.31	60.00	60.00	60.00	60.00	144.57	60.00	144.57	144.57	40.76
Tarsius	134.68	134.68	134.68	134.68	134.68	134.68	134.68	134.68	144.57	134.68	144.57	144.57	134.68
Theropithecus gelada	99.31	99.31	99.31	99.31	25.55	34.11	34.11	43.75	144.57	34.11	144.57	144.57	60.00
Varecia variegata	144.57	144.57	144.57	144.57	144.57	144.57	144.57	144.57	103.32	144.57	41.50	122.02	144.57

	Hapalemur	*Hylobates*	*Indri indri*	*Lagothrix lagothricha*	*Lemur catta*	*Leontopithecus*	*Lepilemur*	*Lophocebus albigena*	*Loris tardigradus*	*Macaca fascicularis*	*Macaca mulatta*	*Macaca nemestrina*	*Mandrillus*
Alouatta caraya	144.57	99.31	144.57	31.10	144.57	45.55	144.57	99.31	144.57	99.31	99.31	99.31	99.31
Ateles	144.57	99.31	144.57	20.54	144.57	45.55	144.57	99.31	144.57	99.31	99.31	99.31	99.31
Cebuella pygmaea	144.57	99.31	144.57	45.55	144.57	31.69	144.57	99.31	144.57	99.31	99.31	99.31	99.31
Cebus	144.57	99.31	144.57	45.55	144.57	42.16	144.57	99.31	144.57	99.31	99.31	99.31	99.31
Cercocebus torquatus	144.57	60.00	144.57	99.31	144.57	99.31	144.57	25.55	144.57	28.52	28.52	28.52	16.07
Cercopithecus	144.57	60.00	144.57	99.31	144.57	99.31	144.57	34.11	144.57	34.11	34.11	34.11	34.11
Chlorocebus aethiops	144.57	60.00	144.57	99.31	144.57	99.31	144.57	34.11	144.57	34.11	34.11	34.11	34.11
Colobus guereza	144.57	60.00	144.57	99.31	144.57	99.31	144.57	43.75	144.57	43.75	43.75	43.75	43.75
Daubentonia madagascariensis	103.32	144.57	103.32	144.57	103.32	144.57	103.32	144.57	122.02	144.57	144.57	144.57	144.57
Erythrocebus patas	144.57	60.00	144.57	99.31	144.57	99.31	144.57	34.11	144.57	34.11	34.11	34.11	34.11
Eulemur	30.39	144.57	62.17	144.57	30.39	144.57	69.26	144.57	122.02	144.57	144.57	144.57	144.57
Galago senegalensis	122.02	144.57	122.02	144.57	122.02	144.57	122.02	144.57	76.00	144.57	144.57	144.57	144.57
Gorilla gorilla	144.57	40.76	144.57	99.31	144.57	99.31	144.57	60.00	144.57	60.00	60.00	60.00	60.00
Hapalemur	0.00	144.57	62.17	144.57	19.86	144.57	69.26	144.57	122.02	144.57	144.57	144.57	144.57
Hylobates	144.57	0.00	144.57	99.31	144.57	99.31	144.57	60.00	144.57	60.00	60.00	60.00	60.00
Indri indri	62.17	144.57	0.00	144.57	62.17	144.57	69.26	144.57	122.02	144.57	144.57	144.57	144.57
Lagothrix lagothricha	144.57	99.31	144.57	0.00	144.57	45.55	144.57	99.31	144.57	99.31	99.31	99.31	99.31
Lemur catta	19.86	144.57	62.17	144.57	0.00	144.57	69.26	144.57	122.02	144.57	144.57	144.57	144.57
Leontopithecus	144.57	99.31	144.57	45.55	144.57	0.00	144.57	99.31	144.57	99.31	99.31	99.31	99.31
Lepilemur	69.26	144.57	69.26	144.57	69.26	144.57	0.00	144.57	122.02	144.57	144.57	144.57	144.57
Lophocebus albigena	144.57	60.00	144.57	99.31	144.57	99.31	144.57	0.00	144.57	28.52	28.52	28.52	25.55
Loris tardigradus	122.02	144.57	122.02	144.57	122.02	144.57	122.02	144.57	0.00	144.57	144.57	144.57	144.57
Macaca fascicularis	144.57	60.00	144.57	99.31	144.57	99.31	144.57	28.52	144.57	0.00	7.96	15.93	28.52
Macaca mulatta	144.57	60.00	144.57	99.31	144.57	99.31	144.57	28.52	144.57	7.96	0.00	15.93	28.52
Macaca nemestrina	144.57	60.00	144.57	99.31	144.57	99.31	144.57	28.52	144.57	15.93	15.93	0.00	28.52
Mandrillus	144.57	60.00	144.57	99.31	144.57	99.31	144.57	25.55	144.57	28.52	28.52	28.52	0.00
Miopithecus talapoin	144.57	60.00	144.57	99.31	144.57	99.31	144.57	34.11	144.57	34.11	34.11	34.11	34.11
Nasalis larvatus	144.57	60.00	144.57	99.31	144.57	99.31	144.57	43.75	144.57	43.75	43.75	43.75	43.75
Nycticebus coucang	122.02	144.57	122.02	144.57	122.02	144.57	122.02	144.57	54.75	144.57	144.57	144.57	144.57
Nycticebus pygmaeus	122.02	144.57	122.02	144.57	122.02	144.57	122.02	144.57	54.75	144.57	144.57	144.57	144.57
Otolemur crassicaudatus	122.02	144.57	122.02	144.57	122.02	144.57	122.02	144.57	76.00	144.57	144.57	144.57	144.57
Pan troglodytes	144.57	40.76	144.57	99.31	144.57	99.31	144.57	60.00	144.57	60.00	60.00	60.00	60.00
Papio hamadryas	144.57	60.00	144.57	99.31	144.57	99.31	144.57	13.06	144.57	28.52	28.52	28.52	25.55
Perodicticus potto	123.47	146.03	123.47	146.03	123.47	146.03	123.47	146.03	66.83	146.03	146.03	146.03	146.03
Pithecia	144.57	60.00	144.57	99.31	144.57	99.31	144.57	43.75	144.57	43.75	43.75	43.75	43.75
Pongo pygmaeus	144.57	99.31	144.57	45.55	144.57	42.16	144.57	99.31	144.57	99.31	99.31	99.31	99.31
Procolobus badius	144.57	40.76	144.57	99.31	144.57	99.31	144.57	60.00	144.57	60.00	60.00	60.00	60.00
Propithecus	62.17	144.57	40.35	144.57	62.17	144.57	69.26	144.57	122.02	144.57	144.57	144.57	144.57
Saimiri	144.57	99.31	144.57	45.55	144.57	42.16	144.57	99.31	144.57	99.31	99.31	99.31	99.31
Semnopithecus	144.57	60.00	144.57	99.31	144.57	99.31	144.57	43.75	144.57	43.75	43.75	43.75	43.75
Symphalangus syndactylus	144.57	14.76	144.57	99.31	144.57	99.31	144.57	60.00	144.57	60.00	60.00	60.00	60.00
Tarsius	144.57	134.68	144.57	134.68	144.57	134.68	144.57	134.68	144.57	134.68	134.68	134.68	134.68
Theropithecus gelada	144.57	60.00	144.57	99.31	144.57	99.31	144.57	13.06	144.57	28.52	28.52	28.52	25.55
Varecia variegata	41.50	144.57	62.17	144.57	41.50	144.57	69.26	144.57	122.02	144.57	144.57	144.57	144.57

	Miopithecus talapoin	*Nasalis larvatus*	*Nycticebus coucang*	*Nycticebus pygmaeus*	*Otolemur crassicaudatus*	*Pan troglodytes*	*Papio hamadryas*	*Perodicticus potto*	*Pithecia*	*Pongo pygmaeus*	*Procolobus badius*
Alouatta caraya	99.31	99.31	144.57	144.57	144.57	99.31	99.31	146.03	99.31	45.55	99.31
Ateles	99.31	99.31	144.57	144.57	144.57	99.31	99.31	146.03	99.31	45.55	99.31
Cebuella pygmaea	99.31	99.31	144.57	144.57	144.57	99.31	99.31	146.03	99.31	42.16	99.31
Cebus	99.31	99.31	144.57	144.57	144.57	99.31	99.31	146.03	99.31	40.39	99.31
Cercocebus torquatus	34.11	43.75	144.57	144.57	144.57	60.00	25.55	146.03	43.75	99.31	60.00
Cercopithecus	28.01	43.75	144.57	144.57	144.57	60.00	34.11	146.03	43.75	99.31	60.00
Chlorocebus aethiops	28.01	43.75	144.57	144.57	144.57	60.00	34.11	146.03	43.75	99.31	60.00
Colobus guereza	43.75	32.55	144.57	144.57	144.57	60.00	43.75	146.03	24.23	99.31	60.00
Daubentonia madagascariensis	144.57	144.57	122.02	122.02	122.02	144.57	144.57	123.47	144.57	144.57	144.57
Erythrocebus patas	28.01	43.75	144.57	144.57	144.57	60.00	34.11	146.03	43.75	99.31	60.00
Eulemur	144.57	144.57	122.02	122.02	122.02	144.57	144.57	123.47	144.57	144.57	144.57
Galago senegalensis	144.57	144.57	76.00	76.00	38.03	144.57	144.57	77.45	144.57	144.57	144.57
Gorilla gorilla	60.00	60.00	144.57	144.57	144.57	20.25	60.00	146.03	60.00	99.31	30.41
Hapalemur	144.57	144.57	122.02	122.02	122.02	144.57	144.57	123.47	144.57	144.57	144.57
Hylobates	60.00	60.00	144.57	144.57	144.57	40.76	60.00	146.03	60.00	99.31	40.76
Indri indri	144.57	144.57	122.02	122.02	122.02	144.57	144.57	123.47	144.57	144.57	144.57
Lagothrix lagothricha	99.31	99.31	144.57	144.57	144.57	99.31	99.31	146.03	99.31	45.55	99.31
Lemur catta	144.57	144.57	122.02	122.02	122.02	144.57	144.57	123.47	144.57	144.57	144.57
Leontopithecus	99.31	99.31	144.57	144.57	144.57	99.31	99.31	146.03	99.31	42.16	99.31
Lepilemur	144.57	144.57	122.02	122.02	122.02	144.57	144.57	123.47	144.57	144.57	144.57
Lophocebus albigena	34.11	43.75	144.57	144.57	144.57	60.00	13.06	146.03	43.75	99.31	60.00
Loris tardigradus	144.57	144.57	54.75	54.75	76.00	144.57	144.57	66.83	144.57	144.57	144.57
Macaca fascicularis	34.11	43.75	144.57	144.57	144.57	60.00	28.52	146.03	43.75	99.31	60.00
Macaca mulatta	34.11	43.75	144.57	144.57	144.57	60.00	28.52	146.03	43.75	99.31	60.00
Macaca nemestrina	34.11	43.75	144.57	144.57	144.57	60.00	28.52	146.03	43.75	99.31	60.00
Mandrillus	34.11	43.75	144.57	144.57	144.57	60.00	25.55	146.03	43.75	99.31	60.00
Miopithecus talapoin	0.00	43.75	144.57	144.57	144.57	60.00	34.11	146.03	43.75	99.31	60.00
Nasalis larvatus	43.75	0.00	144.57	144.57	144.57	60.00	43.75	146.03	32.55	99.31	60.00
Nycticebus coucang	144.57	144.57	0.00	18.36	76.00	144.57	144.57	66.83	144.57	144.57	144.57
Nycticebus pygmaeus	144.57	144.57	18.36	0.00	76.00	144.57	144.57	66.83	144.57	144.57	144.57
Otolemur crassicaudatus	144.57	144.57	76.00	76.00	0.00	144.57	144.57	77.45	144.57	144.57	144.57
Pan troglodytes	60.00	60.00	144.57	144.57	144.57	0.00	60.00	146.03	60.00	99.31	30.41
Papio hamadryas	34.11	43.75	144.57	144.57	144.57	60.00	0.00	146.03	43.75	99.31	60.00
Perodicticus potto	146.03	146.03	66.83	66.83	77.45	146.03	146.03	0.00	146.03	146.03	146.03
Pithecia	43.75	32.55	144.57	144.57	144.57	60.00	43.75	146.03	0.00	99.31	60.00
Pongo pygmaeus	99.31	99.31	144.57	144.57	144.57	99.31	99.31	146.03	99.31	0.00	99.31
Procolobus badius	60.00	60.00	144.57	144.57	144.57	30.41	60.00	146.03	60.00	99.31	0.00
Propithecus	144.57	144.57	122.02	122.02	122.02	144.57	144.57	123.47	144.57	144.57	144.57
Saimiri	99.31	99.31	144.57	144.57	144.57	99.31	99.31	146.03	99.31	40.39	99.31
Semnopithecus	43.75	26.69	144.57	144.57	144.57	60.00	43.75	146.03	32.55	99.31	60.00
Symphalangus syndactylus	60.00	60.00	144.57	144.57	144.57	40.76	60.00	146.03	60.00	99.31	40.76
Tarsius	134.68	134.68	144.57	144.57	144.57	134.68	134.68	146.03	134.68	134.68	134.68
Theropithecus gelada	34.11	43.75	144.57	144.57	144.57	60.00	10.80	146.03	43.75	99.31	60.00
Varecia variegata	144.57	144.57	122.02	122.02	122.02	144.57	144.57	123.47	144.57	144.57	144.57

	Propithecus	*Saimiri*	*Semnopithecus*	*Symphalangus syndactylus*	*Tarsius*	*Theropithecus gelada*	*Varecia variegata*
Alouatta caraya	144.57	45.55	99.31	99.31	134.68	99.31	144.57
Ateles	144.57	45.55	99.31	99.31	134.68	99.31	144.57
Cebuella pygmaea	144.57	42.16	99.31	99.31	134.68	99.31	144.57
Cebus	144.57	38.62	99.31	99.31	134.68	99.31	144.57
Cercocebus torquatus	144.57	99.31	43.75	60.00	134.68	25.55	144.57
Cercopithecus	144.57	99.31	43.75	60.00	134.68	34.11	144.57
Chlorocebus aethiops	144.57	99.31	43.75	60.00	134.68	34.11	144.57
Colobus guereza	144.57	99.31	32.55	60.00	134.68	43.75	144.57
Daubentonia madagascariensis	103.32	144.57	144.57	144.57	144.57	144.57	103.32
Erythrocebus patas	144.57	99.31	43.75	60.00	134.68	34.11	144.57
Eulemur	62.17	144.57	144.57	144.57	144.57	144.57	41.50
Galago senegalensis	122.02	144.57	144.57	144.57	144.57	144.57	122.02
Gorilla gorilla	144.57	99.31	60.00	40.76	134.68	60.00	144.57
Hapalemur	62.17	144.57	144.57	144.57	144.57	144.57	41.50
Hylobates	144.57	99.31	60.00	14.76	134.68	60.00	144.57
Indri indri	40.35	144.57	144.57	144.57	144.57	144.57	62.17
Lagothrix lagothricha	144.57	45.55	99.31	99.31	134.68	99.31	144.57
Lemur catta	62.17	144.57	144.57	144.57	144.57	144.57	41.50
Leontopithecus	144.57	42.16	99.31	99.31	134.68	99.31	144.57
Lepilemur	69.26	144.57	144.57	144.57	144.57	144.57	69.26
Lophocebus albigena	144.57	99.31	43.75	60.00	134.68	13.06	144.57
Loris tardigradus	122.02	144.57	144.57	144.57	144.57	144.57	122.02
Macaca fascicularis	144.57	99.31	43.75	60.00	134.68	28.52	144.57
Macaca mulatta	144.57	99.31	43.75	60.00	134.68	28.52	144.57
Macaca nemestrina	144.57	99.31	43.75	60.00	134.68	28.52	144.57
Mandrillus	144.57	99.31	43.75	60.00	134.68	25.55	144.57
Miopithecus talapoin	144.57	99.31	43.75	60.00	134.68	34.11	144.57
Nasalis larvatus	144.57	99.31	26.69	60.00	134.68	43.75	144.57
Nycticebus coucang	122.02	144.57	144.57	144.57	144.57	144.57	122.02
Nycticebus pygmaeus	122.02	144.57	144.57	144.57	144.57	144.57	122.02
Otolemur crassicaudatus	122.02	144.57	144.57	144.57	144.57	144.57	122.02
Pan troglodytes	144.57	99.31	60.00	40.76	134.68	60.00	144.57
Papio hamadryas	144.57	99.31	43.75	60.00	134.68	10.80	144.57
Perodicticus potto	123.47	146.03	146.03	146.03	146.03	146.03	123.47
Pithecia	144.57	99.31	32.55	60.00	134.68	43.75	144.57
Pongo pygmaeus	144.57	40.39	99.31	99.31	134.68	99.31	144.57
Procolobus badius	144.57	99.31	60.00	40.76	134.68	60.00	144.57
Propithecus	0.00	144.57	144.57	144.57	144.57	144.57	62.17
Saimiri	144.57	0.00	99.31	99.31	134.68	99.31	144.57
Semnopithecus	144.57	99.31	0.00	60.00	134.68	43.75	144.57
Symphalangus syndactylus	144.57	99.31	60.00	0.00	134.68	60.00	144.57
Tarsius	144.57	134.68	134.68	134.68	0.00	134.68	144.57
Theropithecus gelada	144.57	99.31	43.75	60.00	134.68	0.00	144.57
Varecia variegata	62.17	144.57	144.57	144.57	144.57	144.57	0.00

APPENDIX C

BOX PLOTS OF PELVIC MEASURES FOR PAIRWISE COMPARISON ANALYSES

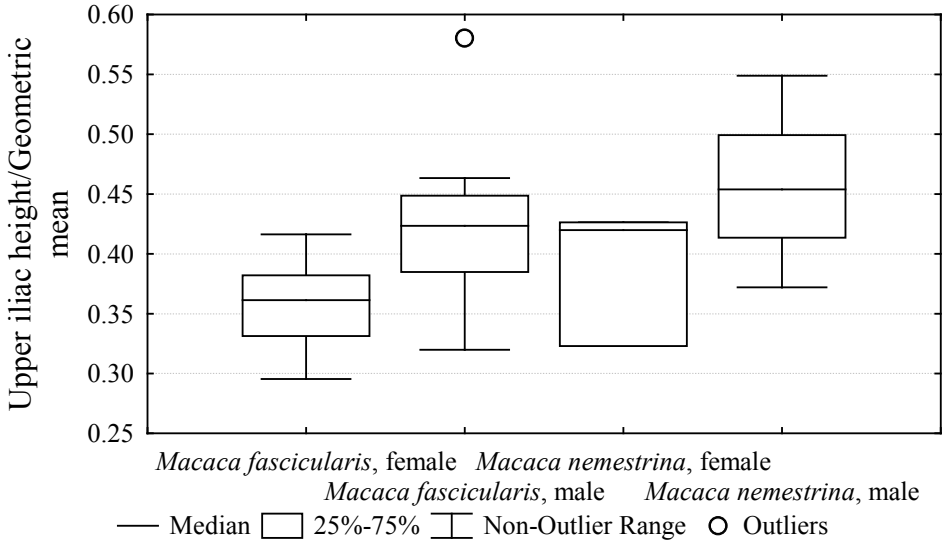
Upper iliac height/Geometric mean
0.60
0.55
0.50
0.45
0.40
0.35
0.30
0.25
Macaca fascicularis, female
Macaca nemestrina, female
Macaca fascicularis, male
Macaca nemestrina, male
Median
25%-75%
Non-Outlier Range
Outliers

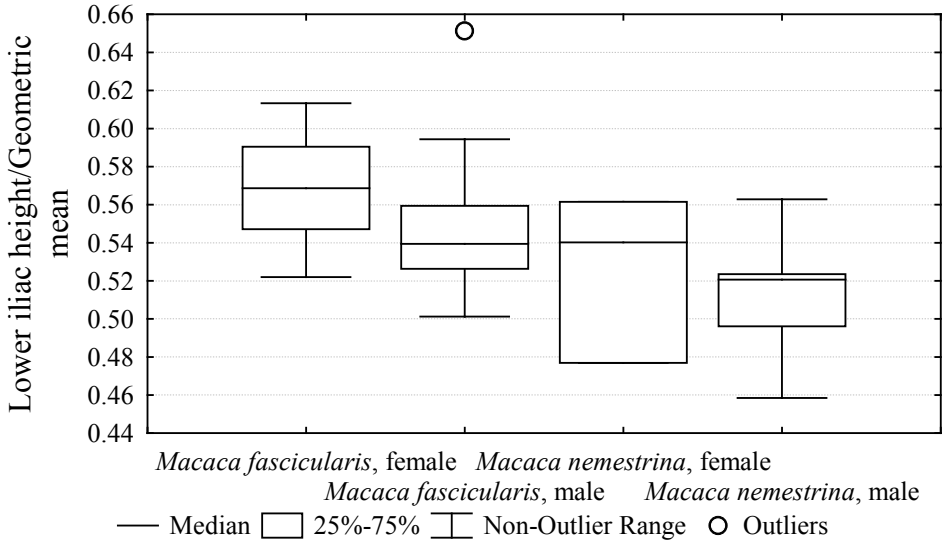
Lower iliac height/Geometric mean
0.66
0.64
0.62
0.60
0.58
0.56
0.54
0.52
0.50
0.48
0.46
0.44
Macaca fascicularis, female
Macaca nemestrina, female
Macaca fascicularis, male
Macaca nemestrina, male
Median
25%-75%
Non-Outlier Range
Outliers

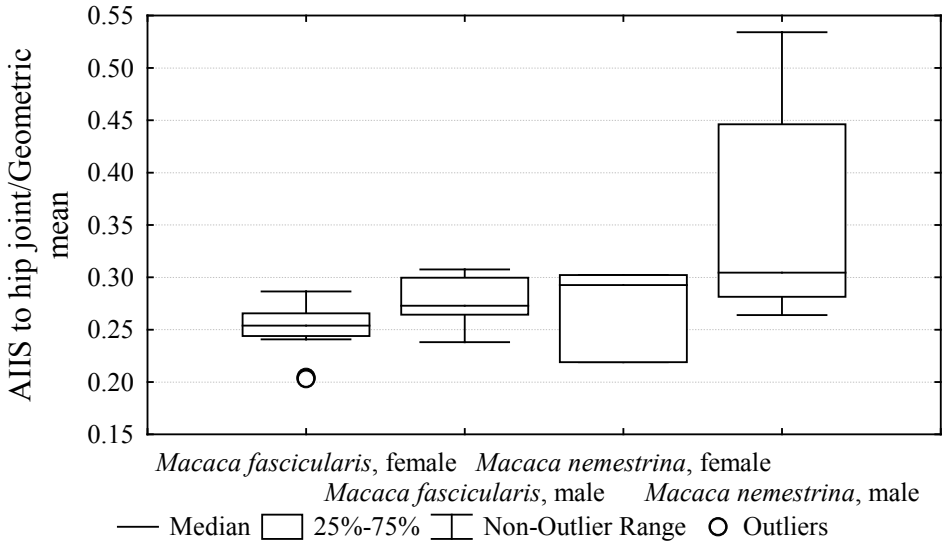
AIIS to hip joint/Geometric mean
0.55
0.50
0.45
0.40
0.35
0.30
0.25
0.20
0.15
Macaca fascicularis, female
Macaca nemestrina, female
Macaca fascicularis, male
Macaca nemestrina, male
Median
25%-75%
Non-Outlier Range
Outliers

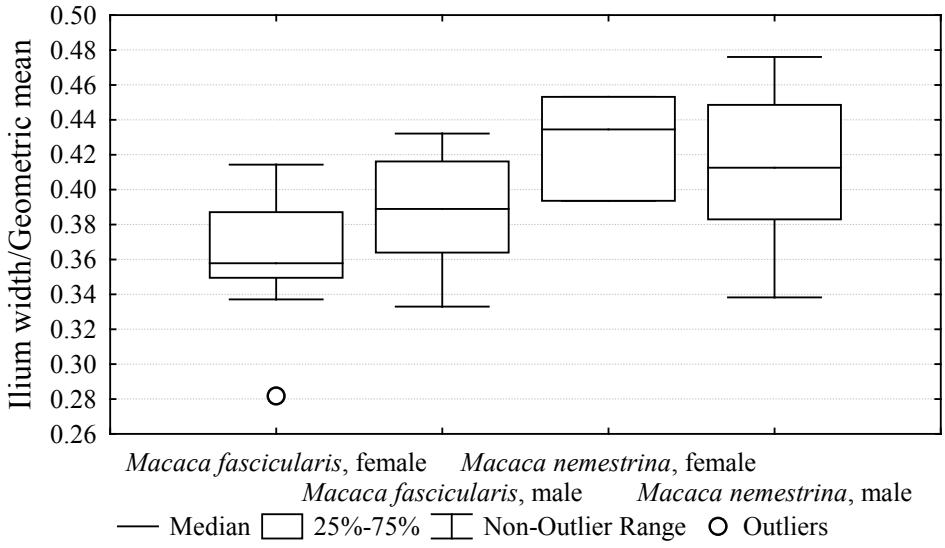
Ilium width/Geometric mean
0.50
0.48
0.46
0.44
0.42
0.40
0.38
0.36
0.34
0.32
0.30
0.28
0.26
Macaca fascicularis, female
Macaca nemestrina, female
Macaca fascicularis, male
Macaca nemestrina, male
Median
25%-75%
Non-Outlier Range
Outliers

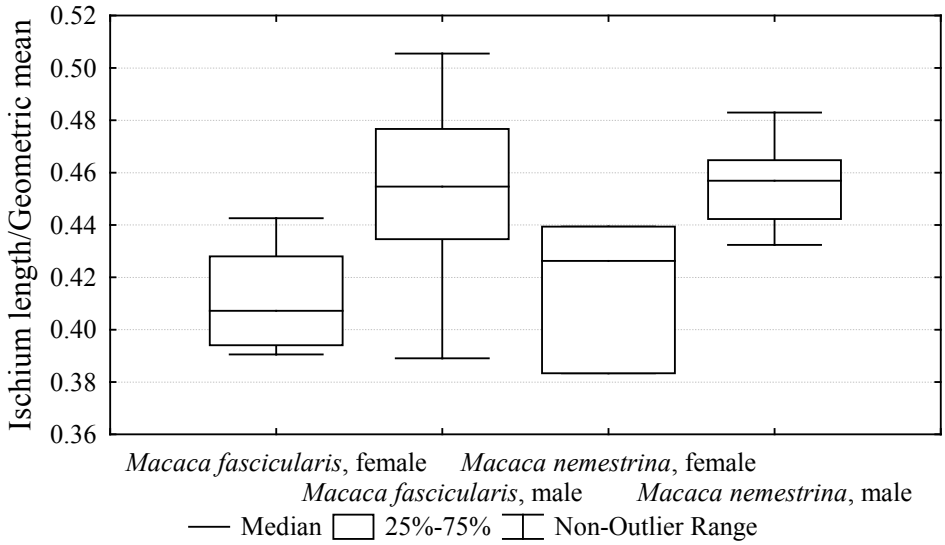
Ischium length/Geometric mean
0.52
0.50
0.48
0.46
0.44
0.42
0.40
0.38
0.36
Macaca fascicularis, female
Macaca nemestrina, female
Macaca fascicularis, male
Macaca nemestrina, male
Median
25%-75%
Non-Outlier Range

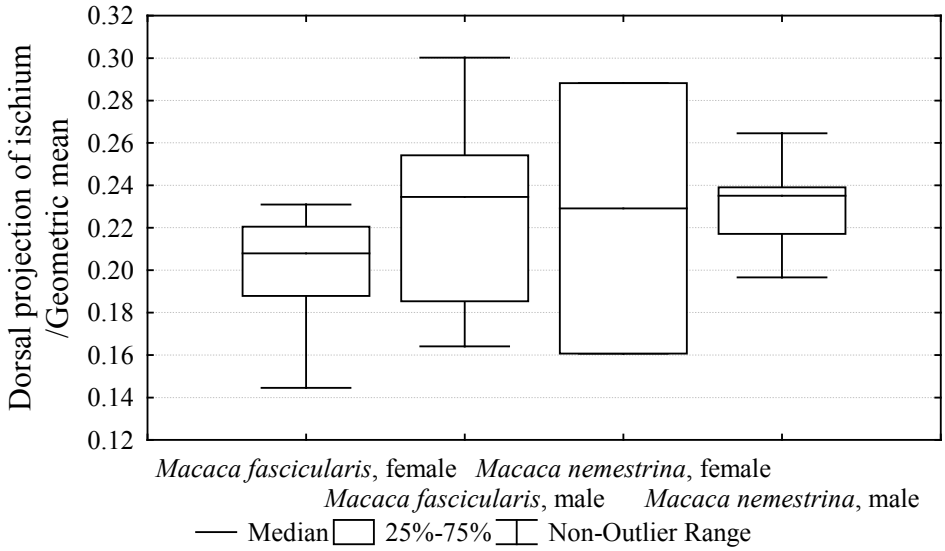
Dorsal projection of ischium /Geometric mean
0.32
0.30
0.28
0.26
0.24
0.22
0.20
0.18
0.16
0.14
0.12
Macaca fascicularis, female
Macaca nemestrina, female
Macaca fascicularis, male
Macaca nemestrina, male
Median
25%-75%
Non-Outlier Range

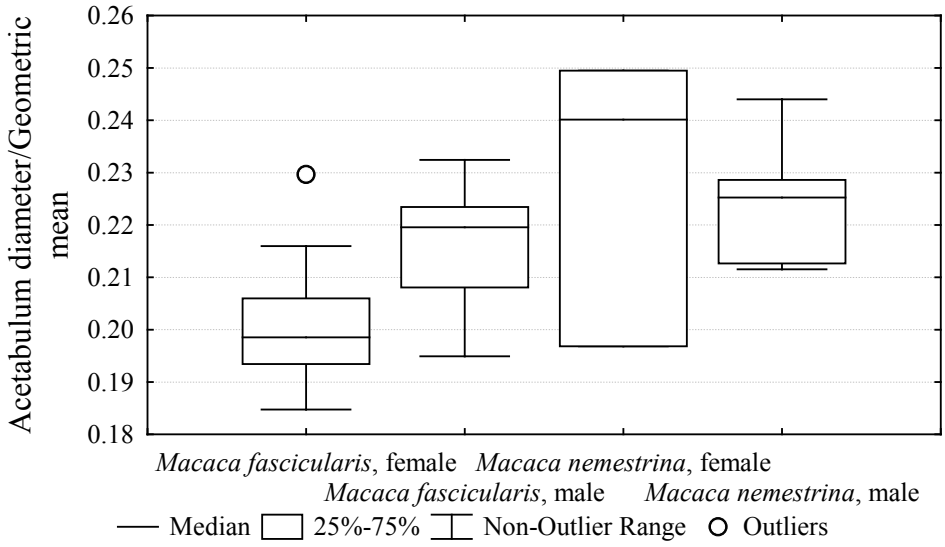
Acetabulum diameter/Geometric mean
0.26
0.25
0.24
0.23
0.22
0.21
0.20
0.19
0.18
Macaca fascicularis, female
Macaca nemestrina, female
Macaca fascicularis, male
Macaca nemestrina, male
Median
25%-75%
Non-Outlier Range
Outliers

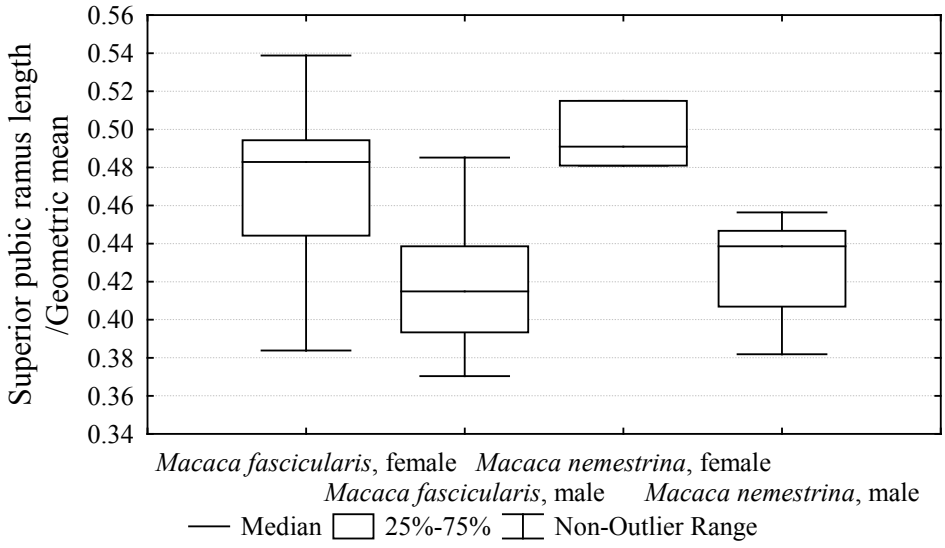
Superior pubic ramus length /Geometric mean
0.56
0.54
0.52
0.50
0.48
0.46
0.44
0.42
0.40
0.38
0.36
0.34
Macaca fascicularis, female
Macaca nemestrina, female
Macaca fascicularis, male
Macaca nemestrina, male
Median
25%-75%
Non-Outlier Range

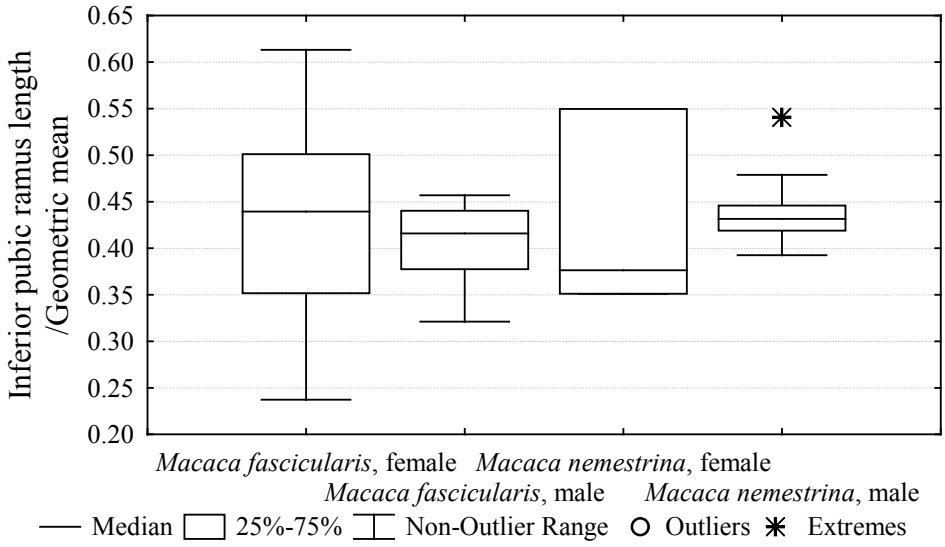
Inferior pubic ramus length
/Geometric mean
0.65
0.60
0.55
0.50
0.45
0.40
0.35
0.30
0.25
0.20
Macaca fascicularis, female
Macaca nemestrina, female
Macaca fascicularis, male
Macaca nemestrina, male
Median
25%-75%
Non-Outlier Range
Outliers
Extremes

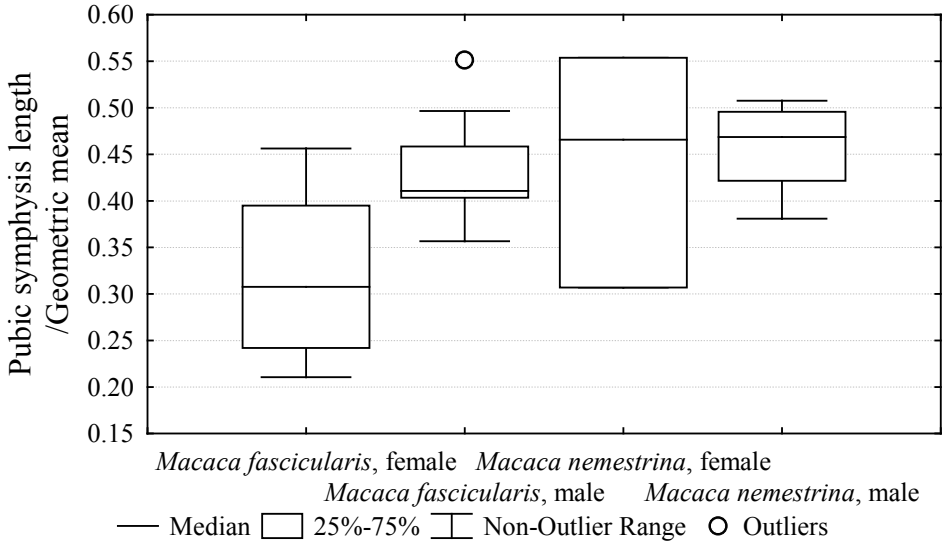
Pubic symphysis length
/Geometric mean
0.60
0.55
0.50
0.45
0.40
0.35
0.30
0.25
0.20
0.15
Macaca fascicularis, female
Macaca nemestrina, female
Macaca fascicularis, male
Macaca nemestrina, male
Median
25%-75%
Non-Outlier Range
Outliers

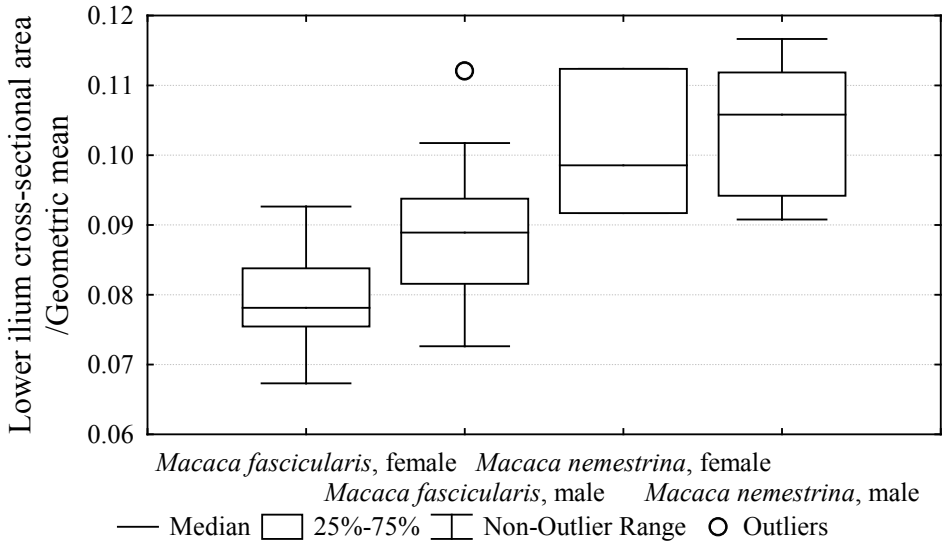
Lower ilium cross-sectional area /Geometric mean
0.12
0.11
0.10
0.09
0.08
0.07
0.06
Macaca fascicularis, female
Macaca nemestrina, female
Macaca fascicularis, male
Macaca nemestrina, male
Median
25%-75%
Non-Outlier Range
Outliers

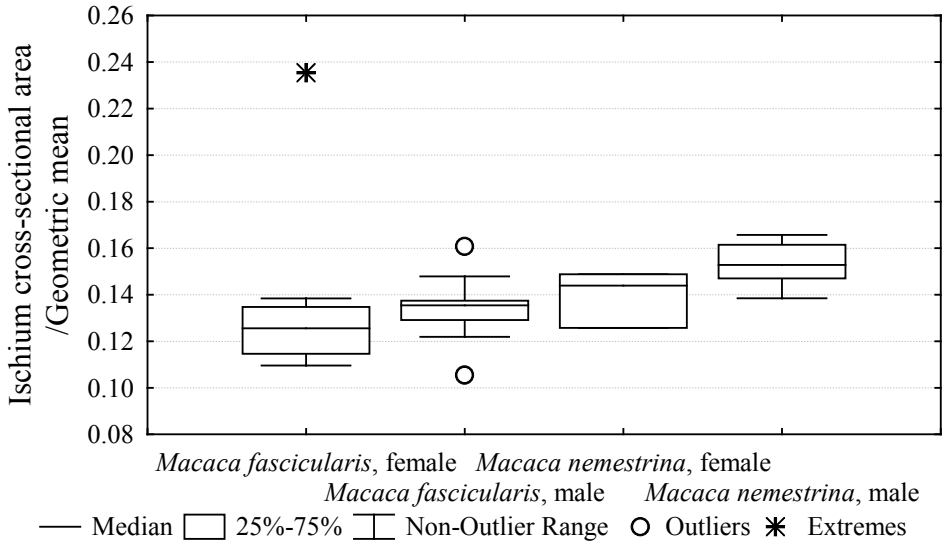
Ischium cross-sectional area /Geometric mean
0.26
0.24
0.22
0.20
0.18
0.16
0.14
0.12
0.10
0.08
Macaca fascicularis, female
Macaca nemestrina, female
Macaca fascicularis, male
Macaca nemestrina, male
Median
25%-75%
Non-Outlier Range
Outliers
Extremes

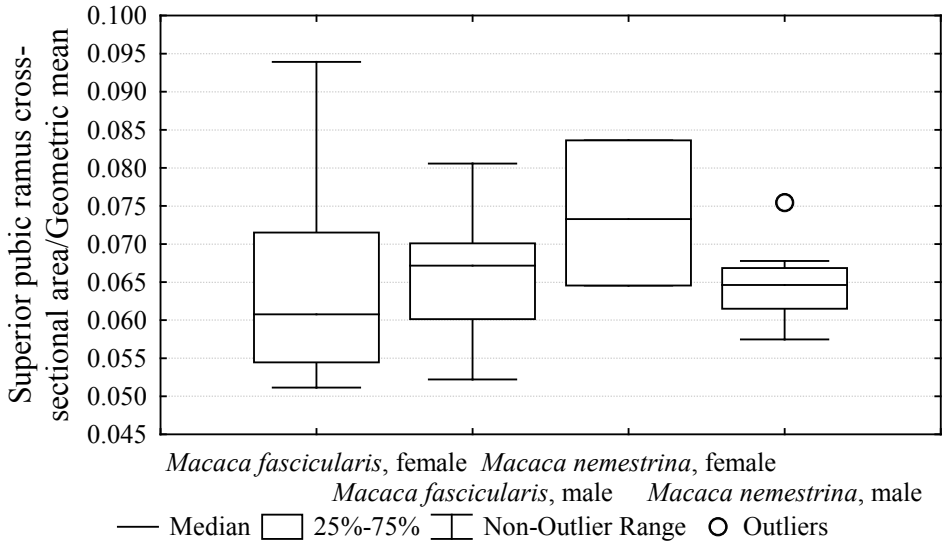
Superior pubic ramus cross-sectional area/Geometric mean
0.100
0.095
0.090
0.085
0.080
0.075
0.070
0.065
0.060
0.055
0.050
0.045
Macaca fascicularis, female
Macaca nemestrina, female
Macaca fascicularis, male
Macaca nemestrina, male
Median
25%-75%
Non-Outlier Range
Outliers

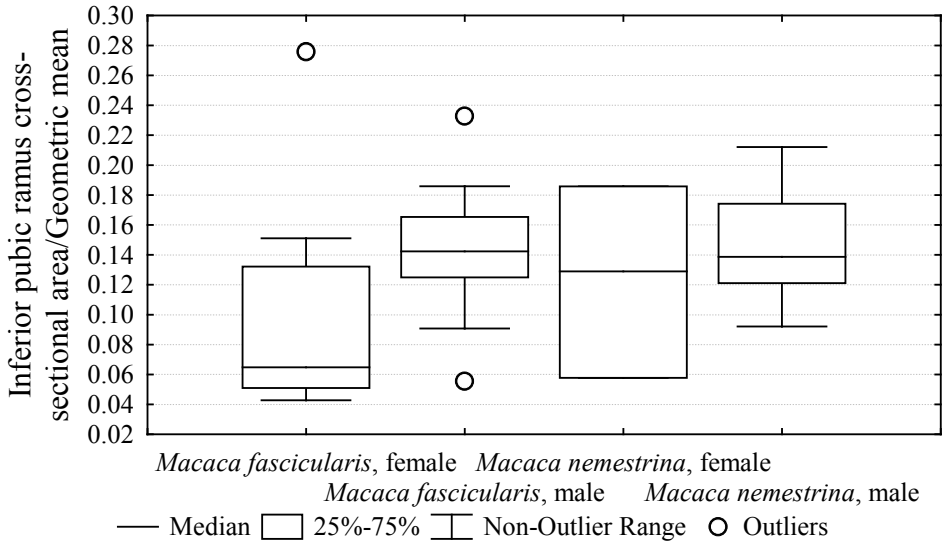
Inferior pubic ramus cross-sectional area/Geometric mean
0.30
0.28
0.26
0.24
0.22
0.20
0.18
0.16
0.14
0.12
0.10
0.08
0.06
0.04
0.02
Macaca fascicularis, female
Macaca nemestrina, female
Macaca fascicularis, male
Macaca nemestrina, male
Median
25%-75%
Non-Outlier Range
Outliers

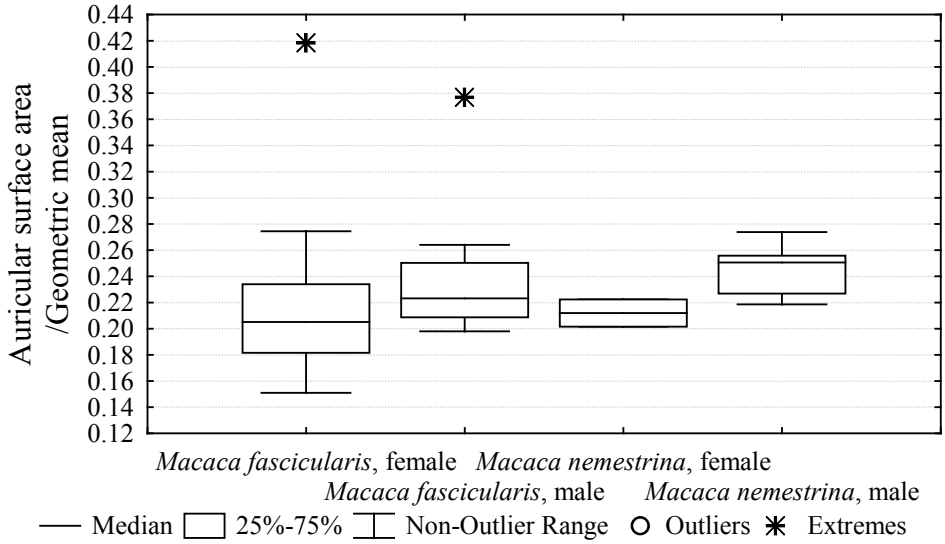
Auricular surface area /Geometric mean
0.44
0.42
0.40
0.38
0.36
0.34
0.32
0.30
0.28
0.26
0.24
0.22
0.20
0.18
0.16
0.14
0.12
Macaca fascicularis, female
Macaca nemestrina, female
Macaca fascicularis, male
Macaca nemestrina, male
Median
25%-75%
Non-Outlier Range
Outliers
Extremes

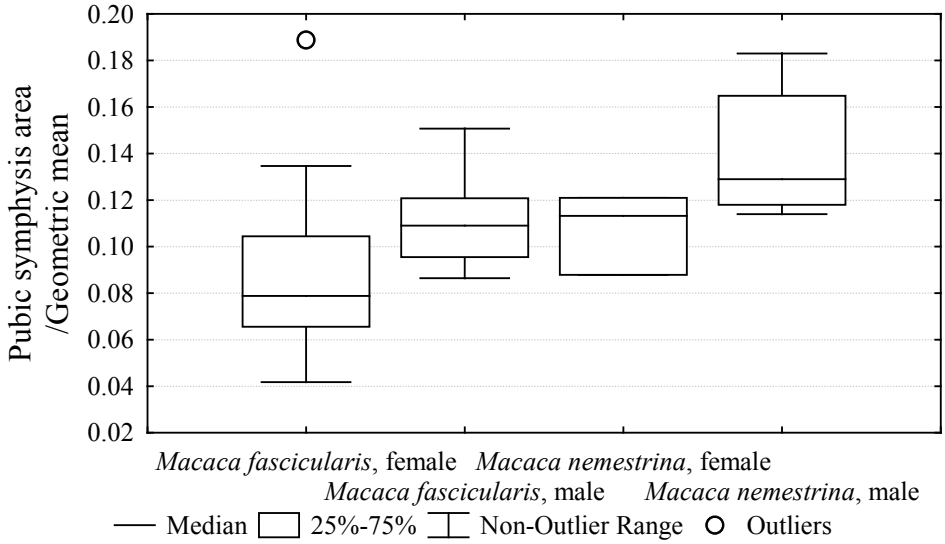
Pubic symphysis area /Geometric mean
0.20
0.18
0.16
0.14
0.12
0.10
0.08
0.06
0.04
0.02
Macaca fascicularis, female
Macaca nemestrina, female
Macaca fascicularis, male
Macaca nemestrina, male
Median
25%-75%
Non-Outlier Range
Outliers

M. FASCICULARIS V. *PAPIO HAMADRYAS*

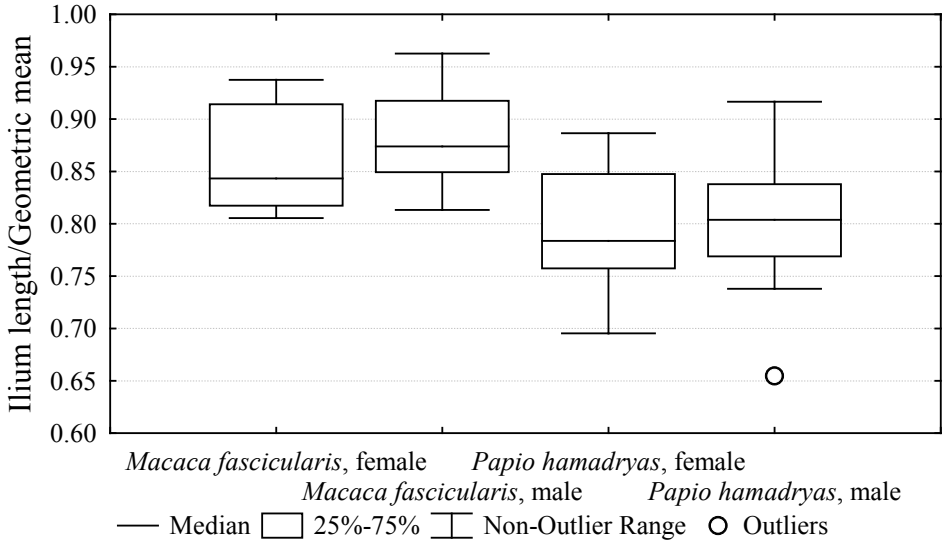

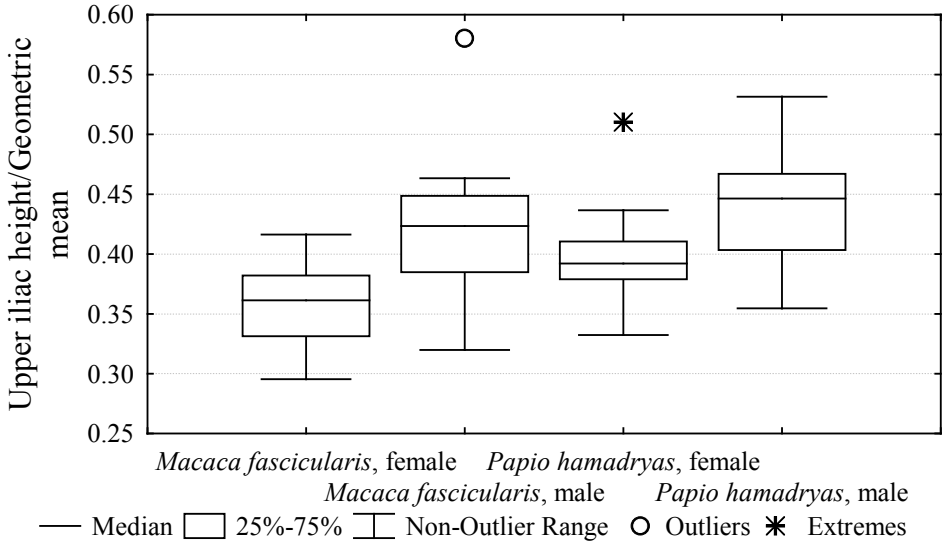

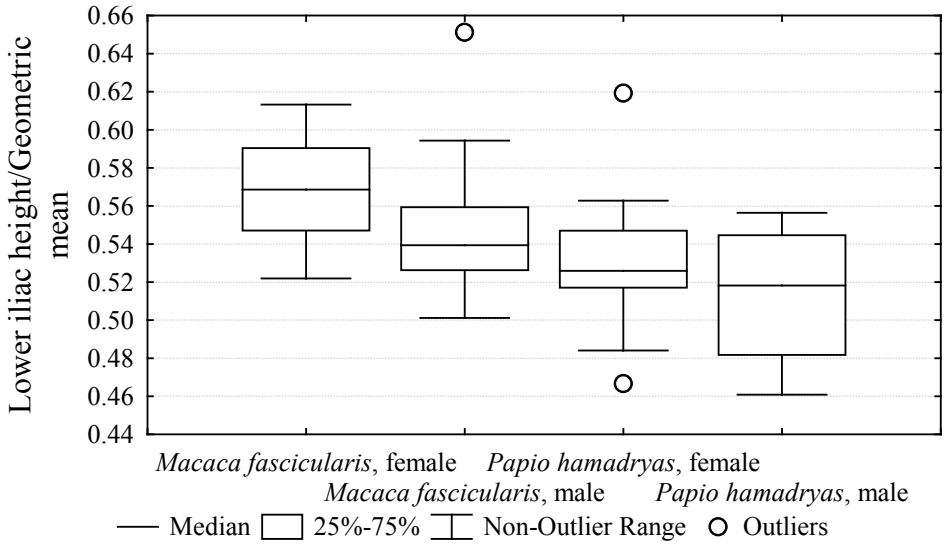
Lower iliac height/Geometric mean
0.66
0.64
0.62
0.60
0.58
0.56
0.54
0.52
0.50
0.48
0.46
0.44
Macaca fascicularis, female
Papio hamadryas, female
Macaca fascicularis, male
Papio hamadryas, male
Median
25%-75%
Non-Outlier Range
Outliers

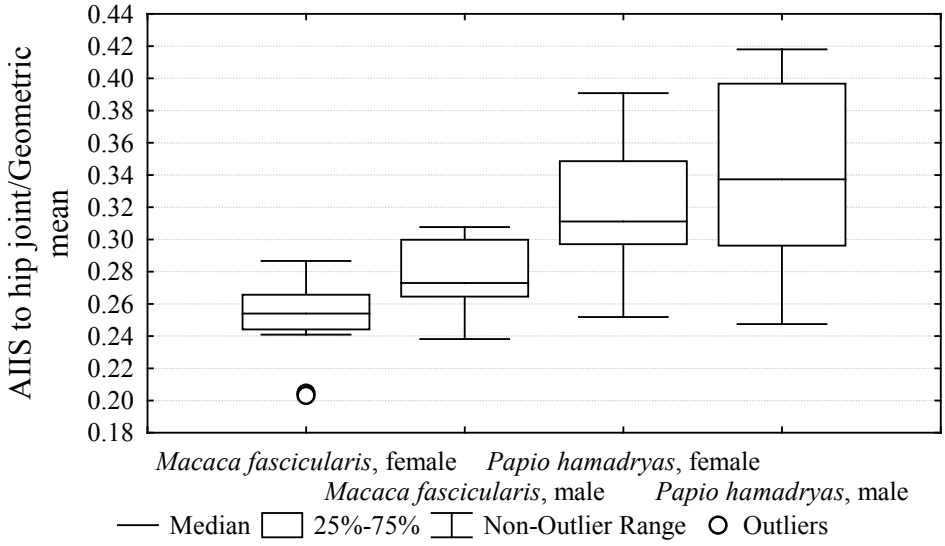
AIIS to hip joint/Geometric mean
0.44
0.42
0.40
0.38
0.36
0.34
0.32
0.30
0.28
0.26
0.24
0.22
0.20
0.18
Macaca fascicularis, female
Papio hamadryas, female
Macaca fascicularis, male
Papio hamadryas, male
Median
25%-75%
Non-Outlier Range
Outliers

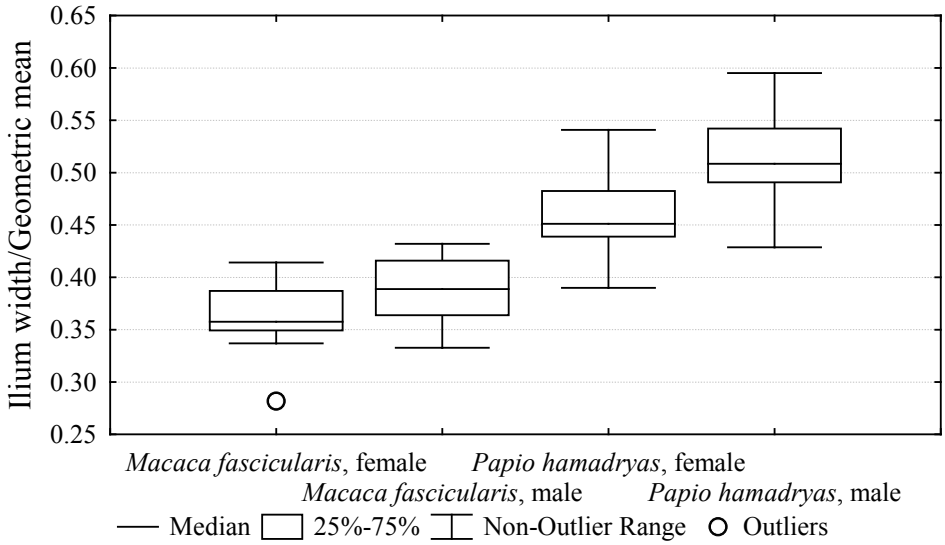
Ilium width/Geometric mean
0.65
0.60
0.55
0.50
0.45
0.40
0.35
0.30
0.25
Macaca fascicularis, female
Papio hamadryas, female
Macaca fascicularis, male
Papio hamadryas, male
Median
25%-75%
Non-Outlier Range
Outliers

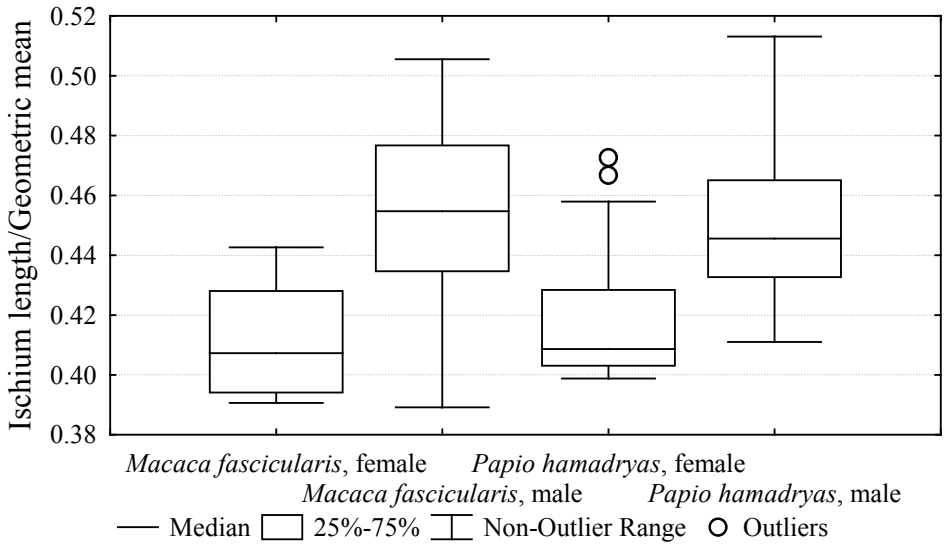
Ischium length/Geometric mean
0.52
0.50
0.48
0.46
0.44
0.42
0.40
0.38
Macaca fascicularis, female
Papio hamadryas, female
Macaca fascicularis, male
Papio hamadryas, male
Median
25%-75%
Non-Outlier Range
Outliers

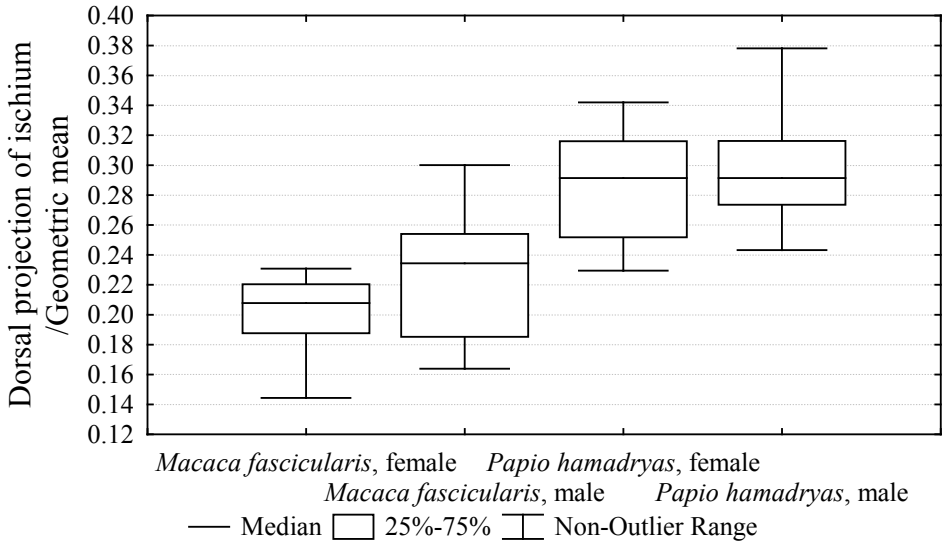
Dorsal projection of ischium /Geometric mean
0.40
0.38
0.36
0.34
0.32
0.30
0.28
0.26
0.24
0.22
0.20
0.18
0.16
0.14
0.12
Macaca fascicularis, female
Papio hamadryas, female
Macaca fascicularis, male
Papio hamadryas, male
Median
25%-75%
Non-Outlier Range

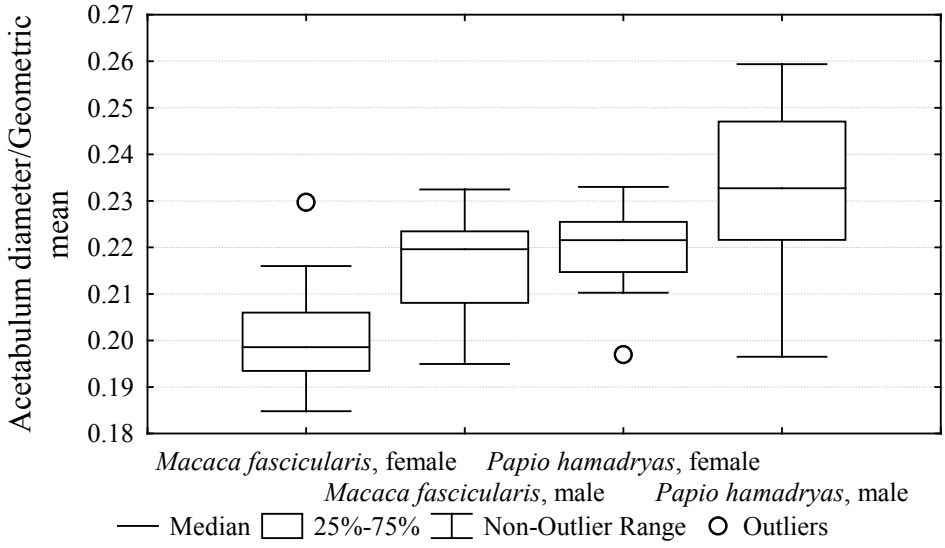
Acetabulum diameter/Geometric mean
0.27
0.26
0.25
0.24
0.23
0.22
0.21
0.20
0.19
0.18
Macaca fascicularis, female
Papio hamadryas, female
Macaca fascicularis, male
Papio hamadryas, male
Median
25%-75%
Non-Outlier Range
Outliers

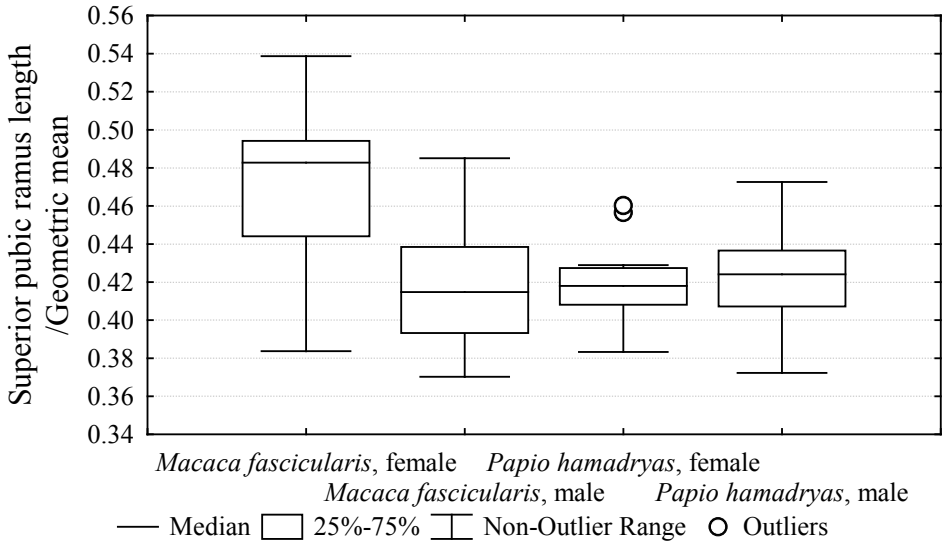
Superior pubic ramus length
/Geometric mean
0.56
0.54
0.52
0.50
0.48
0.46
0.44
0.42
0.40
0.38
0.36
0.34
Macaca fascicularis, female
Papio hamadryas, female
Macaca fascicularis, male
Papio hamadryas, male
Median
25%-75%
Non-Outlier Range
Outliers

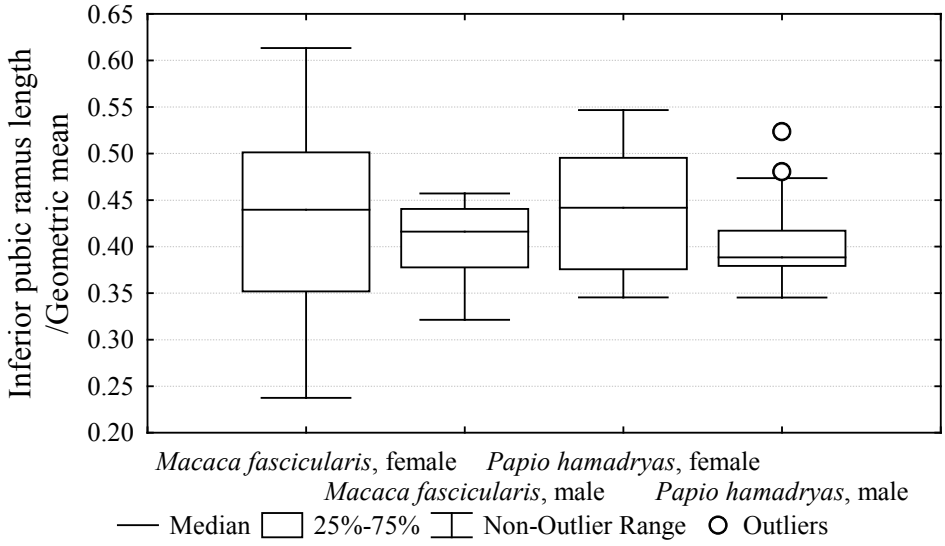
Inferior pubic ramus length
/Geometric mean
0.65
0.60
0.55
0.50
0.45
0.40
0.35
0.30
0.25
0.20
Macaca fascicularis, female
Papio hamadryas, female
Macaca fascicularis, male
Papio hamadryas, male
Median
25%-75%
Non-Outlier Range
Outliers

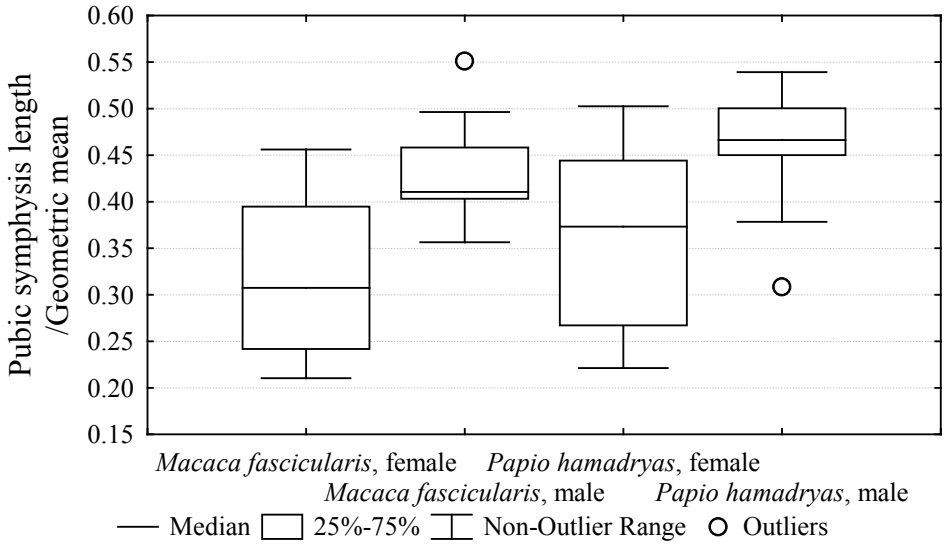
Pubic symphysis length
/Geometric mean
0.60
0.55
0.50
0.45
0.40
0.35
0.30
0.25
0.20
0.15
Macaca fascicularis, female
Papio hamadryas, female
Macaca fascicularis, male
Papio hamadryas, male
Median
25%-75%
Non-Outlier Range
Outliers

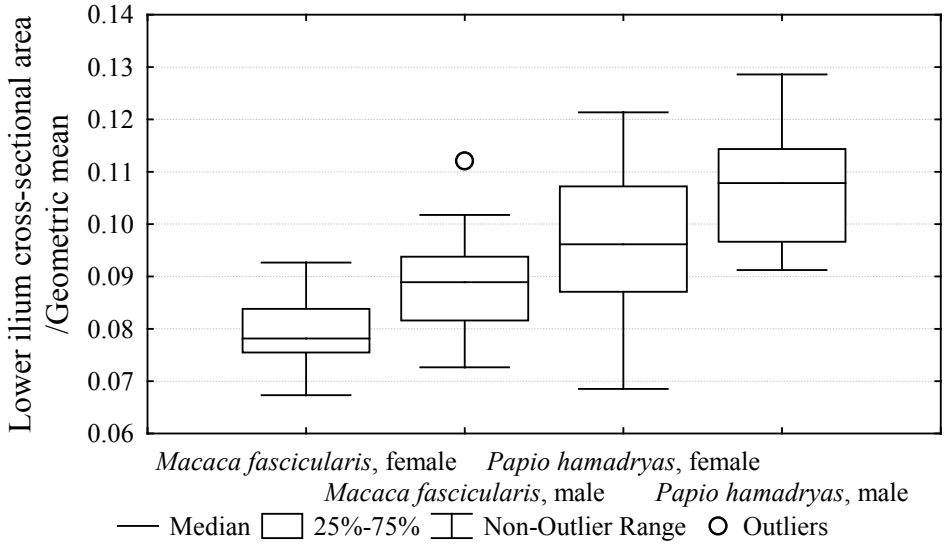
Lower ilium cross-sectional area
/Geometric mean
0.14
0.13
0.12
0.11
0.10
0.09
0.08
0.07
0.06
Macaca fascicularis, female
Papio hamadryas, female
Macaca fascicularis, male
Papio hamadryas, male
Median
25%-75%
Non-Outlier Range
Outliers

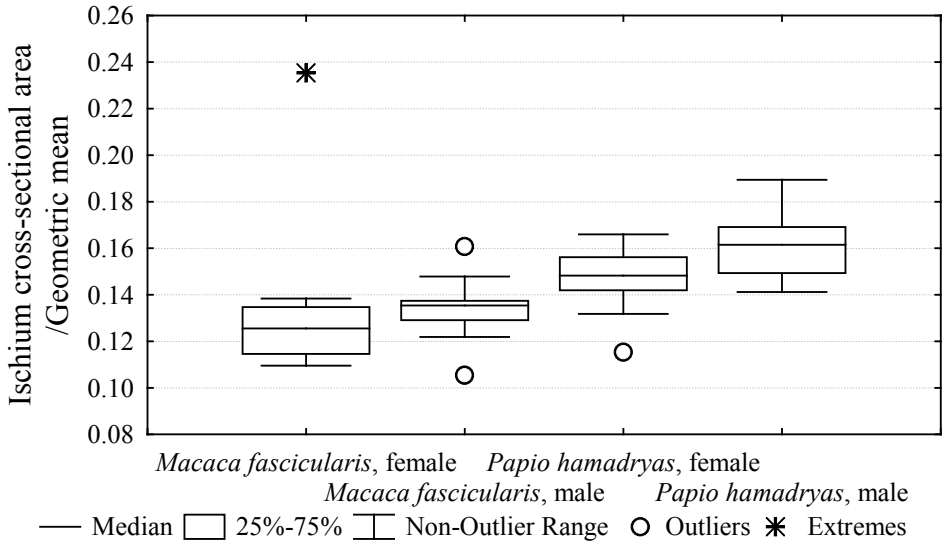
Ischium cross-sectional area /Geometric mean
0.26
0.24
0.22
0.20
0.18
0.16
0.14
0.12
0.10
0.08
Macaca fascicularis, female
Papio hamadryas, female
Macaca fascicularis, male
Papio hamadryas, male
Median
25%-75%
Non-Outlier Range
Outliers
Extremes

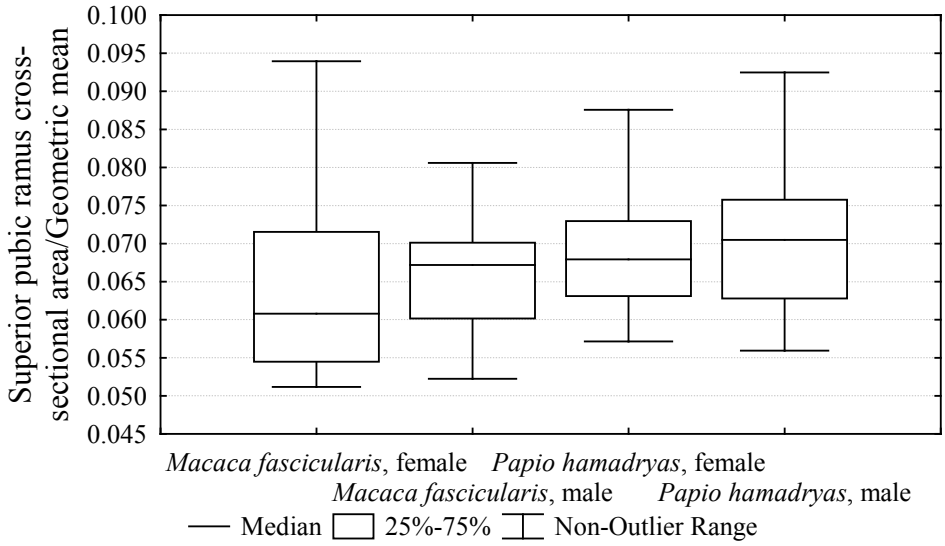
Superior pubic ramus cross-sectional area/Geometric mean
0.100
0.095
0.090
0.085
0.080
0.075
0.070
0.065
0.060
0.055
0.050
0.045
Macaca fascicularis, female
Papio hamadryas, female
Macaca fascicularis, male
Papio hamadryas, male
Median
25%-75%
Non-Outlier Range

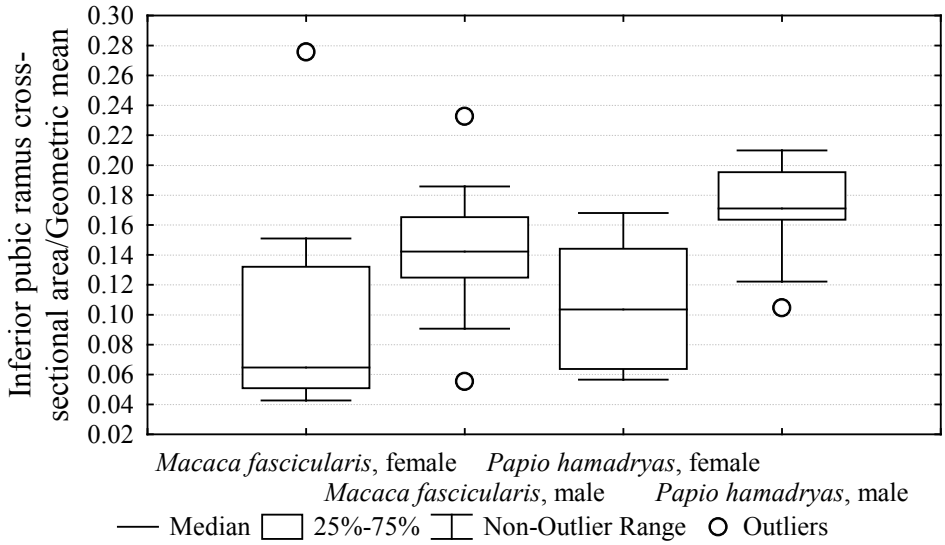
Inferior pubic ramus cross-sectional area/Geometric mean
0.30
0.28
0.26
0.24
0.22
0.20
0.18
0.16
0.14
0.12
0.10
0.08
0.06
0.04
0.02
Macaca fascicularis, female
Papio hamadryas, female
Macaca fascicularis, male
Papio hamadryas, male
Median
25%-75%
Non-Outlier Range
Outliers

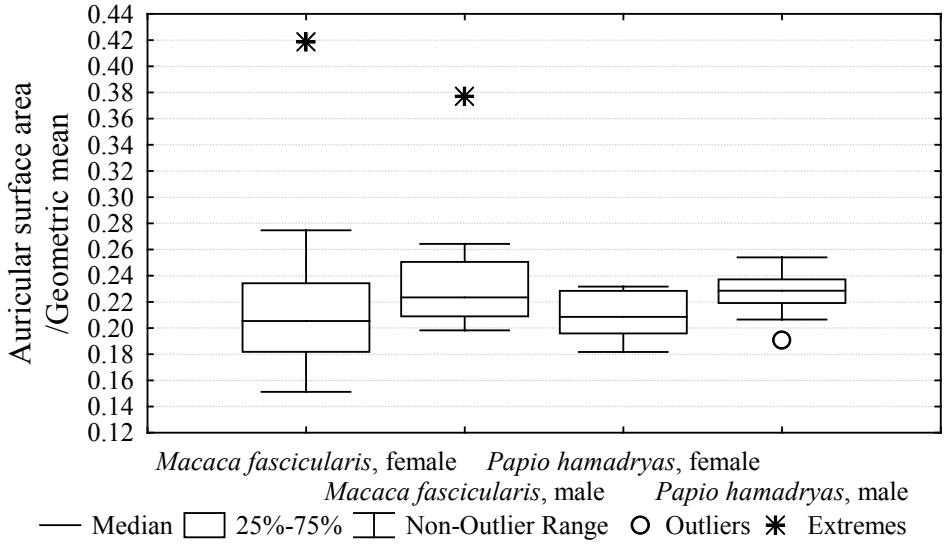
Auricular surface area /Geometric mean
0.44
0.42
0.40
0.38
0.36
0.34
0.32
0.30
0.28
0.26
0.24
0.22
0.20
0.18
0.16
0.14
0.12
Macaca fascicularis, female
Papio hamadryas, female
Macaca fascicularis, male
Papio hamadryas, male
Median
25%-75%
Non-Outlier Range
Outliers
Extremes

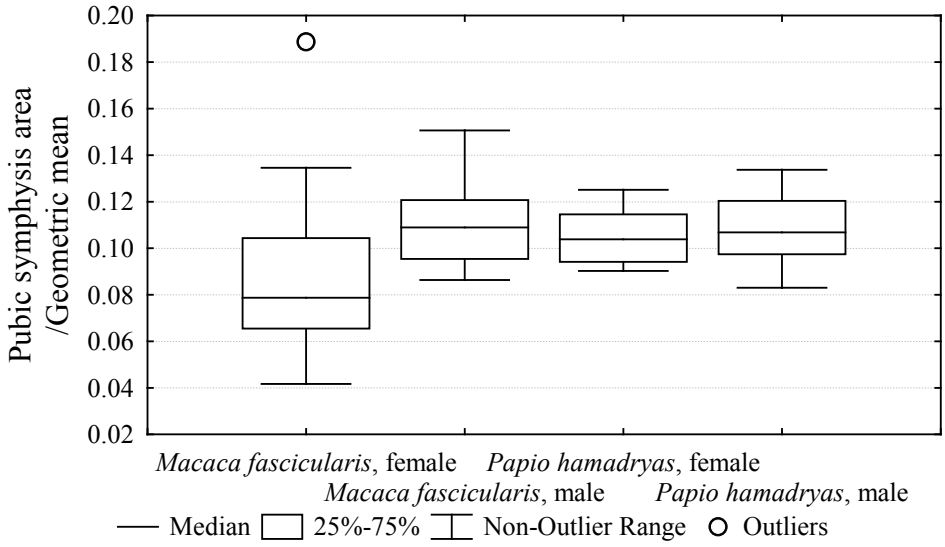
Pubic symphysis area
/Geometric mean
0.20
0.18
0.16
0.14
0.12
0.10
0.08
0.06
0.04
0.02
Macaca fascicularis, female
Papio hamadryas, female
Macaca fascicularis, male
Papio hamadryas, male
Median
25%-75%
Non-Outlier Range
Outliers

GALAGO SENEGALENSIS V. *OTOLEMUR CRASSICAUDATUS*

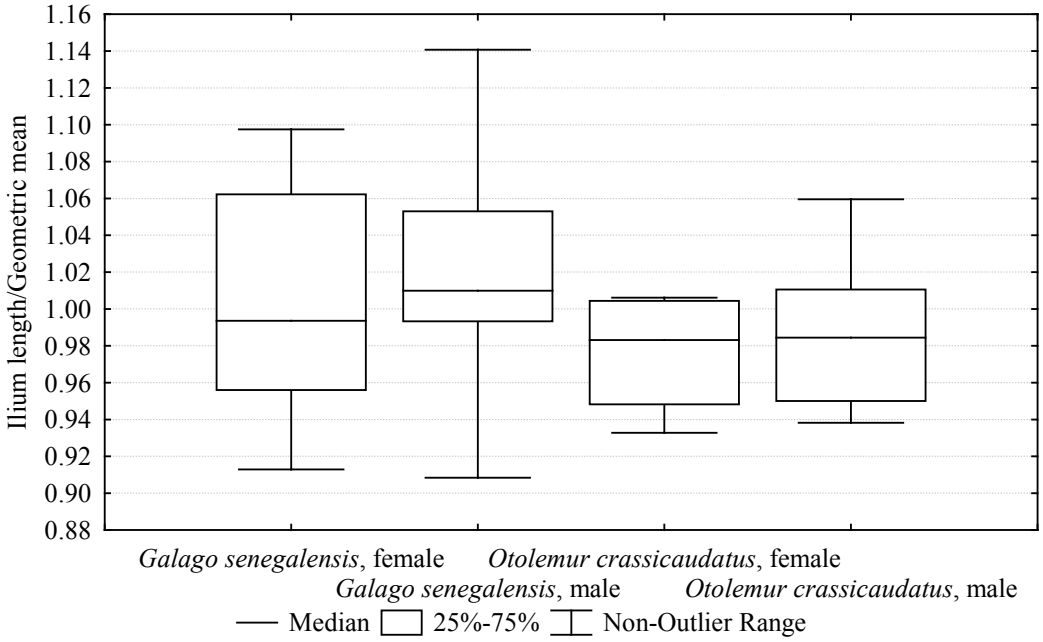

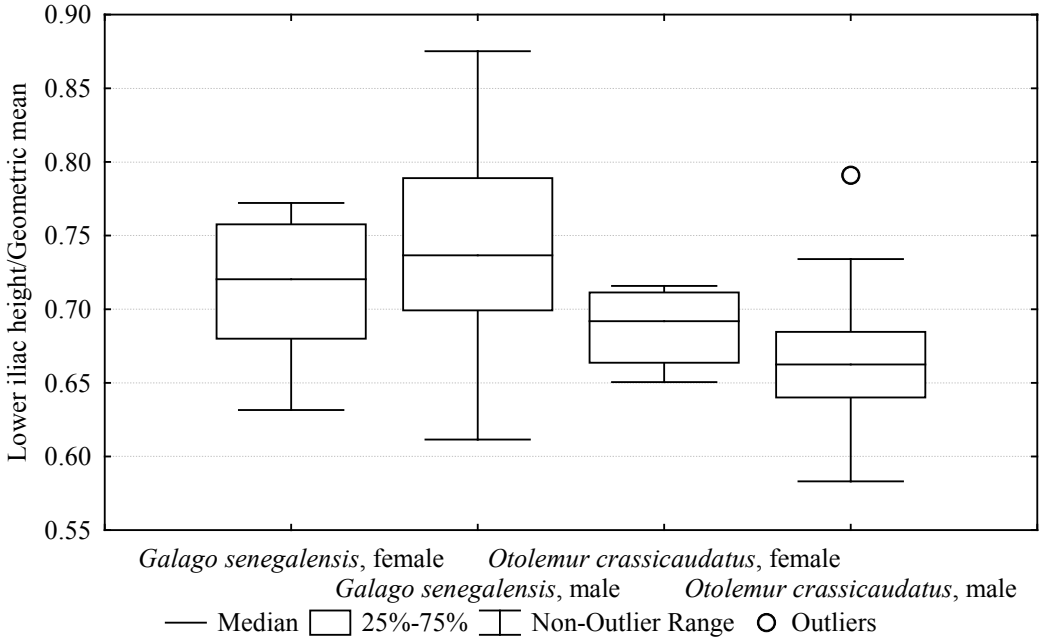
Lower iliac height/Geometric mean
0.90
0.85
0.80
0.75
0.70
0.65
0.60
0.55
Galago senegalensis, female
Otolemur crassicaudatus, female
Galago senegalensis, male
Otolemur crassicaudatus, male
Median
25%-75%
Non-Outlier Range
Outliers

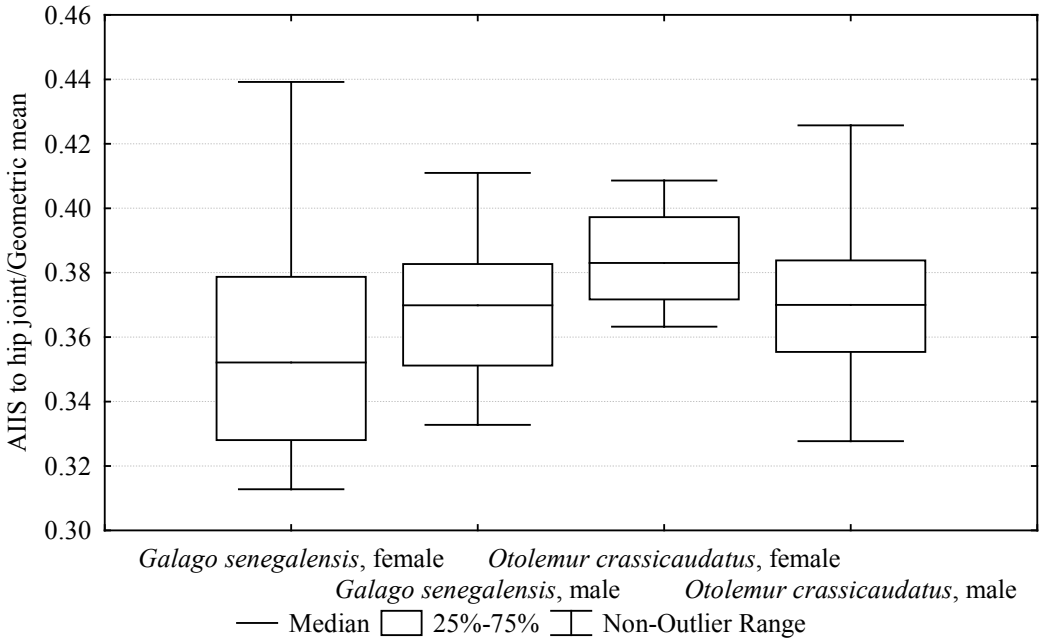
AIIS to hip joint/Geometric mean
0.46
0.44
0.42
0.40
0.38
0.36
0.34
0.32
0.30
Galago senegalensis, female
Otolemur crassicaudatus, female
Galago senegalensis, male
Otolemur crassicaudatus, male
Median
25%-75%
Non-Outlier Range

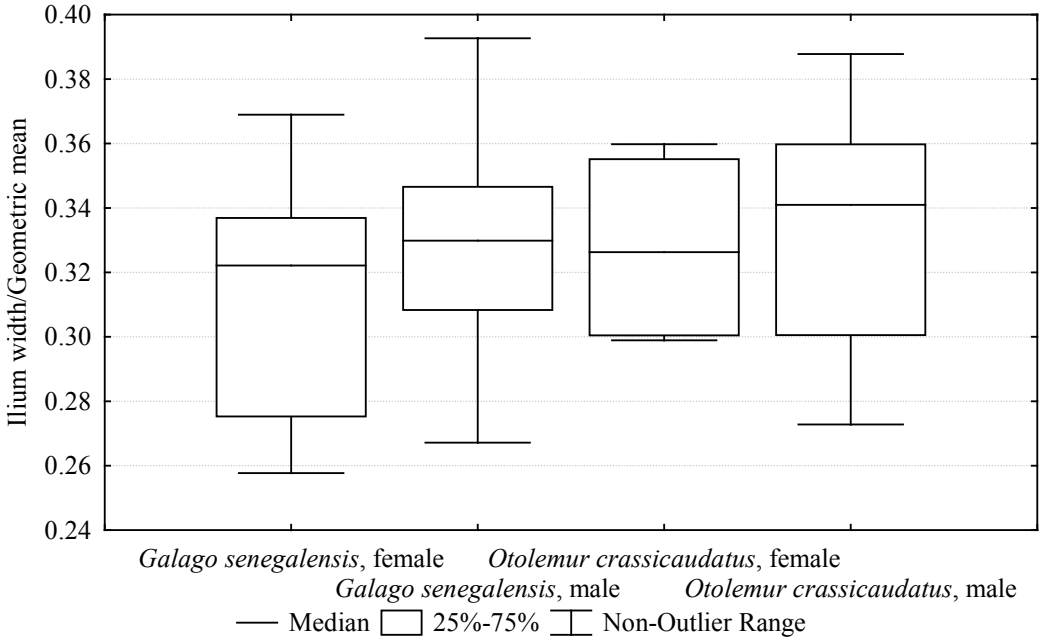
Ilium width/Geometric mean
0.40
0.38
0.36
0.34
0.32
0.30
0.28
0.26
0.24
Galago senegalensis, female
Otolemur crassicaudatus, female
Galago senegalensis, male
Otolemur crassicaudatus, male
Median
25%-75%
Non-Outlier Range


Ischium length/Geometric mean
0.48
0.46
0.44
0.42
0.40
0.38
0.36
0.34
0.32
0.30
0.28
0.26
Galago senegalensis, female
Otolemur crassicaudatus, female
Galago senegalensis, male
Otolemur crassicaudatus, male
Median
25%-75%
Non-Outlier Range
Outliers
Extremes

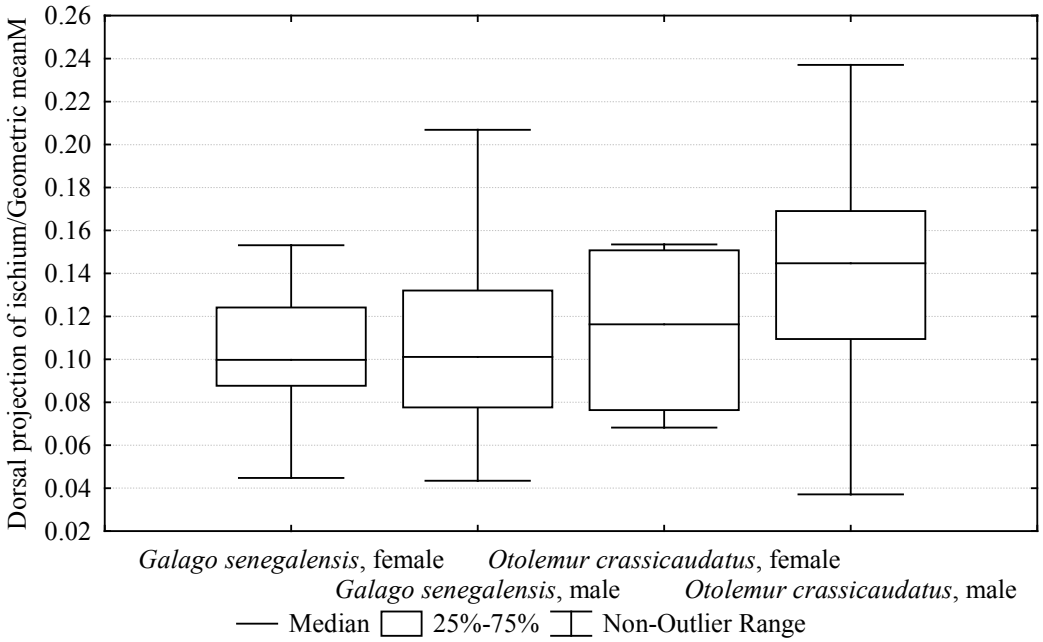
Dorsal projection of ischium/Geometric meanM
0.26
0.24
0.22
0.20
0.18
0.16
0.14
0.12
0.10
0.08
0.06
0.04
0.02
Galago senegalensis, female
Otolemur crassicaudatus, female
Galago senegalensis, male
Otolemur crassicaudatus, male
Median
25%-75%
Non-Outlier Range

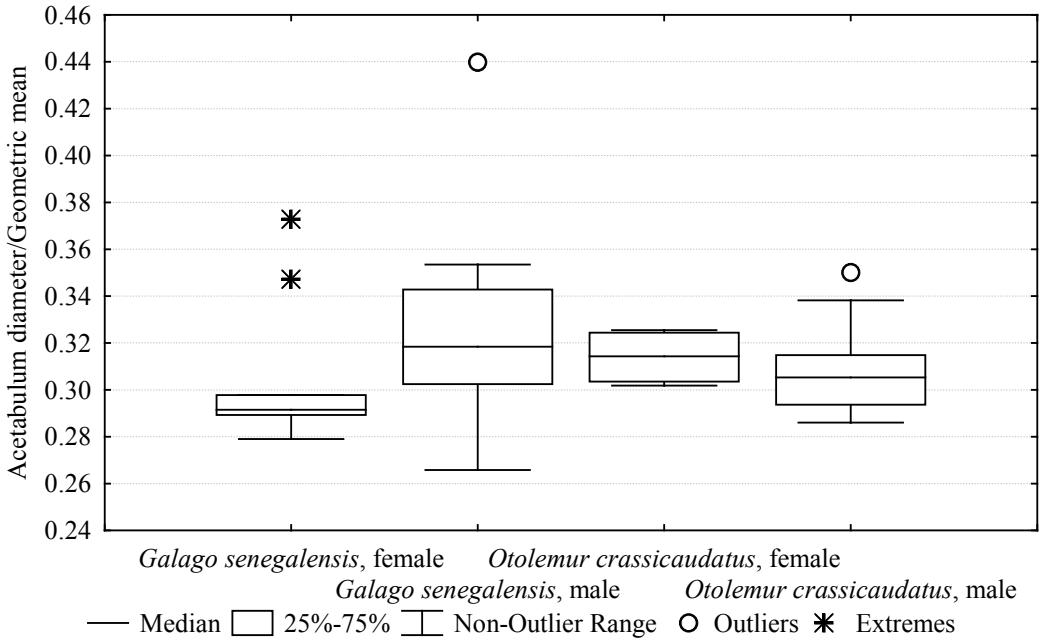
Acetabulum diameter/Geometric mean
0.46
0.44
0.42
0.40
0.38
0.36
0.34
0.32
0.30
0.28
0.26
0.24
Galago senegalensis, female
Otolemur crassicaudatus, female
Galago senegalensis, male
Otolemur crassicaudatus, male
Median
25%-75%
Non-Outlier Range
Outliers
Extremes

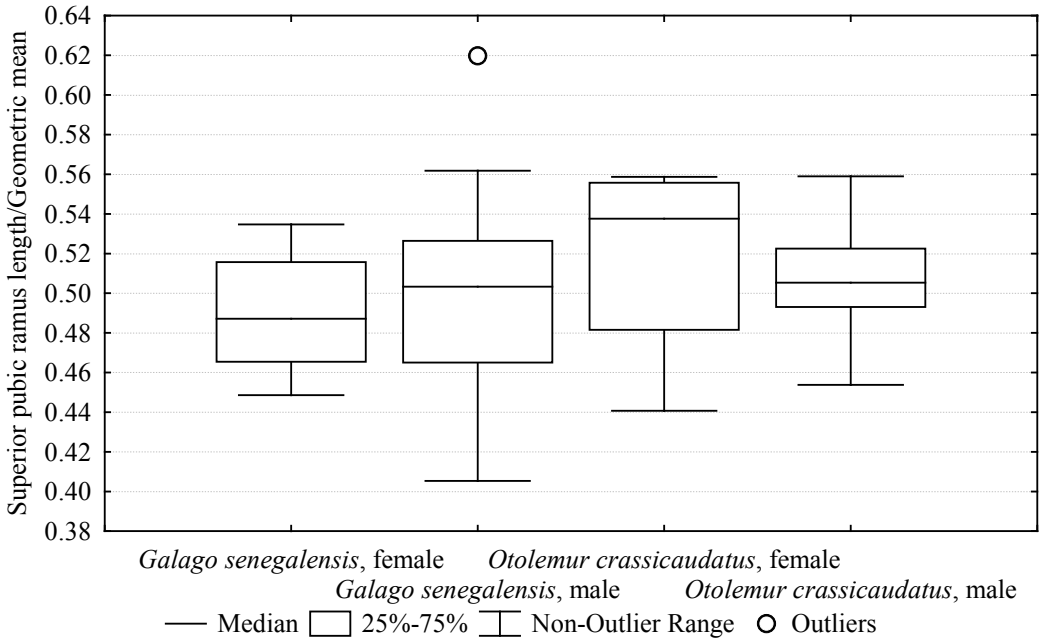
Superior pubic ramus length/Geometric mean
0.64
0.62
0.60
0.58
0.56
0.54
0.52
0.50
0.48
0.46
0.44
0.42
0.40
0.38
Galago senegalensis, female
Otolemur crassicaudatus, female
Galago senegalensis, male
Otolemur crassicaudatus, male
Median
25%-75%
Non-Outlier Range
Outliers

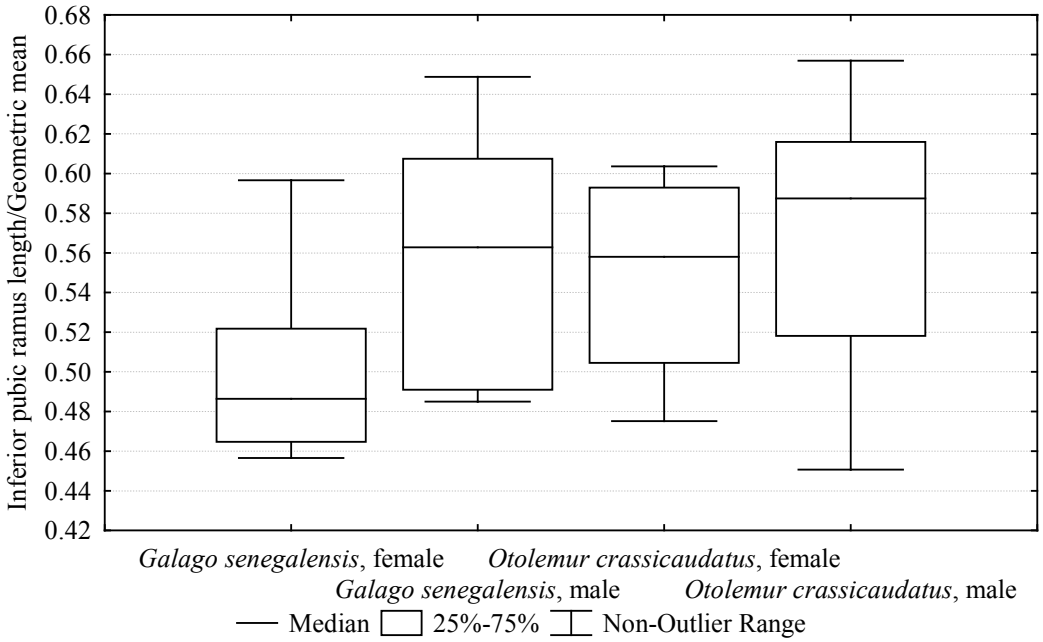
Inferior pubic ramus length/Geometric mean
0.68
0.66
0.64
0.62
0.60
0.58
0.56
0.54
0.52
0.50
0.48
0.46
0.44
0.42
Galago senegalensis, female
Otolemur crassicaudatus, female
Galago senegalensis, male
Otolemur crassicaudatus, male
Median
25%-75%
Non-Outlier Range

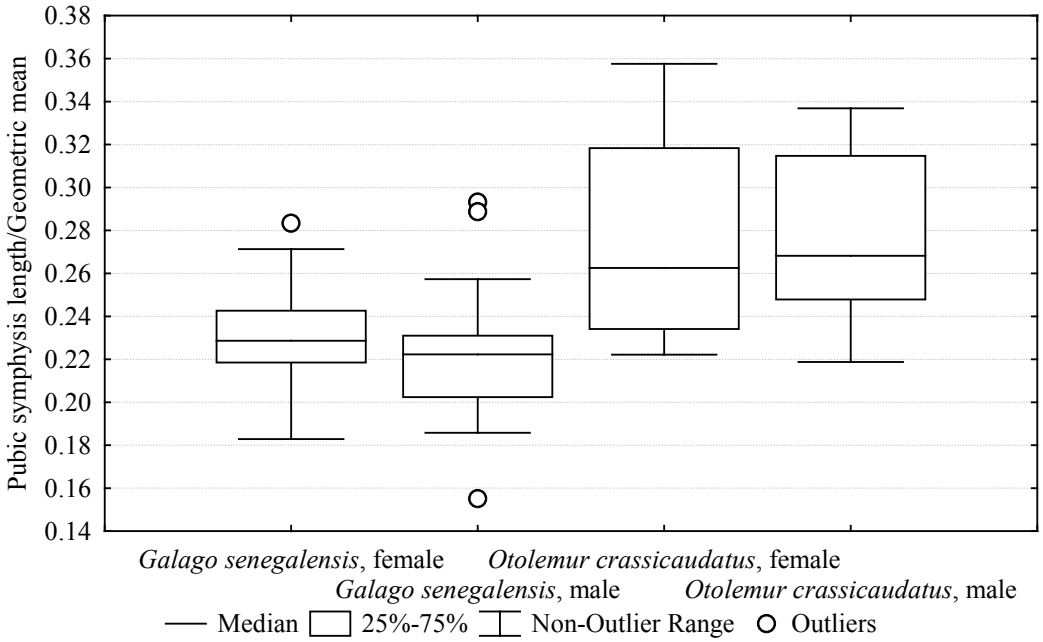
Pubic symphysis length/Geometric mean
0.38
0.36
0.34
0.32
0.30
0.28
0.26
0.24
0.22
0.20
0.18
0.16
0.14
Galago senegalensis, female
Otolemur crassicaudatus, female
Galago senegalensis, male
Otolemur crassicaudatus, male
Median
25%-75%
Non-Outlier Range
Outliers

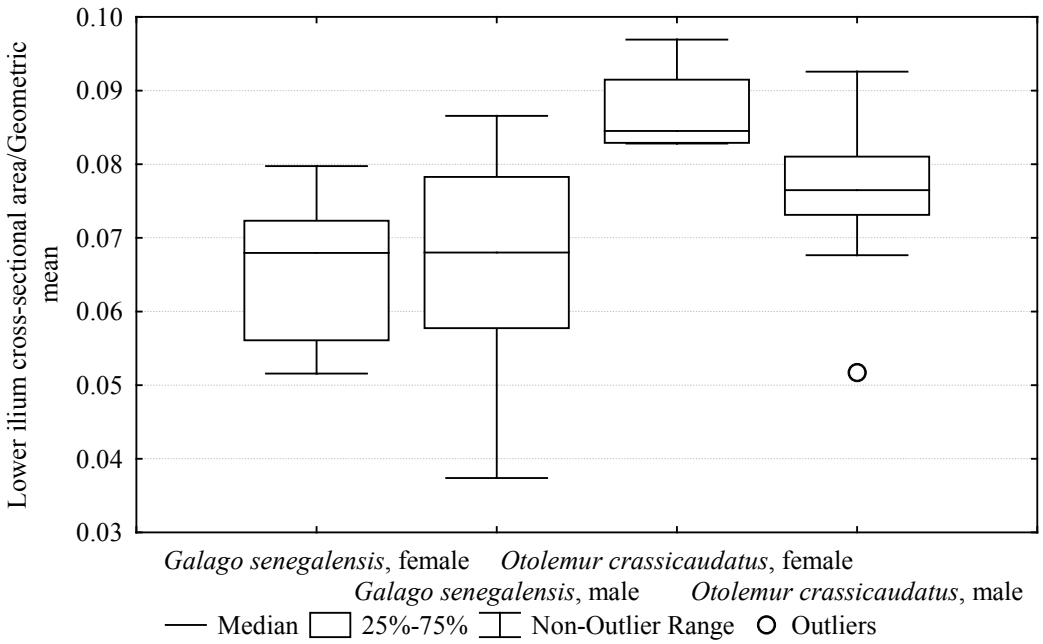
Lower ilium cross-sectional area/Geometric mean
0.10
0.09
0.08
0.07
0.06
0.05
0.04
0.03
Galago senegalensis, female
Otolemur crassicaudatus, female
Galago senegalensis, male
Otolemur crassicaudatus, male
Median
25%-75%
Non-Outlier Range
Outliers

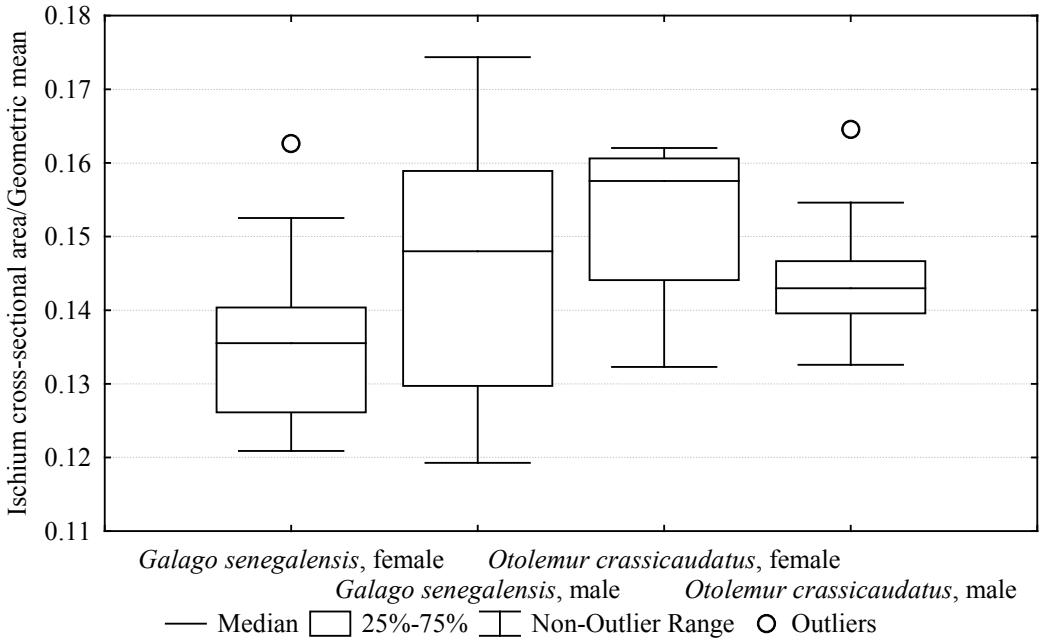
Ischium cross-sectional area/Geometric mean
0.18
0.17
0.16
0.15
0.14
0.13
0.12
0.11
Galago senegalensis, female
Otolemur crassicaudatus, female
Galago senegalensis, male
Otolemur crassicaudatus, male
Median
25%-75%
Non-Outlier Range
Outliers

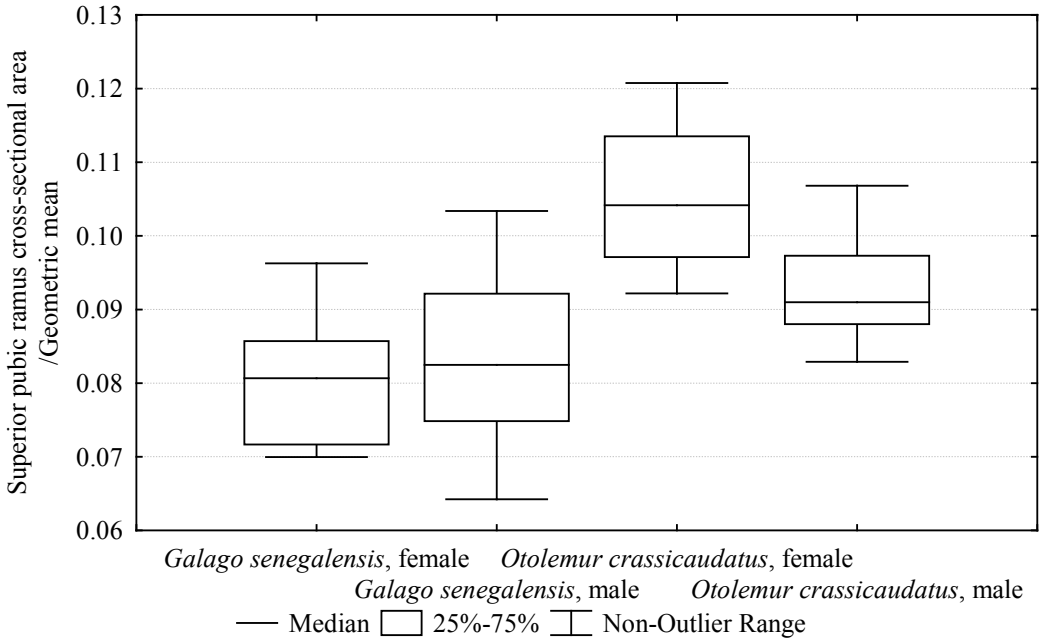
Superior pubic ramus cross-sectional area
/Geometric mean
0.13
0.12
0.11
0.10
0.09
0.08
0.07
0.06
Galago senegalensis, female
Otolemur crassicaudatus, female
Galago senegalensis, male
Otolemur crassicaudatus, male
Median
25%-75%
Non-Outlier Range

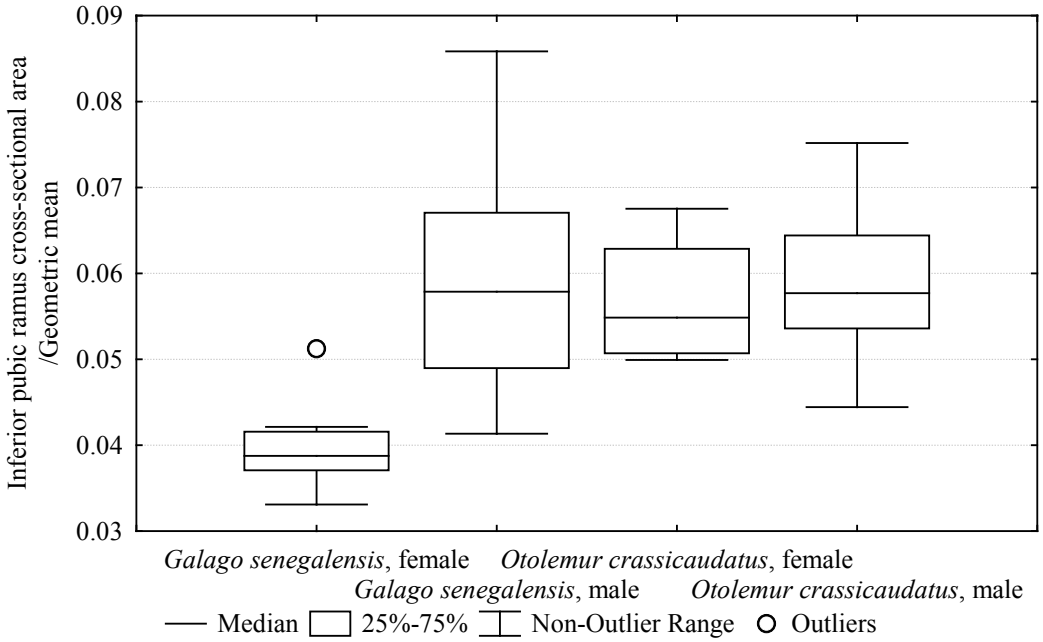
Inferior pubic ramus cross-sectional area /Geometric mean
0.09
0.08
0.07
0.06
0.05
0.04
0.03
Galago senegalensis, female
Otolemur crassicaudatus, female
Galago senegalensis, male
Otolemur crassicaudatus, male
Median
25%-75%
Non-Outlier Range
Outliers


Auricular surface area/Geometric mean
0.27
0.26
0.25
0.24
0.23
0.22
0.21
0.20
0.19
0.18
Galago senegalensis, female
Otolemur crassicaudatus, female
Galago senegalensis, male
Otolemur crassicaudatus, male
Median
25%-75%
Non-Outlier Range

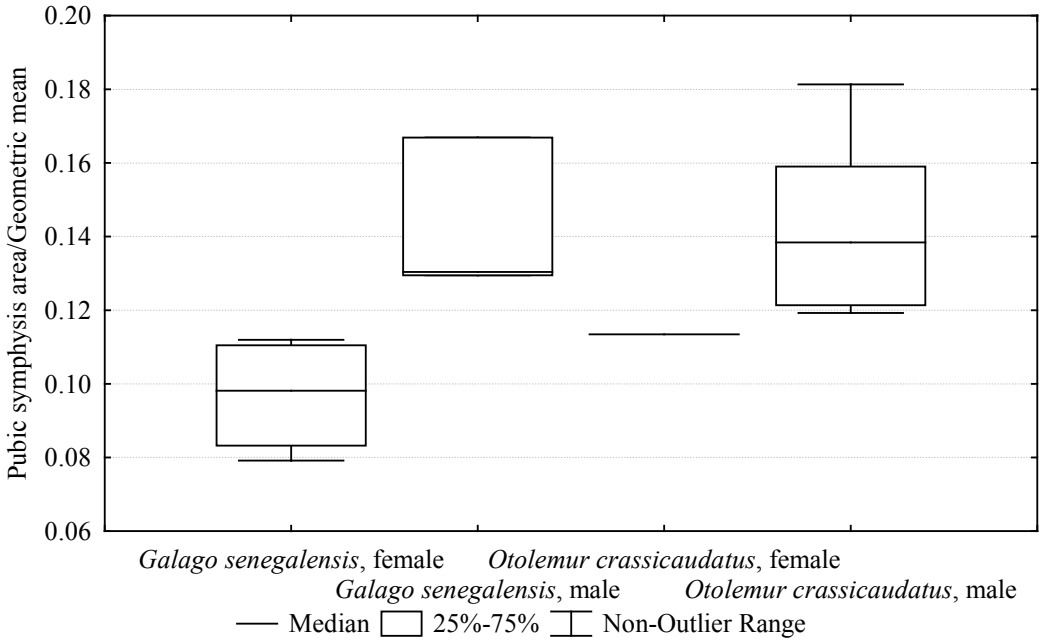
0.20
0.18
0.16
0.14
0.12
0.10
0.08
0.06
Pubic symphysis area/Geometric mean
Galago senegalensis, female
Otolemur crassicaudatus, female
Galago senegalensis, male
Otolemur crassicaudatus, male
Median
25%-75%
Non-Outlier Range

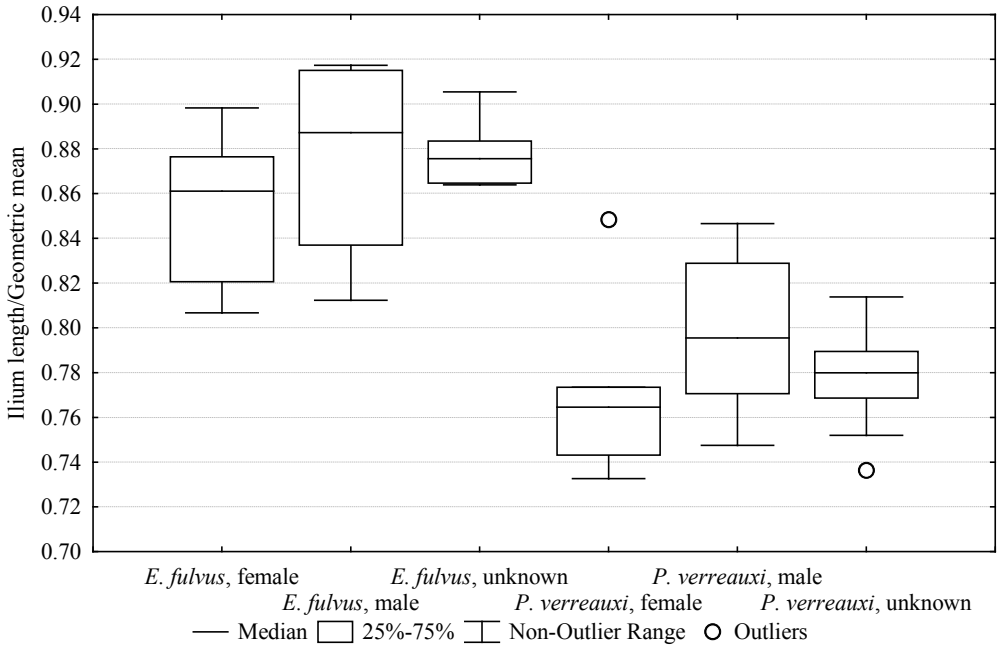
Ilium length/Geometric mean
0.94
0.92
0.90
0.88
0.86
0.84
0.82
0.80
0.78
0.76
0.74
0.72
0.70
E. fulvus, female
E. fulvus, unknown
P. verreauxi, male
E. fulvus, male
P. verreauxi, female
P. verreauxi, unknown
Median
25%-75%
Non-Outlier Range
Outliers

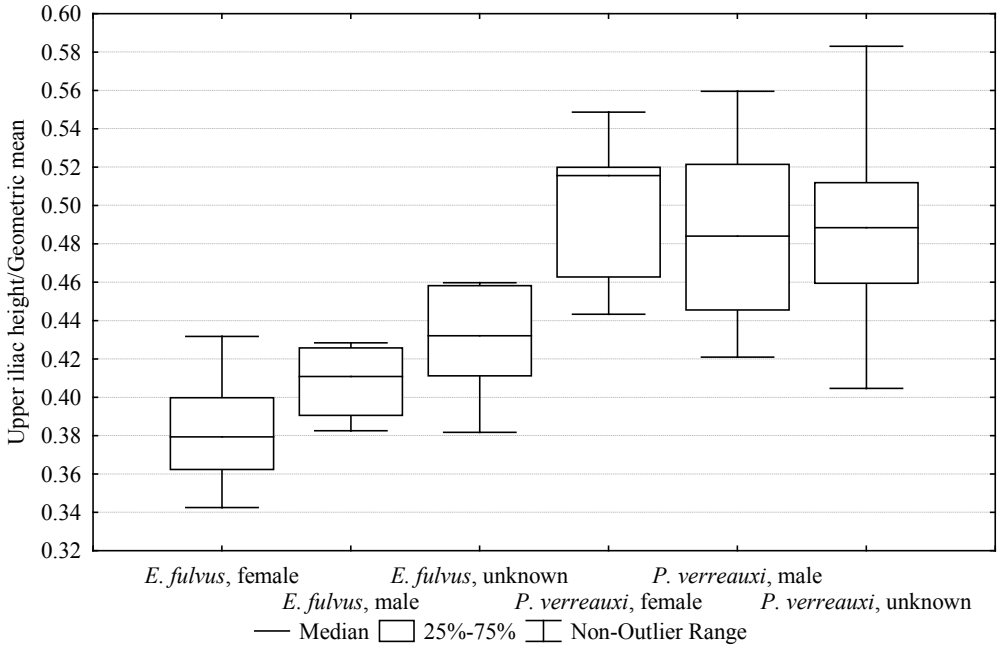
Upper iliac height/Geometric mean
0.60
0.58
0.56
0.54
0.52
0.50
0.48
0.46
0.44
0.42
0.40
0.38
0.36
0.34
0.32
E. fulvus, female
E. fulvus, unknown
P. verreauxi, male
E. fulvus, male
P. verreauxi, female
P. verreauxi, unknown
Median
25%-75%
Non-Outlier Range

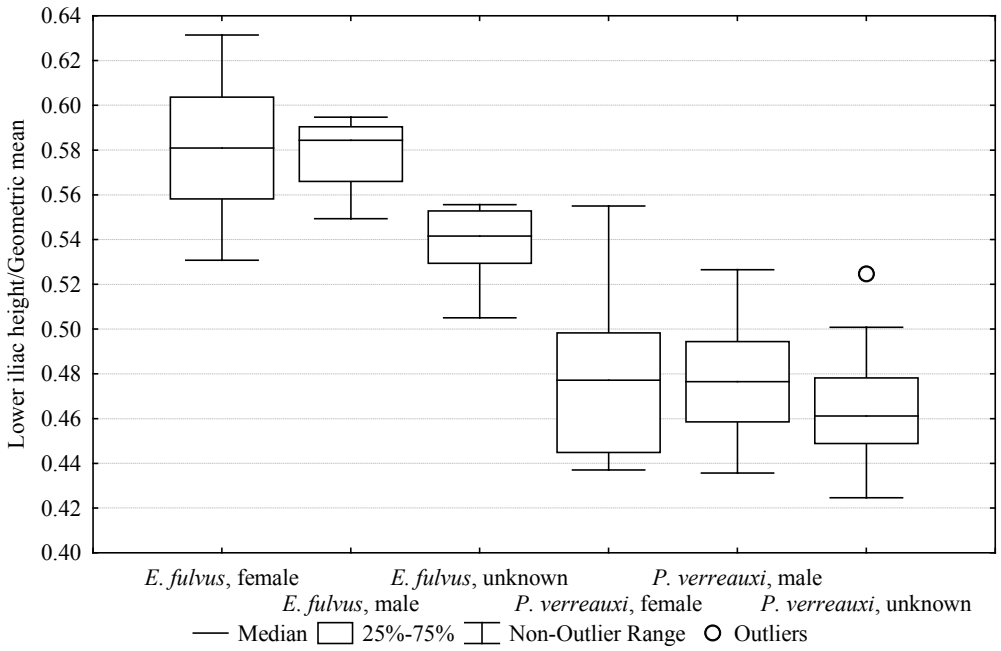
Lower iliac height/Geometric mean
0.64
0.62
0.60
0.58
0.56
0.54
0.52
0.50
0.48
0.46
0.44
0.42
0.40
E. fulvus, female
E. fulvus, unknown
P. verreauxi, male
E. fulvus, male
P. verreauxi, female
P. verreauxi, unknown
Median
25%-75%
Non-Outlier Range
Outliers

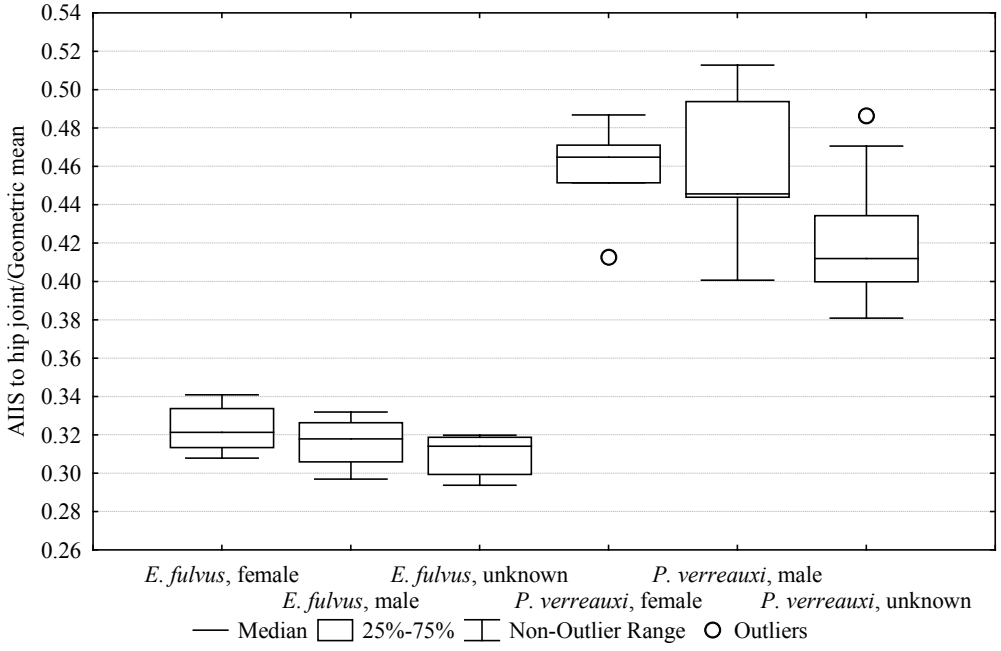
AIIS to hip joint/Geometric mean
0.54
0.52
0.50
0.48
0.46
0.44
0.42
0.40
0.38
0.36
0.34
0.32
0.30
0.28
0.26
E. fulvus, female
E. fulvus, unknown
P. verreauxi, male
E. fulvus, male
P. verreauxi, female
P. verreauxi, unknown
Median
25%-75%
Non-Outlier Range
Outliers

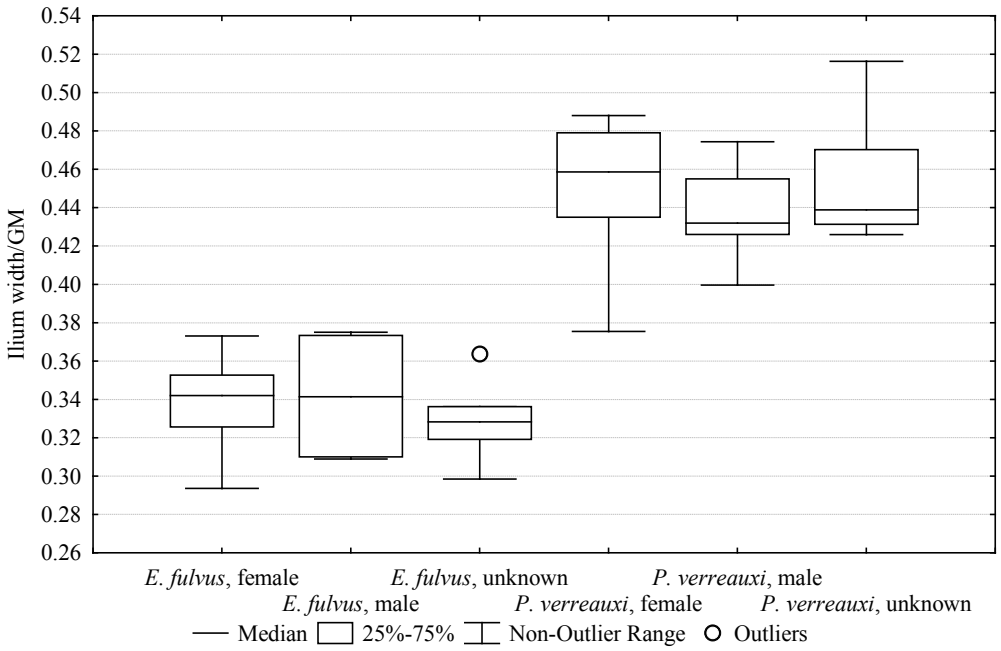
Ilium width/GM
0.54
0.52
0.50
0.48
0.46
0.44
0.42
0.40
0.38
0.36
0.34
0.32
0.30
0.28
0.26
E. fulvus, female
E. fulvus, unknown
P. verreauxi, male
E. fulvus, male
P. verreauxi, female
P. verreauxi, unknown
Median
25%-75%
Non-Outlier Range
Outliers

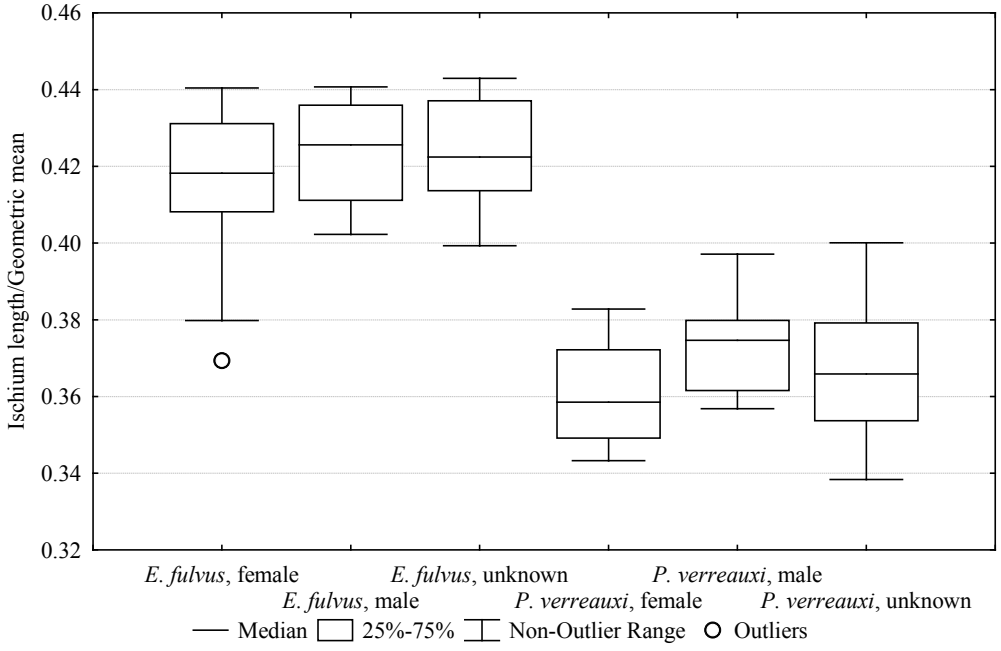
Ischium length/Geometric mean
0.46
0.44
0.42
0.40
0.38
0.36
0.34
0.32
E. fulvus, female
E. fulvus, unknown
P. verreauxi, male
E. fulvus, male
P. verreauxi, female
P. verreauxi, unknown
Median
25%-75%
Non-Outlier Range
Outliers

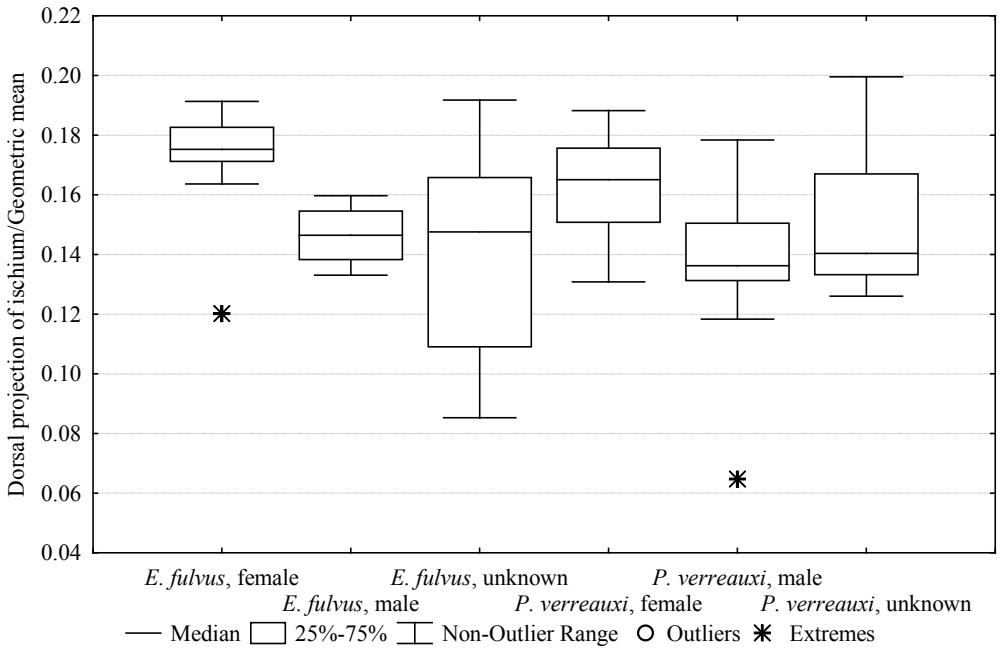
Dorsal projection of ischium/Geometric mean
0.22
0.20
0.18
0.16
0.14
0.12
0.10
0.08
0.06
0.04
E. fulvus, female
E. fulvus, male
E. fulvus, unknown
P. verreauxi, female
P. verreauxi, male
P. verreauxi, unknown
Median
25%-75%
Non-Outlier Range
Outliers
Extremes

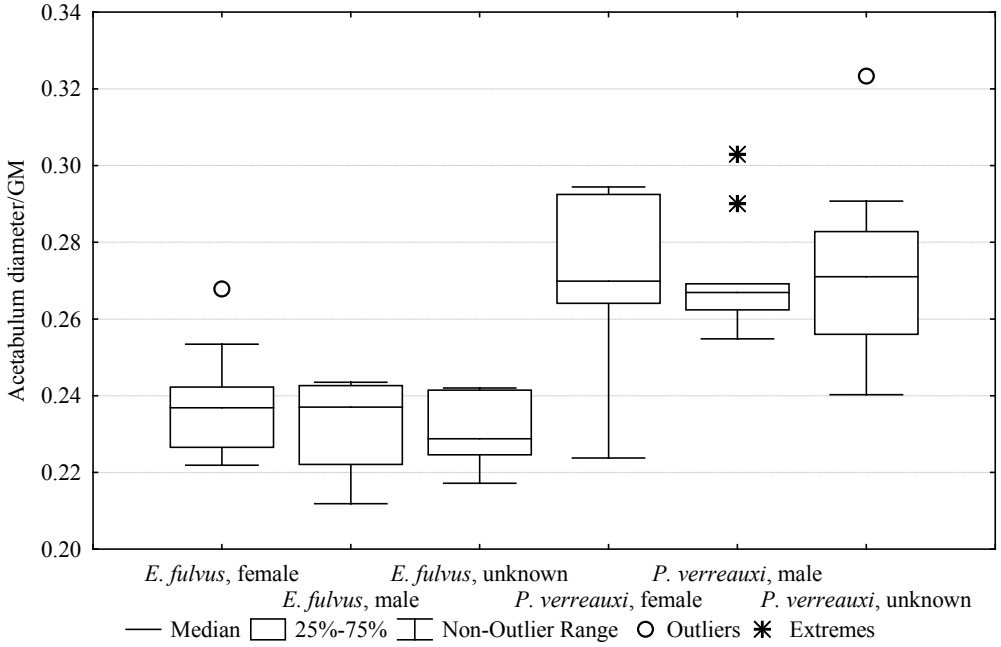
Acetabulum diameter/GM
0.34
0.32
0.30
0.28
0.26
0.24
0.22
0.20
E. fulvus, female
E. fulvus, male
E. fulvus, unknown
P. verreauxi, female
P. verreauxi, male
P. verreauxi, unknown
Median
25%-75%
Non-Outlier Range
Outliers
Extremes

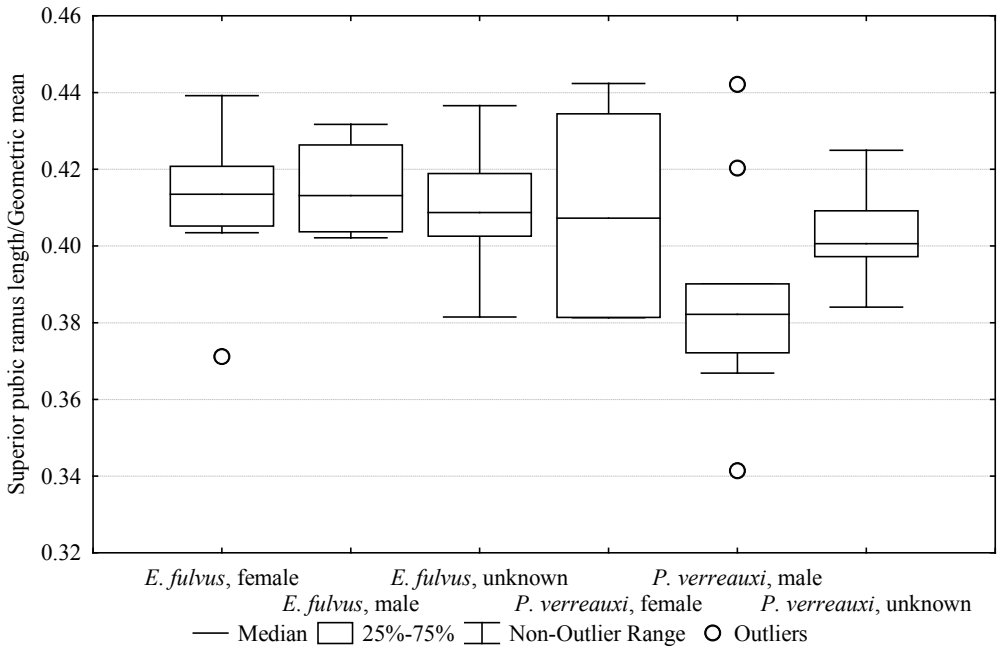
Superior pubic ramus length/Geometric mean
0.46
0.44
0.42
0.40
0.38
0.36
0.34
0.32
E. fulvus, female
E. fulvus, male
E. fulvus, unknown
P. verreauxi, female
P. verreauxi, male
P. verreauxi, unknown
Median
25%-75%
Non-Outlier Range
Outliers

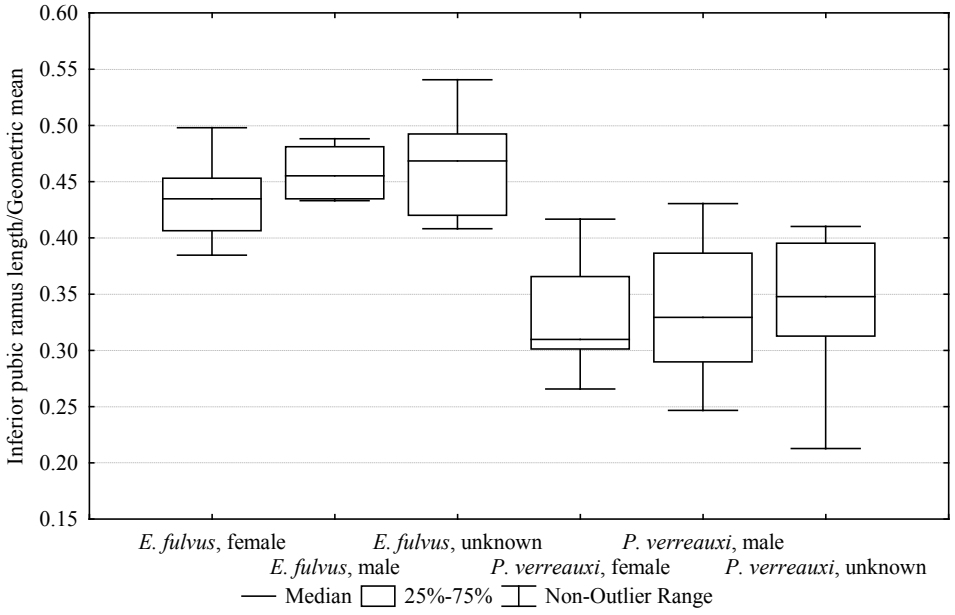
Inferior pubic ramus length/Geometric mean
0.60
0.55
0.50
0.45
0.40
0.35
0.30
0.25
0.20
0.15
E. fulvus, female
E. fulvus, male
E. fulvus, unknown
P. verreauxi, female
P. verreauxi, male
P. verreauxi, unknown
Median
25%-75%
Non-Outlier Range

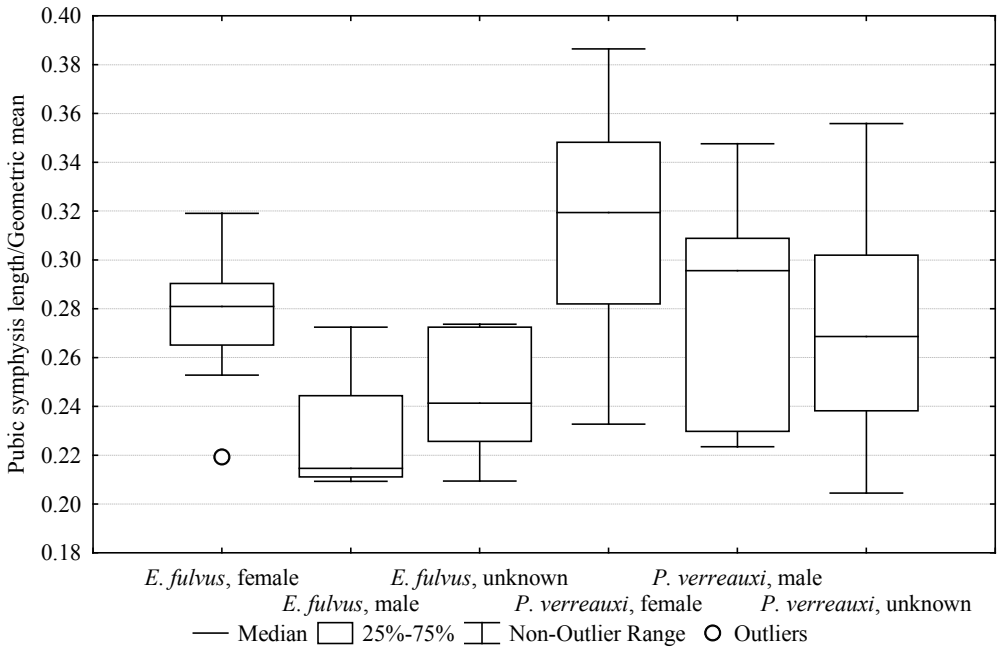
Pubic symphysis length/Geometric mean
0.40
0.38
0.36
0.34
0.32
0.30
0.28
0.26
0.24
0.22
0.20
0.18
E. fulvus, female
E. fulvus, unknown
P. verreauxi, male
E. fulvus, male
P. verreauxi, female
P. verreauxi, unknown
Median
25%-75%
Non-Outlier Range
Outliers

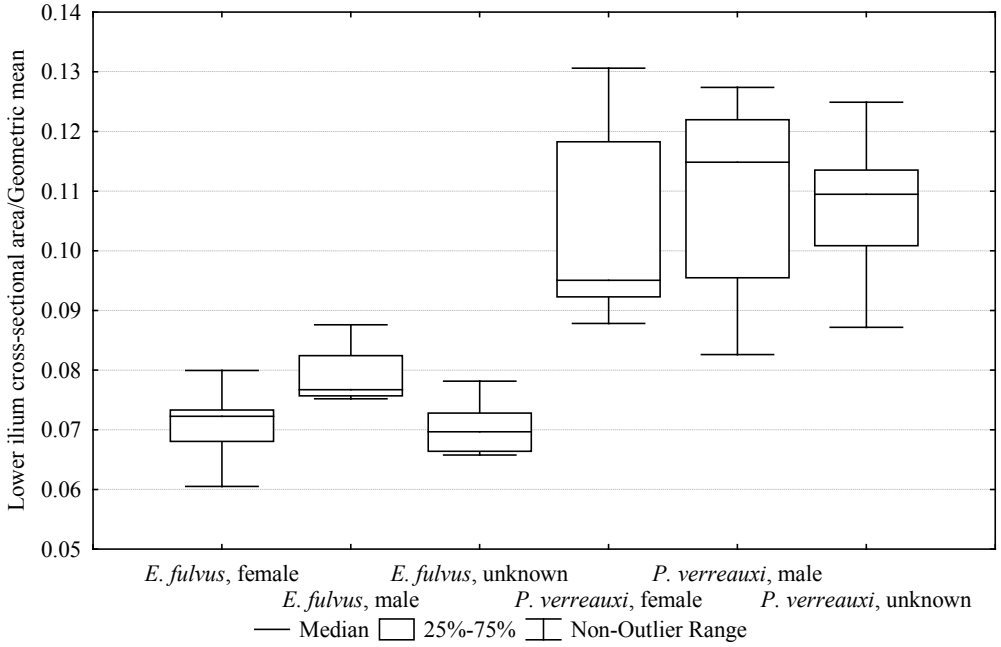
Lower ilium cross-sectional area/Geometric mean
0.14
0.13
0.12
0.11
0.10
0.09
0.08
0.07
0.06
0.05
E. fulvus, female
E. fulvus, unknown
P. verreauxi, male
E. fulvus, male
P. verreauxi, female
P. verreauxi, unknown
Median
25%-75%
Non-Outlier Range

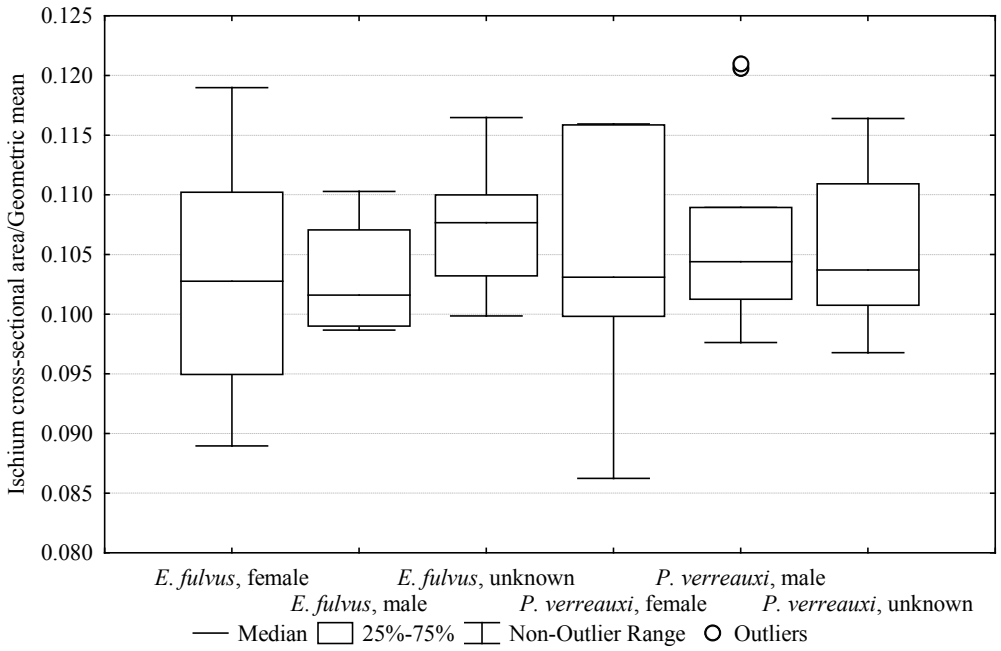
Ischium cross-sectional area/Geometric mean
0.125
0.120
0.115
0.110
0.105
0.100
0.095
0.090
0.085
0.080
E. fulvus, female
E. fulvus, male
E. fulvus, unknown
P. verreauxi, female
P. verreauxi, male
P. verreauxi, unknown
Median
25%-75%
Non-Outlier Range
Outliers

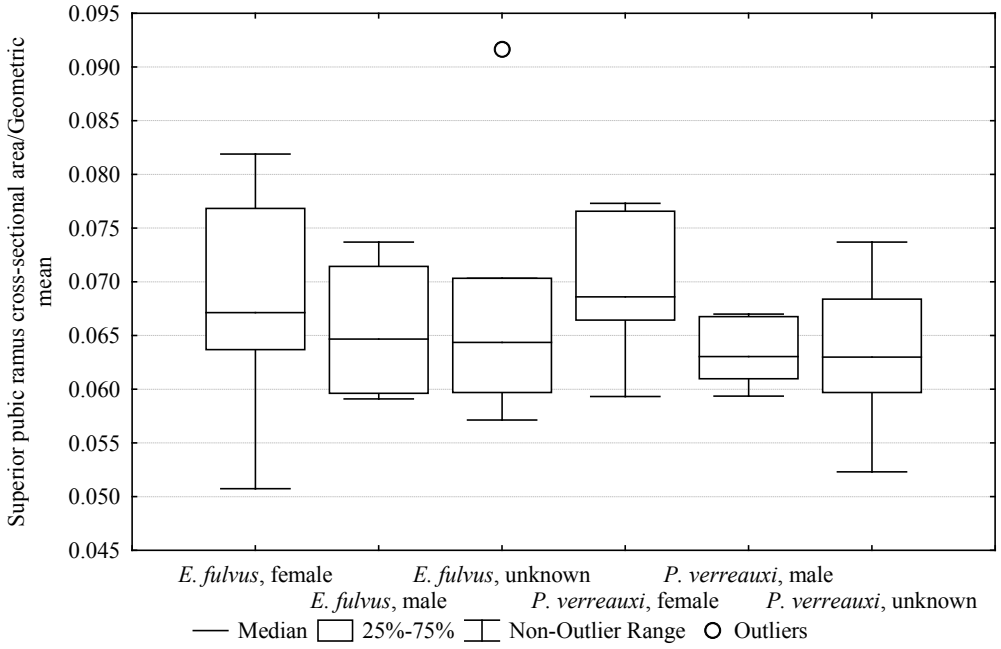
Superior pubic ramus cross-sectional area/Geometric mean
0.095
0.090
0.085
0.080
0.075
0.070
0.065
0.060
0.055
0.050
0.045
E. fulvus, female
E. fulvus, male
E. fulvus, unknown
P. verreauxi, female
P. verreauxi, male
P. verreauxi, unknown
Median
25%-75%
Non-Outlier Range
Outliers

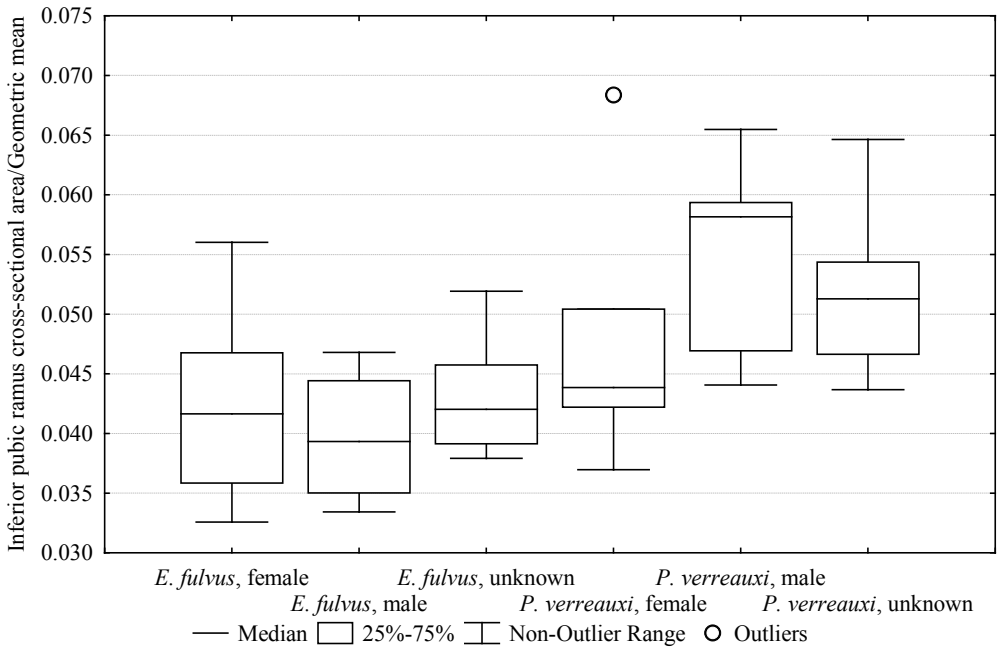
Inferior pubic ramus cross-sectional area/Geometric mean
0.075
0.070
0.065
0.060
0.055
0.050
0.045
0.040
0.035
0.030
E. fulvus, female
E. fulvus, male
E. fulvus, unknown
P. verreauxi, female
P. verreauxi, male
P. verreauxi, unknown
Median
25%-75%
Non-Outlier Range
Outliers

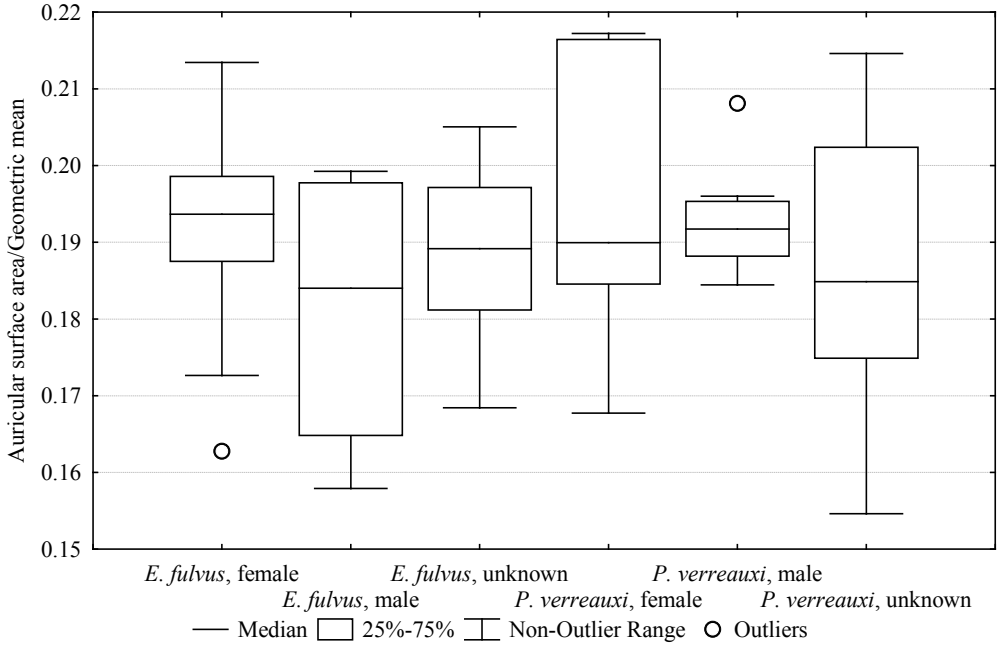
Auricular surface area/Geometric mean
0.22
0.21
0.20
0.19
0.18
0.17
0.16
0.15
E. fulvus, female
E. fulvus, male
E. fulvus, unknown
P. verreauxi, female
P. verreauxi, male
P. verreauxi, unknown
Median
25%-75%
Non-Outlier Range
Outliers

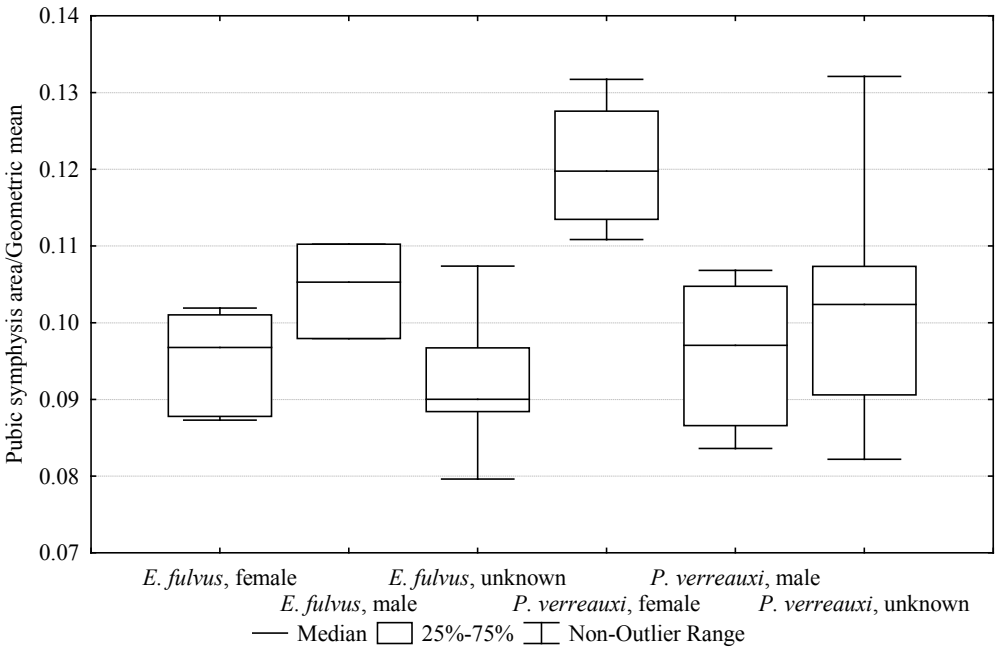
0.14
0.13
0.12
0.11
0.10
0.09
0.08
0.07
Pubic symphysis area/Geometric mean
E. fulvus, female
E. fulvus, male
E. fulvus, unknown
P. verreauxi, female
P. verreauxi, male
P. verreauxi, unknown
Median
25%-75%
Non-Outlier Range

PROPITHECUS VERREAUXI V. *VARECIA VARIEGATA*

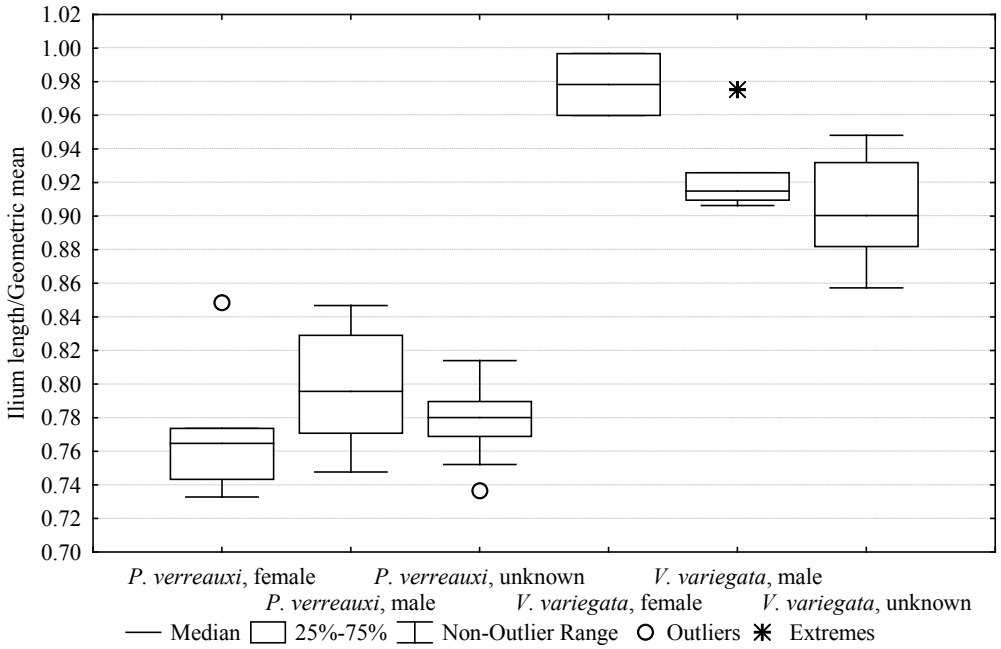

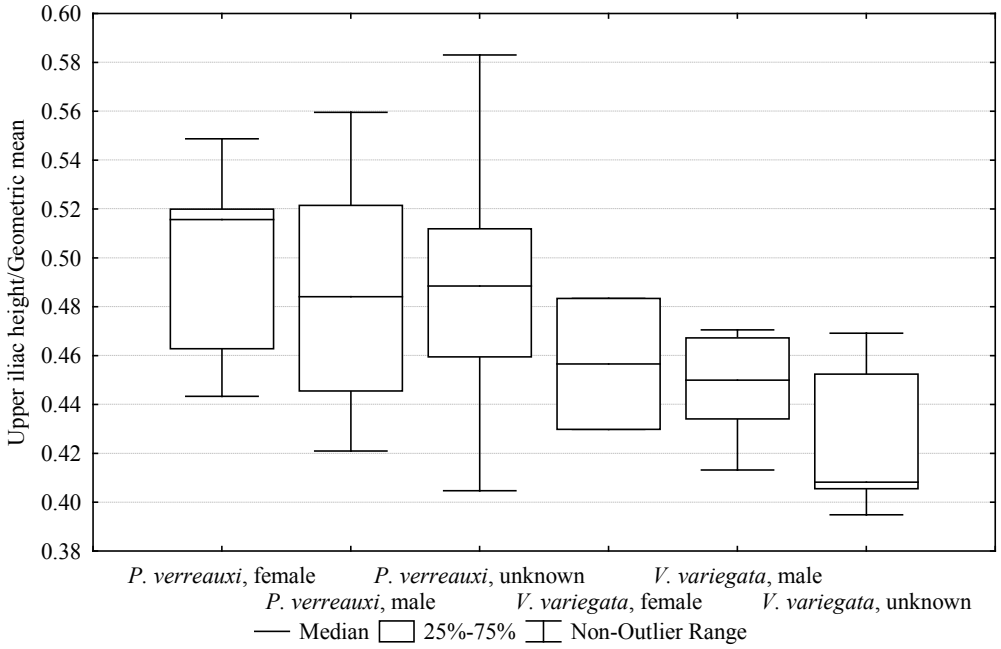

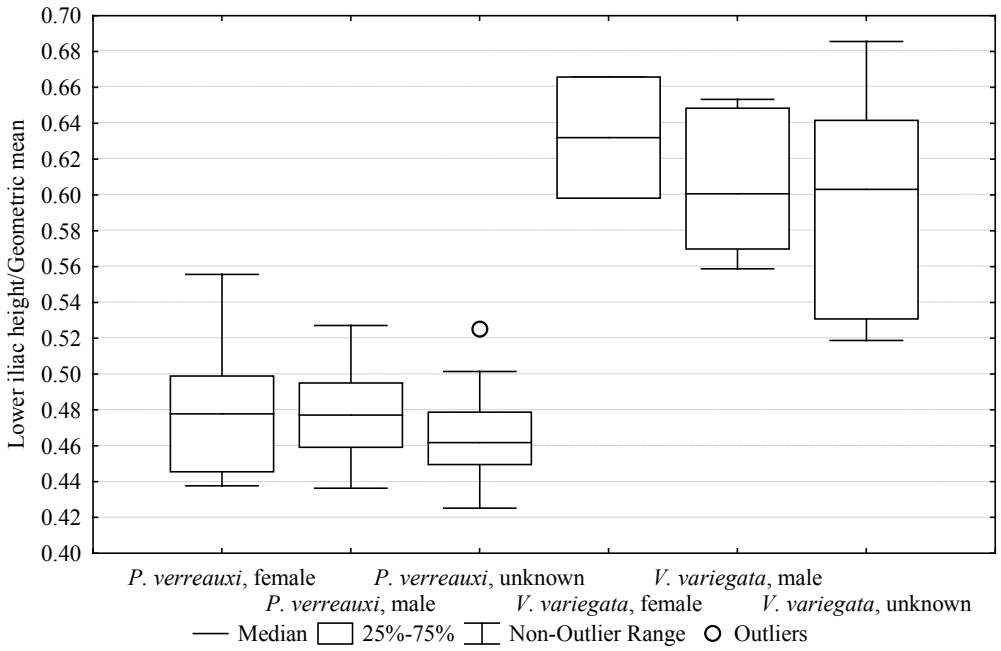
Lower iliac height/Geometric mean
0.70
0.68
0.66
0.64
0.62
0.60
0.58
0.56
0.54
0.52
0.50
0.48
0.46
0.44
0.42
0.40
P. verreauxi, female
P. verreauxi, unknown
V. variegata, male
P. verreauxi, male
V. variegata, female
V. variegata, unknown
Median
25%-75%
Non-Outlier Range
Outliers

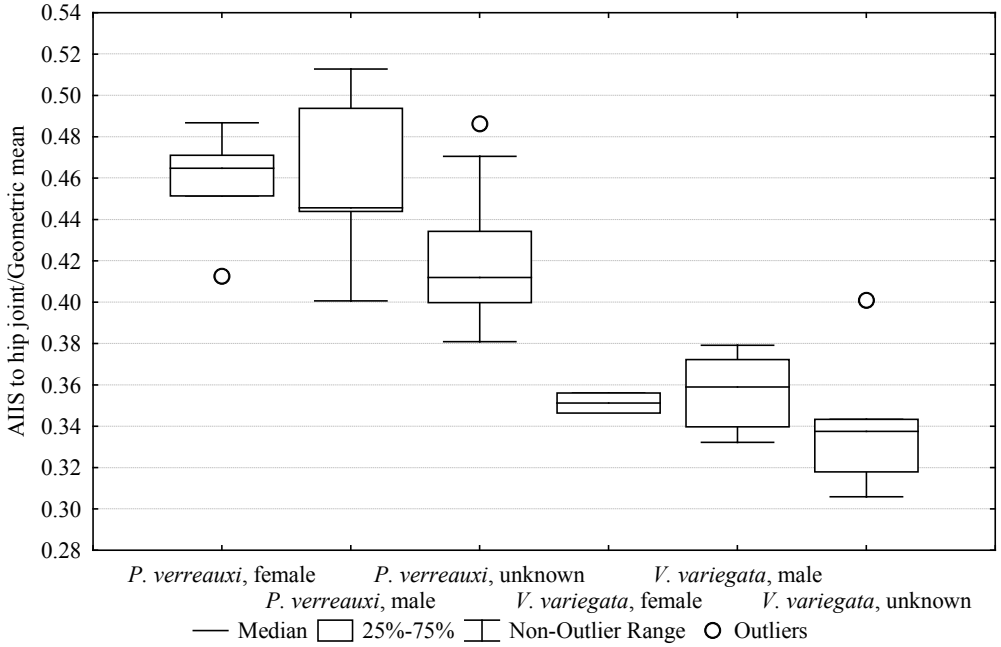
AIIS to hip joint/Geometric mean
0.54
0.52
0.50
0.48
0.46
0.44
0.42
0.40
0.38
0.36
0.34
0.32
0.30
0.28
P. verreauxi, female
P. verreauxi, unknown
V. variegata, male
P. verreauxi, male
V. variegata, female
V. variegata, unknown
Median
25%-75%
Non-Outlier Range
Outliers

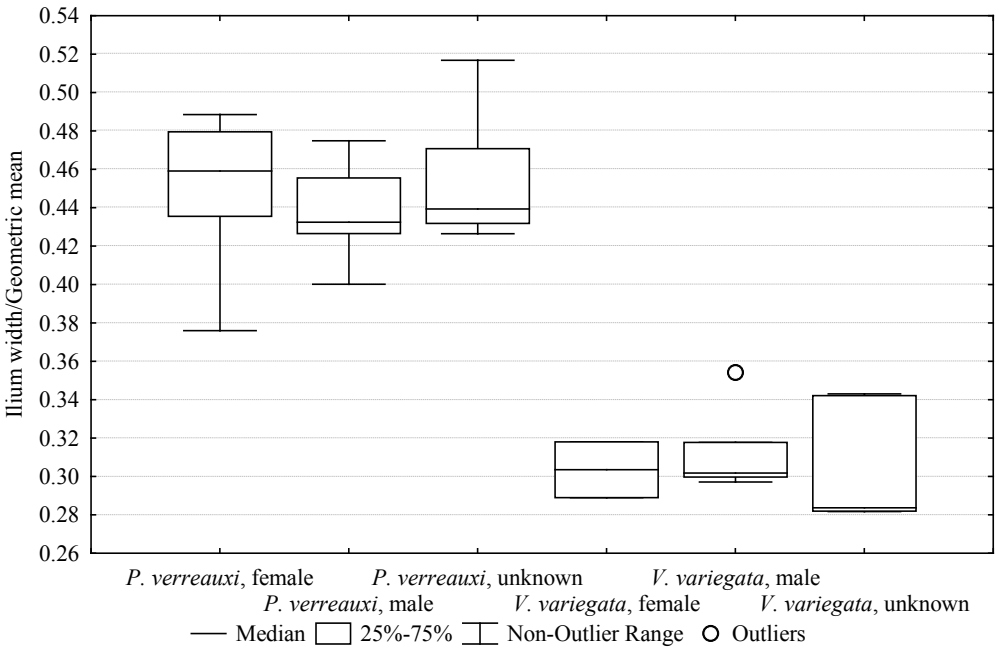
0.54
0.52
0.50
0.48
0.46
0.44
0.42
0.40
0.38
0.36
0.34
0.32
0.30
0.28
0.26
Ilium width/Geometric mean
P. verreauxi, female
P. verreauxi, unknown
V. variegata, male
P. verreauxi, male
V. variegata, female
V. variegata, unknown
Median
25%-75%
Non-Outlier Range
Outliers

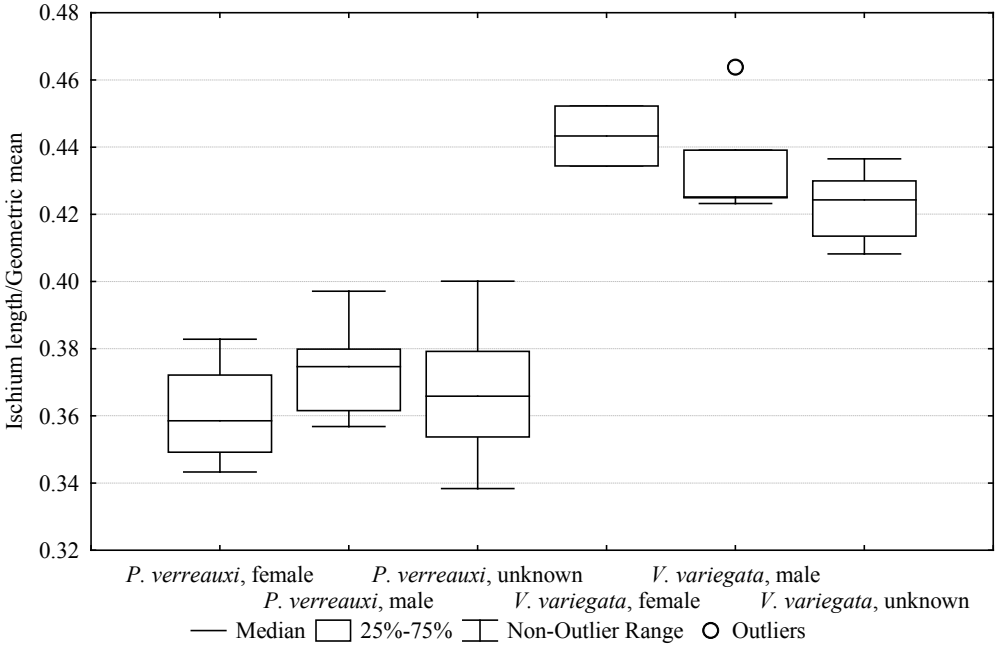
0.48
0.46
0.44
0.42
0.40
0.38
0.36
0.34
0.32
Ischium length/Geometric mean
P. verreauxi, female
P. verreauxi, unknown
V. variegata, male
P. verreauxi, male
V. variegata, female
V. variegata, unknown
Median
25%-75%
Non-Outlier Range
Outliers

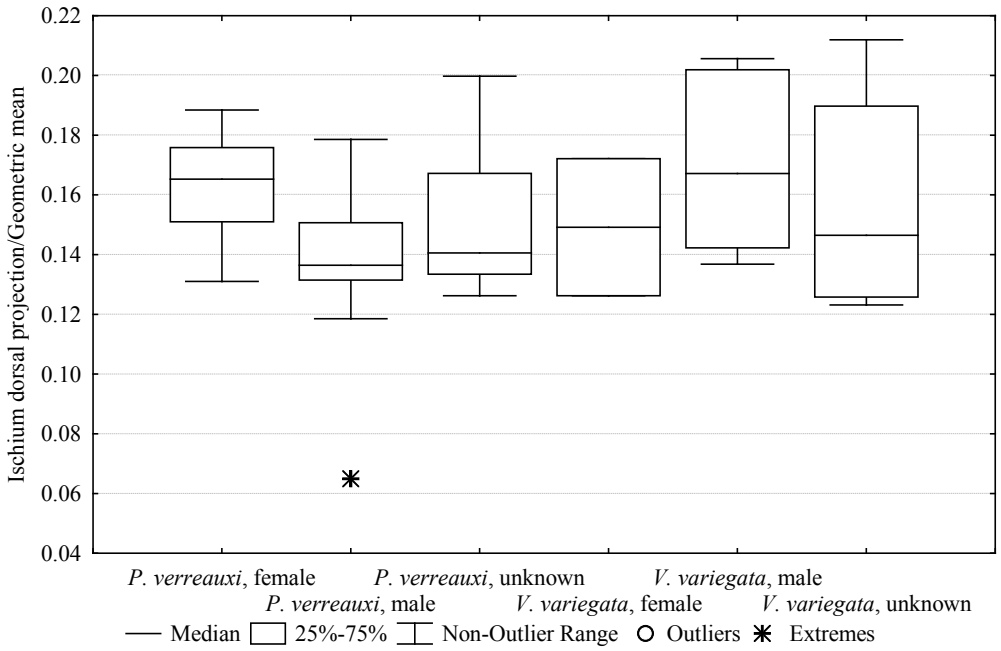
Ischium dorsal projection/Geometric mean
0.22
0.20
0.18
0.16
0.14
0.12
0.10
0.08
0.06
0.04
P. verreauxi, female
P. verreauxi, unknown
V. variegata, male
P. verreauxi, male
V. variegata, female
V. variegata, unknown
Median
25%-75%
Non-Outlier Range
Outliers
Extremes

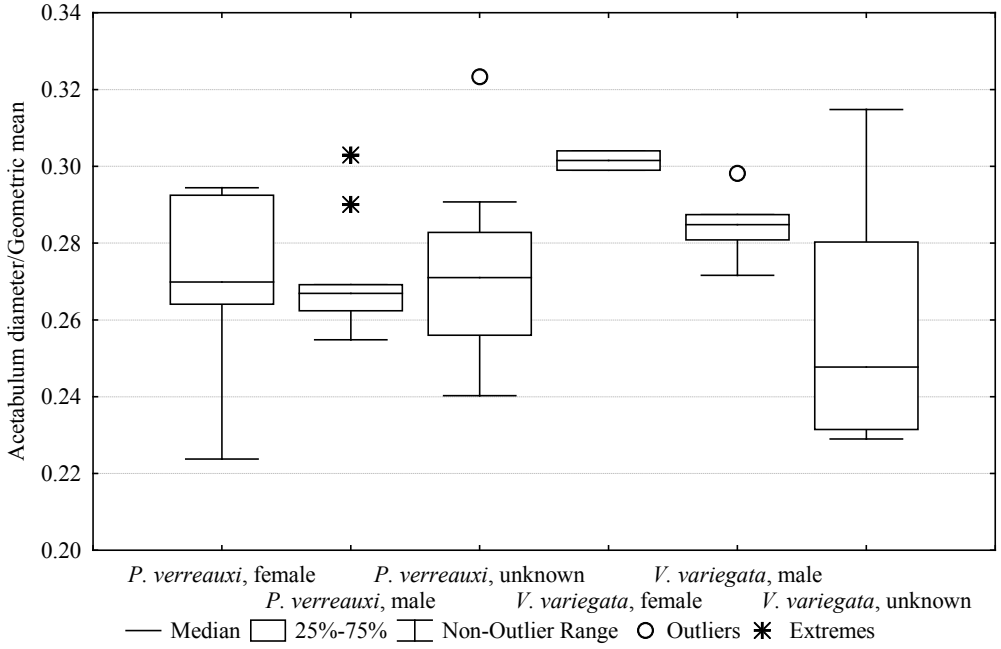
Acetabulum diameter/Geometric mean
0.34
0.32
0.30
0.28
0.26
0.24
0.22
0.20
P. verreauxi, female
P. verreauxi, unknown
V. variegata, male
P. verreauxi, male
V. variegata, female
V. variegata, unknown
Median
25%-75%
Non-Outlier Range
Outliers
Extremes

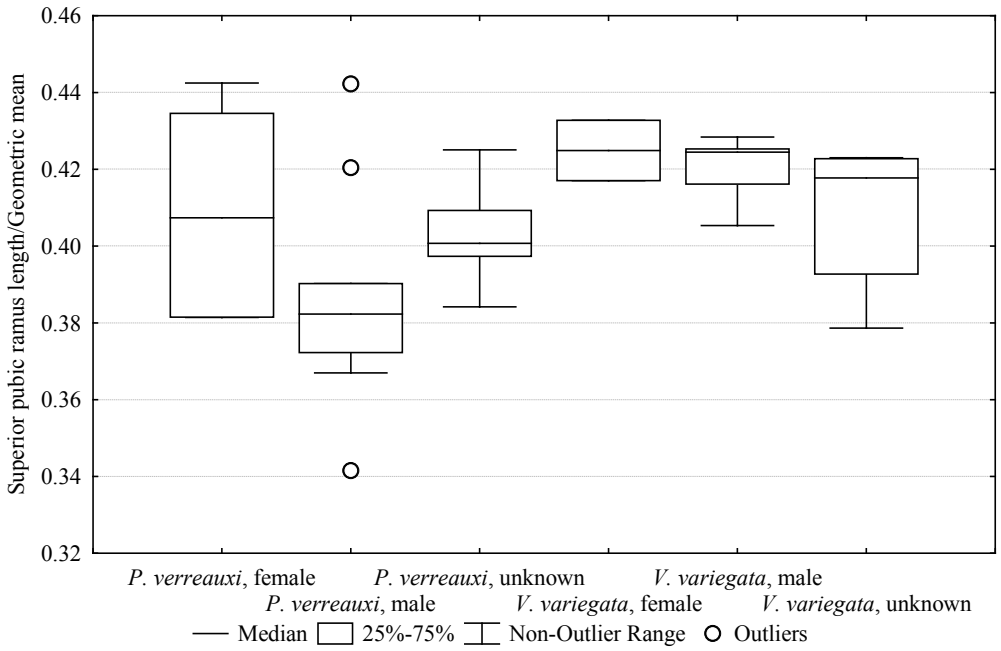
Superior pubic ramus length/Geometric mean
0.46
0.44
0.42
0.40
0.38
0.36
0.34
0.32
P. verreauxi, female
P. verreauxi, unknown
V. variegata, male
P. verreauxi, male
V. variegata, female
V. variegata, unknown
Median
25%-75%
Non-Outlier Range
Outliers

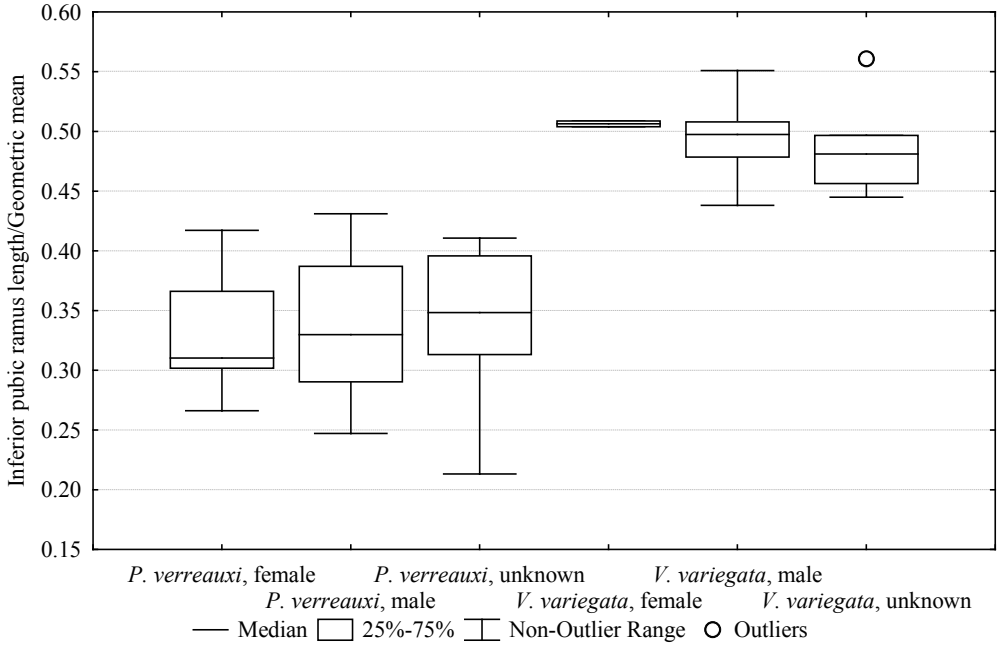
Inferior pubic ramus length/Geometric mean
0.60
0.55
0.50
0.45
0.40
0.35
0.30
0.25
0.20
0.15
P. verreauxi, female
P. verreauxi, unknown
V. variegata, male
P. verreauxi, male
V. variegata, female
V. variegata, unknown
Median
25%-75%
Non-Outlier Range
Outliers

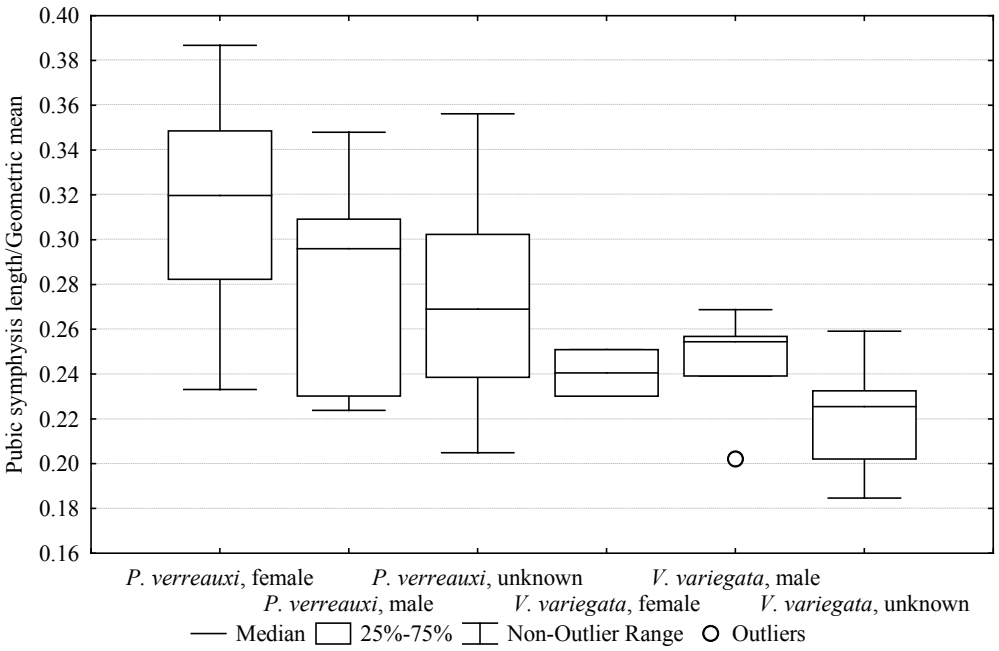
Pubic symphysis length/Geometric mean
0.40
0.38
0.36
0.34
0.32
0.30
0.28
0.26
0.24
0.22
0.20
0.18
0.16
P. verreauxi, female
P. verreauxi, unknown
V. variegata, male
P. verreauxi, male
V. variegata, female
V. variegata, unknown
Median
25%-75%
Non-Outlier Range
Outliers

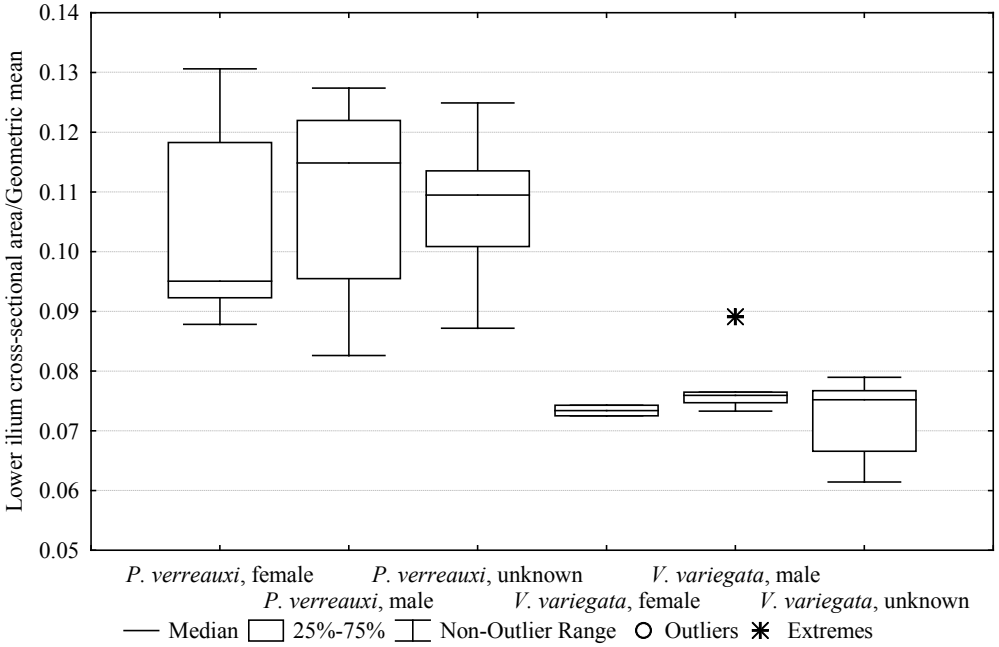
Lower ilium cross-sectional area/Geometric mean
0.14
0.13
0.12
0.11
0.10
0.09
0.08
0.07
0.06
0.05
P. verreauxi, female
P. verreauxi, unknown
V. variegata, male
P. verreauxi, male
V. variegata, female
V. variegata, unknown
Median
25%-75%
Non-Outlier Range
Outliers
Extremes

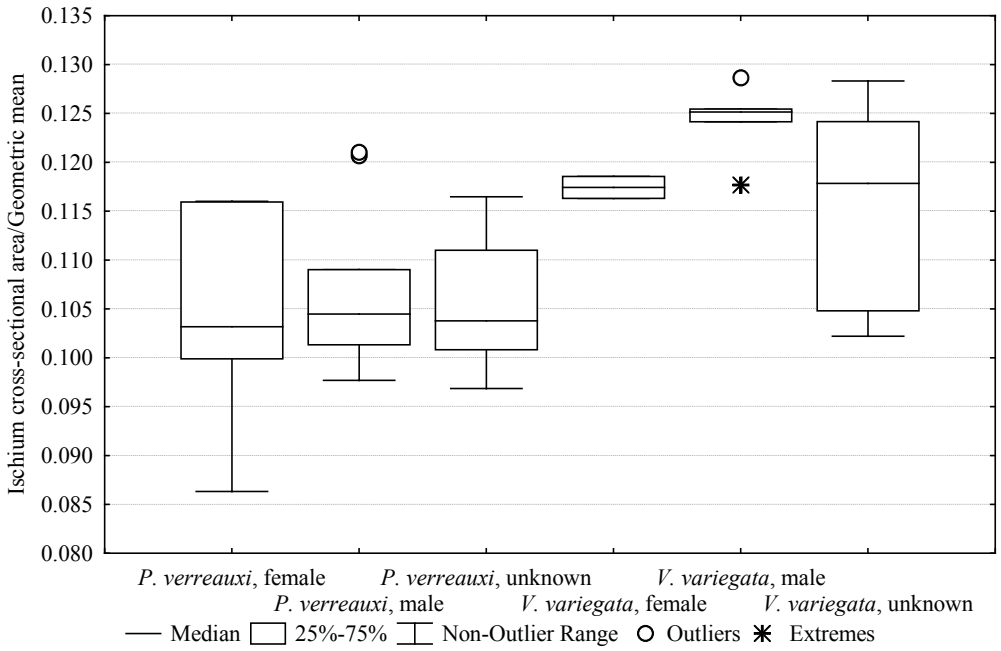
Ischium cross-sectional area/Geometric mean
0.135
0.130
0.125
0.120
0.115
0.110
0.105
0.100
0.095
0.090
0.085
0.080
P. verreauxi, female
P. verreauxi, unknown
V. variegata, male
P. verreauxi, male
V. variegata, female
V. variegata, unknown
Median
25%-75%
Non-Outlier Range
Outliers
Extremes

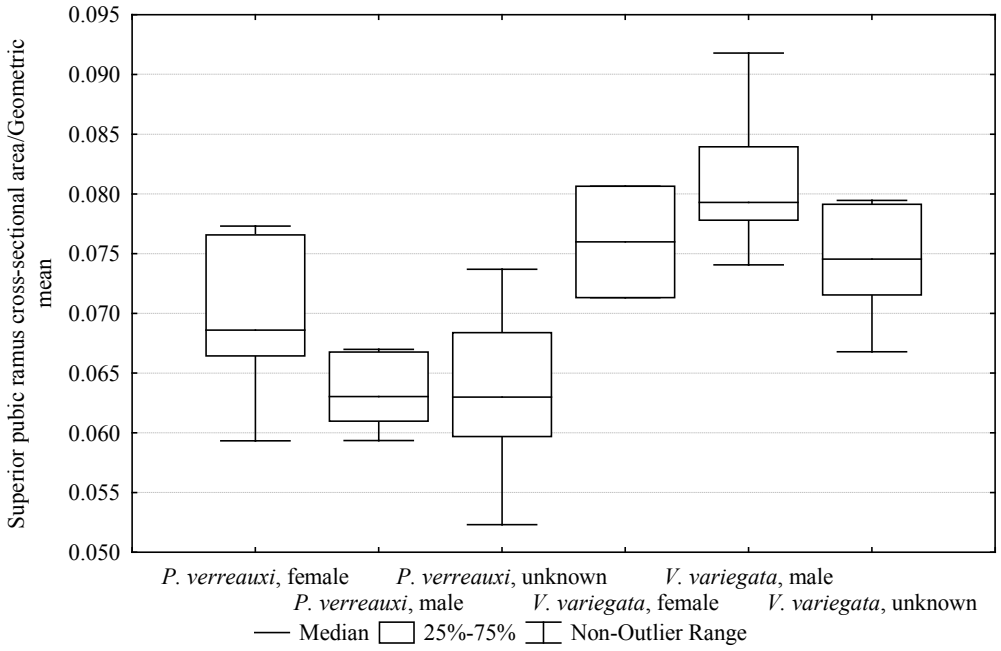
Superior pubic ramus cross-sectional area/Geometric mean
0.095
0.090
0.085
0.080
0.075
0.070
0.065
0.060
0.055
0.050
P. verreauxi, female
P. verreauxi, unknown
V. variegata, male
P. verreauxi, male
V. variegata, female
V. variegata, unknown
Median
25%-75%
Non-Outlier Range

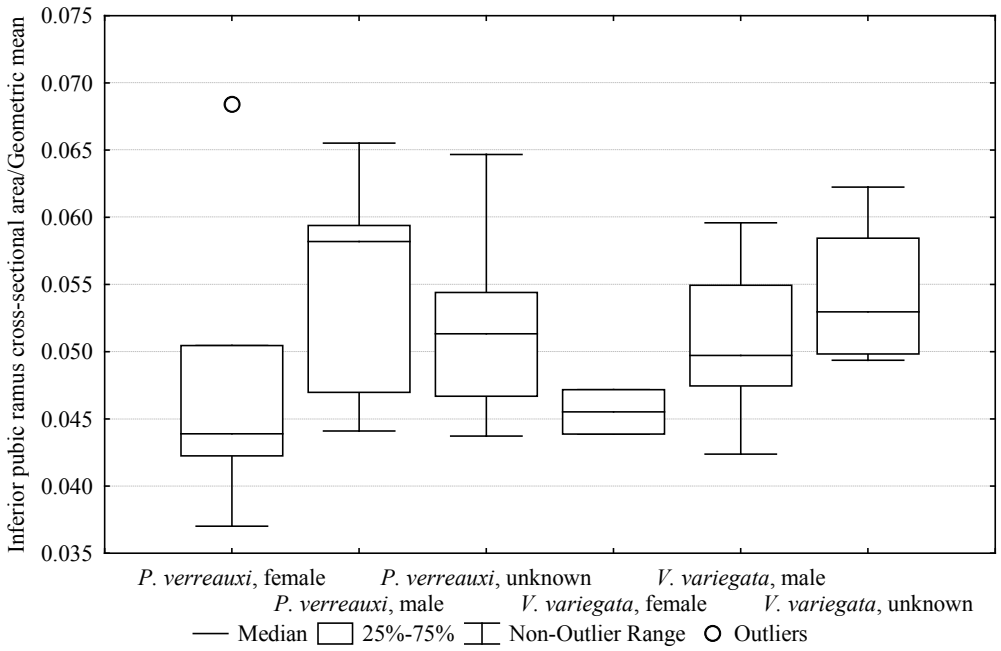
Inferior pubic ramus cross-sectional area/Geometric mean
0.075
0.070
0.065
0.060
0.055
0.050
0.045
0.040
0.035
P. verreauxi, female
P. verreauxi, unknown
V. variegata, male
P. verreauxi, male
V. variegata, female
V. variegata, unknown
Median
25%-75%
Non-Outlier Range
Outliers

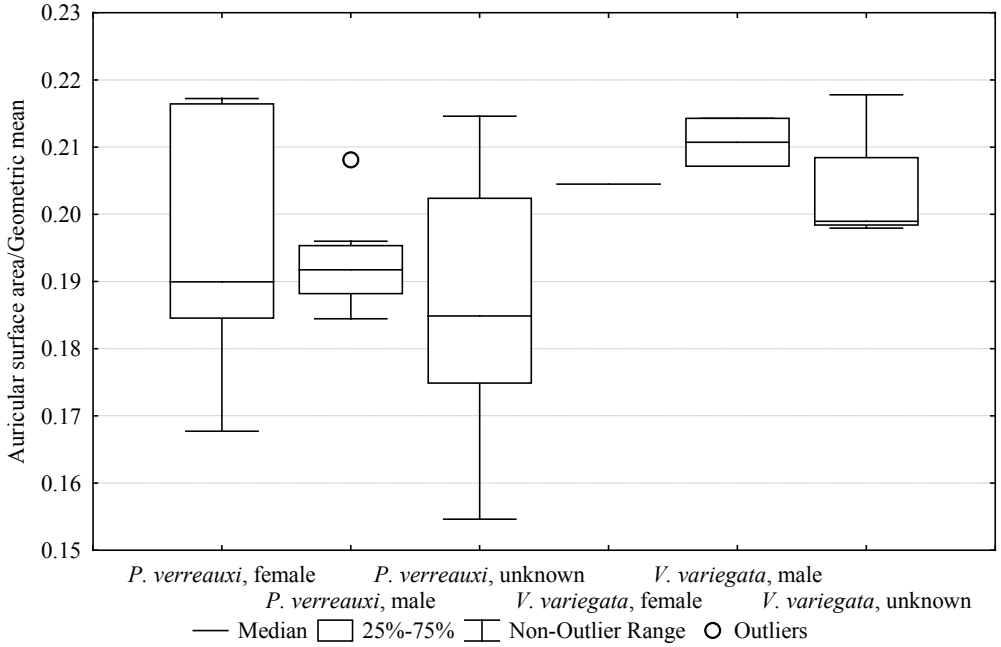
Auricular surface area/Geometric mean
0.23
0.22
0.21
0.20
0.19
0.18
0.17
0.16
0.15
P. verreauxi, female
P. verreauxi, unknown
V. variegata, male
P. verreauxi, male
V. variegata, female
V. variegata, unknown
Median
25%-75%
Non-Outlier Range
Outliers

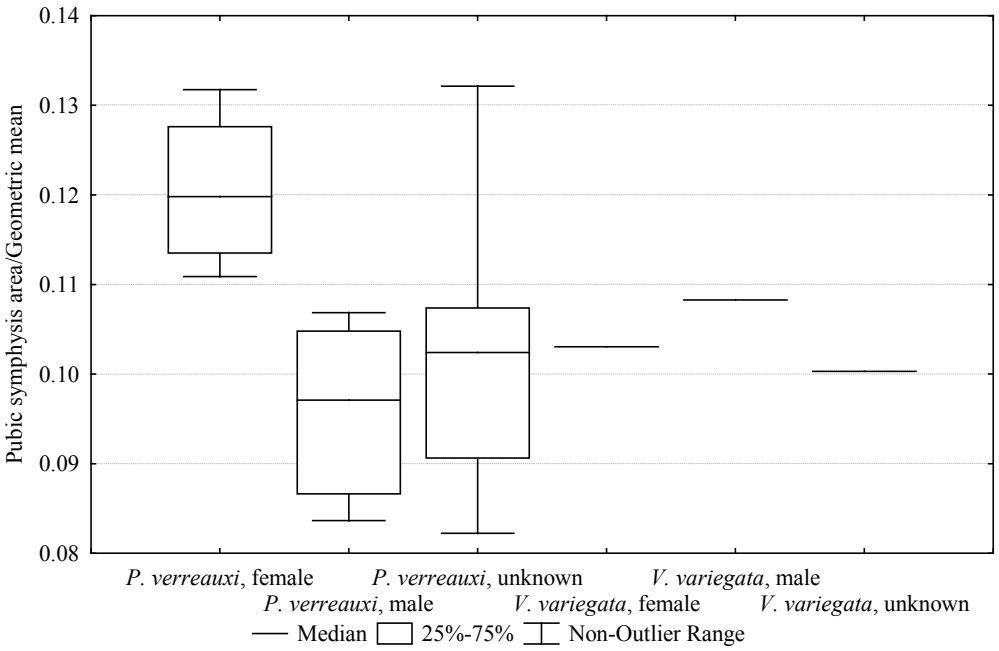
0.14
0.13
0.12
0.11
0.10
0.09
0.08
Pubic symphysis area/Geometric mean
P. verreauxi, female
P. verreauxi, unknown
V. variegata, male
P. verreauxi, male
V. variegata, female
V. variegata, unknown
Median
25%-75%
Non-Outlier Range

APPENDIX D

POST HOC MULTIPLE COMPARISONS TABLES FOR UNIVARIATE ANALYSES

Ilium length/GM: Multiple Comparisons p values (2-tailed)
Kruskal-Wallis test: H (2, N = 25) = 6.45 p =.0399

	AQ	TQ	VCL
AQ		0.035332	1.000000
TQ	0.035332		0.377682
VCL	1.000000	0.377682	

Lower iliac height/GM: Multiple Comparisons p values (2-tailed)
Kruskal-Wallis test: H (2, N = 25) = 10.13 p =.0063

	AQ	TQ	VCL
AQ		0.005999	1.000000
TQ	0.005999		0.083124
VCL	1.000000	0.083124	

Ilium width/GM: Multiple Comparisons p values (2-tailed)
Kruskal-Wallis test: H (2, N = 25) = 12.64 p =.0018

	AQ	TQ	VCL
AQ		0.002705	1.000000
TQ	0.002705		0.017501
VCL	1.000000	0.017501	

Ischium length/GM: Multiple Comparisons p values (2-tailed)
Kruskal-Wallis test: H (2, N = 25) =11.81 p =.0027

	AQ	TQ	VCL
AQ		1.000000	0.004293
TQ	1.000000		0.009345
VCL	0.004293	0.009345	

Dorsal projection of ischium/GM: Multiple Comparisons p values (2-tailed)
Kruskal-Wallis test: H (2, N = 25) = 14.59 p =.0007

	AQ	TQ	VCL
AQ		0.034344	0.286443
TQ	0.034344		0.000547
VCL	0.286443	0.000547	

Inferior pubic ramus length/GM: Multiple Comparisons p values (2-tailed)
Kruskal-Wallis test: H (2, N = 25) = 8.05 p =.0179

	AQ	TQ	VCL
AQ		0.014809	0.453046
TQ	0.014809		0.854870
VCL	0.453046	0.854870	

Pubic symphysis length/GM: Multiple Comparisons p values (2-tailed)
Kruskal-Wallis test: H (2, N = 25) = 7.44 p =.0242

	AQ	TQ	VCL
AQ		0.620093	0.243352
TQ	0.620093		0.019259
VCL	0.243352	0.019259	

Lower ilium cross-sectional area/GM: Multiple Comparisons p values (2-tailed)
Kruskal-Wallis test: H (2, N = 25) = 6.31 p =.0426

	AQ	TQ	VCL
AQ		0.075996	1.000000
TQ	0.075996		0.105339
VCL	1.000000	0.105339	

Ischium cross-sectional area/GM: Multiple Comparisons p values (2-tailed)
Kruskal-Wallis test: H (2, N = 25) = 12.79 p =.0017

	AQ	TQ	VCL
AQ		0.043378	0.429296
TQ	0.043378		0.001503
VCL	0.429296	0.001503	

Inferior pubic ramus cross-sectional area/GM: Multiple Comparisons p values (2-tailed)
Kruskal-Wallis test: H (2, N = 25) = 14.21 p =.0008

	AQ	TQ	VCL
AQ			
TQ	0.052524		
VCL	0.222880	0.000594	

Anteroposterior diameter/GM: Multiple Comparisons p values (2-tailed)
Kruskal-Wallis test: H (7, N = 46) = 25.42 p =.0006

	AQ/Susp.	Susp.	AQ/Leap.	AQ	AQ/TQ	TQ	VCL	AQ/Slow climb
AQ/Susp.								
Susp.	1.00							
AQ/Leap.	1.00	1.00						
AQ	1.00	1.00	1.00					
AQ/TQ	1.00	1.00	1.00	1.00				
TQ	0.20	0.24	1.00	0.28	1.00			
VCL	1.00	1.00	1.00	1.00	1.00	0.45		
AQ/Slow climb	1.00	1.00	0.04	0.42	0.06	0.0005	1.00	

Inter-ASIS distance/GM: Multiple Comparisons p values (2-tailed)
Kruskal-Wallis test: H (7, N = 46) = 22.63 p =.0020

	AQ/Susp.	Susp.	AQ/Leap.	AQ	AQ/TQ	TQ	VCL	AQ/Slow climb
AQ/Susp.								
Susp.	1.00							
AQ/Leap.	1.00	1.00						
AQ	1.00	0.36	1.00					
AQ/TQ	1.00	1.00	1.00	1.00				
TQ	1.00	1.00	1.00	0.12	1.00			
VCL	1.00	1.00	1.00	1.00	1.00	1.00		
AQ/Slow climb	1.00	0.007	0.50	1.00	0.40	0.002	0.56	

Biacetabular distance/GM: Multiple Comparisons p values (2-tailed)
Kruskal-Wallis test: H (7, N = 46) = 21.30 p =.0034

	AQ/Susp.	Susp.	AQ/Leap.	AQ	AQ/TQ	TQ	VCL	AQ/Slow climb
AQ/Susp.								
Susp.	1.00							
AQ/Leap.	1.00	1.00						
AQ	1.00	1.00	1.00					
AQ/TQ	1.00	1.00	1.00	1.00				
TQ	1.00	1.00	1.00	1.00	1.00			
VCL	1.00	0.08	0.04	1.00	0.07	0.09		
AQ/Slow climb	1.00	0.81	0.63	1.00	0.84	1.00	1.00	

Sacral width/GM: Multiple Comparisons p values (2-tailed)
Kruskal-Wallis test: H (7, N = 46) = 18.53 p =.0098

	AQ/Susp.	Susp.	AQ/Leap.	AQ	AQ/TQ	TQ	VCL	AQ/Slow climb
AQ/Susp.								
Susp.	1.00							
AQ/Leap.	1.00	0.08						
AQ	1.00	0.62	1.00					
AQ/TQ	1.00	0.87	1.00	1.00				
TQ	1.00	1.00	1.00	1.00	1.00			
VCL	1.00	1.00	0.24	1.00	1.00	1.00		
AQ/Slow climb	1.00	1.00	0.04	0.37	0.57	1.00	1.00	

Pelvis length/GM: Multiple Comparisons p values (2-tailed)
Kruskal-Wallis test: H (7, N = 46) = 23.44 p =.0014

	AQ/Susp.	Susp.	AQ/Leap.	AQ	AQ/TQ	TQ	VCL	AQ/Slow climb
AQ/Susp.								
Susp.	1.00							
AQ/Leap.	1.00	0.11						
AQ	0.57	0.01	1.00					
AQ/TQ	1.00	0.16	1.00	1.00				
TQ	1.00	1.00	1.00	0.82	1.00			
VCL	1.00	1.00	1.00	0.79	1.00	1.00		
AQ/Slow climb	0.40	0.02	1.00	1.00	1.00	0.77	0.68	